



194

PROGRESS IN
BRAIN RESEARCH

Brain Machine Interfaces
Implications For Science,
Clinical Practice And Society

EDITED BY
JENS SCHOUENBORG
MARTIN GARWICZ
NILS DANIELSEN

SERIES EDITORS

STEPHEN G. WAXMAN

*Bridget Marie Flaherty Professor of Neurology
Neurobiology, and Pharmacology;*

*Director, Center for Neuroscience & Regeneration/Neurorehabilitation Research
Yale University School of Medicine
New Haven, Connecticut
USA*

DONALD G. STEIN

*Asa G. Candler Professor
Department of Emergency Medicine
Emory University
Atlanta, Georgia
USA*

DICK F. SWAAB

*Professor of Neurobiology
Medical Faculty, University of Amsterdam;
Leader Research team Neuropsychiatric Disorders
Netherlands Institute for Neuroscience
Amsterdam
The Netherlands*

HOWARD L. FIELDS

*Professor of Neurology
Endowed Chair in Pharmacology of Addiction
Director, Wheeler Center for the Neurobiology of Addiction
University of California
San Francisco, California
USA*

Elsevier
Radarweg 29, PO Box 211, 1000 AE Amsterdam, The Netherlands
Linacre House, Jordan Hill, Oxford OX2 8DP, UK
360 Park Avenue South, New York, NY 10010-1710

First edition 2011

Copyright © 2011 Elsevier B.V. All rights reserved

No part of this publication may be reproduced, stored in a retrieval system or transmitted in any form or by any means electronic, mechanical, photocopying, recording or otherwise without the prior written permission of the publisher

Permissions may be sought directly from Elsevier's Science & Technology Rights Department in Oxford, UK: phone (+44) (0) 1865 843830; fax (+44) (0) 1865 853333; email: permissions@elsevier.com. Alternatively you can submit your request online by visiting the Elsevier web site at <http://elsevier.com/locate/permissions>, and selecting *Obtaining permission to use Elsevier material*

Notice

No responsibility is assumed by the publisher for any injury and/or damage to persons or property as a matter of products liability, negligence or otherwise, or from any use or operation of any methods, products, instructions or ideas contained in the material herein. Because of rapid advances in the medical sciences, in particular, independent verification of diagnoses and drug dosages should be made

Library of Congress Cataloging-in-Publication Data

A catalog record for this book is available from the Library of Congress

British Library Cataloguing in Publication Data

A catalogue record for this book is available from the British Library

ISBN: 978-0-444-53815-4
ISSN: 0079-6123

For information on all Elsevier publications
visit our website at elsevierdirect.com

Printed and bound in Great Britain

11 12 13 14 10 9 8 7 6 5 4 3 2 1

Working together to grow
libraries in developing countries

www.elsevier.com | www.bookaid.org | www.sabre.org

ELSEVIER

BOOK AID
International

Sabre Foundation

Progress in Brain Research
Volume 194, Pages 2-282 (2011)
Brain Machine Interfaces: Implications for Science, Clinical Practice and Society
Edited by Jens Schouenborg, Martin Garwicz and Nils Danielsen

ISBN: 978-0-444-53815-4

CONTENTS

Series Editors

Page ii

► Abstract |  PDF (20 K)

Copyright Page

Page iv

 PDF (36 K)

List of Contributors

Pages v-viii

► Abstract |  PDF (27 K)

Preface

Page ix

Jens Schouenborg, Martin Garwicz, Nils Danielsen

Chapter 1 - Making the lifetime connection between brain and machine for restoring and enhancing function

Pages 1-25

Philip Kennedy, Dinal Andreasen, Jess Bartels, Princewill Ehirim, Hui Mao, Meel Velliste, Thomas Wichmann, Joe Wright

► Abstract |  Purchase PDF - \$31.50

Chapter 2 - Out of the frying pan into the fire—the P300-based BCI faces real-world challenges

Pages 27-46

Sonja C. Kleih, Tobias Kaufmann, Claudia Zickler, Sebastian Halder, Francesco Leotta, Febo Cincotti, Fabio Aloise, Angela Riccio, Cornelia Herbert, Donatella Mattia, Andrea Kübler

► Abstract |  Purchase PDF - \$31.50

Chapter 3 - Toward a whole-body neuroprosthetic

Pages 47-60

Mikhail A. Lebedev, Miguel A.L. Nicolelis

► Abstract |  Purchase PDF - \$31.50

Chapter 4 - Biocompatible multichannel electrodes for long-term neurophysiological studies and clinical therapy

—Novel concepts and design

Pages 61-70

Jens Schouenborg

Chapter 5 - Deep brain stimulation: BCI at large, where are we going to?

Pages 71-82

Alim Louis Benabid, Thomas Costecalde, Napoleon Torres, Cecile Moro, Tetiana Aksanova, Andrey Eliseyev, Guillaume Charvet, Fabien Sauter, David Ratel, Corinne Mestais, Pierre Pollak, Stephan Chabardes

► Abstract |  Purchase PDF - \$31.50

Chapter 6 - Deep brain stimulation: emerging indications

Pages 83-95

Travis S. Tierney, Tejas Sankar, Andres M. Lozano

Chapter 7 - Development of neuromodulation treatments in a large animal model—Do neurosurgeons dream of electric pigs?

Pages 97-103

J.C. Sørensen, M.S. Nielsen, F. Rosendal, D. Deding, K.S. Ettrup, K.N. Jensen, R.L. Jørgensen, A.N. Glud, K. Meier, L.M. Fitting, A. Møller, A.K.O. Alstrup, L. Østergaard, C.R. Bjarkam

► Abstract |  Purchase PDF - \$31.50

Chapter 8 - A few examples of the contribution of animal research in rodents for clinical application of deep brain stimulation

Pages 105-116

Christelle Baunez

► Abstract |  Purchase PDF - \$31.50

Chapter 9 - Cochlear implants: matching the prosthesis to the brain and facilitating desired plastic changes in brain function

Pages 117-129

Blake S. Wilson, Michael F. Dorman, Marty G. Woldorff, Debara L. Tucci

► Abstract |  Purchase PDF - \$31.50

Chapter 10 - Multimodal, longitudinal assessment of intracortical microstimulation

Pages 131-144

Andrew Koivuniemi, Seth J. Wilks, Andrew J. Woolley, Kevin J. Otto

Chapter 11 - The functional consequences of chronic, physiologically effective intracortical microstimulation

Pages 145-165

Rebecca A. Parker, Tyler S. Davis, Paul A. House, Richard A. Normann, Bradley Greger

► Abstract |  Purchase PDF - \$31.50

Chapter 12 - Reducing surface area while maintaining implant penetrating profile lowers the brain foreign body response to chronically implanted planar silicon microelectrode arrays

Pages 167-180

John L. Skousen, Sr. Mary Elizabeth Merriam, Onnap Srivannavit, Gaytri Perlin, Kensall D. Wise, Patrick A. Tresco

► Abstract |  Purchase PDF - \$31.50

Chapter 13 - Can histology solve the riddle of the nonfunctioning electrode?: Factors influencing the biocompatibility of brain machine interfaces

Pages 181-189

Cecilia Eriksson Linsmeier, Jonas Thelin, Nils Danielsen

► Abstract |  Purchase PDF - \$31.50

Chapter 14 - Changes in CNS structures after spinal cord lesions: implications for BMI

Pages 191-202

M. Martinez, S. Rossignol

Chapter 15 - Modeling the potentiality of spinal-like circuitry for stabilization of a planar arm system

Pages 203-213

George A. Tsianos, Giby Raphael, Gerald E. Loeb

► Abstract |  Purchase PDF - \$31.50

Chapter 16 - Advances in the use of electrical stimulation for the recovery of motor function

Pages 215-225

Dejan B. Popović, Mirjana B. Popović

Chapter 17 - Intraspinal microstimulation for the recovery of function following spinal cord injury

Pages 227-239

Jeremy A. Bamford, Vivian K. Mushahwar

► Abstract |  Purchase PDF - \$31.50

Chapter 18 - Interfacing neurons with carbon nanotubes:: (re)engineering neuronal signaling

Pages 241-252

Alessandra Fabbro, Giada Cellot, Maurizio Prato, Laura Ballerini

► Abstract |  Purchase PDF - \$31.50

Chapter 19 - Nanomodified surfaces and neurite outgrowth

Pages 253-262

Martin Kanje, Fredrik Johansson

► Abstract |  Purchase PDF - \$31.50

Chapter 20 - Direct local polymerization of poly(3,4-ethylenedioxythiophene) in rat cortex

Pages 263-271

Liangqi Ouyang, Rylie Green, Kathleen E. Feldman, David C. Martin

► Abstract |  Purchase PDF - \$31.50

Subject Index

Pages 273-280

Volume in series

Pages 281-282

List of Contributors

- L. Østergaard, Center for Functionally Integrated Neuroscience (CFIN), Aarhus University Hospital, Århus C, Denmark
- T. Aksenova, Clinatec Institute, Commissariat à l'Energie Atomique, Joseph Fourier University, Grenoble, France
- F. Aloise, Neuroelectrical Imaging and BCI Lab, Fondazione Santa Lucia IRCCS, Rome, Italy
- A.K.O. Alstrup, PET Center, Aarhus University Hospital, Århus C, Denmark
- D. Andreasen, Neural Signals Inc., Duluth, and Georgia Institute of Technology, Atlanta, GA, USA
- L. Ballerini, Life Science Department, Center for Neuroscience B.R.A.I.N., University of Trieste, TS, Italy
- J.A. Bamford, Department of Cell Biology and the Centre for Neuroscience, Faculty of Medicine & Dentistry, University of Alberta, Edmonton, AB, Canada
- J. Bartels, Neural Signals Inc., Duluth, GA, USA
- C. Baunez, Laboratoire de Neurobiologie de la Cognition (LNC), Université de Provence; CNRS, UMR6155, and Aix-Marseille Université, Marseille, France
- A.L. Benabid, Clinatec Institute, Commissariat à l'Energie Atomique, Joseph Fourier University, Grenoble, France
- C.R. Bjarkam, Center for Experimental Neuroscience (CENSE), Department of Neurosurgery, Aarhus University Hospital, Århus C, Denmark
- G. Cellot, Life Science Department, Center for Neuroscience B.R.A.I.N., University of Trieste, TS, Italy
- S. Chabardes, Clinatec Institute, Commissariat à l'Energie Atomique, Joseph Fourier University, Grenoble, France
- G. Charvet, Clinatec Institute, Commissariat à l'Energie Atomique, Joseph Fourier University, Grenoble, France
- F. Cincotti, Neuroelectrical Imaging and BCI Lab, Fondazione Santa Lucia IRCCS, Rome, Italy
- T. Costecalde, Clinatec Institute, Commissariat à l'Energie Atomique, Joseph Fourier University, Grenoble, France
- N. Danielsen, Neuronano Research Centre, Lund University, Lund, Sweden
- T.S. Davis, Department of Bioengineering, University of Utah, Salt Lake City, UT, USA
- D. Deding, Center for Experimental Neuroscience (CENSE), Department of Neurosurgery, Aarhus University Hospital, Århus C, Denmark
- M.F. Dorman, Department of Speech and Hearing Science, Arizona State University, Tempe, AZ, USA
- P. Ehirim, Department of Neurosurgery, Gwinnett Medical Center, Lawrenceville, GA, USA
- A. Eliseyev, Clinatec Institute, Commissariat à l'Energie Atomique, Joseph Fourier University, Grenoble, France
- K.S. Ettrup, Center for Experimental Neuroscience (CENSE), Department of Neurosurgery, Aarhus University Hospital, Århus C, Denmark

- A. Fabbro, Life Science Department, Center for Neuroscience B.R.A.I.N., University of Trieste, TS, Italy
- K.E. Feldman, Department of Materials Science and Engineering, The University of Delaware, Newark, DE, USA
- L.M. Fitting, Center for Experimental Neuroscience (CENSE), Department of Neurosurgery, Aarhus University Hospital, Århus C, Denmark
- A.N. Glud, Center for Experimental Neuroscience (CENSE), Department of Neurosurgery, Aarhus University Hospital, Århus C, Denmark
- R. Green, Graduate School of Biomedical Engineering, University of New South Wales, Sydney, NSW, Australia
- B. Greger, Department of Bioengineering, University of Utah, Salt Lake City, UT, USA
- S. Halder, Department of Medical Psychology and Behavioral Neurobiology, University of Tübingen, Tübingen, Germany
- C. Herbert, Department of Psychology I, University of Würzburg, Würzburg, Germany
- P.A. House, Department of Neurosurgery, University of Utah School of Medicine, Salt Lake City, UT, USA
- R.L. Jørgensen, Center for Experimental Neuroscience (CENSE), Department of Neurosurgery, Aarhus University Hospital, Århus C, Denmark
- K.N. Jensen, Center for Experimental Neuroscience (CENSE), Department of Neurosurgery, Aarhus University Hospital, Århus C, Denmark
- F. Johansson, Department of Biology, University of Lund, Sölvegatan, LU, Sweden
- A. Kübler, Department of Psychology I, University of Würzburg, Würzburg, and Department of Medical Psychology and Behavioral Neurobiology, University of Tübingen, Tübingen, Germany
- M. Kanje, Department of Biology, University of Lund, Sölvegatan, LU, Sweden
- T. Kaufmann, Department of Psychology I, University of Würzburg, Würzburg, Germany
- P. Kennedy, Neural Signals Inc., Duluth, GA, USA
- S.C. Kleih, Department of Psychology I, University of Würzburg, Würzburg, Germany
- A. Koivuniemi, The Weldon School of Biomedical Engineering, Purdue University, West Lafayette, and Indiana University School of Medicine, Indianapolis, IN, USA
- M.A. Lebedev, Department of Neurobiology, and Duke Center for Neuroengineering, Duke University, Durham, NC, USA
- F. Leotta, Neuroelectrical Imaging and BCI Lab, Fondazione Santa Lucia IRCCS, Rome, Rome, Italy
- C.E. Linsmeier, Neuronano Research Centre, Lund University, Lund, Sweden
- G.E. Loeb, Department of Biomedical Engineering, University of Southern California, Los Angeles, CA, USA
- A.M. Lozano, Division of Neurosurgery, Toronto Western Hospital, Toronto, Ontario, Canada
- A. Møller, PET Center, and Center for Functionally Integrated Neuroscience (CFIN), Aarhus University Hospital, Århus C, Denmark
- H. Mao, Department of Radiology, Emory University, Atlanta, GA, USA
- D.C. Martin, Department of Materials Science and Engineering, The University of Delaware, Newark, DE, USA
- M. Martinez, Department of Physiology, Groupe de Recherche sur le Système Nerveux Central, Faculty of Medicine, Université de Montréal, SensoriMotor Rehabilitation Research Team of the Canadian Institute for Health Research, Montréal, Québec, Canada
- D. Mattia, Neuroelectrical Imaging and BCI Lab, Fondazione Santa Lucia IRCCS, Rome, Rome, Italy

- K. Meier, Center for Experimental Neuroscience (CENSE), Department of Neurosurgery, Aarhus University Hospital, Århus C, Denmark
- Sr. M.E. Merriam, Department of Electrical Engineering and Computer Science, University of Michigan, Ann Arbor, MI, USA
- C. Mestais, Clinatec Institute, Commissariat à l'Energie Atomique, Joseph Fourier University, Grenoble, France
- C. Moro, Clinatec Institute, Commissariat à l'Energie Atomique, Joseph Fourier University, Grenoble, France
- V.K. Mushahwar, Department of Cell Biology and the Centre for Neuroscience, Faculty of Medicine & Dentistry, University of Alberta, Edmonton, AB, Canada
- M.A.L. Nicolelis, Department of Neurobiology; Duke Center for Neuroengineering; Department of Biomedical Engineering, and Department of Psychology and Neuroscience, Duke University, Durham, NC, USA; Edmond and Lily Safra International Institute of Neuroscience, Natal, Brazil, and Fellow, Center for Neuroprosthetics, École Polytechnique Fédérale de Lausanne, Lausanne, Switzerland
- M.S. Nielsen, Center for Experimental Neuroscience (CENSE), Department of Neurosurgery, Aarhus University Hospital, Århus C, Denmark
- R.A. Normann, Department of Bioengineering, University of Utah, Salt Lake City, UT, USA
- K.J. Otto, The Weldon School of Biomedical Engineering, and Department of Biological Sciences, Purdue University, West Lafayette, IN, USA
- L. Ouyang, Department of Materials Science and Engineering, The University of Delaware, Newark, DE, USA
- R.A. Parker, Interdepartmental Program in Neuroscience, University of Utah, Salt Lake City, UT, USA
- G. Perlin, Department of Electrical Engineering and Computer Science, University of Michigan, Ann Arbor, MI, USA
- P. Pollak, Clinatec Institute, Commissariat à l'Energie Atomique, Joseph Fourier University, Grenoble, France
- D.B. Popović, Faculty of Electrical Engineering, University of Belgrade, BE, Serbia, and Aalborg University, Center for Sensory-Motor Interaction, AA, Denmark
- M.B. Popović, Faculty of Electrical Engineering, University of Belgrade; Institute for Multidisciplinary Research, BE, Serbia, and Aalborg University, Center for Sensory-Motor Interaction, AA, Denmark
- M. Prato, Department of Chemical and Pharmaceutical Sciences, University of Trieste, TS, Italy
- G. Raphael, Advanced Brain Monitoring Inc., Carlsbad, CA, USA
- D. Ratel, Clinatec Institute, Commissariat à l'Energie Atomique, Joseph Fourier University, Grenoble, France
- A. Riccio, Neuroelectrical Imaging and BCI Lab, Fondazione Santa Lucia IRCCS, Rome, Rome, Italy
- F. Rosendal, Center for Experimental Neuroscience (CENSE), Department of Neurosurgery, Aarhus University Hospital, Århus C, Denmark
- S. Rossignol, Department of Physiology, Groupe de Recherche sur le Système Nerveux Central, Faculty of Medicine, Université de Montréal, SensoriMotor Rehabilitation Research Team of the Canadian Institute for Health Research, Montréal, Québec, Canada
- J.C. Sørensen, Center for Experimental Neuroscience (CENSE), Department of Neurosurgery, Aarhus University Hospital, Århus C, Denmark
- T. Sankar, Division of Neurosurgery, Toronto Western Hospital, Toronto, Ontario, Canada

- F. Sauter, Clinatec Institute, Commissariat à l'Energie Atomique, Joseph Fourier University, Grenoble, France
- J. Schouenborg, Neuronano Research Center, Experimental Medical Science and The Nanometer Consortium, Lund University, Lund, Sweden
- J.L. Skousen, Department of Bioengineering, University of Utah, Salt Lake City, UT, USA
- O. Srivannavit, Department of Electrical Engineering and Computer Science, University of Michigan, Ann Arbor, MI, USA
- J. Thelin, Neuronano Research Centre, Lund University, Lund, Sweden
- T.S. Tierney, Division of Neurosurgery, Toronto Western Hospital, Toronto, Ontario, Canada
- N. Torres, Clinatec Institute, Commissariat à l'Energie Atomique, Joseph Fourier University, Grenoble, France
- P.A. Tresco, Department of Bioengineering, University of Utah, Salt Lake City, UT, USA
- G.A. Tsianos, Department of Biomedical Engineering, University of Southern California, Los Angeles, CA, USA
- D.L. Tucci, Duke Hearing Center Duke University Medical Center (DUMC), and Department of Surgery, Division of Otolaryngology—Head and Neck Surgery, DUMC, Durham, NC, USA
- M. Velliste, Neural Signals Inc., Duluth, GA, and Department of Neurobiology, University of Pittsburgh, Pittsburgh, PA, USA
- T. Wichmann, Department of Neurology, Emory University, Atlanta, GA, USA
- J. Wright, Neural Signals Inc., Duluth, GA, USA
- S.J. Wilks, The Weldon School of Biomedical Engineering, Purdue University, West Lafayette, IN, USA
- B.S. Wilson, Duke Hearing Center, Duke University Medical Center (DUMC); Department of Surgery, Division of Otolaryngology—Head and Neck Surgery, DUMC, and Department of Electrical and Computer Engineering, Duke University, Durham, NC, USA
- K.D. Wise, Department of Electrical Engineering and Computer Science, University of Michigan, Ann Arbor, MI, USA
- M.G. Woldorff, Department of Psychiatry; Department of Psychology and Neuroscience; Department of Neurobiology, and Center for Cognitive Neuroscience, Duke University, Durham, NC, USA
- A.J. Woolley, Department of Biological Sciences, Purdue University, West Lafayette, IN, USA
- C. Zickler, Department of Medical Psychology and Behavioral Neurobiology, University of Tübingen, Tübingen, Germany

Preface

Over the past 10–15 years, the research field of brain machine interfaces, or neural interfaces, has exploded with spectacular demonstrations of its enormous clinical potential, such as thought-controlled robots, deep brain stimulation to relieve symptoms in Parkinson’s disease, depression, and Alzheimer’s disease, cochlear implants to restore hearing, and devices for spinal cord stimulation to alleviate chronic pain. With their impressive spatial and temporal resolution, modern neural interfaces also harbor the potential to revolutionize the understanding of how the central nervous system processes, stores, and retrieves information. The symposium *Brain Machine Interfaces—Implications for Science, Clinical Practice and Society* held in Ystad, Sweden, in August 2010 brought together many leading actors in the field to assess the state of the art. As the neural interface research field is interdisciplinary in its nature, the meeting covered a broad range of aspects such as microelectronic technology, mathematical modeling, biocompatibility, pharmacology, neurophysiological research, clinical applications, and upcoming ethical issues. As became evident from the meeting, critical issues for future development and research include how to achieve biocompatible neural interfaces with minimal effects on the tissue and that remain functional for long time periods. Still, neural interfaces produce considerable tissue reactions that may not only cause reorganization of the nervous tissue but also put a limit to the lifetime of the interface. Another critical issue is how to best handle the upcoming ethical questions that will inevitably follow when multichannel electrode implants for deep brain stimulation reach the level of performance that allow widespread clinical use. To solve these fundamental, but very complex, problems, there is a need for coordinated research in material science, organic chemistry, nano- and microtechnology, neurobiology, neurochemistry, neurophysiology, and neuroethics. We would like to see the forum provided by the Ystad symposium as a stepping stone for such a coordinated and constructive effort.

Jens Schouenborg
Martin Garwicz
Nils Danielsen

CHAPTER 1

Making the lifetime connection between brain and machine for restoring and enhancing function

Philip Kennedy^{†,*}, Dinal Andreasen^{†,‡}, Jess Bartels[†], Princewill Ehirim[§], Hui Mao[¶], Meel Velliste^{†,||}, Thomas Wichmann[#] and Joe Wright[†]

[†] Neural Signals Inc., Duluth, GA, USA

[‡] Georgia Institute of Technology, Atlanta, GA, USA

[§] Department of Neurosurgery, Gwinnett Medical Center, Lawrenceville, GA, USA

[¶] Department of Radiology, Emory University, Atlanta, GA, USA

^{||} Department of Neurobiology, University of Pittsburgh, Pittsburgh, PA, USA

[#] Department of Neurology, Emory University, Atlanta, GA, USA

Abstract: A reliable neural interface that lasts a lifetime will lead to the development of neural prosthetic devices as well as the possibility that brain function can be enhanced. Our data demonstrate that a reliable neural interface is best achieved when the surrounding neuropil grows into the electrode tip where it is held securely, allowing myelinated axons to be recorded using implanted amplifiers. Stable single and multiunits were recorded from three implanted subjects and classified according to amplitudes and firing rates. In one paralyzed and mute subject implanted for over 5 years with a double electrode in the speech motor cortex, the single units allowed recognition of over half the 39 English language phonemes detected using a variety of decoding methods. These single units were used by the subject in a speech task where vowel phonemes were recognized and fed back to the subject using audio output. Weeks of training resulted in an 80% success rate in producing four vowels in an adaptation of the classic center-out task used in motor control studies. The importance of using single units was shown in a different task using pure tones that the same subject heard and then sung or hummed in his head. Feedback was associated with smoothly coordinated unit firings. The plasticity of the unit firings was demonstrated over several sessions first without, and then with, feedback. These data suggest that units can be reliably recorded over years, that there is an inverse relationship between single unit firing rate and amplitude, that pattern recognition decoding paradigms can allow phoneme recognition, that single units appear more important than multiunits when precision is important, and that units are plastic in their functional relationships. These characteristics of a reliable neural interface are essential for the development of neural prostheses and also for the future enhancement of human brain function.

*Corresponding author.

Tel.: +1-770-476-1744; Fax: +1-770-476-1745

E-mail: phil@neuralsignals.com

Keywords: brain computer interfacing; brain machine interfacing; neurotrophic electrode; long-term human recording; speech prosthesis; single unit recording; multi-unit recording; local field potentials.

Introduction

For obvious ethical reasons, few studies have been carried out aiming to understand the electrophysiological properties of neurons in the human cortex. Thus far, such information has come from acute, intraoperative microelectrode recordings (Breshears et al., 2009), or by using electrodes that were placed on the cortex for a few weeks prior to surgical resection of epileptic foci (Berger, 1996). An additional source of such information, which has appeared in the past decade, is data from two research groups who have reported long-term recordings using electrodes that were implanted for brain-computer interfacing (Hochberg et al., 2006; Kennedy and Bakay, 1998; Paninski et al., 2004; Serruya et al., 2002), or for speech prosthetics (Guenther et al., 2009). The available studies have largely focused on using recorded signals in neural prosthetic applications. In fact, none of the groups involved with long-term implants in humans has reported on the fundamental properties of human cortical neurons over the long-term and the functional properties of these units. This chapter focuses on the neurophysiologic properties of units recorded from the human motor cortex using data extracted from recordings in three subjects who were implanted with the neurotrophic electrode (NE) for up to 5 years, and with a cumulative experience of 13 years (Bartels et al., 2008). NEs consist of ultrathin Teflon-coated gold wires whose tips are ensheathed in a small cone-shaped glass enclosure which contains neurotrophic factors (Kennedy, 1989). As demonstrated by histological studies, neurons grow neurites into the glass compartment where they undergo myelination (Kennedy et al., 1992). Recordings can then be made from the myelinated neurites “trapped” within the electrode tip. The neuropil within the tip stabilizes after 3–4 months, allowing long-term

recordings for many years (still recording over 5 years), and perhaps indefinitely. Our goal is a lifetime of recording from each electrode.

A major focus of this report presented at the brain-machine interface conference in Ystad, Sweden on August 26, 2010 is the basic aspects of the neurophysiology of the human cortex recorded over many years. Data are available from three subjects in whom the basic firing characteristics are reported. The data demonstrate that single units have a very wide range of firing rates, a wide range of amplitudes, and an inverse relationship between amplitude and firing rate. These results are similar across all subjects. In two subjects, we report on unit firings over long time periods (4 and 5 years), and in one subject, we report on data decoding techniques that used perievent time histograms (PETHs), linear discriminant analysis (LDA), flexible discriminant analysis (FDA), and support vector machine (SVM) analyses to identify over half the 38 tested English phonemes using a data set derived from several recording sessions over a few weeks from our locked-in subject implanted 2 years prior (Brumberg et al., 2011). This same subject at year 4 was able to produce vowel phonemes in a speech paradigm that involved first listening to the vowel pair and then speaking it in his head. The audio output produced the vowel sounds, and a display showed the subject the vowel trajectories in a 2D formant frequency plane (Guenther et al., 2009). With training over many sessions, the subject could produce the vowel pair correctly 80% of the time within a session consisting of 10 trials. We also report here the ability of the subject to listen to a sound and then hum or sing it without and then with feedback of one unit. Feedback optimally consisted of a direct correlation between audio volume and unit firing rate. With this paradigm, the patterns of firings of many single units, but not multiunits, became exquisitely coordinated.

The ongoing recording from human cortical neurons for development of prostheses should produce an unprecedented wealth of basic data relevant to understanding *human* cortical neurophysiology. Obviously, a better understanding of neurophysiologic properties of the human cortex is important in efforts to build neural prosthetic devices that need control signals based on these recordings. In addition, enhancement of human brain function is predicated on understanding the basic physiology of the human brain and how it can be manipulated to optimize a connection directly to the Internet, for example. Human brain enhancement takes on some urgency when considering Ray Kurzweil's prediction that by 2045, intelligent machines will (a) surpass human intelligence, (b) be considered equal to humans, and (c) accorded the same rights as humans (Kurzweil, 2005). One way to delay this moment of singularity is to enhance the capability of the human brain by providing instantaneous access to information, increase external or internal memory storage, and increase mathematical capabilities. However, the limiting factors will likely not be technological such as a reliable neural interface, but rather our limited understanding of how the brain could assimilate and handle extraordinary amounts of information and how it can process such information into an intelligible form.

Methods

Subjects

The experiments described here were carried out in five paralyzed and communication-impaired subjects, as part of a program to develop the use of the NE to control a communication system or, more recently, a speech synthesizer. Subject ER is 26 years old and suffered a brainstem stroke at age 16. His recordings are ongoing 5 years after implantation with a view to develop a speech prosthesis (Brumberg et al., 2009; Guenther et al., 2009). Subject JR was 52 years

old and also suffered a brainstem stroke. He has provided much data on brain to computer communication using single units (Kennedy et al., 2000) or local field potentials (Kennedy et al., 2004a,b). Subject DJ, 46 years old, has amyotrophic lateral sclerosis and provided data during an implantation shortened by nonclosure of the incision. Data from another subject (MH), 53 years old, provided data for a few weeks similar to that reported here (Kennedy and Bakay, 1998). The fifth subject (TT), 42 years old, had mitochondrial myopathy that affected his brain soon after implantation so little useful data were obtained despite a 4.5-year survival. Subjects were implanted with electrodes and data recording hardware, and recordings were carried out, starting several months later, and continued for over 5 years in one subject (ER) (Table 1).

Neurotrophic electrode

The “NE” is a surgically implanted electrode that enables recordings of neuronal activity from single neurons in the brain for many years. The electrode was developed for use in paralyzed human patients to provide lifetime control signals for brain-machine interfaces. A full description of the electrode and associated electronic components has recently been published along with assembly and implantation instructions (Bartels et al., 2008). Two key features will be elucidated briefly. The first is the electrode tip, shown in Fig. 1a. The electrode consists of a small glass cone whose inner surface is coated with proprietary growth factors. The tip of the electrode is 50 μm in diameter, while the upper end (where the wires enter) is 300–400 μm in diameter. Three wires, insulated up to their tips (arrows in diagram) which are spaced by 500 μm , are shown entering the glass conical tip and held in place with methacrylate glue. The electrode can contain two wires (subject JR), three wires (subject ER), or four wires (Subject DJ who also had a second 2-wire electrode). Over the course of several

Table 1. List of implanted subjects

Subjects	Age	Disease	Residual capabilities	Arm hand	Speech	Date of implant	Duration	Outcome
ER	26	BSS	Eyes up slowly for “yes,” down for “no”		***	Dec 22, 2004	6+ years	Ongoing speech decoding
DJ	42	ALS	Slight movement in right hand, face, eyes	***		Nov 25, 2002	3 months	Single units/EMG
TT	39	MM	Eye movements	***		Jul 24, 1999	4.5 years	Too diseased
JR	53	BSS	Slight facial and eye movements	***		Dec 24, 1998	4 years	First Cyborg
MH	54	ALS	Slight eye movements	***		Dec 4, 1996	76 days	Controlled unit firings

***area of motor cortex implanted.

weeks postimplantation of the electrode, neurons from different areas of cortex send processes into the electrode which become myelinated (Kennedy et al., 1992). Electrical potentials can be recorded, from the wires, starting 2–3 weeks after electrode implantation and stabilized at 3–4 months. Since we use bipolar recording amplifiers, the location of the recorded neurite influences the shape of the recorded action potential, specifically its amplitude. The closer a neurite is to a wire, the larger its action potential. Proximity to a given wire can be discerned from the initial deflection of the action potential. Neurites close to one wire will depolarize in the direction opposite to the depolarizing direction of neurites close to the other wire. Neurites located precisely midway between the wires will not be recorded at all, as the direction of the initial depolarization is in “both” directions and hence produces a net zero change in charge. The initial depolarization direction provides some initial spatial separation and eases the task of isolating single units. The second key feature of the NE is shown at the upper end of the cone in Fig. 1a where the first coils of one wire are illustrated. All wires are coiled to allow electrode movements in all three directions, a feature that is essential for minimizing stress on the electrode, which greatly improves the stability and longevity of the recorded signals.

In vivo impedance measurements are typically in the range of 50–750 kΩ at 1 kHz and are rarely available after implantation. However, in subject ER, we had to surgically exchange his implanted electronics 2 years after implantation which required exposure of the electrode connector. Impedance measurements at that time showed an impedance of approximately 70 kΩ (at 1000 Hz) across the wires.

Implant targeting, surgical implantation, and implanted electronic package

As described in detail elsewhere (Bartels et al., 2008), the implantation target was chosen based on brain activation maps obtained from functional MRI scans during imagined active speech articulatory movements (ER) or imagined hand movements (in JR and DJ) while using rest or no movement as the control condition. The surgical implantation sites were targeted using a 3D stereotaxic method. The electronics package, containing a power induction receiving coil, regulators, one or two amplifiers, calibration circuits, and FM transmitters, was implanted subcutaneously on the skull. A coil induction system was used to power the electronic components during recording sessions, by placing a powered coil over

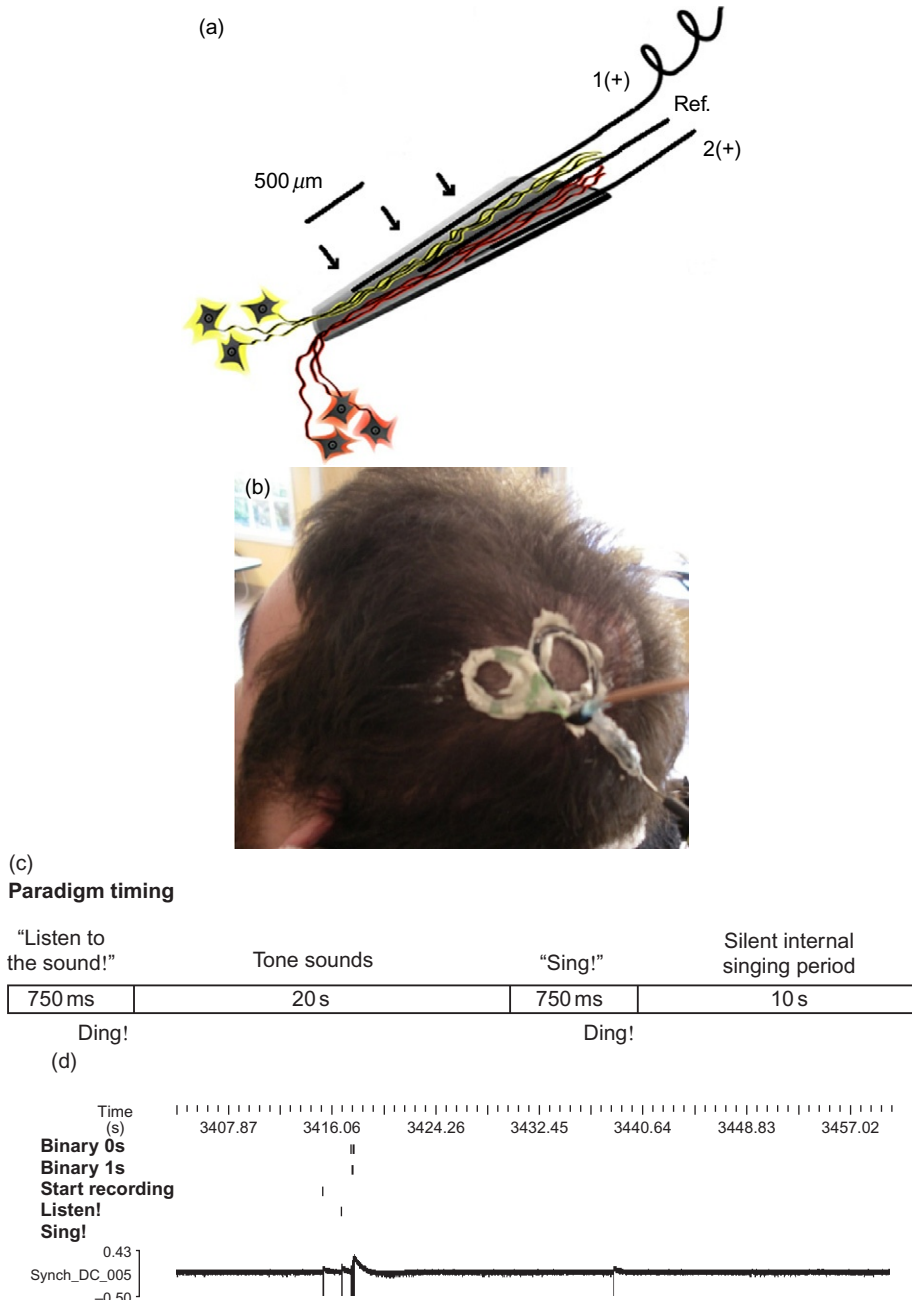


Fig. 1. (a) Overview of the neurotrophic electrode tip. All three wires are coiled for strain relief. Neurons send neurites into and through the cone. Arrows indicate the positions of the wire tips, 500 μm apart. (b) Two FM receiving coils are shown on the left side of subject ER's head. The power induction coil is on the right (not shown). All coils are held in position with EC2 white electrode paste (Grass Electronics Inc.). (c, d) The paradigm used in these studies is described in detail in the text.

the subcutaneous resonant coil. The FM transmitters were used to send the brain signals to external receivers via other coils that were secured to the shaved scalp as shown in Fig. 1b.

Recording methodology, artifact rejection, and spike sorting

As described in our previous publications (Brumberg et al., 2009; Kennedy et al., 2000), the implanted custom-made amplifiers have gains of about 100 \times , bandpassed with filter settings of 4–4000 Hz. The recorded signals were used to FM-modulate a 30–50 MHz signal that was then transmitted through the skin, and received via Win Radios (WinRadio Corp., 15 Stamford Road, Oakleigh 3166, Australia). The modulated signals were further amplified (100 \times ; BMA 200, CWE Inc., Ardmore, PA, USA). The signals were archived on a digital tape recorder (CDAT16, SCSI 16 channel; Cygnus, Delaware Water Gap, PA, USA) at a sampling rate of 20 kHz. The continuous data streams were archived, and a second channel digitally bandpassed at 300–6000 Hz to provide a steady baseline signal for single unit separation. Artifacts induced by discontinuities or sharp transients in the continuous data stream were detected using user-determined signal slope thresholds. In case such artifacts occur, the recording was interrupted (inputs grounded) for a user-determined duration that can last between milliseconds and minutes.

The neuronal signals were sorted into individual spike clusters using commercial software (Cheetah, Neuralynx Inc., Boseman, MO, USA). To distinguish between single and multiunits, interspike interval histograms (ISIHs) were constructed (Fig. 4). Parameters describing cluster features were saved in a file that is used at each recording session. After an initial stabilization phase, it was possible to use the same cluster parameters throughout the recording period. Clusters were nonoverlapping. In the functional data reported here for subject ER, the cluster

parameter file was set up in November 2008 and the data were collected during winter and spring 2009. The cluster parameter file used for data collected in 2007 from subject ER was similar but had to be refined due to reimplantation of the implanted electronics (but not the electrode).

Data collection sessions

The data reported here for subject JR were collected during sessions when he was performing a spelling task as reported previously (Kennedy et al., 2000). The data for subject DJ were collected during a task in which he was making slight pressure movements with his right hand digits while recording from motor cortical area 4. For subject ER, the task needs to be described in full detail as follows.

Subject ER was a 26-year-old male patient, locked-in due to a brainstem stroke in 1999 (at the age of 16 years). He communicated by moving his eyes up for “yes” and down for “no.” The patient was implanted with the NE into his left motor or premotor cortex on December 22, 2004. Data collection recording sessions began on a 3 day per week schedule 3 months after implantation and continued until the fall of 2009. The subject took modafinil (Provigil, Cephalon Inc.) to enhance wakefulness 30 min before any data were collected. The session was terminated if the subject became fatigued as determined by questioning and by observing eye closure. He indicated that he enjoyed the sessions, though they were strenuous for him, requiring considerable mental effort. To minimize fatigue, he listened to music for approximately 2–3 min after each 2–3 min of data collection. The music tended to aid his concentration. During most sessions, his father remained with him to encourage him, stretch his limbs (for comfort and to minimize spasms), and suction his throat as necessary.

In 2007, we tested his hearing using pure tones and found that he could hear up to 13 kHz. In the sessions reported here, background sounds were minimized except for the unavoidable sounds of

computer fans and other electronics. During suctioning of his pharynx using a loud suction machine, recordings were discontinued.

For data collection during tone presentation, blocks of 10 trials, each lasting 31.5 s were employed. Each trial consisted of either a silent control trial or a pure tone followed by either a silent control or a “sing/hum” period where he “sang” (internally) as shown in Fig. 1c. A 750-ms computer instruction to listen was followed by a 200-ms sound to focus his attention, and then a tone was played for 20 s. After this, a “sing” instruction was given, followed by another sound, followed by a silent period during which he sang internally. Figure 1d shows the actual synchronized codes over time, with the “binary 0s and 1s” coding for the specific tone, the “Start recording” indicating recording onset for the block, and “Listen!” and “Sing!” marking their respective onsets with millisecond timing. During the internal singing period (but not the listening period), he received (1) no feedback, (2) feedback of a tone each time a recorded unit fired, or (3) feedback in the form of a tone whose volume varied directly with unit firing. He was questioned after each trial as to whether or not he sang internally, or stayed silent as requested for the control period. He indicated “yes” with upward eye movements, or moved his eyes down for “no.” These responses and other parameters were logged. Ten trials were attempted, but he sometimes showed signs of fatigue before completion of the full trial series. All transitions and codes for the presentations were sent from the instructional computer to the Neuralynx computer and recorded along with the neural data. For data collection during phoneme identification, the basic paradigm is similar to the tone data collection as depicted in Fig. 1c. The difference is that a phoneme, vowel or consonant, is substituted for the tone. In other words, the subject listened to a phoneme and then spoke the phoneme in his head. The timings differ with the “listen” period being 5 s and the “speak” period 10 s. Using a center-out task similar to that used in motor

control studies, it was possible to detect four vowel phonemes. The paradigm involved the computer first sounding out two vowels such as “uh”—“ah,” or “uh”—“iy,” or “uh”—“oo.” The subject then said these in his head, and the pattern of firing was analyzed using the LDA technique. The resultant output was heard by the subject and also translated into movement of a cursor on a screen corresponding to the position of the vowels in 2D formant frequency space (that was essentially the 2D movement space, commonly used in motor control studies). The subject’s task was to move from the center “uh” to one of the corner vowels. Details are in Guenther et al. (2009).

Data analysis

The data were digitized by the Neuralynx software during the recording sessions or afterwards by playing it back from the tape. The data included the synchronized codes along with single units and continuous data streams. The cluster parameter file that sorted the spikes online was not changed throughout the data collection period. The data were first examined using NeuroExplorer software (NEX, from Plexon Technologies, Dallas, TX). ISIIs were generated to distinguish single from multiunit recordings (Fig. 4). Signals were classified as “single units” if ISIs were at least 0.5 ms in duration. Spikes were narrow, presumably due to the fact that they originate from axons, and so can fire close together in time producing the narrow ISIIs.

For the tonal and phoneme data analysis, perievent time histograms were used to average the firing rates during 10 s immediately before (listen phase) and after the ding for the “sing” phase for tone periods as well as for the silent control periods. Normalized data were averaged in each of the 10-s data segments consisting of listen, control, or speak or sing. Two tailed “*t*”-tests (at $p < 0.05$) were used to compare values within and between sessions as described in the

section “Results.” To detect differences between the trends in firing rate values over a session, the firing rates were subtracted from each other across the session. These rates were converted to absolute values if the differences were negative. The values were summed, and the average of these differences and their standard deviations were found to be distributed in a Gaussian fashion and then subjected to two-tailed *t*-tests. Populations of values were compared between sessions. The null hypothesis stated that there should be no differences between the means and one standard deviation from the mean. *p* values less than 0.05 were accepted as rejecting the null hypothesis. Data reported here in JR and DJ were analyzed only for their spike rates and shapes, and not therefore subject to statistical analysis as were the functional data in ER.

Results

Unit amplitudes and firing rates

Multiunit potentials recorded with the NE range in amplitude from 15 to 50 μ Vs (Fig. 2a). Possible single units based on similar amplitudes are shown as letters in the data for subject ER (Fig. 2a, bottom right). Data from another subject (MH) had five similar small amplitude units as already reported (Kennedy and Bakay, 1998). Subject JR had 19 large single units and subject ER had 20. Subject DJ did not remain implanted long enough to give a final reliable count.

In addition to the low-amplitude signals illustrated in Fig. 2a, higher-amplitude signals were also found (Fig. 2b) with amplitudes ranging over 100 μ Vs. These were sufficiently consistent in JR who used them to control a computer cursor (Kennedy et al., 2000). As seen in the lower panel of Fig. 2b for subject ER who was implanted with the three-wire electrode (the center wire acted as reference), large units found on the tracing from one wire (channel 2)

were largely not seen on the adjacent wire (channel 1). The units, though large, were seen on only one wire and hence had to be close to that wire because of the configuration of the wires shown in Fig. 1a. The largest units, however, could be detected by both wires as shown by the only unit on channel 1 for subject ER in Fig. 2b. In other segments of data shown in Fig. 2c, however, there were large units recorded by both channels. These units had to be close to the center reference wire in order to be recorded by both channels. The initial fast phases of depolarization point inward toward each other. This can only happen when the unit is common to both wires by being close to the center reference wire because the amplifiers have fixed but opposite polarities. In addition, the amplitudes are not equal, strongly suggesting that the units were off-center to the reference wire, that is, closer to one wire or the other of the active (nonreference) wires.

Although these large units were useful in subject JR, they were not consistent enough in the other subjects to be useful prosthetic controllers. Hence the remainder of the reported data deals with the low-amplitude multiunits and their extracted single units in subject ER.

Large units often fired very slowly, while smaller units tended to show faster firing rates. Specific firing rates are illustrated for subject JR in Fig. 3a who was implanted in the hand area of motor cortex. Examples of the units are shown in a column on the right side of the figure, and the firing rates are shown over a 15-s period. Bin size is 100 ms with frequency shown on the abscissa. In contrast, the smaller units for subject ER (illustrated in Fig. 2a above) were faster firing in general and again can be divided into four groups of units, with firing rates inversely related to unit amplitudes as shown in Fig. 3b. The groups are itemized as slow firing, medium firing, fast firing, and fastest firing.

These illustrated units were single units as determined by ISIIs shown in Fig. 4. The inter-spike intervals of these units dropped to zero at

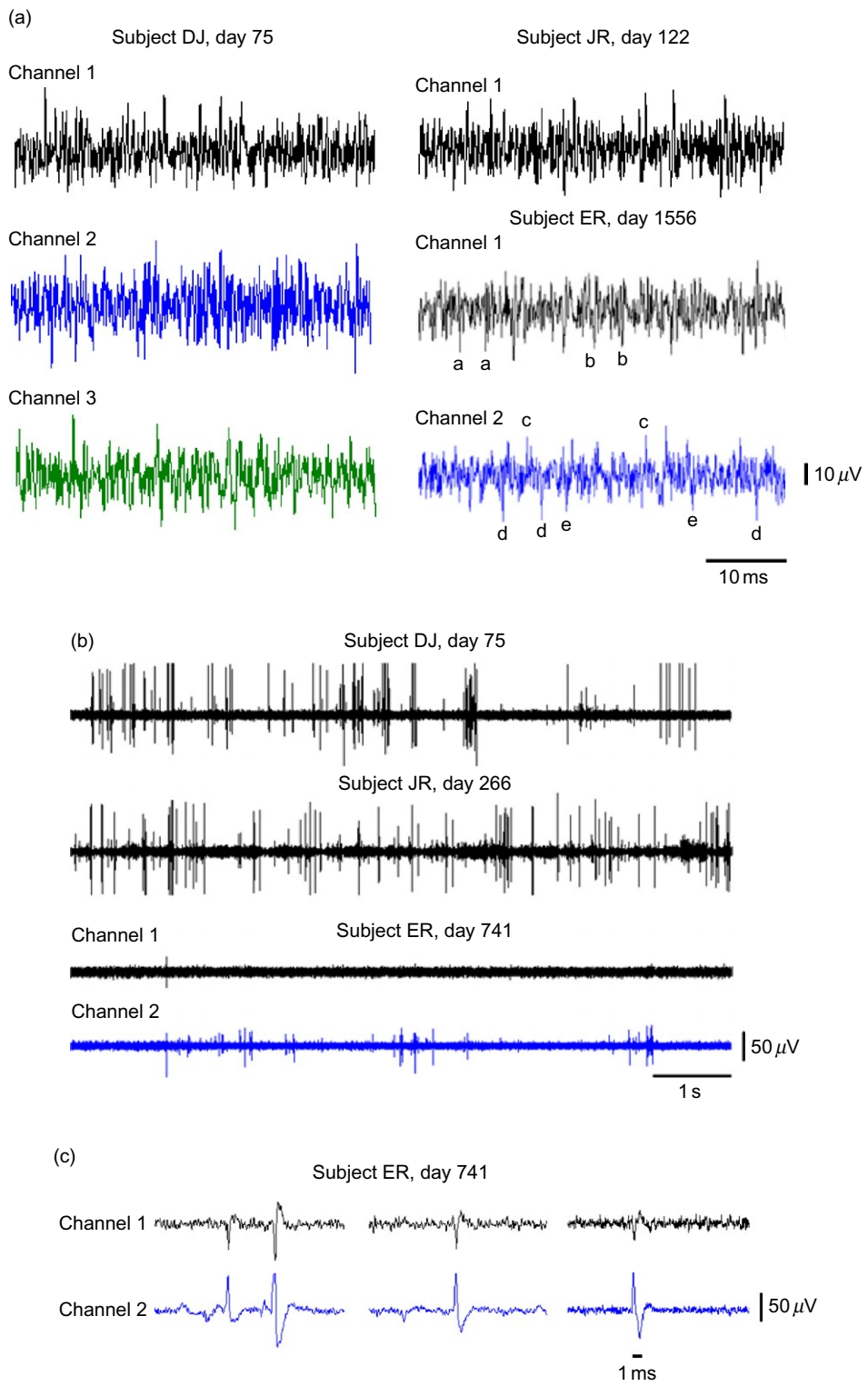


Fig. 2 (Continued)

time zero or close to zero, implying that there was little or no firing within a millisecond, implying they were single units. This only applies to those with sufficiently high firing rates. Because of the density of the multiunit data, many units could not be separated into singletons. Thus about half the units remained as multiunits.

Phoneme identification and speech production

As described in the conference talk, we identified over half the English phonemes from this one electrode using what were single units as identified by ISIH criteria. These analyses were performed offline using PETHs, SVMs, LDA, and FDA. The results were similar for all methods used as described in detail by [Brumberg et al. \(2011\)](#). One of these analytic techniques (LDA) was used online to detect vowel phonemes in real time. The method is described above. In moving from vowel to vowel, he achieved 80% success with practice over several months. Errors decreased, move times shortened, and the end point error decreased over the sessions. Improvements were seen within and between sessions. Detailed results have been published in [Guenther et al. \(2009\)](#).

An issue of great interest in the field is the functional role of single units and whether or not these are more or less important than multiunits. In subject ER, we had a unique

opportunity to correlate firing rates of single and multiunits with “silent” vocalization to determine their relative contributions to tuning patterns as described in Introduction. These studies were performed over 10 days from day 1546 to 1556. The ISIH technique was applied to the data from those days (1556 and 1546), and the same single and multiunits were found from session to session as illustrated in [Fig. 4](#). As described in the section “[Methods](#),” the cluster definition file was not changed over this period.

Single units more important than multiunits for precision tuning

When interrogated, ER indicated that he “sang in his head” most of the time. During these “singing” studies, he was most enthusiastic when provided with loud tonal feedback of his (assumed) output. This was achieved by directly relating loudspeaker volume to unit firing rate. The issue here was not whether or not he “sang in his head,” but how the firing rates of single and multiunits compare during these “singing” periods. We chose a tone at 523 Hz (C5: one octave above middle C) because this tone appeared to produce an increase in firing rate of unit ch2-09 when tested in 2007. Additionally, we also tested tone 262 Hz (C4: middle “C”). Nine tones were initially tested without feedback to determine if there was any modulation in firing rates of any units. These tones were 110, 131, 220,

Fig. 2. (a) Left panel: 42 ms of continuous multidata from subject DJ from the three channels recorded 75 days after implantation on October 25, 2002. Right panel top: 42 ms of continuous multidata from subject JR 122 days after implantation. Right panel bottom: examples of 42 ms of continuous multiunit data from each channel in subject ER. Possible single units are labeled as shown. The letter labels do not correspond to units in later figures and are meant only to highlight wave shapes similar in amplitude recorded on day 1556 after implantation. (b) Top panel: units from subject DJ recorded on day 75. Middle panel: units recorded from JR on day 266. Note the various amplitudes of larger units that fired infrequently. Bottom panel: units from subject ER that fired infrequently on only one channel (blue). There is physiological crosstalk between the channels, but not with the third channel (not shown). See next figure and text for explanation. (c) Physiological crosstalk between channels 1 and 2 inside the electrode. Note the depolarization spikes face each other. For full explanation see text.

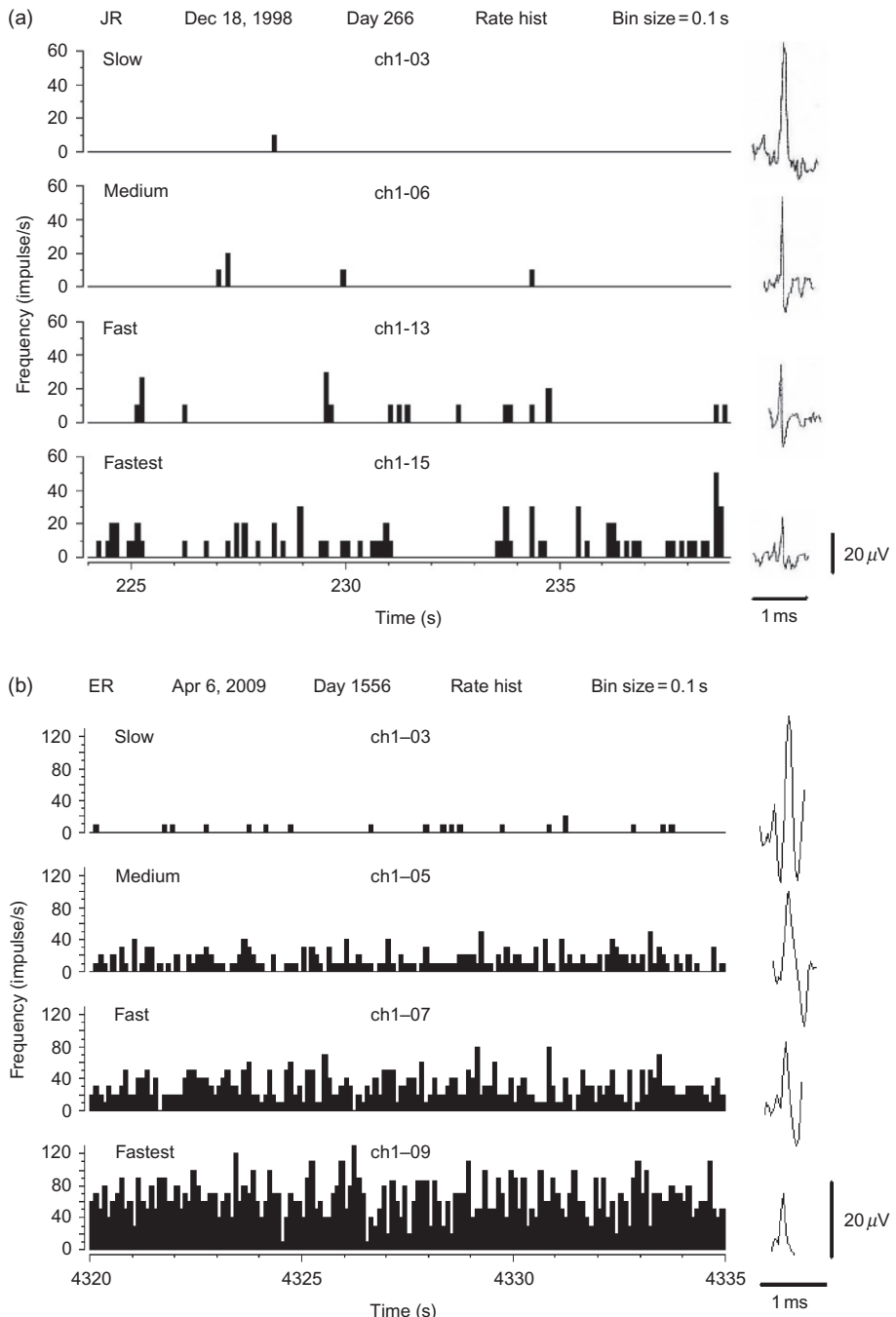


Fig. 3. (a) Firing rate histograms of units with different amplitudes are illustrated for the large units illustrated in Fig. 2a for subject JR. Note the scale differences between these data and those in (b). (b) Firing rate histograms of units illustrated in Fig. 2a for subject ER. Data recorded at rest. Note the scale difference between unit sizes in (a) and (b).

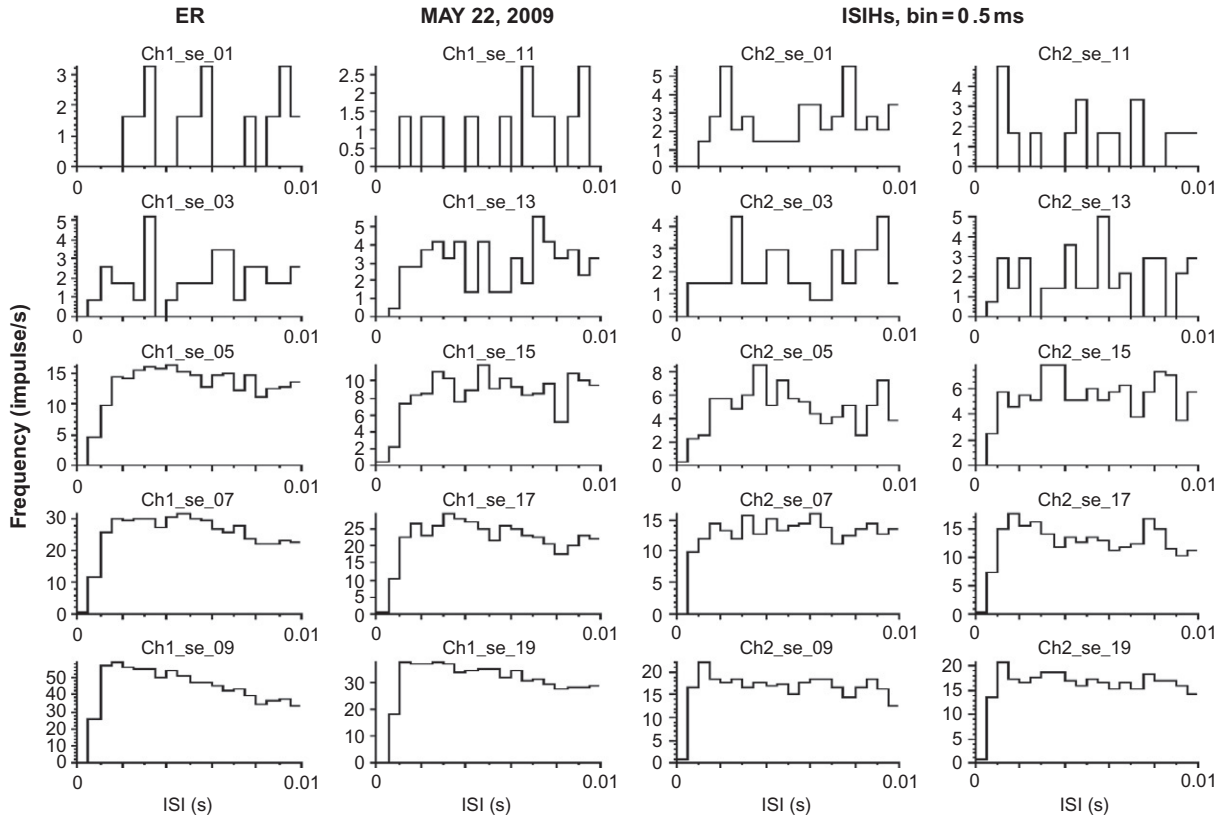


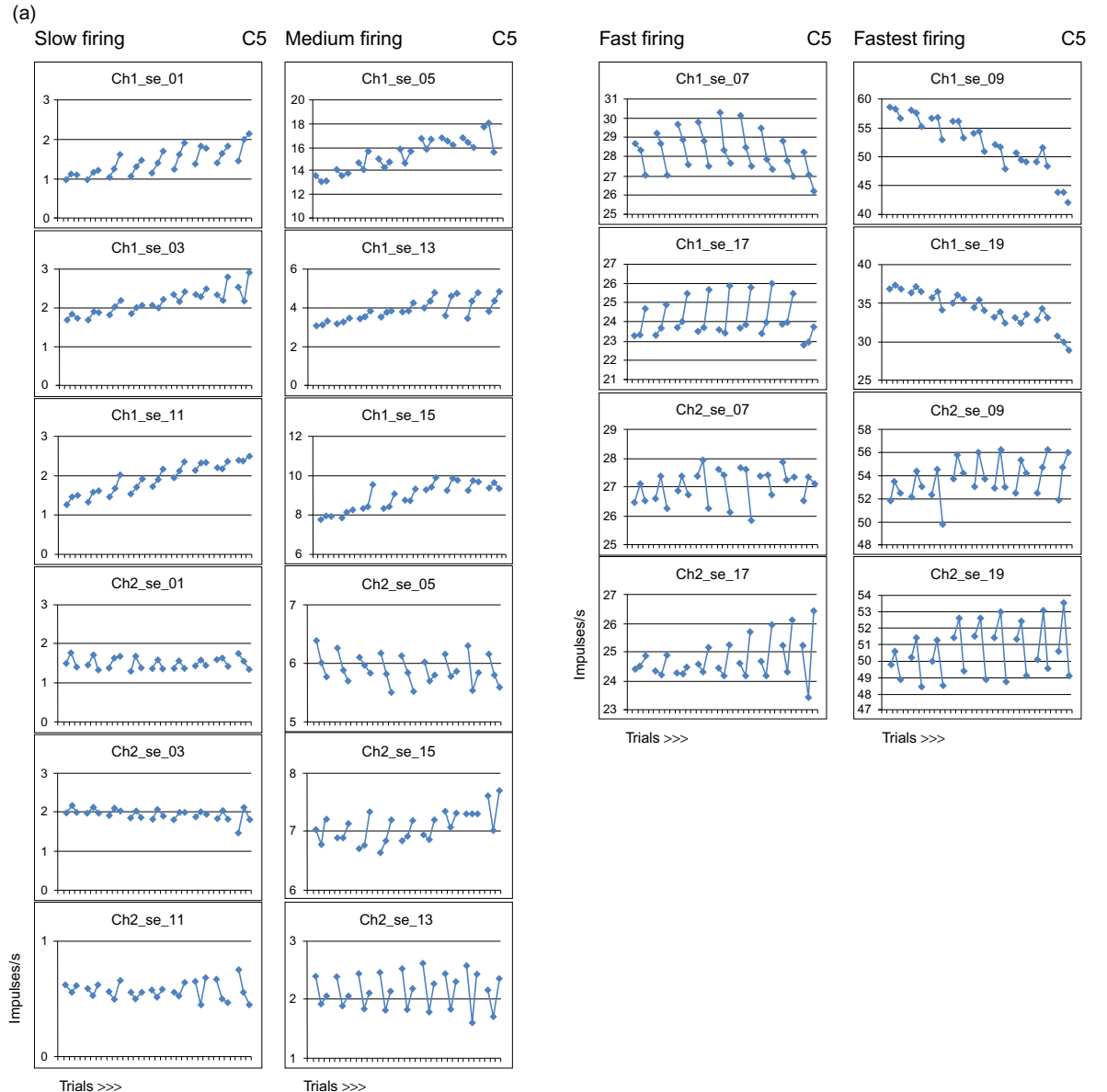
Fig. 4. Interspike interval histograms (ISIH) of 20 units whose rates fall to zero between zero time and 1 ms, implying that each one is a single unit. Data are from day 1602 (May 22, 2009), subject ER.

247, 262, 440, 494, 523, 880, and 988 Hz that spanned four diatonic scales as notes A–C.

On day 1556, he was provided with feedback of the tone through the speaker each time unit ch2-09 fired. The volume of the tone feedback was directly related to the firing rate. To the subject, it seemed like he was actually singing or humming (vocalizing) the tone as loudly as he could. The results for the identified single units are shown in Fig. 5a for the four classes of units. There were nine trials in each session. In each trial, as described in the section “[Methods](#),” the firing rates were averaged over a listen period, a control period, and a “sing” period. Thus the data appear as “V” shapes in the figures. For many units,

there was a progressive smoothing of this pattern as the session progressed. There was a remarkable consistency in most units, even those that were slow firing with average rates of a few Hz, as shown in the figure. The data for tone C4 (middle C) demonstrated a similar smoothing of firing rates (Fig. 5b). Many units responded differently to the different tones (e.g., ch1-01, ch1-03, ch2-13, ch2-17, ch2-19). Interestingly, unit ch2-09, which was the unit fed back as the tone, had averaged firing rates during the control (silent) periods that were higher than those during the listen or sing periods. However, toward the end of the session, the firing rates during the “sing” period increased to levels higher than the

controls. In addition, the medium firing rate units (second column) appeared to be the least well tuned. Finally, for the fastest units, ch1-09 and ch1-19 have rates that drop off gradually as the session progressed.



In contrast to the single unit data, the multiunit data produce little if any smooth tuning. These dramatic findings are illustrated in Fig. 5c and d for tones 523 and 262 Hz, respectively. These data were collected at the same session as the

Fig. 5 (Continued)

(b)

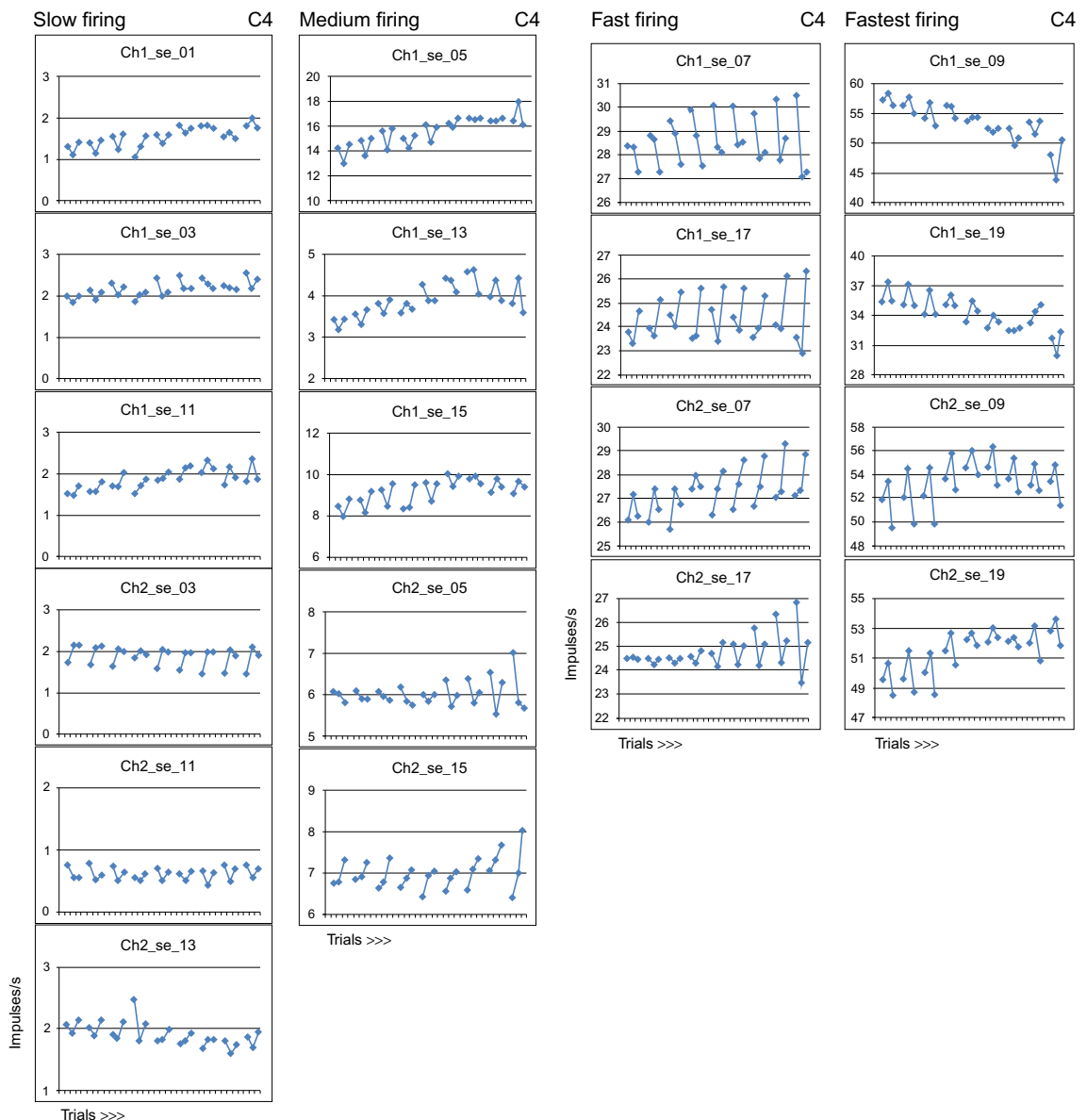


Fig. 5 (Continued)

(c)

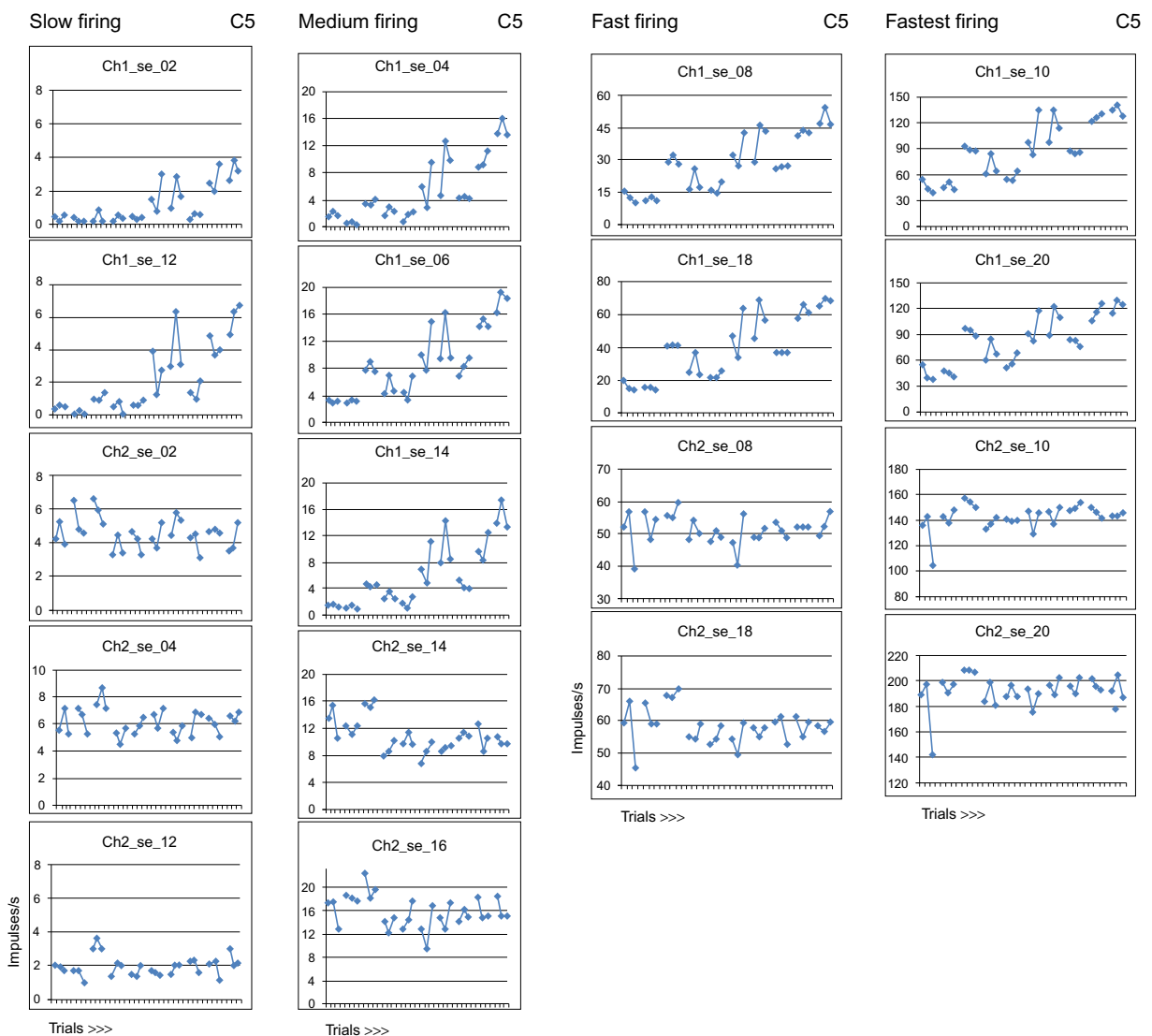


Fig. 5 (Continued)



Fig. 5. (a) Averaged firing rates of the four classes of units during the listen, control, and sing periods appeared as mainly "V"-shaped triplets for tone 523 Hz. (b) Similar data presentation for firing rates for tone 262 Hz. (c) Similar data presentation for multiunit data for one 523 Hz. (d) Similar data presentation for multiunit data for 262 Hz. All data are from day 1556 in subject ER.

single units. These units could not be separated into single units and are multiunits as determined by the ISIH plot (not illustrated).

Plasticity of single unit firings

These data also demonstrate the gradual smoothing of the firing rates over several sessions. This intersession improvement in tuning performance was very obvious in most units. For tone 523 Hz, three sessions preceded the most tuned session (day 1556). The first two sessions on days 1546 and 1549 were performed with no feedback, and the nontuned firing rates are illustrated in Fig. 6a. Feedback of ch2-09 unit firing was provided as a 523-Hz tone on day 1553 (third column in the figure). A pattern of tuning did begin to appear. However, the smooth tuning did not fully appear until volume-related feedback was presented (with the volume increasing as the firing rate increased). These presentations were successfully presented later as intrasession randomized feedback versus no feedback with similar, though not so strong results. The examples represent a sample from each of the four different types of units. For tone 262 Hz, two preceding sessions provided data on intersession tuning changes. The results were similar as shown.

Statistical analysis

To statistically analyze the variability in these data, the averaged values and one SD of three units (ch2-09, ch2-13, ch2-17) were obtained as described in the section “[Methods](#).“ These values were then compared for each condition (listen, control, ing) across the sessions (days 1549, 1553, 1556) for tone 523 Hz, using a two-tailed *t*-test, and plotted in Fig. 6c. The results demonstrate statistically significant differences for all conditions and all units tested between day 1549 (no feedback) and 1556 (volume-related feedback). Statistically,

significant differences were seen for most conditions when day 1553 was included.

Discussion

Cellular origins of single units

The different unit amplitudes and firing frequencies illustrated in Figs. 2 and 3 for the four different units need to be interpreted in light of the design features of the NE shown in Fig. 1. The relevant feature of the electrode is that growth into the tip occurs from upper cortical layers as well as from lower layers, as demonstrated in histological analyses of rat and monkey implants where tissue was consistently found to form a bridge throughout the glass tip and connect to the surrounding neuropil above and below the openings ([Kennedy et al., 1992](#)). Thus we should expect connections with neurons from different cortical layers. The electrode records axonal (not somatic) potentials. Because animal experiments have shown that 3 weeks or longer after implantation, all intercone fibers become myelinated ([Kennedy et al., 1992](#)), it is reasonable to assume that the signals recorded in this study were generated by myelinated axons.

Although the signal amplitude is in part dependent on the spatial separation between the axon and the electrodes, it appears likely that large amplitude units arise from large-diameter axons of corticospinal tract neurons, while small amplitude units may derive from axons of small interneurons. This is further supported by the observation that large-amplitude potentials fired slowly, while small-amplitude potentials fired at higher frequency: primate corticospinal tract neurons are known to fire more slowly than interneurons ([Chang and Luebke, 2007](#); [Gonzalez-Burgos et al., 2005](#); [Zaitsev et al., 2009](#)).

The four types of units illustrated in Figs. 2 and 3 are taken at rest, but the firing rates shown in Figs. 4–6 are analyzed during the vocalization (singing) task and are thus a better reflection of

the active firing rates of the different neurons. We are not claiming they are maximal firing rates because we cannot be sure these are optimally task related. The results of studies of cortical neurons in primate (Chang and Luebke, 2007), cat (Chen et al., 1996), and rat (Schwindt et al., 1997) are not easily transferable to the present results in humans, as all the former studies were

performed in slice preparations (including the monkey studies) using intracellular recording and stimulation. Nevertheless, they confirm the interpretation of the rate/amplitude inverse correlation for neurons in different cortical layers, namely that fast firing units are interneurons and slow firing units are larger neurons that, presumably, give rise to the corticospinal tract.

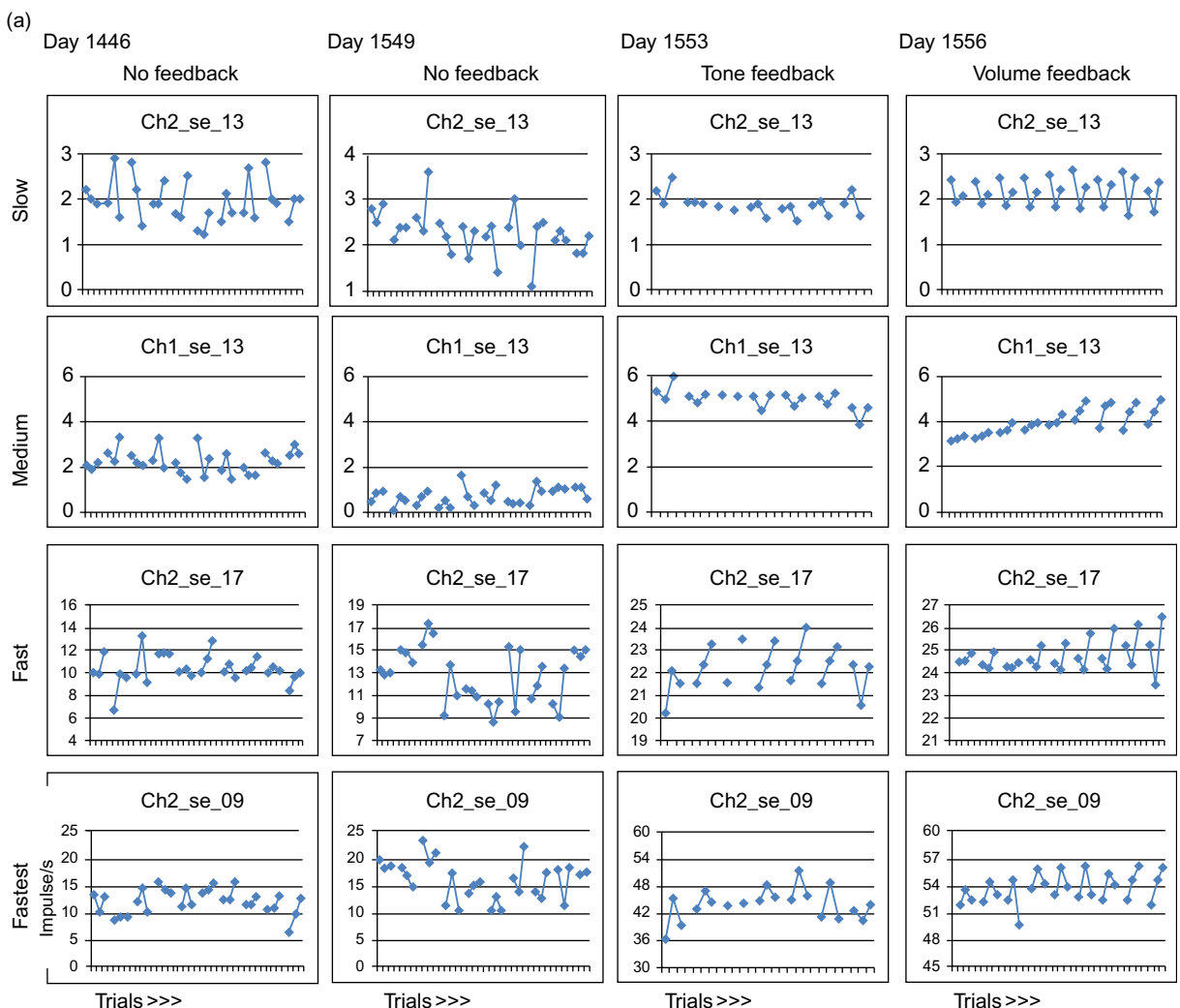


Fig. 6 (Continued)

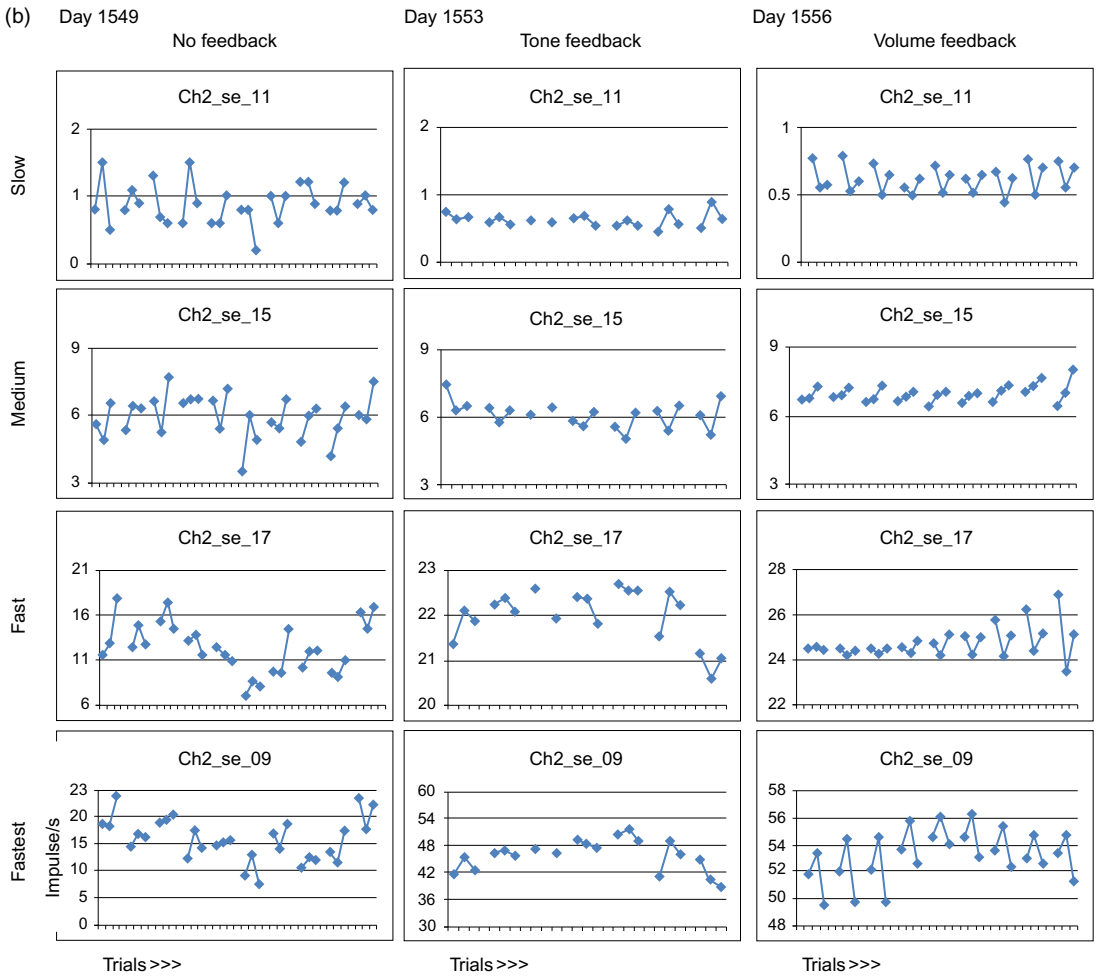


Fig. 6 (Continued)

The separation of multiunits has been hampered by the limited number of recording surfaces inside the cone tip. This disadvantage has long been recognized, and a new design under development involves microfabrication of a flexible polyimide micromachined version with 4, 8, 12, or 16 recording surfaces within the tip. This is expected to provide fewer units per channel easing the task of separation of units and, with a larger number of channels, increasing the yield per electrode. For example, with only 20 single units in ER's two-

channel electrode, 160 units would be available if 10 units were available per channel in a 16-channel electrode. With fewer units per channel, separation into single units ought to be simplified.

Large-amplitude units

Units with amplitudes above 50 μ V were found mainly in subject JR and used by him to drive the cursor (Kennedy et al., 2000). They were also

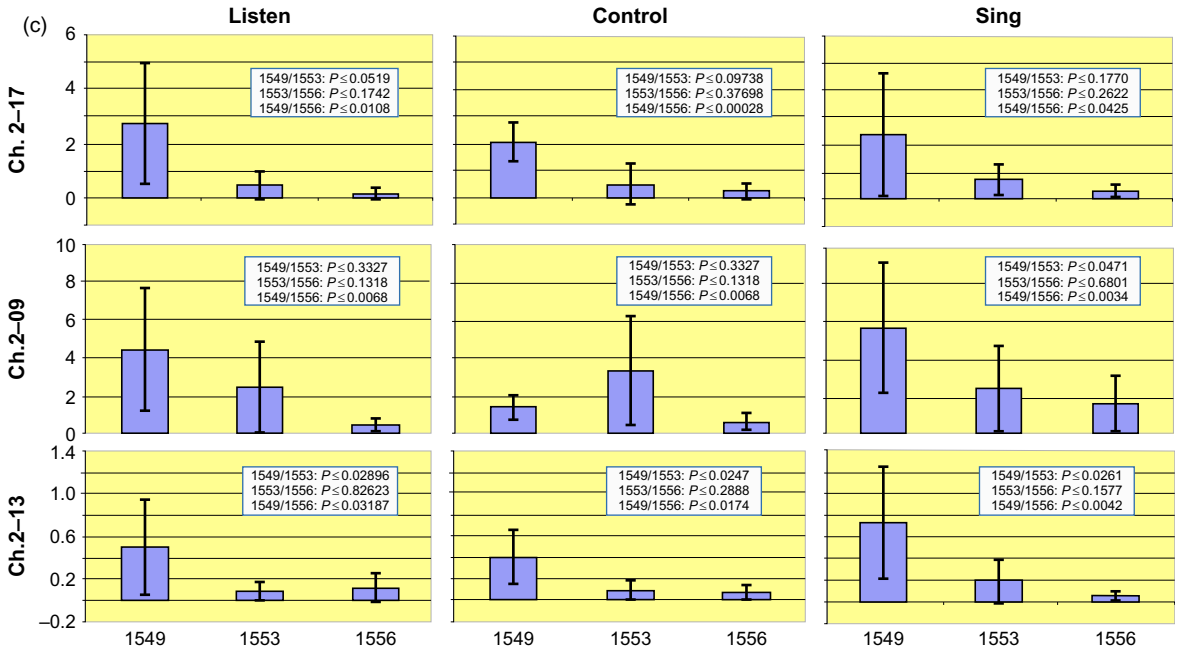


Fig. 6. (a) Data from units followed over four sessions demonstrating the tuning over that period with no feedback (days 1546 and 1549), unit feedback (day 1553), and feedback of volume directly related to unit firing frequency (day 1556). The best tuned units in each of the four classes are illustrated here. Data for tone 523 Hz. (b) Similar data form days 1449 (no data for 1446), 1553, and 1556 for tone 262 Hz. (c) Plots of mean and 1 SD of the variance of firing frequencies during the listen control and sing data over the 3 days, 1549, 1553, and 1556, for tone 262 Hz. Details in text: p values are within each plot. Note the statistically significant decrease in variance between data on day 1549 compared to data on day 1556.

seen in subjects DJ and ER as shown in Fig. 2b though they fired so infrequently as to be functionally useless in these subjects. They did, however, provide information during the listen/sing task discussed above. These large units were recorded at the same time as the smaller-amplitude units mentioned above in all subjects. Although the origin of these large slow-firing units is far from clear, they were stable across recording sessions and are therefore not likely to be artifacts. According to the rationale discussed above, these giant units probably originate from axons of corticospinal tract neurons. Precedence is found for these large units in monkey recordings using the NE. For example, Fig. 5 of Kennedy and Bakay (1997) illustrates that a large

unit appeared only when the monkey was subject to both cortical stimulation close to the NE and simultaneously given caffeine. It is possible to speculate that similar circumstances also resulted in the appearance of the giant potentials in this study: subject JR required multiple medications which may have contributed to the consistent appearance of the large units described in the section “Results.”

Stability

We distinguished single units from multiunits using ISIIs as shown in Fig. 4. The single units recorded near the beginning and at the end of

the testing period for the presented data (days 1546–1556) are similar in firing rate characteristics shown in Figs. 2 and 3. The cluster parameter file was not changed during this sampling period, providing evidence for the stability of the recording. The duration of this stability is demonstrated by the ISIHS of single and multiunits acquired on day 1609, several months later (not illustrated). Data have been collected over many months during the first 5 years of implantation. It is highly unlikely that repeated detection of phonemes (Brumberg et al., 2011) and the gradual learning of vowel production over many months (Guenther et al., 2009) could have been done with unstable units, whether single or multiunits.

In addition, ISIH-identified single units had to remain stable to allow the gradual appearance of tuning over several sessions and within sessions as described in Fig. 6. It would not be possible for such fine tuning of single units to occur if the overall system was unstable: if the system was unstable as *might* be suggested by the data from days 1546 and 1549 (Fig. 6), and the system then underwent stabilization *by chance* on days 1553 and 1556 to produce tuning of single units, then the multiunits ought to have stabilized and tuned, too. In this sense, the consistent differences between the multiunits and single unit recordings are an internal control for the stability of the recordings.

Some units within each of the four types of units preferentially demonstrated tuning as illustrated in Figs. 5a and b and described in the section “Results.” Of particular interest is that within each group, some units did not tune. One interpretation of this is that the unit tuning might be specific to the tone presented to the subject. The finding of differential responses to different tones producing tuning in the same unit tends to support this claim of specificity. An example of this effect is found by comparing unit ch2-19 in Fig. 5a responding to the 523-Hz tone with the same unit in Fig. 5b responding to the 262-Hz tone. Another interesting example is ch2-17: with

tone 523 Hz, the firing rates for “listen” and sing are oppositely related to the rates produced during tone 262 Hz. It is also interesting that the rates tended to increase as the sessions progressed. This effect may have reflected adaptive changes related to recurring presentation of the stimulus, or the interest and enthusiasm of the subject perhaps. Of interest, also is the gradual reduction of firing rate in the two fastest units (ch1-09 and ch1-19) toward the end of the session when other units continued to fire vigorously and some to increase their firing rates especially during the “sing” period (examples include ch1-13, ch2-17, and ch2-09 [the unit fed back]). Of importance too is that this is a consistent effect seen for both tone presentations. One could speculate that these fast units are interneurons that are active during the tuning process, and once that process is complete, they are no longer required for effective tuning functionality so their firing rates decrease.

Feedback

Feedback is well documented in monkey studies as an important factor in learning to control devices such as virtual targets (Taylor et al., 2002) or robotic arms (Velliste et al., 2008). In the present studies, there were substantial changes in the firing rates over the four recording sessions. This plasticity appeared to be feedback dependent as shown in Fig. 6a where two sessions were devoted to no feedback and no plastic changes occurred. Presumably, the auditory feedback was directed through the external auditory nerve to the brain stem, lateral geniculate nucleus to the auditory cortex, and hence through Wernicke’s cortex to the expressive speech motor cortex, where we are presumably recording from neuritic processes of the neurons related to articulation. These are the same units that were active during phoneme detection (Brumberg et al., 2009) and vowel production (Guenther et al., 2009). The common variable between these three

functions is articulation, so it seems reasonable to assume that in all studies, recordings were derived from units related to articulatory movements.

The role of unit ch2-09 in this feedback loop is of interest. The initial feedback session on day 1553 consisted of the production of the tone each time unit ch2-09 fired. The final session on day 1556 consisted of an increase in volume as unit ch2-09 fired. Even though the activity of unit ch2-09 was used to generate the feedback, it was not the most vigorous firing unit as shown in the figure. Its rate did increase for the final trials during the 523-Hz tone presentation but not during the 262-Hz tone presentation. In addition, its firing rate during the control period was higher than during the listen or sing periods for both tone presentations. With *a priori* knowledge of the results, tone 523 Hz would have been better matched to unit ch2-17 and tone 262 Hz better matched to unit ch2-15, possibly producing even stronger modulations. One implication of these data is that the units *not* being used for feedback became more strongly modulated during the feedback sessions, suggesting they are specifically related to the articulatory movements required to produce that tone.

Auditory neurons

During the “listen” period, the subject was asked to passively listen to the tone. To remember it for the subsequent “sing” period, other processes would have to occur, including transfer of the auditory information into working memory. The data in [Figs. 5 and 6](#) demonstrate differences in average firing rates between the listen and “sing” periods for both tones. The fact that some listen rates were also tuned may suggest that the tuning process was more than passive. This would appear to imply that “listen”-related neurons (auditory neurons) are present in cortical motor area in humans. Auditory neurons are not traditionally expected to be present in the motor area,

but recent monkey data suggest that the neural dynamics of ventral premotor cortex are involved in the processing steps that link sensation and decision making during auditory discrimination ([Lemus et al., 2009](#)). In addition, multisensory units (vision and proprioception) have recently been reported in monkey area 4 ([Suminski et al., 2009](#)).

Mirror neurons

The possibility to an alternative interpretation to auditory-related neurons in motor cortex is that these units may arise from mirror neurons, and not from auditory units. The present study cannot definitively address this topic, but this possibility is raised because (a) the units may have fired in anticipation of “singing” (mirroring singing) and (b) the modulations during the “silent” control periods of the task were NOT similar, or only rarely similar, to that during active listening; if the listen period had been completely passive, listening and control firing rates should have been similar. This implies that the listening period modulations could have been something other than listening, and mirror neuronal activity is a possible explanation. There is some evidence in human imaging studies that mirror neurons exist in the human brain ([Skipper et al., 2007](#); [Turella et al., 2009](#)). Attention and emotional factors may have played a role here as well ([Kennedy, 2010](#)).

Functionality of single versus multiunits

One enlightening basic observation was unexpectedly provided by examining a major issue in the field of neural prosthetics. This issue concerns the utility of multiunits as compared to single units. There is evidence that recorded single units are equivalent to multiunits when determining preferred directions of firing in a center-out task performed by monkeys ([Frasier et al., 2009](#)).

These data were obtained from Rhesus Macaque primary motor cortex using a chronic recording system, the Utah Array (Rousche and Normann, 1998), which recorded one or several units at the end of each of 96 tines. The task required the monkeys to move a cursor within a two-dimensional plane in eight directions under visual guidance. The recorded units were either sorted into single units or allowed to remain as multiunits. The results indicated no difference in performance between the use of single and multiunits, suggesting equivalence in the utility of such units. These results contrast with data presented here from human speech motor or premotor cortex recordings during the performance of listen/“sing” tasks in which we found that the firing rates of single units, but not multiunits, developed smoothly tuned patterns of firing related to auditory inputs, thus indicating non-equivalence of single and multiunits.

Neural prosthetic implications

Even though these data deal with basic electrophysiological characteristics of cortical neural activity, the results have important implications for the development of neural prosthetic devices. For prosthetic applications, the cortical control signals need to endure the lifetime of the subject, must be functionally stable, and must be trainable, that is, show plasticity. Ideally, such plasticity or adaption would occur with minimal training of the subject.

None of the existing chronic tine-type electrode designs have yet been shown capable of surviving many years of use with stable units. The 5-year life span to date of the NE is clearly a step in the right direction, however, and is substantially longer than that of other types of electrodes in humans (Hochberg et al., 2006) or monkeys (Carmena et al., 2003; Nicolelis et al., 2003; reviewed by Kennedy, 2006). Functional stability over time has been achieved with this and other electrodes, as highlighted in this chapter. It is also clear that

“stability” in this context refers not simply to the ability to record units but to the ability to discriminate and hold single units to drive a function. The evidence for functional stability comes from the present results demonstrating that a much higher degree of specificity in auditory/vocalization tuning can be extracted from single neuron information than from information provided by multiple unit recordings. Thus, for functional stability in a neural prosthetic that requires *precise* control such as that of individual digits movements or speech, single units may be essential. However, for functions that do not require precise control, signals derived from multiunits, local field potentials, or EEG signals may be adequate.

Decoding algorithms work best with information from multiple simultaneously recorded signal sources. In this regard, the NE performs quite well, with 20 single units per electrode. However, design modification of the electrode presently underway will make it possible to implant many more electrodes of smaller size, record many more channels per electrode and even with fewer units per channel, the yield of single units will increase into the hundreds.

It is desirable that the recorded neurons be highly trainable, with minimal effort. Despite the long time spent training the subject in the use of the speech prosthesis (Brumberg et al., 2011; Guenther et al., 2009), the data presented here suggest that tuning can occur within a single session. This would encourage the view that training will be much briefer in future.

Thus, the NE is beginning to fulfill all the requirements for a neural prosthetic recording system. The present data provide evidence that single units continue to be recorded over years, that these units can be used to recognize phonemes, that these phonemes can be used to drive a speech synthesizer in real time, that feedback is important to produce coordinated firings of single units in a “sing” task, and that plasticity is possible. The data support the notion that long-term recording systems are more reliable when the neuropil grows into and becomes

incorporated into the electrode than when an attempt is made to incorporate the electrode into the brain. Such developments in human prosthetics are expected to reveal a wealth of important basic electrophysiological cortical recording data which will drive developments of prostheses. In addition, it raises the probability of using reliable neural interfaces for neural enhancement. Thus in the future, with more electrodes and decoding paradigms, it may be possible to provide neural enhancement to both patients and nonpatients.

Acknowledgments

Support: This work was supported by a Grant from the NIDCD, NIH, R44 DC007050.

The authors would like to publicly acknowledge the continued strong support of this research by the subject and his family. We would like to particularly acknowledge the support of the subject's father who was present at all sessions reported here and who supplied encouragement to the subject and to us. The authors also acknowledge Prof. Thomas Wichmann for his critique of the chapter. We also acknowledge the role of Dr. Roy Bakay in the implantation of subject JR.

References

- Bartels, J. L., Andreasen, D., Ehirim, P., Mao, H., Seibert, S., Wright, E. J., et al. (2008). Neurotrophic electrode: Method of assembly and implantation into human motor speech cortex. *Journal of Neuroscience Methods*, 174(2), 168–176.
- Berger, M. S. (1996). Minimalism through intraoperative functional mapping. *Clinical Neurosurgery*, 43, 324–337.
- Breshears, J., Sharma, M., Anderson, N. R., Rashid, S., & Leuthardt, E. C. (2009). Electrocorticographic frequency alteration mapping of speech cortex during an awake craniotomy: Case report. *Stereotactic and Functional Neurosurgery*, 88(1), 11–15.
- Brumberg, J. S., Andreasen, D., Bartels, J. L., Ehirim, P., Guenther, F. H., Mao, H., et al. (2011). Classification of intended phoneme production from chronic intracortical microelectrode recordings in speech motor cortex. *Journal of Neural Engineering, Frontiers in Neuroscience*, 5(65), 1–14.
- Brumberg, J. S., Kennedy, P. R., & Guenther, F. H. (2009). Artificial speech synthesizer control by brain-computer interface. *Proceedings of the 10th annual conference of the international speech communication association, presented at the interspeech 2009*, Brighton, UK: International Speech Communication Association.
- Carmena, J. M., Lebedev, M. A., Crist, R. E., O'Doherty, J. E., Santucci, D. M., Dimitrov, D. F., et al. (2003). Learning to control a brain-machine interface for reaching and grasping by primates. *PloS Biology*, 1(2), 193–208.
- Chang, Y. M., & Luebke, J. I. (2007). Electrophysiological diversity of layer 5 pyramidal cells in the prefrontal cortex of the rhesus monkey: *in vitro* slice studies. *Journal of Neurophysiology*, 98(5), 2622–2632.
- Chen, W., Zhang, J. J., Hu, G. Y., & Wu, C. P. (1996). Electrophysiological and morphological properties of pyramidal and non-pyramidal neurons in the cat motor cortex *in vitro*. *Neuroscience*, 73(1), 39–55.
- Frasier, G. W., Chase, S. M., Whitford, A., & Schwartz, A. B. (2009). Control of a brain-computer interface without spike sorting. *Journal of Neural Engineering*, 6(5), 055004.
- Gonzalez-Burgos, G., Krimer, L. S., Povysheva, N. V., Barrioneuvo, G., & Lewis, D. A. (2005). Functional properties of fast spiking interneurons and their synaptic connections with pyramidal cells in primate dorsolateral frontal cortex. *Journal of Neurophysiology*, 93(2), 942–953.
- Guenther, F. H., Brumberg, J. S., Wright, E. J., Nieto-Castanon, A., Tourville, J. A., Panko, M., et al. (2009). A wireless brain-machine interface for real-time speech synthesis. *PLoS One*, 4(12), e8218.
- Hochberg, L. R., Serruya, M. D., Friehs, G. M., Mukand, J. A., Saleh, M., Caplan, A. H., et al. (2006). Neuronal ensemble control of prosthetic devices by a human with tetraplegia. *Nature*, 442(7099), 164–171.
- Kennedy, P. R. (1989). The cone electrode: A long-term electrode that records from neurites grown onto its recording surface. *Journal of Neuroscience Methods*, 29, 181–193.
- Kennedy, P. R. (2006). Comparing electrodes for use as cortical control signals: Tiny tines, tiny wires or tiny cones on wires: Which is best? In *The biomedical engineering handbook*. (3rd ed.). *The electrical engineering handbook series*, (Vol. 1. Boca Raton: CRS/Taylor and Francis.
- Kennedy, P. R. (2010). Changes in emotional state modulate the firing rates of human neural signals during long-term recording with the neurotrophic electrode. *Neurocase*.
- Kennedy, P. R., Andreasen, D. S., Ehirim, P., King, B., Kirby, T., Mao, H., et al. (2004). Using human extra-cortical

- local field potentials to control a switch. *Journal of Neural Engineering*, 1, 72–77.
- Kennedy, P. R., & Bakay, R. A. E. (1997). Activity of single action potentials in monkey motor cortex during long-term task learning. *Brain Research*, 760, 251–254.
- Kennedy, P. R., & Bakay, R. A. E. (1998). Restoration of neural output from a paralyzed patient by direct brain connection. *NeuroReport*, 9, 1707–1711.
- Kennedy, P. R., Bakay, R. A. E., Moore, M. M., Adams, K., & Goldwaith, J. (2000). Direct control of a computer from the human central nervous system. *IEEE Transactions on Rehabilitation Engineering*, 8(2), 198–202.
- Kennedy, P. R., Kirby, T., Moore, M. M., King, B., & Mallory, A. (2004). Computer control using human intracortical local field potentials. *IEEE Transactions on Neural Systems and Rehabilitation Engineering*, 12(3), 339–344.
- Kennedy, P. R., Mirra, S., & Bakay, R. A. E. (1992). The cone electrode: Ultrastructural studies following long-term recording. *Neuroscience Letters*, 142, 89–94.
- Kurzweil, R. (2005). *The Singularity is Near*. Penguin Group.
- Lemus, L., Hernández, A., & Romo, R. (2009). Neural encoding of auditory discrimination in ventral premotor cortex. *Proceedings of the National Academy of Sciences of the United States of America*, 106(34), 14640–14645.
- Nicolelis, M. A. L., Dimitrov, D., Carmena, J. M., Crist, R., Lehew, G., Kralik, J. D., et al. (2003). Chronic, multisite, multielectrode recordings in macaque monkeys. *Proceedings of the National Academy of Sciences of the United States of America*, 100(19), 11041–11046.
- Paninski, L., Fellows, M. R., Hatsopoulos, N. G., & Donoghue, J. P. (2004). Spatiotemporal of motor cortical neurons for hand position and velocity. *Journal of Neurophysiology*, 91, 515–532.
- Rousche, P. J., & Normann, R. A. (1998). Chronic recording capability of the Utah Intracortical Electrode Array in cat sensory cortex. *Journal of Neuroscience Methods*, 82(1), 1–15.
- Schwindt, P., O'Brien, J. A., & Crill, W. (1997). Quantitative analysis of firing properties of pyramidal neurons from layer 5 of rat sensorimotor cortex. *Journal of Neurophysiology*, 77 (5), 2484–2498.
- Serruya, M. D., Hatsopoulos, N. G., Paninski, L., Fellows, M. R., & Donoghue, J. P. (2002). Instant neural control of a movement signal. *Nature*, 416(6877), 141–142.
- Skipper, J. I., Goldin-Meadow, S., Nusbaum, H. C., & Small, S. L. (2007). Speech-associated gestures, Broca's area, and the human mirror system. *Brain and Language*, 101(3), 260–277.
- Suminski, A. J., Tkach, D. C., & Hatsopoulos, N. G. (2009). Exploiting multiple sensory modalities in brain-machine interfaces. *The Journal of Neuroscience*, 30(50), 16777–16787.
- Taylor, D. M., Tillery, S. I., & Schwartz, A. B. (2002). Direct cortical control of 3D neuroprosthetic devices. *Science*, 296 (5574), 1829–1832.
- Turella, L., Pierno, A. C., Tubaldi, F., & Castiello, U. (2009). *Mirror neurons in humans: Consisting or confounding evidence?* 108(1), 10–21.
- Velliste, M., Perel, S., Spalding, M. C., Whitford, A. S., & Schwartz, A. B. (2008). Cortical control of a prosthetic arm for self-feeding. *Nature*, 453(7198), 1098–1101.
- Zaitsev, A. V., Povysheva, N. V., Gonzalez-Burgos, G., Rotaru, D., Fish, K. N., Krimer, L. S., et al. (2009). Interneuron diversity in layers 2–3 of monkey prefrontal cortex. *Cerebral Cortex*, 19(7), 1597–1615.

CHAPTER 2

Out of the frying pan into the fire—the P300-based BCI faces real-world challenges

Sonja C. Kleih[†], Tobias Kaufmann[†], Claudia Zickler[‡], Sebastian Halder[‡],
Francesco Leotta[§], Febo Cincotti[§], Fabio Aloise[§], Angela Riccio[§], Cornelia Herbert[†],
Donatella Mattia[§] and Andrea Kübler^{†,‡,*}

[†] Department of Psychology I, University of Würzburg, Würzburg, Germany

[‡] Department of Medical Psychology and Behavioral Neurobiology, University of Tübingen,
Tübingen, Germany

[§] Neuroelectrical Imaging and BCI Lab, Fondazione Santa Lucia IRCCS, Rome, Rome, Italy

Abstract: Brain–computer interfaces (BCIs) have been investigated for more than 20 years. Many BCIs use noninvasive electroencephalography as a measurement technique and the P300 event-related potential as an input signal (P300 BCI). Since the first experiment with a P300 BCI system in 1988 by Farwell and Donchin, not only data processing has improved but also stimuli presentation has been varied and a plethora of applications was developed and refined. Nowadays, these applications are facing the challenge of being transferred from the research laboratory into real-life situations to serve motor-impaired people in their homes as assistive technology.

Keywords: brain–computer interface; P300; ERP; visual; BCI application; ALS.

Introduction

Brain–computer interfaces (BCIs) allow for communication and control by real-time translation of brain activity into commands for output devices (Birbaumer et al., 2008; Donoghue, 2008; Kübler

and Müller, 2007). In a BCI system, the brain signal is acquired, digitized, and classified for translation of predefined features in the electroencephalography (EEG) into output signals (see the section “Classification” under “P300”) to control, for example, a spelling device for communication (Farwell and Donchin, 1988; Nijboer et al., 2008a). Being independent from muscle activation, the reestablishment of communication and facilitation of daily life activities for people in the locked-in state (Laureys et al., 2005)

*Corresponding author.

Tel.: +49-931-31-80179; Fax: +49-931-31-87059
E-mail: andrea.kuebler@uni-wuerzburg.de

or with severe motor disabilities due to different progressive muscular diseases such as amyotrophic lateral sclerosis (ALS; [Rowland and Shneider, 2001](#)) has been the primary motivation of BCI research. Since the presentation of BCI for communication ([Farwell and Donchin, 1988](#); see the section “[P300](#)”) more than 20 years ago, not only BCIs for communication were investigated thoroughly and progressed further (see the section “[BCI applications](#)”), but also a plethora of new applications has been developed such as assistive domotic technologies (see the section “[BCI applications](#)”) and applications for leisure activities, like BCIs for Internet browsing and painting (see the section “[BCI applications](#)”). Most recently, it is also tried to establish BCI systems for the detection of consciousness in nonresponsive patients (DECODER project: www.decoderproject.eu; [Kübler and Kotchoubey, 2007](#)), thus increasing the number of potential user groups and the clinical relevance of BCIs. Due to its reliability ([Fabiani et al., 1987](#)) and its relatively low computational requirements ([Lotte et al., 2007](#)), the majority of current BCI applications is based on the noninvasively measurable P300 evoked potential as input signal. As a result of the tremendous amount of research invested in determining influencing factors on the P300-BCI and improving performance in the past 10 years, we are now able to present the first P300-BCI review. Additionally, we will also present some preliminary data from our current P300-BCI research.

P300

The P300 event-related potential (ERP) is a positive voltage deflection of the electrocortical potential linked in time with a rare event that initiates sensory and mental processing ([Fabiani et al., 1987](#); [Pritchard, 1981](#)). The P300 occurs 300–500 ms poststimulus as a result of attending or responding to target, task-relevant, visual, auditory, or somatosensory stimuli and reaches its

maximum amplitude over central-parietal areas (see [Fig. 1a and b](#)).

The typical task for eliciting a P300 is the odd-ball paradigm ([Sutton et al., 1965](#)). The subject is presented with a sequence of frequent nontarget stimuli interspersed with infrequent (odd) target stimuli. The occurrence of the rare target stimulus elicits a P300. By focusing attention on the rare target stimulus (e.g., by keeping a mental count of its occurrence), the P300 amplitude can be increased and therefore classified more easily. It is well established that the lower the probability of an attended stimulus, the larger is the amplitude of the P300 ([Gonsalvez and Polich, 2002](#)). In the first report about visual P300 BCI-based communication, the “P300 Speller” ([Farwell and Donchin, 1988](#)), 4 healthy subjects were instructed to spell words on a computer screen by selecting letters from a letter matrix with six rows and six columns (36 characters). An adapted matrix with seven rows and seven columns is shown in [Fig. 2](#).

Rows and columns of the matrix flashed randomly, and the participant focused attention on the letter to be selected. In one sequence of 12 flashes (six rows, six columns), the target character flashed only twice (one column, one row) and, thus, constituted an oddball and elicited a P300. The same basic mechanism for spelling is used in P300-based BCI applications that evolved much later. Compared to other BCI input signals such as slow cortical potentials (SCPs; [Birbaumer et al., 1999](#); [Kübler et al., 2001, 2004](#); [Lutzenberger et al., 1979, 1982](#); [Neumann and Birbaumer, 2003](#)) and sensorimotor rhythms (SMRs; [Blankertz et al., 2010a](#); [Nijboer et al., 2008b](#); [Pfurtscheller, 1992](#); [Pfurtscheller and Neuper, 2005](#)), P300 BCIs have the advantage of the P300 signal being independent from learning and being quickly and robustly classifiable (see the section “[Classification](#)” under “[P300](#)”) even in patients with neurodegenerative disease and in real-world conditions implying a noisy and possibly distracting environment ([Kübler et al., 2008](#); [Münßinger et al., 2010](#); [Nijboer et al., 2008a](#)).

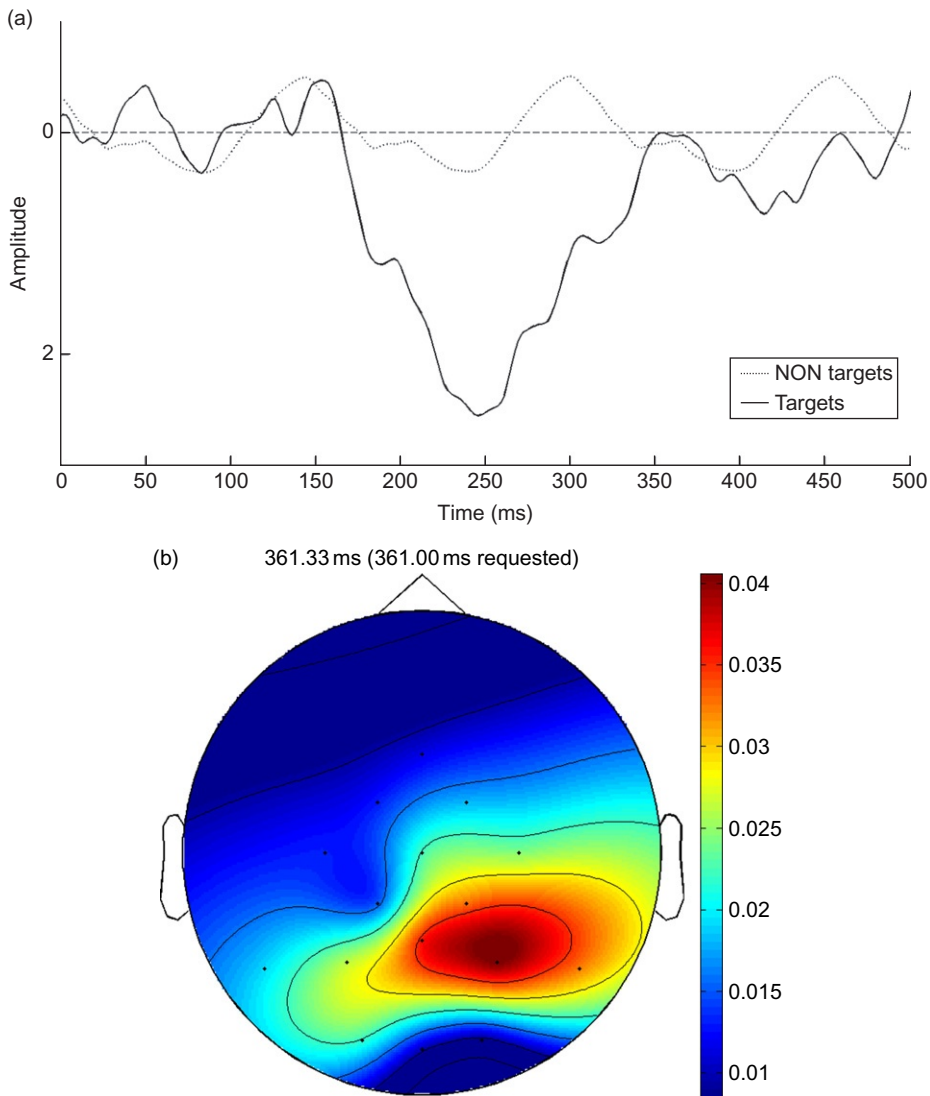


Fig. 1. (a) P300 amplitude at 300 ms. (b) Activation of P300 at centro-parietal regions of the brain.

Classification

The signal processing involved in a BCI can be generally described as the sequence of three steps: signal conditioning, feature extraction, and classification. The procedures that are utilized in a P300-BCI are described in the following sections.

Signal conditioning

Signal conditioning is aiming at discarding those components of the EEG signal that contaminate useful features, which reflect the intention of the BCI user. Selection is performed according to frequency and spatial characteristics of

Brain (R)							
B	A	B	C	D	E	F	G
H	I	J	K	L	M	N	
O	P	Q	R	S	T	U	
V	W	X	Y	Z	1	2	
3	4	5	6	7	8	9	
0	@	.	Sp	!	,	Ö	
Ä	Ü	?	o	()	END	

Fig. 2. Letter matrix used in a P300 BCI for communication. Rows and columns contain the letters of the alphabet, several punctuation marks, and the numbers 0–9.

components. Other conditioning methods can include template matching to remove or reject artifacts or both, but they are not commonly applied in P300-BCI systems. Frequency filtering is used in all P300 studies to avoid effects of off-band artifacts such as line noise, muscular activity, and baseline fluctuations. There is a substantial variation in the cutoff for low pass filtering, some examples being 12 Hz (Hoffmann et al., 2008), 20 Hz (Halder et al., 2010), 30 Hz (Furdea et al., 2009; Guger et al., 2009a; Schreuder et al., 2010; Townsend et al., 2010), 50 Hz (Klobassa et al., 2009), and 70 Hz (Nijboer et al., 2008a). This variation in low pass cutoff frequencies indicates that there is still some disagreement in the BCI community on what the optimal cutoff frequency is. Studies on the frequency composition of the P300 using wavelets have shown an extent from 0 to 32 Hz with the strongest contributions ranging from components of 8 Hz and lower (Demiralp et al., 2001). In contrast to their advantageous effect on sensorimotor rhythm BCI data, commonly used spatial filters such as common average reference (CAR) or Laplacians offer little advantage over the raw signal due to the broad spatial distribution of the P300 (McFarland et al., 1997). It has been demonstrated, for example, that, when using stepwise linear

discriminant analysis (SWLDA) as classifier, using CAR instead of, for example, ear reference has no positive effect on classification rates (Krusienski et al., 2008).

Feature extraction

Numerical values extracted from the EEG for classification purposes in a BCI paradigm are referred to as features. P300 BCI features used for classification are extracted from the time domain of the EEG signal. In other BCI paradigms, such as those based on motor imagery (SMR), features are extracted in the frequency domain. The set of EEG channels from different scalp locations that is used in the measurement adds to the feature set in the spatial domain. A single instance (i.e., trial) of the spatiotemporal feature set can be extracted for each epoch (usually, equivalent to an EEG time segment of 1000-ms length) following a stimulus. The feature set can be described as a matrix of EEG potential values, whose dimension is given by the number of samples belonging to the epoch multiplied by the number of acquired channels. It is common to run a moving average filter over each EEG segment after which the data are

decimated to reduce the dimensionality of the feature set (Krusienski et al., 2008). This feature reduction lowers the risk of overfitting and makes feature selection for algorithms such as SWLDA easier. A detailed mathematical definition of the features used in P300 BCI classification can be found in Blankertz et al. (2010b) and Krusienski et al. (2006).

Classification

Classification in an oddball paradigm such as used for control of the P300 Speller is a binary task of detecting the presence or absence of the ERP (Farwell and Donchin, 1988). As ERPs appear reliably stable over trials, even though highly masked by the ongoing EEG, features can be assumed to be linearly separable. Therefore, linear classification methods, such as SWLDA, described below, can obtain reliable classification results.

Stepwise linear discriminant analysis

In SWLDA, a classification model is built step by step. In each step, spatiotemporal features are added and their contribution to the classification is scored. The features that contribute best are then included into the discrimination function and the analysis proceeds with the next step (forward SWLDA). However, backward SWLDA includes all spatiotemporal features at the beginning and step by step eliminates those that contribute least. A combination of both forward and backward SWLDA was shown to obtain good results (Furdea et al., 2009; Krusienski et al., 2008). Krusienski et al. (2006) compared SWLDA to other classification methods such as support vector machines, Pearson's correlation method (PCM), and Fisher's linear discriminant (FLD) and concluded that SWLDA obtains best results. For this reason, SWLDA is widely used as classification method for P300 BCI. However, other classification approaches exist and are listed in the next section.

Other classification approaches

A broad variety of other methods were introduced for P300 classification, for example, other linear discriminant methods such as FLD (Krusienski et al., 2006) or as recently described by Blankertz et al. (2010b) modifications of linear discriminant analysis (LDA) such as shrinkage LDA and other linear methods such as PCM or linear support vector machine (Krusienski et al., 2006). Besides this, there are also nonlinear machine learning approaches such as Gaussian kernel support vector machines (Krusienski et al., 2006), convolutional neural networks (Cecotti and Graser, 2011), and hidden Markov models (Rastjoo and Arabalibeik, 2009) to name just a few. For a detailed description of these methods, the reader is referred to the respective publications (e.g., Anderson et al., 2007; Dornhege et al., 2007; Hill et al., 2007).

Performance with a P300 BCI depends on the reliability of signal detection. The noisier the signal, the more stimulus presentations are necessary. This implies that the signal detection rate can be increased by the number of stimulus repetitions. This renders the P300 BCI particularly appealing for application in people with cortical neurodegeneration, which affects the amplitude, latency, and localization of the P300 ERP, because simply an increase of the number of target stimulus presentations can be beneficial, albeit at the cost of speed.

BCI applications

P300 BCI-based communication

P300-based BCIs were used very successfully for communication not only in healthy participants who reached spelling accuracies of up to 100% offline (Donchin et al., 2000; Guger et al., 2009a) and online (Kleih et al., 2010) but also severely motor-impaired users could communicate with the P300 BCI. Sellers and Donchin (2006)

introduced a four-choice paradigm (including the four choices “yes,” “no,” “pass,” “end”), and their results indicate that participants with ALS could communicate with a visual P300 BCI system with an accuracy of up almost 70%. When using the full matrix P300 speller (see Fig. 2), not only are users enabled to produce unique spontaneous messages (Nijboer et al., 2008a) but also reliable long-term communication is possible (Nijboer et al., 2008a). After 10 weeks of training, ALS patients spelled between 1.5 and 4.1 characters/min which equals an information transfer rate of 4.8 and 19.2 bits/min (Nijboer et al., 2008a). In summary, successful use of BCIs for communication purpose was demonstrated plenty of times and research led to considerable progress in the field. However, today BCI systems are no longer considered only as a means of interpersonal communication, but as an assistive technology able to restore user’s autonomy and independence (Millán et al., 2010). In the following, we provide an overview of such P300 BCI-controlled applications.

BCIs for environmental control

Following the goal of linking BCIs to assistive technology appliances, the potential of the BCI systems for environmental control has been explored in virtual reality (VR) environments, which was a successful strategy for user training (Bayliss, 2003; Guger et al., 2009b). But the feasibility of a domotic controller interconnecting the BCI with electrical devices, such as TV, DVD player, or lights, could also be demonstrated out of a VR environment (Aloise et al., 2006, 2009; Babiloni et al., 2009; Baldoni et al., 2009; Cincotti et al., 2008). Piccione et al. (2006), for example, used the advantage of the P300 speller matrix that all characters could possibly be replaced by symbols for environmental control, therefore simultaneously offering a large number of possible choices to the user. In their work, tetraplegic

participants steered a cursor on a computer screen by focusing on the arrow that would initiate the according cursor movement (up, down, left, right). Participants reached an average accuracy of 68.6% (Piccione et al., 2006) with an average bit rate of 7.7 bits/min. When choosing one of six subsequently flashing images indicating control over different home environment devices (TV, phone, etc.; Hoffmann et al., 2008), performances of up to 100% in healthy and disabled users were reported. Information transfer rates were on average 15.9 for disabled and 29.3 for able-bodied subjects (Hoffmann et al., 2008). Aloise et al. (2008) also used icons representing the corresponding control actions that users can perform on electrical appliances available in their environment. To overcome the limit in possible commands available on a single screen, they also reorganized the stimulation interface in different submenus related to all available applications, therefore allowing for easier environmental BCI-based control. But besides environmental control, the aspect of mobility and its improvement was also judged to be one of the most important ones among experienced users of assistive technology (Zickler et al., 2009). And BCI research has indeed attempted to provide a mobility solution for patients by developing a BCI-controlled wheelchair independent from residual motor movement (Iturrate et al., 2009; Pires and Nunes, 2002). Research to date showed that a wheelchair can be successfully directed using BCI with the P300 input signal, but a mobility solution does not mean to approach a destination only; it can also mean to bring objects closer within reach. Krusienski et al. (2010) developed a robotic interface for manipulating objects based on commands delivered from a modified P300 Speller application which will be improved further in the future.

As shown here, research has developed communication and control solutions, but still the question of the transfer of these solutions into a real-life environment stayed. A recent contribution by Sellers and colleagues demonstrated the

successful long-term independent home use (2.5 years) of an ERP BCI system by an ALS patient who was intensively supported by his family and caregivers. He reported to use his BCI system for reading, writing, and environmental control. Performance on average was 83%, and the patient stated not being able to live his life the way he does without the BCI. Therefore, the practicability of a BCI system for severely disabled people was demonstrated in this single case report, promising a significant contribution to quality of life, restoring independence in social interaction, and at work (Sellers et al., 2010). But also another form of autonomous participation in the social environment was established recently in BCI research: BCI applications for creative expression and e-inclusion (EU TOBI project: www.tobi-project.org).

BCIs for creative expression and e-inclusion

BCI-based brain painting

In an effort to go beyond communication with a BCI, the artist Adi Hösle together with the University of Tübingen designed the brain painting application (Kübler et al., 2008). The 6×8 speller matrix was replaced with symbols for colors, color intensities, shape (circles and squares), etc. (see Fig. 3a). In a pilot study, the artist himself and a woman with ALS proved the general feasibility of the application and showed that they could produce paintings (e.g., see Fig. 4a–c). To verify that the paintings were not a result of random selection, the artist reproduced one of his paintings.

In a first evaluation study, the accuracy and user friendliness of the brain painting application was assessed by ten healthy subjects and three persons with ALS (Münßinger et al., 2010). In healthy subjects, the comparison between the P300-Spelling application (copy-spelling task; Kübler et al., 2001) and the P300-brain painting

application (copy-painting task) revealed significantly lower accuracies (92% vs. 81%) and P300-amplitudes for the brain painting application (Münßinger et al., 2010). Two of the three ALS patients showed high accuracies in both tasks (89%/100% vs. 95%/89%). To reduce complexity, an adapted black and white brain painting matrix (see Fig. 3b) was developed and tested with healthy subjects. No drop in accuracy and P300-amplitudes was found (Münßinger et al., 2010).

The adapted black and white matrix is currently evaluated with regard to performance and satisfaction by potential end users of BCI with severe disabilities. Participants underwent copy-spelling, copy-painting, and at least five free painting sessions in which they could spend up to 2 h painting pictures. Preliminary results for four users with severe disabilities revealed comparable results for copy-spelling, copy-painting, and free painting ranging between 80% and 100%. And even though the use of electrode gel puts the burden of washing the hair after every BCI session (which might be quite exhausting for a severely disabled person), users reported to be satisfied with the application and three users would like to use brain painting one to two times per week. Most recently, the brain painting application could be offered to a woman diagnosed with ALS about 5 years ago (see Fig. 5a). She used to be a painter but had to give up her profession due to loss of motor function. Provided with brain painting, she said: “I am deeply moved to tears. I have not been able to paint for more than 5 years. Today I again had butterflies in my stomach, a feeling that I have missed so much, so much. I was so sad, I was plagued by fears of loss, I was in shock because I could not paint. For me the picture I have created is so very typical me, no other paints like I do (which is not to say that I am the best). No one else paints in my style, and despite five years of absence, I’m simply an artist again; I’m back to life!” This convincingly demonstrated that BCI can make a real difference to patients’ life. She gave us the permission to

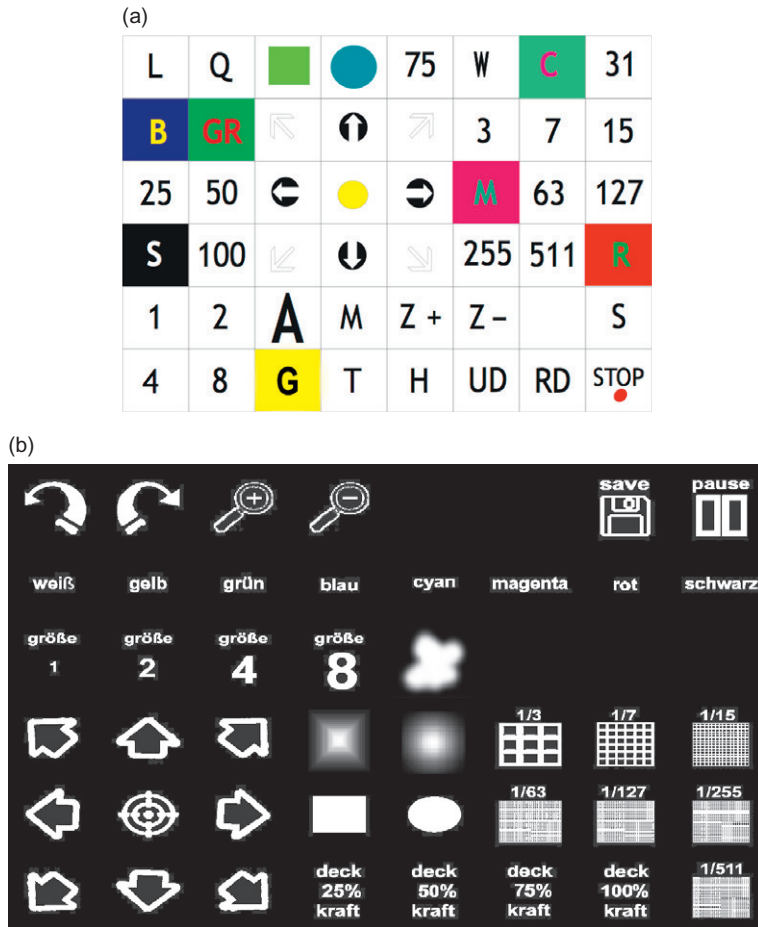


Fig. 3. (a) The colored brain painting matrix. (b) The adapted black and white brain painting matrix.

publish her first brain painting in this chapter (see Fig. 5b).

BCI-based Internet browsing

The past two decades have witnessed the continuous evolution of the Internet from an information container (for educational or informative purposes) to a real service provider allowing users to perform everyday tasks (e.g., shopping

or communication) operated by means of Web browser. Such a trend offers new opportunities for a more fulfilling everyday life experience, social interaction, and thus, inclusion for physically impaired users. An Internet browser controlled via a P300-based BCI has been recently proposed by Mugler et al. (2008, 2009) (see Fig. 6a and b).

The BCI-based Web browsing system was validated first with healthy volunteers ($N=10$) who achieved an average accuracy of 90%, and

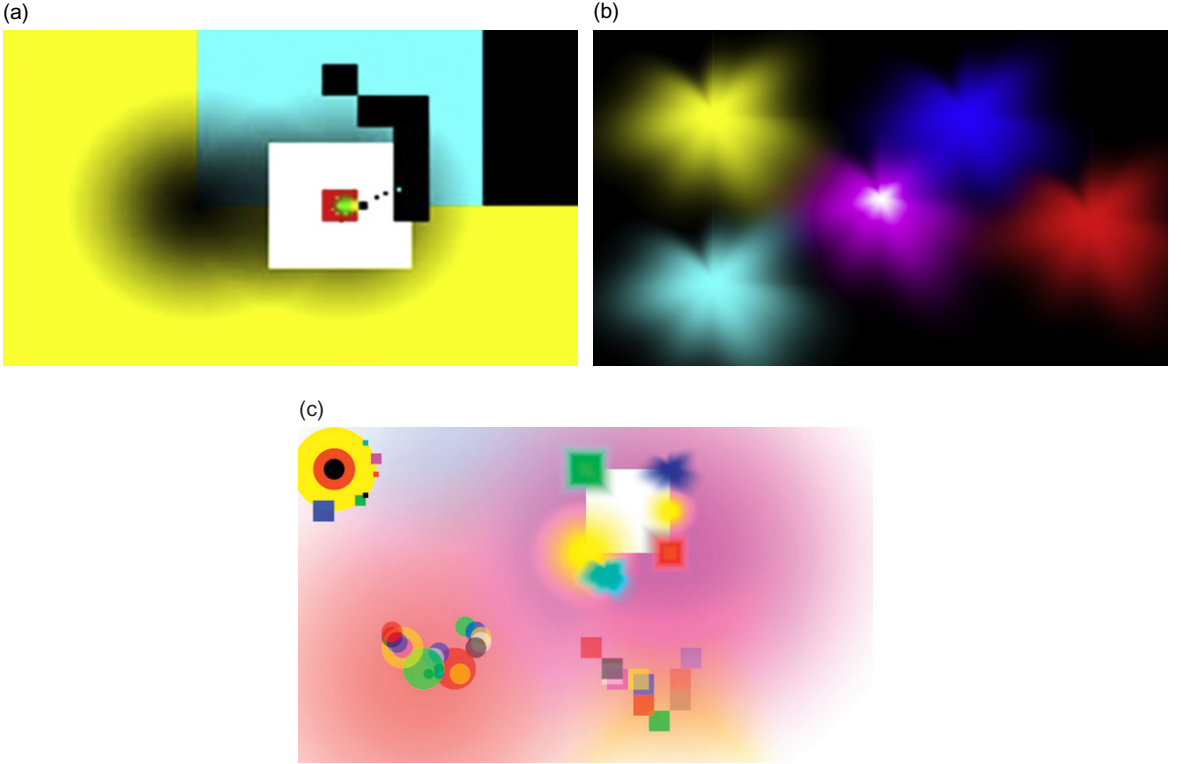


Fig. 4. (a) One of the early paintings produced by Adi Hösle. (b, c) Paintings produced by the patients AW and AE during the current evaluation study.

second with three ALS patients who controlled the BCI system with an accuracy of 73% on average (Mugler et al., 2010). The design of the system was based on a set of guidelines which represents an extension of the requirements described by Mankoff et al. (2002) to define the salient features of “true Web access.” The interface exploits Mozilla Firefox as Web browser, and a keyboard shortcut is associated with each link of the current Web page; the shortcuts are directly displayed on the browser window. A P300 speller matrix placed on a separate screen with respect to that of the browser allows for the stimulation. This matrix gives not only the possibility to choose a specific link by typing the associated shortcut but it also allows the user to enter in a read mode where only the commands necessary to scroll the current

page are enabled. This design provides a way to conciliate the asynchronous nature of the Web surfing task with the (so far) synchronous nature of the P300 BCI Web browser.

A different approach to a P300-BCI-controlled Web surfing has been proposed by Sirvent et al. (2010). The authors implemented a system based on two different P300 speller matrices (a keyboard, a virtual mouse with an associated distance control), placed in a different area of the browser screen. The use of a virtual mouse allowed for the Web access (Sirvent et al., 2010). The system was quantitatively validated with five healthy subjects who achieved an accuracy of 93% on average (Sirvent et al., 2010). A most recent development (Riccio et al., 2010) for Web surfing

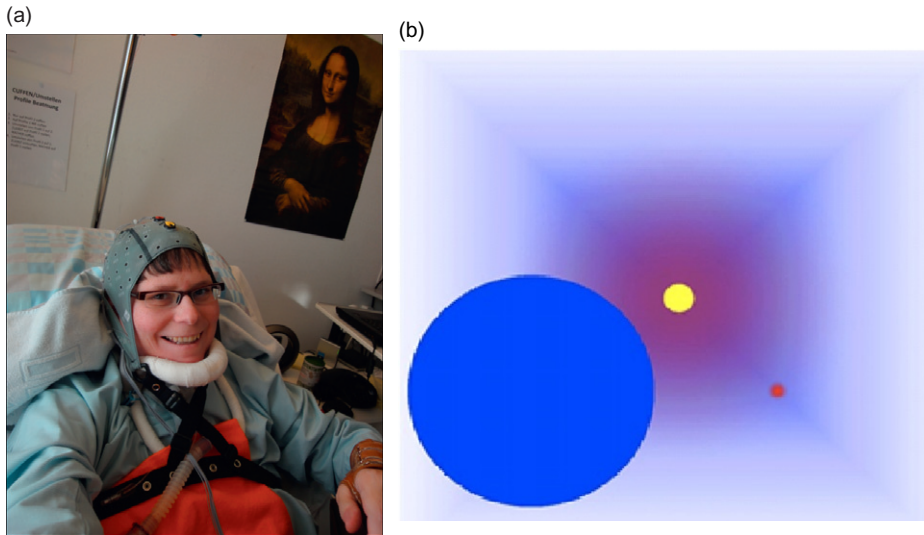


Fig. 5. (a) ALS patient connected to the BCI system for brain painting. (b) First brain painting produced by the ALS patient.

operated via BCI technology includes a P300-based brain transducer, implemented in the BCI2000 platform (Schalk et al., 2004) and the QualiWorld accessibility software (QualiLife SA, Paradiso, Switzerland). In this solution, dedicated software allows for a visual stimulation delivered in two different modalities: a double screen mode (similar to the modality used by Mugler et al., 2010) and an overlaid mode in which the BCI stimulation is placed upon the browser surface (see Fig. 7).

In this latter modality, the P300 stimulation is superimposed on the commands and links provided by the Web browser; thus, no extra letter matrix window is needed for the user. Red dots mark directly the link they would open if chosen; the user focuses therefore on the blinking of red dots instead of flashing characters in a speller matrix. This condition should diminish the workload for a user as switching attention to two separate screens/windows is not required in this approach. Moreover, head movement which is required to operate BCI-based browsing with two screens is not

or less necessary (depending on the size of the screen), rendering this browser more feasible for severely impaired users.

So far, we mainly dealt with classification, presentation, and applications with regard to the P300-based BCI, and performance can be affected by either of these aspects. We may refer to these aspects of BCI as external. However, performance is also influenced by internal states of the BCI user, such as physiological influencing variables or his or her motivational and emotional state, and only few studies are available that investigated the impact of these physiological and psychological variables.

Influences on BCI performance

As a P300 BCI constitutes an interaction between the BCI user (who controls the BCI) and the BCI itself as a machine (training a classifier), there are two possible sources that might influence BCI performance: (1) the BCI system and (2) the BCI user.

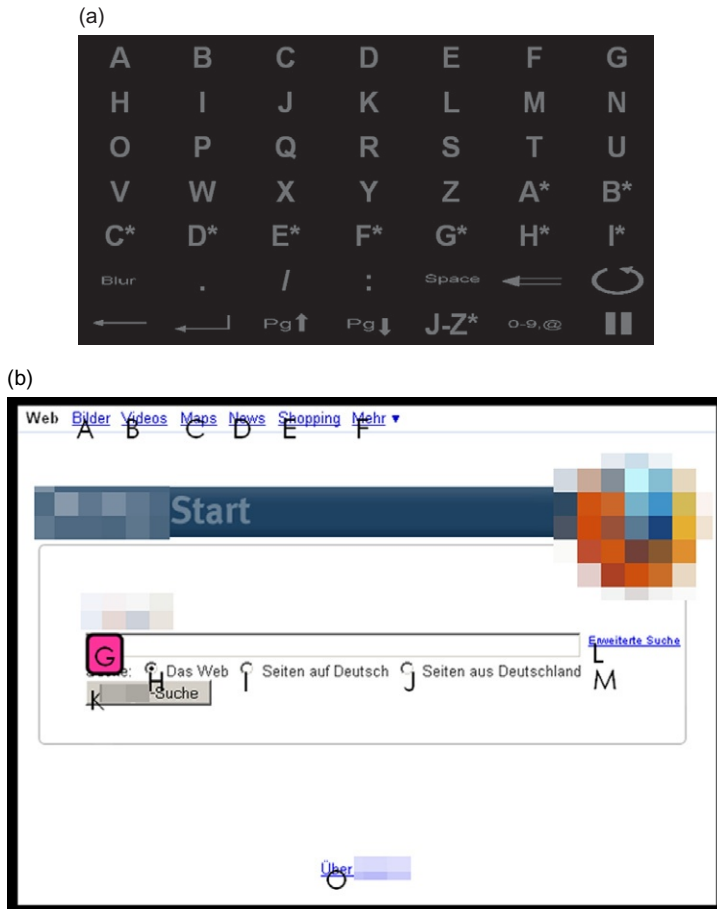


Fig. 6. Double screen of the P300 Web browser: the stimulation screen (a) and the browser screen (b).

The BCI system

Up to now, the communication speed of a visual P300 BCI is, compared to natural communication speed, relatively slow. Various attempts were undertaken to improve BCI performance addressing speed and accuracy for facilitated communication. For example, various electrode montages were applied (Hoffmann, 2007; Kaper et al., 2004; Krusienski et al., 2008). Overall, the use of between six and ten central and occipitoparietal electrodes is recommended (Hoffmann, 2007, Krusienski et al., 2008) and

proven to achieve equal performance compared to an electrode setup with more electrodes. Also, other factors were varied such as the interstimulus interval (Sellers et al., 2006), matrix size (Pineda et al., 2003; Sellers et al., 2006), and various signal processing methods (see the section “Classification” under “P300”) to improve BCI performances. Sellers et al. (2006) reported a 3×3 matrix to be more suitable to achieve higher accuracies while a 6×6 matrix yields a higher information transfer rate. Other research did not find the size of the matrix to be a significant factor in terms of accuracy (Pineda et al., 2003).

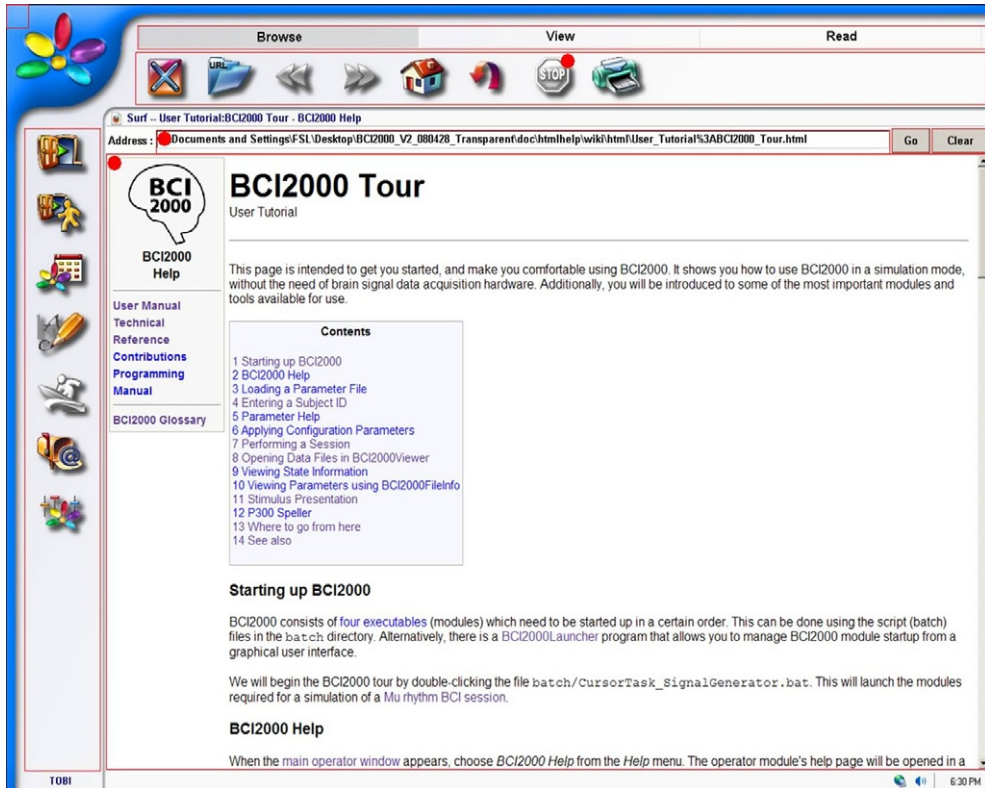


Fig. 7. The P300-based Web browsing prototype in the overlaid mode. Links on this Web page can be chosen by attending to the red dot with which a link is overlaid.

Concerning the ISI, higher P300 amplitudes were reported with longer ISIs of 1200 ms or more (Gonsalvez and Polich, 2002). In line with this result (Gonsalvez and Polich, 2002), higher accuracy was found with a decrease of stimulus rate (McFarland et al., 2010), while on the contrary, Sellers et al. (2006) found a shorter ISI of 175 ms to lead to a more accurate result. Additionally to matrix size and ISI, the P300-based stimulus presentation was experimentally investigated. Takano et al. (2009) found a blue/green chromatic flashing of the speller matrix to be advantageous concerning accuracy compared to the usually used gray/white matrix. Townsend et al. (2010) investigated a novel presentation

way, the checkerboard paradigm (CBP) with an 8×9 matrix containing 72 items. In the CBP, the items flash in random groups of six items and the adjacent items cannot be included in the same flash group. This paradigm was tested on 18 able-bodied adults and 3 ALS patients and revealed higher accuracy in the CBP (92%) compared to the classical row/column paradigm (77%). As performance with a visual speller deteriorates when users switch from directly fixating a target (overt attention) to paying attention to targets in the visual periphery (covert attention, Brunner et al., 2010), a new matrix for P300 BCI use was suggested by Treder and Blankertz (2010) which should still allow for high performances in case

of covert attention (e.g., for people whose eye movement is impaired; [Treder and Blankertz, 2010](#)). Bearing in mind that in ALS patients the oculomotor control can deteriorate, the dichotomous Hex-o-Spell ([Blankertz et al., 2007](#); [Williamson et al., 2009](#)) was adapted as an ERP device ([Treder and Blankertz, 2010](#)). Around one circle in the middle of the screen, six hexagons were arranged. Each of the hexagons contained five letters of the alphabet and was randomly highlighted. When chosen, this hexagon expanded the letters contained in it into the other six hexagons including the backspace option in one empty hexagon. It was found that, in both, the usual matrix and the Hex-o-Spell, performances of up to 100% were achieved, even though the Hex-o-Spell version allowed for this performance level faster (lower number of sequences). In covert, attention performances of up to 60% were found using the Hex-o-Spell compared to 40% for the matrix version of the speller. As all reported results were obtained offline, online trials with disabled users are awaited to judge the potential advantage of the Hex-o-Spell for P300 BCI use.

The BCI user

Although the P300 ERP was shown to be a reliable and feasible signal for brain–computer interfaces, interindividual differences in BCI performance occur that are not yet fully understood. For users that do not succeed in controlling a P300 BCI at high accuracy level, other BCI approaches such as the SMR-based BCI might result in better control. Especially for patients that are dependent on such communication systems, both reliable control and a minimum error rate are a crucial issue and thus choice of the right BCI system is essential. Predictors that are on the one hand easy to measure and on the other hand reliable over time and across participants help to fasten the process of choosing the right system.

Recently, different predictors based on psychological ([Kleih et al., 2010](#); [Nijboer et al., 2010](#)) and physiological signals ([Kaufmann et al., submitted for publication](#)) were investigated.

Psychological variables

Already in 2001 ([Kübler et al., 2001](#)), the hypothesis of psychological variables possibly influencing and explaining interindividual differences in BCI performance was stated. Up to now, it has been shown that highly motivated healthy BCI users present with higher P300 amplitudes compared to less motivated subjects ([Kleih et al., 2010](#)). The influence of psychological variables was also supported in a sample of ALS patients ([Nijboer et al., 2010](#)). In two of six ALS participants, the motivational components *challenge* and *mastery confidence* were positively related to BCI performance, while *incompetence fear* was found to negatively influence BCI performance in one ALS participant when using the P300 BCI. This result suggests an influence of motivation on performance in the P300 BCI; however, more experimentally controlled studies are needed to clarify the effect of psychological variables on BCI performance and to draw valid conclusions and possibly adjust BCI training protocols.

Physiological predictors

Controlling an oddball paradigm in a P300 BCI requires the ability to focus attention and thus requires inhibition of attention drifts to irrelevant stimuli. Recently, heart rate variability (HRV), a peripheral physiological parameter linked to such inhibitory control, was shown to be an indicator for performance in a P300 BCI. Autonomic balance (ratio of low- and high-frequency band of HRV, [Task Force of the European Society of Cardiology and The North American Society of Pacing and Electrophysiology, 1996](#)) and other

HRV measures were associated with BCI performance such that subjects with higher HRV performed better ($r=-0.52$, $n=25$, $p<0.01$). As HRV is recorded during a 5-min resting period and only requires three electrocardiogram electrodes if not only a polar watch (Nunan et al., 2009), HRV also fulfills the important criteria of rapid assessment. If with HRV, a reliable predictor for BCI performance could be identified, this would certainly be interesting not only for P300 BCIs based on the visual input modality but also for BCIs based on the auditory or vibrotactile modality which might put a higher effort concerning attention, on the BCI user.

Nonvisual P300-based BCI systems

As severely impaired patients might also have problems with eye movements or vision in general, BCI research has attempted to establish BCIs which rely on nonvisual modalities such as auditory (Furdea et al., 2009; Halder et al., 2010; Hill et al., 2005; Klobassa et al., 2009; Kübler et al., 2009; Nijboer et al., 2008b; Sellers and Donchin, 2006; Schreuder et al., 2010) or tactile BCIs (Brouwer and van Erp, 2010; Cincotti et al., 2007; Müller-Putz et al., 2006). In these nonvisual BCIs, the target stimulus could be a higher pitch tone presented in a stream of lower pitched standard tones (auditory paradigm) or a vibrotactile stimulation on the waist of a participant with a distinguishably higher or lower frequency compared to the standard stimulation delivered by other sensors around the waist (Brouwer and van Erp, 2010). A binary-choice auditory P300 BCI for communication was introduced by Halder et al. (2010). In their paradigm, the authors used one frequent tone (standard tone, pink noise) and two target tones differing in loudness, pitch, or direction (left or right ear), all presented to healthy participants via stereo headphones. Participants had to attend to a pre-defined target tone and to ignore all deviant stimuli. Results revealed, on average, a

communication accuracy of 70% and a communication speed of 2.46 bits/min with 75% of the participants ($n=20$). In another approach, it was tried to use the spatial location of a stimulus as the discriminating cue (Schreuder et al., 2010). Eight speakers were arranged in a circle around the participant (45° distance) who had to attend to the sound presented from one spatial location. With this setup, accuracies of above 90% and bit rates of 17.39 bits/min were achieved offline. But also more complex communication was investigated using the auditory P300 BCI. In Sellers and Donchin's work (2006), three ALS patients used the auditory four-choice speller ("yes," "no," "pass," "end") with accuracies between 54% and 65%. To be able to use the full range of the letter matrix, Furdea et al. (2009) cued a 5×5 matrix with combinations of auditory presented numbers indicating rows and columns. With this approach, 10 out of 13 participants achieved accuracies between 70% and 100%. The proof of principle of this speller (Furdea et al., 2009) could also be shown with ALS patients (Kübler et al., 2009) who achieved accuracies of up to 70%. The idea of replacing the flashing procedure of the letter matrix by cuing matrix rows and columns with auditory sounds was also followed by others. Klobassa and colleagues (2010) used sounds like, for example, a bell or a buzz to indicate first which row and afterward which column to chose for letter selection and found an accuracy of 75% or more in four out of ten participants. Höhne et al. (2010) used a combination of spatial location of sounds and pitch variation, leading to a nine class BCI system which was also embedded in a predictive text system. This system worked for 10 out of 12 participants with an accuracy of 69.5% (Höhne et al., 2010). Not only has the auditory modality been investigated, but also tactile BCIs are recently developed. Using vibrating elements, each covering an area of 1×2 cm around the waist of participants, who had to pay attention to one of these elements, revealed successful classification of between 58% and 73% (Brouwer and van Erp, 2010). Therefore, future research should on the

basis of these promising results try to develop non-visual BCI systems that allow for an even higher classification accuracy as nonvisual paradigms might especially be useful for the detection or even communication with patients who are diagnosed with a disorder of consciousness (DOC; Giacino et al., 2002; Monti et al., 2010a). DOC is a challenging neurological condition in which little or no capacity for behavioral expression renders the assessment of residual cognitive function, performance fluctuations, and awareness very difficult (Laureys, et al., 2004; Monti et al., 2010a; van Boxtel et al., 2010). Therefore, the distinction between people with DOC and people with completely locked-in state (CLIS) is demanding as from a behavioral assessment point of view, both conditions look very much alike, thus causing a misdiagnosis rate of up to 40% (Schnakers et al., 2009). Thus, there is an urgent need to establish paradigms with which unequivocal detection of consciousness in nonresponsive patients with DOC or CLIS can be achieved and, second, to provide these patients with a robust and easy means of communication in case consciousness is preserved (e.g., CLIS). BCI technology as a part of such an approach could give these patients and their relatives a possibility for interpersonal communication and interaction. Indeed, a promising paradigm was introduced by Schnakers et al. (2009) when they found that the ERP response of a woman when listening to her own name was significantly higher compared to the ERP response to other names. This result was obtained 2 weeks before first signs of consciousness could be detected on a behavioral level. Kotchoubey et al. (2009) found that out of 26 patients diagnosed with permanent vegetative state, seven reacted to an emotional stimulus presented in an oddball paradigm. The authors cautiously conclude that by presentation of emotional stimuli (in this case, the prosody of the words) to DOC patients, conclusions might be drawn about their cognitive functioning level (Kotchoubey et al., 2009). Further, by means of magnetic resonance imaging (MRI), yes/no communication could already be established

with a DOC patient, while four more patients out of the total sample of 54 could actively modulate their brain activity (Monti et al., 2010b). But despite this tremendous progress in research and possible diagnosis, up to now, no means of communication could be developed that was useful for DOC patients at the bedside. Therefore, BCI technology could offer an easy-to-use tool at bedside and holds promising possibilities for nonresponsive patients. Thus, research is aiming at the development of a hierarchical EEG-based approach which will allow for the detection of consciousness and potentially also for the establishment of communication and intentional environmental control in DOC patients (DECODER project: www.decoderproject.eu).

BCI faces the real-world challenge: user experiences with state-of-the-art technology

The lives of patients can be positively influenced by BCI technology already today as demonstrated by the patient examples in this review (see the sections “[BCIs for environmental control](#)” and “[BCI-based brain painting](#)”). But, as BCI users themselves report ([Zickler et al., submitted for publication](#)), there are still obstacles that need to be addressed for further facilitation of BCI technology use in daily life. One of the most obvious and challenging problems is the montage of the electrode cap. Albeit eight electrodes are sufficient for a P300-based BCI system, still cables have to be connected from the electrodes to the amplifiers and to the computer which is a setup that is judged to be complicated and bulky ([Zickler et al., submitted for publication](#)). Moreover, electrode gel is mandatory which requires later hair washing and thus adds strain on the patient and caregiver. Novel developments toward wireless data transmission ([Lin et al., 2010](#)) and (semi)dry electrodes ([Volosyak, et al., 2010](#)) will hopefully solve these problems and would very likely constitute a major step toward regular home use of BCI. Another problem

reported by patients testing BCI is the slowness of the BCI system as compared to other assistive technology ([Zickler et al., submitted for publication](#)). Users reported that they would like a faster system that could also integrate wheelchair control. A very positively rated aspect of the P300-based BCI was that no training is required. The development of alternative classification (e.g., [Blankertz et al., 2010b](#)) or stimulation methods (e.g., [Takano et al., 2009; Townsend et al., 2010](#)) could possibly further enhance BCI speed and support an easier and faster brain-machine interaction.

Conclusion

After 20 years of research on the P300 BCI, we can convincingly state that tremendous progress toward real-world applications has been achieved. The P300 BCI is only moderately influenced by psychological factors such as mood and motivation and, most importantly, by neurodegeneration. This is due to the classification by SWLDA and the improvement of classification with increasing number of averages. Therefore, also people with disease can benefit from the P300 BCI as possible difficulties with detection of the P300 signal can easily be overcome by increasing the stimulation time, albeit at the cost of communication speed. The P300 BCI may constitute a measure of social inclusion as it provides access to the Internet and allows for emailing and environmental control. As the possibility of communication with the P300 BCI was widely demonstrated, the field was open for the development of new applications for entertainment which culminated in brain painting. With brain painting, individuals with severe motor impairment and those in the locked-in state are offered the opportunity to express themselves creatively and in a nonverbal dimension. Evaluation of BCI applications at the users' home also revealed its caveats: speed, technical complexity, and the cap, thus outlining pressing fields for further research. As BCIs went out of the frying pan

into the fire facing use in real-world situations, new questions and problems can be addressed and solved.

Acknowledgments

This work is supported by the European ICT Program Project FP7-224631 and ICT Program Project FP7-247919. This chapter only reflects the authors' views and funding agencies are not liable for any use that may be made of the information contained herein.

References

- Aloise, F., Babiloni, F., Marciani, M. G., Morelli, D., Paolucci, S., Oriolo, G., et al. (2006). *Brain-operated assistive devices: The ASPICE Project*, Pisa, Italy.
- Aloise, F., Ferriero, D., Ruiu, A., Santucci, G., Catarci, T., Mattia, D., Babiloni, F., Cincotti, F., et al. (2009). *Controlling domotic appliances via a dynamical P300-based Brain Computer interface*. AAATE'09, Florence 31 August - 2 September 2009.
- Aloise, F., Marchionni, S., Romito, G., Brouwer, A. M., van Erp, J., Mattia, D., et al. (2008). *P300-based brain computer interface: To operate domotic appliance*. 4th BCI Workshop, Graz.
- Anderson, C. W., Kirby, M. J., Hundley, D. R., & Knight, J. N. (2007). Classification of time-embedded EEG using short-time principal component analysis. In G. Dornhege, J. del, R. Millán, T. Hinterberger, D. J. McFarland & K. R. Müller (Eds.), *Toward brain-computer interfacing* (pp. 261–278). Cambridge, MA: MIT Press.
- Babiloni, F., Cincotti, F., Marciani, M., Salinari, S., Astolfi, L., Aloise, F., et al. (2009). On the use of brain-computer interfaces outside scientific laboratories toward an application in domotic environments. *International Review of Neurobiology*, 86, 133–146.
- Baldoni, R., Di Ciccio, C., Mecella, M., Patrizi, F., Querzoni, L., Santucci, G., et al. (2009). *An embedded middleware platform for pervasive and immersive environments for-all*. SECON Workshops, pp. 1–3.
- Bayliss, J. D. (2003). Use of the evoked potential P3 component for control in a virtual apartment. *IEEE Transactions on Neural Systems and Rehabilitation Engineering*, 11, 113–116.
- Birbaumer, N., Ghanayim, N., Hinterberger, T., Iversen, I., Kotchoubey, B., Kübler, A., et al. (1999). A spelling device for the paralysed. *Nature*, 398(6725), 297–298.

- Birbaumer, N., Murguialday, A. R., & Cohen, L. (2008). Brain-computer interface in paralysis. *Current Opinion in Neurology*, 21(6), 634–638.
- Blankertz, B., Krauledat, M., Dornhege, G., Williamson, J., Murray-Smith, R., & Müller, K. R. (2007). A note on brain actuated spelling with the berlin brain- computer interface. In C. Stephanidis (Ed.), *Universal access in HCI, part II, HCII 2007, volume 4555 of LNCS* (pp. 759–768). Berlin, Heidelberg: Springer.
- Blankertz, B., Lemm, S., Treder, M., Haufe, S., & Müller, K.-R. (2011). Single-trial analysis and classification of ERP components—A tutorial. *Neuroimage*, 56(2), 814–825. doi:10.1016/j.neuroimage.2010.06.048.
- Blankertz, B., Sannelli, C., Halder, S., Hammer, E. M., Kübler, A., Müller, K. R., et al. (2010b). Neurophysiological predictor of SMR-based BCI performance. *Neuroimage*, 51(4), 1303–1309.
- Brouwer, A. M., & van Erp, J. B. F. (2010). A tactile P300 brain-computer interface. *Front Neuroprocessor*, 4, 1–11.
- Brunner, P., Joshi, S., Briskin, S., Wolpaw, J. R., Bischof, H., & Schalk, G. (2010). Does the ‘P300’ speller depend on eye gaze? *Journal of Neural Engineering*, 7, 1–9.
- Cecotti, H., & Gräser, A. (2011). Convolutional neural networks for P300 detection with application to brain-computer interfaces. *IEEE Transactions on Pattern Analysis and Machine Intelligence*, 33(3), 433–445. doi:10.1109/TPAMI.2010.125.
- Cincotti, F., Kauhanen, L., Aloise, F., Palomaki, T., Caporaso, N., Jylänki, P., et al. (2007). Vibrotactile feedback for brain-computer interface operation. *Computational Intelligence and Neuroscience*, 2007, 48937. doi:10.1155/2007/48937.
- Cincotti, F., Mattia, D., Aloise, F., Bufalari, S., Schalk, G., Oriolo, G., et al. (2008). Non-invasive brain-computer interface system: Towards its application as assistive technology. *Brain Research Bulletin*, 75, 796–803.
- Demiralp, T., Ademoglu, A., Comerchero, M., & Polich, J. (2001). Wavelet analysis of P3a and P3b. *Brain Topography*, 13(4), 251–267.
- Donchin, E., Spencer, K. M., & Wijesinghe, R. (2000). The mental prosthesis: Assessing the speed of a P300-based brain-computer interface. *IEEE Transactions on Rehabilitation Engineering*, 8(2), 174–179.
- Donoghue, J. P. (2008). Bridging the gap to the world: A perspective on neural interface systems. *Neuron*, 60, 511–521.
- Dornhege, G., Krauledat, M., Müller, K.-R., & Blankertz, B. (2007). General signal processing and machine learning tools for BCI analysis. In G. Dornhege, J. del R. Millán, T. Hinterberger, D. J. McFarland & K.-R. Müller (Eds.), *Toward brain-computer interfacing* (pp. 207–234). Cambridge, MA: MIT Press.
- Fabiani, M., Gratton, G., Karis, D., & Donchin, E. (1987). Definition, identification and reliability of measurement of the P300 component of the event-related brain potential. In P. K. Ackles, J. R. Jennings & M. G. H. Coles (Eds.), *Advances in psychophysiology* (pp. 1–79). Greenwich, CT: JAI Press.
- Farwell, L. A., & Donchin, E. (1988). Talking off the top of your head: Toward a mental prosthesis utilizing event-related brain potentials. *Electroencephalography and Clinical Neurophysiology*, 70(6), 510–523.
- Furdea, A., Halder, S., Krusinski, D. J., Bross, D., Nijboer, F., Birbaumer, N., et al. (2009). An auditory oddball (P300) spelling system for brain-computer interfaces. *Psychophysiology*, 46(3), 617–625.
- Giacino, J. T., Ashwal, S., Childs, N., Cranford, R., Jennett, B., Katz, D. I., et al. (2002). The minimally conscious state: Definition and diagnostic criteria. *Neurology*, 58, 349–353.
- Gonsalvez, C. L., & Polich, J. (2002). P300 amplitude is determined by target-to-target interval. *Psychophysiology*, 39, 388–396.
- Guger, C., Daban, S., Sellers, E., Holzner, C., Krausz, G., Carabalona, R., et al. (2009a). How many people are able to control a P300-based brain-computer interface (BCI)? *Neuroscience Letters*, 462(1), 94–98.
- Guger, C., Holzner, C., Grönegrass, C., Edlinger, G., & Slater, M. (2009b). Brain-Computer Interface for Virtual Reality Control. *Proceedings of ESANN 2009* (pp. 443–448).
- Halder, S., Rea, M., Andreoni, R., Nijboer, F., Hammer, E. M., Kleih, S. C., et al. (2010). An auditory oddball brain-computer interface for binary choices. *Clinical Neurophysiology*, 121(4), 516–523.
- Hill, N. J., Lal, T. N., Bierig, K., Birbaumer, N., & Schölkopf, B. (2005). An auditory paradigm for brain-computer interfaces. In L. Saul, Y. Weiss & L. Bottou (Eds.), *Advances in Neural Information Processing Systems*, (Vol. 17), (pp. 569–576). Cambridge, MA, USA: MIT Press.
- Hill, N. J., Lal, T. N., Tangermann, M., Hinterberger, T., Widman, G., Elger, C. E., et al. (2007). Classifying event-related desynchronization in EEG, ECg, and MEG signals. In G. Dornhege, J. del R. Millán, T. Hinterberger, D. J. McFarland & K.-R. Müller (Eds.), *Toward brain-computer interfacing* (pp. 235–260). Cambridge, MA: MIT Press.
- Hoffmann, U. (2007). *Bayesian machine learning applied in a Brain-Computer Interface for disabled users*. Dissertation. Ecole Polytechnique Federale de Lausanne.
- Hoffmann, U., Vesin, J., Ebrahimi, T., & Diserens, K. (2008). An efficient P300-based brain-computer interface for disabled subjects. *Journal of Neuroscience Methods*, 167(1), 115–125.
- Höhne, J., Schreuder, M., Blankertz, B., & Tangermann, M. (2010). Two-dimensional auditory P300 Speller with predictive text system. *Conference Proceedings: IEEE Engineering in Medicine and Biology Society*, 1, 4185–4188.
- Iturrate, I., Antelis, J. M., Kübler, A., & Minguez, J. (2009). A noninvasive brain-actuated wheelchair based on a P300 neurophysiological protocol and automated navigation. *IEEE Transactions on Robotics*, 25(3), 614–627.

- Kaper, M., Meinicke, P., Grossekathofer, U., Lingner, T., & Ritter, H. (2004). Support vector machines for the P300 speller paradigm. *IEEE Transactions on Biomedical Engineering*, 51(6), 1073–1076.
- Kaufmann, T., Vögele, C., Sütterlin, S., Lukito, S., & Kübler, A. (submitted for publication). Effects of cardiac autonomic balance on performance in a P300 Brain Computer Interface.
- Kleih, S. C., Nijboer, F., Halder, S., & Kübler, A. (2010). Motivation modulates the P300 amplitude during brain-computer interface use. *Clinical Neurophysiology*, 121(7), 1023–1031.
- Klobassa, D. S., Vaughan, T. M., Brunner, P., Schwartz, N. E., Wolpaw, J. R., Neuper, C., et al. (2009). Toward a high-throughput auditory P300-based brain-computer interface. *Clinical Neurophysiology*, 120(7), 1252–1261.
- Kotchoubey, B., Kaiser, J., Bostanov, V., Lutzenberger, W., & Birbaumer, N. (2009). Recognition of affective prosody in brain-damaged patients and healthy controls: A neurophysiological study using EEG and whole-head MEG. *Cognitive, Affective, & Behavioral Neuroscience*, 9(2), 153–167.
- Krusienski, D. J., Cox, D., & Shih, J. (2010). Control of a robotic manipulator using EEG and ECoG signals. *Conference Paper presented at the TOBI: Tools for Brain-Computer Interaction Workshop 2010*, Graz, Austria.
- Krusienski, D. J., Sellers, E. W., Cabestaing, F., Bayoudh, S., McFarland, D. J., Vaughan, T. M., et al. (2006). A comparison of classification techniques for the P300 speller. *Journal of Neural Engineering*, 3(4), 299–305.
- Krusienski, D. J., Sellers, E. W., McFarland, D. J., Vaughan, T. M., & Wolpaw, J. R. (2008). Toward enhanced P300 speller performance. *Journal of Neuroscience Methods*, 167(1), 15–21.
- Kübler, A., Furdea, A., Halder, S., Hammer, E. M., Nijboer, F., & Kotchoubey, B. (2009). A brain-computer interface controlled auditory event-related potential (p300) spelling system for locked-in patients. *Annals of the New York Academy of Sciences*, 1157, 90–100.
- Kübler, A., Halder, S., Furdea, A., & Hösle, A. (2008). Brain painting—BCI meets art. *Proceedings of the 4th International Brain-Computer Interface Workshop and Training Course*, pp. 361–366.
- Kübler, A., & Kotchoubey, B. (2007). Brain-computer interfaces in the continuum of consciousness. *Current Opinion in Neurology*, 20, 643–649.
- Kübler, A., Kotchoubey, B., Kaiser, J., Wolpaw, J. R., & Birbaumer, N. (2001). Brain-computer communication: Unlocking the locked in. *Psychological Bulletin*, 127(3), 358–375.
- Kübler, A., & Müller, K.-R. (2007). An introduction to brain-computer interfacing. In G. Dornhege, J. del R. Millán, T. Hinterberger, D. J. McFarland & K.-R. Müller (Eds.), *Toward brain-computer interfacing* (pp. 1–26). Cambridge, MA: MIT Press.
- Kübler, A., Neumann, N., Wilhelm, B., Hinterberger, T., & Birbaumer, N. (2004). Brain-computer predictability of brain-computer communication. *Journal of Psychophysiology*, 18(2–3), 121–129.
- Laureys, S., Owen, A., & Schiff, N. D. (2004). Brain function in coma, vegetative state, and related disorders. *Lancet Neurology*, 9, 537–546.
- Laureys, S., Pellas, F., Van Eeckhout, P., Ghorbel, S., Schnakers, C., Perrin, F., et al. (2005). The locked-in syndrome: What is it like to be conscious but paralyzed and voiceless? *Progress in Brain Research*, 150, 495–511.
- Lin, C. T., Ko, L. W., Chang, M. H., Duann, J. R., Chen, J. Y., Su, T. P., et al. (2010). Review of wireless and wearable electroencephalogram systems and brain-computer interfaces—A mini-review. *Gerontology*, 56(1), 112–119.
- Lotte, F., Congedo, M., Lecuyer, A., Lamarche, F., & Arnaldi, B. (2007). A review of classification algorithms for EEG-based brain-computer interfaces. *Journal of Neural Engineering*, 4(2), R1–R13.
- Lutzenberger, W., Elbert, T., Rockstroh, B., & Birbaumer, N. (1979). The effects of self-regulation of slow cortical potentials on performance in a signal detection task. *The International Journal of Neuroscience*, 9(3), 175–183.
- Lutzenberger, W., Elbert, T., Rockstroh, B., & Birbaumer, N. (1982). Biofeedback produced slow brain potentials and task performance. *Biological Psychology*, 14(1–2), 99–111.
- Mankoff, J., Day, A., Moore, M., & Batra, U. (2002). Web accessibility for low bandwidth input. *Proceedings of ASSETS*. pp. 88–96 Edinburgh, ACM Press.
- McFarland, D. J., McCane, L. M., David, S. V., & Wolpaw, J. R. (1997). Spatial filter selection for EEG-based communication. *Electroencephalography and Clinical Neurophysiology*, 103(3), 386–394.
- McFarland, D. J., Sarnacki, W. A., Townsend, G., Vaughan, T., & Wolpaw, J. R. (2011). The P300-based brain-computer interface (BCI): Effects of stimulus rate. *Clinical Neurophysiology*, 122(4), 731–737. doi:10.1016/j.clinph.2010.10.029.
- Millán, J. del R., Rupp, R., Müller-Putz, G.-R., Murray-Smith, R., Giugliemma, C., Tangermann, M., et al. (2010). Combining brain-computer interfaces and assistive technologies: State-of-the-art and challenges. *Frontiers in Neuroscience*, 4(161), 1–15.
- Monti, M., Laureys, S., & Owen, A. M. (2010a). The vegetative state. *British Medical Journal*, 341, 292–296.
- Monti, M. M., Vanhaudenhuyse, A., Coleman, M. R., Boly, M., Pickard, J. D., Tshibanda, L., et al. (2010b). Willful modulation of brain activity in disorders of consciousness. *The New England Journal of Medicine*, 362, 579–589.
- Mugler, E., Bensch, M., Halder, S., Rosenstiel, W., Bogdan, M., Birbaumer, N., et al. (2008). Control of an internet browser using the P300 event-related potential. *International Journal of Bioelectromagnetism*, 10(1), 56–63.

- Mugler, E. M., Ruf, C. A., Halder, S., Bensch, M., & Kübler, A. (2010). Design and implementation of a P300-based brain-computer interface for controlling an internet browser. *IEEE Transactions on Neural Systems and Rehabilitation Engineering*, 18(6), 599–609.
- Müller-Putz, G. R., Scherer, R., Neuper, C., & Pfurtscheller, G. (2006). Steady-state somatosensory evoked potentials: Suitable brain signals for brain-computer interfaces? *IEEE Transactions on Neural Systems and Rehabilitation Engineering*, 14(1), 30–37.
- Münbinger, J. I., Halder, S., Kleih, S. C., Furdea, A., Raco, V., Hösle, A., & Kübler, A. (2010). Brain Painting: first evaluation of a new brain-computer interface application with ALS-patients and healthy volunteers. *Frontiers in Neuroprosthetics*, 4(182), doi:10.3389/fnins.2010.00182.
- Neumann, N., & Birbaumer, N. (2003). Predictors of successful self control during brain-computer communication. *Journal of Neurology, Neurosurgery, and Psychiatry*, 74(8), 1117–1121.
- Nijboer, F., Birbaumer, N., & Kübler, A. (2010). The Influence of Psychological State and Motivation on Brain-Computer Interface Performance in Patients with Amyotrophic Lateral Sclerosis – a Longitudinal Study. *Frontiers in Neuroscience*, 4. doi:10.3389/fnins.2010.00055.
- Nijboer, F., Furdea, A., Gunst, I., Mellinger, J., McFarland, D. J., Birbaumer, N., et al. (2008a). An auditory brain-computer interface (BCI). *Journal of Neuroscience Methods*, 167(1), 43–50.
- Nijboer, F., Sellers, E. W., Mellinger, J., Jordan, M. A., Matuz, T., Furdea, A., et al. (2008b). A P300-based brain-computer interface for people with amyotrophic lateral sclerosis. *Clinical Neurophysiology*, 119(8), 1909–1916.
- Nunan, D., Donovan, G., Jakovljevic, D. G., Hodges, L., Sandercock, G. R. H., & Brodie, D. A. (2009). Validity and reliability of short-term heart-rate variability from the Polar S810. *Medicine and Science in Sports and Exercise*, 41(1), 243–250.
- Pfurtscheller, G. (1992). Event-related synchronization (ERS): An electrophysiological correlate of cortical areas at rest. *Electroencephalography and Clinical Neurophysiology*, 83(1), 62–69.
- Pfurtscheller, G., & Neuper, C. (2005). EEG-based brain-computer interfaces. In E. Niedermeyer & F. da Silva (Eds.), *Electroencephalography: Basic principles, clinical applications, and related fields*. (5th ed.). Philadelphia: Lippincott Williams & Wilkins.
- Piccione, F., Giorgi, F., Tonin, P., Priftis, K., Giove, S., Silvoni, S., et al. (2006). P300-based brain computer interface: Reliability and performance in healthy and paralysed participants. *Clinical Neurophysiology*, 117(3), 531–537.
- Pineda, J. A., Silverman, D. S., Vankov, A., & Hestenes, J. (2003). Learning to control brain rhythms: Making a brain-computer interface possible. *IEEE Transactions on Neural Systems and Rehabilitation Engineering*, 11(2), 181–184.
- Pires, G., & Nunes, U. (2002). A wheelchair steered through voice commands and assisted by a reactive fuzzy-logic controller. *Journal of Intelligent and Robotic Systems*, 34(3), 301–314.
- Pritchard, W. S. (1981). Psychophysiology of P300. *Psychological Bulletin*, 89(3), 506–540.
- Rastjoo, A., & Arabalibeik, H. (2009). Evaluation of hidden Markov model for P300 detection in EEG signal. *Studies in Health Technology and Informatics*, 142, 265–267.
- Riccio, A., Leotta, F., Aloise, F., Bianchi, L., Mattia, D., & Cincotti, F. (2010). Evaluation of a P300 overlaid stimulation for controlling an assistive technology software. *Conference proceedings of Fourth International TOBI BCI Meeting*, Rome, Italy.
- Rowland, L. P., & Shneider, N. A. (2001). Medical progress: Amyotrophic lateral sclerosis. *The New England Journal of Medicine*, 344(22), 1688–1700.
- Schalk, G., McFarland, D., Hinterberger, T., Birbaumer, N., & Wolpaw, J. R. (2004). BCI2000: A general-purpose brain-computer interface (BCI) system. *IEEE Transactions on Biomedical Engineering*, 51(6), 1034–1043.
- Schnakers, C., Vanhaudenhuyse, A., Giacino, J., Ventura, M., Boly, M., Majerus, S., et al. (2009). Diagnostic accuracy of the vegetative and minimally conscious state: Clinical consensus versus standardized neurobehavioral assessment. *BMC Neurology*, 9, 35.
- Schreuder, M., Blankertz, B., & Tangermann, M. (2010). A new auditory multi-class brain computer interface paradigm: Spatial hearing as an informative cue. *PLoS One*, 5(4), e9813.
- Sellers, E. W., & Donchin, E. (2006). A P300-based brain-computer interface: Initial tests by ALS patients. *Clinical Neurophysiology*, 117(3), 538–548.
- Sellers, E. W., Krusinski, D. J., McFarland, D. J., Vaughan, T. M., & Wolpaw, J. R. (2006). A P300 event-related potential brain-computer interface (BCI): The effects of matrix size and inter stimulus interval on performance. *Biological Psychiatry*, 73, 242–252.
- Sellers, E. W., Vaughan, T. M., & Wolpaw, J. R. (2010). A brain-computer interface for long-term independent home use. *Amyotrophic Lateral Sclerosis*, 11, 449–455.
- Sirvent, J. L., Azorín, J. M., Iáñez, E., Úbeda, A., & Fernández, E. (2010). P300-based brain-computer interface for internet browsing. In Y. Demazeau, F. Dignum, J. M. Corchado, J. Bajo, R. Corchuelo, E. Corchado, F. Fernández-Riverola, V. J. Julián, P. Pawlewski & C. Andrew (Eds.), *Trends in practical applications of agents and multiagent*

- systems.* 71, (pp. 615–622). Berlin, Heidelberg: Springer Berlin Heidelberg.
- Sutton, S., Braren, M., Zubin, J., & John, E. R. (1965). Evoked-potential correlates of stimulus uncertainty. *Science*, 150(700), 1187–1188.
- Takano, K., Komatsu, T., Hata, N., & Nakajima, Y. (2009). Visual stimuli for the P300 brain-computer interface: A comparison of white/gray and green/blue flicker matrices. *Clinical Neurophysiology*, 120, 1562–1566.
- Task Force of the European Society of Cardiology and The North American Society of Pacing and Electrophysiology, (1996). Heart rate variability—Standards of measurement, physiological interpretation, and clinical use. *European Heart Journal*, 17, 354–381.
- Townsend, G., LaPallo, B. K., Boulay, C. B., Krusienski, D. J., Frye, G. E., Hauser, C. K., et al. (2010). A novel P300-based brain-computer interface stimulus presentation paradigm: Moving beyond rows and columns. *Clinical Neurophysiology*, 121(7), 1109–1120.
- Treder, M. S., & Blankertz, B. (2010). (C)overt attention and visual speller design in an ERP-based brain-computer interface. *Behavioral and Brain Functions*, 6(1), 28. doi:10.1186/1744-9081-6-28.
- van Boxtel, J. J. A., Tsuchiya, N., & Koch, C. (2010). Consciousness and attention: On sufficiency and necessity. *Frontiers in Psychology*, 1, 217, doi:10.3389/fpsyg.2010.00217.
- Volosyak, I., Valbuena, D., Malechka, T., Peuscher, J., & Gräser, A. (2010). Brain-computer interface using water-based electrodes. *Journal of Neural Engineering*, 7, 066007, doi:10.1088/1741-2560/7/6/066007.
- Williamson, J., Murray-Smith, R., Blankertz, B., Krauledat, M., & Müller, K. R. (2009). Designing for uncertain, asymmetric control: Interaction design for brain-computer interfaces. *International Journal of Human-Computer Studies*, 67(10), 827–841.
- Zickler, C., Di Donna, V., Kaiser, V., Al-Khadairy, A., Kleih, S. C., Kübler, A., et al. (2009). BCI applications for people with disabilities: Defining user needs and user requirements. *Paper presented at the AAATE 25th Conference*, Florence, Italy.
- Zickler, C., Riccio, A., Leotta, F., Hillian-Tress, S., Halder, S., Holz, E., et al. (submitted for publication). BCI and Assistive Technology: BCI as input channel in a standard assistive technology ICT-software. *Clinical EEG*.

References to projects

- DECODER project: EU project in the 7th Framework programme. ICT-2009.7.2. Full title: Deployment of Brain-Computer Interfaces for the Detection of Consciousness in Non-Responsive Patients. www.decoderproject.eu.
- TOBI project: EU project in the 7th Framework programme. ICT-2007-224631. Full title: Tools for Brain-Computer Interaction. www.tobi-project.org.

CHAPTER 3

Toward a whole-body neuroprosthetic

Mikhail A. Lebedev^{†,‡} and Miguel A. L. Nicolelis^{†,‡,§,¶,||,#,*}

[†] Department of Neurobiology, Duke University, Durham, NC, USA

[‡] Duke Center for Neuroengineering, Duke University, Durham, NC, USA

[§] Department of Biomedical Engineering, Duke University, Durham, NC, USA

[¶] Department of Psychology and Neuroscience, Duke University, Durham, NC, USA

^{||} Edmond and Lily Safra International Institute of Neuroscience, Natal, Brazil

^{*} Fellow, Center for Neuroprosthetics, École Polytechnique Fédérale de Lausanne, Lausanne, Switzerland

Abstract: Brain–machine interfaces (BMIs) hold promise for the restoration of body mobility in patients suffering from devastating motor deficits caused by brain injury, neurological diseases, and limb loss. Considerable progress has been achieved in BMIs that enact arm movements, and initial work has been done on BMIs for lower limb and trunk control. These developments put Duke University Center for Neuroengineering in the position to develop the first BMI for whole-body control. This whole-body BMI will incorporate very large-scale brain recordings, advanced decoding algorithms, artificial sensory feedback based on electrical stimulation of somatosensory areas, virtual environment representations, and a whole-body exoskeleton. This system will be first tested in nonhuman primates and then transferred to clinical trials in humans.

Keywords: brain–machine interface; brain–machine–brain interface; intracortical microstimulation; bidirectional brain–machine interface; neuroprosthetic feedback; artificial sensation; active touch; locomotion; functional electrical stimulation; bimanual; multielectrode implant; primary motor cortex; primary somatosensory cortex; exoskeleton; posture; balance.

Introduction

Brain–machine interfaces (BMIs) (Andersen et al., 2004; Birbaumer and Cohen, 2007; Fetz, 2007; Lebedev and Nicolelis, 2006; Nicolelis,

2001; Nicolelis and Lebedev, 2009; Schwartz et al., 2006; Wessberg et al., 2000) offer a translational solution to the problem of restoring mobility to millions of people who suffer from paralysis caused by neurological injuries, neurodegenerative diseases, or limb loss (Paddock, 2009). Only limited treatment options are available to these patients, and often their condition cannot be improved or ameliorated (Dobkin and Havton,

*Corresponding author.

Tel.: +1-919-684-4580; Fax: 919.668.0734
E-mail: nicoleli@neuro.duke.edu

2004; Fouad and Pearson, 2004). BMIs hold promise to revolutionize the treatment of paralysis, as they strive to repair the damaged neural circuitry by bypassing the site of the lesion and establishing direct neural control of artificial tools by the activity of intact brain areas, such as the primary motor cortex (M1), which in many cases remain capable of generating motor commands despite being disconnected from the body effectors (Mattia et al., 2009). BMI research has expanded rapidly during the past decade (Lebedev and Nicolelis, 2006; Nicolelis and Lebedev, 2009), generating high expectations for potential clinical applications. Proof-of-concept BMIs have been tested in rodents (Chapin et al., 1999), nonhuman primates (Carmena et al., 2003; Moritz et al., 2008; Taylor et al., 2002; Velliste et al., 2008; Wessberg et al., 2000), and human subjects (Allison et al., 2007; Birbaumer and Cohen, 2007; Hochberg et al., 2006; Kennedy and Bakay, 1998; Patil et al., 2004; Pfurtscheller and Neuper, 2006). BMI systems developed at the Duke University Center for Neuroengineering (DUCN) during the past 12 years have made it possible to control many motor functions by neuronal ensemble activity recorded with chronic implants, ranging from arm reaching and grasping movements (Carmena et al., 2003; Lebedev et al., 2005; Wessberg et al., 2000) to bipedal locomotion (Cheng et al., 2007a; Fitzsimmons et al., 2009). Moreover, recently we have demonstrated for the first time brain-machine-brain interfaces (BMBIs) that incorporate somatosensory feedback loops that transmit information from the actuator to the brain (O'Doherty et al., 2009, 2010). These developments have put us in the position to develop the first whole-body neuroprosthetic for severely paralyzed patients.

Whole-body neuroprosthetic

Previous BMI studies focused predominantly on behavioral tasks in which an artificial actuator enacted upper extremity movements, such as

reaching and grasping. Except for a few studies (Fitzsimmons et al., 2009; Pfurtscheller et al., 2006; Prilutsky et al., 2005), virtually no attempts have been made to translate BMI technology to tasks enacting motor functionality of lower extremities and the trunk. Yet, deficits or the complete loss of the ability to walk presents a considerable problem for millions of patients worldwide. Such motor deficits commonly result from spinal cord injury (Dietz, 2001; Rossignol et al., 2007; Scivoletto and Di Donna, 2009) and neurological diseases (Boonstra et al., 2008; Pearson et al., 2004). Surveys of paraplegic patients showed that they prioritized walking and trunk stability among desired mobility functions (Anderson, 2004; Brown-Triolo et al., 2002). Quadriplegic patients prioritized arm and hand function (Anderson, 2004). Thus, developing neural prosthetic devices for restoration of leg mobility is as important as developing neuroprosthetics of the arm and hand, and for some categories of patients, it is one of their main priorities in terms of rehabilitation gain. In this context, a whole-body neuroprosthetic device would clearly have a major impact on the community of people suffering from many types of body paralysis.

As it defines its strategic mission for the next decade, the DUCN has elected as its main priority to construct, test, and implement a clinical version of a whole-body BMI. We envision a whole-body BMI as a neuroprosthetic system in which neuronal ensemble activity sampled simultaneously from multiple cortical areas controls the actuators that generate movements of both upper and lower extremities (Winans et al., 2010). In theory, the actuators can be implemented as a whole-body exoskeleton or a set of devices for functional electrical stimulation (FES). As the main project, the DUCN has opted for the first solution, building a whole-body exoskeleton in partnership with Dr. Gordon Cheng's group at the Technical University of Munich.

In our efforts to implement the first whole-body neuroprosthetic device for clinical use, the

first step will be to test a monkey version of such a BMI. This prototype will take into account all findings and technological developments obtained by our laboratory during the past decade. We expect that this whole-body BMI will provide animals with the ability to navigate a virtual environment through the control of a realistic representation of a monkey body. All the movements of this life-like computational avatar will be enacted by the animal's brain activity. Indeed, in this experimental paradigm, monkeys will learn to control the avatar's body movements under BMI control and to perform a series of tasks that require both upper and lower limb coordinated movements, including reaching and grasping virtual objects, selecting objects with different texture, bimanual object manipulation, and autonomous bipedal locomotion. Once monkeys achieve a high degree of proficiency in interacting with such a whole-body BMI in a virtual environment, the same technology will be then transferred to control a real whole-body exoskeleton that the animals will wear. These latter primate experiments, in which animals learn to control an exoskeleton through a BMI, will be developed in parallel with the creation of a virtual environment for patients that will use magnetoencephalography to generate the type of brain-derived signals needed for these patients to learn how to operate a realistic avatar of their own body (see Fig. 1). Through this sequence of animal and clinical experiments, we intend to generate a prototype neural prosthetic device for whole-body control which will be then translated to clinical trials and, eventually, enable severely paralyzed people to walk again by 2016.

Below, we review recent results obtained at the DUCN that support our contention that a whole-body BMI can be implemented by this deadline.

BMI components

The basic components of a BMI system are exemplified by the now classical paradigm that enacts direct control of robotic arm reaching

movements based on the combined cortical activity of hundreds of cortical neurons (Carmena et al., 2003; Lebedev and Nicolelis, 2006; Lebedev et al., 2005; Nicolelis and Lebedev, 2009; Wessberg et al., 2000). In this BMI paradigm, the electrical activity of large populations of motor cortical neurons is recorded by chronically implanted multielectrode arrays and converted into control signals that drive a robotic arm. Concurrently, visual and/or somatosensory feedback signals from the robot are delivered back to the brain as either natural visual stimuli or, as in our recent demonstrations, intracortical microstimulation (ICMS) of the primary somatosensory cortex (S1) (Lebedev and Nicolelis, 2006; O'Doherty et al., 2009, 2010). The processing of neuronal ensemble activity is performed by a series of real-time BMI decoding algorithms which translate a myriad of neuronal spikes into the kinematic and dynamic parameters required to generate the robotic arm's movements, according to the voluntary motor intentions of the subject. The BMI setup also includes the data acquisition system, the computer cluster running multiple decoding models in real time, the robot arm, the visual display, and a sensory feedback loop from the actuator to the brain.

Large-scale neuronal recordings

The major prerequisite for the performance of a neuroprosthetic device to be versatile, accurate, and stable, and to allow simultaneous motor control of both lower and upper extremities, is that multiple brain areas should be implanted and large-scale neuronal activity sampled from those areas simultaneously during operation of a whole-body BMI (Nicolelis and Lebedev, 2009; Nicolelis et al., 2003). During the past two decades, advanced electrophysiological methods have allowed recording from progressively larger samples of single neurons in behaving animals (Churchland et al., 2007; Nicolelis and Ribeiro, 2002; Nicolelis et al., 1995, 2003). With the

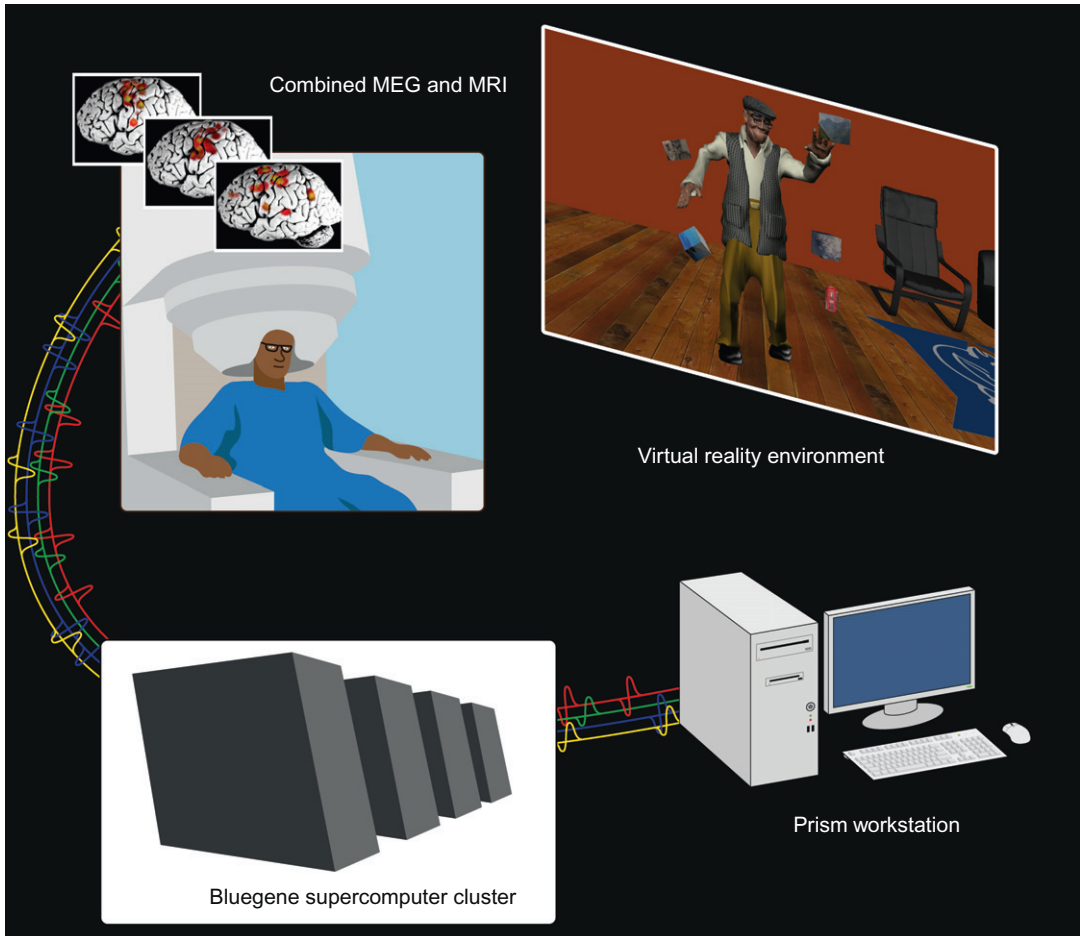


Fig. 1. Schematic illustration of a human whole-body neuroprosthetic based on magnetoencephalographic recordings and functional magnetic resonance imaging that enables a paralyzed human to operate a realistic avatar of their own body in a virtual environment. Brain signals are processed by a powerful computer cluster and converted into commands that drive a life-like avatar. This technology will be used to develop and test a brain-controlled whole-body navigation system and will be eventually translated into a mind-operated whole-body exoskeleton.

present generation of planar multielectrode arrays, which can be chronically implanted in the brain, we can record the extracellular electrical activity of several hundreds of cortical cells simultaneously in a behaving rhesus monkey (Carmena et al., 2003; Fitzsimmons et al., 2009; Lebedev et al., 2005; Nicolelis et al., 2003). Due to a rapid progress in the methods for large-scale recordings (Nicolelis et al., 2003), the number of simultaneously sampled

neural channels is expected to rise to several thousands in the next decade. Indeed, recently, we have started to employ a new type of device, called the three-dimensional (3D) recording cube, which provides recording sites throughout the vertical shaft of each microwire bundle. Preliminary results suggest that such a 3D recording cube could allow neuronal yield to reach several tens of thousands of neurons in the near future. Given that

our previous studies have clearly demonstrated that the accuracy of extraction of motor intentions from the brain improves with the number of neurons recorded (Carmena et al., 2003; Lebedev et al., 2007; Nicolelis and Lebedev, 2009; Santucci et al., 2005; Wessberg et al., 2000), and given that the number of required neurons increases as more motor parameters are simultaneously extracted (Fitzsimmons et al., 2009), the advent of the 3D recording cube, and other technologies like it, could prove vital for the translation of experimental discoveries into clinical practice. Incidentally, the central experimental finding obtained through BMI research, the confirmation that distributed ensembles of neurons define the true physiological unit of the mammalian central nervous system (Nicolelis and Lebedev, 2009), will also play a major role in the road that will take us to clinical fruition.

A brief description may help clarify the imposing need for increasing the size of cortical recording samples in order to obtain the level of motor control needed to operate a whole-body exoskeleton. Currently, our most sophisticated BMIs provide a peak signal-to-noise ratio (SNR) of 10 dB using approximately 100 neurons (Fitzsimmons et al., 2009; Li et al., 2009). This corresponds to 5 bits/s bandwidth. In our estimation, SNRs of about 20–30 dB are needed for a neuroprosthetic device to generate useful movements (see Fig. 2). Assuming that noise decreases as the inverse of the square root of the number of neurons, a tenfold increase in the number of simultaneously recorded neurons is needed to achieve an improvement of 10 dB. A control signal with 20-dB fidelity will then require 1000 neurons recorded simultaneously. For achieving our long-term goal of reaching an SNR of 40 dB, and control a whole-body exoskeleton, recording samples between 50,000–100,000 cortical neurons will be needed. Further, to control the movements of multiple prosthetic limbs, each of which requires enacting of many degrees-of-freedom (DOF), a whole-body neuroprosthetic will call for even higher neuronal samples. Thus, demands for large samples of neurons, located in multiple

cortical areas, will remain a central bottleneck for the development of clinical neuroprosthetics for the foreseeable future.

Another key issue to be dealt with is the question of the longevity of chronic multielectrode recordings. Heretofore, our state-of-the-art multielectrode implants reliably sample large-scale extracellular cortical electrical activity for at least 2 years in rhesus monkeys (Fitzsimmons et al., 2009) and at least 6.5 years in New World monkeys, like the owl monkey (Sandler et al., 2005). We have used a variety of designs for such multielectrode probes. Typically, electrode penetration sites are spaced with a 1-mm separation. The electrodes can be fixed or movable. In our recent design, we arranged stainless steel microwires into subsets (pairs or triplets) sitting inside guiding tubes (Winans et al., 2010). Each subset can be moved independently driven by a microscrew. Given that the electrodes in each subset have different lengths, the array samples from a 3D volume; that is, how we started to test what became known as the 3D recording cube. Currently, we are using this new cube design as a base for the development of the next-generation implants that will increase the number of recording channels to about 1500 per cube. That is because a 10×10 array will gain up to 15 recording contacts per vertical component, using micro-wire assemblies of different lengths. Further, to minimize the displacement of the nervous tissue and to minimize microglial and other immune responses to the foreign material during the surgical implantation of these recording cubes, we will be removing the structural elements after implantation, leaving only small diameter microwires within the neuronal tissue. Small-diameter microwires will be guided into the brain with a strong central shaft which will be removed later. To distinguish the type of cortical activity obtained with this new technology, we have coined the term very large scale brain activity (VLSBA), meaning extracellular neuronal activity generated by populations of more than 50,000 single neurons recorded simultaneously. By developing the means

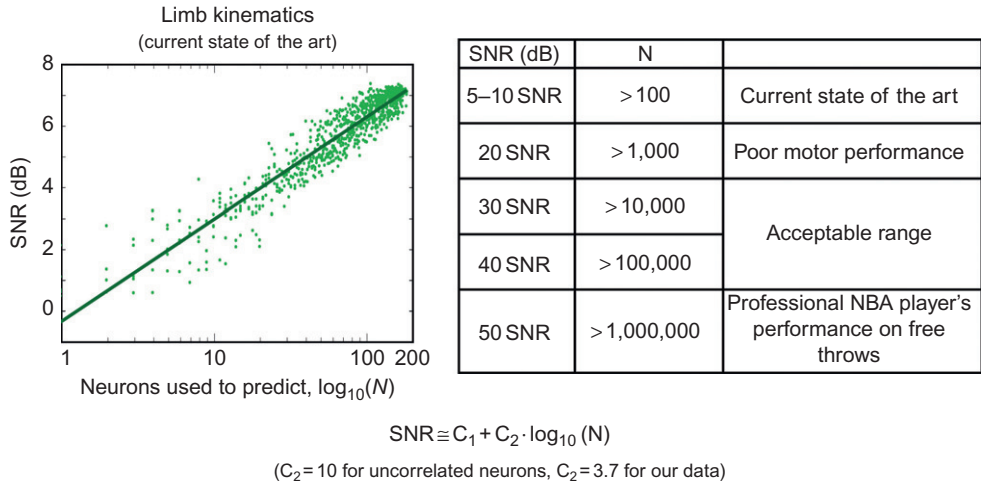


Fig. 2. An estimation of the dependency of the BMI signal-to-noise ratio (SNR) on the neuronal ensemble size. The scatter plot on the left shows a linear dependency of the SNR (in dB) on the logarithm of the number of neurons recorded. The data from Fitzsimmons et al. (2009) was used to construct this plot. This dependency is in correspondence with the equation shown at the bottom. The table on the right shows the estimates of the number of neurons needed to achieve certain performance benchmarks.

to record from VLSBA, we expect to generate the type of motor control signals that will be capable of driving a whole-body BMI.

BMI decoders

The success of any BMI system depends to a significant degree on the choice of BMI decoders that extract motor parameters from the sample of neuronal electrical activity recorded in real time. In our current studies, online processing of large-scale brain activity is achieved through an integrated BMI suite that incorporates the recording and stimulation hardware, as well as a computer cluster employed for all real-time processing of the massive stream of neurophysiological data generated in each of these experimental sections (Fitzsimmons et al., 2009; O'Doherty et al., 2009). This BMI suite can simultaneously run several neuronal decoders, including the unscented Kalman filter (Li et al., 2009), the Wiener filter, multiple artificial neural networks, and discrete state Bayesian algorithms (Li et al.,

2010). Each motor parameter can be extracted by one of these filters or can represent a mixture of the outputs of individual decoders. During the extraction or arm reaching movements, the unscented Kalman filter outperforms the other decoding algorithms (Li et al., 2010). This decoder is based on nonlinear models of neural tuning and prior knowledge about movement patterns. It is also enhanced by a short history of the arm movements. We have also developed a multiple model-switching paradigm (Fitzsimmons et al., 2009) that uses different submodels to extract motor variables in particular behavioral states (e.g., reaching vs. grasping or walking forward vs. walking backward). The simplest switching model consists of three linear decoding models: a model for predicting state 1 (e.g., walking forward), a model for state 2 (e.g., walking backward), and the paradigm predictor model (the switch). When the paradigm predictor determines a particular state, an appropriate submodel is used to produce the output, and when a different state is detected, the other submodel is used.

In the most straightforward implementation of BMI decoding, the kinematics of several limb joints is extracted from the combined neuronal electrical activity and converted into movements of the particular mechanical, electronic or virtual actuator employed in the experiment at hand. This general approach, however, is not optimal for clinical applications of BMIs because the user is required to control each DOF continuously and independently. In a more practical solution, the control over an external actuator is shared between the subject brain's activity and robotic controls (Kim et al., 2005). During this shared control, the subject's brain is in charge primarily of high-order control of movements (when to initiate movement and where to move), whereas the low-level coordination of the movement is performed by an autonomous controller.

Recently, we have developed a BMI decoder that autonomously adjusts its performance during long-term recordings and compensates for non-stationarities in neuronal inputs (Li et al., 2010). This decoder uses a Bayesian regression self-training method for updating the parameters for an unscented Kalman filter. To allow updates on subsets of neurons and to allow addition of newly discovered neurons, we approximated the probability distribution on the tuning model parameters using a factorized distribution and computed the Bayesian regression solution. We tested the performance of this filter in rhesus monkeys that learned to perform reaching movements under the BMI control. Over the course of 29 days, Bayesian regression self-training maintained control accuracy better than decoding without updates. This BMI decoder will be used in the whole-body BMI to provide long-term stability.

Bimanual control

A whole-body neuroprosthetic will have to enable independent control of two prosthetic arms. Such BMI control has not been achieved before. The majority of BMIs developed so far

involved only a single actuator (computer cursor or a robotic arm) that enacted arm reaching movements under the control of the subject's brain activity. We are currently exploring the use of BMIs for bimanual actuator control. As in other applications, the starting point in developing a bimanual BMI is to understand the neurophysiological processes that underlie bimanual behaviors in multiple cortical areas. Bimanual operations engage neuronal populations which are different from those engaged by unimanual movements (Kazennikov et al., 1999; Nakajima et al., 2007; Obhi and Goodale, 2005; Rokni et al., 2003; Rouiller et al., 1994). When both arms are involved, motor areas are activated in both hemispheres, and greater interhemispheric interactions occur. Five cortical areas involved in interlimb coordination are of particular interest for bimanual BMIs: dorsal premotor cortex (PMd), cingulate motor area, supplementary motor area, posterior parietal cortex, and M1 (Kermadi et al., 2000).

We have conducted preliminary experiments to investigate if rhesus monkeys could learn bimanual control of a life-like avatar. In these experiments, one monkey learned to manipulate two joysticks to move two avatar hands toward virtual objects. This learning occurred rapidly, suggesting that the monkey readily associated itself with the avatar. This observation strengthens our expectation that monkeys will be able to learn to control such bimanual movements through a BMI, without engaging any overt movements of their limbs.

Bipedal locomotion

Our laboratory pioneered BMIs that reproduce kinematics of leg movements during bipedal locomotion (Fitzsimmons et al., 2009). Previously, both BMI research and neurophysiological studies in awake, behaving monkeys focused predominantly on the behavioral tasks that involved arm movements and arm representation in the brain.

Neurophysiology of lower extremity control has been virtually neglected in nonhuman primates. Yet, a complete loss of the ability to walk is commonly caused by spinal cord injury (Dietz, 2001; Rossignol et al., 2007; Scivoletto and Di Donna, 2009), neurological diseases (Boonstra et al., 2008; Pearson et al., 2004), and limb loss (Pasquina et al., 2006). Developing a neuroprosthetic for lower limb control will clearly be very important for the treatment of whole-body paralysis.

In our initial study on the BMI for bipedal locomotion, rhesus monkeys walked bipedally on a treadmill (Fitzsimmons et al., 2009). We tracked leg movements using a video-based tracking system developed in our laboratory (Peikon et al., 2009). Leg kinematics and EMGs of leg muscles were extracted from linearly combined cortical ensemble activity in real time using a modified Wiener filter algorithm (Carmena et al., 2003; Haykin, 2002; Lebedev et al., 2005; Wessberg et al., 2000). Recording implants were placed in the leg representation area of M1. We found that the individual neuronal firing rates were highly variable from step to step. However, after the activity of many (several hundreds) neurons was combined using 100-ms bins, accurate extractions of the kinematics of leg movements (X, Y coordinates of the joints, joint angles) were produced. Walking parameters could be extracted using neuronal activity recorded in either M1 or S1 contralateral to the right leg, as well as ipsilateral M1.

Simultaneous extraction of many parameters of bipedal locomotion essentially depended on the size of the neuronal population. In this analysis, random neuronal subpopulations were pooled from the entire recorded population and used to predict several locomotion parameters simultaneously. The accuracy of simultaneous predictions was characterized by the normalized accuracy for the least well-predicted parameter. We found that smaller neuronal populations could predict only a few parameters simultaneously, and larger populations were required for predicting many parameters. Moreover, larger

neuronal populations were required to predict complex patterns of walking compared to more simple walking patterns. For example, the number of neurons required to achieve 95% of maximum prediction accuracy for the X position of the ankle clearly increased when walking conditions of higher complexity were required to complete a task (intermittent walking forward and backward, walking at different speeds). On average, 60 neurons were sufficient for predicting constant-speed walking in the forward direction. However, 90 neurons were needed to achieve this level of accuracy for variable-speed, forward walking, 95 neurons were required for extracting backward walking at constant speed, 115 neurons were required for predicting backward walking at variable speed, and extracting variable-speed bidirectional walking required 110 neurons.

Using our BMI for extracting patterns of bipedal locomotion, we demonstrated BMI control of bipedal walking in a robot (Cheng et al., 2007a) in real time. To achieve this goal, real-time predictions of monkey leg kinematics, derived from combined cortical activity, were transmitted through a dedicated Internet connection to ATR laboratories, in Kyoto, Japan, where our collaborators led by Cheng and Kawato set their humanoid 51-DOF robot (CB-1, manufactured by SARCOS) to reproduce monkey locomotion patterns. Back at our laboratory at Duke University, the monkey received continuous visual feedback of the robot's movements on a video screen placed in front of the animal. As we had observed in the case of BMI control of upper-limb extremities, after the treadmill was stopped, the monkey continued to use its brain activity to sustain bipedal walking in the robot without moving its own biological legs. This result supports our suggestion that a paralyzed person will be able to control a device for locomotion (e.g., an exoskeleton) with his/her cortical activity alone, without the need to produce overt body movements.

Posture and balance

Whole-body neuroprosthetics will not only have to produce stereotypical stepping but also adapt to postural control. As an advancement toward this goal, we have developed a proof-of-concept BMI for postural control (Tate et al., 2009). In these experiments, monkeys first learned to maintain an upright posture on a platform. Then, the platform moved abruptly, generating a postural perturbation. The platform was driven either periodically, allowing the animal to anticipate the upcoming perturbation, or with a random time delay between movements so that the animal could not anticipate when the next displacement would occur. By analyzing samples of simultaneously recorded cortical neurons, we observed that cells recorded in the leg representation of M1 and S1 clearly modulated their firing rate in response to platform displacement. These modulations were directionally tuned. Linear BMI decoders were applied to extract the kinematics of platform movements from cortical ensemble activity. We found that the decoder performance was different, depending on whether the platform movements were anticipated or unanticipated. Anticipated displacements were extracted with higher accuracy than unanticipated. These results suggest that cortical control over posture and balance can be added to a whole-body BMI. Optimal operation of such control probably can be aided by a shared control scheme (Kim et al., 2005).

Functional electrical stimulation

FES that activates the subject's own muscles may be implemented in future whole-body neuroprosthetics. FES devices have been already introduced to clinical practice as therapies for leg paralysis (Barbeau et al., 2002; Dobkin, 2007; Peckham et al., 1988; Thrasher and Popovic, 2008) along with robotic orthoses (Colombo et al., 2000; Dollar and Herr, 2008; Ferris et al., 2007). The first publications on a FES device for

helping to achieve an upright posture date back to the 1960s (Kantrowitz, 1960). Also in the 1960s, FES of the common peroneal nerve was introduced to correct foot drop during the swing phase of the gait (Liberson et al., 1961). At present, a variety of FES methods are available for stimulation of multiple muscle groups using superficial or intramuscular electrodes. In particular, FES systems have been shown to have positive therapeutic effects in patients with incomplete spinal cord injury (Thrasher and Popovic, 2008).

We suggest that FES technology can be incorporated in BMIs for the restoration of walking and balance. In support of this suggestion, we have already obtained reliable predictions of the EMGs of leg muscles during locomotion (Fitzsimmons et al., 2009) from the combined electrical activity of populations of M1 and S1 cortical neurons. Our next objective is to build a BMI-driven FES system that produces bipedal locomotion patterns by converting cortical ensemble activity into stimulation patterns that drive leg muscles. This approach can be used alone or in combination with robotic orthoses, such as exoskeletons.

Sensorized neuroprosthetic

Recently, we have reported our findings on the first BMBI. Such a paradigm expands on traditional BMIs by adding an artificial somatosensory feedback channel that can deliver artificially created tactile signals, generated by either real sensors placed in a robotic hand or virtual ones added to an avatar arm, directly to the somatosensory cortex, via ICMS. In our first study on this subject (Fitzsimmons et al., 2007), we investigated whether multichannel ICMS of S1 could be discriminated by owl monkeys and whether ICMS is suitable for long-term usage. Owl monkeys were implanted with multielectrode arrays in several cortical areas, whereas S1 implants were employed to deliver spatiotemporal patterns of ICMS. The behavioral task progressed from a simple requirement of detecting

the presence of ICMS to the goal of discriminating spatiotemporal patterns created using four electrode pairs. We found that owl monkeys could learn to discriminate spatiotemporal patterns of ICMS of increasing complexity and guide their arm reaching movements based on this discrimination. Moreover, spatiotemporal ICMS was efficient for many months. Interestingly, monkeys got progressively better in learning novel microstimulation patterns. This result suggests that ICMS was incorporated in their brains as a new sensory channel and that they could generalize the general rule applied to communicate directly with their brains.

In a series of studies conducted in rhesus monkeys, we used ICMS to guide monkeys' behavior when they performed BMI-reaching tasks (O'Doherty et al., 2009, 2010). We followed our usual paradigm of training a BMI decoder during a manually performed task and then switched to brain control (Carmena et al., 2003; Lebedev et al., 2005). The tasks consisted of acquiring visual targets with a computer cursor or a life-like avatar hand. We recorded simultaneously the electrical activity of 50–200 neurons in M1 and PMd. The monkeys learned to perform in BMI control with and without using the joystick. The innovative feature of these experiments was that ICMS of the S1 cortex was added to the BMI as an artificial sensory feedback. In the first study that implemented this approach (O'Doherty et al., 2009), ICMS served as a directional cue. It informed the monkeys to which direction they had to move. To avoid an interference of ICMS electrical artifacts with BMI extractions, we segregated the stimulation and recording epochs. Monkeys operated such a BMI with approximately the same accuracy as reported previously for simpler BMI designs.

Moreover, in our recent study (O'Doherty et al., 2010), ICMS served as an artificial sense of active touch, as it conveyed to the monkeys the properties of virtual objects that the actuator (computer cursor or a virtual image of a monkey arm) touched. Monkeys controlled an avatar arm with a BMI that derived motor commands

from the M1 activity. ICMS patterns were delivered to S1 each time the avatar touched virtual objects. Monkeys learned to search through sets of visually identical objects and select those with particular textures. These results suggest that future clinical neuroprosthetics can implement ICMS feedback to generate somatic perceptions from prosthetic limbs.

In our future work, we will incorporate multiple channel ICMS feedback in the BMIs for locomotion and whole-body control. We will also work on the incorporation of an artificial sense of position. Position sense is very important for clinical applications because ideal prosthetic limbs should feel as if they are natural extensions of the users' bodies. Normally, positional signals are provided by muscles, joints, and skin afferents. This information ascends to the sensory areas of the brain where it is processed using different coordinate frames, such as body- and external space-centered coordinates (Maravita et al., 2003; Matthews, 1988). Given this complexity of cortical processing of proprioceptive information (Longo et al., 2010), it would be difficult for an artificial position sense to achieve such precise mapping from the arm joints to the brain somatosensory map. Additionally, certain centrally generated components of normal position sense, such as corollary discharges (Crapse and Sommer, 2008), would be difficult to incorporate in such an implementation. Because of these foreseen difficulties in the straightforward implementation of an artificial position sense, we chose a simpler approach in which stimulation of S1 is not initially coupled to the orientation of the limb position but instead represents 3D spatial locations to which the subject is required to reach. In this approach, the subject starts with learning how ICMS of cortical somatotopic representations of the body is mapped to a 3D space. Such experimental design bears similarity to the studies on sensory substitution in which visual information was conveyed by the stimulation of skin surfaces (Bach-y-Rita, 1983; Bach-y-Rita and Kercel, 2003; Bach-y-Rita et al., 1969). We expect that similar to sensory

substitution using peripheral stimulation, training with stimulation of the somatosensory areas of the brain will eventually give rise to an artificial position sense that represents external space.

In addition to ICMS as the method to sensorize a whole-body BMI, optogenetic methods will be probably, extensively used in the future. Optogenetics is based on genetically modified ion channels that respond directly to light (Zhang et al., 2007). These light-gated ion channels, such as Channelrhodopsin-2 (Chr-2), allow precise, millisecond control of specific neurons (Boyden et al., 2005; Zhang et al., 2006). This technique eliminates most of the key problems associated with ICMS: there is no associated electrical artifact to interfere with the electrophysiological recordings, nor any tissue damage from the current injection. It also allows for finer control of the spatial pattern of activation. BMBIs that incorporate optogenetic stimulators would be superior to current designs in both the specificity and the long-term performance of the sensory loop and the quality of neuronal recordings.

A whole-body exoskeleton

In our research program, the definitive demonstration of a whole-body neuroprosthetic will involve a subject that is able to use his/her VLSBA to control movements of an exoskeleton that encases the entire body. Currently, we have all components needed for this demonstration. We have demonstrated BMIs for arm reaching and leg locomotion in separate experiments. We have also implanted leg and arm representations of the sensorimotor cortex in both hemispheres (Winans et al., 2010). The exoskeleton technology required for this demonstration already exists, and a prototype for our initial testing in monkeys is close to be completed. In our primate studies, such exoskeleton will be attached to the monkey using bracelets molded in the shape of the monkey's limbs. The basic design and controller will be based on the humanoid robot, CB-1 (Cheng et al., 2007a,b). This exoskeleton will provide a rich sensory feedback stream to

the BMI setup, including measurements of joints position and velocity, as well as torque, ground contacts, and orientations. In the BMI mode, the exoskeleton will guide the monkey's limbs with smooth motions, while monitoring its range of motions to ensure it is within the safety limits. This upcoming demonstration will provide the first prototype of a neural prosthetic device that would allow, one day in the near future, paralyzed people to recover a wide range of desired mobility functions.

References

- Allison, B. Z., Wolpaw, E. W., & Wolpaw, J. R. (2007). Brain-computer interface systems: Progress and prospects. *Expert Review of Medical Devices*, 4, 463–474.
- Andersen, R. A., Musallam, S., & Pesaran, B. (2004). Selecting the signals for a brain-machine interface. *Current Opinion in Neurobiology*, 14, 720–726.
- Anderson, K. D. (2004). Targeting recovery: Priorities of the spinal cord-injured population. *Journal of Neurotrauma*, 21, 1371–1383.
- Bach-y-Rita, P. (1983). Tactile vision substitution: Past and future. *The International Journal of Neuroscience*, 19, 29–36.
- Bach-y-Rita, P., Collins, C. C., Saunders, F. A., White, B., & Scadden, L. (1969). Vision substitution by tactile image projection. *Nature*, 221, 963–964.
- Bach-y-Rita, P., & Kercel, W. (2003). Sensory substitution and the human-machine interface. *Trends in Cognitive Sciences*, 7, 541–546.
- Barbeau, H., Ladouceur, M., Mirbagheri, M. M., & Kearney, R. E. (2002). The effect of locomotor training combined with functional electrical stimulation in chronic spinal cord injured subjects: Walking and reflex studies. *Brain Research. Brain Research Reviews*, 40, 274–291.
- Birbaumer, N., & Cohen, L. G. (2007). Brain-computer interfaces: Communication and restoration of movement in paralysis. *The Journal of Physiology*, 579, 621–636.
- Boonstra, T. A., van der Kooij, H., Munneke, M., & Bloem, B. R. (2008). Gait disorders and balance disturbances in Parkinson's disease: Clinical update and pathophysiology. *Current Opinion in Neurology*, 21, 461–471.
- Boyden, E. S., Zhang, F., Bamberg, E., Nagel, G., & Deisseroth, K. (2005). Millisecond-timescale, genetically targeted optical control of neural activity. *Nature Neuroscience*, 8, 1263–1268.
- Brown-Triolo, D. L., Roach, M. J., Nelson, K., & Triolo, R. J. (2002). Consumer perspectives on mobility: Implications for neuroprostheses design. *Journal of Rehabilitation Research and Development*, 39, 659–669.

- Carmena, J. M., Lebedev, M. A., Crist, R. E., O'Doherty, J. E., Santucci, D. M., Dimitrov, D. F., et al. (2003). Learning to control a brain-machine interface for reaching and grasping by primates. *PLoS Biology*, 1, E42.
- Chapin, J. K., Moxon, K. A., Markowitz, R. S., & Nicolelis, M. A. L. (1999). Real-time control of a robot arm using simultaneously recorded neurons in the motor cortex. *Nature Neuroscience*, 2, 664–670.
- Cheng, G., Fitzsimmons, N. A., Morimoto, J., Lebedev, M. A., Kawato, M., & Nicolelis, M. A. L. (2007). *Bipedal locomotion with a humanoid robot controlled by cortical ensemble activity*. Annual Meeting of the Society for Neuroscience. San Diego, California.
- Cheng, G., Hyon, S. H., Morimoto, J., Ude, A., Hale, J. G., Colvin, G., et al. (2007). CB: A humanoid research platform for exploring neuroscience. *Advanced Robotics*, 21, 1097–1114.
- Churchland, M. M., Yu, B. M., Sahani, M., & Shenoy, K. V. (2007). Techniques for extracting single-trial activity patterns from large-scale neural recordings. *Current Opinion in Neurobiology*, 17, 609–618.
- Colombo, G., Joerg, M., Schreier, R., & Dietz, V. (2000). Treadmill training of paraplegic patients using a robotic orthosis. *Journal of Rehabilitation Research and Development*, 37, 693–700.
- Crapse, T. B., & Sommer, M. A. (2008). Corollary discharge across the animal kingdom. *Nature Reviews. Neuroscience*, 9, 587–600.
- Dietz, V. (2001). Spinal cord lesion: Effects of and perspectives for treatment. *Neural Plasticity*, 8, 83–90.
- Dobkin, B. H. (2007). Brain-computer interface technology as a tool to augment plasticity and outcomes for neurological rehabilitation. *The Journal of Physiology*, 579, 637–642.
- Dobkin, B. H., & Havton, L. A. (2004). Basic advances and new avenues in therapy of spinal cord injury. *Annual Review of Medicine*, 55, 255–282.
- Dollar, A. M., & Herr, H. (2008). Lower extremity exoskeletons and active orthoses: Challenges and state-of-the-art. *IEEE Transactions on Robotics*, 24, 144–158.
- Ferris, D. P., Sawicki, G. S., & Daley, M. A. (2007). A physiologist's perspective on robotic exoskeletons for human locomotion. *International Journal of Humanoid Robotics*, 4, 507–528.
- Fetz, E. E. (2007). Volitional control of neural activity: Implications for brain-computer interfaces. *The Journal of Physiology*, 579, 571–579.
- Fitzsimmons, N. A., Drake, W., Hanson, T. L., Lebedev, M. A., & Nicolelis, M. A. L. (2007). Primate reaching cued by multi-channel spatiotemporal cortical microstimulation. *The Journal of Neuroscience*, 27, 5593–5602.
- Fitzsimmons, N. A., Lebedev, M. A., Peikon, I. D., & Nicolelis, M. A. L. (2009). Extracting kinematic parameters for monkey bipedal walking from cortical neuronal ensemble activity. *Frontiers in Integrative Neuroscience*, 3, 3.
- Fouad, K., & Pearson, K. (2004). Restoring walking after spinal cord injury. *Progress in Neurobiology*, 73, 107–126.
- Haykin, S. (2002). *Adaptive filter theory* (4th ed.). Upper Saddle River, NJ: Prentice Hall.
- Hochberg, L. R., Serruya, M. D., Friehs, G. M., Mukand, J. A., Saleh, M., Caplan, A. H., et al. (2006). Neuronal ensemble control of prosthetic devices by a human with tetraplegia. *Nature*, 442, 164–171.
- Kantrowitz, A. (1960). Electronic physiological aids: A report of the Maimonides Hospital, Brooklyn, New York, 75–77.
- Kazennikov, O., Hyland, B., Corboz, M., Babalian, A., Rouiller, E. M., & Wiesendanger, M. (1999). Neural activity of supplementary and primary motor areas in monkeys and its relation to bimanual and unimanual movement sequences. *Neuroscience*, 89, 661–674.
- Kennedy, P. R., & Bakay, R. A. (1998). Restoration of neural output from a paralyzed patient by a direct brain connection. *Neuroreport*, 9, 1707–1711.
- Kermadi, I., Liu, Y., & Rouiller, E. M. (2000). Do bimanual motor actions involve the dorsal premotor (PMd), cingulate (CMA) and posterior parietal (PPC) cortices? Comparison with primary and supplementary motor cortical areas. *Somatosensory and Motor Research*, 17, 255–271.
- Kim, H. K., Biggs, S. J., Schloerb, D. W., Carmena, J. M., Lebedev, M. A., Nicolelis, M. A. L., et al. (2005). Continuous shared control stabilizes reach and grasping with brain-machine interfaces. *IEEE Transactions on Biomedical Engineering*, 53, 1164–1173.
- Lebedev, M. A., Carmena, J. M., O'Doherty, J. E., Zacksenhouse, M., Henriquez, C. S., Principe, J. C., et al. (2005). Cortical ensemble adaptation to represent velocity of an artificial actuator controlled by a brain-machine interface. *The Journal of Neuroscience*, 25, 4681–4693.
- Lebedev, M. A., Fitzsimmons, N. A., Drake, W., Lehew, G., Dimitrov, D. F., & Nicolelis, M. A. L. (2007). Decoding bipedal locomotion patterns from cortical ensemble activity in rhesus monkeys. In *Proceedings of the Society for Neuroscience Annual Meeting*, 33, 517–523, San Diego, CA.
- Lebedev, M. A., & Nicolelis, M. A. L. (2006). Brain-machine interfaces: Past, present and future. *Trends in Neurosciences*, 29, 536–546.
- Li, Z., O'Doherty, J. E., Lebedev, M. A., Nicolelis, M. A. L. (2010) Closed-loop adaptive decoding using bayesian regression self-training. *Proceedings of the Society for Neuroscience Annual Meeting*, vol. 383.101, San Diego, CA, USA.
- Li, Z., O'Doherty, J. E., Hanson, T. L., Lebedev, M. A., Henriquez, C. S., & Nicolelis, M. A. L. (2009). Unscented Kalman filter for brain-machine interfaces. *PLoS One*, 4, e6243.
- Liberson, W. T., Holmquest, H. J., Scot, D., & Dow, M. (1961). Functional electrotherapy: Stimulation of the peroneal nerve synchronized with the swing phase of the gait

- of hemiplegic patients. *Archives of Physical Medicine and Rehabilitation*, 42, 101–105.
- Longo, M. R., Azanon, E., & Haggard, P. (2010). More than skin deep: Body representation beyond primary somatosensory cortex. *Neuropsychologia*, 48, 655–668.
- Maravita, A., Spence, C., & Driver, J. (2003). Multisensory integration and the body schema: Close to hand and within reach. *Current Biology*, 13, R531–R539.
- Matthews, P. B. (1988). Proprioceptors and their contribution to somatosensory mapping: Complex messages require complex processing. *Canadian Journal of Physiology and Pharmacology*, 66, 430–438.
- Mattia, D., Cincotti, F., Astolfi, L., de Vico Fallani, F., Scivoletto, G., Marcianni, M. G., et al. (2009). Motor cortical responsiveness to attempted movements in tetraplegia: Evidence from neuroelectrical imaging. *Clinical Neurophysiology*, 120, 181–189.
- Moritz, C. T., Perlmutter, S. I., & Fetz, E. E. (2008). Direct control of paralysed muscles by cortical neurons. *Nature*, 456, 639–642.
- Nakajima, T., Mushiake, H., Inui, T., & Tanji, J. (2007). Decoding higher-order motor information from primate non-primary motor cortices. *Technology and Health Care*, 15, 103–110.
- Nicolelis, M. A. L. (2001). Actions from thoughts. *Nature*, 409, 403–407.
- Nicolelis, M. A. L., Chapin, J. K., & Lin, R. C. (1995). Development of direct GABAergic projections from the zona incerta to the somatosensory cortex of the rat. *Neuroscience*, 65, 609–631.
- Nicolelis, M. A. L., Dimitrov, D., Carmena, J. M., Crist, R., Lehew, G., Kralik, J. D., et al. (2003). Chronic, multisite, multielectrode recordings in macaque monkeys. *Proceedings of the National Academy of Sciences of the United States of America*, 100, 11041–11046.
- Nicolelis, M. A. L., & Lebedev, M. A. (2009). Principles of neural ensemble physiology underlying the operation of brain-machine interfaces. *Nature Reviews Neuroscience*, 10, 530–540.
- Nicolelis, M. A. L., & Ribeiro, S. (2002). Multielectrode recordings: The next steps. *Current Opinion in Neurobiology*, 12, 602–606.
- Obhi, S. S., & Goodale, M. A. (2005). Bimanual interference in rapid discrete movements is task specific and occurs at multiple levels of processing. *Journal of Neurophysiology*, 94, 1861–1868.
- O'Doherty, J. E., Ifft, P. J., Zhuang, K. Z., Lebedev, M. A., & Nicolelis, M. A. L. (2010). Brain-machine-brain interface using simultaneous recording and intracortical microstimulation feedback. In *Proceedings of the Society for Neuroscience Annual Meeting*. vol. 899.15, San Diego, CA, USA.
- O'Doherty, J. E., Lebedev, M. A., Hanson, T. L., Fitzsimmons, N. A., & Nicolelis, M. A. L. (2009). A brain-machine interface instructed by direct intracortical microstimulation. *Frontiers in Integrative Neuroscience*, 3, 1–10.
- Paddock, C. (2009). Paralysis affects more Americans than previously thought. In *Medical news today*. <http://www.medicalnewstoday.com/articles/146819.php>.
- Pasquina, P. F., Bryant, P. R., Huang, M. E., Roberts, T. L., Nelson, V. S., & Flood, K. M. (2006). Advances in amputee care. *Archives of Physical Medicine and Rehabilitation*, 87, S34–S43 quiz S44–S35.
- Patil, P. G., Carmena, J. M., Nicolelis, M. A. L., & Turner, D. A. (2004). Ensemble recordings of human subcortical neurons as a source of motor control signals for a brain-machine interface. *Neurosurgery*, 55, 27–35, discussion 35–28.
- Pearson, O. R., Busse, M. E., van Deursen, R. W., & Wiles, C. M. (2004). Quantification of walking mobility in neurological disorders. *QJM*, 97, 463–475.
- Peckham, P. H., Keith, M. W., & Freehafer, A. A. (1988). Restoration of functional control by electrical stimulation in the upper extremity of the quadriplegic patient. *The Journal of Bone and Joint Surgery. American Volume*, 70, 144–148.
- Peikon, I. D., Fitzsimmons, N. A., Lebedev, M. A., & Nicolelis, M. A. L. (2009). Three-dimensional, automated, real-time video system for tracking limb motion in brain-machine interface studies. *Journal of Neuroscience Methods*, 180, 224–233.
- Pfurtscheller, G., Leeb, R., Keinrath, C., Friedman, D., Neuper, C., Guger, C., et al. (2006). Walking from thought. *Brain Research*, 1071, 145–152.
- Pfurtscheller, G., & Neuper, C. (2006). Future prospects of ERD/ERS in the context of brain-computer interface (BCI) developments. *Progress in Brain Research*, 159, 433–437.
- Prilutsky, B. I., Sirota, M. G., Gregor, R. J., & Beloozerova, I. N. (2005). Quantification of motor cortex activity and full-body biomechanics during unconstrained locomotion. *Journal of Neurophysiology*, 94, 2959–2969.
- Rokni, U., Steinberg, O., Vaadia, E., & Sompolinsky, H. (2003). Cortical representation of bimanual movements. *The Journal of Neuroscience*, 23, 11577–11586.
- Rossignol, S., Schwab, M., Schwartz, M., & Fehlings, M. G. (2007). Spinal cord injury: Time to move? *The Journal of Neuroscience*, 27, 11782–11792.
- Rouiller, E. M., Babalian, A., Kazennikov, O., Moret, V., Yu, X. H., & Wiesendanger, M. (1994). Transcallosal connections of the distal forelimb representations of the primary and supplementary motor cortical areas in macaque monkeys. *Experimental Brain Research*, 102, 227–243.

- Sandler, A. J., Kralik, J. D., Dewey, K. S., & Nicolelis, M. A. L. (2005). Long-term neuronal recordings from nonhuman primates. In *Society for Neuroscience Annual Meeting 31*, 402.8, Washington, DC.
- Santucci, D. M., Kralik, J. D., Lebedev, M. A., & Nicolelis, M. A. L. (2005). Frontal and parietal cortical ensembles predict single-trial muscle activity during reaching movements in primates. *The European Journal of Neuroscience*, 22, 1529–1540.
- Schwartz, A. B., Cui, X. T., Weber, D. J., & Moran, D. W. (2006). Brain-controlled interfaces: Movement restoration with neural prosthetics. *Neuron*, 52, 205–220.
- Scivoletto, G., & Di Donna, V. (2009). Prediction of walking recovery after spinal cord injury. *Brain Research Bulletin*, 78, 43–51.
- Tate, A. J., Lebedev, M. A., & Nicolelis, M. A. L. (2009). Neural activity associated with changes in posture in rhesus macaques. In *Proceedings of the Society for Neuroscience Annual Meeting*. vol. 181.7, Chicago, IL, USA.
- Taylor, D. M., Tillery, S. I., & Schwartz, A. B. (2002). Direct cortical control of 3D neuroprosthetic devices. *Science*, 296, 1829–1832.
- Thrasher, T. A., & Popovic, M. R. (2008). Functional electrical stimulation of walking: Function, exercise and rehabilitation. *Annales de Réadaptation et de Médecine Physique*, 51, 452–460.
- Velliste, M., Perel, S., Spalding, M. C., Whitford, A. S., & Schwartz, A. B. (2008). Cortical control of a prosthetic arm for self-feeding. *Nature*, 453, 1098–1101.
- Wessberg, J., Stambaugh, C. R., Kralik, J. D., Beck, P. D., Laubach, M., Chapin, J. K., et al. (2000). Real-time prediction of hand trajectory by ensembles of cortical neurons in primates. *Nature*, 408, 361–365.
- Winans, J. A., Tate, A. J., Lebedev, M. A., & Nicolelis, M. A. L. (2010). Extraction of leg kinematics from the sensorimotor cortex representation of the whole body. In *Proceedings of the Society for Neuroscience Annual Meeting*. vol. 294.7, San Diego, CA, USA.
- Zhang, F., Aravanis, A. M., Adamantidis, A., de Lecea, L., & Deisseroth, K. (2007). Circuit-breakers: Optical technologies for probing neural signals and systems. *Nature Reviews Neuroscience*, 8, 577–581.
- Zhang, F., Wang, L. P., Boyden, E. S., & Deisseroth, K. (2006). Channelrhodopsin-2 and optical control of excitable cells. *Nature Methods*, 3, 785–792.

CHAPTER 4

Biocompatible multichannel electrodes for long-term neurophysiological studies and clinical therapy—Novel concepts and design

Jens Schouenborg*

*Neuronano Research Center, Experimental Medical Science and The Nanometer Consortium,
Lund University, Lund, Sweden*

Abstract: Chronic neural interfaces that are both structurally and functionally stable inside the brain over long time periods and that have minimal effects on the physiological conditions of the neural tissue to be studied hold great promise to become invaluable research and clinical tool in the near future. In this chapter, I will briefly review the state of the art of neural interfaces and the concepts behind our recent research and development of ultrathin multichannel electrodes.

Keywords: In vivo neurophysiology; Brain Machine Interface; Neural interface; Tissue engineering; Deep Brain Stimulation; Chronic recordings; Multichannel electrodes; Pain; Biocompatibility.

The physiological state

Normal information processing and learning in the brain and spinal cord happen only in physiological conditions. Deviations from the normal state, such as changes in exocrine and endocrine hormone levels (Haas and Canli, 2008), infections, anesthesia, or trauma (Binder, 1986), impair these processes. Much of our present knowledge on how neuronal networks process, store, and recall information comes from short-term electrophysiological *in vivo* studies in anesthetized animals, decerebrated spinal

animals, *in vitro* tissue slices that are disconnected from the rest of the nervous system or from tissue cultures, that is, conditions that are far from physiological. Consequently, little is known about the normal dynamic information processing in neural networks in physiological conditions, or about altered network processing underlying, for instance, learning and recall of memory (Schouenborg, 2008) or chronic pain (Dolgin, 2010; Woolf, 2010). Multichannel electrodes that can be implanted in the brain for long periods of time and communicate, through recording and stimulations, with a large number of neurons in physiological conditions thus offer to revolutionize the understanding of fundamental brain functions.

*Corresponding author.

Tel.: +4-646-222-7756; Fax: +4-646-222-7752

E-mail: jens.schouenborg@med.lu.se

State of the art

A number of electrode implant constructs have been designed since the start of the neural interface field. Perhaps the most well known are the Utah array electrode (Campbell et al., 1991; Parker et al., this issue; Schwartz, 2004), the Michigan electrode and its later versions (Drake et al., 1988; Kipke et al., 2003; Williams et al., 1999), the tetrode (Jog et al., 2002), the cone electrode (Kennedy, 1989; Kennedy et al., 1992, 2002), and plain wire constructions (Carmena et al., 2003; Chapin et al., 1999). These electrode constructions have permitted the recordings of numerous neurons in awoken animals. As shown already in the 1960s by Fetz and colleagues, the brain can learn to use implanted electrodes to control external devices, demonstrating a considerable plastic capacity. These pioneering studies have been followed up by demonstrations that rats and monkeys can learn to use implanted electrodes in the brain to control robotic arms (Carmena et al., 2003; Chapin et al., 1999) and, perhaps most spectacularly, that paraplegic humans can learn to use electrode implants to communicate with computers (Hatsopoulos et al., 2005; Kennedy et al., 2000). However, it is a different matter to reveal how the brain functions in the normal condition and during disease processes. This requires electrode implants that themselves do not disturb or cause significant reorganization in the tissue and that provide stable recordings/stimulations from the same neurons over long periods of time.

A common concern in the neural interface field is that implanted multichannel electrodes for recordings usually deteriorate over time, although there are examples of very long-lasting recordings in the literature (Tresco and Gerhardt, 2008). There is still no clear consensus as to why deterioration occurs. A related concern has been that neuronal recordings are usually not stable over time. Few studies have therefore attempted recordings of the response patterns in the same neurons over long periods of time. Moreover, the recorded amplitudes of neural spikes are usually much lower than what can be accomplished in acute experiments. As the

spike amplitude partly depends on the distance between electrode and neurons, this may suggest that chronically implanted electrodes are usually not located close to viable neurons. This, in turn, may indicate that neurons close to an electrode either become electrically insulated from the recording electrode or deactivated due to the trauma and subsequent tissue processes caused by the electrode implant. From a clinical perspective, the focus has been on stimulation of nervous tissue, for example, deep brain stimulation and spinal cord stimulation (Benabid et al., this issue; Tierney et al., this issue), rather than recording. Currently, relatively large electrodes (in the millimeter scale) are used, with consequent large spread of current in the tissue resulting in a lack of specific stimulation effects and sometimes marked side effects. Also, stimulation intensity often needs to be increased over time to reach the desired therapeutic effect.

A widened concept of biocompatibility

The issue of biocompatibility of a neural interface is not only limited to the material it is made of but also includes its size, mechanical properties, and anchorage. Common to all implants is that the surgical procedures during implantation cause a trauma to the tissue which, in turn, triggers an acute tissue response that can last for weeks. In the case of implantations into the central nervous tissue, the acute tissue response includes activation of microglia and astrocytes (Biran et al., 2005; Eriksson Linsmeier et al., this issue; Skousen et al., this issue; Winslow and Tresco, 2010). This acute response is a normal pathophysiological response with a purpose to restore normal tissue conditions. However, despite the use of biocompatible surface materials of the implants, the acute tissue response is usually followed by a chronic tissue response that may even escalate with time. It is commonly assumed that a chronic tissue response can lead to functional “encapsulation” of electrodes and thereby loss of electrode functions. Moreover, migration of microglia toward the electrode implant may,

conceivably, displace neurons away from the electrodes causing smaller amplitudes from recorded units (Purcell et al., 2009). However, from the few studies that exist on the relation between recording quality and tissue response, no clear correlation has been found (Polikov et al., 2005; Skousen et al., this issue). In fact, there does not even seem to be a clear correlation between the number of neurons located adjacent to the electrodes and the number of unit recordings obtained.

A common denominator for most electrodes used today is that they are rather rigid and attached to the skull or the skeleton. During normal life, the brain and spinal cord exhibit considerable movements relative to the cranium and vertebrae, respectively, due to forces caused by respiration and heart beats and to forces caused by accelerations and rotations of the body. It is conceivable that the resulting micromotions between the tethered electrodes and nearby tissue lead to continuous microinjuries that can sustain long-term activation of glia cells such as astrocytes or microglia. Micromotions between electrode and tissue also lead to recording instabilities and may contribute to smaller recording amplitudes. From acute experiments, using sharp microelectrodes, it is well known that in order to obtain stable extracellular recordings, the electrode should not be positioned close to the membrane, as local tissue movements caused by blood pressure changes and respiration, despite precautions to stabilize the skull or vertebrae, may easily cause rupture of the neuron membranes and consequent leakage of ions. Hence, if the electrode is not stable in the tissue, only distant neurons with much smaller amplitudes will eventually be recorded from.

During the past 5 years, the Neuronano Research Center has focused on developing ultra thin and flexible electrodes that can be anchored in the tissue. A basic assumption already from the start was that micromotion between electrode and tissue, as discussed above, must be minimal. In a 12-week follow-up study published recently, we found significant tissue displacement and neuronal reorganization adjacent to stiff electrodes

anchored in the skull (Eriksson Linsmeier et al., this issue; Thelin et al., 2011). These were more pronounced in the anterior-posterior axis than in the mediolateral axis, suggesting that the implanted electrodes during daily life move relative to the tissue primarily along this axis. Moreover, neurons around the electrode were abnormally flat (Fig. 1). Such neurons may not function normally albeit apparently staying alive. Moreover, the tissue responses did not decline between the 6th and 12th week postimplantation. By contrast, electrodes that were not tethered to the skull showed much less tissue response, declining tissue response, and no derangement of neurons nearby. The tissue responses were also clearly dependent on the size of the implant, being much more intense for larger electrodes. The combination of small and untethered electrodes is especially favorable. In a parallel study, we found that tissue responses to nanowires (thickness about 200 nm) injected into the striatum decline over a 12-week follow-up period (Linsmeier et al., 2009).

A complexity with micromotions is that they are not uniform in the tissue. For example, blood pressure changes will cause a propagating wave of tissue movements. An electrode that cannot elastically move with the tissue in a direction of the axis of the electrode will therefore exhibit micromotions if it is located close to a large vessel. Hence, electrodes should ideally be very small and flexible in 3D. To avoid slow drift in location of the electrodes in the tissue, electrodes presumably also need to be anchored in the tissue. Our development has therefore been focused to achieve these goals. Below, I will provide a brief résumé of our recent work.

Novel electrode constructs and implantation procedures

A major problem with ultrathin and highly flexible electrodes is how to implant them. Traditionally, relatively thin and straight electrodes (e.g., tungsten wires with a diameter 35–50 μm), but still quite

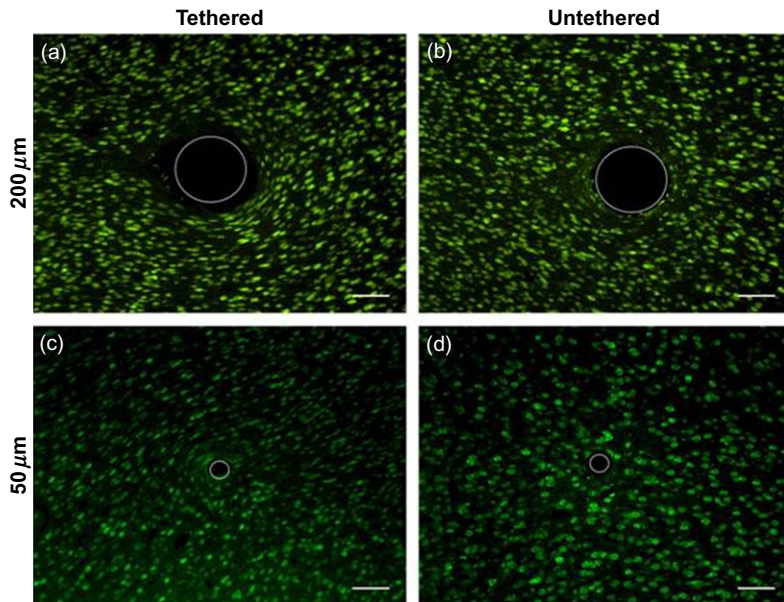


Fig. 1. Long-term effects of electrode implants on nervous tissue. Untethered (right) and tethered to the skull (left) with two different electrode sizes (top: 200 μm , bottom: 50 μm) implanted for 12 weeks in rat cortex cerebri. Note the abnormal morphology around the tethered electrode and the effects of implant size. Neurons stained with NeuN. From [Thelin et al. \(2011\)](#).

stiff, have been guided by a stiff cannula. However, the cannula itself must be much larger than the electrodes and therefore causes more tissue destruction on implantation. Moreover, when withdrawing the guiding cannula, the position of the thin electrodes in the tissue may move due to adhesion to the guiding cannula. Such an arrangement also complicates the issue of connecting multiple electrodes outside the skull.

Electrodes with ultrathin protrusions

To solve the implantation problem, a technique using bundles of electrode leads held together with a nondissolvable glue where each electrode lead has a protruding ultrathin electrode of suitable length directed backwards was therefore developed in our laboratory ([Schouenborg, 2007](#)). This simple construct permitted for the first time very thin electrodes to be pulled into the tissue along a

straight track line (as opposed to being pushed into the tissue, which easily results in deviations from the intended track line). By mounting the electrode protrusions such that they are directed in all dimensions and at different positions along the shaft, a 3D electrode bundle is achieved. In addition, by pulling the electrode bundle slightly backwards after it has been positioned close to the target tissue, the ultrathin protrusions can be made to unfold inside the target tissue. The protrusions themselves functioning as active electrodes (unisolated) and will also have an anchoring effect on the electrode in the tissue, thereby stabilizing the electrode tips with respect to target neurons. This construction was termed the “umbrella electrode.” Another type of electrode with protrusions containing the active sites, termed “ μ -foil,” was developed in parallel by [Köhler et al. \(2009\)](#). This latter electrode construct is manufactured using lithographical methods. The current μ -foil electrode is very thin (<10 μm in thickness) but

extends in the horizontal plane. Its construction is primarily flexible in one dimension, although the protrusions, if made of flexible material, may in addition flex in 2D. Notably, the length of the protrusions of the umbrella electrode and the foil electrode can be made such that their tips will be outside the major tissue response caused by the shank of the electrode, hence connecting with neurons in less disturbed tissue. By stacking folia electrodes, the number of protruding electrodes can be increased. A major advantage of the foil electrode is that it is possible to tailor the dimensions of the protrusion and their spacing with great precision to fit the cytoarchitecture of the target. Initial tests of this construction show promising results as regards signal to noise level of recorded units (Fig. 2), but it remains to be tested in long-term studies.

Surface configurations

The surface configuration of the electrodes is another parameter that needs attention. In a recent study, Johansson et al. (2009) demonstrated that

long-term implants in the sciatic nerve with a porous surface resulted in less tissue response than implants with a smooth surface (Kanje and Johansson, *this issue*). It is conceivable that a porous surface provides improved anchoring in the tissue thereby reducing micromotion. However, also *in vitro* studies, in which the substrate does not move, indicate that neurons tend to avoid smooth surfaces and adhere to and grow along rough or nanostructured surfaces (Kanje and Johansson, *this issue*). The mechanisms of interactions between neurons and surface structures are still poorly understood and clearly warrant further studies.

Matrix-embedded electrodes

While the umbrella electrodes comprise very thin protrusions that may unfold in the tissue, its shank is relatively rigid to permit implantation. To circumvent this problem, we have developed a technique where the individual conductive leads in the shank are held together by a dissolvable/degradable support matrix, thereby providing the necessary strength during implantation (Schouenborg, 2008).

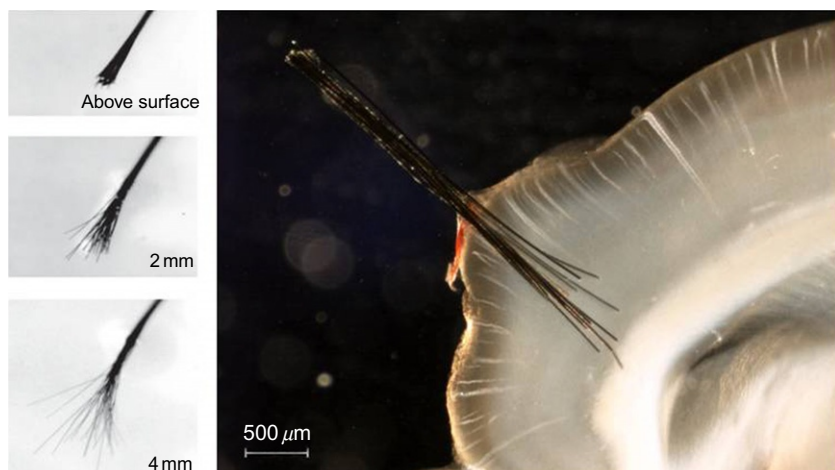


Fig. 2. Gelatin-embedded electrode bundle. Left column shows spread of electrodes on insertion in agar (2% in saline). Right: gelatin-embedded electrode bundle inserted through a narrow opening and spread out in rat cortex to target a larger cortical volume. A slice of cortex cerebri was clarified with methyl salicylate. (from Lind et al., 2010, with permission.)

Gelatin was our first choice as embedding material as it is well known for its biocompatibility. For example, gelatin is used in cell cultures and widely used to encapsulate medical drugs. In the first study, we could demonstrate that it is possible to insert multiple ultrathin (7 and 12 µm in diameter) electrodes through a small opening in the arachnoidea of the cortex cerebri and spread out the electrodes inside the target tissue (Lind et al., 2010) (Fig. 3). In the same study, it was shown that gelatin actually reduces tissue responses following implantation. In fact, implanted pure gelatin shaped as needles could not be traced after 12 weeks postimplantation, whereas a stab wound caused by a metal bar with the same dimensions and insertion depth still produced a clear tissue response at this point in time. Likewise, gelatin-embedded wire bundles tended to show less tissue response than gelatin-coated wire bundles. Importantly, by choosing gelatin or derivates from gelatin to embed electrodes, electrodes of any size (such as nanowires) and configuration can be configurationally locked, and therefore protected, while being implanted into soft tissue (Witteveen et al., 2010). When implanting the electrode in superficially located tissue, one support matrix may be sufficient, but in situations when the electrode bundle is to be implanted in a deep tissue, it can be advantageous to use materials that dissolve with different timecourses, such that the support matrix embedding the proximal parts remains supportive for longer time. After the distal part of the matrix is dissolved, it is possible to spread out the electrodes in the target tissue by pushing the proximal part of the electrodes further into the tissue. Moreover, we have recently obtained recordings from these gelatin-embedded electrodes (12-µm platinum wires insulated with Parylene C), with high signal to noise ratio that remained stable over several days or weeks (Jensen et al., in preparation). As these electrodes were not anchored in the tissue, some drift in unit amplitudes was observed over time in some channels, indicating the need for anchoring in the tissue. Moreover, many of these electrode bundles remained functional, that is, neuronal activity was recorded, after the 6 months end

point. It should be noted that using both the unfolding umbrella electrode and the embedded electrode, it is possible to insert the electrodes through relatively small holes, thus limiting tissue destruction, while targeting a larger volume of tissue (Fig. 4).

The embedding technique led to a subsequent invention of implantable and tissue-anchored electrodes that are for the first time flexible in 3D (Schouenborg, 2011). These electrodes are presently made of ultrathin (4 µm) gold leads and exhibit a wavy or tortuous structure enabling them to follow tissue movements in all three dimensions. Notably, by embedding a 3D flexible electrode in a needle-like hard matrix, it can be introduced into the tissue without substantial deformation during the implantation procedure. These wavy electrodes are equipped with one or more protrusions that serve as active electrodes and/or anchorage points in the tissue. That the electrodes can be configurationally locked in the matrix during the implantation opens up additional possibilities for tailoring their architecture to the target tissue. The optimal configuration of electrode parameters such as number and dimension of protrusions remains to be evaluated. By using compartments within the central parts of the embedding matrix that swell more than the support matrix in the tissue, the individual electrodes can, in addition, be made to unfold inside the tissue. Electrodes that are flexible in 3D may be particularly useful in tissues exhibiting large movements such as the spinal cord or peripheral nerves or tissue that is close to major vessels.

Embedded electrodes with drug delivery

The dissolvable matrix material used to embed ultrathin electrodes can also serve as a vehicle for drugs, nano- or microparticles loaded with drugs, or particles loaded with drugs, virus vectors, etc., to be implanted together with the electrodes. As different effects of the electrode implantation have different time courses,

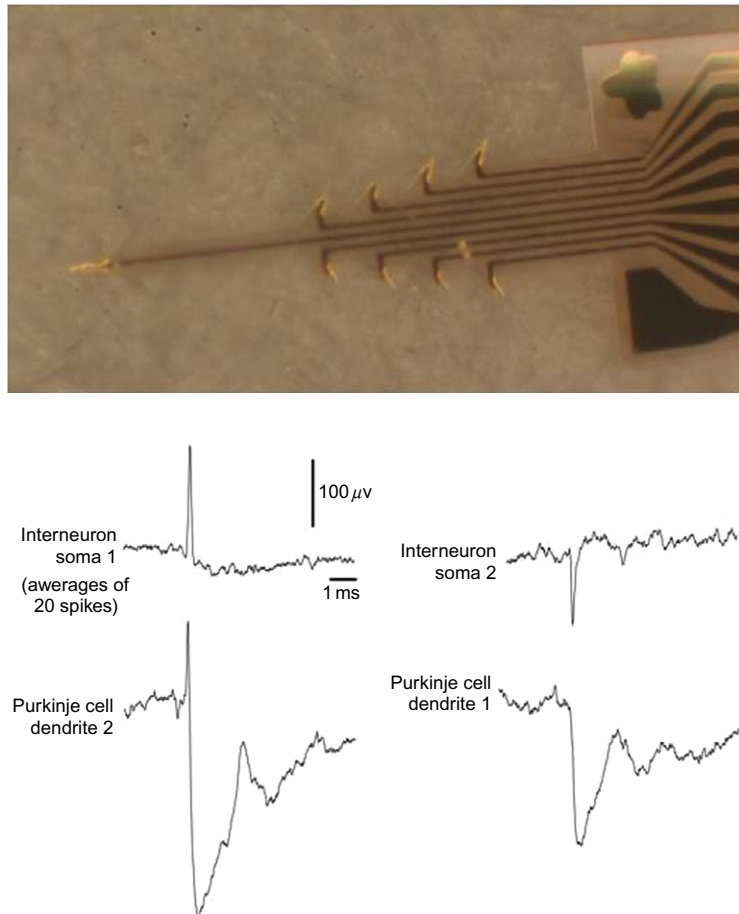


Fig. 3. Prototype of a polymer-based “μ-foil” electrode with nine electrode protrusions. Left: “μ-foil” electrode with distances between protrusions adapted to the layered structure of cerebellum. Right: recordings from rat cerebellar cortex. (modified from [Köhler et al., 2009](#)).

for example, bleedings, activation of astrocytes and microglia, and infections, we recently invented compartmentalized drug-releasing multi-channel electrodes ([Ek et al., 2010](#)) (Fig. 5). This can be used to improve implantation safety. For example, antibiotics may be included at strategic points along the electrode implant to reduce the risk of infections after the implantation. Another strategy may be to reduce the inflammatory response and support neuronal survival caused

by the implant around the active electrode sites. Successful attempts to reduce acute inflammation by incorporating anti-inflammatory drugs in coating materials have been reported ([Mercanini et al., 2010; Zhong and Bellamkonda, 2007](#)). However, it should be kept in mind that, as mentioned above, inflammatory responses may be beneficial in the long run. For this reason, studies to permit the evaluation of anti-inflammatory drug strategies for long-term implants are

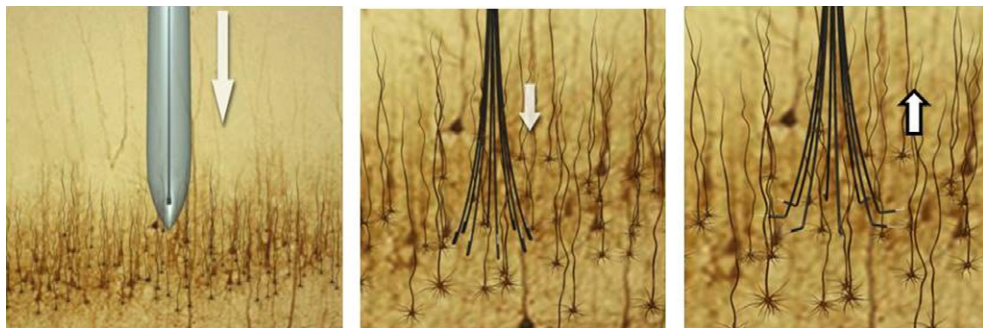


Fig. 4. Schematic of implantation procedure and unfolding of a matrix-embedded “umbrella” electrode bundle. Arrows indicate movements of electrode during implantation.

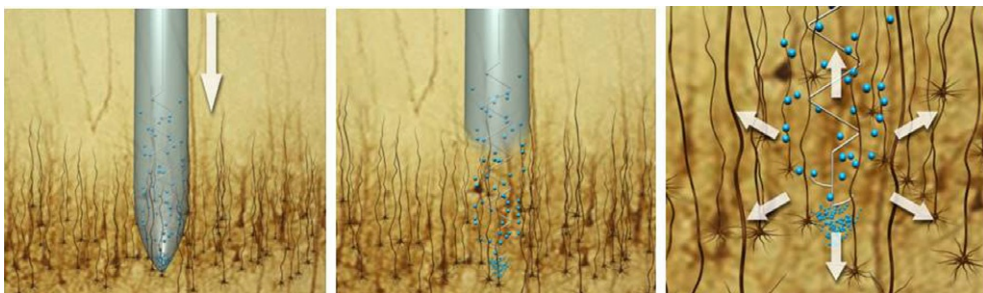


Fig. 5. Schematic of implantation procedure and release of drug-loaded nano- and microparticles embedded in a support matrix of an electrode.

ongoing in our lab. We will also explore the possibilities offered by slow drug release regimes combined with long-term recordings/stimulations of neurons.

Concluding remarks

In conclusion, our development and research on biocompatible neural interfaces that preserve normal physiological conditions in the tissue has resulted in a number of novel ultrathin and flexible constructs that can be implanted and stabilized with respect to soft tissue for long periods of time. These devices provide new opportunities for high-resolution studies on *physiological* information processing- and learning-dependent long-

term changes in functionally defined networks ([Schouenborg, 2008](#)) and to distinguish *pathological* alterations in network functions that occur during, for instance, neurodegenerative diseases. The novel embedding technology allowing combined implantation of complex nanostructured electrodes and compartmentalized local drug release, in addition, provides important new opportunities in advanced pharmacology and drug development. There is, however, a need for a careful, and therefore time-consuming, evaluation on the impact of different types of electrode architecture, surface structures, embedding media and local administration of drugs, on glia and neurons and other tissue constituents such as blood vessels and the blood–brain barrier. This is important not only to provide high-quality research tools

that cause minimal distortion of the information processing in the neural circuits under study but also for subsequent therapeutic use in humans, which requires a high degree of safety and durability.

Finally, it should be kept in mind that, so far, few attempts to combine chronic recordings in awoken animals with neuroanatomical techniques, such as tracers, have been made. This may partly be due to the problems with recording instability from implanted neural interfaces reviewed above, precluding subsequent detailed histological identification. Consequently, with few exceptions, neuronal recordings in awoken animals have been obtained from neurons unidentified with respect to their functional connections in the CNS and histological identity. Thus, an important task in future research will be to achieve stable long-term recordings under physiological conditions from histologically and functionally characterized neural networks.

Acknowledgments

This work was supported by grants from Knut and Alice Wallenbergs foundation, the Swedish Research Council (project grant 01013 and Linneus grant) and the medical faculty of Lund.

References

- Benabid, A. L., Torres, N., Moro, C., Aksanova, T., Costecalde, T., Eliseyev, A., et al. (2011). Deep brain stimulation: BMI at large, where are we going to? *Progress in Brain Research*, 194, 71–82.
- Binder, L. (1986). Persistent symptoms after mild head injury: A review of the postconcussive syndrome. *Journal of Clinical and Experimental Neuropsychology*, 8, 323–346.
- Biran, R., Martin, D. C., Tresco, P. A., et al. (2005). Neuronal cell loss accompanies the brain tissue response to chronically implanted silicon microelectrode arrays. *Experimental Neurology*, 195(1), 115–126.
- Campbell, P. K., Jones, K. E., Huber, R. J., Horch, K. W., & Normann, R. A. (1991). A silicone-based, three-dimensional neural interface: manufacturing processes for an intracortical electrode array. *IEEE Transactions on Bio-medical Engineering*, 38, 758.
- Carmena, J. M., Lebedev, M. A., Crist, R. E., O'Doherty, J. E., Santucci, D. M., et al. (2003). Learning to control a brain-machine interface for reaching and grasping by primates. *PLoS Biology*, 1(2), 193–208.
- Chapin, J. K., Moxon, K. A., Markowitz, R. S., & Nicolelis, M. A. (1999). Real-time control of a robot arm using simultaneously recorded neurons in the motor cortex. *Nature Neuroscience*, 2(7), 664–670.
- Dolgin, E. (2010). Animalgesic effects. *Nature Medicine*, 16 (11), 1237–1240.
- Drake, K. L., Wise, K. D., Farraye, J., Anderson, D. J., & BeMent, S. L. (1988). Performance of planar multisite micropoles in recording extracellular single-unit intracortical activity. *IEEE Transactions on Bio-medical Engineering*, 35, 719–732.
- Ek, F., Danielsen, N., Linsmeier, C. E., Petersson, P., & Schouenborg, J. (2010). Microelectrode and multiple microelectrodes comprising means for releasing drugs into the tissue. WO2010144016 (A1)—2010-12-16 Priority Date: 2009-06-09.
- Eriksson Linsmeier, C., Thelin, J., & Danielsen, N. (2011). Can histology solve the riddle of the non-functioning electrode? Factors influencing the biocompatibility of brain machine interfaces. *Progress in Brain Research*, 194, 181–189.
- Fetz, E. E. (1969). Operant conditioning of cortical unit activity. *Science*, 163, 955–958.
- Haas, B. W., & Canli, T. (2008). Emotional memory function, personality structure and psychopathology: A neural system approach to the identification of vulnerability markers. *Brain Research Reviews*, 58, 71–84.
- Hatsopoulos, N. G., Mukand, J. A., Polykoff, G., Friehs, G. M., & Donoghue, J. P. (2005). Cortically controlled brain-machine interface. *IEEE Engineering in Medicine and Biology 27th Annual Conference*. 0780387414, pp. 7660–7663.
- Jog, M. S., Connolly, C. I., Kubota, Y., Iyengar, D. R., Garrido, L., Harlan, R., et al. (2002). Tetrode technology: Advances in implantable hardware, neuroimaging, and data analysis techniques. *Journal of Neuroscience Methods*, 117 (2), 141–152.
- Johansson, F., Wallman, L., Danielsen, N., Schouenborg, J., & Kanje, M. (2009). Porous silicon as a potential electrode material in a nerve repair setting: Tissue reactions. *Acta Biomateria*, 5(6), 2230–2237.
- Kanje, M., & Johansson, F. (2011). Nanomodified surfaces and neurite outgrowth. *Progress in Brain Research*, 194, 253–262.
- Kennedy, P. R. (1989). The cone electrode: A long-term electrode that records from neurites grown onto its recording surface. *Journal of Neuroscience Methods*, 29(3), 181–193.
- Kennedy, P. R., Bakay, R. A. E., Moore, M. M., Adams, K., Goldwaith, J., et al. (2000). Direct control of a computer

- from the human central nervous system. *Rehabilitation Engineering, IEEE Transactions*, 8, 198–202.
- Kennedy, P. R., Mirra, S. S., & Bakay, R. A. E. (1992). The cone electrode: Ultrastructural studies following long-term recording in rat and monkey cortex. *Neuroscience Letters*, 142, 89–94.
- Kipke, D. R., Vetter, R. J., Williams, J. C., & Hetke, J. F. (2003). *IEEE Transactions on Neural Systems and Rehabilitation Engineering*, 11, 151.
- Köhler, P., Linsmeier, C. E., Thelin, J., Bengtsson, M., Jörntell, H., Garwicz, M., et al. (2009). Flexible multi electrode brain-machine interface for recording in the cerebellum. *Conference Proceedings—IEEE Engineering in Medicine and Biology Society*, 2009, 536–538.
- Lind, G., Linsmeier, C. E., Thelin, J., & Schouenborg, J. (2010). Gelatine-embedded electrodes—A novel biocompatible vehicle allowing implantation of highly flexible microelectrodes. *Journal of Neural Engineering*, 7(4), 046005.
- Linsmeier, C. E., Prinz, C. N., Pettersson, L. M. E., Caroff, P., Samuelson, L., Schouenborg, J., et al. (2009). Nanowire biocompatibility in the brain—Looking for a needle in a 3D stack. *Nano Letters*, 9(12), 4184–4190.
- Mercanzini, A., Reddy, S. T., Velluto, D., Colin, P., Maillard, A., Bensadoun, J.-C., et al. (2010). Controlled release nanoparticle-embedded coatings reduce the tissue reaction to neuroprostheses. *Journal of Controlled Release*, 145(3), 196–202.
- Parker, R. A., Davis, T. S., House, P. A., Normann, R. A., & Greger, B. (2011). The functional consequences of chronic, physiologically effective intracortical micro-stimulation. *Progress in Brain Research*, 194, 145–165.
- Polikov, V. S., Tresco, P. A., & Reichert, W. M. (2005). Response of brain tissue to chronically implanted neural electrodes. *Journal of Neuroscience Methods*, 148(1), 1–18.
- Purcell, E. K., Thompson, D. E., Ludwig, K. A., Kipke, D. R., et al. (2009). Flavopiridol reduces the impedance of neural prostheses in vivo without affecting recording quality. *Journal of Neuroscience Methods*, 183(2), 149–157.
- Schouenborg, J. (2007). Electrode bundle. US2007088417 (A1)—2007-04-19 Priority Date: 2005-10-06, Granted in China.
- Schouenborg, J. (2008). Action-based sensory encoding in spinal sensorimotor circuits. *Brain Research Reviews*, 57(1), 111–117.
- Schouenborg, J. (2008). Electrode array. WO2008091197 (A1)—2008-07-31 Priority Date: 2007-01-23 CN101616630 (A)—2009-12-30 Priority Date: 2007-01-23.
- Schouenborg, J. (2011). Medical electrode, electrode bundle and electrode bundle array. PENDING US2011009728 (A1)—2011-01-13 Priority Date: 2007-12-10.
- Schwartz, A. B. (2004). Cortical neural prosthetics. *Annual Review of Neuroscience*, 27, 487–507.
- Skousen, J. L., Merriam, M. E. Sr., Srivannavit, O., Perlin, G., Wise, K. D., & Tresco, P. A. (2011). Reducing surface area while maintaining implant penetrating profile lowers the brain foreign body response to chronically implanted planar silicon microelectrode arrays. *Progress in Brain Research*, 194, 167–180.
- Thelin, J., Jörntell, H., Psouni, E., Garwicz, M., Schouenborg, J., Danielsen, N., et al. (2011). Implant size and fixation mode strongly influence tissue reactions in the CNS. *PLoS One*, 6(1), e16267.
- Tierney, T. S., Sankar, T., & Lozano, A. M. (2011). Deep brain stimulation: Emerging indications. *Progress in Brain Research*, 194, 83–95.
- Tresco, P. A., & Gerhardt, G. A. (2008). The biotic-abiotic interface. In T. W. Berger et al. (Ed.), *Brain computer interfaces* (pp. 31–45). Springer Science + Business Media B.V., www.Springer.com.
- Williams, J. C., Rennaker, R. L., & Kipke, D. R. (1999). Long term neural recording characteristics of wire microelectrode arrays implanted in cerebral cortex. *Brain Research. Brain Research Protocols*, 4, 303.
- Winslow, B. D., & Tresco, P. A. (2010). Quantitative analysis of the tissue response to chronically implanted microwire electrodes in rat cortex. *Biomaterials*, 31(7), 1558–1567.
- Witteveen, J. A., Suyatin, D. B., Gällentoft, L., Schouenborg, J., Danielsen, N., & Prinz, C. N. (2010). Gelatin/glycerol coating to preserve mechanically compliant nanowire electrodes from damage during brain implantation. *Journal of Vacuum Science & Technology*, 28(6), C6K13–C6K16.
- Woolf, C. J. (2010). Overcoming obstacles to developing new analgesics. *Nature Medicine*, 16(11), 1241–1247.
- Zhong, Y., & Bellamkonda, R. V. (2007). Dexamethasone-coated neural probes elicit attenuated inflammatory response and neuronal loss compared to uncoated neural probes. *Brain Research*, 1148, 15–27.

CHAPTER 5

Deep brain stimulation: BCI at large, where are we going to?

Alim Louis Benabid*, Thomas Costecalde, Napoleon Torres, Cecile Moro, Tetiana Aksenova, Andrey Eliseyev, Guillaume Charvet, Fabien Sauter, David Ratel, Corinne Mestais, Pierre Pollak and Stephan Chabardes

Cinatec Institute, Commissariat à l'Energie Atomique, Joseph Fourier University, Grenoble, France

Abstract: Brain–computer interfaces (BCIs) include stimulators, infusion devices, and neuroprostheses. They all belong to functional neurosurgery. Deep brain stimulators (DBS) are widely used for therapy and are in need of innovative evolutions. Robotized exoskeletons require BCIs able to drive up to 26 degrees of freedom (DoF). We report the nanomicrotechnology development of prototypes for new 3D DBS and for motor neuroprostheses. For this complex project, all compounds have been designed and are being tested. Experiments were performed in rats and primates for proof of concepts and development of the electroencephalogram (EEG) recognition algorithm.

Methods: Various devices have been designed. (A) In human, a programmable multiplexer connecting five tetrapolar (20 contacts) electrodes to one DBS channel has been designed and implanted bilaterally into STN in two Parkinsonian patients. (B) A 50-mm diameter titanium implant, telepowered, including a radioset, emitting ECoG data recorded by a 64-electrode array using an application-specific integrated circuit, is being designed to be implanted in a 50-mm trephine opening. Data received by the radioreceiver are processed through an original wavelet-based Iterative N-way Partial Least Square algorithm (INPLS, CEA patent). Animals, implanted with ECoG recording electrodes, had to press a lever to obtain a reward. The brain signature associated to the lever press (LP) was detected online by ECoG processing using INPLS. This detection allowed triggering the food dispenser.

Results: (A) The 3D multiplexer allowed tailoring the electrical field to the STN. The multiplication of the contacts affected the battery life and suggested different implantation schemes. (B) The components of the human implantable cortical BCI are being tested for reliability and toxicology to meet criteria for chronic implantation in 2012. (C) In rats, the algorithm INPLS could detect the cortical signature with an accuracy of about 80% of LPs on the electrodes with the best correlation

*Corresponding author.

Tel.: +33-680872491/+33-684156692

Fax: +33-4-38785787

E-mail: alimlouis@aol.com; alim-louis.benabid@cea.fr

coefficient (located over the cerebellar cortex), 1% of the algorithm decisions were false positives. We aim to pilot effectors with DoF up to 3 in monkeys.

Conclusion: We have designed multielectrodes wireless implants to open the way for BCI ECoG-driven effectors. These technologies are also used to develop new generations of brain stimulators, either cortical or for deep targets. This chapter is aimed at illustrating that BCIs are actually the daily background of DBS, that the evolution of the method involves a growing multiplicity of targets and indications, that new technologies make possible and simpler than before to design innovative solutions to improve DBS methodology, and that the coming out of BCI-driven neuroprostheses for compensation of motor and sensory deficits is a natural evolution of functional neurosurgery.

Keywords: brain computer interfaces (BCI); deep brain stimulation; animal models; neuroprostheses; motor deficit; sensory deficit; functional neurosurgery; multiple electrodes; electrocorticography; software analysis; motor cortical signatures; rats.

Deep brain stimulation: A genuine brain-device interface

Deep brain stimulation (DBS) is an established neurosurgical method. It has a wide range of indications, due to essentially to its reversibility, adaptability, and low morbidity. There is a frequency-dependent duality of effects: low frequency excites both neurons and axons, while high-frequency selectively “inhibits” clusters of neurons. The precise mechanism is under debate, and recent data could support also an activation of the passing fibers. DBS works through a brain–electrode–machine interface: it is achieved using electrodes implanted into the brain ([Fig. 1a–c](#)) and connected through a wire to a wireless implantable and programmable stimulator.

Current targets for implantation in Parkinson’s disease are essentially the thalamus (VIM), the pallidum (GPI), the subthalamic nucleus (STN, *nucleus subthalamicus*), and the pedunculopontine nucleus (PPN). They are reached through a complex process of targeting, based on neuro-navigation tools, including MRI, atlases, and microrecording providing the signature of the recorded structure, allowing positioning precisely the electrode. During the surgery, it is possible at every level of the exploration to stimulate the traversed structure and to observe the effects of stimulation, which are frequency-dependent with a plateau of efficiency between 10^2 and $10^{3.5}$.

The current main indications are movement disorders, and particularly *Parkinson’s disease*. DBS at high frequency globally mimics the effects of ablation, and both targets which were initially used for lesioning surgeries, such as the thalamus and the pallidum, have been used initially. In 1987, we observed serendipitously the abolition of tremor during the exploration of the thalamic area during an intended thalamotomy for essential tremor when stimulation, used to explore the target area, was equal or higher than 100 Hz ([Benabid et al., 1987](#)). The observation of the reversible, frequency-dependent, intensity-dependent, arrest of tremor was at the basis of the current method of DBS at high frequency (HF-DBS). This method was made applicable, as at that time the necessary equipment (electrodes, connecting wires, and implantable programmable stimulators) was already available from industrial companies, being used at the time for deep brain stimulation for pain, either in the thalamus (VPL, ventro-postero-lateral) or in the (PAG, periaqueductal gray). It became quite quickly clear that this could be a method mimicking and then replacing the lesioning surgery. This new technology was extended in 1992 to the pallidum GPI, which was the other target for lesions ([Siegfried and Lippitz, 1994](#)). The pallidum had been just reintroduced and validated by the team of Laitinen and Hariz ([Laitinen et al., 1992](#)). The stimulation of VIM is essentially efficient on tremor, while the stimulation as well as the lesion

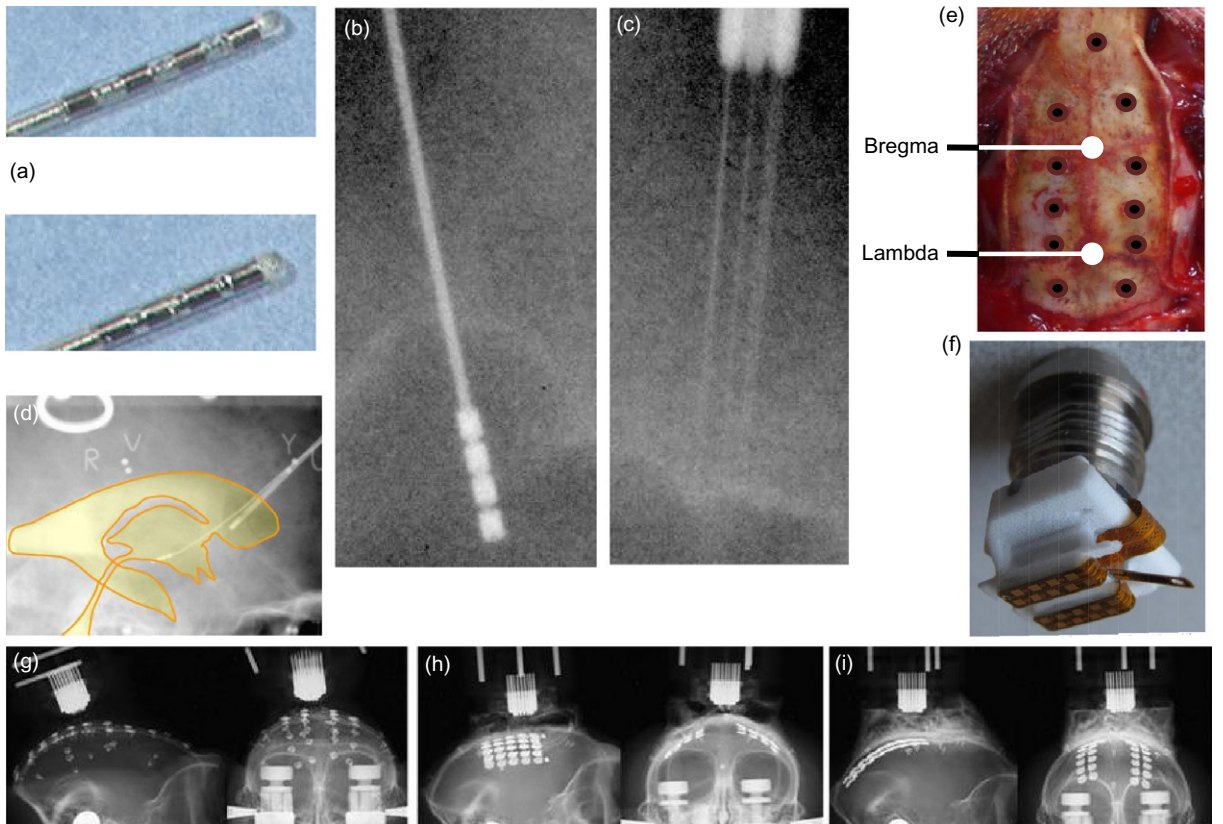


Fig. 1. Electrodes as brain–computer interfaces. (a) DBS electrodes for human, large spacing on the top, small spacing on the bottom. (b) X-ray control of implanted DBS macroelectrode and microelectrode for recording (c). (d) Endoventricular placement of a DBS electrode on the floor of the third ventricle, for treatment of cluster headaches. (e) Placement of transcranial titanium screws in rats. (f) Minielectrode array (platinum on polyimide flex and connector for rats). (g) Primate implant with 32 transcranial titanium screws. (h) Primate implant with bilateral 20 silicone platinum square grids (subdural on right side, and epidural on left side). (i) Primate implant with bilateral 16 silicone platinum strip grids (subdural on right side and epidural on left side).

of the pallidum is essentially efficient on the levodopa-induced dyskinesias (LID). LID are a new disease, an iatrogenic complication of the levodopa treatment, which was not present in the 1950s when Leksell had introduced the pallidotony for the treatment of Parkinson (Svennilson et al., 1960). Due to the unsatisfactory effects of pallidotony on akinesia and rigidity, this target was temporarily abandoned. In 1990, the paper of the group of DeLong (Bergman et al., 1990) highlighted the importance of the STN in the control of motricity. The MPTP monkeys were profoundly improved by the electrolytic destruction of STN with only

temporary dyskinesias. This was nevertheless not very attractive from the neurosurgeons due to the risk of hemiballism (Aebischer and Goddard, 1991). There was then the possibility to alter STN in a more flexible and softer method, using HF-DBS on the basis of the experience gained in VIM and GPi. The work of the group of Bordeaux (Benazzouz et al., 1993) proved in monkeys that the papers of Bergman et al. (1990) and of Aziz et al. (1991) could be replicated using HF-DBS instead of lesions. In 1993, we implanted the first Parkinsonian patient in the STN. This was extremely positive, providing both relief of tremor,

akinesia, and rigidity, and at the same time, the possibility to decrease significantly the drug dosage of anti-Parkinsonian medication. The freezing of gait during ON periods in Parkinsonian patients is not improved by VIM, STN, or pallidum stimulations. Coming from the basic science once again (Jenkinson et al., 2004; Nandi et al., 2002), it has been shown recently that the stimulation of the PPN is efficient on this gait disturbance. What is extremely interesting is the fact that the effect is obtained not at high frequency but at low frequency (25 Hz). The attempt to stimulate at high frequency, to observe what happens, leads to the induction of a ‘slow non-REM sleep’ acutely reversed by interruption of stimulation (Arnulf et al., 2010). This has the interest to document further if needed the specific effect of high frequency and the duality of high and low frequency, which might be used as a potential specificity of the DBS. Of course in these cases, it is necessary to have two sets of electrodes, connected to two different stimulators, one for STN stimulated at high frequency and another for PPN stimulated at 25 Hz.

The second important indication in the field of movement disorder is *dystonia*. The best results are observed in primary, and particularly genetic, forms (DYT 1 mutation) (Vidailhet et al., 2005, 2007, 2009). The time course of the effect is slightly different from that of PD, as quite often there is no clear benefit observable during surgery. This does not help the placement of the electrode, while the benefit becomes progressively established within days or weeks and months. This time course is observed also after pallidotomies, which shows that this particular behavior is disease dependent and not method dependent. Another target is the STN, which has been more largely used by the Chinese neurosurgeons (Sun et al., 2007) with a similar result and (this is an advantage) the observation of immediate effects during surgery, helping them for the correct placement of the electrode. In a limited series of cases, we have implanted altogether GPI and STN, suggesting that there is a cooperative effect of these two targets.

New indications are being currently investigated.

Epilepsy

This is a large domain, which is more difficult to assess because of the specific aspect of the epilepsy (multiple causes, multiple symptomatic profiles, and the difficulty of making any easy judgment because of the long time needed to evaluate the benefit of either surgery or medication). Since 2002 (Benabid et al., 2002; Chabardes et al., 2002), we had stimulated STN and shown that in cases of epilepsy of the motor region, the benefit could be extremely important. The difficulty now is to establish the list of the responding and nonresponding indications. The question of the target also is of importance: the amygdalo hippocampus formation has been targeted by DBS electrodes and has produced some effect (Vonck et al., 2005). We have stimulated hamartomas of the third ventricle responsible for gelastic seizures, which proved to be efficient but induced hormonal side effects due to the proximity of the hypothalamus; the epileptogenic zone has been stimulated with interesting results by the group of Velasco. Very recently, a double-blind study in North America (Fisher et al., 2010) has targeted the anterior nucleus of the thalamus, based on their previous experimental results. They reported an improvement of the seizure frequency by 40% as compared to the controls (14%).

Mental disorders: Obsessive-compulsive disorders (OCD)

This indication, which has been the most successful at the time of the lesioning psychosurgery, was the first to be reused with DBS. Since 1999, Bart Nuttin and his group had replaced the anterior capsulotomy by stimulation of the internal capsule at the same targets where lesions were made (Nuttin et al., 1999). Actually it appeared that the intensity

of stimulation and the extent of the targets were such that, actually, the electrical field reaches a deeper and more posterior target, which turned out to be the nucleus accumbens. Based on that, this has been also used as a target for the OCD (Sturm et al., 2003). In 2002, the group of Paris (Mallet et al., 2002) observed that two Parkinsonian patients treated for their parkinsonism had also their comorbid traits of OCD improved by STN stimulation. A multicenter double-blind prospective study was started, whose results have been published in the *New England Journal of Medicine* (Mallet et al., 2008), showing that STN was a very efficient and practical target for this disease. In Grenoble, where the method was performed under local anesthesia, we had the privilege to observe for the first time in one patient acute changes of the cognitive and behavioral OCD symptoms during surgery when the high-frequency stimulation was turned on and off. This allowed targeting STN in a similar way that for Parkinson's disease.

Depression

Following the observation on PET scan (Mayberg, 2003) that in the acute depression induced by bad news as well as in chronic depression, there was a hypermetabolism in the medial basal frontal, subgenual cortex named the area CG 25. On this basis, the group of Toronto has implanted bilateral electrodes in this area, showing significant benefits following high-frequency stimulation with a decrease in the various scores (Mayberg et al., 2005). We have applied exactly this methodology in our department. In this short series, we observed that extending the area of stimulation to the four contacts of the electrode and increasing the intensity to the maximum available on the stimulator (10.5 V) did not induce side effects but produced a dramatic improvement of the behavior and of the scores allowing even to suppress medication. This was obtained at the expense of the battery life, which is depleted within a period of 1 year (Chabardès et al., 2010).

Tourette's syndrome

The first results were obtained by stimulation of the intralaminar thalamus, close to the target suggested by Riechert some decades ago (Visser-Vandewalle et al., 2003). The internal pallidum GPI has been stimulated mostly (Houeto et al., 2005) with spectacular results on the motor symptoms as well as on the cognitive and behavioral symptoms, with return to an almost normal behavior. More recently (Vilela Filho, 2009), a similar result was obtained in the external pallidum and provided a functional hypothesis to explain these paradoxical results. It is clear that more work is needed to prove that these are two different targets and how they may interact.

Other indications are being under evaluation in the field of psychosurgery

Different targets have been used so far in various "psychiatrics" conditions: stimulation of the posterior hypothalamus for aggressivity, of the anterior hypothalamus for anorexia nervosa and obesity, of the accumbens for addiction, as well as stimulation of the centrum medianum para fascicularis area, for minimally conscious states (Schiff et al., 2007) are currently investigated by different groups. It is clear that, within the next years, several other indications involving several other targets will be confirmed on the basis of the efficiency.

This nevertheless raises ethical concerns: the low morbidity of the method creates the risk of its misuse by inexpert and inexperienced teams or with flexible consideration of ethical concepts. Are there limits in applying DBS to putative indications, suggested by scientific observations, under the pretext we have a "safe" method which could be used, and then canceled and the material withdrawn, if it happens it was not a good idea? For instance, it has been shown (Naqvi et al., 2007) that the traumatic lesion of the right insula could reverse the tobacco addiction of the

patients when they would awaken from their coma. Should this be enough to propose a stimulation of the insula to treat tobacco addiction, considering also that the tobacco addiction might have lethal consequences when inducing lung carcinomas? On the other side, should we refrain to provide a potentially interesting and beneficial advance under the pretext that this might sound quite audacious?

New brain electrode interfaces

Although this is still in the field of deep brain stimulation, electrodes could be placed in a different situation than intraparenchymally. We have (Data not shown) performed in the 1980s low-frequency stimulation of the PAG by catheterization of the aqueduct of Sylvius using a monopolar electrode. This created the same benefits as the intraparenchymal low-frequency stimulation of the PAG (Hosobuchi, 1986; Young and Chambi, 1987), supposed to elevate the production of endorphins by this structure. This method was performed in 16 patients with a satisfactory result at that time and was abandoned, as was the intraparenchymal implantation, because it tended to induce similarly a cross tolerance to morphine. Based on this former experience, we have implanted (data not yet published) patients with cluster headaches to stimulate the target used by the group of Franzini (Franzini et al., 2003), which is the posterior hypothalamus. These two nuclei are close to the midline and just below the ependymal floor of the third ventricle. We have positioned under fluoroscopy the brain stimulation electrodes into the cavity of the third ventricle over this area and obtained in all the implanted patients a complete relief of their cluster headaches, under continuous stimulation (Fig. 1d). There are many other subependymal targets around the third ventricle which could be reached by electrical stimulation in a less invasive manner than intraparenchymally implanting these targets. New electrodes are being designed and

have been patented to adapt to the specific demands of the endoventricular stimulation (width of the third ventricle changing between patients, steerable electrodes allowing to position the electrode in the posterior part of the third ventricle, or on the contrary reaching the infundibulum and the area below the anterior commissure). It becomes clear that new electrodes are needed (and actually are being designed) and that we must also reconsider the biophysics of this situation of an electrode in the CSF instead of in the parenchyma.

Three-dimensional array of electrodes: 3D high-frequency stimulation for field shaping

The purpose is to better cover one symptom or to cover multiple symptoms, and to better control side effects. Implanting this 3D array would allow implanting five electrodes which would be later combined. This would provide time-saving for the surgery, which would be therefore compatible with general anesthesia without losing the important return of the electrophysiological studies during the surgery. This would also allow a better exploration of new targets, where the limits or the efficient parts are not necessarily well determined before implantation in these clinically experimental approaches. We had therefore produced a set of programmable multiplexers (Fig. 2a and b) acting as a switch-board, which were connected to sets of five DBS electrode 3389, implanted in each of the STN (Fig. 2c and d). There was no complication, the usual microsubthalamotomy effect was observed but not enhanced. The cosmetic aspect (Fig. 2b) of these experimental systems obviously requires a phase of miniaturization using nanomicrotechnologies. However, the recent commercial availability of Implantable Programmable Generator (IPGs) with 16 independent channels has made the approach of the multiplexer obsolete.

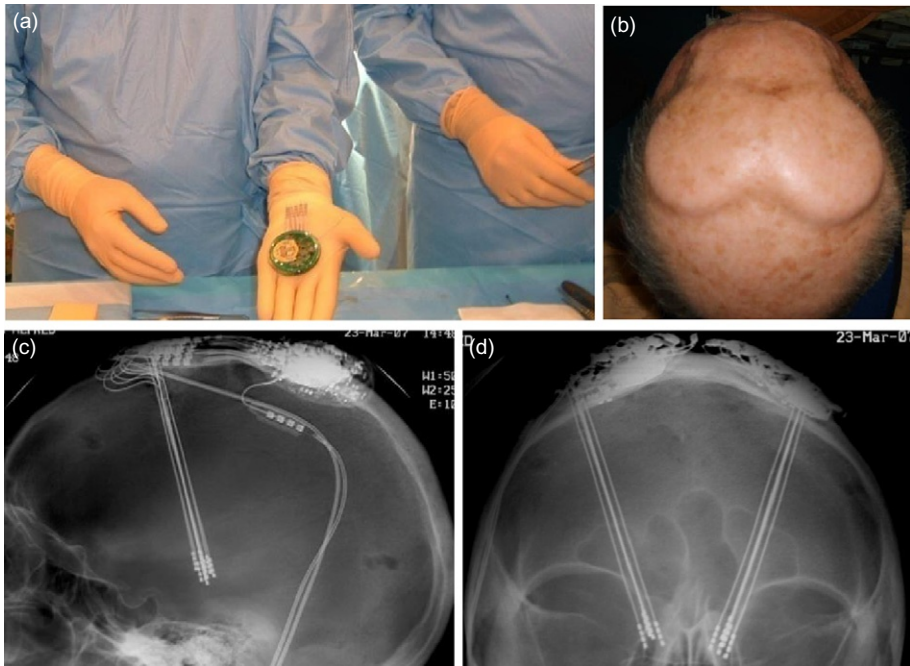


Fig. 2. Multiplexer to connect five DBS tetrpolar electrodes in each STN to a dual programmable IPG. (a) Aspect of the multiplexer at the time of surgery. (b) Subcutaneous programmable multiplexers. (c and d) Postoperative X-rays.

From DBS to ECoG recording: Brain-machine interface neuroprosthetics for deficit compensation

This field has been largely inspired by the pioneers such as Miguel Nicolelis, Donoghue, Schwartz, and Georgopoulos (Donoghue, 2002; Donoghue et al., 1998; Georgopoulos, 1994; Georgopoulos et al., 1989; Nicolelis, 2001, 2003; Nicolelis and Lebedev, 2009; Wang et al., 2010). The goal is to restore mobility to tetraplegics using an (electrocorticographic) ECoG-driven 26 degrees of freedom (DoF) exoskeleton. Our program has compelling requirements. The first human implant is programmed for the first semester 2012. It has to be moderately invasive (which is why ECoG has been chosen), compatible with chronic wireless bilateral implantation, and able to drive at least 26 DoF online (this is why the patient will be equipped with two sets of 64 electrodes), and the software must be

designed in such a way that no or almost no recalibration is needed. The whole system is aimed at driving a wearable motorized exoskeleton with a backpack computer and battery. A parallel approach has been undertaken to validate all the preliminary steps first in rats, then in nonhuman primates, and then in human healthy volunteers to prepare the steps of the implant site localization using functional MRI and magnetoencephalography. The site of the project is at Clinatec, which is a multidisciplinary biomedical research Center at the CEA Grenoble.

Rat BCI program

This part of the program was aimed at showing the feasibility, to start the development of the algorithm, and to emulate a 1 DoF effector. Electrodes have been used as transcranial

titanium screws connected to a multilead connector (Fig. 1e). In the meantime, other systems are being designed which are all made of arrays of flat electrodes using the micronanotechnologies with 16 1-mm² platinum electrodes, mounted on a polyamide basis (Fig. 1f). The positioning of the electrode is being replicated for all animals, allowing establishment of a pertinent functional and anatomical correspondence with each of them. They have been functionally validated by both visual- and sensory-evoked potentials, shown in topoplot representations of the cortically evoked electrical activities. The behavioral experiment is classical, the animal being in a behavioral cage (Fig. 3c), allowed to press on a lever (Fig. 3d) which would trigger the release of the pellet by a reward dispenser. Once the animal is trained, sessions are performed in freely moving and self-paced condition (no clue is given to the animal to go and press on the lever), and in the meantime, the ECoG is recorded simultaneously on all the electrodes. The offline treatment comprises

- (1) back averaging potentials showing the appearance of a motor activity prior to the action of pressing on a lever, which happens mostly on the electrodes over the cerebellum.
- (2) time-frequency spatial analysis using wavelet decomposition shows that the maximal correlation happens on the same type of electrodes recording the activity in the cerebellar cortex. The INPLS software (Eliseyev et al., 2011) has been designed in-house, based on a wavelet transformation of the EEG, and decomposition to reduce the data space dimension from 30,000 to 10 combinations of features (latent variables). A regression function is calculated between the pedal signal and the latent variables, which leads to a predictive function. According to the threshold chosen, this yields to a prediction taking the binary values of zero and one allowing separating the cluster of events (Fig. 3a and b blue crosses) from the cluster of nonevents (Fig. 3a

and b black circles). This has been tested on offline analysis of long-term experiments in freely moving rats, for sessions up to 70 min in animals repeatedly investigated for long periods of several months up to 8 months. In the best experiment, 92% of true positive detections were made, with only one false prediction per 5 min, with a correlation coefficient equal to 0.7 (Fig. 3a). The paradigm was self-paced. About 60% of the time was spent in spurious activities. The pedal is then disconnected from the reward dispenser, which is therefore activated only when the ECoG signature is detected. In these experiments, the lever signal was only used to validate the detection as true lever activation, corresponding to animal's intentions. Along time, probably due to the loss of the quality of the electrode contact against the dura, there was an evolution of the correlation coefficient which went from 0.58 to 0.40 7 months later, corresponding to an increased overlap of the event and nonevent clusters (Fig. 3b).

Primate BCI program

It was aimed at designing the prototype of the implant, making the integration of the algorithm, the multichannel processing, and the extension from 1° to 3° effectors. The animals have been implanted with epi and subdural grids to compare the efficiency and the quality of the results are simultaneously recorded on either 36 or 40 channels. The animal was in the sitting chair with the restriction collard, and the electrodes were connected to a PL900 40 pins connector to the recorders (CEA Biomea and Micromed 64 channels). The animal was allowed to press on a pedal and get the rewards which could be either a pellet to be taken in the receiver or orange juice provided by a cannula close to the mouth. Figure 1g–i shows some of the various electrode implantations which were achieved in different animals.

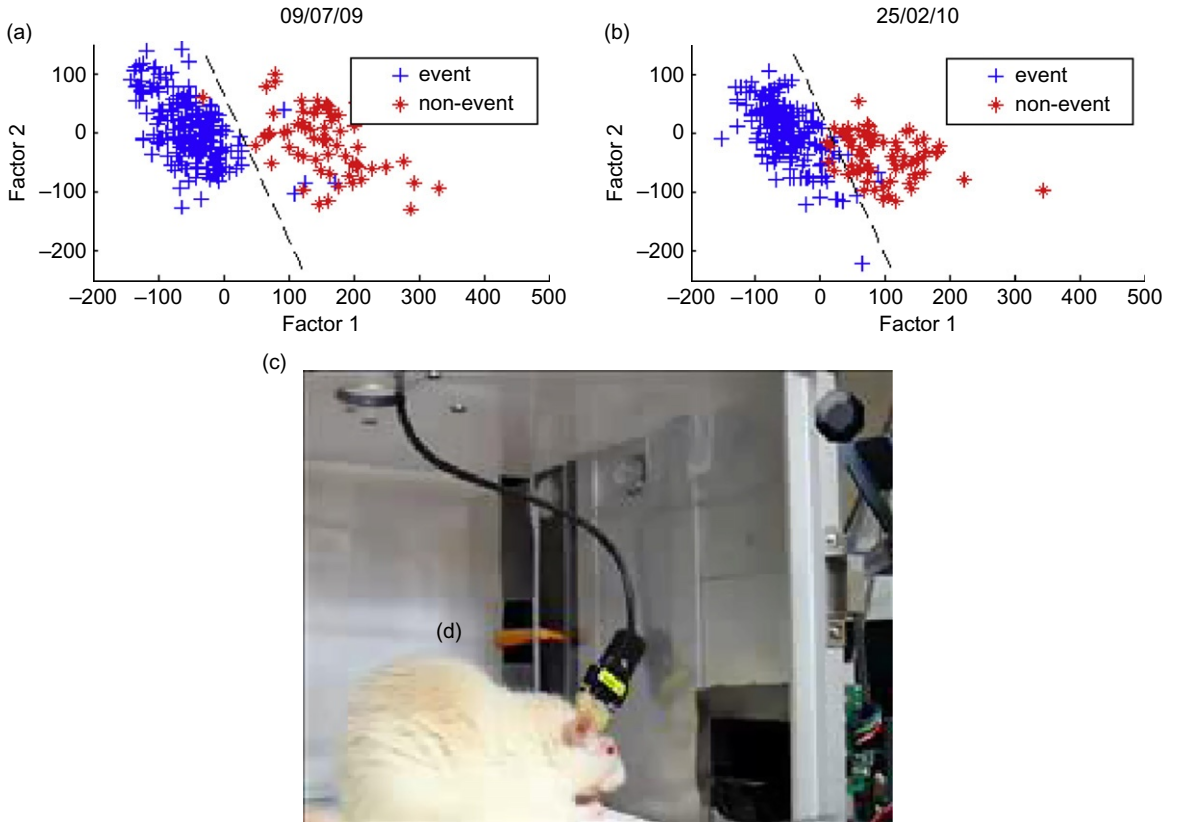


Fig. 3. Rat BCI experiment. (a) Clusterization of the events (blue crosses) and nonevents (black circles) using the INPLS software. (b) In the same animal, 7 months later. (c) Experimental setup: the rat is freely moving in the cage, ECoG is recorded from the titanium transcranial electrodes, and the animal presses the lever (d) spontaneously, on its own, clueless, decision.

The Human BCI program

It is based on the development of the 64 channel implants made of a 5-cm (Fig. 4a-f) diameter titanium cylinder being inserted against the dura (or with the dura resected for subdural implantation) bilaterally implanted and each of them featuring an antenna set (Fig. 4d), comprising a UHF antenna (Fig. 4b), to allow the telepowering of the electronics inside the implant, and the radiofrequency antenna, to export the data to the external receiver. Inside the titanium case, two application-specific integrated circuits aimed

at recording two sets of 32 electrodes are connected to a Zarlink radio emitting module to export the data to the external data processing module. The implants are easily inserted in a 5-cm trephine-made skull opening, with the skin totally closed, allowing long-term monitoring and the capture of ECoG data. In the external set are situated the terminal for reception/emission of the data, then a treatment stage to submit the recorded ECoG data to the algorithm software, interfaced with the command interface to drive the effectors. The effectors will be subsequently upgraded during the training phase.

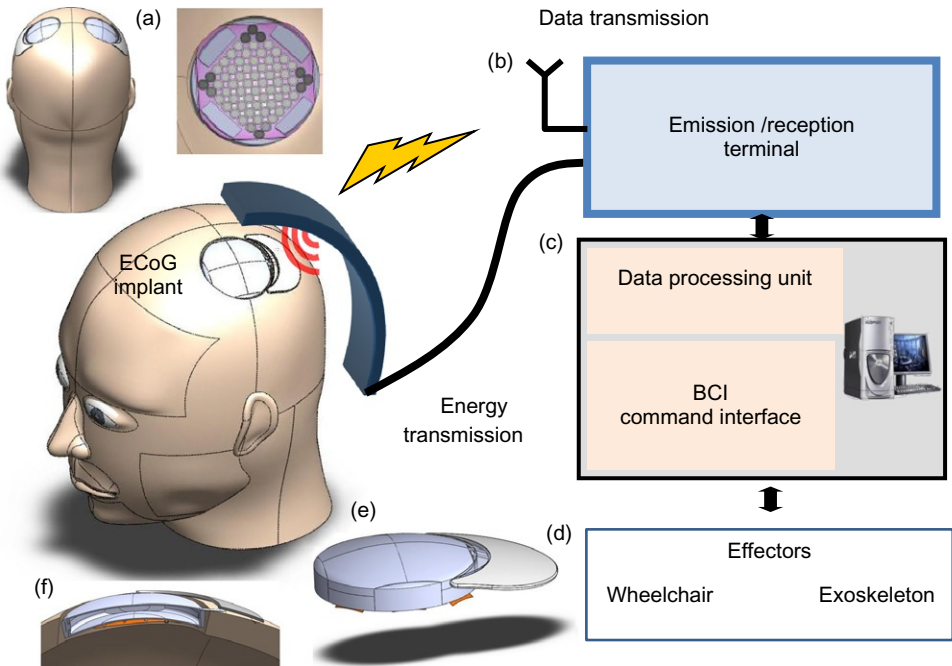


Fig. 4. Human prototype of the 64 ECoG electrode, wireless, telepowered implant for the human BCI project. (a) Bilateral implantation. The 64-electrode array is shown on the inner face of the implant. (b) The first stage of the external system is designed to provide energy for the embedded electronic components EEG recording ASIC, Zarlink radio emitting unit, and to record continuously the ECoG. (c) Processing unit using the INPLS software to detect the feature predicting the motor activity. This stage uses the detected features to initiate command orders to the various DoF of the effectors. (d) Connection to the effectors. (e) Computer-generated image of the implant with the antennas included in the visor of the cap. (f) Schematic drawing of the position of the implant placed in the 5-cm trephine opening of the skull.

A wheelchair with 6 DoF will be used to accommodate the patient with the concept of being able to activate several different components. The final effector will be a motorized exoskeleton very similar to the Japanese HAL system which might be in the first stage adapted to our purposes by replacing the commands coming from the EMG sensors by the commands coming from the command module of the BCI system. Cooperation with CEA LIST, which is the robotic department of CEA, is aimed at taking advantage of these first informations and developing a specifically designed exoskeleton for this application.

Conclusion

Since several decades, functional neurosurgery has integrated the concept of brain-tool, then brain-machine, and finally brain-computer interfaces, all of which have in common a specific area where external human-made devices are in contact with the brain tissue. This crucial part of the interface is of complex nature, made by tissue on one side, and usually a metallic component on the other side, separated by a layer of extracellular fluid. This composite situation is usually considered as a simple juxtaposition of elements,

bypassing more complex phenomena which might happen. They are currently being submitted to a more sophisticated modelization as this interface is probably modifying the signal, either recorded from the brain by the electrode or emitted from the electrode to the brain during stimulation. Brain-computer interfaces used to drive neuroprostheses will be part of functional neurosurgery; this field is in continuity with what was done before by deep brain stimulation or spinal cord stimulation or cortical stimulation. There is no question about how much this will have an important impact on the capability of treatment, which is provided by the development of new technologies, their miniaturization through nanomicrotechnologies, and therefore their decreased invasiveness and their lower morbidity.

References

- Aebischer, P., & Goddard, M. (1991). Treating Parkinson's disease with lesions of the subthalamic nucleus. *Science*, 252, 133–134.
- Arnulf, I., Ferraye, M., Fraix, V., Benabid, A. L., Chabardès, S., Goetz, L., et al. (2010). Sleep induced by stimulation in the human pedunculopontine nucleus area. *Annals of Neurology*, 67, 546–549.
- Aziz, T. Z., Peggs, D., Sambrook, M. A., & Crossman, A. R. (1991). Lesion of the subthalamic nucleus for the alleviation of 1-methyl-4-phenyl-1,2,3,6-tetrahydropyridine (MPTP)-induced parkinsonism in the primate. *Movement Disorders*, 6, 288–292.
- Benabid, A. L., Minotti, L., Koudsie, A., de Saint Martin, A., & Hirsch, E. (2002). Antiepileptic effect of high-frequency stimulation of the subthalamic nucleus (corpus lusii) in a case of medically intractable epilepsy caused by focal dysplasia: A 30-month follow-up: Technical case report.. *Neurosurgery*, 50, 1385–1391 (discussion: 1391–1392).
- Benabid, A. L., Pollak, P., Louveau, A., Henry, S., & de Rougemont, J. (1987). Combined (thalamotomy and stimulation) stereotactic surgery of the VIM thalamic nucleus for bilateral Parkinson disease. *Applied Neurophysiology*, 50, 344–346.
- Benazzouz, A., Gross, C., Feger, J., Boraud, T., & Bioulac, B. (1993). Reversal of rigidity and improvement in motor performance by subthalamic high-frequency stimulation in MPTP-treated monkeys. *The European Journal of Neuroscience*, 5, 382–389.
- Bergman, H., Wichmann, T., & DeLong, M. R. (1990). Reversal of experimental parkinsonism by lesions of the subthalamic nucleus. *Science*, 249, 1436–1438.
- Chabardès, S., Kahane, P., Minotti, L., Koudsie, A., Hirsch, E., & Benabid, A. L. (2002). Deep brain stimulation in epilepsy with particular reference to the subthalamic nucleus. *Epileptic Disorders*, 4(Suppl. 3), 83–93.
- Chabardès, S., Polosan, M., Seigneuret, E., Carron, R., Lhommée, E., Gay, E., et al. (2010). Stimulation cérébrale profonde et CG25 dans les formes graves de dépression. *Société française de neurochirurgie*, Lyon.
- Donoghue, J. P. (2002). Connecting cortex to machines: Recent advances in brain interfaces. *Nature Neuroscience Supplement*, 5, 1085–1088.
- Donoghue, J. P., Sanes, J. N., Hatsopoulos, N. G., & Gaal, G. (1998). Neural discharge and local field potential oscillations in primate motor cortex during voluntary movements. *Journal of Neurophysiology*, 79, 159–173.
- Eliseyev, A., Moro, C., Costecalde, T., Torres, N., Gharbi, S., Mestais, C., et al. (2011). Iterative N-way PLS for binary self-paced BCI in freely moving animals. *Journal of Neural Engineering*, doi: 10.1088/1741-5608/4/046012.
- Fisher, R., Salanova, V., Witt, T., Worth, R., Henry, T., Gross, R., et al. (2010). Electrical stimulation of the anterior nucleus of thalamus for treatment of refractory epilepsy. *Epilepsia*, 51, 899–908.
- Franzini, A., Ferroli, P., Leone, M., & Broggi, G. (2003). Stimulation of the posterior hypothalamus for treatment of chronic intractable cluster headaches: First reported series. *Neurosurgery*, 52, 1095–1099 (discussion: 1099–1101).
- Georgopoulos, A. P. (1994). Population activity in the control of movement. *International Review of Neurobiology*, 37, 103–119.
- Georgopoulos, A. P., Lurito, J. T., Petrides, M., Schwartz, A. B., & Massey, J. T. (1989). Mental rotation of the neuronal population vector. *Science*, 243, 234–236.
- Hosobuchi, Y. (1986). Subcortical electrical stimulation for control of intractable pain in humans. Report of 122 cases (1970–1984). *Journal of Neurosurgery*, 64, 543–553.
- Houeto, J. L., Karachi, C., Mallet, L., Pillon, B., Yelnik, J., Mesnage, V., et al. (2005). Tourette's syndrome and deep brain stimulation. *Journal of Neurology, Neurosurgery, and Psychiatry*, 76, 992–995.
- Jenkinson, N., Nandi, D., Miall, R. C., Stein, J. F., & Aziz, T. Z. (2004). Pedunculopontine nucleus stimulation improves akinesia in a Parkinsonian monkey. *Neuroreport*, 15, 2621–2624.
- Laitinen, L. V., Bergenheim, A. T., & Hariz, M. (1992). Leksell's posteroverentral pallidotomy in the treatment of Parkinson's disease. *Journal of Neurosurgery*, 76, 53–61.
- Mallet, L., Mesnage, V., Houeto, J. L., Pelissolo, A., Yelnik, J., Behar, C., et al. (2002). Compulsions, Parkinson's disease, and stimulation. *The Lancet*, 360, 1302–1304.

- Mallet, L., Polosan, M., Jaafari, N., Baup, N., Welter, M. L., Fontaine, D., et al. (2008). Subthalamic nucleus stimulation in severe obsessive-compulsive disorder. *The New England Journal of Medicine*, 359, 2121–2134 Erratum in: *The New England Journal of Medicine*, 361(10), 1027, 2009 Sep 3.
- Mayberg, H. S. (2003). Positron emission tomography imaging in depression: A neural systems perspective. *Neuroimaging Clinics of North America*, 13, 805–815 Review.
- Mayberg, H. S., Lozano, A. M., Voon, V., McNeely, H. E., Seminowicz, D., Hamani, C., et al. (2005). Deep brain stimulation for treatment-resistant depression. *Neuron*, 45, 651–660.
- Nandi, D., Liu, X., Winter, J., Aziz, T. Z., & Stein, J. F. (2002). Deep brain stimulation of the pedunculopontine region in the normal non human primate. *Journal of Clinical Neuroscience*, 9, 170–174.
- Naqvi, N. H., Rudrauf, D., Damasio, H., & Bechara, A. (2007). Damage to the insula disrupts addiction to cigarette smoking. *Science*, 315, 531–534.
- Nicolelis, M. A. (2001). Actions from thoughts. *Nature*, 409, 403–407.
- Nicolelis, M. A. (2003). Brain-machine interfaces to restore motor function and probe neural circuits. *Nature Reviews Neuroscience*, 4, 417–422.
- Nicolelis, M. A., & Lebedev, M. A. (2009). Principles of neural ensemble physiology underlying the operation of brain-machine interfaces. *Nature Reviews Neuroscience*, 10, 530–540.
- Nuttin, B., Cosyns, P., Demeulemeester, H., Gybels, J., & Meyerson, B. (1999). Electrical stimulation in anterior limbs of internal capsules in patients with obsessive-compulsive disorder. *The Lancet*, 354, 1526.
- Schiff, N. D., Giacino, J. T., Kalmar, K., Victor, J. D., Baker, K., Gerber, M., et al. (2007). Behavioural improvements with thalamic stimulation after severe traumatic brain injury. *Nature*, 448, 600–604.
- Siegfried, J., & Lippitz, B. (1994). Bilateral chronic electrostimulation of ventroposterolateral pallidum: A new therapeutic approach for alleviating all parkinsonian symptoms. *Journal of Neurosurgery*, 35, 1126–1130.
- Sturm, V., Lenartz, D., Kououlousakis, A., Treuer, H., Herholz, K., & Klein, J. C. (2003). The nucleus accumbens: A target for deep brain stimulation in obsessive-compulsive and anxiety-disorders. *Journal of Chemical Neuroanatomy*, 26, 293–299.
- Sun, B., Chen, S., Zhan, S., Le, W., & Krahl, S. E. (2007). Subthalamic nucleus stimulation for primary dystonia and tardive dystonia. *Acta Neurochirurgica. Supplement*, 97 (Pt. 2), 207–214 Review.
- Svennilson, E., Torvik, A., Lowe, R., & Leksell, L. (1960). Treatment of parkinsonism by stereotactic thermolesions in the pallidal region. A clinical evaluation of 81 cases. *Acta Psychiatrica et Neurologica Scandinavica*, 35, 358–377.
- Vidalhet, M., Vercueil, L., Houeto, J. L., Krystkowiak, P., Benabid, A. L., Cornu, P., et al. (2005). Bilateral deep-brain stimulation of the globus pallidus in primary generalized dystonia. *The New England Journal of Medicine*, 352, 459–467.
- Vidalhet, M., Vercueil, L., Houeto, J. L., Krystkowiak, P., Lagrange, C., Yelnik, J., et al. (2007). Bilateral, pallidal, deep-brain stimulation in primary generalised dystonia: A prospective 3 year follow-up study. *Lancet Neurology*, 6, 223–229.
- Vidalhet, M., Yelnik, J., Lagrange, C., Fraix, V., Grabli, D., Thobois, S., et al. (2009). Bilateral pallidal deep brain stimulation for the treatment of patients with dystonia-choreoathetosis cerebral palsy: A prospective pilot study. *Lancet Neurology*, 8, 709–717.
- Vilela Filho, O. (2009). Personal communication on DBS of the External Pallidum, in *Dystonia*.
- Visser-Vandewalle, V., Temel, Y., Boon, P., Vreeeling, F., Colle, H., Hoogland, G., et al. (2003). Chronic bilateral thalamic stimulation: A new therapeutic approach in intractable Tourette syndrome. *Report of three cases. Journal of Neurosurgery*, 99, 1094–1100.
- Vonck, K., Boon, P., Claeys, P., Dedeurwaerdere, S., Achter, R., & Van Roost, D. (2005). Long-term deep brain stimulation for refractory temporal lobe epilepsy. *Epilepsia*, 46(Suppl. 5), 98–99.
- Wang, W., Collinger, J. L., Perez, M. A., Tyler-Kabara, E. C., Cohen, L. G., Birbaumer, N., et al. (2010). Neural interface technology for rehabilitation: Exploiting and promoting neuroplasticity. *Physical Medicine and Rehabilitation Clinics of North America*, 21, 157–178 Review.
- Young, R. F., & Chambi, V. I. (1987). Pain relief by electrical stimulation of the periaqueductal and periventricular gray matter. Evidence for a non-opioid mechanism. *Journal of Neurosurgery*, 66, 364–371.

CHAPTER 6

Deep brain stimulation: emerging indications

Travis S. Tierney, Tejas Sankar and Andres M. Lozano*

Division of Neurosurgery, Toronto Western Hospital, Toronto, Ontario, Canada

Abstract: There are a number of emerging surgical indications for deep brain stimulation. We have shown that modulation of activity within motor, mood, and cognitive circuits has beneficial effects in patients with Parkinson's disease, treatment-resistant depression, and perhaps Alzheimer's type dementia. We review the rationale, safety, and efficacy for each of these indications, focusing on disease mechanisms and relevant data that are necessary to document therapeutic value in each case. The review closes with some thoughts on possible future directions for deep brain stimulation. It is likely that applications for deep brain stimulation will continue to expand as accumulating data establish its safety and efficacy profile in these and other conditions.

Keywords: Alzheimer's disease; deep brain stimulation; depression; Parkinson's disease; pedunculopontine nucleus.

Introduction

This review summarizes targets for deep brain stimulation that are currently emerging as new treatments for Parkinson's disease, refractory depression, and Alzheimer's type dementia. The rationale, safety, and efficacy of each modality are discussed focusing on disease mechanisms

and relevant data that are necessary to document therapeutic value in each case. The review closes with some thoughts on possible future directions for deep brain stimulation.

Parkinson's disease

Clinical interest in deep brain stimulation has its roots in the treatment of Parkinson's disease. Since its renewed inception in the late 1980s, nearly 80,000 patients worldwide have received deep brain stimulation (DBS) with an ongoing accrual of approximately 8000–10,000 new patients per year.

*Corresponding author.

Tel.: +1-416-603-6200; Fax: +1-416-603-5298
E-mail: lozano@uhnres.utoronto.ca

Several recent clinical trials have established the safety and efficacy of pallidal and subthalamic stimulation for Parkinson's disease (Benabid et al., 2005; Deuschl et al., 2006; Weaver et al., 2009; Williams et al., 2010). Although primary parkinsonian symptoms such as tremor (Blahak et al., 2007; Diamond et al., 2007; Hariz et al., 2008), rigidity (Shapiro et al., 2007; Tabbal et al., 2008), and bradykinesia (Dafotakis et al., 2008; Timmermann et al., 2008) respond well to DBS, the major modern indication for surgical intervention in Parkinson's disease is the dose-limiting side effects of prolonged levodopa therapy, that is, motor fluctuations and dyskinesia (Guridi et al., 2008; Moro et al., 2010b). There are also a number of medication-resistant symptoms including gait and postural disturbances that respond only transiently or more variably to standard DBS surgery (Botzel and Kraft, 2010; Hausdorff et al., 2009; Johnsen et al., 2009). Other medically refractory symptoms including speech dysfunction (Castelli et al., 2010; Okun et al., 2009), cognitive impairment (Parsons et al., 2006; York et al., 2008; Zangaglia et al., 2009), and some psychiatric manifestations (Rodrigues et al., 2010; Witt et al., 2008) can, in some cases, be aggravated by surgery.

The recent recognition of debilitating non-motor parkinsonian symptoms has prompted a search for novel surgical interventions. So-called non-levodopa-responsive symptoms are disorders of cognition, mood, gait and posture, sleep, olfaction, autonomic instability, and sexual function (Fig. 1). Over time, nearly all patients with Parkinson's disease develop significant cognitive impairment. Long-term longitudinal studies show that the incidence of dementia is 50% at 10 years and 83% at 20 years (Hely et al., 2008) (Fig. 2). These disturbances are poorly responsive to levodopa and represent major drivers of disability in these patients (Aarsland et al., 2009; Schrag, 2006). In addition, 10 years after the diagnosis of Parkinson's disease, approximately 50% of patients are falling, and at 20 years many of these patients have

suffered a fracture as a consequence of their falls (Hely et al., 2008) (Fig. 3). Because gait impairment and postural instability associated with advanced Parkinson's disease underlie significant mortality and morbidity in this patient population, there has been a great deal of renewed interest in understanding the pathophysiology of gait. This has led directly to the examination of a novel target for deep brain stimulation in Parkinson's disease: the pedunculopontine nucleus and its adjacent areas.

Early work on mechanisms of locomotion by Shik and colleagues in the 1960s first established the location of important neural centers regulating gait (Shik et al., 1969). Decerebrate cats were implanted with arrays of electrodes throughout the neuroaxis, and areas in the brain were found where electrical simulation could initiate locomotion or enhance locomotive behavior (Orlovsky et al., 1966) (Fig. 4). The anatomical location of the so-called midbrain locomotor region was first identified based on these pioneering studies (Garcia-Rill and Skinner, 1987a,b). In bipedal animals, these areas are thought to correspond to the region of the pedunculopontine nucleus complex (Pahapill and Lozano, 2000). Several groups have now begun to implant electrodes in the pedunculopontine nucleus to see whether this approach might be helpful in ameliorating some of the gait disturbances associated with Parkinson's disease (Ferraye et al., 2010; Mazzone et al., 2008; Pereira et al., 2008; Stefani et al., 2007) (Fig. 5). A recent paper by Moro et al. (2010a) documents sustained reduction in falls and freezing in six patients with advanced Parkinson's disease who received a unilateral pedunculopontine stimulator (Table 1). Approximately 100 patients worldwide have now undergone placement of deep brain electrodes into the pedunculopontine nucleus for postural instability. There are, however, several unresolved issues associated with this novel target. For example, it is unclear which neural structures within or around the pedunculopontine nucleus mediate the therapeutic effect. Based

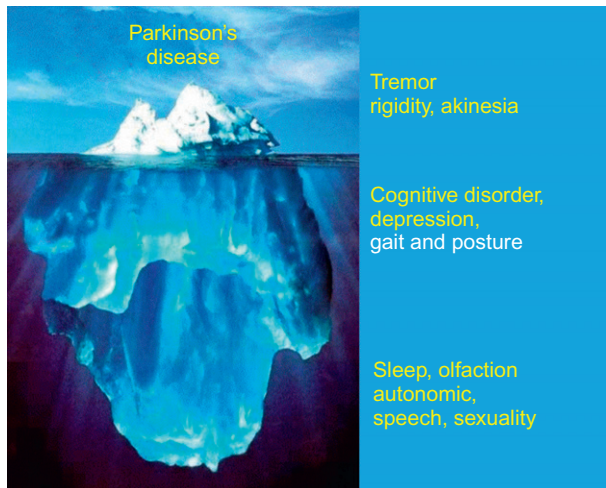


Fig. 1. The well-known cardinal motor symptoms of Parkinson's disease (tremor, rigidity, and akinesia) typically respond well to levodopa therapy. However, there is a large burden of underlying symptoms that do not respond to either medical or convention DBS therapy. It is now becoming widely recognized that these “dopa-nonresponsive” conditions produce significant morbidity as Parkinson's disease advances.

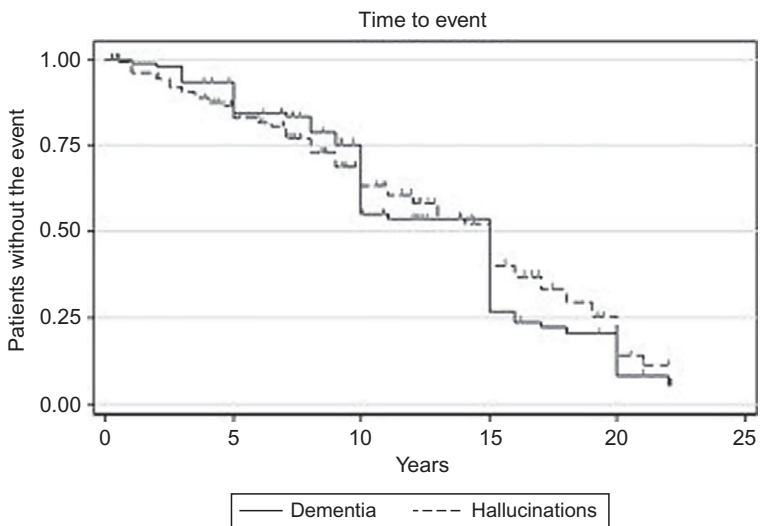


Fig. 2. Kaplan–Meier plot of time to hallucinations and dementia after the diagnosis of Parkinson's disease in 136 patients. (Used with permission from [Hely et al., 2008](#).)

largely on preclinical studies of primates, some groups have suggested that electrical stimulation of cholinergic neurons within the

pedunculopontine nucleus is likely to be the most relevant target ([Karachi et al., 2010](#)), but whether stimulation of the nucleus *per se* or some other

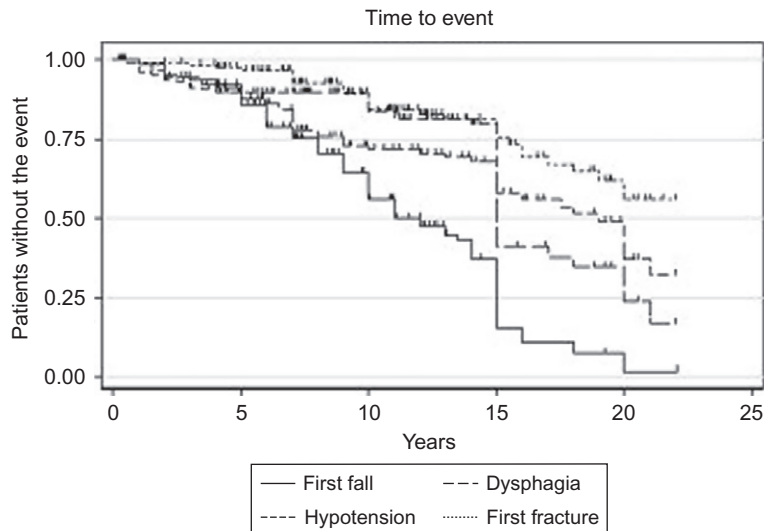


Fig. 3. Kaplan-Meier plot of time to falls, dysphagia, symptomatic postural hypotension, and first fracture in 136 patients with Parkinson's disease. (Used with permission from [Hely et al., 2008](#).)

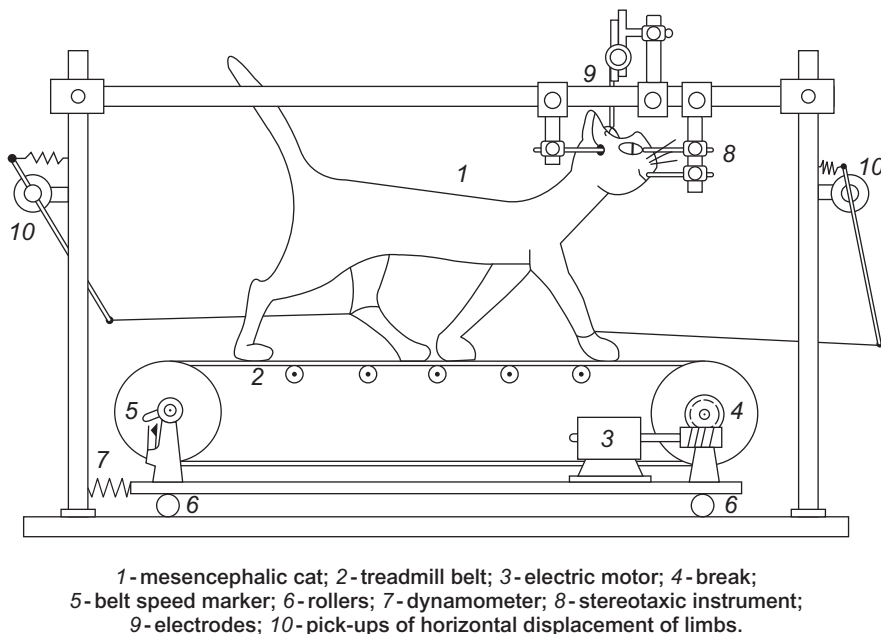


Fig. 4. Schematic drawing from the original 1966 article by Shik and colleagues describing their experimental method used to determine neural centers for locomotor behavior in decerebrate cats. (From [Orlovsky et al., 1966](#).)

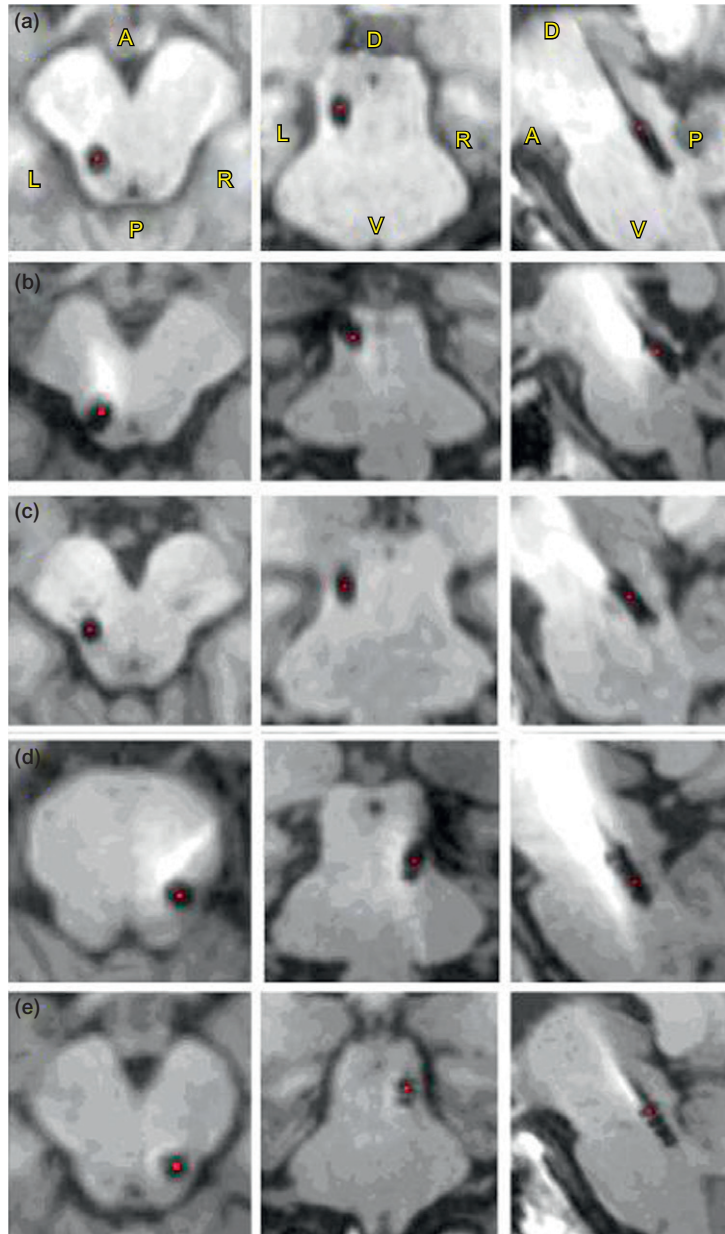


Fig. 5. T1-weighted axial (left column), coronal (middle column), and sagittal (right column) magnetic resonance (MR) images showing the location of the deep brain electrodes within the pedunculopontine nucleus complex in five patients with postural instability associated with advanced Parkinson's disease. The small red dot in each panel marks the location of the active electrode. A, anterior; P, posterior; L, left; R, right; D, dorsal; V, ventral. (Used with permission from Moro et al., 2010a.)

Table 1. Effects of unilateral pedunculopontine nucleus (PPN) DBS on Unified Parkinson Disease Rating Scale (UPDRS) part II subscores (falling and freezing) after 3 and 12 months of stimulation (Used with permission. Modified from [Moro et al., 2010a.](#))

Patient no.	UPDRS-II item 13 (falling)			UPDRS-II item 14 (freezing)		
	Preop	3 mos	12 mos	Preop	3 mos	12 mos
1	4	0	0	3	0	1
2	2	0	1	3	0	3
3	3	2	2	2	2	2
4	3	1	2	2	1	2
5	3	1	0	3	1	2
6	2	2	0	3	2	2
Mean (s.d.)	2.8 (0.7)	0.9 (0.8)	0.8 (0.9)	3.0 (1.0)	1.0 (0.9)	2.0 (1.0)
P-value ^a		0.04	0.02		0.04	0.10

^aCompared to baseline.

adjacent nuclei or white matter tracts is responsible for clinical benefits in humans is not yet firmly established.

Refractory depression

According to the World Health Organization, the disease burden of intractable depression represents one of the major obstacles to human development. Whereas there may be a few million patients with Parkinson's disease, it is estimated that over 121 million people worldwide currently fulfill Diagnostic and Statistical Manual (DSM)-4 criteria for major depression ([World Health Organization, 2001](#)). Of these, roughly 10–20% will fail standard medical, cognitive, and electroconvulsive therapy ([Agency for Health Care Policy and Research, 1993; Fava, 2003](#)). Currently there are several targets for deep brain stimulation that are being proposed for the treatment of intractable major depression. These include the subcallosal cingulum, the inferior thalamic peduncle, the nucleus accumbens, and the anterior limb of the internal capsule. Among these various targets, the largest number of patients have undergone chronic high-frequency stimulation of cingulate white matter tracts near Brodmann's area 25. The rationale for targeting area 25 comes from Positron Emission

Tomography (PET) imaging studies of patients with major depression demonstrating increased blood flow in that region and decreased flow in associated prefrontal and premotor cortical areas (areas 9 and 46) ([Mayberg et al., 1999; Seminowicz et al., 2004](#)) ([Fig. 6a and b](#)). This pattern of activation in depressed patients is largely reversed after successful treatment with antidepressants, cognitive behavioral therapy, or electroconvulsive therapy ([Dougherty et al., 2003; Goldapple et al., 2004; Mayberg et al., 2000; Nobler et al., 2001](#)). Based on these findings, electrodes were implanted into subgenual cingulate area 25 in six patients with treatment-resistant depression ([Mayberg et al., 2005](#)) ([Fig. 7](#)). PET imaging from responding patients showed that deep brain stimulation of area 25 is able to reverse pretreatment blood flow changes in a similar manner and time course as antidepressant medication ([Fig. 6c–f](#)). To date, about 100 patients with major depression have been treated with bilateral stimulation of area 25. The results of a recent single center trial show that 60% of patients responded to the therapy as assessed by a 50% reduction in the Hamilton Rating Scale for Depression (HRSD-17) and a third were in complete remission at 6 months ([Lozano et al., 2008; Fig. 8](#)). At 1 year follow-up, these effects appear to be well maintained. A large double-blinded controlled trial of subcallosal cingulate deep brain

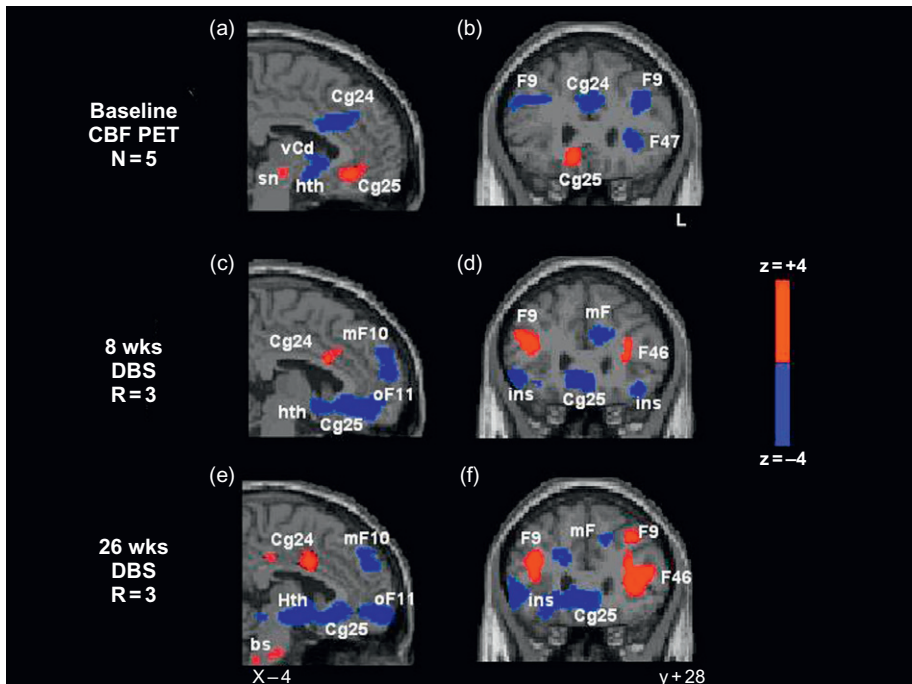


Fig. 6. Changes in regional cerebral blood flow as assessed with PET imaging in patients with treatment-resistant depression before surgery (a, b) and after 8 (c, d) and 26 (e, f) weeks of successful treatment with continuous high-frequency stimulation to the subgenual cingulate gyrus (Brodmann area 25, Cg25). Dorsolateral prefrontal (F9), ventrolateral prefrontal (F47), anterior cingulate (Cg24) cortices, hypothalamus (Hth), anterior insula (ins), medial frontal (mF10), and orbital frontal (oF11), prefrontal (F46). (Used with permission from [Mayberg et al., 2005](#).)

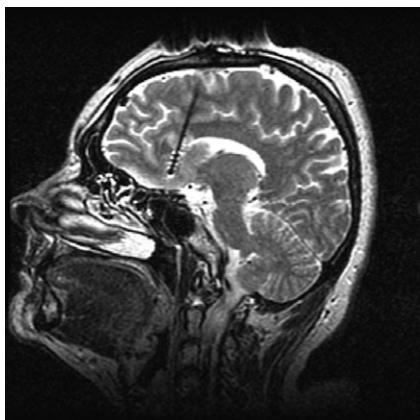


Fig. 7. Sagittal T2-weighted MRI showing the position of a DBS electrode in the subcallosal cingulate gyrus (Brodmann area 25) in a patient with treatment-resistant depression.

stimulation for treatment-resistant depression is currently underway along with several studies aimed at identifying a clinical or imaging marker capable of predicting which patients will have a significant postoperative response.

Alzheimer's type dementia

Alzheimer's disease is the most common form of adult-onset dementia. Worldwide about 27 million people are affected, and its prevalence is predicted to increase significantly as world population ages ([Brookmeyer et al., 2007](#)). The disease is characterized by functional impairment in the neural circuits serving cognitive and memory functions, particularly in the hippocampus/

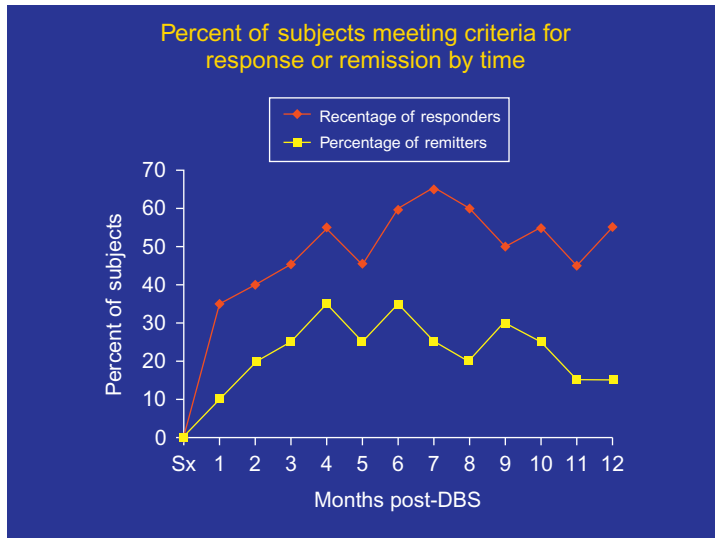


Fig. 8. Patients meeting response criteria (a 50% or greater reduction in the 17-item Hamilton Rating Scale for Depression [HRSD-17]) or remission (scores of seven or less) after high-frequency stimulation of area 25. The proportion of patients responding or reaching remission increased over time to plateau between 6 and 12 months. (Used with permission from [Lozano et al., 2008](#).)

entorhinal cortical complex where the neurodegenerative burden of the disease is highest. Based on a serendipitous clinical observation ([Hamani et al., 2008](#)), we hypothesized that electrical stimulation of the fornix, part of the Papez memory circuit ([Powell et al., 1957; Vann et al., 2009](#)), might be used to improve working memory and cognitive function in patients with Alzheimer's-type dementia. Six patients were recruited for a phase I safety trial ([Laxton et al., 2011](#)) where deep brain stimulators were placed along the anteromedial border of the fornix bundle bilaterally (Fig. 9). After 1 year of chronic high-frequency stimulation, glucose hypometabolism within the temporoparietal cortex that is characteristic of the diseased brain was largely reversed (Fig. 10). Scores on the mini-mental state exam (MMSE) improved for two of the six patients, three others saw a decline, and one was unchanged (Fig. 11). The average rate of decline in the MMSE approaches three points per year ([Mayeux and Sano, 1999](#)), suggesting that the rate of cognitive decline for patients in this study may have been delayed. No adverse effects of stimulation on sleep,

hypothalamic, or endocrine function were detected. No patient developed a stroke, intracranial hemorrhage, or infection during the 12-month follow-up. This pilot study demonstrates the safety and potential efficacy of deep brain stimulation to treat the cognitive decline that accompanies Alzheimer's disease. We are currently working on basic mechanisms of electrical stimulation within this circuit in various animal models and have initiated a large multicenter clinical trial to fully assess the therapeutic effect of this intervention.

Future directions for DBS: optogenetics

In the near future, it may become possible to use light, rather than electrical stimulation, to modulate the activity of neural circuits in patients with DBS-tractable disease. Optogenetic stimulation may be an improved method for activating or inhibiting more precisely the target of therapeutic interest so as to avoid off-target effects that we may now be seeing with the spread of electric

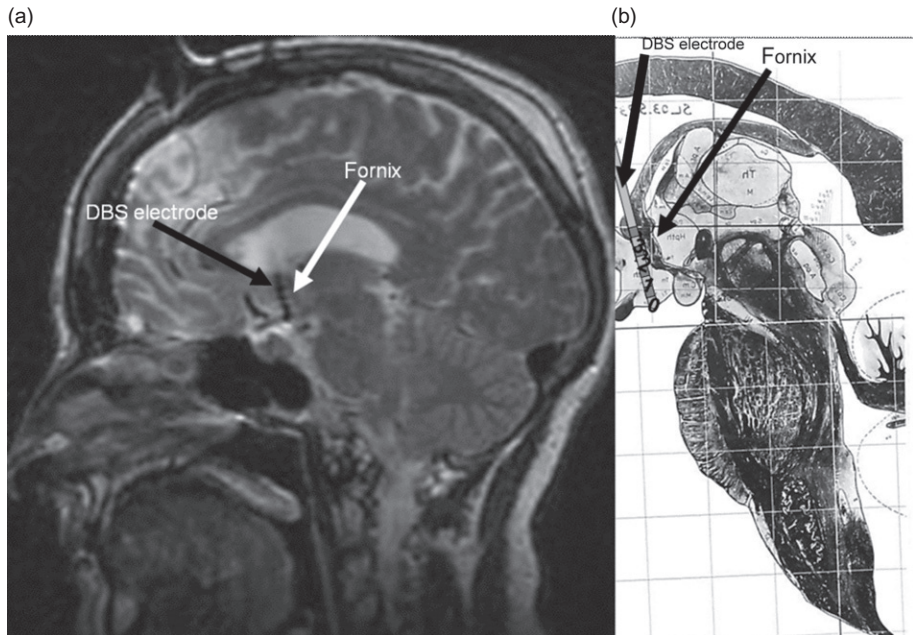


Fig. 9. Sagittal T2-weighted MRI (a) and image from a histological brain atlas (b) depicting the position of a 3387 DBS electrode inserted adjacent to the fornix for the treatment of Alzheimer's type dementia. (Used with permission from Laxton et al., 2011.)

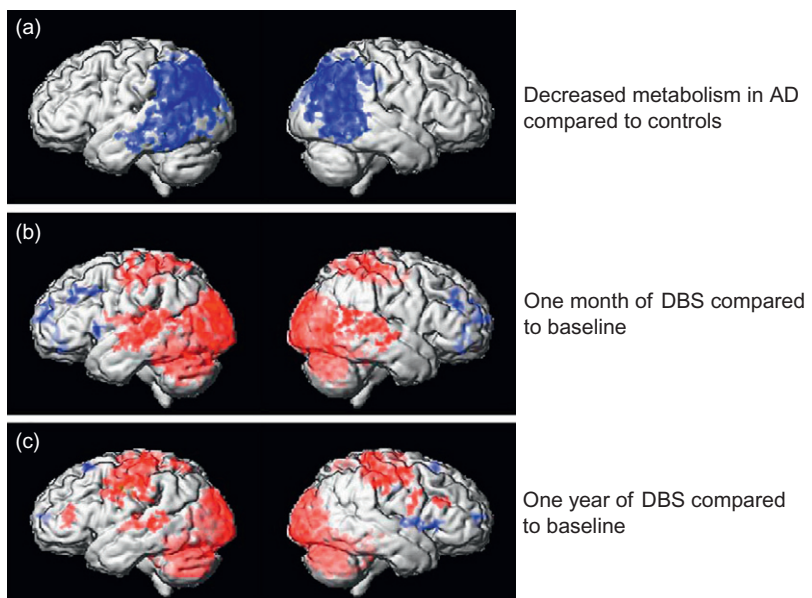


Fig. 10. [18 F]-fluorodeoxyglucose (FDG) PET scans to measure cerebral glucose metabolism at baseline (a) 1 month (b), and 1 year (c) after deep brain stimulation of the fornix in a single patient with Alzheimer's disease. Blue represents areas of decreased glucose uptake and red shows areas of increased glucose utilization between conditions noted on the right. (Used with permission from Laxton et al., 2011.)

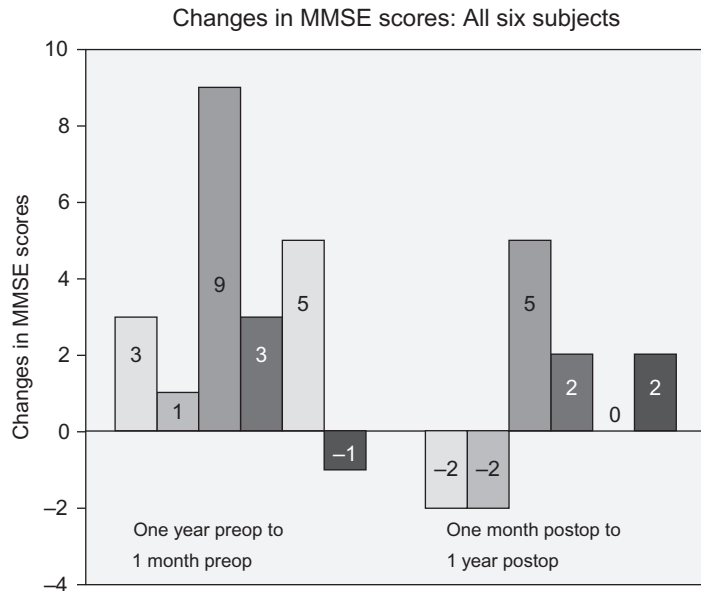


Fig. 11. The first 6 bars on the left show point changes in the mini-metal state exam (MMSE) in the first 11 months before surgery for each of the six patients. Negative numbers represent an improvement, and the top score is 30. The second set of 6 bars on the right shows point changes for the same six patients 11 months after surgery: the first two patients showed modest improvement, three saw worsening scores, and one was unchanged. The average rate of decline on the MMSE for patients with Alzheimer's disease is approximately three points per year. (Used with permission from [Laxton et al., 2011](#).)

charge around a DBS electrode. The selectivity of an optogenetic approach lies in the cellular specificity of viral vectors used to deliver light-sensitive proteins to relevant targets ([Boyden et al., 2005](#); [Nagel et al., 2002](#); [Zhang et al., 2007, 2010](#)). These molecules are light-sensitive plasma membrane channels capable of permitting rapid entry of sodium or chloride with concomitant excitation or inhibition of the neuron ([Han and Boyden, 2007](#)). With this approach, Deisseroth and colleagues have shown that channelrhodopsins or halorhodopsins expressed in the rat motor cortex can drive or inhibit the activity of cortical neurons and that there are behavioral correlates of this neural modulation ([Aravanis et al., 2007](#)). Only those neural elements expressing the light-sensitive protein are stimulated. This may provide greater specificity and reduce the collateral side effects related to electrical stimulation ([Gradinaru et al., 2009](#)).

There are many practical hurdles that would need to be overcome before this technique could be used clinically, but the theoretical advantages of optogenetic stimulation seem quite promising.

Conclusion

There are a number of emerging surgical indications for deep brain stimulation. We have shown that modulation of activity within motor, mood, and cognitive circuits has beneficial effects in patients with Parkinson's disease, major depression, and perhaps Alzheimer's type dementia. It is likely that indications for deep brain stimulation will continue to expand as accumulating data establish its safety and efficacy profile in other conditions. This chapter reviews the rationale and

outcome data for pedunculopontine nucleus stimulation for postural instability associated with advanced Parkinson's disease, Brodmann area 25 stimulation for intractable depression, and fornix stimulation for Alzheimer's type dementia. None of these interventions have yet received FDA approval, but it is hoped that with further study some of these emerging indications will soon become standard of care. With the striking success of deep brain stimulation for the treatment of refractory movement disorders, there is little doubt that we will continue to see similar techniques of neuromodulation applied to treat many other neurologic, psychiatric, and chronic pain conditions.

References

- Aarsland, D., Marsh, L., & Schrag, A. (2009). Neuropsychiatric symptoms in Parkinson's disease. *Movement Disorders*, 24, 2175–2186.
- Agency for Health Care Policy and Research. (1993). *Depression in primary care: Volume 2. Treatment of major depression*. Rockville, USA: Department of Health and Human Services, Public Health Service.
- Aravanis, A. M., Wang, L. P., Zhang, F., Meltzer, L. A., Mogri, M. Z., Schneider, M. B., et al. (2007). An optical neural interface: In vivo control of rodent motor cortex with integrated fiberoptic and optogenetic technology. *Journal of Neural Engineering*, 4, S143–S156.
- Benabid, A. L., Chabardes, S., & Seigneuret, E. (2005). Deep-brain stimulation in Parkinson's disease: Long-term efficacy and safety—What happened this year? *Current Opinion in Neurology*, 18, 623–630.
- Blahak, C., Wohrle, J. C., Capelle, H. H., Bazner, H., Grips, E., Weigel, R., et al. (2007). Tremor reduction by subthalamic nucleus stimulation and medication in advanced Parkinson's disease. *Journal of Neurology*, 254, 169–178.
- Botzel, K., & Kraft, E. (2010). Strategies for treatment of gait and posture associated deficits in movement disorders: The impact of deep brain stimulation. *Restorative Neurology and Neuroscience*, 28, 115–122.
- Boyden, E. S., Zhang, F., Bamberg, E., Nagel, G., & Deisseroth, K. (2005). Millisecond-timescale, genetically targeted optical control of neural activity. *Nature Neuroscience*, 8, 1263–1268.
- Brookmeyer, R., Johnson, E., Ziegler-Graham, K., & Arrighi, H. M. (2007). Forecasting the global burden of Alzheimer's disease. *Alzheimer's & Dementia*, 3, 186–191.
- Castelli, L., Rizzi, L., Zibetti, M., Angrisano, S., Lanotte, M., & Lopiano, L. (2010). Neuropsychological changes 1-year after subthalamic DBS in PD patients: A prospective controlled study. *Parkinsonism & Related Disorders*, 16, 115–118.
- Dafotakis, M., Fink, G. R., Allert, N., & Nowak, D. A. (2008). The impact of subthalamic deep brain stimulation on bradykinesia of proximal and distal upper limb muscles in Parkinson's disease. *Journal of Neurology*, 255, 429–437.
- Deuschl, G., Schade-Brittinger, C., Krack, P., Volkmann, J., Schafer, H., Botzel, K., et al. (2006). A randomized trial of deep-brain stimulation for Parkinson's disease. *The New England Journal of Medicine*, 355, 896–908.
- Diamond, A., Shahed, J., & Jankovic, J. (2007). The effects of subthalamic nucleus deep brain stimulation on parkinsonian tremor. *Journal of the Neurological Sciences*, 260, 199–203.
- Dougherty, D. D., Weiss, A. P., Cosgrove, G. R., Alpert, N. M., Cassem, E. H., Nierenberg, A. A., et al. (2003). Cerebral metabolic correlates as potential predictors of response to anterior cingulotomy for treatment of major depression. *Journal of Neurosurgery*, 99, 1010–1017.
- Fava, M. (2003). Diagnosis and definition of treatment-resistant depression. *Biological Psychiatry*, 53, 649–659.
- Ferraye, M. U., Debu, B., Fraix, V., Goetz, L., Ardouin, C., Yelnik, J., et al. (2010). Effects of pedunculopontine nucleus area stimulation on gait disorders in Parkinson's disease. *Brain*, 133, 205–214.
- Garcia-Rill, E., & Skinner, R. D. (1987a). The mesencephalic locomotor region. I. Activation of a medullary projection site. *Brain Research*, 411, 1–12.
- Garcia-Rill, E., & Skinner, R. D. (1987b). The mesencephalic locomotor region. II. Projections to reticulospinal neurons. *Brain Research*, 411, 13–20.
- Goldapple, K., Segal, Z., Garson, C., Lau, M., Bieling, P., Kennedy, S., et al. (2004). Modulation of cortical-limbic pathways in major depression: Treatment-specific effects of cognitive behavior therapy. *Archives of General Psychiatry*, 61, 34–41.
- Gradinaru, V., Mogri, M., Thompson, K. R., Henderson, J. M., & Deisseroth, K. (2009). Optical deconstruction of parkinsonian neural circuitry. *Science*, 324, 354–359.
- Guridi, J., Obeso, J. A., Rodriguez-Oroz, M. C., Lozano, A. A., & Manrique, M. (2008). L-dopa-induced dyskinesia and stereotactic surgery for Parkinson's disease. *Neurosurgery*, 62, 311–323 discussion 323–325.
- Hamani, C., McAndrews, M. P., Cohn, M., Oh, M., Zumsteg, D., Shapiro, C. M., et al. (2008). Memory enhancement induced by hypothalamic/fornix deep brain stimulation. *Annals of Neurology*, 63, 119–123.
- Han, X., & Boyden, E. S. (2007). Multiple-color optical activation, silencing, and desynchronization of neural activity, with single-spike temporal resolution. *PloS One*, 2, e299.
- Hariz, M. I., Krack, P., Alesch, F., Augustinsson, L. E., Bosch, A., Ekberg, R., et al. (2008). Multicentre European study of thalamic stimulation for parkinsonian tremor:

- A 6 year follow-up. *Journal of Neurology, Neurosurgery, and Psychiatry*, 79, 694–699.
- Hausdorff, J. M., Gruendlinger, L., Scollins, L., O'Herron, S., & Tarsy, D. (2009). Deep brain stimulation effects on gait variability in Parkinson's disease. *Movement Disorders*, 24, 1688–1692.
- Hely, M. A., Reid, W. G., Adena, M. A., Halliday, G. M., & Morris, J. G. (2008). The Sydney multicenter study of Parkinson's disease: The inevitability of dementia at 20 years. *Movement Disorders*, 23, 837–844.
- Johnsen, E. L., Mogensen, P. H., Sunde, N. A., & Ostergaard, K. (2009). Improved asymmetry of gait in Parkinson's disease with DBS: Gait and postural instability in Parkinson's disease treated with bilateral deep brain stimulation in the subthalamic nucleus. *Movement Disorders*, 24, 590–597.
- Karachi, C., Grabli, D., Bernard, F. A., Tande, D., Wattiez, N., Belaid, H., et al. (2010). Cholinergic mesencephalic neurons are involved in gait and postural disorders in Parkinson disease. *The Journal of Clinical Investigation*, 120, 2745–2754.
- Laxton, A. W., Tang-Wai, D. F., McAndrews, M. P., Zumsteg, D., Wennberg, R., Keren, R., et al. (2011). A phase I trial of deep brain stimulation of memory circuits in Alzheimer's disease. *Annals of Neurology*, 68, 521–534.
- Lozano, A. M., Mayberg, H. S., Giacobbe, P., Hamani, C., Craddock, R. C., & Kennedy, S. H. (2008). Subcallosal cingulate gyrus deep brain stimulation for treatment-resistant depression. *Biological Psychiatry*, 64, 461–467.
- Mayberg, H. S., Brannan, S. K., Tekell, J. L., Silva, J. A., Mahurin, R. K., McGinnis, S., et al. (2000). Regional metabolic effects of fluoxetine in major depression: Serial changes and relationship to clinical response. *Biological Psychiatry*, 48, 830–843.
- Mayberg, H. S., Liotti, M., Brannan, S. K., McGinnis, S., Mahurin, R. K., Jerabek, P. A., et al. (1999). Reciprocal limbic-cortical function and negative mood: Converging PET findings in depression and normal sadness. *The American Journal of Psychiatry*, 156, 675–682.
- Mayberg, H. S., Lozano, A. M., Voon, V., McNeely, H. E., Seminowicz, D., Hamani, C., et al. (2005). Deep brain stimulation for treatment-resistant depression. *Neuron*, 45, 651–660.
- Mayeux, R., & Sano, M. (1999). Treatment of Alzheimer's disease. *The New England Journal of Medicine*, 341, 1670–1679.
- Mazzone, P., Sposato, S., Insola, A., Dilazzaro, V., & Scarnati, E. (2008). Stereotactic surgery of nucleus tegmenti pedunculopontine [corrected]. *British Journal of Neurosurgery*, 22(Suppl. 1), S33–S40.
- Moro, E., Hamani, C., Poon, Y. Y., Al-Khairallah, T., Dostrovsky, J. O., Hutchison, W. D., et al. (2010a). Unilateral pedunculopontine stimulation improves falls in Parkinson's disease. *Brain*, 133, 215–224.
- Moro, E., Lozano, A. M., Pollak, P., Agid, Y., Rehncrona, S., Volkmann, J., et al. (2010b). Long-term results of a multi-center study on subthalamic and pallidal stimulation in Parkinson's disease. *Movement Disorders*, 25, 578–586.
- Nagel, G., Ollig, D., Fuhrmann, M., Kateriya, S., Musti, A. M., Bamberg, E., et al. (2002). Channelrhodopsin-1: A light-gated proton channel in green algae. *Science*, 296, 2395–2398.
- Nobler, M. S., Oquendo, M. A., Kegeles, L. S., Malone, K. M., Campbell, C. C., Sackeim, H. A., et al. (2001). Decreased regional brain metabolism after ect. *The American Journal of Psychiatry*, 158, 305–308.
- Okun, M. S., Fernandez, H. H., Wu, S. S., Kirsch-Darrow, L., Bowers, D., Bova, F., et al. (2009). Cognition and mood in Parkinson's disease in subthalamic nucleus versus globus pallidus interna deep brain stimulation: The COMPARE trial. *Annals of Neurology*, 65, 586–595.
- Orlovsky, G. N., Severin, F. V., & Shik, M. L. (1966). Locomotion elicited by midbrain stimulation (trans. Russian). *Proceedings of the Academy of Sciences of the USSR*, 169, 1223–1226.
- Pahapill, P. A., & Lozano, A. M. (2000). The pedunculopontine nucleus and Parkinson's disease. *Brain*, 123(Pt 9), 1767–1783.
- Parsons, T. D., Rogers, S. A., Braaten, A. J., Woods, S. P., & Troster, A. I. (2006). Cognitive sequelae of subthalamic nucleus deep brain stimulation in Parkinson's disease: A meta-analysis. *Lancet Neurology*, 5, 578–588.
- Pereira, E. A., Muthusamy, K. A., De Pennington, N., Joint, C. A., & Aziz, T. Z. (2008). Deep brain stimulation of the pedunculopontine nucleus in Parkinson's disease. Preliminary experience at Oxford. *British Journal of Neurosurgery*, 22(Suppl. 1), S41–S44.
- Powell, T. P. S., Guillory, R. W., & Cowan, W. M. (1957). A quantitative study of the fornix-mammillothalamic system. *Journal of Anatomy*, 91, 419–432.
- Rodrigues, A. M., Rosas, M. J., Gago, M. F., Sousa, C., Fonseca, R., Linhares, P., et al. (2010). Suicide attempts after subthalamic nucleus stimulation for Parkinson's disease. *European Neurology*, 63, 176–179.
- Schrag, A. (2006). Quality of life and depression in Parkinson's disease. *Journal of the Neurological Sciences*, 248, 151–157.
- Seminowicz, D. A., Mayberg, H. S., McIntosh, A. R., Goldapple, K., Kennedy, S., Segal, Z., et al. (2004). Limbic-frontal circuitry in major depression: A path modeling metanalysis. *NeuroImage*, 22, 409–418.
- Shapiro, M. B., Vaillancourt, D. E., Sturman, M. M., Metman, L. V., Bakay, R. A., & Corcos, D. M. (2007). Effects of STN DBS on rigidity in Parkinson's disease. *IEEE Transactions on Neural Systems and Rehabilitation Engineering*, 15, 173–181.

- Shik, M. L., Severin, F. V., & Orlovsky, G. N. (1969). Control of walking and running by means of electrical stimulation of the mesencephalon. *Electroencephalography and Clinical Neurophysiology*, 26, 549.
- Stefani, A., Lozano, A. M., Peppe, A., Stanzione, P., Galati, S., Tropepi, D., et al. (2007). Bilateral deep brain stimulation of the pedunculopontine and subthalamic nuclei in severe Parkinson's disease. *Brain*, 130, 1596–1607.
- Tabbal, S. D., Ushe, M., Mink, J. W., Revilla, F. J., Wernle, A. R., Hong, M., et al. (2008). Unilateral subthalamic nucleus stimulation has a measurable ipsilateral effect on rigidity and bradykinesia in Parkinson disease. *Experimental Neurology*, 211, 234–242.
- Timmermann, L., Braun, M., Groiss, S., Wojtecki, L., Ostrowski, S., Krause, H., et al. (2008). Differential effects of levodopa and subthalamic nucleus deep brain stimulation on bradykinesia in Parkinson's disease. *Movement Disorders*, 23, 218–227.
- Vann, S. D., Tsivilis, D., Denby, C. E., Quamme, J. R., Yonelinas, A. P., Aggleton, J. P., et al. (2009). Impaired recollection but spared familiarity in patients with extended hippocampal system damage revealed by 3 convergent methods. *Proceedings of the National Academy of Sciences of the United States of America*, 106, 5442–5447.
- Weaver, F. M., Follett, K., Stern, M., Hur, K., Harris, C., Marks, W. J. Jr., et al. (2009). Bilateral deep brain stimulation vs best medical therapy for patients with advanced Parkinson disease: A randomized controlled trial. *The Journal of the American Medical Association*, 301, 63–73.
- Williams, A., Gill, S., Varma, T., Jenkinson, C., Quinn, N., Mitchell, R., et al. (2010). Deep brain stimulation plus best medical therapy versus best medical therapy alone for advanced Parkinson's disease (PD SURG trial): A randomised, open-label trial. *Lancet Neurology*, 9, 581–591.
- Witt, K., Daniels, C., Reiff, J., Krack, P., Volkmann, J., Pinsker, M. O., et al. (2008). Neuropsychological and psychiatric changes after deep brain stimulation for Parkinson's disease: A randomised, multicentre study. *Lancet Neurology*, 7, 605–614.
- World Health Organization. Chapter 2: Burden of mental and behavioral disorders.* (2001). In *The WHO report 2001: Mental health, new understanding, New Hope*, <http://www.who.int/whr/2001/en/>. accessed July18, 2011.
- York, M. K., Dulay, M., Macias, A., Levin, H. S., Grossman, R., Simpson, R., et al. (2008). Cognitive declines following bilateral subthalamic nucleus deep brain stimulation for the treatment of Parkinson's disease. *Journal of Neurology, Neurosurgery, and Psychiatry*, 79, 789–795.
- Zangaglia, R., Pacchetti, C., Pasotti, C., Mancini, F., Servello, D., Sinforiani, E., et al. (2009). Deep brain stimulation and cognitive functions in Parkinson's disease: A three-year controlled study. *Movement Disorders*, 24, 1621–1628.
- Zhang, F., Gradinaru, V., Adamantidis, A. R., Durand, R., Airan, R. D., de Lecea, L., et al. (2010). Optogenetic interrogation of neural circuits: Technology for probing mammalian brain structures. *Nature Protocols*, 5, 439–456.
- Zhang, F., Wang, L. P., Brauner, M., Liewald, J. F., Kay, K., Watzke, N., et al. (2007). Multimodal fast optical interrogation of neural circuitry. *Nature*, 446, 633–639.

CHAPTER 7

Development of neuromodulation treatments in a large animal model—Do neurosurgeons dream of electric pigs?

J. C. Sørensen^{†,*}, M. S. Nielsen[†], F. Rosendal[†], D. Deding[†], K. S. Ettrup[†],
K. N. Jensen[†], R. L. Jørgensen[†], A. N. Glud[†], K. Meier[†], L. M. Fitting[†], A. Møller^{‡,§},
A. K. O. Alstrup[‡], L. Østergaard[§] and C. R. Bjarkam[†]

[†] Center for Experimental Neuroscience (CENSE), Department of Neurosurgery, Aarhus University Hospital,
Århus C, Denmark

[‡] PET Center, Aarhus University Hospital, Århus C, Denmark

[§] Center for Functionally Integrated Neuroscience (CFIN), Aarhus University Hospital,
Århus C, Denmark

Abstract: The Göttingen minipig has been established as a translational research animal for neurological and neurosurgical disorders. This animal has a large gyrencephalic brain suited for examination at sufficient resolution with conventional clinical scanning modalities. The large brain, further, allows use of standard neurosurgical techniques and can accommodate clinical neuromodulatory devices such as deep brain stimulation (DBS) electrodes and encapsulated cell biodelivery devices making the animal ideal for basic scientific studies on neuromodulation mechanisms and preclinical tests of new neuromodulation technology for human use. The use of the Göttingen minipig is economical and does not have the concerns of the public associated with the experimental use of primates, cats, and dogs, thus providing a cost-effective research model for translation of rodent data before clinical trials are initiated.

Keywords: neuromodulation; translational neuroscience; large animal models; minipig; mini swine; neurodegenerative disorders; deep brain stimulation; spinal cord stimulation; stem cells; encapsulated cells; stereotaxic surgery; high-tesla MRI.

*Corresponding author.

Tel.: +45-8949-3461; Fax: +45-8949-3410
E-mail: jenssore@rm.dk

Introduction

The aim of our translational research is to examine mechanisms of action and develop new treatment paradigms of neuromodulation in a large nonprimate animal model.

Over the past 14 years, the CENSE group has worked to establish the Göttingen minipig as a research animal for neurological and neurosurgical disorders. The advantage of this animal is that it has a large gyrencephalic brain that can be examined at sufficient resolution using conventional clinical scanning modalities (Andersen et al., 2005; Cumming et al., 2001, 2003; Danielsen et al., 1998, 2000; Watanabe et al., 2001). The large brain, furthermore, enables the use of deep brain stimulation (DBS) electrodes and other neuromodulatory devices for human use, making the animal ideal for preclinical tests of new neuromodulation technology (Bjarkam et al., 2005, 2008, 2010; Dalmose et al., 2004; Fjord-Larsen et al., 2010; Glud et al., 2010; Jensen et al., 2009). The use of the Göttingen minipig is economical and without the concerns of the public, associated with the experimental use of primates, cats, and dogs (Goodman and Check, 2002).

In a minipig model of DBS toward Parkinson's disease, we have examined mechanisms of action of this treatment with positron emission tomography (PET) imaging (Nielsen, 2010). The model has been further developed with quantitative behavioral data and neurostereology (Nielsen, 2010; Nielsen et al., 2009).

Minipig models of stem cell transplantation to the central nervous system (CNS) has been established (Cumming et al., 2001; Danielsen et al., 2000), to serve as a test platform for the *in vivo* characterization of stem cell lines developed toward neurodegenerative diseases and CNS cancer. The model also serves as a test system for new delivery systems for stem cell transfer to the CNS (Bjarkam et al., 2010).

The minipig model is also being used for pre-clinical testing of encapsulated cell biodelivery

(ECB) for neurotrophic factor delivery to the brain (Fjord-Larsen et al., 2010).

Studies concerning the possible role of Brodmann area 25 DBS for depression, hypothalamic DBS in the treatment of adiposity, and pontine DBS toward central bladder regulation dysfunction are ongoing (Dalmose et al., 2004; Ettrup et al., 2010). Finally, we use the minipig to address the mechanisms of action of spinal cord stimulation for pain.

In conclusion, the minipig provides a cost-effective research model allowing further elucidation of rodent data on neuromodulation and safety testing of neuromodulation equipment for human use before clinical patient trials are initiated. The model also allows use and safety testing of neuromodulation equipment for human use. Finally, it provides a platform for the examination of mechanisms of action of neuromodulatory treatments.

The Göttingen minipig as a neurobiological research animal

Pigs have been used for surgical training and as physiological nonprimate research model for several decades at our University center. It was therefore a logical step to use this animal as a translational platform to develop and test neuromodulation treatments intended for human use. As the landrace pigs grow to an inconvenient size (250–300 kg), we chose the Göttingen minipig (20–40 kg adult weight) as our experimental animal for chronic studies, whereas young Landrace animals can be used for acute studies (Bollen et al., 2010). This also lay to rest the public and economical concerns that have hampered the use of primates for neurobiological research (Goodman and Check, 2002).

The Göttingen minipig was originally bred at the University of Göttingen (Germany), from a crossing between the Minnesota minipig and the Vietnamese potbelly swine (Lind et al., 2007).

In 1992, a small colony of the white Göttingen minipig was brought to the Ellegaard farm in Denmark where it is now bread under specific pathogen free conditions. The Göttingen minipig used for our neuromodulation studies are standardized laboratory animals, with a well-defined genetic background and health status. They are mild-tempered, shy, and easy to handle (Bollen et al., 2010).

Neuroimaging in the Göttingen minipig

The minipig has a gyrencephalic, and relatively large, brain, with a weight of 60–90 g (depending on age), and 6 × 5 × 4 cm in adult dimensions (Bjarkam et al., 2005). The cranium of the minipig is pneumatized with a large frontal sinus, which can prove a challenge in both imaging and surgery (Bjarkam et al., 2005). The minipigs are anesthetized, intubated, and maintained on artificial ventilation during all imaging procedures (Ettrup et al., 2011). Human-sized scanner beds fit the minipigs and magnetic resonance imaging (MRI) compatible head holders have been developed for minipig use (Bjarkam et al., 2004, 2005, 2009). At our center, we can use CT, MRI, and PET imaging for visualizing the minipig brain (Andersen et al., 2005; Cumming et al., 2001, 2003; Danielsen et al., 1998, 2000; Rosendal et al., 2009a,b, 2010; Watanabe et al., 2001). The scanning modality depending on the hypotheses and the experimental paradigm.

Neurosurgery in the Göttingen minipig

Just as for the imaging procedures, the minipigs are anesthetized, intubated, and maintained on artificial ventilation during surgical procedures (Ettrup et al., 2011). To facilitate surgery and stereotaxic procedures, the head of the minipig is fixed in a head holder that also functions as an MRI compatible localizer box (Bjarkam et al., 2004, 2005, 2008, 2009). Access to the minipig

brain is achieved with standard neurosurgical technique and instruments, such as high-speed drills, fine tipped aspirators, bipolar coagulation, etc. The equipment used is the same as for human neurosurgical procedures. For stereotaxic, high-precision placement of DBS electrodes, intracerebral microinjections of stem cells, and encapsulated biodelivery devices, a stereotaxic MRI is performed prior to the surgery followed by calculation of the stereotaxic coordinates for the target site (Bjarkam et al., 2004, 2005, 2009). The calculation can be based on an implanted fiducial marker or by external fiducials in the side plates of the head holder. The latter allows import of the MR images into standard neuro-navigation systems (Fig. 1f) and a precision in the stereotaxic targeting that equals that in routine clinical use (Bjarkam et al., 2009). The minipigs tolerate the anesthesia and surgery well and complications (bleeding, infections) are few.

Neural and stem cell transplantation in the Göttingen minipig

In an MPTP minipig model of Parkinson's disease, we have tested the feasibility of neural cell transplantation (Cumming et al., 2001; Danielsen et al., 2000), grafting neural tissue from the ventral mesencephalon of 28-week old pig embryos. The grafts were stereotactically placed in the dopamine-depleted striatum of adult parkinsonian minipigs. PET imaging revealed increased fluorodopa uptake in the transplantation sites, and after 7 months, postmortem analysis revealed surviving grafts (Cumming et al., 2001; Danielsen et al., 2000). Subsequent experimental paradigms have included implantation of stem cells, using a newly developed intracerebral microinjection device (Bjarkam et al., 2010), in the minipig striatum, and stereotaxic implantation of lentiviruses, carrying an alpha-synuclein construct, into the minipig substantia nigra in order to overexpress alpha-synuclein locally in transfected nigral neurons (Glud et al., 2010).



Fig. 1. (a) Adult Göttingen minipig in its pen. (b) Intubated minipig in stereotactic MRI compatible localizer box with fiducial side plates attached. (c) DBS electrode being stereotactically inserted into the minipig hypothalamus by use of Frederic Hayer Company (FHC) micromanipulator (www.fh-co.com) attached to a Surgiplan compatible stereotaxic arch system. (d) Two burr holes with DBS electrodes fixed by titanium microplates to the scull. (e) Implantable impulse generator, with the distal ends of the DBS electrodes attached, being implanted into a subcutaneous pocket above the scapula in the neck region of the minipig. (f) Postoperative control MRI imported into the Surgiplan system showing calculated trajectories for the DBS electrodes and dark artifacts from the tips of the electrodes (seen just above the green target crosshair).

In a series of good laboratory practice (GLP) monitored studies, we have, in collaboration with the biotech company NsGene A/S, shown that nerve growth factor (NGF) and glia derived nerve growth factor (GDNF) producing encapsulated cells survive implantation and expand in their ECB device and that the neurotrophic factors diffuse out into the brain parenchyma in therapeutic amounts (Fjord-Larsen et al., 2010). This has led to a preclinical test in Alzheimer patients.

Deep brain stimulation in the Göttingen minipig

In order to examine the mechanism of action of DBS for Parkinson's disease, we implanted the DBS system for patients into an MPTP minipig model of Parkinson's disease. The DBS was unilateral and resulted in improved motor performance on the side contralateral to the stimulation, leading to rotational behavior (Bjarkam et al., 2005). The PET studies revealed increased blood flow around the stimulation site in the subthalamic nucleus (STN) and increased oxygen uptake in the motor cortex leading us to the hypothesis that DBS for Parkinson's disease results in a normalization of the neural signaling in the basal ganglia system.

Newer paradigms have involved targeting the subgenual area (Brodmann area 25 analogue) in the minipig to establish a DBS treatment model of depression.

We have, likewise, targeted the minipig ventral hypothalamus with DBS to induce satiety in the minipig as a potential treatment for obesity (Fig. 1).

Finally, we have targeted the pontine micturition center and achieved central control of voiding in the minipig (Dalmose et al., 2004; Jensen et al., 2009).

Spinal cord stimulation in the Göttingen minipig

Although spinal cord stimulation is an established clinical treatment for severe chronic pain

syndromes, we have not clarified its mechanism of action. The treatment involves placement of an electrode in the epidural space over spinal cord segments innervating the dermatome inflicted by chronic pain. We have accordingly set out to map the dermatomes of the minipig, and with this neuroanatomical information, we intend to address the mechanism of action of the treatment by functional imaging modalities.

Conclusion and perspectives

Minipigs are increasingly recognized as useful animals for neuromodulation research.

The characteristics that make them particularly useful for this purpose are:

1. Convenient body size for most clinical neuromodulatory and surgical experiments or trials involving repeated collection of blood samples, biopsies, etc.
2. Similarities with the biology of the human, in particular with respect to, for example, brain, immune mechanism, heart and blood vessels, lung, liver and kidney, and physiological stage of the newborn.
3. The ease of handling and housing under confined conditions.
4. The relatively low price at which they can be made available
5. The use of pigs in research is generally accepted in the public.
6. The pig model provides a unique translational platform to develop and test innovative therapeutic approaches whether pharmacologic or surgical.

With the title reference to the novel of Philip K. Dick, we not only dream of electric minipigs but also want to emphasize the potential for translational research and preclinical testing of neuromodulatory treatments that we have uncovered by the use of this animal.

Acknowledgments

The authors gratefully acknowledge the collaboration and technical assistance of Ms. Dorete Jensen, Ms. Trine W Mikkelsen, Mr. Albert Meier, Mr. Mogens Koed, Mr. Graziano Cancian, the staff and researchers at the Institute of Clinical Medicine, Påskehøjgård, and at the animal research center Foulum, Aarhus University, Dr. Lars Wahlberg and the staff at NsGene A/S, Dr. Miles Cunningham, Mc Lean Hospital, Harvard University, Professor Jens Zimmer and the Staff at Institute of Biomedical Research, University of Southern Denmark.

The studies have been supported financially by the Danish Research Council, The Lundbeck Foundation, and the Karen Elise Jensen Foundation.

References

- Andersen, F., Watanabe, H., Bjarkam, C. R., Danielsen, E. H., & Cumming, P. The DaNeX Study Group. (2005). Pig brain stereotaxic standard space: Mapping of cerebral blood flow normative values and effect of MPTP-lesioning. *Brain Research Bulletin*, 66(1), 17–29.
- Bjarkam, C. R., Cancian, G., Glud, A. N., Ettrup, K. S., Østergaard, L., & Sørensen, J. C. (2009). Isocentric MRI-guided stereotaxic procedures in pigs based on a stereotaxic localizer box fitted with an adapted Leksell frame and use of related clinical computer-planning software. *Journal of Neuroscience Methods*, 183(2), 119–126.
- Bjarkam, C. R., Cancian, G., Larsen, M., Rosendal, F., Ettrup, K. S., Zeidler, D., et al. (2004). A MRI-compatible stereotaxic localizer box enables high-precision stereotaxic procedures in quadrupeds. *Journal of Neuroscience Methods*, 139, 293–298.
- Bjarkam, C. R., Glud, A. N., Margolin, L., Reinhart, K., Franklin, R., Deding, D., et al. (2010). Safety and function of a new clinical intracerebral microinjection instrument (IMI) for stem cells and therapeutics examined in the Göttingen minipig. *Stereotactic and Functional Neurosurgery*, 88(1), 56–63.
- Bjarkam, C. R., Jorgensen, R. L., Jensen, K. N., Sunde, N. A., & Sørensen, J. C. (2008). Deep brain stimulation electrode anchoring using BioGlue®, a protective electrode covering, and a titanium microplate. *Journal of Neuroscience Methods*, 168, 151–155.
- Bjarkam, C. R., Larsen, M., Watanabe, H., Røhl, L., Simonsen, C. Z., Pedersen, M., et al. (2005). A porcine model of subthalamic high-frequency deep brain stimulation in Parkinson's disease. In M. J. Willow (Ed.), *Chapter 5 in Parkinson's disease: New research*. New York: Nova Science Publishers, 1-59454-352-6.
- Bollen, P. J. A., Hansen, A. K., & Alstrup, A. K. O. (2010). *The laboratory swine* (2nd ed.). Boca Raton, London, New York, Washington: CRC Press, 0-8493-1035-0.
- Cumming, P., Danielsen, E. H., Vafaee, M., Falborg, L., Steffensen, E., Sorensen, J. C., et al. (2001). Normalization of markers for dopamine innervation in striatum of MPTP-lesioned miniature pigs with intrastratal grafts. *Acta Neurologica Scandinavica*, 103(5), 309–315.
- Cumming, P., Gillings, N. M., Jensen, S. B., Bjarkam, C. R., & Gjedde, A. (2003). Kinetics of the uptake and distribution of the dopamine D_{2/3} agonist (R)-N-[1-11C]n-propylnorapomorphine in brain of healthy and MPTP-poisoned Gottingen miniature pigs. *Nuclear Medicine and Biology*, 30 (5), 547–553.
- Dalmose, A. L., Bjarkam, C. R., Sørensen, J. C., Djurhuus, J. C., & Jørgensen, T. M. (2004). Effects of high frequency deep brain stimulation on urine storage and voiding function in conscious minipigs. *Neurourology and Urodynamics*, 23, 265–272.
- Danielsen, E. H., Cumming, P., Andersen, F., Bender, D., Brevig, T., Falborg, L., et al. (2000). The DaNEX study of embryonic mesencephalic, dopaminergic tissue grafted to a minipig model of Parkinson's disease: Preliminary findings of effect of MPTP poisoning on striatal dopaminergic markers. *Cell Transplantation*, 9, 247–259.
- Danielsen, E. H., Smith, D. F., Poulsen, P. H., Østergaard, L., Gee, A., Ishizu, K., et al. (1998). Positron emission tomography of living brain in minipigs and domestic pigs. *Scandinavian Journal of Laboratory Animal Science*, 25(Suppl. 1), 127–135.
- Ettrup, K. S., Glud, A. N., Orlowski, D., Fitting, L. M., Meier, K., Sørensen, J. C., et al. (2011). Basic surgical techniques in the Göttingen minipig: Intubation, transurethral bladder catheterization, femoral vessel catheterization, and transcardial perfusion. *Journal of Visualized Experiments*, (www.jove.com/details.php?id=2652).
- Ettrup, K., Sørensen, J. C., & Bjarkam, C. R. (2010). The anatomy of the Göttingen minipig hypothalamus. *Journal of Chemical Neuroanatomy*, 39(3), 151–165.
- Fjord-Larsen, L., Kusk, P., Tornøe, J., Juliusson, B., Torp, M., Bjarkam, C. R., et al. (2010). Long-term delivery of nerve growth factor by encapsulated cell biodelivery in the Göttingen minipig basal forebrain. *Molecular Therapy*, 18 (12), 2164–2172.
- Glud, A. N., Hedegaard, C., Nielsen, M. S., Sørensen, J. C., Bendixen, C., Jensen, P. H., et al. (2010). Direct gene transfer in the Göttingen minipig CNS using stereotaxic lentiviral microinjections. *Acta Neurobiologiae Experimentalis*, 70, 1–8.

- Goodman, S., & Check, E. (2002). The great primate debate. *Nature*, 417, 684–687.
- Jensen, K. N., Deding, D., Sørensen, J. C., & Bjarkam, C. R. (2009). Long-term implantation of deep brain stimulation electrodes in the pontine micturition centre of the Göttingen minipig. *Acta Neurochirurgica*, 151(7), 785–794.
- Lind, N. M., Moustgaard, A., Jelsing, J., Vajta, G., Cumming, P., & Hansen, A. K. (2007). The use of pigs in neuroscience: Modeling brain disorders. *Neuroscience and Biobehavioral Reviews*, 31(5), 728–751.
- Nielsen, M. S. (2010). *Progressive Parkinson's disease in the Göttingen minipig based on continuous MPTP intoxication*. PhD thesis, Faculty of Health Sciences, Aarhus University, Denmark.
- Nielsen, M. S., Sørensen, J. C., & Bjarkam, C. R. (2009). The substantia nigra pars compacta of the Göttingen minipig: An anatomical and stereological study. *Brain Structure & Function*, 213(4–5), 481–488.
- Rosendal, F., Chakravarty, M. M., Sunde, N., Rodell, A., Jonsdottir, K. Y., Pedersen, M., et al. (2010). Defining the intercommissural plane and stereotactic coordinates for the basal ganglia in the Göttingen minipig brain. *Stereotactic and Functional Neurosurgery*, 88(3), 138–146.
- Rosendal, F., Frandsen, J., Chakravarty, M. M., Bjarkam, C. R., Pedersen, M., Sangill, R., et al. (2009). New surgical technique reduces the susceptibility artefact at air-tissue interfaces on in vivo cerebral MRI in the Göttingen minipig. *Brain Research Bulletin*, 80(6), 403–407.
- Rosendal, F., Pedersen, M., Sangill, R., Stødkilde-Jørgensen, H., Nielsen, M. S., Bjarkam, C. R., et al. (2009). MRI protocol for in vivo visualization of the Göttingen minipig brain improves targeting in experimental functional neurosurgery. *Brain Research Bulletin*, 79(1), 41–45.
- Watanabe, H., Andersen, F., Simonsen, C. Z., Evans, S. M., Gjedde, A., Cumming, P., et al. (2001). MR-based statistical atlas of the Göttingen minipig brain. *NeuroImage*, 14, 1089–1096.

CHAPTER 8

A few examples of the contribution of animal research in rodents for clinical application of deep brain stimulation

Christelle Baunez^{†,‡,§,*}

[†] Laboratoire de Neurobiologie de la Cognition (LNC), Université de Provence, Marseille, France

[‡] CNRS, UMR6155, Marseille, France

[§] Aix-Marseille Université, Marseille, France

Abstract: In the late 1980s, deep brain stimulation has regained interest for the treatment of neurological disorders. The first spectacular application has been developed for the treatment of Parkinson's disease. This development has been the result of interactions between clinical observations and studies carried out in animal models. Further investigations in animal models have lead to consider not only possible side effects of DBS on nonmotor functions in parkinsonian patients but also DBS as a possible strategy for other diseases, including psychiatric disorders such as obsessive compulsive disorder or addiction.

Keywords: basal ganglia; subthalamic nucleus; nucleus accumbens; lesion; reaction time; attention; motivation; behavior; impulsivity; obsessive compulsive disorder; nonmotor functions.

Introduction

The application of deep brain stimulation (DBS) for the treatment of Parkinson's disease (PD) represents a nice example of interaction between clinical and basic research, which has been reported in Chapter 5.

Following the finding that lesion of the subthalamic nucleus (STN) could alleviate some parkinsonian signs in parkinsonian monkeys (Bergman et al., 1990), Benazzouz and colleagues were the first to show that unilateral STN high-frequency stimulation (HFS) applied in monkeys rendered hemiparkinsonian with 1-methyl-4-phenyl-1,2,3,6-tetrahydropyridine (MPTP) alleviated the muscular rigidity observed in the contralateral forelimb (Benazzouz et al., 1993). This pioneer work was actually at the origin of the idea to

*Corresponding author.

Tel.: +33-41-3550937; Fax.: +33-41-3550958
E-mail: christelle.baunez@univ-provence.fr

apply HFS that had been initiated at the level of the thalamus, into the STN in PD patients. In the intact monkey, it was also shown that STN HFS could induce hyperkinetic movements similar to the hemiballism observed after STN lesions (Beurrier et al., 1997). In contrast to what was described after STN lesions, STN HFS does not seem to induce hyperkinetic movements when applied at certain voltage to MPTP monkeys and when compared to L-3,4-dihydroxyphenylalanine effects (Benazzouz et al., 1996). Application of STN HFS in PD patients was first performed by the group of Benabid in Grenoble, France (Limousin et al., 1995) and is currently used worldwide with great success. However, there are still remaining questions regarding its mechanism of action that are still under investigation in both patients and animal models (see for review Gubellini et al., 2009).

The use of animal models has been carried on further and not only could contribute to highlight some of the possible nonmotor side effects of STN DBS but also helped to assess the possible use of this surgical strategy for the treatment of other disorders such as obsessive compulsive disorder (OCD) and addiction. A few examples focused on the STN will be described in this chapter.

Nonmotor functions in PD

As reported above, the obvious beneficial effect of STN DBS on motor functions lead to extensive development of this therapeutic strategy with little consideration for the possible nonmotor side effects at the beginning, the basal ganglia being mainly considered as motor structures. However, when considering the connectivity of these structures, it is obvious that the STN belongs not only to the so-called motor loop but also to the associative and limbic loops (Alexander et al., 1986). Indeed, the STN receives direct connections from the prefrontal cortex, the ventral pallidum, and indirectly from the nucleus accumbens, all structures well known for their

involvement in nonmotor behavior such as attention, impulsivity, and motivation. It seems then logical to expect nonmotor disturbances after STN inactivation on these nonmotor processes.

STN lesions and DBS in a rat model of PD performing reaction time tasks

STN lesions

Based on Bergman's work in the monkey showing that STN lesion could alleviate some forms of motor deficit in the MPTP parkinsonian model (Bergman et al., 1990), we have first tested the effects of bilateral STN lesions in rats trained to perform a simple reaction time (RT) task. In this task, rats are required to press a lever down and sustain their paw on the lever until the presentation of a light (occurring after a foreperiod of 0.5, 0.75, 1, or 1.25 s), starting a 600 ms period during which the rat has to release the lever (RT). Not only this task allows a good measure of akinesia (lengthened RT), but it requires cognitive processes such as time estimation, attention, control of inhibition, etc. In this experiment, we have shown that lesioning the STN could indeed alleviate akinetic deficits induced by the 6-hydroxydopamine (6-OHDA) dopaminergic depletion, but induced another form of deficit expressed by increased early withdrawal of the lever (see Fig. 1; Baunez et al., 1995). This was the first publication reporting possible side effects of STN inactivation in PD that might be related to nonmotor dysfunctions related to attention or impulsivity.

STN DBS in rat model of PD

The first study published on STN HFS in freely moving rats performing behavioral tasks used unilateral stimulation in a hemiparkinsonian model consisting in a unilateral 6-OHDA lesion of the substantia nigra pars compacta/reticulata. In this

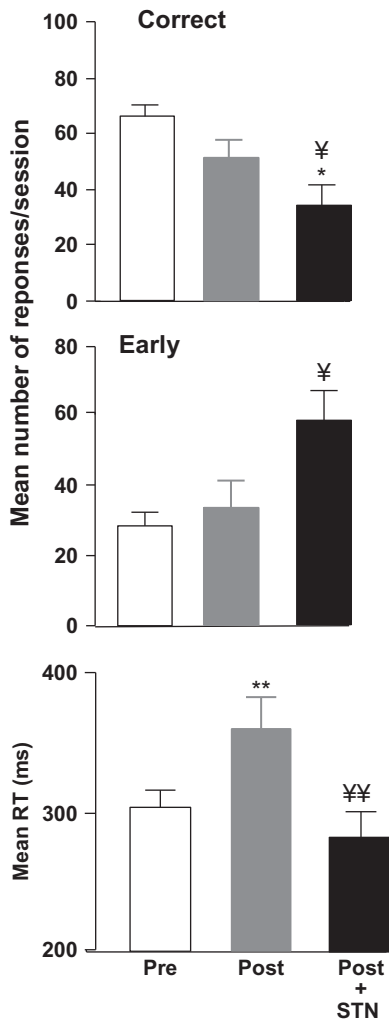


Fig. 1. Effects of STN lesions in a rat model of parkinsonism on the performance in the simple reaction time (RT) task (Baunez et al., 1995). The performance is illustrated in terms of number of correct responses/100 trial session before surgery (pre), after 6-OHDA lesion (pos t), and after STN lesion consecutive to 6-OHDA lesion (post + STN). The dopaminergic depletion of the dorsal striatum induced an akinetic-like deficit characterized by an increased RT. Performing a bilateral lesion of the STN in these animals alleviated this deficit, but affected further the performance in terms of correct responses because of a dramatic increase in the number of early withdrawals of the lever before the occurrence of the light. *, **: significantly different from preoperative performance, Y, YY: significantly different from postoperative performance (6-OHDA lesion effect), $p < 0.05$ and 0.01 , respectively.

work, we assessed both basic motor tasks such as haloperidol-induced catalepsy, apomorphine-induced circling behavior, as well as a choice RT task (Darbaky et al., 2003). The parameters were set at 130 Hz, 60–70 μ s pulse width and intensity set just below the threshold of hyperkinetic movements of the contralateral paw (range: 50–150 μ A). We showed that both the cataleptic state induced by haloperidol and the circling behavior induced by apomorphine in unilateral DA-depleted rats could be alleviated by unilateral STN HFS.

In a choice RT task, the rats were trained to hold their nose in a central hole until the presentation of a light in one of the adjacent holes and then respond by a nose-poke in the appropriate hole (Fig. 2a). After the dopaminergic unilateral depletion, only a few animals remained able to perform the task, as illustrated in Fig. 2b. Unfortunately, the STN HFS did not help the severely impaired animals. Thus, in contrast to the spectacular effect of STN HFS in PD patients, the stimulation applied in the rat could not overcome the profound deficit preventing the animals to perform the task. Interestingly, however, as illustrated in Fig. 2c, for those able to perform the task, STN HFS alleviated the deficit expressed as a decreased ability to initiate a response toward the side contralateral to the DA lesion (Darbaky et al., 2003). Our conclusion was that STN HFS could be beneficial for the treatment of motor deficit, but inefficient when the cognitive load was higher, suggesting that further cognitive studies were necessary and better assessment of cognitive functions in PD patients before and after STN DBS was important.

Interestingly, it has also been shown that bilateral STN HFS could alleviate the premature-responding deficit in a choice RT task at lower current intensity (3 μ A) than that reducing RT and MT (30 μ A) (Temel et al., 2005). This latter study provided the evidence that to treat cognitive and motor deficits, it may be necessary to apply HFS at a different intensity.

The evidences gained from these animal studies (Darbaky et al., 2003; Temel et al., 2005) seem thus

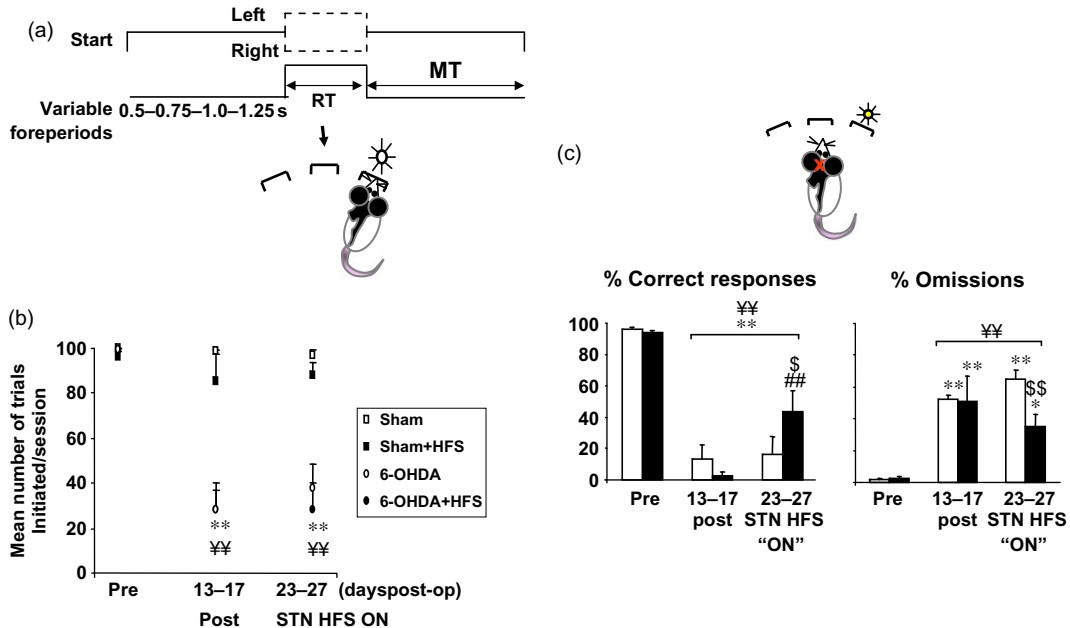


Fig. 2. Effects of STN HFS in a unilateral rat model of parkinsonism on the performance in the choice reaction time (RT) task (Darbaky et al., 2003). (a) Schematic diagram of the task. The rats initiate a trial by a nose-poke in the central hole. They have to hold this nose-poke until the occurrence of a light in one of the adjacent holes (left or right) at the end of the variable foreperiod. Then, rats have to withdraw their nose from the central hole and make a nose-poke in the appropriate (i.e., illuminated) hole to be rewarded by a food pellet. RT and MT (Movement Time) are measured in this task. They correspond respectively to the time elapsing between the occurrence of the light and the exit of the nose from the central hole and to the time elapsing between the exit of the central hole and the detection of the nose in the appropriate adjacent hole. (b) Mean number of the trials initiated per session before surgery (pre), after surgery with no HFS (post), and after surgery with STN HFS activated (STN HFS ON). (c) Performance of the animals still able to work after surgery for the trials in the contralateral side to the surgery. The performance is illustrated as the percentage of correct responses (left) and the percentage of omissions (right; i.e., no response within the 5 s following the presentation of the light).

to confirm that STN HFS applied at parameters inducing beneficial effects on motor functions does not necessarily correlate with beneficial cognitive effects. This observation has also been reported in human patients (Perriol et al., 2006). There are now indeed several studies reporting either further impairment, improvement or no effect by STN DBS in PD patients.

STN lesions and DBS in a rat model of PD performing an attentional task

As mentioned above, STN is connected with the prefrontal cortex (Monakow et al., 1978; Parent

and Hazrati, 1995) via a hyperdirect pathway, although this denomination has been used initially for the motor projections (Nambu, 2004). Inactivation of the STN can therefore be expected to affect “frontal functions” such as attention. This latter function has been investigated after STN lesions and HFS in rats.

STN lesions

We have used the “five-choice serial RT task” in which the animals are trained to wait and detect a brief visual stimulus that can be presented in

five possible various locations. The animals have to divide their attention between these five possible choices and then go and respond by a nose-poke in the appropriate location to obtain a food reward in a food magazine and then initiate the next trial. Using this specific visual attentional task, we have studied the effects of STN lesions first (Baunez and Robbins, 1997), and then of STN lesions combined with a bilateral DA depletion in the dorsal striatum (Baunez and Robbins, 1999a). We first showed that bilateral excitotoxic lesions of the STN induced multiple independent deficits in the task, such as impaired accuracy suggestive of an attentional deficit; an increased level of premature responses suggestive of increased impulsivity; an increased level of perseverative responses toward the response locations and toward the magazine where the animals collect the food reward, suggestive of deficit in response control; and an increased level of motivation for the reward (Baunez and Robbins, 1997). These results were the first to highlight the involvement of STN in cognitive functions. These results were replicated after blockade of the GABA receptors into the STN with muscimol (Baunez and Robbins, 1999b).

When lesioning the DA inputs to the dorsal striatum, we did not affect dramatically the level of performance in the attentional task: although there was a slight impairment in visual attention, most of the deficits were more motor related (omissions, increased latencies). Interestingly, when combining this lesion with STN lesions, the performance was further impaired. One of the most striking effects was observed on perseverative responses toward the food magazine, suggesting an increased level of motivation for the reward (Baunez and Robbins, 1999a). Further, in a study using a disconnection between the medial prefrontal cortex and the STN, by lesioning the prefrontal cortex on one side and the STN on the other side, we have given the first evidence of a functional role for the hyperdirect pathway in the attentional and perseverative deficits observed in this attentional task

(Chudasama et al., 2003). These results were highlighting the fact that inactivating the STN could affect attention and questioned the possibility to affect this function in PD patients subjected to an inactivation by DBS of STN. We then studied how STN HFS could induce similar effects to those observed after the lesion.

STN DBS

In intact and parkinsonian rats, we have tested the effects of bilateral STN HFS and could therefore compare them to those induced by bilateral excitotoxic STN lesions in the visual attentional task described above. For both intact and parkinsonian animals, the effects of STN HFS were slightly different to those induced by STN lesions (Baunez et al., 2007). Accuracy of performance as well as latency to make a correct response was only transiently affected, while no effect on premature responses could be seen (Fig. 3). Interestingly, the perseverative responses on both response location and reward magazine were found, in line with the lesion study. In parkinsonian rats, the subtle deficits recorded in the five-choices RT task were neither further deteriorated by bilateral STN HFS nor alleviated. The most striking effect was observed on the perseverative responses recorded in the food magazine that increased under STN HFS in both intact and DA-depleted rats, suggesting that STN HFS increases motivation for the food reward whatever the integrity of the DA system (Fig. 3; Baunez et al., 2007).

DBS for psychiatric disorders

Impulse control disorders–OCD

STN lesions and ICD

We first showed that bilateral excitotoxic lesions of the STN induced multiple independent deficits

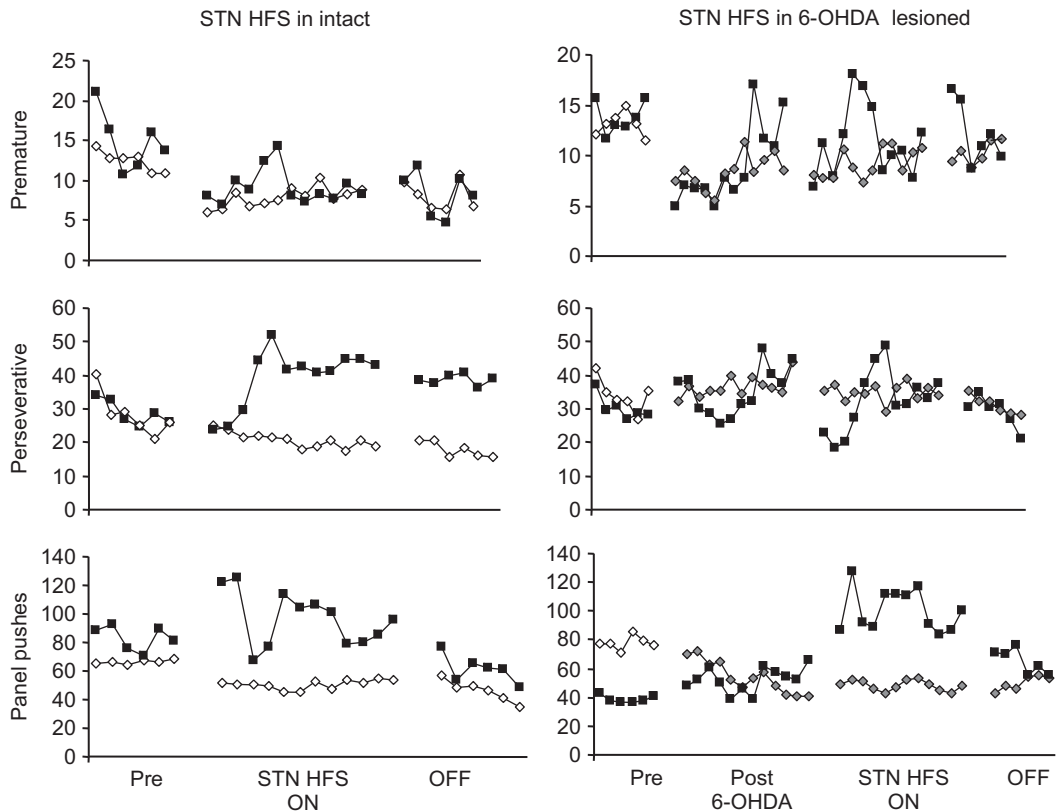


Fig. 3. Effects of bilateral high-frequency stimulation (HFS) of the STN in the five-choice serial reaction time task, applied in intact (left) and 6-OHDA-lesioned rats (right) (Baunez et al., 2007). The performance in the five-choice task is illustrated here for premature responses, perseverative responses, and perseverative entries into the food magazine (panel pushes) at the different stages of the experiment: during a block of six sessions before surgery (pre), during a block of six sessions after surgery without stimulation (post), during the first block of six sessions under STN HFS (stim 1), during the second block of six sessions under STN HFS (stim 2), and during a block of six sessions during which the stimulation was turned OFF (stim OFF). (a) Intact rats subjected (black squares) or not (open diamonds) to STN HFS. (b) 6-OHDA-lesioned animals remaining OFF STN HFS (gray diamonds) and 6-OHDA-lesioned animals subjected to STN HFS (black squares).

in the task, such as impaired accuracy suggestive of an attentional deficit; an increased level of premature responses suggestive of increased impulsivity; an increased level of perseverative responses toward the response locations and toward the magazine where the animals collect the food reward, suggestive of deficit in response control; and an increased level of motivation for the reward (Baunez and Robbins, 1997). These results were the first to highlight the involvement

of STN in cognitive functions. These results were replicated after blockade of the GABA receptors into the STN with muscimol (Baunez and Robbins, 1999b).

In both RT and attentional tasks, STN inactivation increased the number of premature and perseverative responses, suggesting a critical role for STN in the control of impulsivity (see for review Eagle and Baunez, 2010). It has also been reported that STN lesions induce perseverative

lever pressing in a signal attenuation task, a deficit qualified by the authors as “compulsive lever pressing” (Winter et al., 2008a).

Further studies have confirmed that STN lesion increases impulsive action, as expressed by a difficulty for the lesioned rats to stop an ongoing action in a stop-signal task (Eagle et al., 2008). In contrast, in a task measuring impulsive choice, STN lesion can help the animals to wait for a larger reward when given the choice between a small but immediate reward and a large but delayed reward (Winstanley et al., 2005). This latter result was confirmed by another group (Uslaner and Robinson, 2006) and questions whether or not the effect measured is more related to motivation than impulsivity in the task.

STN DBS and ICD

Interestingly, although the lesion of STN induces impulsivity and perseverative behavior, DBS does not always replicate these deficits, as illustrated in Fig. 3 (Baunez et al., 2007). Indeed, when applied in DA-depleted rats, STN HFS did not increase perseverative responses in the holes, but only the perseverations toward the magazine, suggesting that the detrimental effect of STN HFS in PD rats might be more related to motivation than to “compulsion.” Even though STN HFS did not reduce perseveration in our study (Baunez et al., 2007), it has been reported to reduce stereotyped behavior induced by quinpirole in rats (Winter et al., 2008b) or induced by bicuculline, a GABA antagonist, into the limbic GPe in the monkey (Baup et al., 2008). It might explain why, although based on lesion data obtained in rats, we would have argued against the choice of STN as a possible target for the treatment of OCD, the clinical studies using STN DBS report positive results to treat OCD (Mallet et al., 2002, 2008; Haynes and Mallet, 2010). Indeed STN DBS has been reported to abolish compulsions and decrease obsessions in PD patients with OCD comorbidity (Mallet et al., 2002). A recent study has actually shown that PD patients with impulse

control disorders exhibit an activity in the ventral STN that is coherent with premotor frontal cortical activity, highlighting a role for the “associative-limbic” hyperdirect pathway in impulse control disorders (Rodriguez-Oroz et al., 2011).

Based on the topographic organization of the STN (Mallet et al., 2007), when the stimulation was applied at the border of the associative and limbic territories (antero-ventral), HFS has a beneficial effect in OCD patients (Mallet et al., 2008).

Regarding OCD, it is important to note that, to date, animal models have provided little direct contribution since there is a lack of satisfying model combining several aspects of OCD. Although STN lesions seem to induce an “OCD-like” pattern of behavior, associating perseverative behavior, impulse control disorder, there is no indication of any effect on anxiety. A model combining various criteria of diagnosis matching the DSM IV, as was developed for addiction (Deroche-Gammonet et al., 2004), will be necessary for future investigations.

Motivation-addiction

Nucleus accumbens

The involvement of the nucleus accumbens in motivational processes is so-well documented that it seems an obvious place to study when assessing possible surgical targets for the treatment of addiction. Vassoler et al. have recently shown that DBS applied at the level of nucleus accumbens shell could reduce relapse to cocaine, without reducing it for food (Vassoler et al., 2008). Although there were electrophysiological data reporting the possibility for accumbens neurons to respond differentially to natural reward versus drug of abuse such as cocaine (Carelli and Deadwyler, 1994; Carelli et al., 2000), there were no other behavioral data showing dissociation between various types of reward after manipulations within the accumbens. The classical view of the reward system does not

account for this possibility. Therefore, targeting the nucleus accumbens to treat cocaine addiction was never a hypothesis since reducing its activity may affect all forms of motivation. Another recent study has shown that DBS of the nucleus accumbens (at higher current parameters than those applied in the STN) could reduce the preference and consumption of alcohol in alcohol preferring rats (Henderson et al., 2010). In parallel, clinical observations of beneficial effect of DBS in the accumbens on alcoholism in one case (Kuhn et al., 2007) or on smoking in patients treated for OCD or Tourette's syndrome (Kuhn et al., 2009) have been reported. It is to note, however, that a few clinical groups are currently considering, if not assessing, application of DBS in the accumbens of addicts (Stelten et al., 2008).

STN: a possible target

We have first shown that bilateral STN lesion does not increase hunger or affect primary processes of motivation whatever the internal state of the animals (deprived or sated) or the reward (standard animal food, palatable food, alcohol, or i.v. injection of cocaine). STN lesion does not affect these consummatory processes (Baunez et al., 2002, 2005; Lardeux and Baunez, 2008; Rouaud et al., 2010). When assessing motivation by measures of reactivity to stimuli predicting food, we found that STN lesions increase responses to these stimuli (Baunez et al., 2002). This result was further confirmed by another group (Uslaner et al., 2008). We also showed that STN lesion increases willingness to work on a lever to obtain food pellets and increases the score of preference for an environment previously associated with food. In contrast to these results, we found the opposite effects when the reward was cocaine, highlighting a possible role for STN to modulate the reactivity of the reward system with regard to the nature of the reward involved (Baunez et al., 2005). When testing the effects of bilateral STN lesion on motivation for alcohol, we have further

shown that it could also affect motivation in an opposite manner depending on the initial preference of the animals for the reward, STN lesions increasing motivation for alcohol in "high drinker rats," while decreasing it in "low drinkers" (Lardeux and Baunez, 2008).

These results position the STN as an interesting target in the brain where dissociation between motivation for drug and motivation for other types of reward can be made. The dissociation seems to be even more complex than based on the nature of the reward not only since the initial preference for it plays a critical role (Lardeux and Baunez, 2008) but also since electrophysiological recording in the STN has revealed that the specific value of a reward of the same type (i.e., different concentrations of sucrose) is encoded by different neurons in the STN (Lardeux et al., 2009).

STN DBS: the possible strategy?

Very recently, we have tested the effects of bilateral STN HFS on motivation for food and for cocaine. As shown after STN lesions (Baunez et al., 2005), bilateral STN HFS reduces the preference for cocaine and the willingness to work to obtain cocaine (Fig. 4), while in contrast, it increases the preference for food and the willingness to work for food reward (Rouaud et al., 2010). One of the advantages of DBS is the possible reversibility that was tested and confirmed since the motivation to work for cocaine was increased after extinction of the stimulation (Fig. 4) (Rouaud et al., 2010).

These results suggest that not only STN might represent an interesting target for the treatment of cocaine addiction, but STN DBS may be the appropriate strategy to diminish the desire for cocaine, without diminishing other motivated behavior.

Although there are no data available regarding the effects of STN manipulation on motivation in animal models of PD, these results that we have obtained in intact rats are in line with some

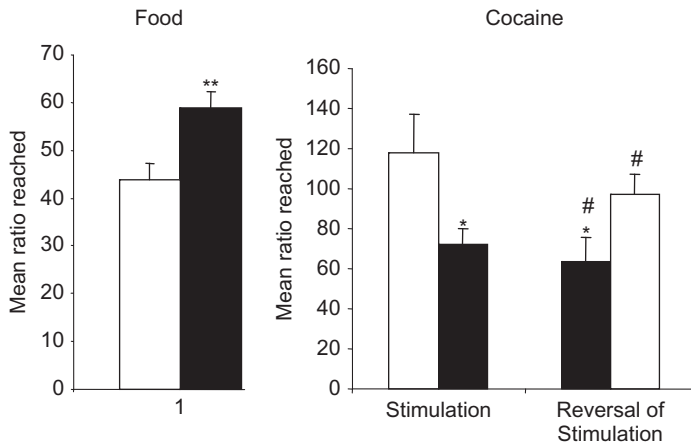


Fig. 4. Effects of bilateral high frequency stimulation (HFS) of the STN on motivation to work to obtain either food (left) or cocaine intraveinously injections (right) in a progressive ratio schedule of reinforcement. The animals are required to press the active lever an increasing number of times (i.e., ratio) to obtain the reward. The last ratio reached is called the breaking point and gives an indication of the motivation for the given reward. Performance is illustrated as the mean ratio reached during 10 sessions under the initial conditions of stimulation (for food and cocaine, left) (OFF $n=8$ and 7 (white bar), respectively, ON $n=14$ and 9 (black bar), respectively, for food and cocaine) and after reversal of the stimulation conditions (former ON group was turned OFF, $n=9$ (right white bar), and former OFF group was turned ON, $n=7$ (right black bar)). Error bars illustrate standard errors (s.e.m.). *: $p < 0.05$ (ANOVA group effect), significant difference between groups STN DBS OFF and STN DBS ON. #: $p < 0.05$ and 0.01, respectively; paired t -test between the initial condition and its reversal. Taken from [Rouaud et al. \(2010\)](#).

clinical observations in PD patients after STN DBS, reporting craving for sweet food in some cases, or decreased addictive behavior toward DAergic treatment ([Witjas et al., 2005](#); [Knobel et al., 2008](#); [Lim et al., 2009](#)).

General conclusion

In conclusion, we have seen through a few examples how animal models can sometimes lead to investigate other aspects of behavior in patients subjected to DBS (nonmotor functions in PD patients) and can sometimes contribute to clinical indication in the best case scenario or to better assessment of possible side effects. In contrast, animal data could sometime lead to conclusions that may have prevented the use of surgical strategy, as in the example of OCD for which STN DBS happens to be efficient. Although one might wonder whether or not

clinical trials are sometimes based on too little rationale, this latter example argues in favor of such a strategy, without questioning the necessity for animal research to carry on.

Acknowledgments

This work has been supported by grants from the Centre National de la Recherche Scientifique (CNRS), the Université de Provence, the Agence Nationale pour la Recherche (ANR-05-JC05_48262 and ANR-09-MNPS-028-01), the MILDT-InCa-INSERM program, and the Fondation pour la Recherche sur le Cerveau.

Abbreviations

6-OHDA	6-hydroxydopamine
BG	basal ganglia
DBS	deep brain stimulation

GPe	external segment of the globus pallidus
HFS	high-frequency stimulation
L-DOPA	L-3,4-dihydroxyphenylalanine
MPTP	1-methyl-4-phenyl-1,2,3,6-tetrahydropyridine
OCD	obsessive compulsive disorder
PD	Parkinson's disease
RT	reaction time
SNC/r	substantia nigra pars compacta/reticulata
STN	subthalamic nucleus

References

- Alexander, G. E., DeLong, M. R., & Strick, P. L. (1986). Parallel organization of functionally segregated circuits linking basal ganglia and cortex. *Annual Review of Neuroscience*, 9, 357–381.
- Baunez, C., & Robbins, T. W. (1997). Bilateral lesions of the subthalamic nucleus induce multiple deficits in an attentional task in rats. *The European Journal of Neuroscience*, 9(10), 2086–2099.
- Baunez, C., & Robbins, T. W. (1999a). Effects of dopamine depletion of the dorsal striatum and further interaction with subthalamic nucleus lesions in an attentional task in the rat. *Neuroscience*, 92(4), 1343–1356.
- Baunez, C., & Robbins, T. W. (1999b). Effects of transient inactivation of the subthalamic nucleus by local muscimol and APV infusions on performance on the five-choice serial reaction time task in rats. *Psychopharmacology (Berlin)*, 141(1), 57–65.
- Baunez, C., Nieoullon, A., & Amalric, M. (1995). In a rat model of parkinsonism, lesions of the subthalamic nucleus reverse increases of reaction time but induce a dramatic premature responding deficit. *The Journal of Neuroscience*, 15 (10), 6531–6541.
- Baunez, C., Amalric, M., & Robbins, T. W. (2002). Enhanced food-related motivation after bilateral lesions of the subthalamic nucleus. *The Journal of Neuroscience*, 22(2), 562–568.
- Baunez, C., Dias, C., Cador, M., & Amalric, M. (2005). The subthalamic nucleus exerts opposite control on cocaine and 'natural' rewards. *Nature Neuroscience*, 8(4), 484–489.
- Baunez, C., Christakou, A., Chudasama, Y., Forni, C., & Robbins, T. W. (2007). Bilateral high-frequency stimulation of the subthalamic nucleus on attentional performance: Transient deleterious effects and enhanced motivation in both intact and parkinsonian rats. *The European Journal of Neuroscience*, 25(4), 1187–1194.
- Baup, N., Grabl, D., Karachi, C., Mounayar, S., Francois, C., Yelnik, J., et al. (2008). High-frequency stimulation of the anterior subthalamic nucleus reduces stereotyped behaviors in primates. *The Journal of Neuroscience*, 28(35), 8785–8788.
- Benazzouz, A., Gross, C., Feger, J., Boraud, T., & Bioulac, B. (1993). Reversal of rigidity and improvement in motor performance by subthalamic high-frequency stimulation in MPTP-treated monkeys. *The European Journal of Neuroscience*, 5(4), 382–389.
- Benazzouz, A., Boraud, T., Feger, J., Burbaud, P., Bioulac, B., & Gross, C. (1996). Alleviation of experimental hemiparkinsonism by high-frequency stimulation of the subthalamic nucleus in primates: A comparison with L-Dopa treatment. *Movement Disorders*, 11(6), 627–632.
- Bergman, H., Wichmann, T., & DeLong, M. R. (1990). Reversal of experimental parkinsonism by lesions of the subthalamic nucleus. *Science*, 249(4975), 1436–1438.
- Beurrier, C., Bezard, E., Bioulac, B., & Gross, C. (1997). Subthalamic stimulation elicits hemiballismus in normal monkey. *Neuroreport*, 8(7), 1625–1629.
- Carelli, R. M., & Deadwyler, S. A. (1994). A comparison of nucleus accumbens neuronal firing patterns during cocaine self-administration and water reinforcement in rats. *The Journal of Neuroscience*, 14(12), 7735–7746.
- Carelli, R. M., Ijames, S. G., & Crumling, A. J. (2000). Evidence that separate neural circuits in the nucleus accumbens encode cocaine versus "natural" (water and food) reward. *The Journal of Neuroscience*, 20(11), 4255–4266.
- Chudasama, Y., Baunez, C., & Robbins, T. W. (2003). Functional disconnection of the medial prefrontal cortex and subthalamic nucleus in attentional performance: Evidence for corticosubthalamic interaction. *The Journal of Neuroscience*, 23(13), 5477–5485.
- Darbaky, Y., Forni, C., Amalric, M., & Baunez, C. (2003). High frequency stimulation of the subthalamic nucleus has beneficial antiparkinsonian effects on motor functions in rats, but less efficiency in a choice reaction time task. *The European Journal of Neuroscience*, 18(4), 951–956.
- Deroche-Gammonet, V., Belin, D., & Piazza, P. V. (2004). Evidence for addiction-like behavior in the rat. *Science*, 305 (5686), 1014–1017.
- Eagle, D. M., & Baunez, C. (2010). Is there an inhibitory-response-control system in the rat? Evidence from anatomical and pharmacological studies of behavioral inhibition. *Neuroscience and Biobehavioral Reviews*, 34(1), 50–72.
- Eagle, D. M., Baunez, C., Hutcheson, D. M., Lehmann, O., Shah, A. P., & Robbins, T. W. (2008). Stop-signal reaction-time task performance: Role of prefrontal cortex and subthalamic nucleus. *Cerebral Cortex*, 18(1), 178–188.
- Gubellini, P., Salin, P., Kerkerian-Le Goff, L., & Baunez, C. (2009). Deep brain stimulation in neurological diseases and experimental models: From molecule to complex behavior. *Progress in Neurobiology*, 89(1), 79–123.

- Haynes, W. I., & Mallet, L. (2010). High-frequency stimulation of deep brain structures in obsessive-compulsive disorder: The search for a valid circuit. *The European Journal of Neuroscience*, 32(7), 1118–1127.
- Henderson, M. B., Green, A. I., Bradford, P. S., Chau, D. T., Roberts, D. W., & Leiter, J. C. (2010). Deep brain stimulation of the nucleus accumbens reduces alcohol intake in alcohol-preferring rats. *Neurosurgical Focus*, 29(2), E12.
- Knobel, D., Aybek, S., Pollo, C., Vingerhoets, F. J., & Berney, A. (2008). Rapid resolution of dopamine dysregulation syndrome (DDS) after subthalamic DBS for Parkinson disease (PD): A case report. *Cognitive and Behavioral Neurology*, 21(3), 187–189.
- Kuhn, J., Lenartz, D., Huff, W., Lee, S., Koulousakis, A., Klosterkoetter, J., et al. (2007). Remission of alcohol dependency following deep brain stimulation of the nucleus accumbens: Valuable therapeutic implications? *Journal of Neurology, Neurosurgery, and Psychiatry*, 78(10), 1152–1153.
- Kuhn, J., Bauer, R., Pohl, S., Lenartz, D., Huff, W., Kim, E. H., et al. (2009). Observations on unaided smoking cessation after deep brain stimulation of the nucleus accumbens. *European Addiction Research*, 15(4), 196–201.
- Lardeux, S., & Baunez, C. (2008). Alcohol preference influences the subthalamic nucleus control on motivation for alcohol in rats. *Neuropsychopharmacology*, 33(3), 634–642.
- Lardeux, S., Pernaud, R., Paleressompoule, D., & Baunez, C. (2009). Beyond the reward pathway: Coding reward magnitude and error in the rat subthalamic nucleus. *Journal of Neurophysiology*, 102(4), 2526–2537.
- Lim, S. Y., O'Sullivan, S. S., Kotschet, K., Gallagher, D. A., Lacey, C., Lawrence, A. D., et al. (2009). Dopamine dysregulation syndrome, impulse control disorders and punding after deep brain stimulation surgery for Parkinson's disease. *Journal of Clinical Neuroscience*, 16(9), 1148–1152.
- Limousin, P., Pollak, P., Benazzouz, A., Hoffmann, D., Le Bas, J. F., Broussolle, E., et al. (1995). Effect of parkinsonian signs and symptoms of bilateral subthalamic nucleus stimulation. *The Lancet*, 345(8942), 91–95.
- Mallet, L., Mesnage, V., Houeto, J. L., Pelissolo, A., Yelnik, J., Behar, C., et al. (2002). Compulsions, Parkinson's disease, and stimulation. *The Lancet*, 360(9342), 1302–1304.
- Mallet, L., Schupbach, M., N'Diaye, K., Remy, P., Bardinet, E., Czernecki, V., et al. (2007). Stimulation of subterritories of the subthalamic nucleus reveals its role in the integration of the emotional and motor aspects of behavior. *Proceedings of the National Academy of Sciences of the United States of America*, 104(25), 10661–10666.
- Mallet, L., Polosan, M., Jaafari, N., Baup, N., Welter, M. L., Fontaine, D., et al. (2008). Subthalamic nucleus stimulation in severe obsessive-compulsive disorder. *The New England Journal of Medicine*, 359(20), 2121–2134.
- Monakow, K. H., Akert, K., & Kunzle, H. (1978). Projections of the precentral motor cortex and other cortical areas of the frontal lobe to the subthalamic nucleus in the monkey. *Experimental Brain Research*, 33(3–4), 395–403.
- Nambu, A. (2004). A new dynamic model of the cortico-basal ganglia loop. *Progress in Brain Research*, 143, 461–466.
- Parent, A., & Hazrati, L. N. (1995). Functional anatomy of the basal ganglia. II. The place of subthalamic nucleus and external pallidum in basal ganglia circuitry. *Brain Research. Brain Research Reviews*, 20(1), 128–154.
- Perriol, M. P., Krystkowiak, P., Defebvre, L., Blond, S., Destee, A., & Dujardin, K. (2006). Stimulation of the subthalamic nucleus in Parkinson's disease: Cognitive and affective changes are not linked to the motor outcome. *Parkinsonism & Related Disorders*, 12(4), 205–210.
- Rodriguez-Oroz, M. C., Lopez-Azcarate, J., Garcia-Garcia, D., Alegre, M., Toledo, J., Valencia, M., et al. (2011). Involvement of the subthalamic nucleus in impulse control disorders associated with Parkinson's disease. *Brain*, 134(Pt 1), 36–49.
- Rouaud, T., Lardeux, S., Panayotis, N., Paleressompoule, D., Cador, M., & Baunez, C. (2010). Reducing the desire for cocaine with subthalamic nucleus deep brain stimulation. *Proceedings of the National Academy of Sciences of the United States of America*, 107(3), 1196–1200.
- Stelten, B. M., Noblesse, L. H., Ackermans, L., Temel, Y., & Visser-Vandewalle, V. (2008). The neurosurgical treatment of addiction. *Neurosurgical Focus*, 25(1), E5.
- Temel, Y., Visser-Vandewalle, V., Aendekerk, B., Rutten, B., Tan, S., Scholtissen, B., et al. (2005). Acute and separate modulation of motor and cognitive performance in parkinsonian rats by bilateral stimulation of the subthalamic nucleus. *Experimental Neurology*, 193(1), 43–52.
- Uslaner, J. M., & Robinson, T. E. (2006). Subthalamic nucleus lesions increase impulsive action and decrease impulsive choice—Mediation by enhanced incentive motivation? *The European Journal of Neuroscience*, 24(8), 2345–2354.
- Uslaner, J. M., Dell'Orco, J. M., Pevzner, A., & Robinson, T. E. (2008). The influence of subthalamic nucleus lesions on sign-tracking to stimuli paired with food and drug rewards: Facilitation of incentive salience attribution? *Neuropsychopharmacology*, 33(10), 2352–2361.
- Vassoler, F. M., Schmidt, H. D., Gerard, M. E., Famous, K. R., Ciraulo, D. A., Kornetsky, C., et al. (2008). Deep brain stimulation of the nucleus accumbens shell attenuates cocaine priming-induced reinstatement of drug seeking in rats. *The Journal of Neuroscience*, 28(35), 8735–8739.
- Winstanley, C. A., Baunez, C., Theobald, D. E., & Robbins, T. W. (2005). Lesions to the subthalamic nucleus decrease impulsive choice but impair autoshaping in rats: The importance of the basal ganglia in Pavlovian conditioning and impulse control. *The European Journal of Neuroscience*, 21(11), 3107–3116.

- Winter, C., Flash, S., Klavir, O., Klein, J., Sohr, R., & Joel, D. (2008a). The role of the subthalamic nucleus in 'compulsive' behavior in rats. *The European Journal of Neuroscience*, 27(8), 1902–1911.
- Winter, C., Mundt, A., Jalali, R., Joel, D., Harnack, D., Morgenstern, R., et al. (2008b). High frequency stimulation and temporary inactivation of the subthalamic nucleus reduce quinpirole-induced compulsive checking behavior in rats. *Experimental Neurology*, 210(1), 217–228.
- Witjas, T., Baumer, C., Henry, J. M., Delfini, M., Regis, J., Cherif, A. A., et al. (2005). Addiction in Parkinson's disease: Impact of subthalamic nucleus deep brain stimulation. *Movement Disorders*, 20(8), 1052–1055.

CHAPTER 9

Cochlear implants: matching the prosthesis to the brain and facilitating desired plastic changes in brain function

Blake S. Wilson^{†,‡,§,*}, Michael F. Dorman[¶], Marty G. Woldorff^{||,#,***,††} and Debara L. Tucci^{†,‡}

[†] Duke Hearing Center, Duke University Medical Center (DUMC), Durham, NC, USA

[‡] Department of Surgery, Division of Otolaryngology—Head and Neck Surgery, DUMC, Durham, NC, USA

[§] Department of Electrical and Computer Engineering, Duke University, Durham, NC, USA

[¶] Department of Speech and Hearing Science, Arizona State University, Tempe, AZ, USA

^{||} Department of Psychiatry, Duke University, Durham, NC, USA

[#] Department of Psychology and Neuroscience, Duke University, Durham, NC, USA

^{**} Department of Neurobiology, Duke University, Durham, NC, USA

^{††} Center for Cognitive Neuroscience, Duke University, Durham, NC, USA

Abstract: The cochlear implant (CI) is one of the great success stories of modern medicine. A high level of function is provided for most patients. However, some patients still do not achieve excellent or even good results using the present-day devices. Accumulating evidence is pointing to differences in the processing abilities of the “auditory brain” among patients as a principal contributor to this remaining and still large variability in outcomes. In this chapter, we describe a new approach to the design of CIs that takes these differences into account and thereby may improve outcomes for patients with compromised auditory brains.

Keywords: cochlear implant; cochlear prosthesis; auditory prosthesis; brain–machine interface; brain plasticity; neural prostheses; hearing; deafness; central auditory processing; auditory cortex.

Introduction

The cochlear implant (CI) is the most successful neural prosthesis developed to date. More than 220,000 people have received a CI or bilateral CIs as of this writing (early 2011). This number

*Corresponding author.

Tel.: +1-919-314-3006; Fax: +1-919-484-9229
E-mail: blake.wilson@duke.edu

exceeds by orders of magnitude the number for all other types of neural prostheses combined. According to the most recent NIH Consensus Statement on CIs in adults and children ([National Institutes of Health, 1995](#)), “A majority of those individuals with the latest speech processors for their implants will score above 80% correct on high-context sentences even without visual cues.” This restoration of function is remarkable and far surpasses that of any other neural prosthesis.

Although the average and top performances of the present-day CIs are spectacular, a large variability in outcomes remains. Patients using the same type of implant device may score almost anywhere in the range of possible scores in tests of speech reception that are more difficult than high-context sentences. Also, a small proportion of patients have low scores even for the relatively easy tests. Accumulating evidence is pointing to differences in brain function among patients as a principal contributor to this remaining variability.

The main purpose of this chapter is to describe a new “top-down” or “cognitive neuroscience” approach to the design of CIs that takes such differences into account. The chapter includes (1) a brief review of the design and performance of the present-day CIs, (2) a summary of the evidence indicating the importance of the brain in determining outcomes with CIs, (3) the description of the new approach, and (4) a list of questions that are raised by the approach.

Present-day cochlear implants

All CI systems now in widespread use include multiple channels of sound processing and multiple sites of stimulation along the length of the cochlea. The aim of these systems is to mimic at least to some extent the “place” or “tonotopic” representation of frequencies in the normal cochlea, that is, by stimulating electrodes near the basal end of the cochlea to indicate the presence of high-frequency sounds and by stimulating

electrodes closer to the apical end to indicate the presence of sounds at lower frequencies.

One of the simpler and most effective designs for achieving this aim, illustrated in [Fig. 1](#), is called the continuous interleaved sampling (CIS) strategy for CIs ([Wilson et al., 1991](#)). Other strategies also are highly effective and are described in [Wilson and Dorman \(2009\)](#). As noted there, most of those other strategies are based on CIS or are variations of CIS.

The CIS strategy filters input sounds into bands of frequencies with a bank of band-pass filters. Envelope variations in the different bands are represented at corresponding electrodes in the cochlea with modulated trains of biphasic electrical pulses. The envelope signals extracted from the band-pass filters are compressed with a non-linear mapping function prior to the modulation, to map the wide dynamic range of audible sounds in the environment (about 100 dB) into the much narrower dynamic range of electrically evoked hearing (stimulus levels needed for eliciting loud percepts typically are only 10 dB higher than the levels needed for eliciting threshold percepts). The output of each band-pass channel is directed to a single electrode, with channels with low-to-high center frequencies assigned to apical-to-basal electrodes, to mimic at least the order, if not the precise locations, of frequency mapping in the normal cochlea. The pulse trains are interleaved in time, so that the pulses across channels and the associated electrodes are nonsimultaneous. This eliminates a principal component of electrode interaction, which otherwise would be produced by direct summation of the electric fields from different (simultaneously stimulated) electrodes. The corner or “cutoff” frequency of the low-pass filter in each envelope detector typically is set at 200 Hz or higher, so that the fundamental frequencies of voiced speech sounds are represented in the modulation waveforms. CIS gets its name from the continuous sampling of the (compressed) envelope signals by rapidly presented pulses that are interleaved across electrodes. As many as 22 channels have been

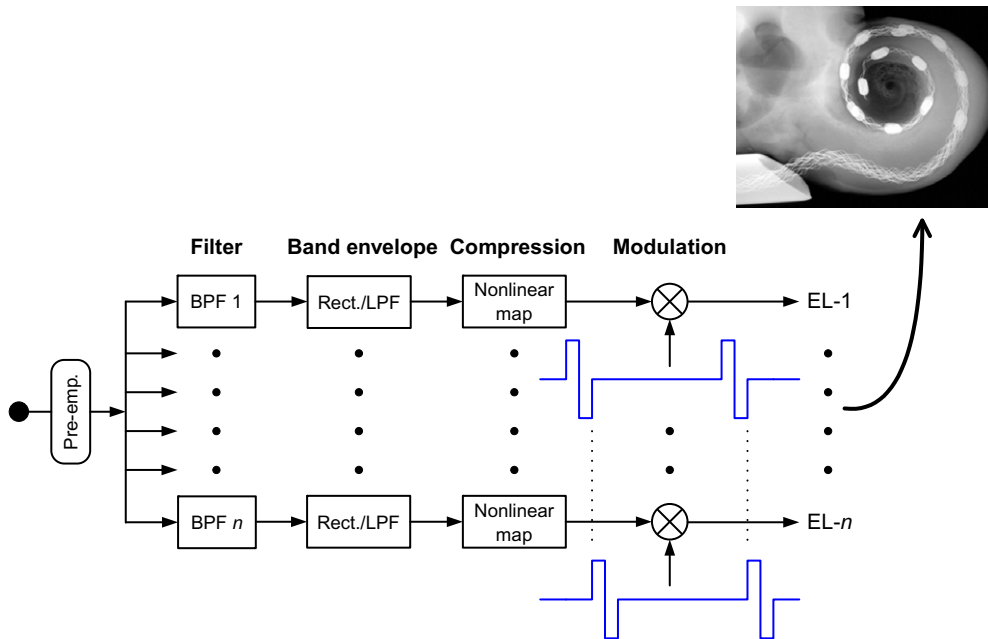


Fig. 1. Block diagram of the continuous interleaved sampling (CIS) strategy. The input to the strategy is indicated by the filled circle in the left-most part of the diagram. Next, a pre-emphasis filter (Pre-emp.) is used to attenuate strong components in speech below 1.2 kHz. This filter is followed by multiple channels of processing. Each channel includes band-pass filtering (BPF), envelope detection, compression, and modulation. The envelope detectors typically use a rectifier (Rect.) followed by a low-pass filter (LPF). A Hilbert transform or a half-wave rectifier without the LPF also may be used. Carrier waveforms for two of the modulators are shown immediately below the two corresponding multiplier blocks (the circles with an "X" within them). The outputs of the multipliers are directed to intracochlear electrodes (EL-1 to EL- n), as illustrated by the X-ray micrograph in the inset. (Block diagram is adapted from Wilson et al. (1991) with the permission of the Nature Publishing Group. Inset is reproduced from Hüttenbrink et al. (2002) with the permission of Lippincott Williams and Wilkins.)

used in CIS implementations to date, although speech reception scores generally do not increase with increases in the number of channels beyond 4–8, for the CIS and the other strategies used in conjunction with the present-day CIs (e.g., Friesen et al., 2001).

Patterns of activity in the auditory nerve produced by the CIS and the other strategies are far different from the patterns found in normal hearing. For example, only a small number of (broadly overlapping and only somewhat independent) sites of stimulation are provided with the strategies, up to a maximum of 22 sites, whereas the number of sites in normal hearing approximates 3500, corresponding to the number

of rows of sensory hair cells distributed along the length of the cochlea. Many additional differences between normal and electrically elicited hearing are described in Wilson and Dorman (2007, 2009).

Despite the differences between the peripheral representations of sound produced by electric versus acoustic stimulation, most CI users are able to understand everyday speech with their restored hearing alone and without the aid of lipreading, although it often requires rather focused attention. Indeed, some patients have speech reception scores that approach—and in many tests match—the scores obtained by subjects with normal hearing (e.g., Wilson and

Dorman, 2007). This result is an existence proof that the present-day CIs can provide enough information at the periphery for excellent understanding of speech in many circumstances. In addition, the result is a testament to the brain, in that the brain is somehow able to reconstruct speech from a decidedly sparse and otherwise unnatural input.

However, a large variability in outcomes remains with the present-day CIs, with widespread distributions of scores, from very low scores to very high scores, for the relatively difficult tests such as recognition of monosyllabic words or of sentences presented in competition with noise. In addition, some patients still have great difficulty even with the easier tests.

A further aspect of the results with the present-day and prior CIs is a general tendency toward improvement in speech reception scores over time, as patients gain experience with their implants. Scores typically continue to improve during the first 3–12 months of implant use, although the period can be even longer for some patients and for difficult tests. In the study by Helms et al. (1997), for example, the average scores for 55 CI patients improved significantly out to 12 months after the first use of the implant, and then plateaued thereafter. These long time courses also indicate a role of the brain in determining outcomes with CIs, in that the times needed to reach asymptotic performance far exceed the times of any possible changes at the periphery and must instead reflect plastic changes in brain organization and function, as the brain “reconfigures” itself over the months to make progressively better use of the impoverished input.

The results reviewed above generally apply to postlingually deafened patients (i.e., patients who lost their hearing after they had acquired language). Results for prelingually deafened patients may be different, depending on the age of implantation. If the implant occurs at an early age, for example, 18 months or less, then the results for the prelingually deafened population are as good

as the better outcomes for the postlingually deafened population (e.g., Niparko et al., 2010). In contrast, implantations after the second or third birthday for the prelingual patients are associated with outcomes that are usually worse than those for the postlingual patients, and the odds for a good outcome are very poor for prelingually deafened persons implanted after 4–6 years of age.

Importance of brain function in determining outcomes

Two positive aspects of brain function have been mentioned: the brain’s ability in some cases to make outstanding use of a sparse input from the periphery, and the brain’s ability in most cases to adapt at least partially to the input over a long time span. These aspects clearly appear to contribute to the present high levels of performance with CIs.

However, damage to the brain can impair performance. Such damage may be produced by a prolonged period of auditory deprivation (Shepherd and Hardie, 2001; Shepherd et al., 2006); cross-modal plasticity in the brains of congenitally or otherwise prelingually deafened children who are implanted after age 3 or thereabouts (Buckley and Tobey, 2010; Giraud and Lee, 2007; Lee et al., 2001); missing the “sensitive period” for normal development of the “auditory brain” for congenitally deaf persons who are implanted after 3.5 years of age (Sharma et al., 2002); various genetic defects; and various diseases such as meningitis and demyelinating disorders. (Cross-modal plasticity in the congenitally deafened cases is the encroachment of the auditory cortical areas by another sensory modality, e.g., vision, and the sensitive period refers to the time window in which especially rapid and large plastic changes in brain function may occur.) The resulting deficits in brain function may underlie at least in part (1) the observed negative correlation between outcomes with CIs and the duration of deafness or severe hearing

loss prior to implantation for postlingually deafened patients (e.g., [Blamey et al., 1996](#)) and (2) the poor outcomes for congenitally or otherwise prelingually deafened persons who are not implanted early in life. In addition, differences in brain function among patients, at least vis-à-vis the functional interaction with the implant, may explain or help to explain the remaining variability in outcomes for the postlingually deafened patients. Results may be good in the fortuitous cases of early implantation for prelingually deafened persons and implantation within a year or so of the first substantial hearing loss for postlingually deafened persons. For all other cases, however, outcomes may be affected by deficits in the ability of the brain to make functional use of the input provided by the implant. These latter cases constitute the majority of CI recipients.

These and many other findings indicating the importance of brain function in determining outcomes with CIs are described in detail in the recent reviews by [Fallon et al. \(2008\)](#), [Giraud and Lee \(2007\)](#), [Kral et al. \(2006\)](#), [Kral and Eggermont \(2007\)](#), [Moore and Shannon \(2009\)](#), [Musiek and Daniels \(2010\)](#), and [Wilson and Dorman \(2009\)](#). In addition, further information about cross-modal plasticity in various brain systems is presented in the review by [Bavelier and Neville \(2002\)](#), and extended discussion about sensitive periods in various brain systems, and on the persistence of some brain plasticity following a sensitive period, is presented in the reviews by [Chen et al. \(2002\)](#), [Irvine et al. \(2006\)](#), [Jäncke \(2009\)](#), and [Knudsen \(2004\)](#).

A “top-down” or “cognitive neuroscience” approach to implant designs

The evidence indicating the importance of the brain in determining outcomes with implants has led to a new way of thinking about the design of CIs. To date, a “bottom-up” approach has been used, in which the goal is to reproduce in so far as possible the normal patterns of neural activity

at the auditory periphery. Great progress has been made with that approach, and further substantial progress is certainly possible, given the large gaps that remain between the normal patterns and the patterns produced by the present-day CIs.

Despite the successes of the bottom-up approach, however, some or even most patients may be underserved by it. In particular, this traditional approach ignores the brain as a part of the overall prosthesis system and, while this may not matter (or matter much) when the brain is perfect or is in the “clean slate” state of the sensitive period and prior to any effects of cross-modal plasticity, ignoring the brain is likely to be detrimental for most other cases.

Concept

An alternative approach is to include the perspective of the brain instead of focusing exclusively on the periphery. This top-down approach asks what the (usually compromised) brain needs as an input in order to perform optimally, and/or to learn how to perform optimally. The answer to this question almost certainly would vary from patient to patient according to the functional abilities of each patient’s auditory brain. In addition, the inputs may depart dramatically from those produced with the bottom-up approach, especially for patients with severe deficits in brain function.

At the outset, one might anticipate that the stimuli prescribed by the top-down approach could be far slower or far sparser or both for many patients, compared with the stimuli derived from the bottom-up approach. In particular, the compromised auditory brain may have greatly degraded abilities to “follow” or otherwise process temporal information from the periphery (e.g., [Fu, 2002](#); [Walton, 2010](#)), or to distinguish among stimulus sites in the cochlea or otherwise process spectral information from the periphery (e.g., [Fallon et al., 2008](#)). These likely deficits

may well intrinsically limit the effective processing of the inputs to the brain provided by the present-day CIs. Instead, a simplification of the inputs may be needed to produce a match between the inputs and the brain's capabilities to process them. Possible simplifications include reductions in (1) the rate of stimulation at each electrode in the implant, along with conjoint reductions in the cutoff frequency of the envelope detectors for each channel and associated electrode (see Fig. 1) and (2) the number of activated electrodes. The choices for the reductions might be guided by psychophysical measures of temporal and spectral acuities for each patient, for example, gap detection, forward masking, or modulation detection for the temporal acuities, and electrode or spectral ripple discrimination for the spectral acuities.

Fortunately, some simplifications could be made while still preserving important information about speech and other sounds. For example, much of the information about speech is contained in envelope variations below 16 Hz in a relatively small number of bands (e.g., Xu and Zheng, 2007). This means that the envelope cutoff frequency could be reduced from the typical 200–400 Hz down to as low as 16 Hz before removing absolutely essential information about speech. Fundamental frequency variations would be discarded in the modulation waveforms, but those variations convey little phonetic information and instead provide information about the speaker's gender and age, declarative versus interrogative intent, and emotion in speech. Except in the cases of tone languages, intelligibility of speech is largely retained when fundamental frequencies are removed from the representation. Thus, the essential aspects for western and other nontonal languages would be preserved using the lower cutoff frequencies for the envelope detectors.

Such sharp reductions in the cutoff frequencies could be accompanied by similarly sharp reductions in the pulse rate at each of the activated electrodes, up to the same proportional

amount. These large reductions in the pulse rate could greatly reduce the likely deleterious effects of prolonged forward masking or otherwise "sluggish" central auditory processing, by allowing the central system to follow inputs that could not be followed before. (The reductions also could improve sensitivity to modulation; see, e.g., Pfingst et al., 2007.) The low frequencies of the envelope variations, and the low pulse rates at each electrode, might fit within or at least approach the temporal processing abilities of a compromised auditory brain, as may be indicated, for example, by one or more of the psychophysical measures mentioned above.

In addition, for speech presented in quiet, as few as four band-pass processing channels are sufficient for high levels of speech recognition (Shannon et al., 1995). Thus, the number of channels and associated active electrodes could be reduced to four in a CI system and still allow the representation of important speech information. As many as 12, 16, or 22 channels and active electrodes are used in the present-day CIs, depending on the particular device and processing strategy. A lower number might fit within or at least approach the spectral (or, more precisely, the tonotopic) processing abilities of a compromised auditory brain.

Of course, higher pulse rates, higher cutoff frequencies for the envelope detectors, and higher numbers of channels could be better for patients who can utilize the additional represented information. The advantages of including information about the fundamental frequency variations have been mentioned. Those advantages would only accrue with the use of the higher pulse rates and cutoff frequencies. In addition, higher numbers of channels may be needed for useful speech reception in other than quiet conditions (Dorman et al., 1998, 2002; Friesen et al., 2001; Shannon et al., 2004), for example, for speech reception in typically noisy environments. More channels are required as well for music reception (Shannon et al., 2004), and information about the fundamental frequency

variations may be essential for conveying critical phonemic contrasts in tone languages. The point here, however, is that great simplifications are possible, before all of the important information about speech is eliminated. In addition, the simplifications could be made using the present-day implant systems and processing strategies, with adjustments in the parameter values for the strategies. Other implant systems or processing strategies could be envisioned, that also would produce marked reductions in the rates of stimulation, the number of sites stimulated, or both, but a useful first step may be made with informed manipulations in the parameter values for the present-day systems and strategies.

The goal in the top-down approach is to provide a good match between what the implant provides and what the brain can most effectively process or “handle,” while still presenting the maximum amount of information possible. Maintaining the quality of the match most likely would require adjustments in the stimuli from time to time, as the brain is not static and can reconfigure itself through plastic changes when presented with stimuli within its processing abilities and with enough experience with those stimuli (Irvine et al., 2006). Such changes are possible for adults as well as children, although the maximum speed and magnitude of the changes during the sensitive period (generally before 2–3 years of age for auditory processing by humans) may far exceed those maxima later in life (e.g., Knudsen, 2004).

Good matches may require simplifications in the stimuli, and the patterns of activity in the auditory nerve evoked by those stimuli, compared with the stimuli derived with the bottom-up approach and used in the present-day CIs. (Certainly, an increase in the complexity of the stimuli would seem to be going in the wrong direction for CI users with compromised auditory brains, both because the stimuli of the present-day CIs include enough information for some users to achieve high levels of speech reception and because psychophysical and other results indicate that the

compromised brains are less able than fully intact brains to process temporal and spectral information.) The simplifications if needed should not be overdone, of course, but should instead be just enough for a match or a helpful approximation to the brain’s abilities, both to preserve the maximum amount of information included in the peripheral representations, and to challenge the brain to work at its limits and thereby encourage desired plastic changes in brain organization and function. Ultimately, with continued adjustments of the stimuli and with continued development of the brain’s processing abilities, both the brain and the stimuli may approach normality. That is, the previously compromised brain may ultimately more closely resemble the fully intact brain in function, and the stimuli may resemble those delivered by the present-day CIs. The critical step may be the first one, in giving the compromised brain an input it can process and thereby start it on a path to (at least partial) recovery.

In some cases, the brain may be so damaged that a good match cannot be achieved, even with huge simplifications in the stimuli. Such brains may be beyond remediation. However, training aimed at improving performance on a basic psychophysical task—involving stimuli that are far simpler than even the simplest of the stimuli described in the preceding paragraphs—may help to “nudge” the highly compromised brain into a position where stimuli of greater complexity could be processed, perhaps up to a point at which a match could then be achieved. Possible psychophysical tasks include electrode discrimination or gap or modulation detection. The idea again is to drive the brain at its limits to invoke desired plastic changes in function. Alternatively, certain drug therapies have promise for “reopening” sensitive periods (Castrén and Rantamäki, 2010; Maya Vetencourt et al., 2008; Thiel, 2007), in which large plastic changes in brain function could be induced, in the directions of increased temporal and spectral processing abilities. (In addition, Tobey et al. (2005) have suggested a pharmacological enhancement of

brain plasticity that does not necessarily involve a reopening of a sensitive period.) Such therapies could reestablish at least temporarily a favorable milieu for rapid and large changes in brain organization and function, and may even allow a partial or full recovery from a preceding cross-modal encroachment by vision or another sense in the areas of cortex normally utilized primarily for the processing of auditory inputs and information.

Measures of brain function

Another important feature of the new approach being proposed here is that measures of brain function might inform or guide the design of processing strategies using consideration of top-down factors. For example, and as described above, psychophysical measures could inform choices for the rate of stimulation, the cutoff frequency of the envelope detectors, and the number of sites to be stimulated in CIs. In addition, electrophysiological or brain imaging measures could be used. Ideally, the selected measures should be simple and inexpensive to apply, and such measures should be predictive of outcomes with CIs.

Many of the psychophysical measures mentioned in the preceding subsection would fulfill these criteria. All of the measures could be made relatively quickly and in clinical settings. In addition, many of them are correlated or strongly associated with outcomes with CIs, including modulation detection (Fu, 2002), gap detection (Hochmair-Desoyer et al., 1985), forward masking (Nelson and Donaldson, 2002), and spectral ripple discrimination (Henry et al., 2005).

In addition, various electrophysiological measures would fulfill the criteria. For example, the latency of the short-latency P₁ wave of the cortical evoked potential to a brief stimulus such as a speech syllable may indicate the functional status of the auditory pathways from the cochlear nucleus to the primary auditory cortex, at least for children (Sharma et al., 2002). The P₁ latencies are associated with outcomes in that

the latencies enter the normal range for prelingually deafened persons implanted at or before 3.5 years of age, but do not typically do so for prelingually deafened persons implanted after their seventh birthday. (Variable results are obtained for the intermediate ages.) As noted previously, CI outcomes are much better for the early-implanted group than for the late-implanted group.

Further electrophysiological measures that may be helpful are the mismatch negativity (MMN) response to a feature “oddball” stimulus or the adaptation of longer-latency cortical responses to repeated stimuli. [Zhang et al. \(2011\)](#) have found, for example, that (1) the MMN response to an oddball tone stimulus is significantly larger in high-performing CI subjects than for CI subjects with moderate or low levels of performance and (2) adaptation in late auditory evoked potentials (the N₁-P₂ wave of the cortical evoked potential) to a tone or speech stimulus is significantly greater in the good versus the moderate-to-poor performers. The MMN response to a tone with a different frequency from the non-oddball stimuli is a measure of the brain’s spectral processing abilities, and MMN responses to oddball speech stimuli are measures of speech discrimination. These MMN and adaptation data require more time to collect and more sophisticated paradigms than the P₁ latencies. However, it is conceivable that, with refinement, these additional tools could be brought within the realm of clinical settings.

For research studies, in which time is not always such a pressing issue, a cascade of electrophysiological measures, such as the one shown in [Fig. 2](#), could be helpful. These various measures probe the functions of different structures in the auditory pathways. The electrically evoked auditory brainstem responses (BERs in the figure) probe the functions of the auditory nuclei in the brainstem up to the inferior colliculus and thalamus, and the different waves in the responses can reflect the functional integrities of the different nuclei. At the other end of the cascade, the

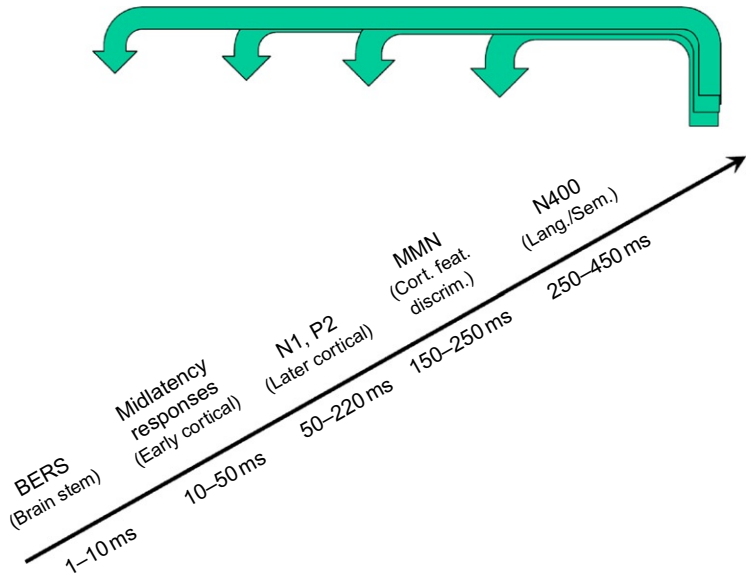


Fig. 2. Hierarchy or cascade of electrophysiological measures (event-related potential (ERP) components) to assess the functional integrity of the auditory pathways and cortices. Abbreviations in the figure include BERs for brainstem evoked responses; MMN for mismatch negativity responses; Cort. feat. discrimin. for Cortical feature discrimination; and Lang./Sem. for Language and Semantic processing. Measures of other auditory ERP components could also be included for additional noninvasive assessment of the functional processing in the auditory pathways. The thick arrows coming in across the top of the figure reflect the potential influence of top-down factors, such as attention, on these various processing stages.

MMN can be used to assess feature discrimination at the cortical level, and the still longer-latency N400 response the cortical processing of language and semantic information.

All or a subset of these measures could be made for individual CI subjects and compared with their speech-reception outcomes and also with the same measures collected for normal-hearing and age-matched controls. (CI subjects with the best performances also could serve as control subjects.) Significant differences between results for the CI subjects versus the control subjects at any point in the cascade would indicate a likely problem for the CI subjects on a site-specific basis. This in turn could be a powerful diagnostic for targeting both training and design efforts to improve results for that site or those sites. Such targeting would not be possible with the psychophysical measures, inasmuch as

they are all “global” measures that only indicate the ability of the auditory brain as a whole to perform certain tasks, as opposed to identifying a particular structure that may be deficient in its processing abilities.

An important aspect of the measures beyond the BERs is that effects of attention or vigilance can be strong (e.g., [Woldorff et al., 1991, 1993](#)). Such effects are indicated in the figure by the arrows at the top. Fortunately, attention and vigilance can be measured and engendered, and thereby used to better understand processes and to facilitate the development of improved training protocols.

The sites at which problems may occur in the ascending auditory pathways and cortices also might be identified with other brain imaging measures. Some brain imaging measures may have sufficient spatial resolution to provide a

crude indication of tonotopic processing at the auditory cortices. In general, however, brain imaging measures are far more time consuming and expensive than the psychophysical and electrophysiological measures described previously. Also, functional magnetic resonance imaging (fMRI) cannot be used in conjunction with CI stimulation for the vast majority of CI patients, because the radio-frequency fields of the MRI machine would interfere with the correct operation of the radio-frequency communication links used in all present-day CI devices ([Seghier et al., 2005](#)).

Feedback in the design process

Measures of brain function also could provide useful feedback in the design process. For example, parameter values for a processing strategy for CIs could be adjusted toward greater and greater simplicity, or otherwise differing parameters, until oddball speech or other stimuli elicit an MMN response. Also, the use of psychophysical measures has been mentioned in the context of setting parameter values.

Once the inputs produced by the CI are simple or suitable enough for the compromised brain to process, then plastic changes in brain function may be anticipated, as experience is gained with the inputs. Such changes could be monitored with periodic psychophysical or electrophysiological measures. A detected improvement in brain function would prompt a new adjustment in the parameter values or even a new choice in the processing strategy, depending on the magnitude of the change. A “closed-loop” process for design could include (1) assessment of the functional abilities of each patient’s auditory brain at the outset, (2) prescription of the stimuli to be delivered by the implant based on the assessment, (3) repeated measures of brain function at periodic intervals or when a change in speech reception performance is noticed by a patient or his or her clinician(s), and (4) when the measures indicate

an improvement in brain function, looping back to step 2 and repeating the process from there. In this way, a good match between the implant and the brain could be maintained at all times, and the expectation would be for continued and linked improvements in the brain’s abilities and the performance of the CI until high performance is achieved or until no further changes in brain function are possible.

Training to facilitate desired plastic changes in brain function

Improvements over time also might be facilitated with directed training. The training could be aimed at discriminating basic psychophysical stimuli at the boundaries of a patient’s abilities. For example, the training could be directed at improving the sensitivity to modulation, which reflects temporal processing in the brain and additionally is strongly correlated with implant outcomes. Improvements in modulation detection could generalize to better speech reception scores and further could indicate the need for repeated adjustments in the parameter values for the CI processing strategy.

The training also could be aimed at improving gap detection, or electrode or spectral ripple discrimination. An improvement in the first of these measures might generalize to better temporal processing abilities in the brain, and an improvement in either of the two remaining measures might generalize to better spectral (or tonotopic) processing abilities.

Alternatively, training aimed at improving speech reception directly may be even more effective, as it uses meaningful stimuli and as the training objective is the “end point” of CI performance. Further, training using complex stimuli such as speech may facilitate desired plastic changes in both temporal and spectral processing abilities of the brain simultaneously. Training using speech as stimuli has been shown to be more effective than training using simpler stimuli

for patients using the present-day CIs and standard parameter values for the processing strategies (Fu and Galvin, 2008). The same may be true for at least some patients using CIs based on the top-down approach to implant designs. However, it is also possible that beginning with simpler discrimination tasks, and then building up to tasks involving more-complex linguistic stimuli, would be more effective.

Training may accelerate possible improvements in brain function and implant performance. In addition, the ultimate asymptotic performance level may be higher with training than without it. Any of multiple training options might be used; the most important aspect may be to force the brain to work at its limits during the training, building appropriately on increasing levels of successes, as this is the most efficient if not the only way to drive the desired plastic changes.

Questions raised by the top-down approach

Development of the top-down approach is in its nascent stages. Questions that are raised by the approach and still not fully answered include the following:

1. How can a sensory prosthesis be best matched to a brain that has been compromised through years of sensory deprivation or other causes?
2. How can brain function be measured in ways that would be helpful for achieving the match?
3. Can a well-designed training procedure accelerate or enhance learning with (or accommodation to) a sensory prosthesis?
4. If so, how can the device be adapted to the desired plastic changes in brain function, to continually provide good matches across time?
5. Can the effects of cross-modal plasticity be reversed, to allow a “reconnection” between a cortical area and its original primary sensory input?
6. Can sensitive periods be reopened, to make the previously damaged brain a “clean slate”

for possible full recovery, perhaps even following cross-modal changes in brain organization?

7. How would the stimuli specified by the top-down and bottom-up approaches differ, and for which population(s) of patients would those differences be the greatest?

These are general questions that relate not only to CIs but also to other neural prostheses. Tentative answers in the context of CIs have been presented in this chapter. Each of the questions can of course be restated as a hypothesis or a set of connected hypotheses. Studies are now underway to evaluate some of the various hypotheses, in tests with CI users and control subjects. In addition, questions 5 and 6 are important in contemporary neuroscience, so those questions are receiving considerable attention from a large number of research teams worldwide. Further information in response to all of the questions listed above may well help to shepherd in a new era in neural prosthesis designs, in which the brain is regarded as a key part of the system.

Acknowledgments

This chapter is based on an invited lecture given at the symposium on *Brain machine interfaces—implications for science, clinical practice, and society*, held in Ystad, Sweden, August 26–29, 2010. Parts of the chapter are drawn or adapted from prior publications (Wilson, 2011; Wilson and Dorman, 2009). B. S. W. is a consultant for MED-EL GmbH of Innsbruck, Austria, one of the three major manufacturers of CI systems. None of the statements in this chapter favor that or any other company.

Abbreviations

BER	brainstem evoked response
CI	cochlear implant
CIS	continuous interleaved sampling

ERP	event related potential
fMRI	functional magnetic resonance imaging
MMN	mismatch negativity (as in MMN responses)

References

- Bavelier, D., & Neville, H. J. (2002). Cross-modal plasticity: Where and how? *Nature Reviews Neuroscience*, 3, 443–452.
- Blamey, P., Arndt, P., Bergeron, F., Bredberg, G., Brimacombe, J., Facer, G., et al. (1996). Factors affecting auditory performance of postlinguistically deaf adults using cochlear implants. *Audiology & Neuro-Otology*, 1, 293–306.
- Buckley, K. A., & Tobey, E. A. (2010). Cross-modal plasticity and speech perception in pre- and postlingually deaf cochlear implant users. *Ear and Hearing*, 32, 2–15.
- Castrén, E., & Rantamäki, T. (2010). The role of BDNF and its receptors in depression and antidepressant drug action: Reactivation of developmental plasticity. *Developmental Neurobiology*, 70, 289–297.
- Chen, R., Cohen, L. G., & Hallet, M. (2002). Nervous system reorganization following injury. *Neuroscience*, 111, 761–773.
- Dorman, M. F., Loizou, P. C., Fitzke, J., & Tu, Z. (1998). The recognition of sentences in noise by normal-hearing listeners using simulations of cochlear-implant signal processors with 6–20 channels. *Journal of the Acoustical Society of America*, 104, 3583–3585.
- Dorman, M. F., Loizou, P. C., Spahr, A. J., & Maloff, E. (2002). A comparison of the speech understanding provided by acoustic models of fixed-channel and channel-picking signal processors for cochlear implants. *Journal of Speech, Language, and Hearing Research*, 45, 783–788.
- Fallon, J. B., Irvine, D. R. F., & Shepherd, R. K. (2008). Cochlear implants and brain plasticity. *Hearing Research*, 238, 110–117.
- Friesen, L. M., Shannon, R. V., Baskent, D., & Wang, X. (2001). Speech recognition in noise as a function of the number of spectral channels: Comparison of acoustic hearing and cochlear implants. *Journal of the Acoustical Society of America*, 110, 1150–1163.
- Fu, Q. J. (2002). Temporal processing and speech recognition in cochlear implant users. *NeuroReport*, 13, 1635–1639.
- Fu, Q. J., & Galvin, J. J. III. (2008). Maximizing cochlear implant patients' performance with advanced speech training procedures. *Hearing Research*, 242, 198–208.
- Giraud, A. L., & Lee, H. J. (2007). Predicting cochlear implant outcome from brain organization in the deaf. *Restorative Neurology and Neuroscience*, 25, 381–390.
- Helms, J., Müller, J., Schön, F., Moser, L., Arnold, W., et al. (1997). Evaluation of performance with the COMBI 40 cochlear implant in adults: A multicentric clinical study. *ORL; Journal for Oto-Rhino-Laryngology and Its Related Specialties*, 59, 23–35.
- Henry, B. A., Turner, C. W., & Behrens, A. (2005). Spectral peak resolution and speech recognition in quiet: Normal hearing, hearing impaired, and cochlear implant listeners. *Journal of the Acoustical Society of America*, 118, 1111–1121.
- Hochmair-Desoyer, I. J., Hochmair, E. S., & Stiglbrunner, H. K. (1985). Psychoacoustic temporal processing and speech understanding in cochlear implant patients. In R. A. Schindler & M. M. Merzenich (Eds.), *Cochlear implants* (pp. 291–304). New York: Raven Press.
- Hüttenbrink, K. B., Zahnert, T., Jolly, C., & Hofmann, G. (2002). Movements of cochlear implant electrodes inside the cochlea during insertion: An x-ray microscopy study. *Otology & Neurotology*, 23, 187–191.
- Irvine, D. R., Fallon, J. B., & Kamke, M. R. (2006). Plasticity in the central auditory system. *Acoustics Australia*, 34, 13–17.
- Jäncke, L. (2009). The plastic human brain. *Restorative Neurology and Neuroscience*, 27, 521–538.
- Knudsen, E. I. (2004). Sensitive periods in the development of the brain and behavior. *Journal of Cognitive Neuroscience*, 16, 1412–1425.
- Kral, A., & Eggermont, J. J. (2007). What's to lose and what's to learn: Development under auditory deprivation, cochlear implants and limits of cortical plasticity. *Brain Research Reviews*, 56, 259–269.
- Kral, A., Tillein, J., Heid, S., Klinke, R., & Hartmann, R. (2006). Cochlear implants: Cortical plasticity in congenital deprivation. *Progress in Brain Research*, 157, 283–313.
- Lee, D. S., Lee, J. S., Oh, S. H., Kim, S. K., Kim, J. W., Chung, J. K., et al. (2001). Cross-modal plasticity and cochlear implants. *Nature*, 409, 149–150.
- Maya Vetencourt, J. F., Sale, A., Viegi, A., Baroncelli, L., De Pasquale, R., O'Leary, O. F., et al. (2008). The antidepressant fluoxetine restores plasticity in the adult visual cortex. *Science*, 320, 385–388.
- Moore, D. R., & Shannon, R. V. (2009). Beyond cochlear implants: Awakening the deafened brain. *Nature Neuroscience*, 12, 686–691.
- Musiek, F. E., & Daniels, S. B. (2010). Central auditory mechanisms associated with cochlear implantation: An overview of selected studies and comment. *Cochlear Implants International*, 11(Suppl. 1), 15–28.
- National Institutes of Health, (1995). Cochlear implants in adults and children. *NIH Consensus Statement*, 13(2), 1–30 (This statement also is available in the JAMA, 274, 1955–1961.).
- Nelson, D. A., & Donaldson, G. S. (2002). Psychophysical recovery from pulse-train forward masking in electric hearing. *Journal of the Acoustical Society of America*, 112, 2932–2947.
- Niparko, J. K., Tobey, E. A., Thal, D. J., Eisenberg, L. S., Wang, N. Y., Quittner, A. L., et al. (2010). Spoken language

- development in children following cochlear implantation. *Journal of the American Medical Association*, 303, 1498–1506.
- Pfingst, B. E., Xu, L., & Thompson, C. S. (2007). Effects of carrier pulse rate and stimulation on modulation detection by subjects with cochlear implants. *Journal of the Acoustical Society of America*, 121, 2236–2246.
- Seghier, M. L., Boëx, C., Lazeyras, F., Sigris, A., & Pelizzzone, M. (2005). FMRI evidence for activation of multiple cortical regions in the primary auditory cortex of deaf subjects users of multichannel cochlear implants. *Cerebral Cortex*, 15, 40–48.
- Shannon, R. V., Fu, Q.-J., & Galvin, J. III (2004). The number of spectral channels required for speech recognition depends on the difficulty of the listening situation. *Acta Oto-Laryngologica Suppl.* 2004, 50–54.
- Shannon, R. V., Zeng, F. G., Kamath, V., Wygonski, J., & Ekelid, M. (1995). Speech recognition with primarily temporal cues. *Science*, 270, 303–304.
- Sharma, A., Dorman, M. F., & Spahr, A. J. (2002). A sensitive period for the development of the central auditory system in children with cochlear implants: Implications for age of implantation. *Ear and Hearing*, 23, 532–539.
- Shepherd, R. K., & Hardie, N. A. (2001). Deafness-induced changes in the auditory pathway: Implications for cochlear implants. *Audiology & Neuro-Otology*, 6, 305–318.
- Shepherd, R. K., Meltzer, N. E., Fallon, J. B., & Ryugo, D. K. (2006). Consequences of deafness and electrical stimulation on the peripheral and central auditory system. In S. B. Waltzman & J. T. Roland, Jr. (Eds.), *Cochlear implants* (pp. 25–39). (2nd ed.). New York: Thieme Medical Publishers.
- Thiel, C. M. (2007). Pharmacological modulation of learning-induced plasticity in human auditory cortex. *Restorative Neurology and Neuroscience*, 25, 435–443.
- Tobey, E. A., Devous, M. D., Sr., Buckley, K., Overton, G., Harris, T., Ringe, W., et al. (2005). Pharmacological enhancement of aural habilitation in adult cochlear implant users. *Ear and Hearing*, 26(Suppl. 4), 45S–56S.
- Walton, J. P. (2010). Timing is everything: Temporal processing deficits in the aged auditory brainstem. *Hearing Research*, 264, 63–69.
- Wilson, B. S. (2011). A ‘top down’ or ‘cognitive neuroscience’ approach to cochlear implant designs and fittings. *Cochlear Implants International*, 12, S35–S39.
- Wilson, B. S., & Dorman, M. F. (2007). The surprising performance of present-day cochlear implants. *IEEE Transactions on Biomedical Engineering*, 54, 969–972.
- Wilson, B. S., & Dorman, M. F. (2009). The design of cochlear implants. In J. K. Niparko, K. I. Kirk, N. K. Mellon, A. M. Robbins, D. L. Tucci & B. S. Wilson (Eds.), *Cochlear implants: Principles & practices* (pp. 95–135). (2nd ed.). Philadelphia: Lippincott Williams and Wilkins.
- Wilson, B. S., Finley, C. C., Lawson, D. T., Wolford, R. D., Eddington, D. K., & Rabinowitz, W. M. (1991). Better speech recognition with cochlear implants. *Nature*, 352, 236–238.
- Woldorff, M. G., Gallen, C. C., Hampson, S. A., Hillyard, S. A., Pantev, C., Sobel, D., et al. (1993). Modulation of early sensory processing in human auditory cortex during auditory selective attention. *Proceedings of the National Academy of Sciences of the United States of America*, 90, 8722–8726.
- Woldorff, M. G., Hackley, S. A., & Hillyard, S. A. (1991). The effects of channel-selective attention on the mismatch negativity wave elicited by deviant tones. *Psychophysiology*, 28, 30–42.
- Xu, L., & Zheng, Y. (2007). Spectral and temporal cues for phoneme recognition in noise. *Journal of the Acoustical Society of America*, 122, 1758–1764.
- Zhang, F., Hammer, T., Banks, H.-L., Benson, C., Xiang, J., & Fu, Q.-J. (2011). Mismatch negativity and adaptation measures of the late auditory evoked potential in cochlear implant users. *Hearing Research*, 275, 17–29.

CHAPTER 10

Multimodal, longitudinal assessment of intracortical microstimulation

Andrew Koivuniemi^{†,§}, Seth J. Wilks[†], Andrew J. Woolley[†] and Kevin J. Otto^{†,‡,*}

[†] *The Weldon School of Biomedical Engineering, Purdue University, West Lafayette, IN, USA*

[‡] *Department of Biological Sciences, Purdue University, West Lafayette, IN, USA*

[§] *Indiana University School of Medicine, Indianapolis, IN, USA*

Abstract: The fundamental obstacle to neuroprostheses based on penetrating microstimulation is the tissue's response to the device insertion and to the application of the electrical stimulation. Our long-term goal is to develop multichannel microstimulation of central nervous tissue for clinical therapy. The overall objective of this research is to identify the optimal parameters for a chronically implanted microstimulation device. In particular, the work presented here focuses on the effects of repeated stimulation and the reactive tissue response on the efficacy of stimulation-driven behavior. To this end, psychophysical experiments were performed using multichannel cortical implants in the auditory cortex of rats. Further, we investigated the effect of the device–tissue interfacial quality on the psychophysical threshold. Here, we report the effects of cortical depth, days postimplant on the psychophysical threshold of auditory cortical microstimulation, along with correlated impedance spectral changes and *post vivo* histology. We expect that these data will further enable neuroprosthetic development.

Keywords: behavioral; impedance spectroscopy; reactive tissue response; histology; cortical depth.

Introduction

Brain machine interfaces (BMIs) aim to transduce information between the world and the subjective experience of the individual. The modern nexus of this dimensional exchange is typically

an electrode. From atop the brain or implanted among the glial cells and neurons, the electrode can passively receive or actively drive the dynamics of the local neural cells. This ability to directly interact with the functional networks of the brain has allowed clinicians to lessen the severity of patients' movement disorders (Benabid et al., 2009), grant volitional control over devices to the paralyzed (Hochberg et al., 2006; Kennedy

*Corresponding author.

Tel.: +1-765-496-1012; Fax: +1-765-496-1912
E-mail: kotto@purdue.edu

and Bakay, 1998), and create visual sensations in the blind (Schmidt et al., 1996).

Nonetheless, one serious and nagging problem for many BMIs is failure of effective transduction, putatively due to the reactive tissue response to the indwelling implanted device. Determining whether electrodes can inhabit the brain for decades and continue to interact and provide valuable information is the most significant BMI hurdle. Efforts to develop the proper signal processing techniques and the most effective stimulation patterns are useful endeavors only if the physical connection between the mind and the machine is viable. The answer to the question of long-term device viability varies based on the application. Indeed, for some BMIs, such as deep brain stimulation (Benabid et al., 2009) and surface cortical stimulation (Dobelle, 2000), the issue seems to be mostly resolved, with devices showing functionality extending well beyond 10 years. Further, some arrays used for recording, such as the neurotrophic electrode (Bartels et al., 2008) and cyberkinetics array (Kim et al., 2008), have also showed functionality in humans for years after the initial implantation. However, for systems that rely on the ability of microelectrodes implanted within the cerebral cortex to record and stimulate highly localized cell populations, this problem remains frustratingly unresolved.

This chapter focuses exclusively on intracortical microstimulation (ICMS) of primary sensory cortical structures. After a brief summary of ICMS, it will set forth what is known about the long-term stability of the sensory effects of ICMS in three parts. The first part will discuss the stability of the *behavioral* effect of microstimulation as a function cortical depth. The second will describe the changes in *electrode impedance* seen during electrical stimulation as a potential approach to elucidating changes seen in the behavioral detection level. The final section will describe postmortem *histological* analysis of interfacing tissue as an alternative approach to understanding the behavioral changes.

Background

Stimulation of various sensory cortices offers a versatile platform for sensory prostheses. The logic for this is as follows: (1) Regions of the brain are responsible for processing information from the outside world and, in doing so, generating a perception in the individual. Thus, all awareness of the outside world is a product of this information processing conducted by the networks of neurons. (2) Electric current can be used to artificially drive the activity of those neurons. This driven activity produces an illusory sensation in the subject, the qualities of which are determined by the region that is stimulated. For example, stimulation of the visual cortex creates a visual illusion. Therefore, given points (1) and (2), electrical stimulation of the sensory cortex could restore vision to the blind, hearing to the deaf, and sensation to the paralyzed.

The first well-documented demonstration of electric cortical stimulation's ability to generate sensory illusions was performed by the neurosurgeon Wilder Penfield (Penfield and Boldrey, 1937). Using simple electrodes applied to what is now referred to as the primary somatosensory cortex, Penfield was able to electrically stimulate conscious patients and have them report the evoked sensations, their location, and quality. In doing so, he was able to generate the iconic sensory homunculus. Penfield continued to study the effects of electrical stimulation on the cortex (Penfield and Mullan, 1957; Penfield and Perot, 1963), but his work tended to focus on higher order structures and was never technologically developed in a way that would lend itself to a sensory prosthesis.

Prosthetic development drove other researchers working in the 1960s and 1970s to systemize the reports of patients receiving cortical stimulation, typically of the primary visual cortex (Brindley and Lewin, 1968; Dobelle and Mladajovsky, 1974). Using surface electrodes placed over the target region, these researchers were able to study the reports of patients and the effects of stimulation

parameters either in an acute experiment that only lasted a few minutes during a surgery (Dobelle et al., 1973) or chronically with patients implanted for years (Dobelle, 2000). While the studies did show that some information could be transferred to individuals and that these effects could last years, the large surface electrodes were too limited in terms of the quality and degree of information transferred to make them a viable prosthetic option.

Building on previous work in nonhuman primates (Bartlett and Doty, 1980), another group attempted to improve upon surface stimulation by using microelectrodes implanted within the visual cortex (Bak et al., 1990; Schmidt et al., 1996). These experiments confirmed that ICMS could be employed to increase the density of stimulation electrodes and that they could deliver more channels of information. They also demonstrated that the amount of electric current required to create a detectable sensation in the stimulated individual was two to three orders of magnitude less for ICMS when compared to surface stimulation.

Since that time, work has focused primarily on animal behavioral models. Because the artificially generated sensations require a conscious agent to report on the generated sensation, animals are trained to perform tasks under known physical stimuli which are subsequently replaced by electrical stimuli. Two excellent examples of such tasks can be found in the somatosensory system (O'Doherty et al., 2009; Romo et al., 1998, 2000), where monkeys have been trained to discriminate between the rate of flutter at their finger tips, and in the visual system, where monkeys have learned to perform a delayed saccade to demonstrate where a light appears in their visual field (Murasugi et al., 1993; Salzman et al., 1990; Tehovnik et al., 2003). After the animals perform these tasks in response to known physical stimuli, the behavior is then reelicited using electrical stimuli.

While such elegant tasks are useful in determining the subjective features of ICMS, simple detection tasks in which the animal indicates the presence of a sensation can also be elucidating (Butovas and Schwarz, 2007; Rousche and Normann, 1999). Such

studies with simpler tasks are useful for evaluating the stimulation parameters that determine the behavioral salience of the electric pulses because experimenters can rapidly explore a variety of factors (Otto et al., 2005a,b). Additionally, such studies could also be helpful in determining the reliability of ICMS in terms of threshold stability. However, systematic exploration of longitudinal detection thresholds for electrical stimulation is lacking, particularly with regard to the cortical depth of the electrode. Wildly fluctuating or steadily rising thresholds are undesirable and must be avoided if ICMS is to become a clinically viable option for treating individuals with sensory deficits. Here, we report recent data from our laboratory that seeks to assess the *reliability* of ICMS.

Experimental overview

In our behavioral paradigm, water-deprived male Sprague-Dawley rats are trained to perform a conditioned avoidance task to detect a sensory stimulus. This protocol was adapted from earlier studies by Heffner and Kelly (Heffner et al., 1994; Kelly et al., 2006) and is described here only briefly.

After 24 h of water deprivation, a rat is placed in a Coulbourn Instruments (Whitehall, PA) behavioral box in a sound isolated chamber. Water flows through an electrically active drinking spout in response to the rat licking the spout. A pure, unmodulated tone is played for 600 ms and acts as a warning. The rat's licking is monitored for the last 200 ms of the warning. If the rat continues to lick during this period, he receives a mild ~ 1 mA cutaneous shock delivered through the spout. The amplitude of the next warning stimulus is then raised and a "miss" is recorded. However, if the rat withdraws from the spout during the last 200 ms of the warning trial, a "hit" is recorded and the amplitude of the next stimulus is lowered. After five to seven detection reversals (changes between series of hits and misses), the mean of the final four reversals is calculated and recorded as the

detection threshold. This is referred to as the “threshold task,” a representative example of which can be seen in Fig. 1c.

To ensure that the rat is maintaining good contact with the spout, warning trials are presented randomly with a 1 in 5 probability, while 4 out of 5 trials are shams in which no warning is presented. If the rat leaves the spout for more than 20% of the sham trials, the series is eliminated from analysis. Once a rat demonstrates that it can consistently perform the task near its putative threshold (Kelly and Masterton, 1977) for a range of frequencies within a single training session, thus generating an audiogram like the one seen in Fig. 1a, it is implanted in its primary auditory cortex (A1) with a single shank, 16 site, 100 μm pitch NeuroNexus (Ann Arbor, MI) microelectrode array in a procedure described in a previous publication (Vetter et al., 2004). During surgery, electrophysiology is performed to ensure that the electrode is placed within the primary auditory cortex and that the site depth is approximately the same for all rats. The electrodes are implanted to span the cortical lamina (Fig. 1b); to confirm cortical depth, local field potentials are recorded, and the current source density is computed to confirm that the electrode array abides in the desired lamina (Müller-Preuss and Mitzdorf, 1984) as seen in Fig. 2.

Behavioral thresholds

Using the adaptive task described above, multiple thresholds can be generated by an animal in a day. Our experimental preparation provides 16 sites linearly over a distance of 1.5 mm, and thus, stimulation can be delivered to all layers of the rat auditory cortex (Paxinos and Watson, 2008), and a behavioral threshold can be generated for all 16 sites in a given rat, each day.

For the experiment presented here, six Sprague-Dawley rats were used (Harlan: Indianapolis, IN) in order to study the effect of electrode site depth on the detection threshold over the first month

after implantation. These data, representing 1273 thresholds, have been analyzed in two ways. The first analysis was performed to show the role of depth on the detection threshold. For the second analysis, the data have been lumped into groups representing four relative cortical depths and displayed by day in order to demonstrate how threshold stability varies over time with cortical depth.

Threshold level varies with depth

Thresholds for all six rats were combined and averaged by electrode site depth. This data is shown in Fig. 3. For the six rats studied, there are three distinct regions in terms of threshold level as follows: The first region is represented by the most superficial sites which are \sim 0–300 μm below the cortical surface and correspond to the first and second lamina (as schematized in Fig. 1b). These sites have the highest threshold levels and are statistically equivalent. The second region represents a linear transition from the superficial region to the third “deep” region, roughly corresponding to third lamina to fifth lamina. Regression analysis of the threshold means for sites 300–1300 μm deep shows a strong linear correlation ($R^2=0.98$) with regard to electrode site depth. The third region contains the deepest sites, corresponding to the transition between the fifth and sixth lamina, and has the lowest thresholds. These findings recapitulate previous microstimulation studies performed in the visual cortex which have demonstrated a similar depth-dependent effect (Bak et al., 1990; DeYoe et al., 2005; Tehovnik and Slocum, 2009).

Threshold stability varies with depth

This experiment also helps to elucidate how the depth of the electrode site affects device performance over time. During the 31 days after electrode placement, there appear to be three distinct phases as seen in Fig. 4. In the first phase,

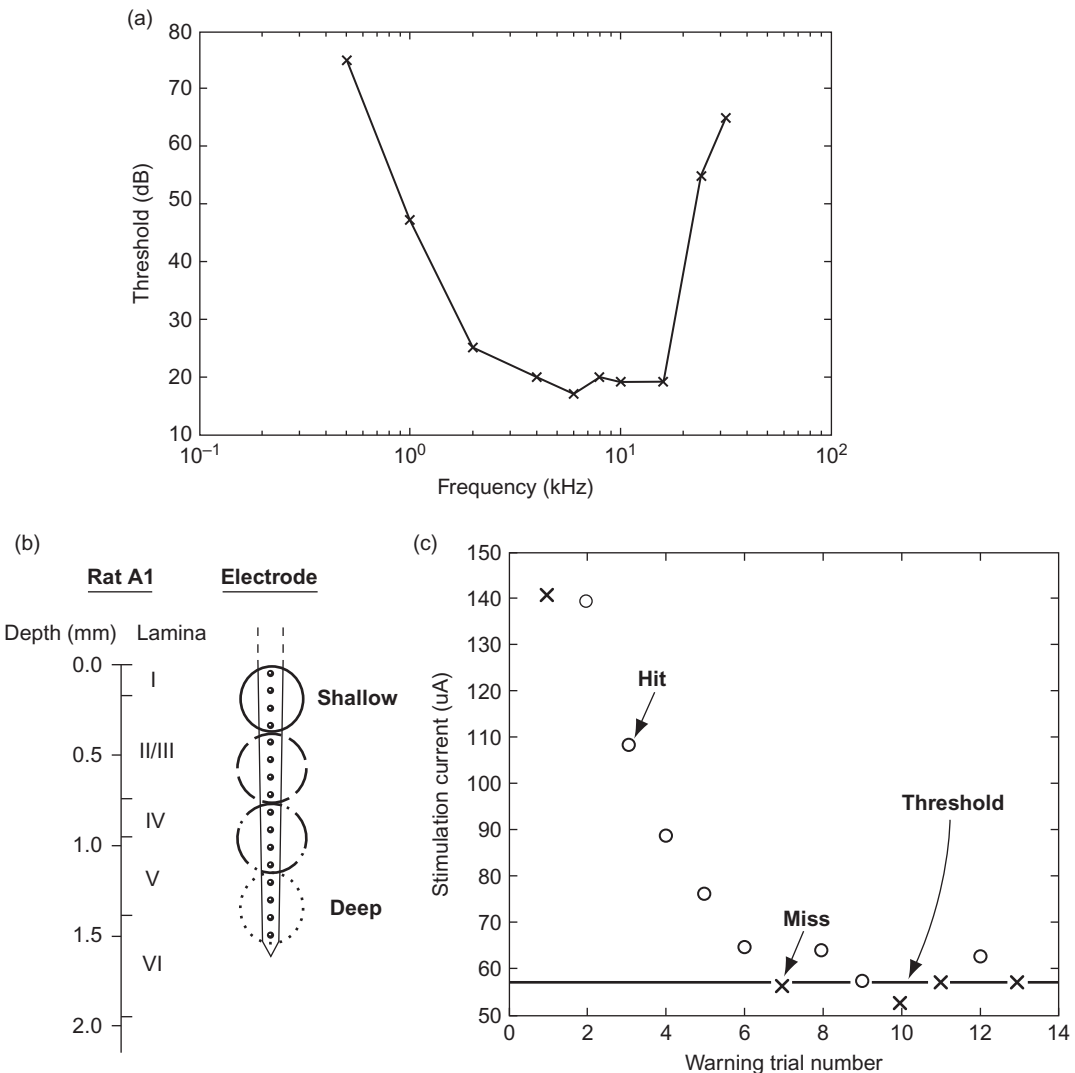


Fig. 1. Experimental background. (a) Sample audiogram generated by a rat in a single day. (b) Schematic representation of rat auditory cortex delineating histological layers as well as relative electrode site placement. (c) Sample rat adaptive threshold task: “○” represents a hit, “×” represents a miss, the bold line represents the threshold estimate.

which represents the first week after implantation, there is a relatively small difference between the superficial sites and the deep sites. Additionally, there is a gradual rise in the thresholds for all sites. In the second phase, which represents roughly the second week after surgery, the

superficial and deep sites begin to separate with threshold levels for the deepest sites declining and the most superficial sites remaining relatively constant. In the third and final phase, thresholds begin to increase again for all but the deepest sites.

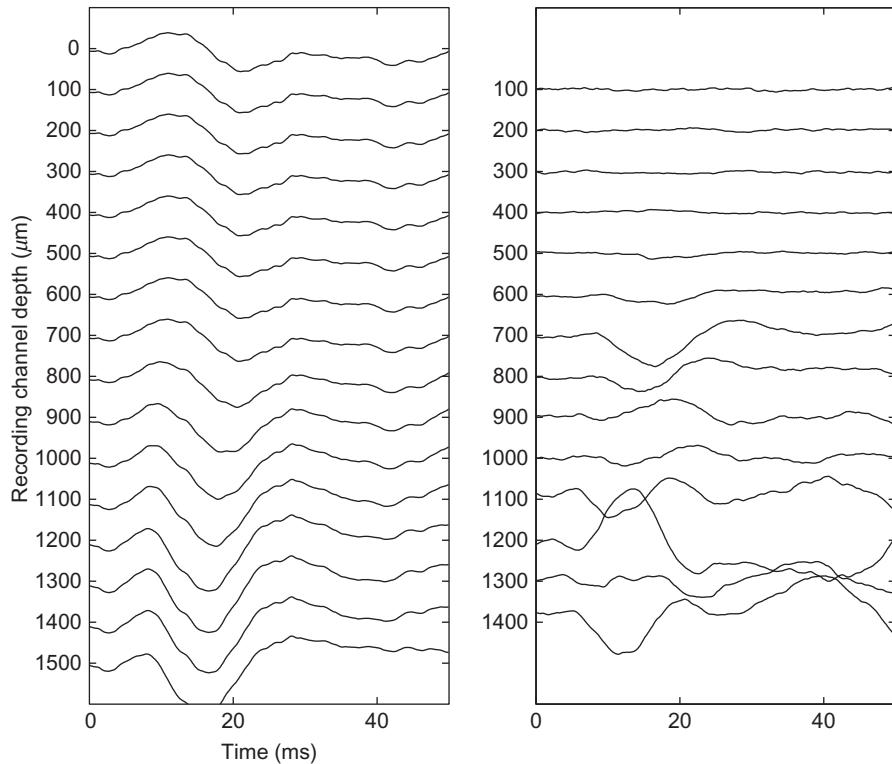


Fig. 2. Sample recording to determine electrode depth location. The left panel shows the averaged local field potentials. The right panel shows the second spatial derivative of the left panel, a method known as current source density analysis (CSD).

Impedance

Implanted electrodes and adjacent tissue form an electrochemical interface that can be characterized via electrochemical measurement techniques. The most common, electrochemical impedance spectroscopy (EIS) measures the impedance magnitude and phase via sinusoidal voltage excitation between the electrode and distant reference at multiple frequencies. EIS provides insight on recording noise levels and safe stimulation levels. Chronic functionality of intracortical microelectrodes requires stable interfacial impedance; however, this is challenging. The reactive tissue response has been shown to affect the impedance at the electrode–tissue interface since encapsulated, damaged tissue display high

impedance ([Williams et al., 2007](#)). Electrical stimulation can further alter the electrical properties of the tissue, as well as the electrode ([Cogan et al., 2004](#); [Weiland and Anderson, 2000](#); [Wilks et al., 2009](#)).

Historical studies show impedance measurements from chronically implanted electrodes showing trends of increasing impedance during the first 2–3 weeks, and then stabilizing, with a reduction in variability between sites and days ([Ludwig et al., 2006](#); [Vetter et al., 2004](#)). This trend corresponds well with the time course of the reactive tissue response ([Williams et al., 2007](#)). [Figure 5a](#) shows average daily 1 kHz impedance magnitude for three probes implanted in three different rats and subjected to daily microstimulation. The impedance increases sharply during the first week after

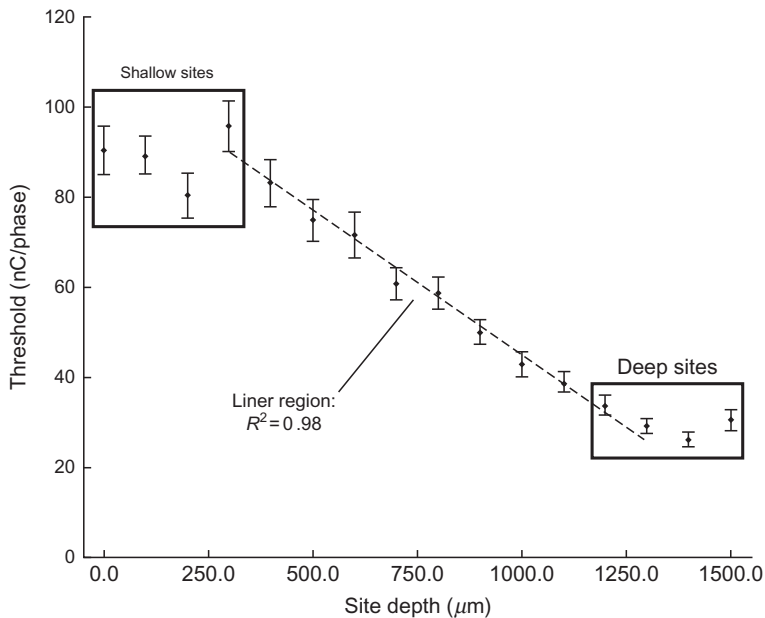


Fig. 3. Mean thresholds for all six rats averaged by electrode site. Points highlighted as “deep” and “shallow” sites have statistically equivalent threshold levels. The linear region represents a transition zone. Regression analysis was performed on the threshold mean from 300 to 1300 μm deep. Error bars show the standard error of the mean.

implantation and then gradually decreases back to baseline after day 21. Rather than stabilizing, impedance magnitude and site-to-site variability increase after this point. A similar trend is observed with the day-to-day changes in behavioral thresholds (Fig. 4).

Pronounced changes in the impedance spectra occur after 2 days postimplant and a subsequent trial of microstimulation. As seen in Fig. 5b, the Nyquist plot becomes gradually less linear over the duration of the implant associated with the progression of the reactive tissue response. The original linearity is partially restored after a trial of microstimulation, similar to that seen with *in vivo* voltage biasing (Otto et al., 2006). As previously seen with the *in vivo* biasing, the reduction in impedance is temporary, and the increase in impedance magnitude and variability after 3 weeks of implantation is most likely attributed to tissue and electrode material damage caused

by microstimulation amplitudes as high as 50–100 μA ($1.6\text{--}3.2 \text{ mC/cm}^2$) which exceed the threshold for neural damage (Shannon, 1992) and iridium oxide damage (Cogan et al., 2004; Wilks et al., 2009).

EIS data can be fit to an equivalent circuit model to enable *in vivo* assessment of both the electrode and tissue. As seen in Fig. 6a, the model comprises a constant phase element (CPE) representing the electrode component, a sealing resistance (R_{en}) representing adsorbed proteins, extracellular resistance (R_{ex}), and parallel RC (resistive/capacitive) components representing cell membranes of the glial sheath (Johnson et al., 2005; Otto et al., 2006). The electrode component is broken down into a magnitude (K) and phase scaling term (α), and the membrane component is lumped into a single scaling term (A_m). Figure 6b shows impedance spectra and fitted model data, as well as individual tissue

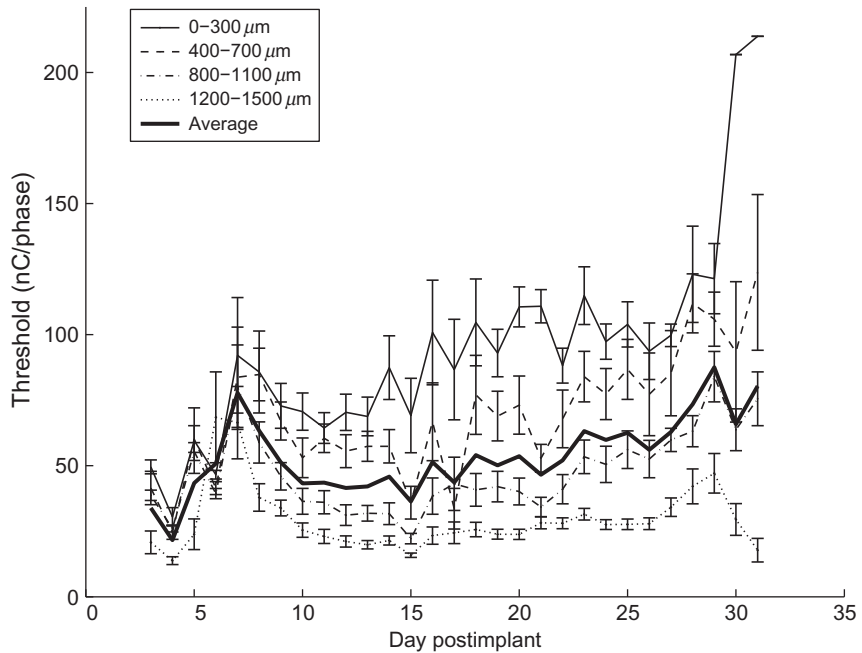


Fig. 4. Mean thresholds (represented on the Y-axis) for all six rats lumped into depth regions and averaged by days postimplant. The threshold, that is, the current amplitude for which the rat's detection probability equaled 50%, is represented in terms of nC per phase, which is the product of the current amplitude and the duration of the first phase. The data represent the first month (31 days) after implantation. In the first week (days 1–7), thresholds tend to rise together. In the second week (days 8–14), thresholds tend to recover with deeper sites decreasing the most. In the final phase, thresholds tend to increase in the superficial sites, while thresholds at deep sites are relatively stable. Error bars show the standard error of the mean.

and electrode model components, pre- and post-microstimulation application. Microstimulation leads to an immediate decrease in impedance with the largest changes occurring in A_m and R_{ex} (Fig. 6c), indicating changes in the encapsulated tissue and extracellular space.

Maintaining a stable, low-impedance interface is important in the continuing functionality of intracortical microelectrodes. Changes in the cellular environment influence the day-to-day impedance changes which are similar to the day-to-day changes in behavioral threshold levels, revealing a complex interaction between the reactive tissue response, changes in electrode properties, and device performance. Repeated microstimulation likely results in additional tissue and electrode damage. However, because the

stimulation seems to necessarily disrupt the tissue response adjacent to the electrode site, it is difficult to systematically study this interaction. Nonetheless, it remains an *a priori* truth that the development of devices and techniques to mitigate adverse tissue responses and deliver non-damaging, behaviorally relevant electrical stimulation to the electrode and tissue is essential to maintain a stable, low-impedance interface and a healthy surrounding neural population.

Histology

To investigate whether and how tissue changes at the electrode interface might be affecting long-term device utility, histological labeling and

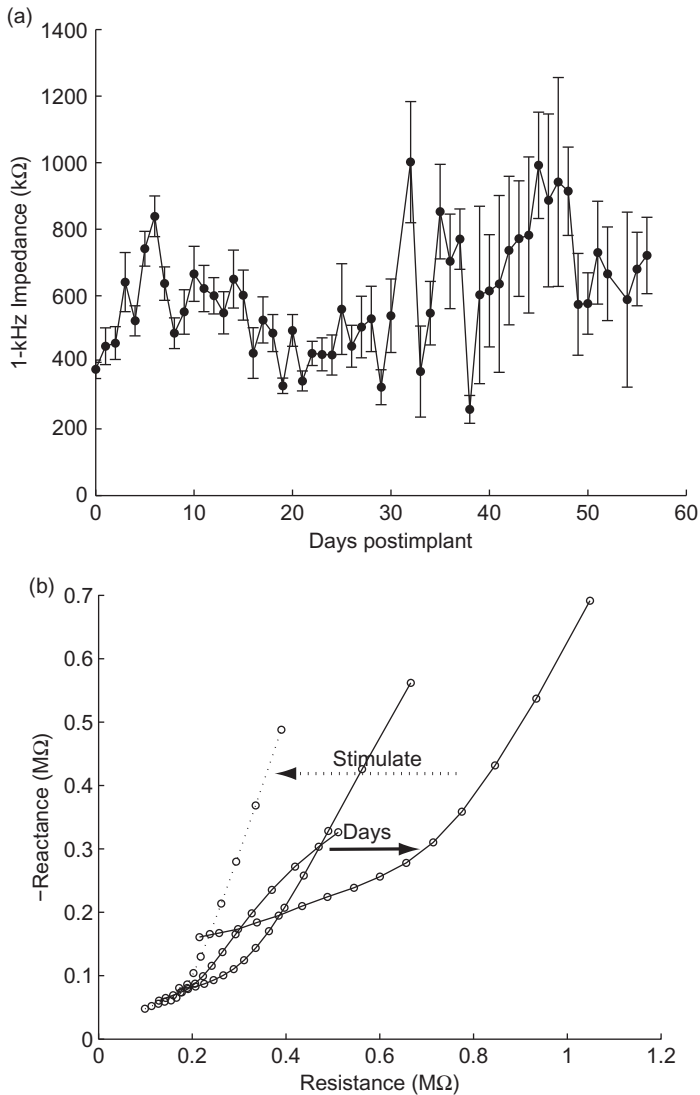


Fig. 5. Impedance stability over time. (a) Mean 1 kHz impedance magnitudes from three electrode arrays implanted in three different rats subjected to daily microstimulation. Consistent across each implantation, the impedance magnitude increases with time postimplant. (b) Nyquist plots from three electrode arrays taken immediately after implantation, 1 and 2 days postimplant (solid lines), and immediately after electrical stimulation (dotted line). This is an example of typical trends in impedance changes after implantation and electrical stimulation.

imaging techniques are often employed (Polikov et al., 2005; Stensaas and Stensaas, 1978; Turner et al., 1999). Microscope-based analysis, akin to traditional pathological analysis, can be

performed on brain tissue to investigate the tissue response in each subject at a single, final time point. Typically, the locations of applied biomarkers relative to explanted-device holes

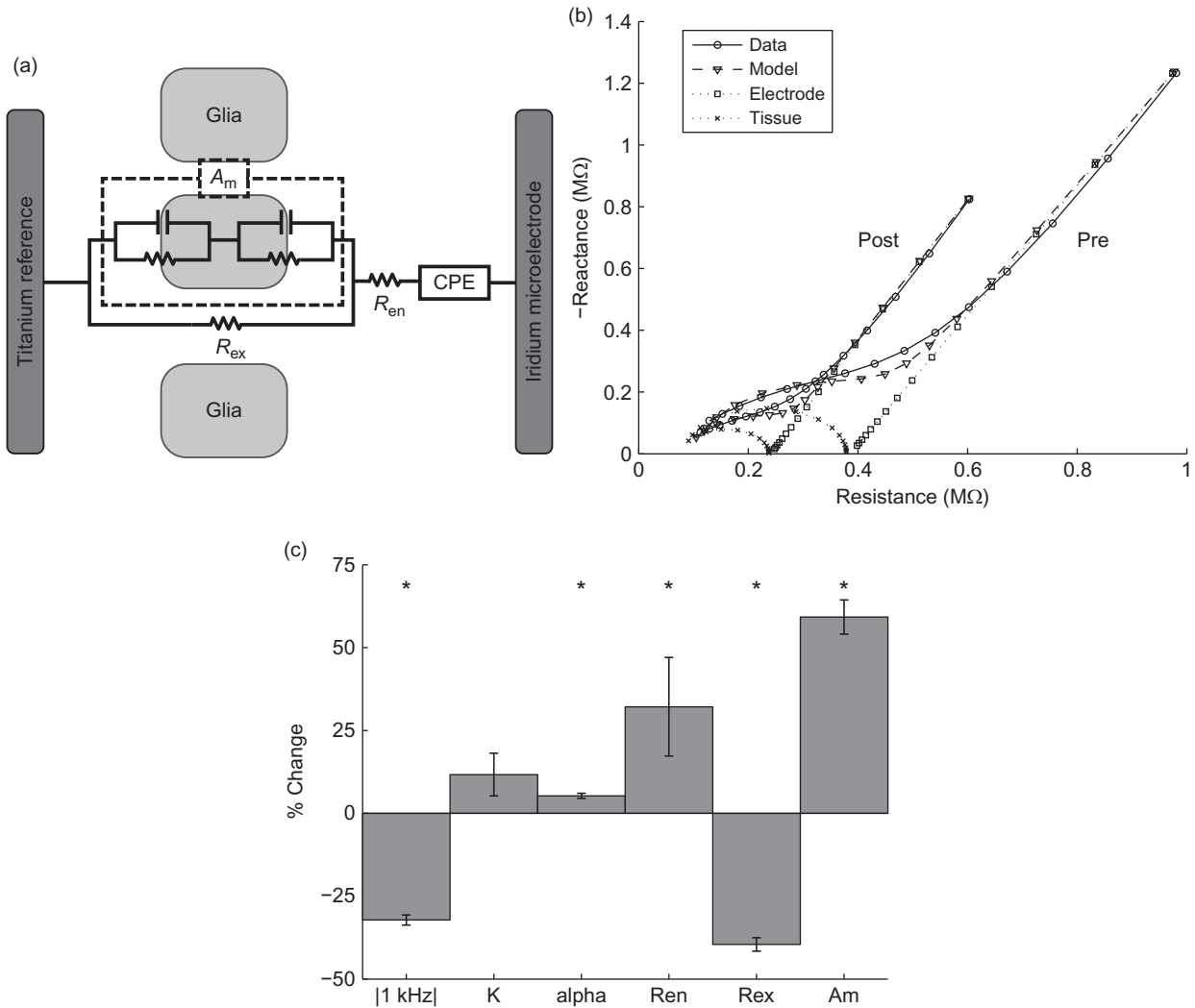


Fig. 6. Modeling effects of stimulation on electrode impedance. (a) Equivalent circuit model of the electrode–tissue interface. (b) Nyquist plots of measured and modeled impedance spectra from an electrode pre- and postmicrostimulation. (c) Significant changes in 1 kHz impedance and model parameters occur pre- and postmicrostimulation, especially for the tissue components R_{en} , R_{ex} , and A_m ($n=350$, paired t -test, $p<0.01$).

within each tissue slice are imaged and analyzed. The reason that devices are explanted from tissue is to avoid dragging or shattering them upon slicing the tissue and to simplify the histological preparation. The tissue is thinly

sliced in order to both improve the even diffusion of applied biomarker labels and avoid limitations on light penetration through the somewhat opaque tissue upon microscope analysis.

While explanting devices and taking thin ($<50\text{ }\mu\text{m}$) tissue slices has provided significant data on the tissue changes that occur around chronic ICMS arrays (McConnell et al., 2009; Turner et al., 1999; Winslow and Tresco, 2010), this method produces tissue with morphological distortion at the interfacing tissue (Holecko et al., 2005). The former location of electrode sites is also difficult to determine once the device has been explanted. Also, because histological labels diffuse from applied solutions into the tissue, surfaces contacting the solution can have increased labeling, leading to possibly misleading label intensity at the surface of explant holes. To avoid these problems, the authors have developed a method to collect, label, and image the *in situ* implanted device and its surrounding tissue.

Figure 7 presents example microscope data taken around an implanted device, left *in situ* within a thicker ($>100\text{ }\mu\text{m}$) histological slice. Using chemical and immunohistochemical labeling techniques, biomarkers for inflammation, specific cell types, and other items of interest can be fluorescently tagged. After labeling, the tissue and devices can then be imaged using a laser scanning confocal microscope. Images taken along the depth of the intact implant (Fig. 7a

and b) allow investigation of tissue changes related to cortical depth. Close investigation of tissue at the device surface or even around individual electrode sites is also performed (Fig. 7c–e), revealing the local distribution of labeled elements relative to the intact electrode–tissue interface.

Conclusion and future work

The development of a functional sensory prosthesis that interfaces directly with the human cortex is a daunting challenge with many obstacles to overcome. However, before any of these may be addressed, it is important to first optimize the electrode design, the implantation technique, and the stimulation parameters.

This chapter reports data and two potential ways of assessing that data. First, the data clearly demonstrate that there is a laminar variation in terms of detection threshold for ICMS in which the deepest sites, roughly corresponding to layers V and VI, are the most sensitive. Second, the data also demonstrate that there is laminar variation in terms of threshold stability over the first month after implantation. Sites that are deepest in cortex maintain their threshold during the 1-month trial

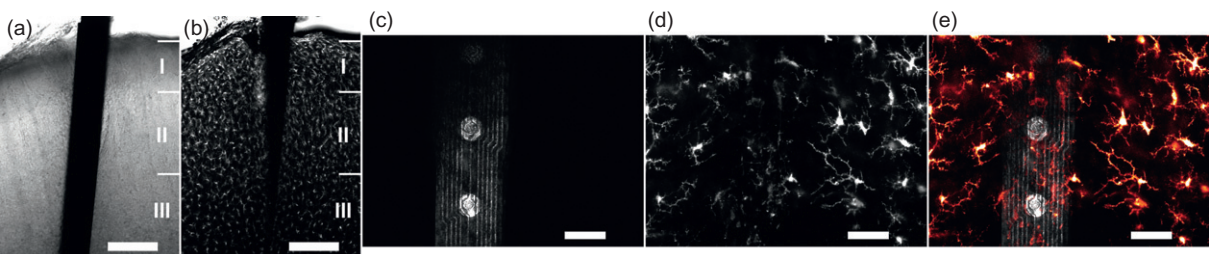


Fig. 7. *In situ* histology to investigate the intact device/tissue interface. (a) Transmission light image showing a microelectrode array captured in fixed brain tissue and imaged by laser confocal microscopy. (b) Microglia, labeled by immunohistochemically tagging the protein Iba1 with the fluorescent marker Alexa Fluor 633, are seen in a single optical section responding in a layer-dependent fashion around this 1-week implanted device. (c) A 10- μm -thick z-stack of images shows the device surface imaged by collecting laser reflectance; (d) microglia at this same location are shown responding to the presence of the device 24 h after implantation. (e) Microglia filopodia investigating the device's surface and neighboring tissue are further presented in this image overlay. Scale bars indicate 200 μm in (a) and (b), and 50 μm in (c–e).

period, while the thresholds for more superficial sites tend to gradually increase. These two facts taken together suggest further investigation of the potential for deep layers to provide consistent stimulation. However, additional work needs to be conducted to determine the source of the laminar variation.

Data addressing the source of the laminar variation may be collected through impedance spectroscopy, which attempts to model the magnitude of the cellular and extracellular tissue response to the implanted electrode. This approach offers an obvious advantage in that it may be performed concurrently with the behavioral task and does not require that the animal be euthanized. A potential hypothesis is that more superficial sites undergo a larger reactive tissue response and, thus, receive the most damage to the neighboring neurons. If this is the case, then those sites should see the greatest increase in impedance levels, signifying that the cellular encapsulation is most virulent at these layers. However, to date, there has not been any strong correlation between electrode impedance values with either site depth or with threshold level. While this may seem to contradict the above hypothesis, it must be noted that the electrical stimulation presents a strong confounding factor by electrical disruption of the glial encapsulation, lowering the impedance as seen in Fig. 6. Future work will focus on refining the model and exploring other parameters that may better correlate with or predict changes in the detection thresholds.

The second potential means of assessing the stability difference between cortical layers is through histology. Using *in situ* techniques which capture the electrode along with the neighboring tissue, we hope to analyze and describe histological markers that could help to explain variations in threshold stability. The primary drawback to this approach is that it requires that the experiment be terminated. Due to the longitudinal behavioral data, animals are often not sacrificed until the device fails or the animal becomes infected. This

has frustrated work to fully analyze these effects; therefore, future work will attempt to perform *in vivo* imaging concurrent with the behavioral and impedance spectroscopy measurements.

Finally, additional future work will seek to expand on these findings by exploring novel, potentially more efficient stimulation waveforms, which have been designed to take advantage of the nonlinearities of the voltage-gated sodium channel (McIntyre and Grill, 2000, 2002). Such pulses, employing asymmetric biphasic morphologies, have been shown to lower detection thresholds in cochlear implant users (van Wieringen et al., 2008). However, to the authors' knowledge, these pulses have never been evaluated in the context of ICMS. Additionally, an effort will be made to determine the behavioral safe limits of high duty electrical stimulation using studies similar in design to other chronic stimulation experiments (McCreery et al., 1997, 2002).

References

- Bak, M. J., Girvin, J. P., et al. (1990). Visual sensations produced by intracortical microstimulation of the human occipital cortex. *Medical & Biological Engineering & Computing*, 28(3), 257–259.
- Bartels, J., Andreasen, D., et al. (2008). Neurotrophic electrode: Method of assembly and implantation into human motor speech cortex. *Journal of Neuroscience Methods*, 174 (2), 168–176.
- Bartlett, J. R., & Doty, R. W. (1980). An exploration of the ability of macaques to detect microstimulation of striate cortex. *Acta Neurobiologiae Experimentalis*, 40(4), 713–727.
- Benabid, A. L., Chabardes, S., et al. (2009). Deep brain stimulation of the subthalamic nucleus for the treatment of Parkinson's disease. *Lancet Neurology*, 8(1), 67–81.
- Brindley, G. S., & Lewin, W. S. (1968). The sensations produced by electrical stimulation of the visual cortex. *The Journal of Physiology*, 196(2), 479–493.
- Butovas, S., & Schwarz, C. (2007). Detection psychophysics of intracortical microstimulation in rat primary somatosensory cortex. *The European Journal of Neuroscience*, 25(7), 2161–2169.
- Cogan, S. F., Guzelian, A. A., et al. (2004). Over-pulsing degrades activated iridium oxide films used for intracortical neural stimulation. *Journal of Neuroscience Methods*, 137 (2), 141–150.

- DeYoe, E. A., Lewine, J. D., et al. (2005). Laminar variation in threshold for detection of electrical excitation of striate cortex by macaques. *Journal of Neurophysiology*, 94(5), 3443–3450.
- Dobelle, W. H. (2000). Artificial vision for the blind by connecting a television camera to the visual cortex. *ASAIO Journal*, 46(1), 3–9.
- Dobelle, W. H., & Mladejovsky, M. G. (1974). Phosphenes produced by electrical stimulation of human occipital cortex, and their application to the development of a prosthesis for the blind. *The Journal of Physiology*, 243(2), 553–576.
- Dobelle, W. H., Stensaas, S. S., et al. (1973). A prosthesis for the deaf based on cortical stimulation. *The Annals of Otology, Rhinology, and Laryngology*, 82(4), 445–463.
- Heffner, H. E., Heffner, R. S., et al. (1994). Audiogram of the hooded Norway rat. *Hearing Research*, 73(2), 244–247.
- Hochberg, L. R., Serruya, M. D., et al. (2006). Neuronal ensemble control of prosthetic devices by a human with tetraplegia. *Nature*, 442(7099), 164–171.
- Holecko, M. M., 2nd, Williams, J. C., et al. (2005). Visualization of the intact interface between neural tissue and implanted microelectrode arrays. *Journal of Neural Engineering*, 2(4), 97–102.
- Johnson, M. D., Otto, K. J., et al. (2005). Repeated voltage biasing improves unit recordings by reducing resistive tissue impedances. *IEEE Transactions on Neural Systems and Rehabilitation Engineering*, 13(2), 160–165.
- Kelly, J. B., Cooke, J. E., et al. (2006). Behavioral limits of auditory temporal resolution in the rat: Amplitude modulation and duration discrimination. *Journal of Comparative Psychology*, 120(2), 98–105.
- Kelly, J. B., & Masterton, B. (1977). Auditory sensitivity of the albino rat. *Journal of Comparative and Physiological Psychology*, 91(4), 930–936.
- Kennedy, P. R., & Bakay, R. A. E. (1998). Restoration of neural output from a paralyzed patient by a direct brain connection. *NeuroReport*, 9(8), 1707–1711.
- Kim, S.-P., et al. (2008). Neural control of computer cursor velocity by decoding motor cortical spiking activity in humans with tetraplegia. *Journal of Neural Engineering*, 5(4), 455.
- Ludwig, K. A., Uram, J. D., et al. (2006). Chronic neural recordings using silicon microelectrode arrays electrochemically deposited with a poly(3,4-ethylenedioxythiophene) (PEDOT) film. *Journal of Neural Engineering*, 3(1), 59–70.
- McConnell, G. C., et al. (2009). Implanted neural electrodes cause chronic, local inflammation that is correlated with local neurodegeneration. *Journal of Neural Engineering*, 6(5), 056003.
- McCreery, D. B., Agnew, W. F., et al. (2002). The effects of prolonged intracortical microstimulation on the excitability of pyramidal tract neurons in the cat. *Annals of Biomedical Engineering*, 30(1), 107–119.
- McCreery, D. B., Yuen, T. G., et al. (1997). A characterization of the effects on neuronal excitability due to prolonged microstimulation with chronically implanted microelectrodes. *IEEE Transactions on Biomedical Engineering*, 44(10), 931–939.
- McIntyre, C. C., & Grill, W. M. (2000). Selective microstimulation of central nervous system neurons. *Annals of Biomedical Engineering*, 28(3), 219–233.
- McIntyre, C. C., & Grill, W. M. (2002). Extracellular stimulation of central neurons: Influence of stimulus waveform and frequency on neuronal output. *Journal of Neurophysiology*, 88(4), 1592–1604.
- Müller-Preuss, P., & Mitzdorf, U. (1984). Functional anatomy of the inferior colliculus and the auditory cortex: Current source density analyses of click-evoked potentials. *Hearing Research*, 16(2), 133–142.
- Murasugi, C. M., Salzman, C. D., et al. (1993). Microstimulation in visual area MT: Effects of varying pulse amplitude and frequency. *The Journal of Neuroscience*, 13(4), 1719–1729.
- O'Doherty, J. E., Lebedev, M., et al. (2009). A brain-machine interface instructed by direct intracortical microstimulation. *Frontiers in Neuroengineering*, 2(7), 1–8.
- Otto, K. J., Johnson, M. D., et al. (2006). Voltage pulses change neural interface properties and improve unit recordings with chronically implanted microelectrodes. *IEEE Transactions on Biomedical Engineering*, 53(2), 333–340.
- Otto, K. J., Rousche, P. J., et al. (2005a). Cortical microstimulation in auditory cortex of rat elicits best-frequency dependent behaviors. *Journal of Neural Engineering*, 2(2), 42–51.
- Otto, K. J., Rousche, P. J., et al. (2005b). Microstimulation in auditory cortex provides a substrate for detailed behaviors. *Hearing Research*, 210(1–2), 112–117.
- Paxinos, G., & Watson, C. (2007). *The rat brain in stereotaxic coordinates*. San Diego, CA: Academic Press.
- Penfield, W., & Boldrey, E. (1937). Somatic motor and sensory representation in the cerebral cortex of man as studied by electrical stimulation. *Brain*, 60, 389–443.
- Penfield, W., & Mullan, S. (1957). Illusions of perception and the temporal cortex. *Transactions of the American Neurological Association 82nd Meeting*: 6–8, discussion 8–9.
- Penfield, W., & Perot, P. (1963). The brain's record of auditory and visual experience. *Brain*, 86, 595–696.
- Polikov, V. S., Tresco, P. A., et al. (2005). Response of brain tissue to chronically implanted neural electrodes. *Journal of Neuroscience Methods*, 148(1), 1–18.
- Romo, R., Hernandez, A., et al. (1998). Somatosensory discrimination based on cortical microstimulation. *Nature*, 392(6674), 387–390.
- Romo, R., Hernandez, A., et al. (2000). Sensing without touching: Psychophysical performance based on cortical microstimulation. *Neuron*, 26(1), 273–278.

- Rousche, P. J., & Normann, R. A. (1999). Chronic intracortical microstimulation (ICMS) of cat sensory cortex using the Utah Intracortical Electrode Array. *IEEE Transactions on Rehabilitation Engineering*, 7(1), 56–68.
- Salzman, C. D., Britten, K. H., et al. (1990). Cortical microstimulation influences perceptual judgements of motion direction. *Nature*, 346(6280), 174–177.
- Schmidt, E. M., Bak, M. J., et al. (1996). Feasibility of a visual prosthesis for the blind based on intracortical microstimulation of the visual cortex. *Brain*, 119(Pt. 2), 507–522.
- Shannon, R. V. (1992). A model of safe levels for electrical stimulation. *IEEE Transactions on Biomedical Engineering*, 39(4), 424–426.
- Stensaas, S. S., & Stensaas, L. J. (1978). Histopathological evaluation of materials implanted in cerebral-cortex. *Acta Neuropathologica*, 41(2), 145–155.
- Tehovnik, E. J., & Slocum, W. M. (2009). Depth-dependent detection of microampere currents delivered to monkey V1. *The European Journal of Neuroscience*, 29(7), 1477–1489.
- Tehovnik, E. J., Slocum, W. M., et al. (2003). Saccadic eye movements evoked by microstimulation of striate cortex. *The European Journal of Neuroscience*, 17(4), 870–878.
- Turner, J. N., Shain, W., et al. (1999). Cerebral astrocyte response to micromachined silicon implants. *Experimental Neurology*, 156(1), 33–49.
- van Wieringen, A., Macherey, O., et al. (2008). Alternative pulse shapes in electrical hearing. *Hearing Research*, 242 (1–2), 154–163.
- Vetter, R. J., Williams, J. C., et al. (2004). Chronic neural recording using silicon-substrate microelectrode arrays implanted in cerebral cortex. *IEEE Transactions on Biomedical Engineering*, 51(6), 896–904.
- Weiland, J. D., & Anderson, D. J. (2000). Chronic neural stimulation with thin-film, iridium oxide electrodes. *IEEE Transactions on Biomedical Engineering*, 47(7), 911–918.
- Wilks, S. J., Richardson-Burns, S. M., et al. (2009). Poly(3,4-ethylenedioxythiophene) as a micro-neural interface material for electrostimulation. *Frontiers in Neuroengineering*, 3 (20), 1–8.
- Williams, J. C., Hippensteel, J. A., et al. (2007). Complex impedance spectroscopy for monitoring tissue responses to inserted neural implants. *Journal of Neural Engineering*, 4, 410–423.
- Winslow, B. D., & Tresco, P. A. (2010). Quantitative analysis of the tissue response to chronically implanted microwire electrodes in rat cortex. *Biomaterials*, 31(7), 1558–1567.

CHAPTER 11

The functional consequences of chronic, physiologically effective intracortical microstimulation

Rebecca A. Parker[†], Tyler S. Davis[‡], Paul A. House[§], Richard A. Normann[‡] and
Bradley Greger^{‡,*}

[†] Interdepartmental Program in Neuroscience, University of Utah, Salt Lake City, UT, USA

[‡] Department of Bioengineering, University of Utah, Salt Lake City, UT, USA

[§] Department of Neurosurgery, University of Utah School of Medicine, Salt Lake City, UT, USA

Abstract: Many studies have demonstrated the ability of chronically implanted multielectrode arrays (MEAs) to extract information from the motor cortex of both humans and nonhuman primates. Similarly, many studies have shown the ability of intracortical microstimulation to impart information to the brain via a single or a few electrodes acutely implanted in sensory cortex of nonhuman primates, but relatively few microstimulation studies characterizing chronically implanted MEAs have been performed. Additionally, device and tissue damage have been reported at the levels of microstimulation used in these studies. Whether the damage resulting from microstimulation impairs the ability of MEAs to chronically produce physiological effects, however, has not been directly tested. In this study, we examined the functional consequences of multiple months of periodic microstimulation via chronically implanted MEAs at levels capable of evoking physiological responses, that is, electromyogram (EMG) activity. The functionality of the MEA and neural tissue was determined by measuring impedances, the ability of microstimulation to evoke EMG responses, and the recording of action potentials. We found that impedances and the number of recorded action potentials followed the previously reported trend of decreasing over time in both animals that received microstimulation and those which did not receive microstimulation. Despite these trends, the ability to evoke EMG responses and record action potentials was retained throughout the study. The results of this study suggest that intracortical microstimulation via MEAs did not cause functional failure, suggesting that MEA-based microstimulation is ready to transition into subchronic (<30 days) human trials to determine whether complex spatiotemporal sensory percepts can be evoked by patterned microstimulation.

*Corresponding author.

Tel.: +1-801-585-5795; Fax: +1-801-581-8966

E-mail: bradley.greger@utah.edu

Keywords: micro-electrode array; motor cortex; feline; electromyogram; impedance; microstimulation.

Introduction

Multielectrode arrays (MEAs) are a promising technology for use in intracortical neuroprosthetics. For such devices to be clinically successful in recording applications, MEAs must be able to acquire sufficient neural data to control an effector device, such as a prosthetic arm, for the life span of the patient. While the action potential recordings currently obtained using MEAs are not stable over these timeframes (Dickey et al., 2009; Linderman et al., 2006; Suner et al., 2005), studies have shown that having well-isolated action potential recordings is not necessary for successfully decoding movements (Fraser et al., 2009; Rivera-Alvidrez et al., 2010). Numerous studies have also demonstrated the utility of MEAs for intracortical motor prosthetic applications in non-human primates (Aggarwal et al., 2009; Musallam, 2004; Nicolelis, 2003; Santhanam et al., 2006; Schwartz et al., 2006; Taylor, 2002; Wessberg, 2000). Further, chronically implanted MEAs have been used to control a variety of effectors in human patients (Hochberg and Donoghue, 2006; Hochberg et al., 2006; Serruya et al., 2002).

MEAs can also potentially be used as a high-resolution interface for the injection of charge directly into brain tissue. Such electrical microstimulation activates neurons, which can generate or modulate a neurophysiological process, such as sensory perception or movement. Numerous studies have evaluated the effects of acute microstimulation on different neural systems. These studies include experiments in the auditory system of rodents (Otto et al., 2005a; Rousche et al., 2003), and the somatosensory system (Romo et al., 1998), visual system (DeYoe, 2005; Murphrey and Maunsell, 2007, 2008; Tehovnik, 2006; Tehovnik and Slocum, 2009), and motor system (Cooke, 2003; Fitzsimmons et al., 2007; Graziano, 2005; Graziano et al., 2002; Salzman et al., 1990; Schmidt and McIntosh, 1990) of nonhuman primates. Only a few studies, however, have

investigated the consequences of chronic intracortical microstimulation to effect through a chronically implanted MEA (Bradley, 2004; Rousche and Normann, 1999). Human studies have demonstrated the ability to evoke percepts through intracortical microstimulation, but these experiments have been limited to intraoperative time frames (Bak et al., 1990) or to a single chronically implanted patient (Schmidt et al., 1996). Significant insight into the perceptual effects of microstimulation was obtained in these few human experiments, suggesting that further studies utilizing microstimulation via high-density MEAs in subchronic clinical trials will be valuable. Prior to transitioning such research into human patients, however, the functional effects of microstimulation must be evaluated in a nonhuman system to demonstrate both safety and efficacy over chronic timescales.

The consequences of chronic microstimulation are disputed. *In vitro* stimulation studies and investigations of the histological response of brain tissue to microstimulation have shown that damage to both device and tissue can arise from microstimulation (Cogan, 2004; McCreery et al., 2010; Merrill et al., 2005; Negi et al., 2010; Troyk et al., 2004). Intracortical stimulating macroelectrodes, such as deep brain stimulating electrodes, have also been shown to cause tissue reactivity with the application of stimulation (Moss, 2004). Despite the damage caused by stimulating macroelectrodes, however, such devices can deliver functional stimulation for years, especially when stimulation is titrated to effect (Deuschl et al., 2006). While histological markers, including antibodies for reactive astrocytes and neurons can indicate that tissue is damaged, histology cannot indicate whether or not stimulation was effective or whether tissue response would have had an effect on performance. Additionally, histology can only be collected at experimental end points, which means that tissue response cannot be tracked through the course of multiple months of

implantation and microstimulation without the sacrifice of many animals at several time points. In order to analyze the performance of microstimulation via microelectrodes over the course of a multiple-month implantation, electrophysiological markers of performance, rather than histological markers of safety, must be used. Electrophysiological markers, such as recorded action potentials, can demonstrate not only the viability of tissue in the vicinity of electrodes, but also that device integrity is maintained.

In this study, we investigate the *in vivo* performance of sputtered iridium oxide film (SIROF) metalized MEAs used to deliver chronic, physiologically effective intracortical microstimulation. Four felines were implanted with MEAs and two were stimulated to physiological effect, as measured by electromyogram (EMG). Functionality was evaluated using impedance measurements, electrophysiological recordings, and the ability of microstimulation to evoke EMG responses, to determine if device and/or tissue damage occurred with periodic microstimulation. Using these measures, we found that microstimulation efficacy could be maintained after several months of implantation and many microstimulation sessions. Further, we found that microstimulation did not appear to adversely impact either impedances or the ability to perform electrophysiological recordings over the course of the study.

Methods

Surgical procedures

Implantations and all other procedures were performed in accordance with protocols approved by the University of Utah Institutional Animal Care and Use Committee. Four felines (*Felis catus*) were used in this study. Felines each had an array implanted in motor cortex (Ghosh, 1997) so that applied stimulation would result in motor response measurable by EMGs recorded in either forelimb or hindlimb muscles. All implants were performed

by the same clinical neurosurgeon to ensure consistency of implant technique and array placement. Anesthesia was induced using ketamine/xylazine and then continued using Isoflurane. Under sterile conditions, a midline incision was performed, and a craniotomy over the targeted area was made by means of a neurosurgical drill. The dura was reflected, and the array was pneumatically inserted into motor cortex (Rousche and Normann, 1992). Following implantation, the titanium percutaneous connector was attached to the skull using bone screws. A dural replacement (DuraGen, Integra Life Sciences, Plainsboro, NJ) was used to cover the array, and silicone polymer (Kwik-cast, World Precision Instruments, Sarasota, FL) was used to fill the craniotomy, if necessary. The scalp was sutured closed and the animal given at least 24 h to recover before data acquisition was attempted.

Electrode arrays

For Felines 1 and 2, arrays were obtained from Cyberkinetics, Inc. (Salt Lake City, UT) with electrode tips that had been coated by EIC Laboratories (Norwood, MA) with SIROFs. For Felines 3 and 4, 96-electrode SIROF Utah Electrode Arrays were commercially obtained from Blackrock Microsystems, Inc. (Salt Lake City, UT). Arrays were manufactured as described elsewhere (Jones et al., 1992) under Design Controls specified by the United States Food and Drug Administration. Electrodes were 1 mm long and spaced 400 μm apart. The SIROF used to coat the conductive electrode tips increased the charge injection capacity of the electrodes and reduced the possibility of electrode dissolution (Cogan, 2008; Cogan et al., 2009). Active electrode tips were $\sim 40 \mu\text{m}$ in length, yielding $\sim 4000 \mu\text{m}^2$ of SIROF surface area per electrode (Negi et al., 2010; VanWagenen, 2004). The remainder of the array was coated with Parylene-C insulation for electrical isolation and biocompatibility. A summary of arrays used is presented in Table 1.

Table 1. Arrays used

Animal	Array material, manufacture date, location	Implant date	Preinsertion impedances (kΩ)
Feline 1	SIROF 2006, Cyberkinetics/EIC	January 2007	Mean 16, Median 11, Min 4, Max 110
Feline 2	SIROF 2006, Cyberkinetics/EIC	October 2008	Mean 23, Median 14, Min 5, Max 160
Feline 3	SIROF 2009, Blackrock Microsystems	July 2009	Mean 50.4, Median 50, Min 42, Max 74
Feline 4	SIROF 2010, Blackrock Microsystems	July 2010	Mean 46.9, Median 47, Min 40, Max 63

Four SIROF arrays were chronically implanted in feline motor cortex. Felines 3 and 4 were microstimulated, while Felines 1 and 2 were used to obtain comparison recording-only data for long-term patterns of 1 kHz impedance and electrophysiological measures of chronic performance.

Data acquisition

A 128-channel Cerebus data acquisition system (Blackrock Microsystems) was used to acquire neural data. The 96 channels of electrode data from the UEA were fed to a front-end amplifier using a Cereport patient cable.

Impedance measurements

One kilohertz (kHz) impedance measurements were made using a routine in the Cerebus data acquisition system. Briefly, a small sinusoidal current at 1 kHz was passed through a reference electrode, and impedance was simultaneously computed on all electrodes. Chronic impedance readings were taken throughout the multiple-month course of implantation in all four felines. Acute impedance readings were also taken pre- and post-stimulation for each microstimulation session in Felines 3 and 4.

Electrophysiological recordings

Neural recordings were obtained from awake felines to examine device performance over time both with and without the application of microstimulation. Felines were placed in a pet carrier inside an electrically shielded chamber to

minimize noise, and connected to the Cerebus. Recordings were made at least weekly in all felines, as well as prior to and following every stimulation session in Felines 3 and 4. Recordings were made in several-minute sessions using band-pass filter settings of 0.3 Hz–7.5 kHz and sampled at 30 kHz in Felines 1–3, and band-pass filter settings of 0.3 Hz–2.5 kHz sampled at 10 kHz in Feline 4 to reduce file size.

Electromyography

EMGs were used periodically in Felines 3 and 4 to test the ability to evoke physiological responses via intracortical microstimulation. Following a control neural data recording, the animal was anesthetized with Telazol administered intramuscularly at 0.01 mg/kg. Sterile, clinical fine-wire electrodes were placed in the biceps femoris muscle of Feline 3 and either the triceps or extensor carpi muscle of Feline 4. Reference electrodes were placed subcutaneously near the intramuscular electrode. EMG activity in response to stimulation was recorded at 2 kHz using the Cerebus data acquisition system described above. For the EMG sessions performed prior to 29/Sep/2009, a MA300-18-002 commercial EMG system (Motion Lab Systems, Baton Rouge, LA) was used. For subsequent EMG sessions, a one-channel AC differential amplifier (DAM 80, World Precision

Instruments) was employed. Stimulus markers were output to Cerebus using in-house LabView code (National Instruments, Austin, TX).

Microstimulation

Six daisy-chained RX-7 stimulators (Tucker-Davis Technologies Inc., Alachua, FL) were used for microstimulation. These stimulators are capable of applying current-controlled waveforms with a voltage excursion of -24 to 24 V. Stimulation was controlled with in-house Matlab (The Mathworks, Natick, MA) and LabView code. Microstimulation was applied to Felines 3 and 4.

Stimulus waveforms

Stimuli were applied in charge-balanced square waveforms to prevent charge buildup (Merrill et al., 2005). For each session, pulses of a square, charge-balanced, biphasic waveform at 0.2 ms per phase were applied in trains of 25, 50, or 100 pulses at 100 Hz, settings chosen for their efficacy at evoking responses in perceptual microstimulation studies (Table 5). Trains of pulses were applied in rounds such that every electrode was stimulated at a given amplitude before the current used to stimulate was increased.

All-channel stimulation

Stimulation was periodically applied to the feline on all 96 electrodes in sequence in rounds of each indicated amplitude in order to determine whether stimulation across all channels affected functionality. In none of these sessions did the feline respond in any manner (e.g., vocalizations or movements) that would indicate an adverse reaction to stimulation while awake (listed as all-channel sessions in Table 2). All-channel stimulation was also performed with the feline anesthetized in order to perform EMG (listed as all-channel EMG sessions

in Table 2). Microstimulating current was increased in rounds over the course of the session to determine the threshold current required to evoke EMG responses on each electrode.

Test of parallel stimulation

To test the effects of synchronous stimulation on multiple electrodes, such as might be applied during a failure of patterned microstimulation, stimulation was applied simultaneously at 25 μ A via 72 electrodes. The animal was disconnected from the experimental apparatus following five trains of stimulation.

Chronic stimulation

Chronic stimulation sessions were applied in two paradigms, low (15/20 μ A) and high (20/25/30/25 μ A), on 15 selected electrodes of the MEA in Felines 3 and 4 (Table 2). These specific 15 electrodes were chosen for microstimulation based on two factors: (1) Spatial distribution of charge application. (2) To stimulate on some electrodes which recorded action potentials and some electrodes which did not (Figs. 5a and 5c). Chronic microstimulation was applied at amplitudes ranging from 15 to 35 μ A over the course of several months (Table 2). Stimulation levels were adjusted based on the results of EMG sessions.

Data analysis

All analyses and statistical tests were performed using custom Matlab code.

Impedance data

Electrodes which recorded 1 kHz impedance values over 2 M Ω on all days were considered

Table 2. Summary of microstimulation sessions

Feline	Figure label (Fig. 5a or c)	Date	Description	Stimulus parameters	Amplitudes	Electrodes
3	1	14/Aug/2009	All-electrode (EMG efficacy test)	5 trains, 50 pulses	5–50 µA in steps of 5 µA	All
3	2	29/Aug/2009	All-electrode (EMG efficacy test)	5 trains, 50 pulses	5–35 µA, steps of 1–µA	43,78,84
3	3	01/Sep/2009 02/Sep/2009	All-electrode stimulation	2 rounds, 5 trains, 25 pulses	20/30, 30/35 µA	All
3	4	07/Sep/2009	Test of parallel stimulation	5 trains, 25 pulses	25 µA	Distributed pattern of 72 electrodes
3	5	14/Sep/2009	All-electrode stimulation	5 trains, 25 pulses	20–35 µA in steps of 5 µA	All
3	6	30/Oct/2009	All-electrode (EMG efficacy test)	10 trains, 25 pulses	20–40 µA in steps of 5 µA	All
3	7	31/Oct/2009–09/Nov/2009	15/20 µA on seven electrodes	100 trains of 25 pulses	15/20 µA	88,89,90,91/ 79,80,81
3	15/20 µA (Teal bars)	11/Oct/2009–03/Dec/2009 (23 sessions)	15/20 µA paradigm	200 trains (two rounds), 25 pulses	15 or 20 µA	20 µA—Electrodes 79,80,81 15 µA—Electrodes 26,28,29,31,39, 40,41,43,89,90,91,92
3	8	04/Dec/2009	All-electrode (EMG efficacy test)	5 trains of 25 pulses	20–40 µA in steps of 5 µA	All
3	20/25/30/25 µA (Blue bars)	05/Dec/2009–13/Jan/2009 (20 sessions)	20/25/30/25 µA paradigm	200/electrode (two rounds), 25 pulses	20, 25, 30, or 35 µA	20 µA—Electrodes 39,40,41,43 25 µA—Electrodes 79,80,81 30 µA—Electrodes 89,90,91,92 35 µA—Electrodes 26,28,29,31
3	9	14/Jan/2010	All-electrode (EMG efficacy test)	5 trains of 25 pulses	100 µA	All
4	1	17/Sep/2010	All-electrode (EMG efficacy test)	5 trains of 25 pulses	5–50 µA in steps of 5 µA	All
4	2	28/Sep/2010	Test for feline response	5 trains of 25 pulses	5–50 µA in steps of 5 µA	All
4	3	01/Oct/2010	All-electrode (EMG efficacy test)	5 trains of 25 pulses	50–100 µA in steps of 10 µA	All

Table 2. Summary of microstimulation sessions (*Continued*)

Feline	Figure label (Fig. 5a or c)	Date	Description	Stimulus parameters	Amplitudes	Electrodes
4	4	28/Oct/2010	All-electrode (EMG efficacy test)	5 trains of 25 pulses	20–60 µA in steps of 10 µA	All
4	5–7	24/Nov/2010–30/Nov/2010	25 µA paradigm	100 trains of 25 pulses	25 µA	1,10,11,32,33,42,43, 66,67,75,76, 79,80,88,89
4	8	01/Dec/2010	All-electrode (EMG efficacy test)	5 trains of 25 pulses	40–100 µA in steps of 10 µA	All
4	9	22/Dec/2010	All-electrode (EMG efficacy test)	5 trains of 25 pulses	50–100 µA in steps of 10 µA	All

Microstimulation was applied to Felines 3 and 4 according to several different stimulus paradigms depending on the goals of microstimulation, for example, to evaluate efficacy or to determine the effects of periodic stimulation on device functionality.

to be out-of-specification and not included in any further analyses. Impedance values over 2 MΩ on a single day were replaced with a 2 MΩ ceiling value. Z-scored impedances were computed by electrode in each feline. The value for an impedance reading of a single electrode in a single dataset was compared to mean value for that electrode across all datasets, and then divided by the standard deviation of all values recorded on that particular electrode. Z-scores were averaged across all electrodes for each dataset. For pre- and poststimulation session impedance readings, median impedances and standard errors were computed. Wilcoxon's signed rank test was applied to demonstrate significant drops in median impedance values immediately pre- and post-all-channel-stimulation in Feline 3. The Komolgorov–Smirnov test was applied in Feline 4 due to the small number of pre/post-stimulation datasets. Wilcoxon's signed rank test was used to demonstrate the significance of acute impedance drops on 15 stimulated channels in both Felines 3 and 4. In Feline 3, the median impedance drops between the first and second chronic stimulation paradigms were compared using Wilcoxon's signed rank test on the last 20 datasets of the first paradigm and all 20 datasets of the second

paradigm. Wilcoxon's signed rank test was also used to determine significance of drops in impedance over time. Impedances for the first and last 30 datasets were compared in Felines 1, 3, and 4, and the first and last 10 datasets were compared in Feline 2 due to the lower number of recording sessions.

Electrophysiological recording data

Action potential recordings were sorted using a PCA-based *t*-distribution algorithm (Shoham, 2003). A threshold for action potentials was subsequently imposed at 70 µV. *t*-tests were performed to quantify changes in the number of electrodes which recorded well-isolated action potentials over time (using the first and last 30 datasets in Felines 1, 3, and 4 and the first and last 10 datasets in Feline 2). Student's *t*-test was also applied to acute pre- and poststimulation number of electrodes which recorded action potentials. The distribution of number of electrodes which recorded action potentials across all microstimulation sessions during pre-stimulation recordings was compared to the immediate post-stimulation distribution for Felines 3 and 4.

Electromyographic data

EMG data was rectified, and a boxcar filter (size 50 ms, stepped per sample) was applied across all recorded twitches evoked by a given amplitude of stimulus via a given electrode on EMG response traces to demonstrate the population-level response to a train of stimulation. The Komolgorov–Smirnov test was applied to the rectified averaged EMG data at –400 to –100 ms prior, and the +100 to +400 ms following, the application of microstimulation.

Results

Chronic 1 kHz impedance

Impedances followed a pattern of increasing after implantation to a peak within the first month in all felines (Figs. 1 and 2). This increase was followed by a decrease over time. The first 30 impedance measurement datasets had higher mean impedance than the last 30 datasets in Felines 1, 3, and 4 ($p < 0.001$, Wilcoxon's signed rank test). Due to the smaller number of datasets in Feline 2, only the 10 first and last datasets were compared, with the same result ($p < 0.05$, Wilcoxon's signed rank test). A summary of impedances is included in Table 3. Impedances over 2 M Ω were considered to be out-of-specification. In Feline 1, three electrodes were out-of-specification. In Feline 4, seven electrodes were out-of-specification. Felines 2 and 3 did not have any out-of-specification electrodes.

Pre- and post-stimulation impedance

Median 1 kHz impedance decreased acutely on 19 of 23 days with the application of daily microstimulation (low paradigm) on 15 electrodes in Feline 3 ($p < 0.01$, Wilcoxon's signed rank test, $n = 23$ sessions; Fig. 3a), as well as acutely on 20 out of 20 days when stimulation (high paradigm)

was not consistently applied on consecutive days ($p < 0.01$, Wilcoxon's signed rank test, $n = 20$ sessions; Fig. 3b). Median acute impedance drops were larger during the high chronic stimulation paradigm than the low paradigm ($p < 0.01$, Wilcoxon's signed rank test). Parallel microstimulation on 72 channels of the MEA in Feline 3 also led to an acute decrease in median impedance ($p < 0.001$, Wilcoxon's signed rank test, $n = 96$ electrodes) on all electrodes of the MEA. Median impedance across the 96 electrodes of the MEA decreased when stimulation was applied simultaneously on 72 electrodes in Feline 3 (Feline 3, $p < 0.05$, $n = 8$ sessions, Wilcoxon's signed rank test). In Feline 4, only five impedance readings were made following all-electrode stimulation sessions. Median impedance decreased following all-electrode stimulation (Komolgorov–Smirnov test, $p < 0.01$, $n = 5$ sessions). Median impedance also decreased significantly on the 15 electrodes that passed current during the three applications of the 25 μ A stimulation paradigm in Feline 4 ($p < 0.001$, Wilcoxon's signed rank test, 15 electrodes over three sessions, $n = 45$).

Action potential recordings

In both nonstimulated and microstimulated felines (Figs. 4 and 5), the number of action potentials recorded from motor cortex followed a previously observed pattern of initially increasing followed by a decrease in numbers over the course of months (Suner et al., 2005). This chronic pattern of action potential recordings was similar between microstimulated and non-microstimulated felines. In nonstimulated Feline 1, the number of action potentials recorded during the plateau period (sessions 30–60) was greater than that recorded during the fade-out period (last 30 datasets, $p < 0.05$, Student's two-sample *t*-test). This same observation was made in the microstimulated Felines 3 and 4 ($p < 0.05$, Student's two-sample *t*-test). In non-microstimulated Feline 2, in which only 39 data acquisition sessions were performed,

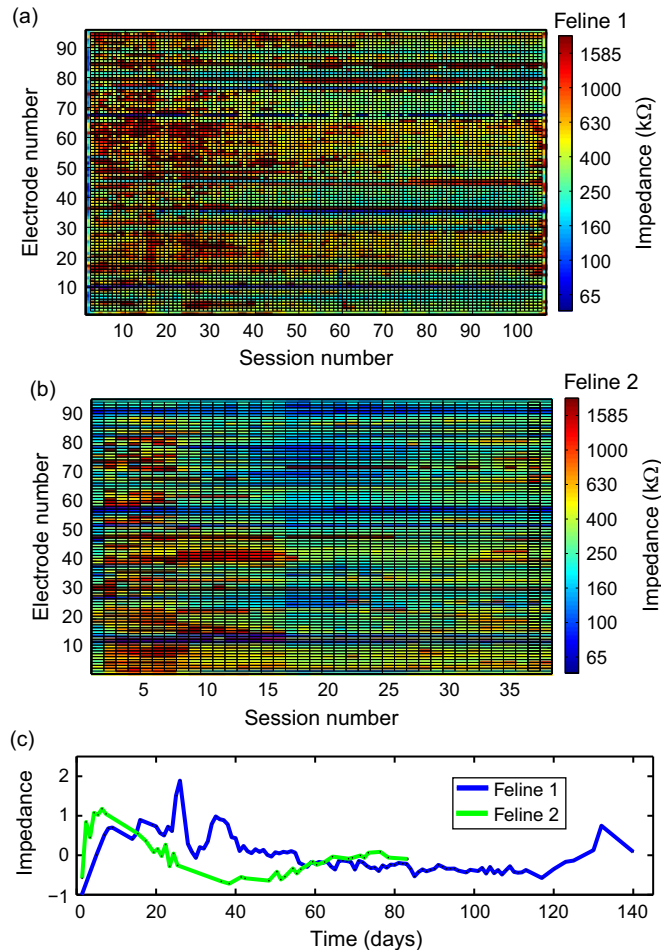


Fig. 1. 1 kHz impedance is variable over chronic timescales. (a, b) 1 kHz impedance measurements were made in the two nonstimulated felines over 8 and 3 months of implantation, respectively. Shown are impedance measurements colored by value. (c) Mean Z-scored impedance over time, in days, for both felines. Both felines exhibited a pattern of increase in impedance following implant that peaked within the first month, followed by a decrease toward preimplantation values ($p < 0.01$, Wilcoxon's signed rank test).

there was no significant change in the number of action potentials recorded between the first and last 10 datasets. All-electrode microstimulation, for example, for feline response tests and EMG sessions, did not lead to an acute decrease in the number of well-isolated action potentials recorded in either microstimulated feline ($p < 0.05$, one-

tailed Student's *t*-test; Feline 3, prestimulation mean=5 action potentials, poststimulation=8 action potentials, $n=8$ sessions; Feline 4, prestimulation mean=60 action potentials, post-stimulation=70 action potentials, $n=6$ sessions). The number of action potentials recorded prior to multielectrode synchronous stimulation in Feline

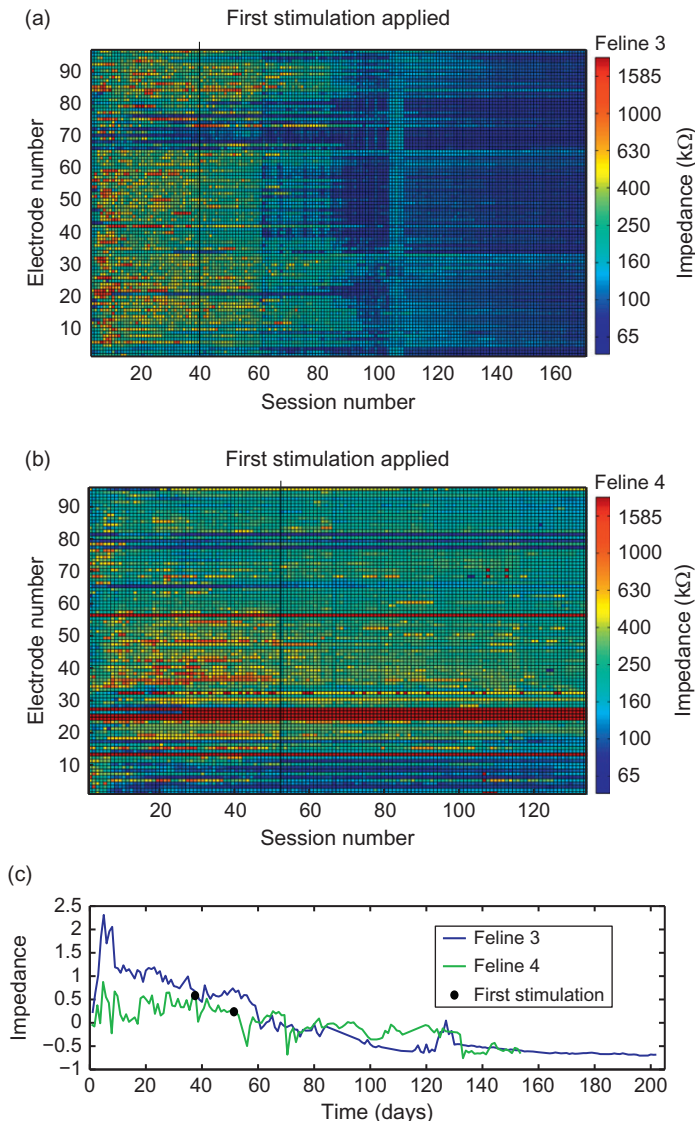


Fig. 2. Microstimulation did not change 1 kHz impedance patterns. (a, b) 1 kHz impedance measurements, colored by value, across all 96 electrodes of the MEA in Felines 3 and 4. Black lines and circles indicate the first application of stimulation. (c) Mean Z-scored impedance over time (prestimulation values shown) over time in days. In both Feline 3 (blue) and Feline 4 (green), impedances dropped toward baseline over time ($p < 0.01$, Wilcoxon's signed rank test).

Table 3. Summary of impedances during implantation

Feline	Mean (kΩ)	Median (kΩ)	Standard deviation (kΩ)	Recording sessions	Electrodes
1	462	353	144	107	93
2	358	285	161	39	96
3	157	91	78	168	96
4	244	99	73	134	89

Impedance values were used as a measure of device performance over the course of implantation and microstimulation. Shown here is summary data on impedances from all four MEAs used in this study.

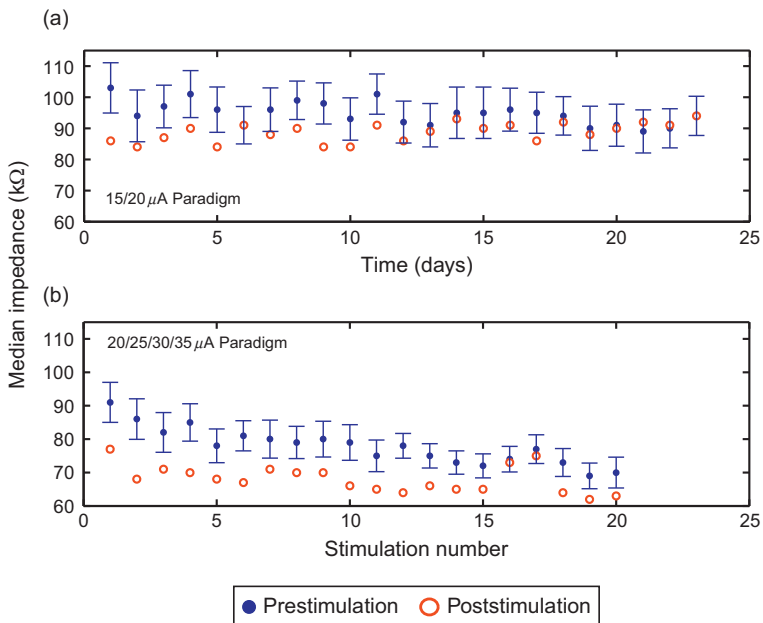


Fig. 3. Microstimulation leads to acute drops in 1 kHz impedance. Median impedance before (blue, with standard error bars) and after (red) microstimulation on the 15 electrodes that passed current into tissue is shown for (a) the low stimulation paradigm, applied daily for 23 days and (b) the high stimulation paradigm, applied 20 times over a 6-week course. Impedance decreased significantly following microstimulation for both stimulus paradigms ($p < 0.01$, Wilcoxon's signed rank test). Impedance drops were larger for the second paradigm ($p < 0.01$, Wilcoxon's signed rank test).

3 was 12, while the number recorded poststimulation was 13, demonstrating that acute parallel synchronous stimulation did not preclude recording ability. A summary of action potential recording data in all four felines is included in Table 4.

Microstimulation in awake felines

For awake stimulation sessions in both Felines 3 and 4, microstimulation was applied to one electrode at a time without anesthesia. No adverse

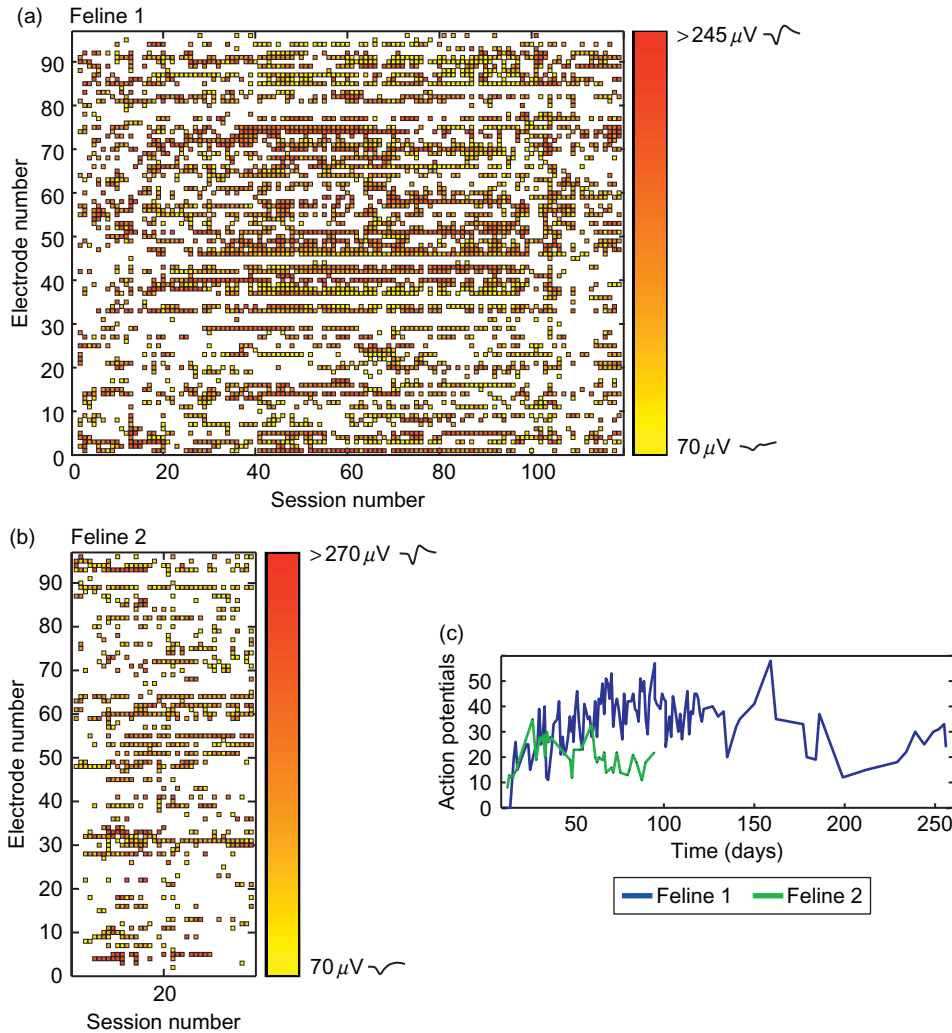


Fig. 4. Action potential amplitudes over chronic timescales. (a and b) Raster plots of thresholded, sorted action potential recordings across the array for the duration of the study for Felines 1 and 2. Each square represents the mean of the furthest cluster from noise as isolated by principle component analysis. Waveforms shown on color bar are samples of action potential shapes isolated at low and high amplitudes. (c) Number of isolated action potentials recorded over time in days. There was an initial increase in the number of action potentials recorded, followed by a significant decrease in Feline 1 by the end of the 8 months of implantation ($p < 0.01$, Student's t -test).

behavioral or physiological responses to such stimulation were observed. For multichannel parallel stimulation in Feline 3, stimulation was synchronously applied to 72 electrodes of the MEA (Table 2;

07/Sep/2009). A bilateral, tonic seizure of <1 min duration resulted from this microstimulation paradigm. Full ambulatory recovery occurred within 5 min of ictus. The animal exhibited neither

behavioral deficits nor spontaneous seizures in the 5 months between seizure induction and termination of the experiment.

Microstimulation to effect

Chronic stimulation was applied on the same 15 electrodes (shown in Fig. 5a) for a total of 43 days in Feline 3 (Table 2). It was possible to evoke

EMG responses via an electrode that performed chronic microstimulation, both after it delivered 23 sessions of stimulation at 15 μ A, and after 20 sessions at 30 μ A (**Fig. 6a**), though this electrode did not record action potentials between EMG sessions. Of the 15 electrodes used for chronic stimulation in Feline 3, four recorded action potentials during the time that chronic stimulation was applied. EMG responses could also be evoked several months apart in time via electrodes that

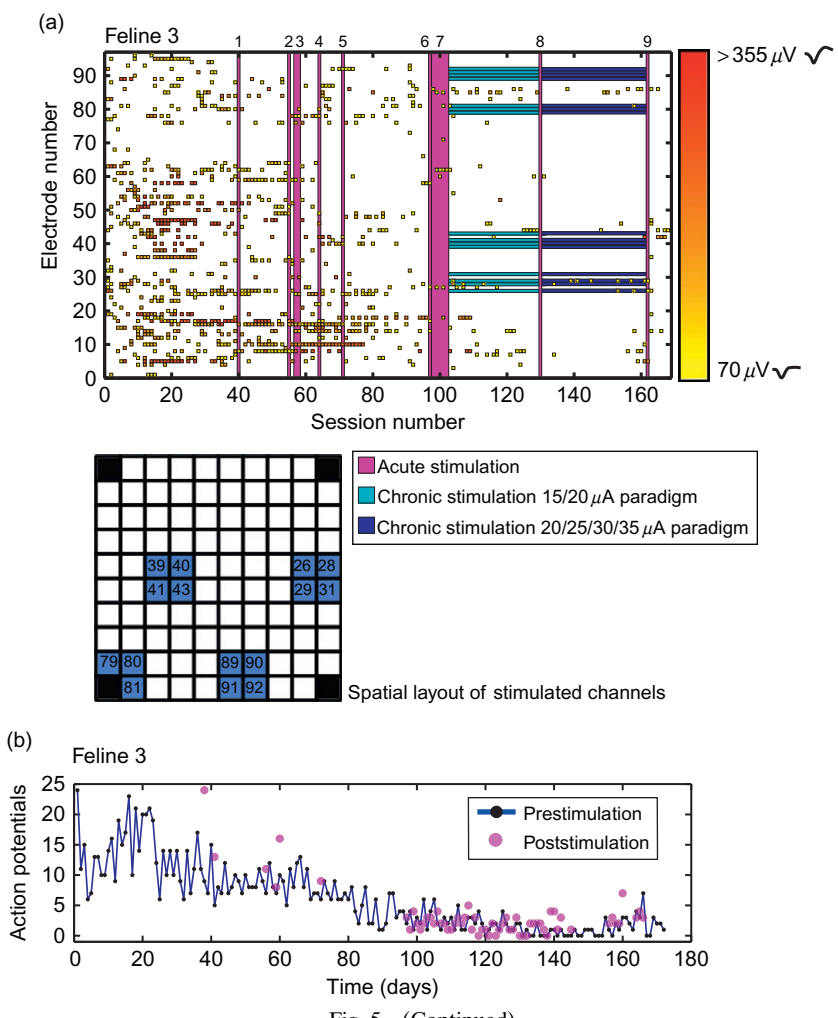


Fig. 5 (Continued)

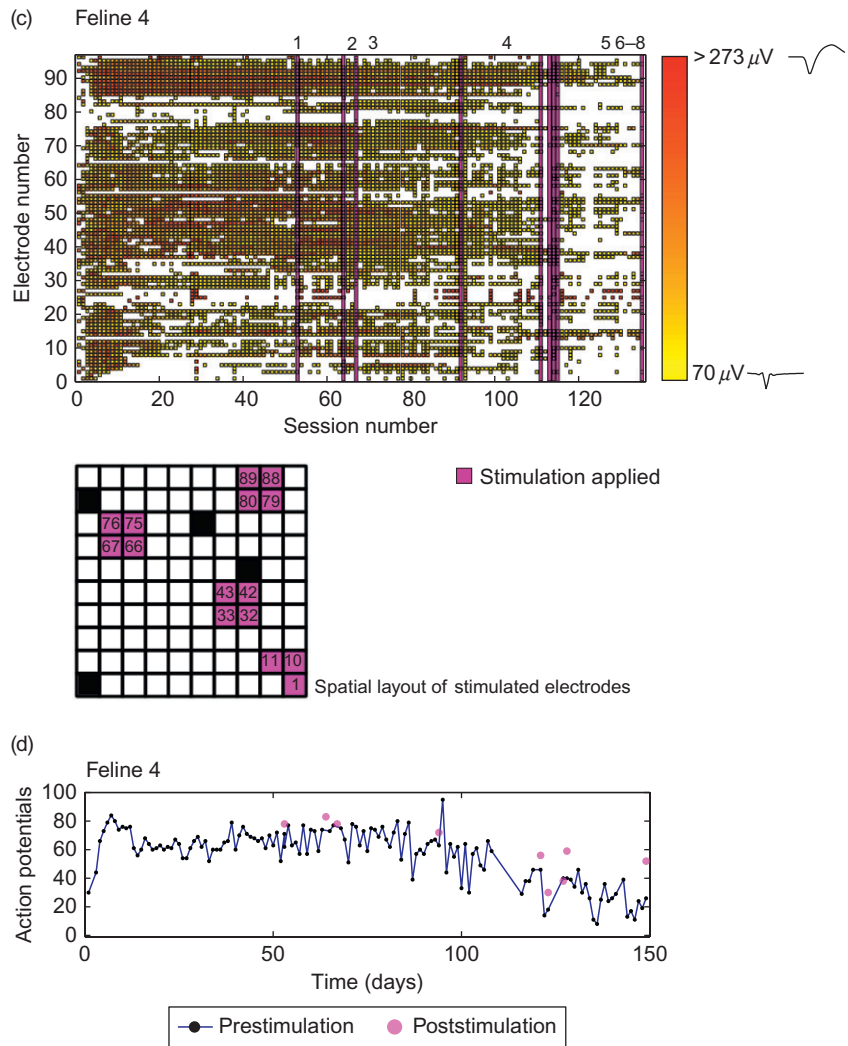


Fig. 5. Microstimulation did not have a clear effect on the number or distribution of action potentials across the array over chronic timescales. (a and c) Raster of action potentials in Felines 3 and 4, color coded by amplitude over recording sessions. Purple bars represent an acute stimulation session, detailed by number in [Table 2](#). Teal bars in Feline 3 represent chronic stimulation at the low stimulation paradigm listed in [Table 2](#), while blue bars represent the high stimulation paradigm applied to the 15 electrodes highlighted. Grids show the spatial layout of electrodes stimulated, blue in Feline 3 and purple in Feline 4. Waveforms shown on color bar are samples of action potential shapes isolated at low and high amplitudes. (b, d) Number of action potentials recorded both over time before (blue) and after (purple) microstimulation in Felines 3 and 4. While the number of action potentials overall did decrease significantly by the end of the experiment in both felines ($p < 0.01$, Student's t -test), the number of action potentials isolated acutely, that is, before and after individual stimulation sessions, did not decrease ($p < 0.05$, Student's t -test).

Table 4. Summary of thresholded action potential amplitudes

Feline	Number of recording sessions	Mean number of electrodes which recorded action potentials, all sessions	Mean number of electrodes which recorded action potentials, first 30 sessions	Mean number of electrodes which recorded action potentials, last 30 sessions
1	123	34	38	33
2	39	20	18 (first 10 sessions)	17 (last 10 sessions)
3	168	6	9	2
4	135	57	73	40

Electrophysiological data recorded from each MEA was used as a chronic measure of device performance. Shown are summary statistics for all four MEAs used in this study.

recorded action potentials in both microstimulated felines (Fig. 6b and c), though these electrodes did not deliver chronic microstimulation (three electrodes in Feline 3, two electrodes in Feline 4). In Feline 3, 13 electrodes evoked electromyographic responses at 10–35 μ A on 14/Aug/2009, seven electrodes evoked responses between 20 and 40 μ A on 04/Dec/2009, and 11 electrodes evoked responses at 100 μ A on 14/Jan/2009 ($p < 0.05$, Komolgorov–Smirnov test). While responses were evoked at currents of <40 μ A during the second month of implantation in Feline 3, 100 μ A current was required to evoke responses during the sixth month of implantation. Currents higher than 100 μ A were not tested due to the voltage excursion limitation of the stimulator. Of the electrodes which evoked responses in Feline 3, two consistently evoked responses throughout all EMG sessions. In Feline 4, eight electrodes evoked EMG responses at 60–80 μ A on 01/Oct/2010, two electrodes evoked responses at 60 μ A on 28/Oct/2010, and eight electrodes evoked responses at 60–100 μ A on 22/Dec/2010. Of the electrodes that evoked EMG responses in Feline 4, two retained the ability to evoke responses throughout the experiments performed.

Discussion

Many studies have shown that intracortical microstimulation to effect can be performed in nonhuman primate, feline, and other model

systems for many sensory modalities (see Table 5). In most of these studies, stimulation was performed acutely on a single electrode in order to evaluate behavioral responses to stimulation. Few of these studies examined the chronic response to stimulation, and still fewer evaluated the long-term consequences of stimulation in a functional context. In this study, we found that chronic, intracortically implanted MEAs could stimulate to effect on multiple electrodes over the course of several months. By evaluating device performance using electrophysiological data, stimulation ability, and 1 kHz impedance, we found that effective stimulation via chronically implanted MEAs did not appear to destroy either the device or underlying cortical tissue.

The stimulation applied in this study was in the 5–100 μ A range. While this exceeds the stimulus amplitudes that have been used in many *in vitro* studies that reported electrode damage with long-term pulsing, and several rodent studies that evoked behavioral response (Cogan, 2004; Houweling and Brecht, 2007; McCreery et al., 2010; Tehovnik, 1996), it is equivalent to the stimulus amplitudes that have been used to evoke perceptual or other effects in felines, macaques, and humans (see Table 5), as well as in other rodent studies (Otto et al., 2005b; Tehovnik, 1996). Some of these studies have noted damage to the tissue surrounding the electrodes using histological markers. While these histological markers indicate that tissue surrounding the electrodes reacted to stimulation, they cannot demonstrate whether or

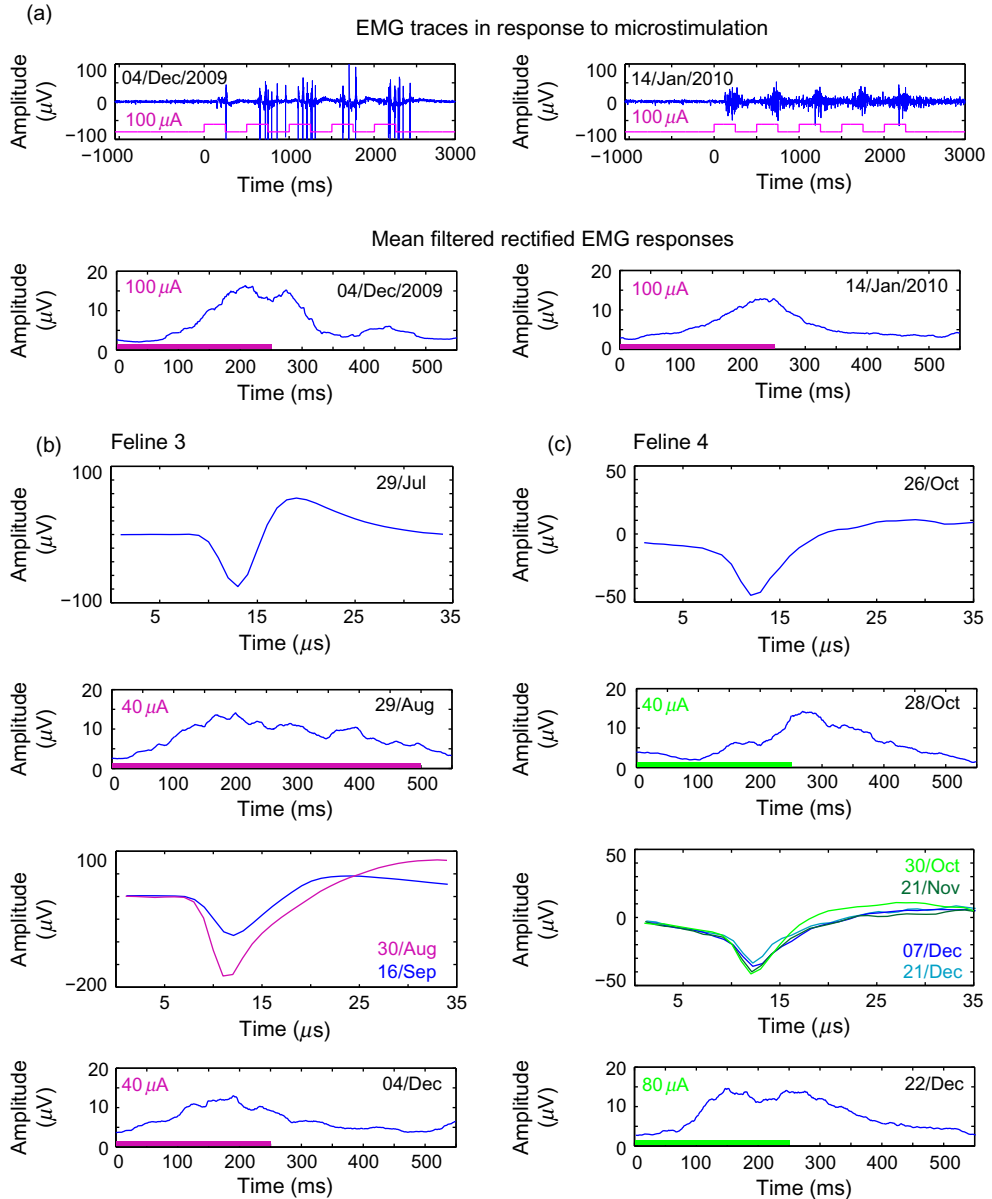


Fig. 6. Chronically stimulated electrodes maintained the ability to stimulate to effect for multiple months. (a) Sample EMG recordings from both 04/Dec/2009 and 14/Jan/2009 evoked by stimulation on and electrode which applied current at 15 and 30 μ A, according to the chronic paradigms detailed in Table 2, with the respective filtered mean rectified EMG responses below. Blue represents the recorded EMG response, while purple represents the pulses applied. (b) Sample action potentials recorded before and between electromyographic sessions during which responses were evoked at 40 μ A in Feline 3. Colored bars along the time axis mark the application of microstimulation. (c) Sample action potentials recorded before and between EMG sessions in Feline 4. Dates of action potential recordings or stimulation and amplitude of stimulation applied are noted in each panel.

Table 5. Summary of selected intracortical microstimulation studies

Citation	Model system	Electrode type	Reporter of efficacy	Current range applied	Frequency (Hz)	Impedance range 1 kHz	Damage?
Murphrey and Maunsell (2008)	Macaque	Platinum/iridium, single electrode	Behavioral task (visual)	Up to 50 µA	200	0.2–1.5 MΩ	No
Murphrey and Maunsell (2007)	Macaque	Platinum/iridium, single electrode	Behavioral task (visual)	3–12 µA	200	0.2–1.5 MΩ	No
McCreery et al. (2010)	Feline	Activated iridium, 16 microelectrode array	N/A	10–20 µA	50	Not reported	Yes
McCreery et al. (2002)	Feline	Activated iridium, 16 microelectrode array	Evoked potentials in medulla	0–32 µA	50	0.2–1.5 MΩ	No
Graziano (2005)	Macaque	Tungsten, single microelectrode	Arm movements	5–100 µA	100–250	1–2 MΩ	No
Graziano et al. (2002)	Macaque	Tungsten, single microelectrode	Arm movements	Up to 150 µA	200	0.5–2 MΩ	No
Tehovnik et al. (2003)	Macaque	Platinum/iridium, single microelectrodes	Behavioral task (visual)	Up to 30 µA	200	1–2 MΩ	No
Tehovnik et al. (2002)	Macaque	Platinum/iridium, single microelectrodes	Behavioral task (visual)	Up to 40 µA	200	1–1.5 MΩ	No
Romo et al. (2000)	Macaque	Platinum/tungsten, seven microelectrodes	Behavioral task (flutter discrimination)	65–100 µA	50–200	1–1.5 MΩ	No
Romo et al. (1998)	Macaque	Platinum/tungsten, seven microelectrodes	Behavioral task (flutter discrimination)	65–100 µA	50–200	1–1.5 MΩ	No
Rousche and Normann (1999)	Feline	Platinum, 96 electrode Utah Electrode Array	Behavioral task (auditory)	100 µA	25–2000	30–149 kΩ	No
Torab et al. (2011)	Macaque	SIROF, 96 electrode Utah Electrode Array	Behavioral task (visual)	0–96 µA	200	40 kΩ–2 MΩ	No
Bradley (2004)	Macaque	Iridium, 192 electrode array	Behavioral task (visual)	12–20 µA	200	80 kΩ–1.6 MΩ	No
Bak et al. (1990)	Human	Iridium, arrays of 1–3 electrodes	Verbal report (visual percepts)	20 µA–2 mA	100	Not reported	No
Schmidt et al. (1996)	Human	Iridium, 12 single electrodes, 13 paired electrodes	Verbal report (visual percepts)	1–80 µA	200	Not reported	No

The stimulus amplitudes and parameters applied in this study were similar to those used in other microstimulation experiments which evoked sensory percepts. Shown are sample studies for comparison.

not stimulation affected device performance. By using electrophysiological markers such as recorded action potentials and ability to evoke physiological responses, we were able to demonstrate sustained functionality, including action potential recording, which implies tissue viability in the recording radius of the microelectrode tips.

The chronic changes in impedance observed in our experiments followed a pattern which has been previously noted in the literature. Mean impedance of passively implanted microelectrodes tends to increase over the first weeks of implantation, followed by a decrease over time (Williams et al., 2007). The causes of this pattern remain unclear, though it could result from ongoing processes of the tissue response to implanted devices. We observed this trend during the first weeks of implantation, followed by a continued decrease in impedance throughout the duration of the experiments in both passively implanted felines. The same phenomenon has also been observed in deep brain stimulation studies, where current was applied via chronically implanted macroelectrodes over time (Lempka et al., 2009). Important to note is that the impedances of both microstimulated and nonstimulated felines followed the same general pattern over time. The application of microstimulation did not drive electrode impedances out-of-specification, that is, $>2\text{ M}\Omega$, as might be expected in the case of device failure or catastrophic tissue damage over time.

We also observed short-term decreases in impedance on stimulating electrodes with the application of microstimulation, which are reported to occur both *in vivo* and *in vitro* (Otto et al., 2006). These changes in impedance could reflect tissue response, for example, disruption of the glial scar by microstimulation. Impedance changes may also reflect processes of device damage known to occur with stimulation, such as dissolution of metallization or damage to electrode insulation. Finally, decreases could also indicate processes of electrochemical activation, which would change the valence state of the stimulating SIROF. The repeatability of the short-term

impedance drops, with subsequent recovery, suggests that reversible electrochemical activation rather than cumulative damage may be reflected by these short-term changes in impedance values. The second chronic microstimulation paradigm in Feline 3 yielded larger acute impedance drops. This could be a result of either the increased current used to stimulate, or the increased time between stimulation sessions which would allow impedances to return to baseline. This further supports the idea that reversible electrochemical processes, rather than damage, contribute to observed impedance drops. Further, the maintained ability to stimulate and record indicates that any damage that may have occurred with microstimulation did not preclude device functionality. Importantly, catastrophic changes in impedance, which might indicate device damage or tissue death, did not occur with the application of stimulation.

The microstimulation amplitudes used in this study never evoked seizure-like or aberrant electrical activity when performed on a single electrode. Further, no adverse behavioral responses occurred with the application of microstimulation in awake animals at $50\text{ }\mu\text{A}$. However, a seizure did result from multielectrode simultaneous stimulation (Table 2; 07/Sep/2009) at $25\text{ }\mu\text{A}$. Though no long-term device performance or physiological deficits were noted following this simultaneous multielectrode microstimulation, clearly the induction of a seizure event is unacceptable for any neural prosthetic application. In order to evoke complex spatiotemporal sensory percepts, interleaved multielectrode stimulation will need to be performed; it remains unknown how many electrodes can be simultaneously used without adverse physiological consequences. Patterns of stimulation can be sparsely distributed in both space and time, but must also be able to convey useful sensory information. An acceptable, safe balance between spatiotemporal patterns of microstimulation which convey useful sensory information and those which result in seizure must be found. Additionally, mechanisms to

prevent unacceptably dense microstimulation will need to be implemented in the stimulation control electronics for human sensory prostheses to ensure that this failure mode does not occur.

It is unclear if complex spatiotemporal percepts can be evoked by patterned intracortical microstimulation. Testing patterned microstimulation in nonhuman primates is challenging (Bradley, 2004; Torab et al., 2011). It will be more efficiently addressed by means of psychophysical experiments conducted in human volunteers. Our ability to stimulate to effect and record electrophysiological data over multiple months demonstrated that tissue in the recording radius of the MEA remained viable after many months, and that the device maintained functionality over this time. These results suggest that microstimulation is ready for the next step in the development of sensory prosthetics, namely sub-chronic clinical trials in human subjects. Such trials will allow researchers to optimize stimulation parameters that are best at evoking sensory percepts, and will greatly speed the development of devices for the benefit of human patients.

Acknowledgments

Supported in part by an Unrestricted Grant from Research to Prevent Blindness, Inc., New York, NY, to the Department of Ophthalmology & Visual Sciences, University of Utah.

Additional support from NIH Training Grant 5T32DC008553-02 and NIH R01 EY019363-01.

The authors would also like to thank Rick VanWagenen and Blackrock Microsystems for their ongoing support.

Abbreviations

EMG	electromyogram
MEA	multielectrode array
SIROF	sputtered iridium oxide film

References

- Aggarwal, V., Tenore, F., Acharya, S., Schieber, M. H., & Thakor, N. V. (2009). Cortical decoding of individual finger and wrist kinematics for an upper-limb neuroprosthesis. *Conference Proceedings—IEEE Engineering in Medicine and Biology Society, 2009*, 4535–4538.
- Bak, M., Girvin, J. P., Hambrecht, F. T., Kufta, C. V., Loeb, G. E., & Schmidt, E. M. (1990). Visual sensations produced by intracortical microstimulation of the human occipital cortex. *Medical & Biological Engineering & Computing, 28*, 257–259.
- Bradley, D. C. (2004). Visuotopic mapping through a multi-channel stimulating implant in primate V1. *Journal of Neurophysiology, 93*, 1659–1670.
- Cogan, S. (2004). Over-pulsing degrades activated iridium oxide films used for intracortical neural stimulation. *Journal of Neuroscience Methods, 137*, 141–150.
- Cogan, S. F. (2008). Neural stimulation and recording electrodes. *Annual Review of Biomedical Engineering, 10*, 275–309.
- Cogan, S., Ehrlich, J., Plante, T., Smirnov, A., Shire, D., Gingerich, M., et al. (2009). Sputtered iridium oxide films for neural stimulation electrodes. *Journal of Biomedical Materials Research. Part B, Applied Biomaterials, 89*, 353–361.
- Cooke, D. F. (2003). Complex movements evoked by microstimulation of the ventral intraparietal area. *Proceedings of the National Academy of Sciences of the United States of America, 100*, 6163–6168.
- Deuschl, G., Herzog, J., Kleiner-Fisman, G., Kubu, C., Lozano, A. M., Lyons, K. E., et al. (2006). Deep brain stimulation: Postoperative issues. *Movement Disorders, 21*, S219–S237.
- Deyoe, E. A. (2005). Laminar variation in threshold for detection of electrical excitation of striate cortex by macaques. *Journal of Neurophysiology, 94*, 3443–3450.
- Dickey, A. S., Suminski, A., Amit, Y., & Hatsopoulos, N. G. (2009). Single-unit stability using chronically implanted multielectrode arrays. *Journal of Neurophysiology, 102*, 1331–1339.
- Fitzsimmons, N. A., Drake, W., Hanson, T. L., Lebedev, M. A., & Nicolelis, M. A. L. (2007). Primate reaching cued by multi-channel spatiotemporal cortical microstimulation. *The Journal of Neuroscience, 27*, 5593–5602.
- Fraser, G. W., Chase, S. M., Whitford, A., & Schwartz, A. B. (2009). Control of a brain-computer interface without spike sorting. *Journal of Neural Engineering, 6*, 055004.
- Ghosh, S. (1997). Cytoarchitecture sensorimotor areas cat cerebral cortex. *Journal of Comparative Neurology, 388*, 354–370.
- Graziano, M. S. A. (2005). Arm movements evoked by electrical stimulation in the motor cortex of monkeys. *Journal of Neurophysiology, 94*, 4209–4223.

- Graziano, M. S. A., Taylor, C. S., & Moore, T. (2002). Complex movements evoke microstimulation precentral cortex. *Neuron*, 34, 841–851.
- Hochberg, L., & Donoghue, J. (2006). Sensors for brain-computer interfaces. *IEEE Engineering in Medicine and Biology Magazine: The Quarterly Magazine of the Engineering in Medicine & Biology Society*, 25, 32–38.
- Hochberg, L. R., Serruya, M. D., Friehs, G. M., Mukand, J. A., Saleh, M., Caplan, A. H., et al. (2006). Neuronal ensemble control of prosthetic devices by a human with tetraplegia. *Nature*, 442, 164–171.
- Houweling, A. R., & Brecht, M. (2007). Behavioural report of single neuron stimulation in somatosensory cortex. *Nature*, 451, 65–68.
- Jones, K. E., Campbell, P. K., & Normann, R. A. (1992). A glass/silicon composite intracortical electrode array. *Annals of Biomedical Engineering*, 20, 423–437.
- Lempka, S. F., Miocinovic, S., Johnson, M. D., Vitek, J. L., & McIntyre, C. C. (2009). In vivoimpedance spectroscopy of deep brain stimulation electrodes. *Journal of Neural Engineering*, 6, 046001.
- Linderman, M. D., Gilja, V., Santhanam, G., Afshar, A., Ryu, S., Meng, T. H., et al. (2006). Neural recording stability of chronic electrode arrays in freely behaving primates. *Conference Proceedings—IEEE Engineering in Medicine and Biology Society*, 1, 4387–4391.
- McCreery, D. B., Agnew, W. F., & Bullara, L. A. (2002). The effects of prolonged intracortical microstimulation on the excitability of pyramidal tract neurons in the cat. *Annals of Biomedical Engineering*, 30, 107–119.
- McCreery, D., Pikov, V., & Troyk, P. R. (2010). Neuronal loss due to prolonged controlled-current stimulation with chronically implanted microelectrodes in the cat cerebral cortex. *Journal of Neural Engineering*, 7, 036005.
- Merrill, D. R., Bikson, M., & Jefferys, J. G. R. (2005). Electrical stimulation of excitable tissue: Design of efficacious and safe protocols. *Journal of Neuroscience Methods*, 141, 171–198.
- Moss, J. (2004). Electron microscopy of tissue adherent to explanted electrodes in dystonia and Parkinson's disease. *Brain*, 127, 2755–2763.
- Murphy, D. K., & Maunsell, J. H. R. (2007). Behavioral detection of electrical microstimulation in different cortical visual areas. *Current Biology*, 17, 862–867.
- Murphy, D. K., & Maunsell, J. H. R. (2008). Electrical microstimulation thresholds for behavioral detection and saccades in monkey frontal eye fields. *Proceedings of the National Academy of Sciences of the United States of America*, 105, 7315–7320.
- Musallam, S. (2004). Cognitive control signals for neural prosthetics. *Science*, 305, 258–262.
- Negi, S., Bhandari, R., Rieth, L., van Wagenen, R., & Solzbacher, F. (2010). Neural electrode degradation from continuous electrical stimulation: Comparison of sputtered and activated iridium oxide. *Journal of Neuroscience Methods*, 186, 8–17.
- Nicolelis, M. A. L. (2003). Chronic, multisite, multielectrode recordings in macaque monkeys. *Proceedings of the National Academy of Sciences of the United States of America*, 100, 11041–11046.
- Otto, K. J., Johnson, M. D., & Kipke, D. R. (2006). Voltage pulses change neural interface properties and improve unit recordings with chronically implanted microelectrodes. *IEEE Transactions on Biomedical Engineering*, 53, 333–340.
- Otto, K., Rousche, P., & Kipke, D. (2005a). Microstimulation in auditory cortex provides a substrate for detailed behaviors. *Hearing Research*, 210, 112–117.
- Otto, K. J., Rousche, P. J., & Kipke, D. R. (2005b). Cortical microstimulation in auditory cortex of rat elicits best-frequency dependent behaviors. *Journal of Neural Engineering*, 2, 42–51.
- Rivera-Alvidrez, Z., Kalmar, R. S., Ryu, S. I., & Shenoy, K. V. (2010). Low-dimensional neural features predict muscle EMG signals. *Conference Proceedings—IEEE Engineering in Medicine and Biology Society*, 1, 6027–6033.
- Romo, R., Hernandez, A., Zainos, A., Brody, C. D., & Lemus, L. (2000). Sensing without touching: Psychophysical performance based on cortical microstimulation. *Neuron*, 26, 273–278.
- Romo, R., Hernandez, A., Zainos, A., & Salinas, E. (1998). Somatosensory discrimination based on cortical microstimulation. *Nature*, 392, 387–390.
- Rousche, P. J., & Normann, R. A. (1992). A method for pneumatically inserting an array of penetrating electrodes into cortical tissue. *Annals of Biomedical Engineering*, 20, 413–422.
- Rousche, P. J., & Normann, R. A. (1999). Chronic intracortical microstimulation (ICMS) of cat sensory cortex using the Utah Intracortical Electrode Array. *IEEE Transactions on Rehabilitation Engineering*, 7, 56–68.
- Rousche, P. J., Otto, K. J., Reilly, M. P., & Kipke, D. R. (2003). Single electrode micro-stimulation of rat auditory cortex: An evaluation of behavioral performance. *Hearing Research*, 179, 62–71.
- Salzman, C. D., Britten, K. H., & Newsome, W. T. (1990). Cortical microstimulation influences perceptual judgements of motion direction. *Nature*, 346, 174–177.
- Santhanam, G., Ryu, S. I., Yu, B. M., Afshar, A., & Shenoy, K. V. (2006). A high-performance brain-computer interface. *Nature*, 442, 195–198.
- Schmidt, E. M., Bak, M. J., Hambrecht, F. T., Kufta, C. V., O'Rourke, D. K., & Vallabhanath, P. (1996). Feasibility of a visual prosthesis for the blind based on intracortical microstimulation of the visual cortex. *Brain*, 119(Pt. 2), 507–522.

- Schmidt, E. M., & McIntosh, J. S. (1990). Microstimulation mapping of precentral cortex during trained movements. *Journal of Neurophysiology*, 64, 1668–1682.
- Schwartz, A., Cui, X., Weber, D., & Moran, D. (2006). Brain-controlled interfaces: Movement restoration with neural prosthetics. *Neuron*, 52, 205–220.
- Serruya, M. D., Hatsopoulos, N. G., Paninski, L., Fellows, M. R., & Donoghue, J. P. (2002). Instant neural control of a movement signal. *Nature*, 416, 141–142.
- Shoham, S. (2003). Robust, automatic spike sorting using mixtures of multivariate t-distributions. *Journal of Neuroscience Methods*, 127, 111–122.
- Suner, S., Fellows, M. R., Vargas-Irwin, C., Nakata, G. K., & Donoghue, J. P. (2005). Reliability of signals from a chronically implanted, silicon-based electrode array in non-human primate primary motor cortex. *IEEE Transactions on Neural Systems and Rehabilitation Engineering*, 13, 524–541.
- Taylor, D. M. (2002). Direct cortical control of 3D neuroprosthetic devices. *Science*, 296, 1829–1832.
- Tehovnik, E. J. (1996). Electrical stimulation of neural tissue to evoke behavioral responses. *Journal of Neuroscience Methods*, 65, 1–17.
- Tehovnik, E. J. (2006). Direct and indirect activation of cortical neurons by electrical microstimulation. *Journal of Neurophysiology*, 96, 512–521.
- Tehovnik, E. J., & Slocum, W. M. (2009). Background luminescence affects the detection of microampere currents delivered to macaque striate cortex. *The European Journal of Neuroscience*, 30, 263–271.
- Tehovnik, E. J., Slocum, W. M., & Schiller, P. H. (2002). Differential effects of laminar stimulation of V1 cortex on target selection by macaque monkeys. *The European Journal of Neuroscience*, 16, 751–760.
- Tehovnik, E. J., Slocum, W. M., & Schiller, P. H. (2003). Saccadic eye movements evoked by microstimulation of striate cortex. *The European Journal of Neuroscience*, 17, 870–878.
- Torab, K., Davis, T. S., Warren, D. J., House, P. A., Normann, R. A., & Greger, B. (2011). Multiple factors may influence the performance of a visual prosthesis based on intracortical microstimulation: nonhuman primate behavioral experimentation. *Journal of Neural Engineering*, 8, 035001 (13 pp).
- Troyk, P., Detlefsen, D., Cogan, S., Ehrlich, J., Bak, M., McCreery, D., et al. (2004). “Safe” charge-injection waveforms for iridium oxide (AIROF) microelectrodes. *Conference Proceedings—IEEE Engineering in Medicine and Biology Society*, 6, 4141–4144.
- Vanwagenen, R. (2004). *Micro-electrode impedance model*. Salt Lake City, UT: Cyberkinetics, Inc.
- Wessberg, J., Stambaugh, C. R., Kralik, J. D., Beck, P. D., Laubach, M., Chapin, J. K., et al. (2000). Real-time prediction of hand trajectory by ensembles of cortical neurons in primates. *Nature*, 408(6810), 361–365.
- Williams, J. C., Hippenstein, J. A., Dilgen, J., Shain, W., & Kipke, D. R. (2007). Complex impedance spectroscopy for monitoring tissue responses to inserted neural implants. *Journal of Neural Engineering*, 4, 410–423.

CHAPTER 12

Reducing surface area while maintaining implant penetrating profile lowers the brain foreign body response to chronically implanted planar silicon microelectrode arrays

John L. Skousen[†], Sr. Mary Elizabeth Merriam[‡], Onnap Srivannavit[‡], Gaytri Perlin[‡],
Kensall D. Wise[‡] and Patrick A. Tresco^{†,*}

[†] Department of Bioengineering, University of Utah, Salt Lake City, UT, USA

[‡] Department of Electrical Engineering and Computer Science, University of Michigan, Ann Arbor, MI, USA

Abstract: A consistent feature of the foreign body response (FBR), irrespective of the type of implant, is persistent inflammation at the biotic–abiotic interface signaled by biomarkers of macrophage/microglial activation. Since macrophage-secreted factors shape the foreign body reaction, implant designs that reduce macrophage activation should improve biocompatibility and, with regard to recording devices, should improve reliability and longevity. At present, it is unclear whether the goal of seamless integration is possible or whether electrode developers can modulate specific aspects of the FBR by intentionally manipulating the constitutive properties of the implant. To explore this area, we studied the chronic brain FBR to planar solid silicon microelectrode arrays and planar lattice arrays with identical penetrating profiles but with reduced surface area in rats after an 8-week indwelling period. Using quantitative immunohistochemistry, we found that presenting less surface area after equivalent iatrogenic injury is accompanied by significantly less persistent macrophage activation, decreased blood brain barrier leakiness, and reduced neuronal cell loss. Our findings show that it is possible for implant developers to modulate specific aspects of the FBR by intentionally manipulating the constitutive properties of the implant. Our results also support the theory that the FBR to implanted electrode arrays, and likely other implants, can be explained by the presence of macrophages at the biotic–abiotic interface, which act as a sustained delivery source of bioactive agents that diffuse into the adjacent tissue and shape various features of the brain FBR. Further, our findings suggest that one method to improve the recording consistency and lifetime of implanted

*Corresponding author.

Tel.: 801-587-9263; Fax: +1-801-5855151

E-mail: patrick.tresco@utah.edu

microelectrode arrays is to design implants that reduce the amount of macrophage activation at the biotic–abiotic interface and/or enhance the clearance or impact of their released factors.

Keywords: inflammation; blood brain barrier; electrode; neural prosthesis.

Introduction

Numerous studies have shown that using implanted microelectrode arrays, consciously modulated neural signals can be recorded in both animal subjects as well as human patients for periods of time ranging from months to multiple years, and that these recorded signals can be used to control a number of external devices (Hochberg et al., 2006; Kennedy et al., 2004; Kruger et al., 2010; Musallam et al., 2004; Nicolelis et al., 2003). Despite these promising results, achieving widespread clinical application of this technology requires improving recording consistency over a clinically relevant time frame. A widely accepted theory in the field is that the foreign body response (FBR) that the brain mounts against implanted microelectrodes contribute to the observed recording instability, currently limiting clinical application.

Over 60 years of studies have described consistent, stereotypic features of the brain FBR that occur irrespective of the type of implant, species studied, or implantation method. A key feature of the FBR is persistent inflammation at the biotic–abiotic interface signaled by biomarkers for activated microglia and macrophages (Biran et al., 2005; Stensaas and Stensaas 1976; Winslow and Tresco, 2010; Winslow et al., 2010). Surrounding this, a region consisting of hypertrophic astrocytes, fibroblasts, and meningeal cells has been observed (Biran et al., 2005, 2007; Collias and Manuelidis 1957; Edell et al., 1992; Schmidt et al., 1993; Schultz and Willey 1976; Seymour and Kipke 2007; Shain et al., 2003; Stensaas and Stensaas, 1976, 1978; Szarowski et al., 2003). Associated with the region of inflammation and reactive gliosis, studies also have described a decrease in the local nerve fiber

and neuronal cell body densities surrounding implanted devices (Biran et al., 2005, 2007; Collias and Manuelidis 1957; Edell et al., 1992; Schultz and Willey 1976; Stensaas and Stensaas, 1976, 1978; Winslow and Tresco, 2010; Winslow et al., 2010). We have shown that persistent inflammation and neuronal loss do not accompany stab wound injuries made with recording devices, indicating that these responses are associated with the continual presence of the implant and are not solely a result of iatrogenic injury related to device implantation (Biran et al., 2005).

More recent studies have built upon these observations and shown that, as observed in many neurodegenerative disorders, the local blood brain barrier (BBB) is compromised and decreases in myelin are observed in the tissue immediately surrounding the recording device (Winslow et al., 2010; Winslow and Tresco, 2010). These findings suggest new possible mechanisms for the observed recording instability including an altered local ionic milieu leading to neuronal silencing, decreased neuronal conduction, and/or compromised synaptic stability. Further, our findings using single shaft recording devices did not support several previous hypotheses for FBR-associated recording failure mechanisms, including progressive increases in astrocyte encapsulation or progressive neuronal loss within the recording zone, indicating that at least for certain recording device designs, neuroinflammatory sequelae are likely involved in chronic recording inconsistency.

Despite our increased understanding of the brain's response to microelectrodes and how it might influence recording consistency, it is still unclear if the goal of seamless integration into nervous tissue is possible and whether future electrode designers can modulate specific aspects of

the FBR by intentionally manipulating the constitutive properties of the implant (Edell et al., 1992; Seymour and Kipke 2007; Stice et al., 2007; Szarowski et al., 2003; Thelin et al., 2011). Based on the available evidence, it is likely that the tissue reaction to implanted electrodes is modulated by the sustained delivery of bioactive factors that are released into the adjacent tissue by activated macrophages that occupy and move to and from the biotic–abiotic interface over the indwelling period (Biran et al., 2005). If macrophage-secreted factors shape the tissue reaction, then implant architectures that reduce macrophage activation should reduce the magnitude of the FBR and hence improve biocompatibility. To begin testing this hypothesis, using quantitative immunohistochemical methods, we studied the brain tissue reaction to planar silicon microelectrode arrays with identical penetrating profiles, but different amounts of exposed surface implanted chronically in the rat brain.

Methods

Microelectrodes

Silicon microelectrode arrays were supplied by the Center for Wireless Integrated Microsystems at the University of Michigan. Both styles of microelectrodes had identical penetrating profiles with shanks that were 300 μm wide \times 12 μm thick and 3.45 mm in length including a tapered tip (Fig. 1). Surface area measurements were calculated from SolidWork (Dassault Systèmes SolidWorks Corp., Concord, MA) models of the implanted portion of the two styles of microelectrode arrays. To facilitate handling, the microelectrodes were attached to a 0.25-mm diameter stainless steel wire with a UV-curable, medical-grade adhesive (MD-1187-M, Dymax, Torrington, CT) at the bond pads. All electrodes were cleaned by immersion in 70% ethanol and rinsed several times in sterile DI water, followed by sterilization with ethylene oxide. Sterilized

samples were allowed to outgas for at least 48 h prior to implantation.

Animal surgery

All procedures involving animals were conducted in accordance with the University of Utah Institutional Animal Care and Use Committee (IACUC). Methods used were similar to those described previously (Winslow et al., 2010; Winslow and Tresco, 2010). Briefly, male Sprague Dawley rats (225–250 g, $n=4$ solid, $n=5$ lattice) were anesthetized via an intraperitoneal injection of ketamine (65 mg/kg), xylazine (7.5 mg/kg), and acepromazine (0.5 mg/kg). Animals' heads were shaved and disinfected with 70% IPA and betadyne prior to being transferred to a stereotactic frame. A midline incision, extending the length of the skull, was made along with a 3 mm diameter burr hole at –3.2 mm to bregma, and 2.0 mm lateral to bregma under stereotactic control. A single microelectrode array was stereotactically implanted into the center of the hole in the same orientation of each animal with the 300 μm -wide face oriented perpendicular to the midline to a depth of 3 mm from the top of the cortex, penetrating CA1 of the hippocampus. Electrodes were then fixed to the skull with a custom-fabricated polyurethane grommet using a UV-curable, medical-grade adhesive (Biran et al., 2007; Kim et al., 2004).

Euthanasia and tissue preparation

At 8 weeks postimplantation, animals were terminally anesthetized via an IP injection of ketamine (70 mg/kg) and xylazine (30 mg/kg) and then transcardially perfused with PBS at 50 ml/min followed by 4% paraformaldehyde in PBS. Following perfusion fixation, solid electrodes were carefully retrieved from tissue using microdissection forceps, while fine surgical scissors were used to cut through the lattice electrodes and release them

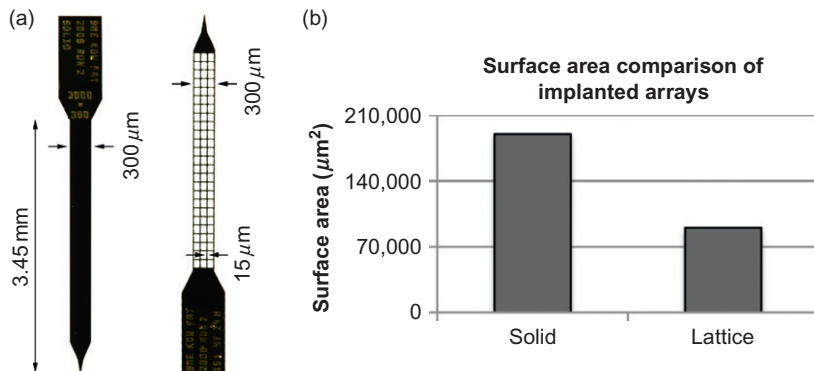


Fig. 1. (a) Representative image of the 300 μm -wide planar solid and 300 μm -wide planar lattice microelectrode arrays used in the study. Both styles of electrodes were 12 μm thick. (b) Calculated surface area exposed to brain microenvironment when implanted to a depth of 3 mm that includes all surface areas measurements including all edges of the lattice.

from their polyurethane grommets, leaving the lattice electrode shanks embedded in brain tissue throughout all subsequent processing steps. Retrieved brains were postfixed with 4% paraformaldehyde for 24 h at 4 °C. Brains were then equilibrated in 30% sucrose. Following equilibration, brains were serially sectioned in the horizontal plane at 30 μm thickness with a cryostat (Leica Microsystems, Bannockburn, IL).

Immunohistochemistry

Serial sections were processed using indirect immunohistochemistry for CD68 (ED-1, 0.5 mg/ml, AbD Serotec, Raleigh, NC) to assess activated microglia/macrophages, rat IgG (2.0 mg/ml, Southern Biotech, Birmingham, AL) for BBB dysfunction, GFAP (2.4 mg/ml, DAKO, Carpinteria, CA) for astrocytes, and NeuN (2.0 mg/ml, Millipore, Billerica, MA) for neuronal nuclei using previously published conditions (Winslow and Tresco, 2010; Winslow et al., 2010). In brief, antibodies were diluted in a blocking solution consisting of 4% (v/v) goat serum (Invitrogen, Carlsbad, CA), 0.5% (v/v) Triton-X 100, and 0.1% (w/v) sodium azide. Free-floating tissue sections were batch treated for 1 h in blocking solution at room temperature, followed by incubation with primary antibodies

overnight at 4 °C. After three rinses in PBS at room temperature to remove excess antibody (1 h/rinse), appropriate fluorescently labeled secondary antibodies were applied in block for 1 h at room temperature, followed by three washes in PBS (1 h/rinse). All sections were also counterstained with DAPI (10 mM) to identify cell nuclei. Tissue sections were mounted on microscope slides with Fluormount-G (Southern Biotech) and cover-slipped.

Quantitative analysis

Fluorescent images of tissue sections from layers III–VI of the cortex were captured with a Coolsnap digital camera and a Nikon Eclipse E600 microscope, using identical exposure times and conditions which were optimized for each immunomarker. All fluorescent images were lightfield corrected and background subtracted using primary controls prior to quantification (Biran et al., 2005).

The staining intensity for each immunomarker was quantified, averaged, and compared using a custom LabView-based image analysis program (National Instruments, Austin, TX) as described

previously (Kim et al., 2004; Winslow and Tresco, 2010; Winslow et al., 2010). In brief, fluorescent intensity as a function of distance from the implant site is extracted using a horizontal array of line profiles spanning the implant site. At each point along the lines, an anti-alias pixel extraction algorithm was used to derive the pixel intensity of the line profile arrays per section. The intensity profiles for a given immunomarker from one section for each layer, III–VI, were averaged to obtain an average intensity profile for a given animal. The average intensity profile for a given animal was then averaged with other animal profiles receiving the same type of implant to obtain an average intensity profile for each cohort (solid or lattice).

In order to quantify changes in neuronal cell body distribution in the presumptive recording zone and in the tissue surrounding the device, the density of neuronal nuclei was calculated by counting the number of NeuN/Dapi+ cells in discrete bins every 50 μm from the device interface out to 500 μm in what appeared to be normal, undisturbed tissue. The number of neuronal nuclei per bin was then divided by the bin area to determine the average neuronal nuclear density as an estimate of the number of neuronal cell bodies surrounding the device.

Statistical analysis

The area under the curve of each average intensity profile for each immunomarker as well as the average neuronal nuclear density at 50 μm intervals from the device interface was compared across cohorts ($n=4$ for solids and $N=5$ for lattices) using a one-way ANOVA and Tukey post hoc tests by means of an SPSS software package (IBM, Somers NY), with significance considered at $p<0.05$. All data are Mean \pm SD.

Results

Consistent with previous reports, explanted 300 μm solid microelectrodes had minimal cell

attachment (data not shown). These cells were primarily CD68⁺ with small numbers of GFAP⁺ cells. We did not observe any NeuN⁺ cells attached to explanted microelectrodes. We did, however, observe DAPI⁺ nuclei that were not associated with either CD68⁺ or GFAP⁺ immunoreactivity, indicating the presence of other cell types. We observed no disruption of the tissue interface surrounding sectioned silicon lattice microelectrodes that remained embedded in tissue. Previously, we observed significant amounts of tissue that was immunohistochemically positive for CD68, GFAP, NF200, and MAP-2 associated with other explanted lattice electrode designs.

CD68, a lysosomal enzyme found in activated mononuclear phagocytes, was used to identify microglia/macrophage activation near the implant site of 300 μm solid and lattice microelectrode arrays. We observed CD68⁺ immunoreactivity surrounding both styles of microelectrodes (Fig. 2a and c). Despite having a larger penetrating profile than previously studied planar solid microelectrode arrays, the distribution of CD68⁺ tissue surrounding 300 μm solid arrays was similar to that described previously (Biran et al., 2005; Winslow et al., 2010). Punctate CD68⁺ immunoreactivity primarily was localized adjacent to and within the electrode track. Immunoreactivity was greatest along the 300 μm face of the planar electrode, as opposed to the 12 μm edges (Fig. 2a). For lattice electrodes, we observed punctate CD68⁺ immunoreactivity primarily at the interface of the 15 \times 12 μm silicon ribs and to a lesser extent spanning the distance between ribs (Fig. 2c). When the relative intensity profiles for CD68 were compared, we observed a significant reduction in immunoreactivity surrounding the 300 μm lattice arrays within the first 0–50 and 50–100 μm (Fig. 2e) compared to solid controls.

To assess BBB dysfunction associated with microelectrode implantation, sections were reacted with antisera against rat IgG. In uninjured rat cortex, IgG is restricted to the vasculature and removed upon perfusing the animal (Azzi et al., 1990; Seitz et al., 1985). However, in cases of

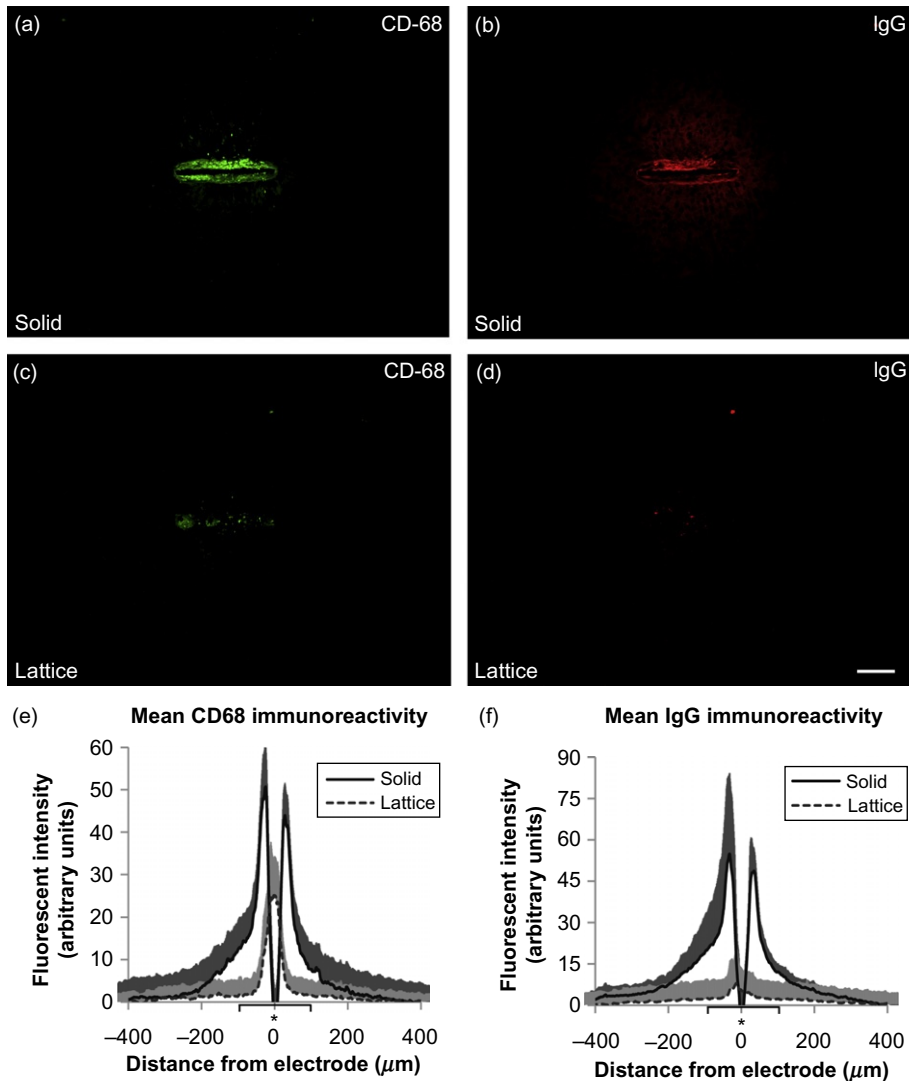


Fig. 2. Chronic macrophage/microglial response and estimate of blood brain barrier dysfunction adjacent to implanted solid and lattice silicon microelectrode arrays. (a and c) Representative horizontal sections showing CD68 immunoreactivity to (a) 300 μm planar solid and (c) 300 μm planar lattice arrays. (b and d) Representative horizontal sections through the implantation tract of a 300 μm planar, solid shank array (b), and a 300 μm planar lattice array (d) showing the distribution of IgG. (e and f) The results of a quantitative image analysis showing that lattice silicon microelectrode arrays with reduced surface area had a significantly reduced macrophage activation and blood brain barrier leakiness to IgG within the presumptive recording zone or first 100 μm from the center of the electrode. (*) denotes significant difference with $p < 0.05$. Data shown as mean \pm SD. Scale bar = 100 μm .

BBB dysfunction, IgG leaks through the vasculature and remains in tissue after perfusion (Aihara et al., 1994). Figure 2b and d shows representative

images of the IgG immunoreactivity surrounding solid and lattice electrodes, respectively. Lattice microelectrode arrays showed significantly

reduced BBB dysfunction within the first 100 μm from the center of the electrode compared to solid controls (Fig. 2f).

The astrocyte-specific intermediate filament marker GFAP was used to identify astrocytic hypertrophy surrounding implanted devices. Figure 3 shows representative images and quantitative analysis of GFAP immunoreactivity near solid and lattice microelectrode arrays. Similar to previous findings, both designs showed diffuse astrocytic hypertrophy near the device (Biran et al., 2007; Winslow et al., 2010). We observed a significant amount of GFAP⁺ tissue ingrowth through the lattice architecture. Except for this ingrowth, no significant differences were observed in the GFAP immunoreactivity between the two designs.

Antibodies against NeuN were used to identify neuronal nuclei to examine the density of neuronal cell bodies near implanted devices. Representative images for NeuN immunoreactivity surrounding solid and lattice arrays are shown in Fig. 4a and b. The density of neuronal nuclei surrounding both styles of devices was quantified in discrete bins every 50 μm from the implant site through manual counting and is shown in Fig. 4c. As observed previously, there was a significant reduction in neuronal cell body density compared to the density in uninjured tissue of approximately 60% and 10% surrounding 300 μm solid arrays within the first 50 and 100 μm , respectively. In contrast, there was significantly less reduction, roughly 10%, surrounding lattice arrays within the first 50 μm and no observable reduction

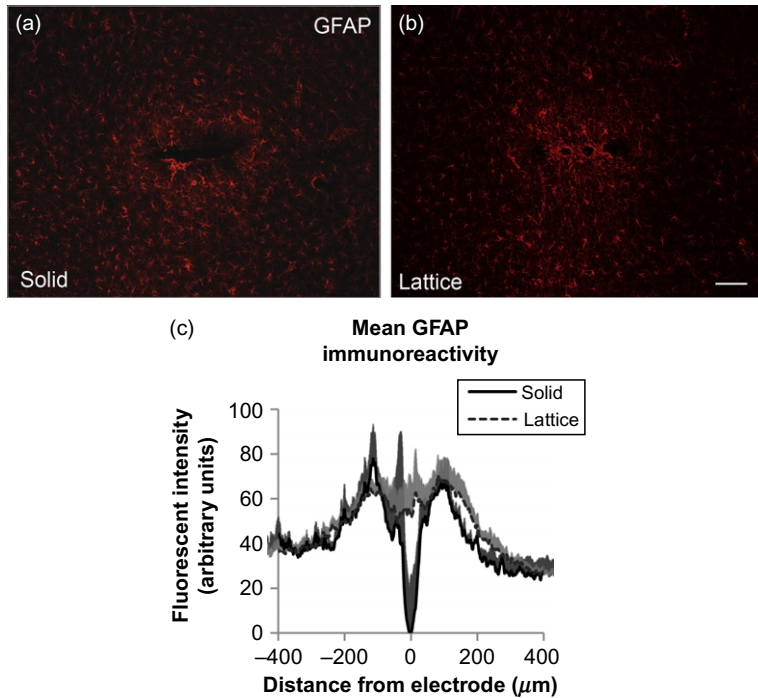


Fig. 3. Chronic astrocyte response to implanted silicon microelectrode arrays. (a and b) Representative horizontal sections showing GFAP immunoreactivity adjacent to (a) 300 μm planar solid and (b) 300 μm planar lattice arrays. (c) The results of a quantitative image analysis showing that both designs exhibited astrocytic hypertrophy surrounding the device, which differed in the significant amount of tissue ingrowth through the lattice architecture. Data shown as mean \pm SD. Scale bar = 100 μm .

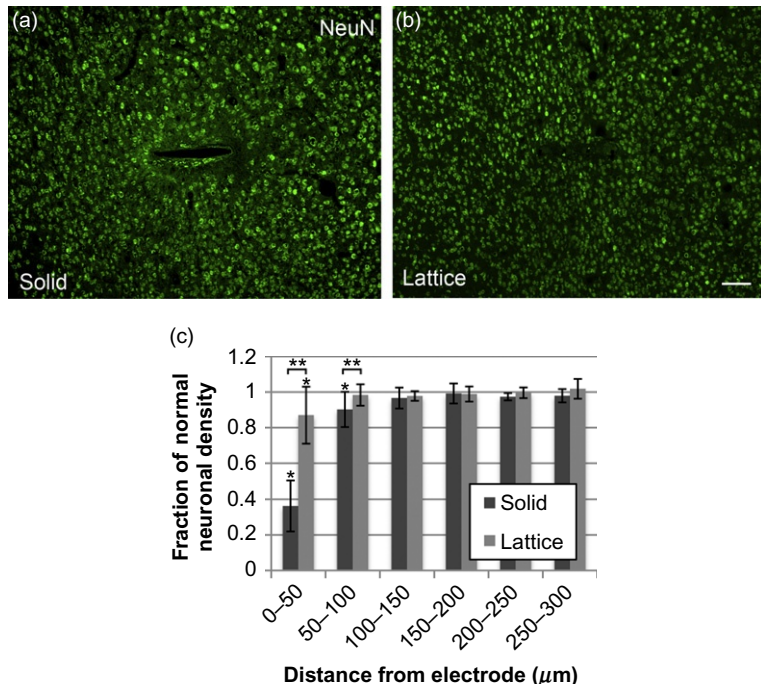


Fig. 4. Representative horizontal images of NeuN^+ nuclei around (a) solid and (b) lattice microelectrodes. (c) Neuronal density is plotted as a function of 50- μm bins from 0 to 250 μm from the microelectrode interface. Values were normalized to the average density of NeuN^+ neurons observed in normal tissue 400–500 μm from the electrode interface, and are therefore expressed as fraction of control. (*) denotes significant difference compared to normal neuronal density and (**) denotes differences between solid and lattice cohorts; both comparisons are $p < 0.05$. Data shown as mean \pm SD. Scale bar = 100 μm .

between 50 and 100 μm compared to uninjured tissue (Biran et al., 2007).

Discussion

In this study, we demonstrate that altering the exposed surface area of an implanted microelectrode array while maintaining a similar penetrating profile is sufficient to significantly change the classic hallmarks of the chronic FBR including reducing the degree of inflammation, reducing BBB leakiness, and reducing the amount of neuronal cell body loss. Our findings are supported by several recent studies looking at either planar (Seymour and Kipke, 2007) or cylindrical devices (Stice et al., 2007; Thelin et al., 2011). Seymour

and Kipke found significant differences in the neuronal and nonneuronal cell response between a parylene-based electrode's larger shank and an adjoining thin lateral platform connected to the main shaft (Seymour and Kipke, 2007), while both Stice et al. and Thelin et al. found significant differences in classic hallmarks of the FBR between microwires of different diameters (Stice et al., 2007; Thelin et al., 2011). Our results agree with these observations and disagree with Szarowski et al. who studied the FBR to a variety of devices with different cross-sectional areas, geometries, and roughnesses and concluded that the tissue response was independent of electrode properties (Szarowski et al., 2003). In contrast to the study by Seymour and Kipke, here we used quantitative methods to investigate specific

cellular and molecular features of the FBR rather than quantifying all nonneuronal cells as a single category, which allows us to determine which aspects of the brain FBR are affected by changes in implant architecture. Further, by studying the response to two planar devices with identical penetrating profiles, we have also negated the influence of implant curvature and the extent of iatrogenic injury that is unavoidable when comparing cylindrical microwire devices of different diameters (Stice et al., 2007; Thelin et al., 2011).

As described earlier, a key feature of the FBR to conventional microelectrode array designs is persistent inflammation at the biotic–abiotic interface signaled by biomarkers for activated microglia and macrophages (Biran et al., 2005; Stensaas and Stensaas 1976; Winslow and Tresco, 2010; Winslow et al., 2010). This observation is also supported by studies showing persistent inflammation surrounding other devices implanted into the central and peripheral nervous system including deep brain stimulating electrodes (Burbaud et al., 2002; Caparros-Lefebvre et al., 1994; Chou et al., 2004; Haberler et al., 2000; Henderson et al., 2002; Jarraya et al., 2003; Moss et al., 2004; Nielsen et al., 2007; Pilitsis et al., 2008), numerous designs of hydrocephalic shunts (Del Bigio 1998; Ellis et al., 2008; Thomale et al., 2010; Woodruff et al., 1986), and peripheral nerve electrodes (Branner et al., 2004). In this study, we observed a similar pattern of inflammation 8 weeks after implantation, a time point when recording inconsistency has been reported (Liu et al., 1999, 2006; Ludwig et al., 2006; Rennaker et al., 2005, 2007). The observation is signaled by similar CD68⁺ immunoreactivity, surrounding 300 μm -wide, planar, solid silicon microelectrode arrays to that described around smaller, 100 μm -wide, planar, solid silicon microelectrode arrays (Biran et al., 2005, 2007; Winslow et al., 2010).

The planar, silicon, lattice microelectrode arrays used here had identical penetrating profiles but exhibited significantly less inflammation-related biomarker distribution in the tissue

surrounding the implanted arrays compared to solid shank designs. This finding is supported by *in vivo* work from Sanders et al. showing that single small-diameter polymer fibers elicit minimal macrophage encapsulation (Sanders et al., 2000). Additionally, Seymour and Kipke's work showed qualitative differences between macrophage morphology and the amount of CD11b immunoreactivity surrounding different surface geometries contained within the same implant (Seymour and Kipke, 2007). Sanders et al. suggested that the minimal encapsulation observed in their model may have been caused by a threshold surface area effect or a critical surface curvature, where below a certain threshold of cell–material contact or above a critical curvature, there is insufficient mechanotransduction to induce macrophage activation (Sanders et al., 2000). Seymour and Kipke also proposed that a critical surface area concept may play a role in their results but favored the theory of mechanical property differences between the adjoining lattice and the primary solid shank as the explanation (Seymour and Kipke, 2007). We favor a critical surface area concept model. However, we do not believe that differences in mechanics between solid and lattice designs play as large of a role as attributed previously due to the similarity in findings between the soft, flexible parylene/SU-8-based structures used by Seymour and Kipke and our silicon-based arrays that are orders of magnitude stiffer.

Based on our findings, we propose a model that takes into account the quantity of soluble factors released by immune cells interacting with the device surface along with soluble factor diffusive distribution and clearance at the biotic/abiotic interface. Figure 5a shows a schematic of a two-dimensional model that includes macrophage-secreted soluble factors as the dominant remodeling force of tissue surrounding a cross section of a virtual device. Available evidence indicates that these macrophage-secreted soluble factors not only shape the foreign body reaction but also likely are responsible for neural and BBB dysfunction caused by a mixture of released

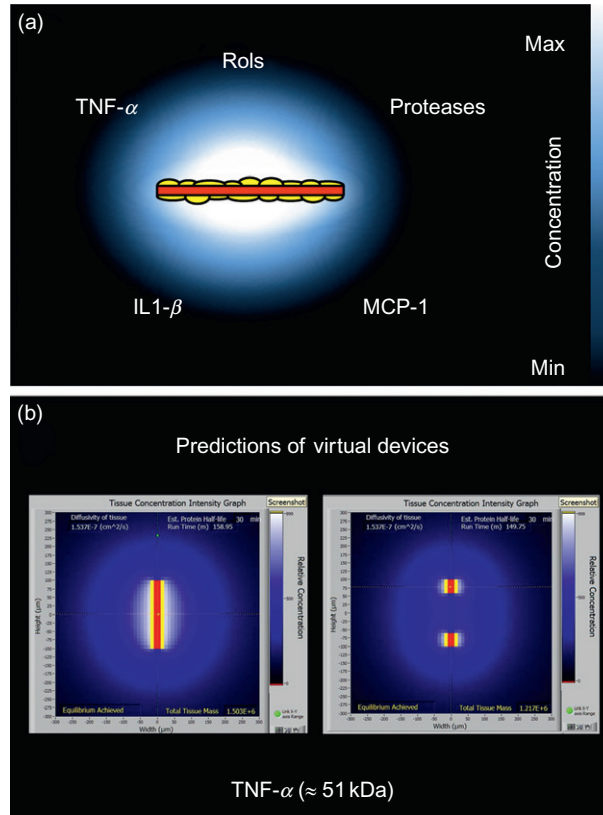


Fig. 5. (a) Schematic of 2D model of how implant architecture influences the brain tissue foreign body response. Here, we show a rectangular cross section through a typical impermeable, planar, electrode array (red) with a single layer of macrophages (yellow) at its surface and the soluble factor distribution (white to blue gradient) which dominates tissue remodeling during the indwelling period. The model takes into account the impermeable nature of the implant, which reflects and effectively doubles the concentration of molecules released at its surface. Coupled with the hindered diffusion present in brain tissue, supraphysiological levels of macrophage derived soluble factors result. The concentration gradient of these soluble factors surrounding the device is controlled by a combination of the diffusion and various clearance mechanisms. (b) Theoretical distribution of the macrophage-released soluble factor TNF- α surrounding cross sections of (left) solid and (right) lattice virtual devices (red) with similar penetrating profiles but differing amounts of exposed surface. Decreasing the surface area that is exposed to macrophages of the right-hand device by using a lattice structure decreases the source of soluble factors released into the adjacent tissue. The corresponding decrease in released soluble factor concentration due to a lessened source is further enhanced by increased distance between the two sources.

proinflammatory and cytotoxic cytokines such as IL-1B, IL-6, and TNF- α (Block et al., 2007; Cammer, 2000; Chao et al., 1995; Hanisch and Kettenmann, 2007; Quagliarello et al., 1991). While the cytophysiological sensitivity of adjacent neurons and glial cell types to these and other

macrophage-secreted factors has been established, the finer features of the picture are still emerging. Figure 5b shows what we believe is responsible for the results presented in this work by showing a theoretical distribution of one macrophage-released soluble factor, TNF- α ,

surrounding cross sections of two virtual devices with similar penetrating profiles but differing amounts of exposed surface.

Another specific feature of the brain FBR we examined in this work was BBB integrity. Recent studies from our lab have described disruption of BBB integrity, indicated by the presence of autologous IgG in the brain parenchyma, surrounding both microwire and planar silicon recording devices (Winslow and Tresco, 2010; Winslow et al., 2010). Under normal conditions, autologous IgG is excluded from the brain parenchyma (Azzi et al., 1990; Seitz et al., 1985) but has been observed following BBB disruption (Aihara et al., 1994). This disruption of the BBB alters the local ionic milieu and may influence chronic recording consistency through neuronal silencing or alterations in conduction velocity. Similar to previous studies from our group, we observed significant BBB disruption, indicated by the presence of autologous IgG in the brain parenchyma, surrounding solid arrays with significantly less disruption surrounding planar lattice microelectrodes with reduced surface area.

In accordance with our previous findings, the observed immunoreactivity for autologous IgG surrounding both styles of implanted arrays roughly colocalized with CD68 immunoreactivity (Winslow and Tresco, 2010; Winslow et al., 2010). This observation and that of decreased BBB disruption surrounding the lattice implants that also exhibited reduced macrophage activation further support our idea that macrophage-released factors and macrophage trafficking to and from the implant through adjacent post-capillary venules (Crane et al., 2003; Xu et al., 2003) may underlie changes in BBB integrity, as well as explain some observations labeled as recording inconsistency.

Consistent with previous studies of neuronal viability surrounding recording devices, we observed a reduction in neuronal nuclei within the recoding zone surrounding solid arrays (Biran et al., 2005, 2007; Collias and Manueldis, 1957; Edell et al., 1992; Schultz and Willey, 1976;

Stensaas and Stensaas, 1976, 1978; Winslow and Tresco, 2010; Winslow et al., 2010). We found a more normal distribution of neuronal nuclei surrounding the lattice microelectrode arrays compared to solid devices of the same size and shape. This observation of reduced neuronal loss surrounding implants with reduced macrophage activation also supports our group's hypothesis that implant design can be used to reduce the amount of macrophage activation at the biotic-abiotic interface and reduce the impact of their released factors, which should improve recording consistency and the lifetime of implanted microelectrode arrays.

Of interest was our observation that, except for astrocytic integration through the lattice structure, we found no significant difference between the relative GFAP intensity between the two designs studied. The relative intensity and spatial distribution of GFAP immunoreactivity were similar to that seen with other types of devices implanted in the CNS (Biran et al., 2005, 2007; Collias and Manueldis, 1957; Edell et al., 1992; Schmidt et al., 1993; Schultz and Willey, 1976; Stensaas and Stensaas, 1976, 1978; Szarowski et al., 2003). Astrocyte hypertrophy surrounding implanted microelectrodes has been put forward as a major contributor to chronic recording inconsistencies and failure (Liu et al., 1999). Previous work from our lab using single microwires and single shaft, planar silicon microelectrode arrays indicated that the spatial distribution of GFAP does not increase with time over the indwelling period and did not support the “increase in astrogliosis over time hypothesis” as a dominant or general biologically related failure mechanism for this type of microelectrode recording device (Winslow et al., 2010; Winslow and Tresco, 2010). It is not clear if this observation will hold for multishaft penetrating arrays with more complicated geometries.

With regards to the observed integration of astrocytes through the device, Seymour and Kipke have suggested that this response may better anchor lattice architectures in place (Seymour

and Kipke, 2007). However, it should also be noted that complications might arise from the significant amount of tissue integrated through the lattice structure if the device ever needs to be explanted due to infection or other adverse clinical event, especially with larger multishank devices. Therefore, further efforts may be needed to find alternative methods other than open lattice architectures to reduce device-associated inflammation, while preventing significant tissue ingrowth and the complication associated with implant retrieval should that be necessary.

Conclusion

In this study, we show that it is possible for electrode developers to modulate specific aspects of the brain tissue FBR by intentionally manipulating the shape of the implant. The results of our work also support our theory that the FBR to implanted electrode arrays, and likely other devices, can be explained by the persistence of activated macrophages at the biotic–abiotic interface, which act as a sustained delivery source of bioactive agents that diffuse into the adjacent tissue and shape other features of the FBR including recruitment of macrophages, BBB dysfunction, local areas of demyelination, and a sustained reduction in the local number of neuronal cell bodies. Further, our findings suggest that one method to improve recording consistency and lifetime of implanted microelectrode arrays is to design implants that reduce the amount of macrophage activation at the biotic–abiotic interface and or improve the clearance or impact of their released factors.

Acknowledgment

Research funding supported by the National Institutes of Health R01 NS0467700.

References

- Aihara, N., Tanno, H., et al. (1994). Immunocytochemical localization of immunoglobulins in the rat brain: Relationship to the blood-brain barrier. *The Journal of Comparative Neurology*, 342(4), 481–496.
- Azzi, G., Bernaudin, J. F., et al. (1990). Permeability of the normal rat brain, spinal cord and dorsal root ganglia microcirculations to immunoglobulins G. *Biology of the Cell*, 68(1), 31–36.
- Biran, R., Martin, D. C., et al. (2005). Neuronal cell loss accompanies the brain tissue response to chronically implanted silicon microelectrode arrays. *Experimental Neurology*, 195(1), 115–126.
- Biran, R., Martin, D. C., et al. (2007). The brain tissue response to implanted silicon microelectrode arrays is increased when the device is tethered to the skull. *Journal of Biomedical Materials Research. Part A*, 82(1), 169–178.
- Block, M. L., Zecca, L., et al. (2007). Microglia-mediated neurotoxicity: Uncovering the molecular mechanisms. *Nature Reviews. Neuroscience*, 8(1), 57–69.
- Branner, A., Stein, R. B., et al. (2004). Long-term stimulation and recording with a penetrating microelectrode array in cat sciatic nerve. *IEEE Transactions on Biomedical Engineering*, 51(1), 146–157.
- Burbaud, P., Vital, A., et al. (2002). Minimal tissue damage after stimulation of the motor thalamus in a case of chorea-acanthocytosis. *Neurology*, 59(12), 1982–1984.
- Cammer, W. (2000). Effects of TNFalpha on immature and mature oligodendrocytes and their progenitors in vitro. *Brain Research*, 864(2), 213–219.
- Caparros-Lefebvre, D., Ruchoux, M. M., et al. (1994). Long-term thalamic stimulation in Parkinson's disease: Postmortem anatomoclinical study. *Neurology*, 44(10), 1856–1860.
- Chao, C. C., Hu, S., et al. (1995). Glia, cytokines, and neurotoxicity. *Critical Reviews in Neurobiology*, 9(2–3), 189–205.
- Chou, K. L., Forman, M. S., et al. (2004). Subthalamic nucleus deep brain stimulation in a patient with levodopa-responsive multiple system atrophy. Case report. *Journal of Neurosurgery*, 100(3), 553–556.
- Collias, J. C., & Manuelidis, E. E. (1957). Histopathological changes produced by implanted electrodes in cat brains; comparison with histopathological changes in human and experimental puncture wounds. *Journal of Neurosurgery*, 14(3), 302–328.
- Crane, I. J., Xu, H., et al. (2003). Effect of anti-macrophage inflammatory protein-1alpha on leukocyte trafficking and disease progression in experimental autoimmune uveoretinitis. *European Journal of Immunology*, 33(2), 402–410.
- Del Bigio, M. R. (1998). Biological reactions to cerebrospinal fluid shunt devices: A review of the cellular pathology. *Neurosurgery*, 42(2), 319–325, discussion 325–316.

- Edell, D. J., Toi, V. V., et al. (1992). Factors influencing the biocompatibility of insertable silicon microshafts in cerebral cortex. *IEEE Transactions on Biomedical Engineering*, 39(6), 635–643.
- Ellis, M. J., Kazina, C. J., et al. (2008). Treatment of recurrent ventriculoperitoneal shunt failure associated with persistent cerebrospinal fluid eosinophilia and latex allergy by use of an “extracted” shunt. *Journal of Neurosurgery. Pediatrics*, 1(3), 237–239.
- Haberler, C., Alesch, F., et al. (2000). No tissue damage by chronic deep brain stimulation in Parkinson’s disease. *Annals of Neurology*, 48(3), 372–376.
- Hanisch, U. K., & Kettenmann, H. (2007). Microglia: Active sensor and versatile effector cells in the normal and pathologic brain. *Nature Neuroscience*, 10(11), 1387–1394.
- Henderson, J. M., Pell, M., et al. (2002). Postmortem analysis of bilateral subthalamic electrode implants in Parkinson’s disease. *Movement Disorders*, 17(1), 133–137.
- Hochberg, L. R., Serruya, M. D., et al. (2006). Neuronal ensemble control of prosthetic devices by a human with tetraplegia. *Nature*, 442(7099), 164–171.
- Jarraya, B., Bonnet, A. M., et al. (2003). Parkinson’s disease, subthalamic stimulation, and selection of candidates: A pathological study. *Movement Disorders*, 18(12), 1517–1520.
- Kennedy, P. R., Kirby, M. T., et al. (2004). Computer control using human intracortical local field potentials. *IEEE Transactions on Neural Systems and Rehabilitation Engineering*, 12(3), 339–344.
- Kim, Y. T., Hitchcock, R. W., et al. (2004). Chronic response of adult rat brain tissue to implants anchored to the skull. *Biomaterials*, 25(12), 2229–2237.
- Kruger, J., Caruana, F., et al. (2010). Seven years of recording from monkey cortex with a chronically implanted multiple microelectrode. *Frontiers in Neuroengineering*, 3, 6.
- Liu, X., McCreery, D. B., et al. (1999). Stability of the interface between neural tissue and chronically implanted intracortical microelectrodes. *IEEE Transactions on Rehabilitation Engineering*, 7(3), 315–326.
- Liu, X., McCreery, D. B., et al. (2006). Evaluation of the stability of intracortical microelectrode arrays. *IEEE Transactions on Neural Systems and Rehabilitation Engineering*, 14(1), 91–100.
- Ludwig, K. A., Uram, J. D., et al. (2006). Chronic neural recordings using silicon microelectrode arrays electrochemically deposited with a poly(3,4-ethylenedioxythiophene) (PEDOT) film. *Journal of Neural Engineering*, 3(1), 59–70.
- Moss, J., Ryder, T., et al. (2004). Electron microscopy of tissue adherent to explanted electrodes in dystonia and Parkinson’s disease. *Brain*, 127(Pt 12), 2755–2763.
- Musallam, S., Corneil, B. D., et al. (2004). Cognitive control signals for neural prosthetics. *Science*, 305(5681), 258–262.
- Nicolelis, M. A., Dimitrov, D., et al. (2003). Chronic, multisite, multielectrode recordings in macaque monkeys. *Proceedings of the National Academy of Sciences of the United States of America*, 100(19), 11041–11046.
- Nielsen, M. S., Bjarkam, C. R., et al. (2007). Chronic subthalamic high-frequency deep brain stimulation in Parkinson’s disease—A histopathological study. *European Journal of Neurology*, 14(2), 132–138.
- Pilitsis, J. G., Chu, Y., et al. (2008). Postmortem study of deep brain stimulation of the anterior thalamus: Case report. *Neurosurgery*, 62(2), E530–E532, discussion E532.
- Quagliarello, V. J., Wispelwey, B., et al. (1991). Recombinant human interleukin-1 induces meningitis and blood-brain barrier injury in the rat. Characterization and comparison with tumor necrosis factor. *The Journal of Clinical Investigation*, 87(4), 1360–1366.
- Rennaker, R. L., Miller, J., et al. (2007). Minocycline increases quality and longevity of chronic neural recordings. *Journal of Neural Engineering*, 4(2), L1–L5.
- Rennaker, R. L., Street, S., et al. (2005). A comparison of chronic multi-channel cortical implantation techniques: Manual versus mechanical insertion. *Journal of Neuroscience Methods*, 142(2), 169–176.
- Sanders, J. E., Stiles, C. E., et al. (2000). Tissue response to single-polymer fibers of varying diameters: Evaluation of fibrous encapsulation and macrophage density. *Journal of Biomedical Materials Research*, 52(1), 231–237.
- Schmidt, S., Horch, K., et al. (1993). Biocompatibility of silicon-based electrode arrays implanted in feline cortical tissue. *Journal of Biomedical Materials Research*, 27(11), 1393–1399.
- Schultz, R. L., & Willey, T. J. (1976). The ultrastructure of the sheath around chronically implanted electrodes in brain. *Journal of Neurocytology*, 5(6), 621–642.
- Seitz, R. J., Heininger, K., et al. (1985). The mouse blood-brain barrier and blood-nerve barrier for IgG: A tracer study by use of the avidin-biotin system. *Acta Neuropathologica*, 68(1), 15–21.
- Seymour, J. P., & Kipke, D. R. (2007). Neural probe design for reduced tissue encapsulation in CNS. *Biomaterials*, 28(25), 3594–3607.
- Shain, W., Spataro, L., et al. (2003). Controlling cellular reactive responses around neural prosthetic devices using peripheral and local intervention strategies. *IEEE Transactions on Neural Systems and Rehabilitation Engineering*, 11(2), 186–188.
- Stensaas, S. S., & Stensaas, L. J. (1976). The reaction of the cerebral cortex to chronically implanted plastic needles. *Acta Neuropathologica*, 35(3), 187–203.
- Stensaas, S. S., & Stensaas, L. J. (1978). Histopathological evaluation of materials implanted in the cerebral cortex. *Acta Neuropathologica*, 41(2), 145–155.
- Stice, P., Gilletti, A., et al. (2007). Thin microelectrodes reduce GFAP expression in the implant site in rodent somatosensory cortex. *Journal of Neural Engineering*, 4(2), 42–53.

- Szarowski, D. H., Andersen, M. D., et al. (2003). Brain responses to micro-machined silicon devices. *Brain Research*, 983(1–2), 23–35.
- Thelin, J., Jornell, H., et al. (2011). Implant size and fixation mode strongly influence tissue reactions in the CNS. *PLoS One*, 6(1), e16267.
- Thomale, U. W., Hosch, H., et al. (2010). Perforation holes in ventricular catheters—is less more? *Child's Nervous System*, 26(6), 781–789.
- Winslow, B. D., Christensen, M. B., et al. (2010). A comparison of the tissue response to chronically implanted Paraffylene-C-coated and uncoated planar silicon microelectrode arrays in rat cortex. *Biomaterials*, 31(35), 9163–9172.
- Winslow, B. D., & Tresco, P. A. (2010). Quantitative analysis of the tissue response to chronically implanted microwire electrodes in rat cortex. *Biomaterials*, 31(7), 1558–1567.
- Woodruff, W. W., Jr., Yeates, A. E., et al. (1986). Ventricular shunt therapy of the brain: Long-term rubber-catheter-induced inflammation. *Radiology*, 158(1), 171–174.
- Xu, H., Forrester, J. V., et al. (2003). Leukocyte trafficking in experimental autoimmune uveitis: Breakdown of blood-retinal barrier and upregulation of cellular adhesion molecules. *Investigative Ophthalmology & Visual Science*, 44(1), 226–234.

CHAPTER 13

Can histology solve the riddle of the nonfunctioning electrode?: Factors influencing the biocompatibility of brain machine interfaces

Cecilia Eriksson Linsmeier¹, Jonas Thelin^{*1} and Nils Danielsen

Neuronano Research Centre, Lund University, Lund, Sweden

Abstract: Neural interfaces hold great promise to become invaluable clinical and diagnostic tools in the near future. However, the biocompatibility and the long-term stability of the implanted interfaces are far from optimized. There are several factors that need to be addressed and standardized when improving the long-term success of an implanted electrode. We have chosen to focus on three key factors when evaluating the evoked tissue responses after electrode implantation into the brain: implant size, fixation mode, and evaluation period. Further, we show results from an ultrathin multichannel wire electrode that has been implanted in the rat cerebral cortex for 1 year.

To improve biocompatibility of implanted electrodes, we would like to suggest that free-floating, very small, flexible, and, in time, wireless electrodes would elicit a diminished cell encapsulation. We would also like to suggest standardized methods for the electrode design, the electrode implantation method, and the analyses of cell reactions after implantation into the CNS in order to improve the long-term success of implanted neural interfaces.

Keywords: cell morphology; brain; electrode; neural cell; micromotion; cell encapsulation.

General background

When implanting a functional brain machine interface (BMI), it is possible to record from, or stimulate, central nervous tissue over long periods of time providing a unique basis for diagnosing, and treating, patients with neurodegenerative or psychiatric disorders, as well as for characterizing fundamental neural mechanisms in animal models

*Corresponding author.

Tel.: +46-46-2227781; Fax: +46-46-2227756
E-mail: jonas.thelin@med.lu.se

¹These authors have contributed equally to the study.

(Benabid, 2007; Benabid et al., 2009; Kipke et al., 2008; Mushahwar et al., 2007). However, the biocompatibility and the long-term stability of the implanted interfaces are far from optimized. It is well known that the implantation procedure is associated with a certain amount of local tissue damage, and the implant itself subsequently elicits both acute and chronic reactions in the surrounding tissue (Biran et al., 2005; Winslow and Tresco, 2010). These tissue responses may have detrimental effects on the long-term function of the electrode. The reactions can be seen as a zone of many different cell types, mainly activated astroglial cells surrounding a core of activated microglia adjacent to the implant surface. Hence, the encapsulation tissue that forms and surrounds the interface acts to electrically insulate the neural interface from nearby neurons, thus leading to higher impedance (see Marin and Fernandez, 2010 for recent review). In this zone of gliosis (the reactive capsule), a reduction of neuronal density has been demonstrated (Edell et al., 1992; Kim et al., 2004). The cause of the neuronal reduction has not yet been fully understood; it is uncertain if they die or migrate away (Biran et al., 2005) or just simply are being pushed further out by the reactive capsule.

Biocompatibility is widely defined as “the ability of a material to perform with an appropriate host response in a specific application” (Williams, 2008). When designing a neural interface, many parameters have to be considered, for example, material, size, shape, stiffness, surface topography (microstructure), and surface energy. It is also of uttermost importance to consider the state of the host, the surgical technique, the mechanical loading, the tethering inside the brain tissue, and also the shear forces, when designing a neural interface that should be able to function for a long time period, in extreme cases, the expected lifetime of the experimental animal or the patient. Unfortunately, there is no general consensus about how the different parameters discussed above will affect the biocompatibility of different

BMIs; some of the recent reported findings are contradictory. This hampers the development of the field.

Implant size

Some authors have suggested that long-term tissue responses (more than 2 weeks) are independent of implant size (Szarowski et al., 2003), while others have reported that smaller diameter implants induce a smaller astrocytic reaction than larger devices (Stice et al., 2007). In a nonquantitative immunohistochemical study, three different implants with various shapes and sizes were compared for up to 12 weeks after implantation (Szarowski et al., 2003). It was claimed that device size was the major factor to early tissue responses, but that the responses after 4 weeks were similar for all devices. The intriguing question of size was specifically addressed by Stice et al. (2007). This study demonstrated that glial fibrillary acidic protein (GFAP) expression was significantly smaller for 12 μm diameter implants as compared to 25 μm implants at the longer evaluation period, that is, 4 weeks. Notably, the relative importance of implant size and fixation mode and the possible interplay between the two factors have not been established or quantified.

Fixation mode

In previous studies, one of the factors deemed to be important for minimizing the unwanted tissue reactions is the use of untethered, rather than tethered, electrodes. The rationale for this approach is to minimize the motion between electrode and brain tissue caused by the normal movements of the brain within the skull cavity due to forces induced by respiration and circulation (Biran et al., 2007). A tethered design may also allow invasion of unwanted cells such as meningeal fibroblasts into the brain tissue (Biran et al., 2007; Kim et al., 2004). However, although there seems

to be consensus that untethered implants elicit a smaller tissue reaction than tethered ones, it is still unclear if the actual neuronal numbers differ between the two fixation modes. In a quantitative immunohistochemical study using rather large implants (Kim et al., 2004), it was shown that tethered implants induced a significantly larger astrocytic and microglial response at 4 weeks, compared to nontethered ones. In a quantitative follow-up study comparing tethered, and untethered silicon microelectrodes during 1–4 weeks (Biran et al., 2007), it was demonstrated that tethered electrodes induced a more severe astrocytic and microglial response. Immunohistochemical staining for neurofilaments showed a reduced expression for tethered electrodes, suggesting a reduced neuronal density, but no actual cell counts were presented (Biran et al., 2007). Although this research group had previously demonstrated that tethered electrode implantation induced a reduced neuronal density using cell counting methods, about 40%, and this was most obvious within a 100 µm radius from the implant (Biran et al., 2005). However, in this study it should be noted that the evaluation period was rather short, 2–4 weeks (Biran et al., 2005). In another recent study, it was shown that stainless microwires implanted and tethered to the skull induced a persistent inflammation over a 12-week evaluation period, but the reactive gliosis and the reduction in neuronal density within a 50 µm radius from the implant were not progressive (Winslow and Tresco, 2010). Taken together, these findings underscore the need for a systematic study comparing the two fixation modes by evaluating the overall elicited tissue reactions and specifically addressing in quantitative terms the issue of neuronal numbers close to the implants over rather long evaluation periods (see below).

Functional distance

Further, the functional distance between neurons and recording/stimulation sites and the stability

of this distance over time is one of the key factors determining long-term function of neural interfaces. The distance over which spiking activity of individual neurons can be followed rarely exceeds 50 µm (Purcell et al., 2009), rendering less neurophysiological relevant situations when the electrode–neuron distance is over 50 µm. Hence, if the functional distance is increased, either by loss of neurons in close vicinity to the electrode or by a progressively growing glial capsule, the function of the electrode will be compromised. The formation of a glial capsule may also *per se* jeopardize electrode function by increasing the electrical resistance/impedance. These changes must therefore be minimized to ensure the long-term high-quality recordings necessary for analysis of processes such as memory formation, or maintained stimulation efficacy necessary for obtaining adequate and stable therapeutic effects in the clinical context.

Implantation time

Electrodes implanted in humans are expected to function for a very long time, in some cases, nearly a whole lifetime and human and primate studies have shown that electrodes can function for several years (Hochberg et al., 2006; Nicolelis et al., 2003). In rabbits, 6-month follow-up periods have been used (Edell et al., 1992). Most experimental rat studies use rather short evaluation periods with an emphasis on 2–4 weeks (Biran et al., 2005, 2007; Kim et al., 2004; Stice et al., 2007; Szarowski et al., 2003), even though some studies have follow-up periods up to 16 weeks (McConnell et al., 2009). Since changes over time are important when evaluating how the characteristics of the implant influence the tissue, we have recently published an article focusing on quantifying the relative importance and potential interactions between implant size and fixation modes over relatively long time periods in the experimental setting (Thelin et al., 2011).

Implant size versus fixation mode over time

In this study by Thelin et al., a total of 24 adult female Sprague-Dawley rats were divided into four groups (implant diameter: 200 vs. 50 μm , fixation mode: tethered vs. untethered) and two different time points were chosen (6 and 12 weeks). To evaluate the evoked tissue reactions of the different implants, we used GFAP (labels an astrocyte-specific intermediate filament, which is upregulated in activated astrocytes), ED1 (CD68; a marker for activated microglia), and NeuN (a marker for neuronal nuclei; see Fig. 1; Thelin et al., 2011).

The analysis was divided into three steps. First, in order to establish the relative importance of individual experimental variables on the tissue reaction including number of neurons, effects of implant *fixation mode* and *diameter*, *time-point* after implantation, and *distance* from implant were analyzed. There were significant multivariate main effects of all experimental variables described above (Thelin et al., 2011).

Second, in order to find the optimal implant configuration in this study, effects of the four actual implant types—tethered or untethered with small or large diameter, respectively—were compared. Progressively less-activated astrocytes and microglia were found as one advanced from a 200- μm tethered electrode to a 200- μm untethered, further to a 50- μm tethered, and finally a 50- μm untethered electrode, where the least number of activated astrocytes was found (see Fig. 2; Thelin et al., 2011).

In a third step, further addressing outcomes of the implantation that may be expected to influence recording or stimulation characteristics, the shapes of neurons surrounding the implant cavity and the size and shape of the cavity itself were examined. We found an alteration in the shape and organization of nerve cells (flattened neurons in a whirl-like pattern close to the implant) surrounding the tethered implants which has not been described previously. When quantifying the area of the different cavities, we found a significant ($p < 0.01$) enlargement in relation to actual

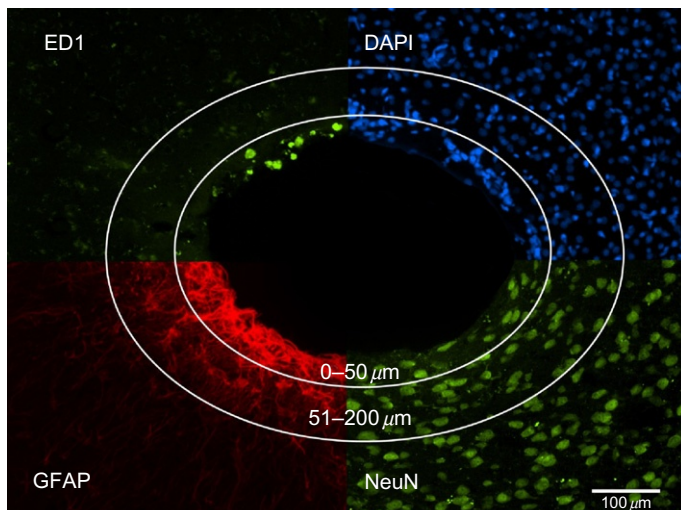


Fig. 1. The picture is a montage visualizing the four different markers used, ED1 (activated microglia), DAPI (all cell bodies), GFAP (astrocytes), and NeuN (neuronal nuclei), in rat cortex surrounding an implant. The circles illustrate two different regions of interest.

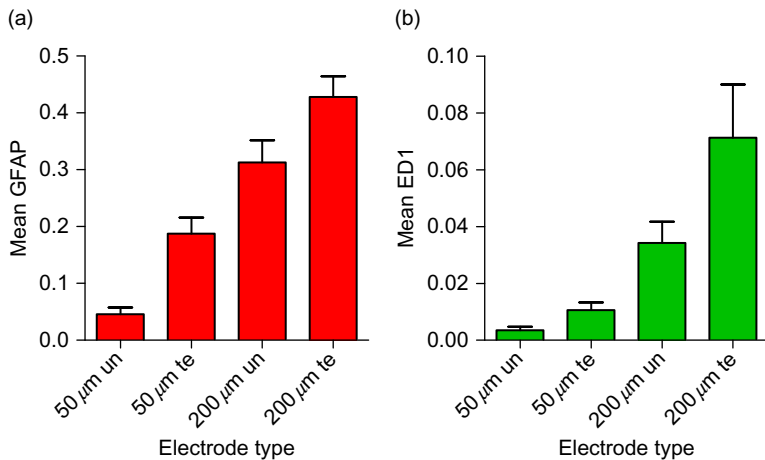


Fig. 2. (a) Quantified GFAP density surrounding (0–200 μm) the implants with respect to fixation mode (un=untethered and te=tethered) and size (50 or 200 μm) of the implant after 12 weeks. (b) Quantified ED1 density surrounding (0–200 μm) the implants with respect to fixation mode (un=untethered and te=tethered) and size (50 or 200 μm) of the implant after 12 weeks. The columns indicate the mean and bars show the standard error of the mean.

implant size made by tethered implants regardless of diameter ([Thelin et al., 2011](#)).

Relation between neurons and reactive cell capsule

As pointed out in the introduction, there are several potential sources of variability when evaluating function of different microelectrodes such as geometry, insertion method, substrate composition, insulation material, and size. However, for all electrodes, whether it is a recording or a stimulation electrode, the goal is to be as close to the neurons as possible. Although everyone agrees that it is of course the neurons that are the cells of interest, many previous studies primarily concentrate on activated astrocytes and other glial cells when studying the results after implantation to the central nervous tissue ([Holecko et al., 2005; Kreutzberg, 1996; Turner et al., 1999](#)). Although it is suggested, and probably likely, that the glial scar compromises recording quality by impeding ion diffusion through the extracellular space and reduces neuronal density

within the recording radius of the microelectrodes, this assumption has never been proven ([Ward et al., 2009](#)). The question is, is the measurement of inflammation and the reactive cell capsule a good marker for the number of neurons in the proximity of the electrode and subsequently recording quality?

In order to try to answer this methodological important question, we analyzed the tissue sections obtained in our recently published article ([Thelin et al., 2011](#)) further. Specifically, we wanted to establish if there was a correlation between activated astrocytes and microglia, and the number of neurons close to the implanted electrode. If such a correlation could be established, it could simplify the evaluation of new electrode designs by making arduous cell counting procedures less necessary. The area analyzed was the region within a 25 μm radius from the electrode. Previously, it has been shown that this region is the most interesting electrophysiological zone, and this region is also where the glial scar is most pronounced. Neural density (number of NeuN positive cells per μm²) within this zone was plotted against the intensity of the two

markers for astrocytes (GFAP) and activated microglia (ED1), respectively, and the linear correlation was calculated (see Fig. 3). The evaluation showed, regardless of electrode size, that after 6 weeks of implantation, the correlation was almost nonexistent with r^2 values of 0.02 for astrocytes and 0.06 for activated microglia. After 12 weeks, when the tissue reaction is believed to be stabilized, the astrocytic response had a correlation value of $r^2=0.12$ to the number of neurons, and for the activated microglial cells, the correlation was $r^2=0.18$ (see Fig. 3). These low correlation values suggest that the inflammatory markers commonly used, GFAP and ED1, are not good indicators of how many neurons that are in the vicinity of the electrode.

It should be noted that when evaluating the DAPI staining (labeling all cell nuclei), it is evident that there are many unidentified cells in close vicinity of the implanted electrodes that could be important for the impedance and also the general functionality of the electrode. We believe that future studies have to focus on identifying all involved cell components.

Further, we noted that, in our hands, an automated quantification of neurons using the area of immunofluorescence resulted in errors and unreliable results due to artifacts and background staining. This finding makes it necessary to count each individual neuron to establish

reliable numbers of neurons within the analyzed area. Counting neurons is a time-consuming effort and it is also necessary to use certain methodologies to establish true differences between different experimental situations (Coggeshall and Lekan, 1996). One promising method is to monitor the tissue response *in vivo* indirectly by measuring the electric properties of the surrounding tissue. Because the reactive cell capsule is much less conductive than unaffected neural tissue, impedance measurements can be used to monitor the extent and progress of the formation of the glial capsule (Johnson et al., 2005; Otto et al., 2006). The progress of the scar formation can then be correlated to histological analyses of the tissue.

Strategies for a tethered design

In our previous study, we found that the brain movements in relation to the skull had a significant impact on the tissue surrounding the electrodes (Thelin et al., 2011). When electrodes were tethered to the skull, the motions of the underlying tissue caused cavities and compression of the surrounding tissue. Interestingly, an untethered 50- μm electrode exhibited very weak inflammatory response after 12 weeks indicating that a small-sized electrode that can move with

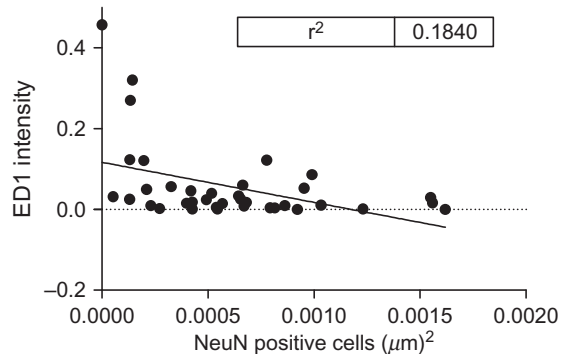
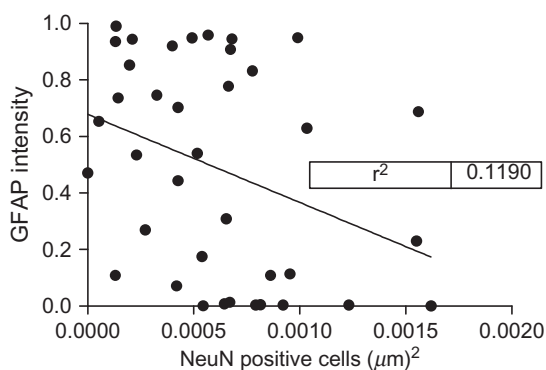


Fig. 3. The correlation plots between neural density and the two inflammatory markers GFAP and ED1 after 12 weeks.

the tissue seems to be gentler to the surrounding tissue (Thelin et al., 2011). However, as all existing electrodes today need some kind of connection to electronics, most of them have a tethered design (Ward et al., 2009). One strategy to minimize the problem with tissue motions in relation to the electrode is to make the electrode as flexible as possible. In our laboratory, we have developed a wire electrode that consists of 28 (12 μm thick) platinum/iridium wires that are believed to be flexible enough to move with the tissue. However, very flexible electrodes are difficult to insert through the Pia Mater, and thus a new method of implantation was developed (Lind et al., 2010). Using gelatine as a water-soluble backbone to the thin flexible wires allows us to implant the flexible wires. The wires are organized in a tight bundle with a diameter of proximally 200 μm (see Fig. 4). When the bundle is inserted into the tissue, the gelatine starts to dissolve and the individual wires start to fan out in the tissue. This allows for a dramatic increase in the area that is contacted by the wires, that is, from an area of 31,000 μm^2 at the surface of the cortex to an area of 280,000 μm^2 approximately 0.5 mm down in the tissue. This is an increase of 900%. The actual area at the tip of the wires is

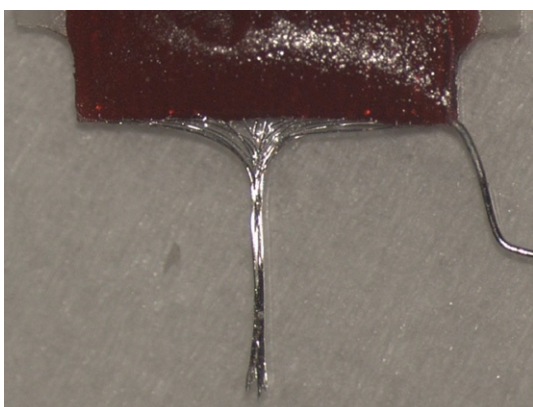


Fig. 4. The newly developed 12 μm wire electrode. The 28 wires are arranged in a bundle ($\sim 200 \mu\text{m}$ in diameter), held together with a very thin layer of gelatine.

very difficult to estimate, as there is no clear boundary indicating where the wires have been in the cortex after implantation. When this type of electrode was left in the rat cortex for almost a year (354 days), we found that the tissue response was very limited at the tips (see Fig. 5). The 12 μm wires exhibit no clear GFAP staining or ED1 positive cells at the tips. These findings indicate that 12 μm diameter electrodes are small enough to not elicit a significant chronic tissue response, that is, GFAP and ED1 positive cells; however, there might be a transient response at earlier time points. Further, our results suggest that the neurons seem to be unaffected in morphology and are situated very close to the electrodes. The ongoing inflammatory response reported by others seems to be significantly reduced when the electrodes are small and have the ability to follow the movements of the brain.

Conclusions

Electrode size seems to be of importance for the elicited cell response. Small devices evoke less cell reactions.

The negative effects of using tethered designs can be limited by downsizing the electrode size.

For future biocompatibility studies, it is necessary to analyze each involved cell component (astrocytes, microglia, oligodendrocytes, and neurons) separately using well-established methods and antibodies.

It seems necessary to count neurons manually to establish the number of neurons within an area. The recommendations for cell counting should be followed. To only rely on the immunofluorescently stained area for estimations of neuronal density is not recommended, since it does not correspond with the actual number of neurons.

Try to use as long evaluation periods as possible in order to establish more accurate tissue response studies.

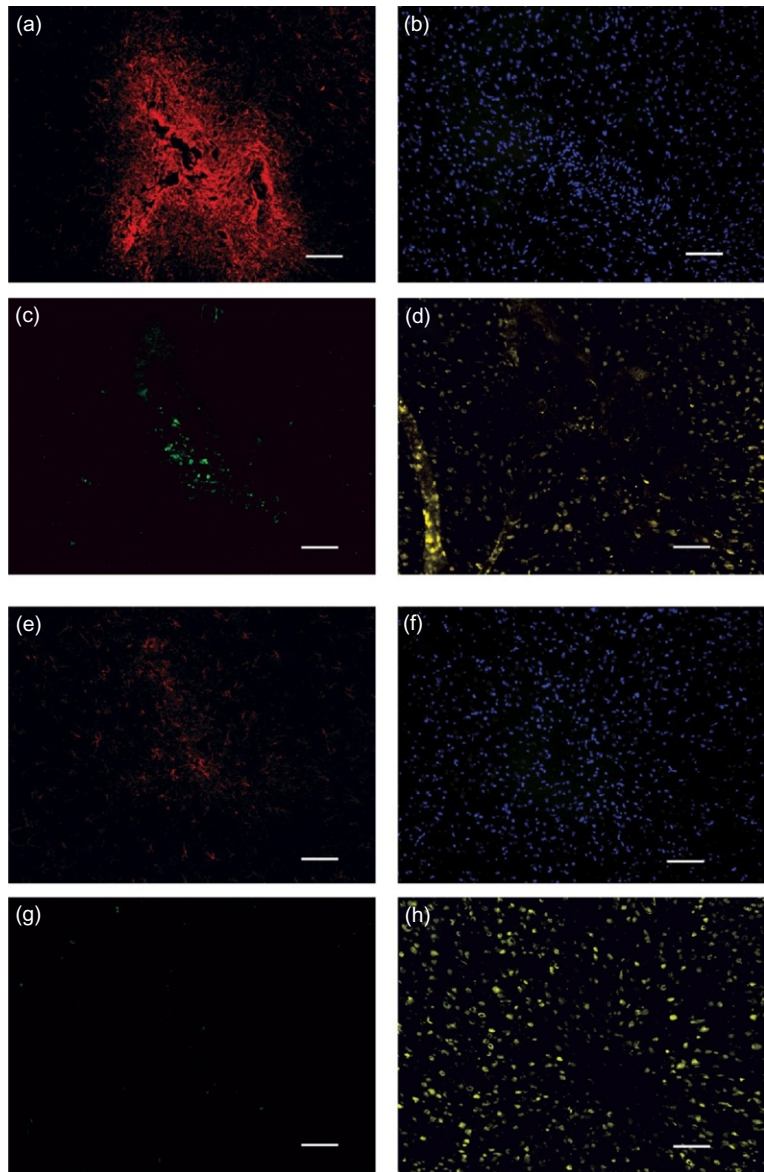


Fig. 5. Showing representative images of horizontal sections (perpendicular to the implantation tract) of the rat cortex 1 year after electrode implantation. Visualizing four different immunohistochemical stainings, in red (a, e)=GFAP, in yellow (d, h)=NeuN, in green (c, g)=ED1, and in blue (b, f)=DAPI, showing the spatial and temporal reactivity surrounding the twenty-eight 12 μm wires. Sections (a-d) are from a depth of 300 μm and (e-h) from 1500 μm below the surface of the cortex. The 1500 μm depth corresponds to where the tips of the 12 μm wires were located. Scale bar 100 μm .

Acknowledgments

We thank Suzanne Rosander and Agneta San Martin for excellent technical assistance. The project was sponsored by The Royal Physiographic Society in Lund, The Magnus Bergvall Foundation, The Knut and Alice Wallenberg Foundation (project number: KAW 2004-0119), and a Linné grant (project number: 600012701) from the Swedish Research Council.

References

- Benabid, A. L. (2007). What the future holds for deep brain stimulation. *Expert Review of Medical Devices*, 4(6), 895–903.
- Benabid, A. L., Chabardes, S., et al. (2009). Deep brain stimulation of the subthalamic nucleus for the treatment of Parkinson's disease. *Lancet Neurology*, 8(1), 67–81.
- Biran, R., Martin, D. C., et al. (2005). Neuronal cell loss accompanies the brain tissue response to chronically implanted silicon microelectrode arrays. *Experimental Neurology*, 195(1), 115–126.
- Biran, R., Martin, D. C., et al. (2007). The brain tissue response to implanted silicon microelectrode arrays is increased when the device is tethered to the skull. *Journal of Biomedical Materials Research*, A82(1), 169–178.
- Coggeshall, R. E., & Lekan, H. A. (1996). Methods for determining numbers of cells and synapses: A case for more uniform standards of review. *The Journal of Comparative Neurology*, 364(1), 6–15.
- Edell, D. J., Toi, V. V., et al. (1992). Factors influencing the biocompatibility of insertable silicon microshafts in cerebral cortex. *IEEE Transactions on Biomedical Engineering*, 39(6), 635–643.
- Hochberg, L. R., Serruya, M. D., et al. (2006). Neuronal ensemble control of prosthetic devices by a human with tetraplegia. *Nature*, 442(7099), 164–171.
- Holecko, M. M., 2nd, Williams, J. C., et al. (2005). Visualization of the intact interface between neural tissue and implanted microelectrode arrays. *Journal of Neural Engineering*, 2(4), 97–102.
- Johnson, M. D., Otto, K. J., et al. (2005). Repeated voltage biasing improves unit recordings by reducing resistive tissue impedances. *IEEE Transactions on Neural Systems and Rehabilitation Engineering*, 13(2), 160–165.
- Kim, Y. T., Hitchcock, R. W., et al. (2004). Chronic response of adult rat brain tissue to implants anchored to the skull. *Biomaterials*, 25(12), 2229–2237.
- Kipke, D. R., Shain, W., et al. (2008). Advanced neurotechnologies for chronic neural interfaces: New horizons and clinical opportunities. *The Journal of Neuroscience*, 28(46), 11830–11838.
- Kreutzberg, G. W. (1996). Microglia: A sensor for pathological events in the CNS. *Trends in Neurosciences*, 19(8), 312–318.
- Lind, G., Linsmeier, C. E., et al. (2010). Gelatine-embedded electrodes—A novel biocompatible vehicle allowing implantation of highly flexible microelectrodes. *Journal of Neural Engineering*, 7(4), 046005.
- Marin, C., & Fernandez, E. (2010). Biocompatibility of intracortical microelectrodes: Current status and future prospects. *Frontiers in Neuroengineering*, 3, 8.
- McConnell, G. C., Rees, H. D., et al. (2009). Implanted neural electrodes cause chronic, local inflammation that is correlated with local neurodegeneration. *Journal of Neural Engineering*, 6(5), 056003.
- Mushahwar, V. K., Jacobs, P. L., et al. (2007). New functional electrical stimulation approaches to standing and walking. *Journal of Neural Engineering*, 4(3), S181–S197.
- Nicolelis, M. A., Dimitrov, D., et al. (2003). Chronic, multisite, multielectrode recordings in macaque monkeys. *Proceedings of the National Academy of Sciences of the United States of America*, A100(19), 11041–11046.
- Otto, K. J., Johnson, M. D., et al. (2006). Voltage pulses change neural interface properties and improve unit recordings with chronically implanted microelectrodes. *IEEE Transactions on Biomedical Engineering*, 53(2), 333–340.
- Purcell, E. K., Thompson, D. E., et al. (2009). Flavopiridol reduces the impedance of neural prostheses *in vivo* without affecting recording quality. *Journal of Neuroscience Methods*, 183(2), 149–157.
- Stice, P., Gilletti, A., et al. (2007). Thin microelectrodes reduce GFAP expression in the implant site in rodent somatosensory cortex. *Journal of Neural Engineering*, 4(2), 42–53.
- Szarowski, D. H., Andersen, M. D., et al. (2003). Brain responses to micro-machined silicon devices. *Brain Research*, 983(1–2), 23–35.
- Thelin, J., Jörntell, H., et al. (2011). Implant size and fixation mode strongly influence tissue reactions in the CNS. *PLoS One*, 6(1), e16267.
- Turner, J. N., Shain, W., et al. (1999). Cerebral astrocyte response to micromachined silicon implants. *Experimental Neurology*, 156(1), 33–49.
- Ward, M. P., Rajdev, P., et al. (2009). Toward a comparison of microelectrodes for acute and chronic recordings. *Brain Research*, 1282, 183–200.
- Williams, D. F. (2008). On the mechanisms of biocompatibility. *Biomaterials*, 29(20), 2941–2953.
- Winslow, B. D., & Tesco, P. A. (2010). Quantitative analysis of the tissue response to chronically implanted microwire electrodes in rat cortex. *Biomaterials*, 31(7), 1558–1567.

CHAPTER 14

Changes in CNS structures after spinal cord lesions: implications for BMI

M. Martinez and S. Rossignol*

Department of Physiology, Groupe de Recherche sur le Système Nerveux Central, Faculty of Medicine, Université de Montréal, SensoriMotor Rehabilitation Research Team of the Canadian Institute for Health Research, Montréal, Québec, Canada

Abstract: It is well established that a spinal circuitry can generate locomotor movements of the hindlimbs in absence of descending supraspinal inputs. This is based, among others, on the observation that after a complete spinalization, cats can walk with the hindlimbs on a treadmill. Does this spinal pattern generator (CPG) also participate in the recovery of locomotion after a partial spinal cord lesion (SCI)? After such SCI, functional reorganization can occur spontaneously along the whole neuraxis, namely the spinal cord circuitry below the lesion (CPG) and in supraspinal structures still partially connected to the spinal cord. This review focuses mainly on the capacity of the spinal and supraspinal structures to reorganize spontaneously after incomplete SCI in animals (rats and cats). BMI approaches to foster recovery of functions after various types of SCI should take into account these changes at the various levels of the CNS.

Keywords: spinal cord injury; central pattern generator; plasticity; cortex; locomotion; BMI.

Brain machine interface (BMI) may eventually offer viable solutions to the problem of recovery of sensorimotor functions after partial spinal cord injuries (SCIs). Indeed, it might be very appealing to consider that a device could be designed to bridge the gap made by the spinal lesion and somehow transmit or relay signals to the severed cord.

Other BMI approaches may aim at stimulating sensorimotor pathways to potentiate weak remaining descending commands. Finally, one could stimulate the spinal cord itself electrically with or without a pharmacological potentiation. Before any of these solutions become a reality, it should be realized that after a SCI, plastic changes occur throughout the central nervous system (CNS) and BMI must take into account these changes. In this context, understanding the normal CNS control of sensorimotor functions is essential but knowing how

*Corresponding author.

Tel.: +1-514-343-6371; Fax: +1-514-343-6113
E-mail: serge.rossignol@umontreal.ca

pathophysiological processes alter the properties of the CNS structures involved in their control is crucial. Indeed, stimulated areas of the brain and spinal cord might have changed and alternative pathways might have become more or less prominent in the control of a given function such as locomotion.

There is a large corpus of evidence showing that some degree of functional recovery occurs spontaneously after incomplete SCI, thus indicating that reorganizations within different CNS structures can compensate for the disruption of pathways subserving the altered functions. After incomplete SCI, reorganization can occur spontaneously along the whole neuraxis since part of the spinal cord circuitry remains intact and still partially connected with cortical and subcortical structures through remnant fibers. Such plastic changes might occur in preexisting circuits by modification of synaptic efficiency or could involve the formation of new circuits through sprouting and anatomical reorganizations.

This review will focus mainly on the capacity of the spinal and supraspinal systems to reorganize spontaneously after incomplete SCI in animals. Given the fact that this is a large topic reviewed in more detail elsewhere (Rossignol, 2006; Rossignol and Frigon, 2011; Rossignol et al., 2006, 2009), we will concentrate on major changes in supraspinal structures, in descending pathways as well as in changes occurring within the spinal cord itself below the SCI as illustrated in Fig. 1.

Reorganization of cortical areas after incomplete SCI

In response to incomplete SCI, the sensorimotor cortex can undergo a dramatic reorganization. Somatosensory (S1) and motor (M1) maps remodeling can be used to gain insight into the capacity of sensorimotor systems to reorganize in response to SCI. Regardless of the species used, a spinal lesion targeting the dorsal column pathways or the entire hemicord (Fig. 2a) induced an immediate

abolishment of somatosensory-evoked responses in the deprived area within the S1 cortex corroborating the loss of tactile perception (Jain et al., 1995, 1997; Martinez et al., 2009, 2010; Onifer et al., 2005). A few weeks later (see Fig. 2b and c), the cortical areas deprived of their prevailing sensory afferents became responsive to sensory stimuli applied to contiguous skin territories, whose afferent pathways were not affected by the spinal lesion (Jain et al., 1997; Martinez et al., 2009, 2010), as also found after nerve lesion or limb amputation (Calford and Tweedale, 1988, 1991; Faggin et al., 1997; Merzenich and Jenkins, 1993). Reorganizations also occurred in the M1 cortex, but, since the topographic organization is less clear, the interpretation of changes is more difficult (see Fig. 2d). One month after a bilateral lesion of the corticospinal tract at the thoracic spinal level in rats, intracortical stimulation that normally evoked hindlimb responses was found to evoke responses in the forelimbs, the trunk, and whiskers which are classically represented in adjacent cortical territories (Fouad et al., 2001). In the same vein, 1 month after a unilateral C4–C5 hemisection, a drastic reduction of the overall M1 map size as well as an overrepresentation of the forelimb muscles whose motoneurons were localized rostrally to the hemisection was observed (Martinez et al., 2010; see Fig. 2e). Similar results were observed after motor nerve sections (Donoghue et al., 1990; Franchi and Veronesi, 2004; Sanes et al., 1990; Schmidlin et al., 2004), indicating that cortical territories controlling intact body parts tend to enlarge and invade cortical areas that have lost their peripheral targets. Interestingly, an elegant study combining several functional imagery techniques in rats with cervical spinal cord lateral hemisections showed that the intact sensorimotor cortex (ipsilesional) also underwent a drastic reorganization (Ghosh et al., 2009). More specifically, the cortex developed an enhanced representation of the unimpaired forepaw by 12 weeks after SCI, a change hypothesized to result from an increased use of the intact forelimb. It is, however, unclear whether the changes of activity in cortical regions

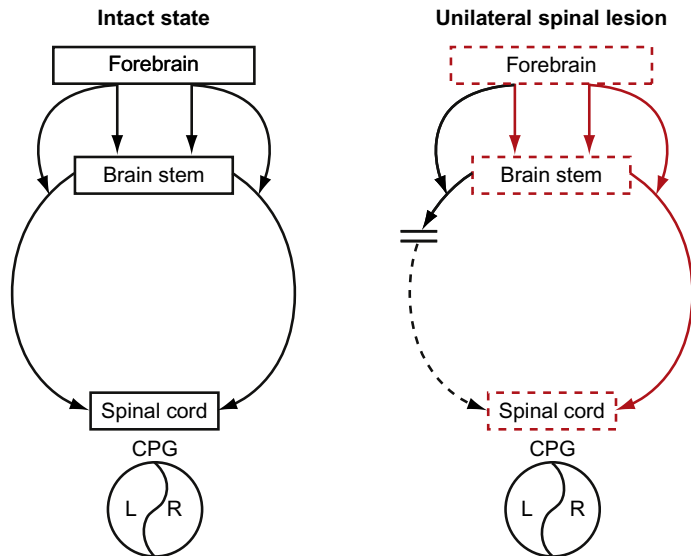


Fig. 1. General scheme of locomotor control in intact state (left panel) and after unilateral spinal cord hemisection (right panel). In normal state (left panel), various descending pathways from the forebrain act directly and/or through connections in the brainstem on the spinal cord to initiate or modulate the locomotor pattern for goal-directed behaviors. The spinal cord contains a network of interneurons capable of generating the basic locomotor pattern of flexor and extensor motoneurons on both sides (L, left; R, right; the spinal central pattern generator or CPG). After a unilateral spinal lesion (right panel), the communication between supraspinal and spinal structures is disrupted on one side and reorganizations occur at both supraspinal and spinal levels so that locomotion can be reexpressed.

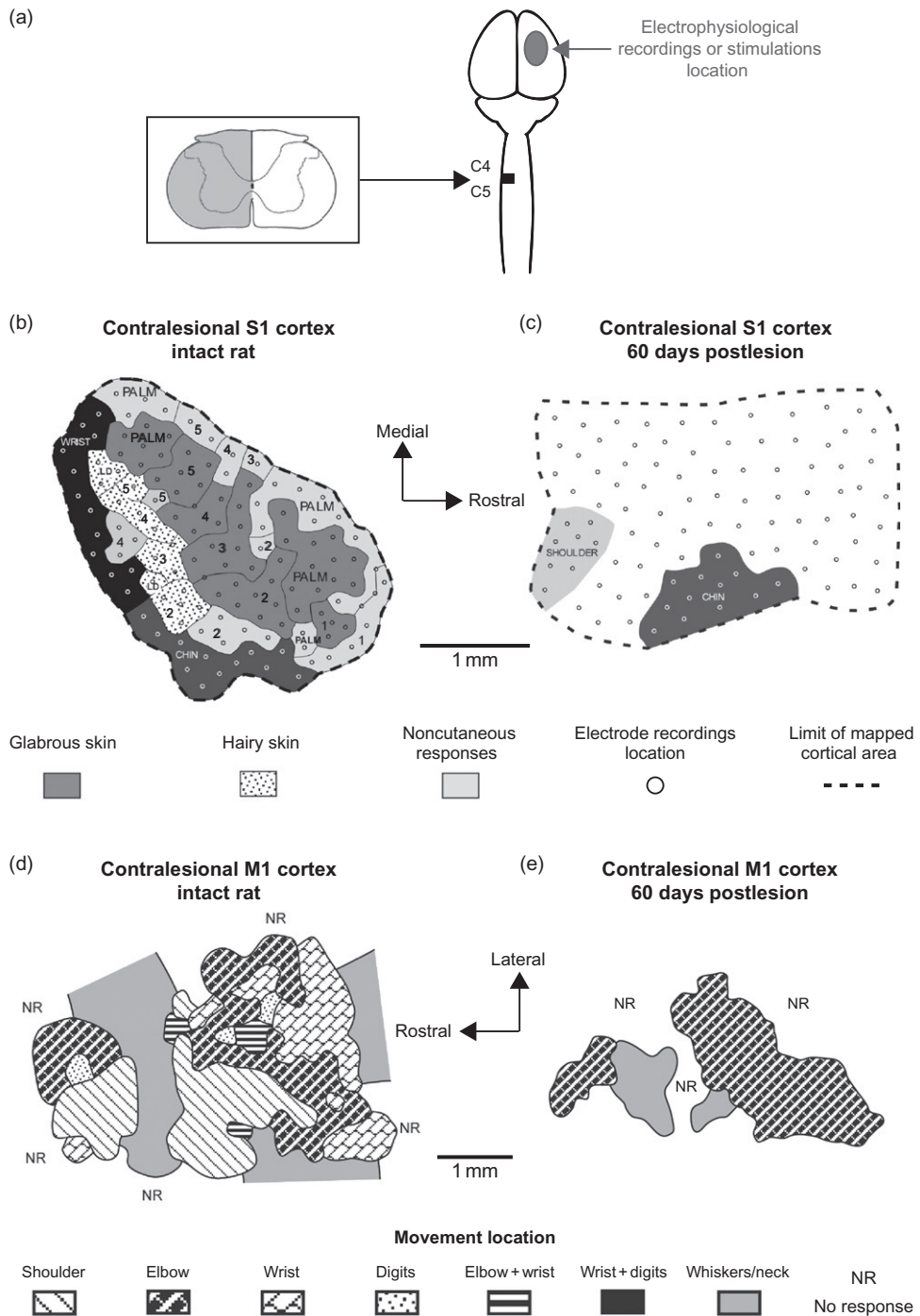
causally contribute to the functional recovery or if they are induced by the development of behavioral strategies. They can, however, be considered to reflect compensatory changes in functional connectivity between the cortex and periphery that can sometimes be attributable to anatomical reorganization of neural circuits.

Reorganization of descending pathways after incomplete SCI

Physiological compensatory mechanisms: synaptic efficiency changes

SCI induce major synaptic efficiency changes within sensorimotor networks, mainly in the vicinity of the lesion. The loss of part or all of efferent

inputs leads to structural changes relative to the number, size, or distribution of synaptic contacts within interneurons (including propriospinal) and motoneurons. An example of synaptic changes after SCI has been demonstrated by comparing the synaptophysin immunoreactivity (Ir), a synaptic marker, in intact versus lesioned spinal tissues (Nacimiento et al., 1995). In the intact tissue, motoneurons are surrounded by synaptophysin Ir, while they are depleted for several weeks in the lesioned territory. After the third month, however, synaptophysin expression was similar in the intact and lesioned tissues thus suggesting that new synapses formed on motoneurons soma. Although the origin of these new synapses is uncertain, they could arise from interneurons or sensory afferents transmitting tactile and proprioceptive signals.



Modifications in synaptic efficiency can also be due to neurotransmission changes within neuronal networks. GABA, the main CNS inhibitory neurotransmitter, has a presynaptic inhibitory action on primary afferents and on postsynaptic membranes of interneurons and motoneurons (Alvarez et al., 1996). After complete SCI, GABA neurotransmission is increased in the spinal cord below the injury site as measured from increase in synthesizing enzymes, resulting in altered inhibition during the postlesion period (Tillakaratne et al., 2000). Along the same line, upregulation of different monoaminergic receptors such as alpha-1, alpha-2 noradrenergic receptors, and 5-HT1A receptors were observed in the lumbar region in the first month after a complete SCI (Giroux et al., 1999). These changes in synaptic efficiency and neurotransmission may be important during the period of postlesion recovery.

In addition, the propriospinal system, including short and long neurons, is known to, respectively, interconnect spinal segments as well as the brainstem and the spinal cord (Sherrington and Laslett, 1903). In intact and in the presence of staggered bilateral hemisections in *in vitro* neonatal rats preparations, these propriospinal neurons have been shown to be sufficient in transmitting the descending locomotor command signals from the brainstem (Cowley et al., 2008; Zaporozhets et al., 2006), suggesting that the efficiency of the latter is increased after SCI which may contribute to the rerouting of descending commands through sprouting as we will detail later (Bareyre et al., 2004).

Compensation by remnant fibers (sprouting)

In cats submitted to a unilateral thoracic hemisection (Pike et al., 1929), a spontaneous recovery of the affected hindlimb was observed and it was hypothesized that “the mechanism which takes over control of movements of the limb lying below the level of the lesion includes motor fibers coming down on the opposite side of the spinal cord, and commissural neurons lying on the spinal cord below the level of lesion.” Up to now, such a hypothesis of a compensatory role of remnant fibers is prevalent. Indeed, after a subtotal midthoracic cord section which spared the left lateral and ventral funiculi, the subsequent lumbar commissurotomy or left thoracic spinal hemisection was shown to abolish the locomotor recovery of rats, suggesting again that spared descending fibers could reach the sublesional spinal cord and mediate locomotor recovery (Harris et al., 1994). Tract tracing and immunocytochemical studies of the corticospinal axons projections after thoracic unilateral hemisection suggested an increased projection from the undamaged corticospinal tract to the denervated side of the spinal cord (Aoki et al., 1988, 1991; Goldstein et al., 1997). Indeed, a recent study in rats subjected to a cervical unilateral hemisection showed that corticospinal axons from the intact cortex (i.e., ipsilesional) sprouted to recross the midline, innervating the spinal segments below the injury in both cervical and lumbar segments. These midline-crossing axons from the cervical spinal segments revealed the formation of a new forelimb representation in the ipsilesional cortex

Fig. 2. Changes in primary somatosensory (S1) and motor (M1) cortices representations after unilateral spinal hemisection in rats. (a) Schematic view of the injury model used. The damaged spinal tissue is represented in gray (left panel) and the diagram of the rat head shows the field of view (in gray, right panel) used to detect responses in S1 cortex after contralateral forepaw stimulation or to evoke forepaw movements after M1 cortex microstimulations. (b–e) Changes in the organization of the contralateral S1 and M1 forepaw representation following cervical spinal cord hemisection. Individual cortical S1 and M1 maps obtained from intact (b and d) and spinal injured (c and e) rats. (c) Potentials evoked from somatosensory stimulation were abolished in the contralateral forepaw areas 60 days after the spinal hemisection. Note the expansion of the chin representation within the adjacent forepaw cortical sectors. Numbers 1–5, digits 1–5; LD, large dorsum. (e) M1 cortex microstimulations evoked little forepaw movements 60 days after spinal cord hemisection and the size of M1 forepaw representation was drastically reduced. Note the overrepresentation of elbow movements and the increase of NR territories. Modified with permission from Martinez et al. (2010).

(Ghosh et al., 2009). In addition, lesion targeting the dorsal component of the corticospinal tract at cervical level in rats was shown to induce sprouting of ventral corticospinal axons that reconnected pools of cervical motoneurons (Weidner et al., 2001). These anatomical rearrangements were accompanied by the recovery of forelimb motor capacities. After a thoracic unilateral hemisection in rats, the reticulospinal axons coursing through the intact side of the cord and therefore spared by the lesion were found to sprout in lumbar segments and this intraspinal plasticity paralleled the locomotor recovery (Ballermann and Fouad, 2006).

Regeneration of damaged fibers

In the adult mammalian CNS, the damaged fibers have a very limited capacity to regenerate. After a spinal lesion at the thoracic level disrupting the corticospinal fibers in adult rats, the axons, disrupted from their cellular target, degenerated massively and failed to regenerate (Bregman et al., 1989). Such a report has also been made for the other descending motor tracts. Indeed, after a cervical hemisection or a thoracic transection in rats, the rubro- and reticulospinal fibers, respectively, were unable to regenerate within the damaged tissue as well as in the host tissue caudal to the spinal lesion (Houle and Jin, 2001; Menei et al., 1998). Nevertheless, recent studies have shown that the damaged motor axons have the capacity to regenerate spontaneously and form new circuits in response to spinal lesions. Transected axons from the hindlimb motor cortex have been found to sprout into the cervical gray matter after a dorsal thoracic hemisection where they made contact and formed new synapses to short and long propriospinal neurons. These propriospinal neurons were also shown to innervate the lumbar motor neurons, the original targets of the damaged corticospinal fibers, thus creating a new anatomo-functional intraspinal circuit (Bareyre et al., 2004). After a dorsal hemisection at thoracic level in rats, it was recently shown that axotomized corticospinal axons from the hindlimb sensorimotor

cortex sprouted in the cervical spinal cord on fibers from the unaffected forelimb cortex such as the hindlimb cortex became responsive to forelimb inputs (Ghosh et al., 2010). Another study has demonstrated, by using similar lesion model in mice interrupting the dorsal and dorsolateral components of the corticospinal tracts, that some ventral axons expressed collaterals in the spinal segments rostral to the lesion. These collaterals bypassed the lesion via the ventral funiculus and formed terminal arborizations within the caudal spinal segments (Steward et al., 2008).

Changes in the spinal circuitry after SCI

Complete SCI and the role of spinal CPG

In many species, some recovery of hindlimb locomotion can be observed after a complete spinal cord section (Grillner, 1981; Rossignol, 1996). Since locomotion can be expressed in kittens spinalized before having “learned” to walk, it must be concluded that this behavior is genetically determined (Forssberg et al., 1980a,b; Grillner, 1973). In adults, hindlimb locomotion is subtended by a spinal circuitry (central pattern generator, CPG) that can operate even when isolated from descending command signals or afferent information (Grillner and Zanger, 1979) when stimulated by the noradrenergic precursor levo 3,4-dihydroxyphénylalanine (L-DOPA). In adult cats, noadrenergic agonists such as clonidine can evoke locomotion within minutes of a complete spinalization (Forssberg and Grillner, 1973) illustrating that the spinal CPG can immediately evoke hindlimb locomotion without the need for elaborate circuit reorganization when proper stimulation is provided (in this case, noradrenergic receptor stimulation) after SCI.

Without such neurotransmitter replacement, hindlimbs of cats with a complete SCI will be flaccid for several days or even weeks, in some cases, and only faint rhythmic movements are observed without foot placement and weight support. At this

stage, noradrenergic agonists can enhance markedly the walking pattern and increase step length and foot placement as well as hindquarter weight support. Locomotor training started early after a complete section using noradrenergic stimulation can accelerate the recovery of hindlimb stepping (Chau et al., 1998a,b). When cats have recovered spontaneous (no drug stimulation) hindlimb locomotion on a treadmill, various agonists and antagonists of neurotransmitters can exert modulatory effects on the kinematics and electromyographic (EMG) parameters (Rossignol et al., 1995). Of interest for any work attempting to revive the spinal cord through pharmacological means after SCI is the fact that the spinal receptors of various neurotransmitters synthesized in the brainstem (and therefore depleted after a complete section) are upregulated for several months after the lesion and then return to their baseline value after about 6 months (Giroux et al., 1999). It should also be mentioned that the effects of drugs (agonists and antagonists) differ importantly depending on the state of excitability of these receptors. For instance, clonidine or yohimbine will have significantly different effects when injected intrathecally in the normal, partially lesioned or completely lesioned cat (Giroux et al., 1998). Thus, if any BMI device is coupled to a pharmacological intervention, the latter should take these time-varying excitability changes after various types of spinal lesions. The changes in the excitability of receptors can be profound as recently demonstrated (Murray et al., 2010). Indeed serotonergic receptors can become constitutive after spinal lesions which will lead to a state of hyperexcitability of motoneurons that can facilitate locomotion but also may lead to unwarranted symptoms such as spasticity.

Spinal localization of the locomotor CPG

Knowing how the spinal CPG is organized and where it is located should be of paramount importance in the design of BMI devices to restore

locomotion. Besides pharmacological stimulation of spinal circuits as summarized above, electrical stimulation can be envisaged as a means of reactivating the spinal CPG either by intraspinal stimulation or by stimulation of sensory afferents. In the first case, the intraspinal stimulation seeks to activate motoneuron pools through an activation of the motoneurons themselves or through local microcircuits including local afferent inputs or local descending inputs (Guèvremont et al., 2006; Saigal et al., 2004; Stein and Mushahwar, 2005). With electrical stimulation of sensory afferents (peripheral nerves or dorsal roots accessed by epidural stimulation), the aim is to activate the CPG through already existing connections with interneurons (Lavrov et al., 2008). Such epidural stimulation can evoke rather striking bipedal locomotion in the rat when coupled to serotonergic stimulation (Courtine et al., 2009). We have also used intraspinal electrical stimulation of the spinal cord in 1-week SCI decerebrate cats injected with clonidine. With a systematic exploration of the cord, we also found that dorsal areas were the most effective (1 mm lateral and 1 mm deep) in evoking locomotion and that this stimulation could be effective when applied to several segmental lumbosacral levels. However, we also found that the integrity of midlumbar segmental levels was necessary to induce locomotion with intraspinal or dorsal root stimulation (Barthélemy et al., 2006, 2007). This finding was consistent with earlier work showing that these midlumbar segments occupy a strategic role in spinal locomotion. Indeed, we had shown that pharmacological blockade by yohimbine of these segments abolished clonidine-evoked locomotion (Marcoux and Rossignol, 2000). Further, when a second complete spinalization was performed at L3–L4 in cats having recovered hindlimb locomotion after a first spinal section at T13, it was impossible to evoke locomotion although other rhythmic activities such as fast paw shake could be observed (Langlet et al., 2005). More recent work also showed that these midlumbar segments may be important even for decerebrate walking, suggesting that these premotoneuronal segments

play an important role in generating locomotion (Delivet-Mongrain et al., 2008).

Whether some segments contain neural circuits necessary for locomotion as stated above or whether certain segments are more excitable than others for the generation of locomotion (Kiehn, 2006), the design of implantable stimulating devices should take into account such regionalization to increase their effectiveness.

Involvement of the spinal circuitry after incomplete SCI

The above sections summarize various observations leading to the conclusion that there is a spinal CPG responsible for spinal locomotion and that this circuitry can be modulated by various pharmacological agents, sensory afferents, and intrinsic premotoneuronal inputs. It is reasonable to ask whether these mechanisms also apply to hindlimb locomotion generated after partial SCI.

One important finding in this respect is that hindlimb locomotion can be expressed quite readily after various types of partial SCI involving either bilateral dorsal/dorsolateral tracts (Jiang and Drew, 1996) or bilateral ventral/ventrolateral tracts (Brustein and Rossignol, 1998, 1999). The fact that none of the tracts appear essential for triggering hindlimb locomotion suggests that indeed the spinal circuitry plays an important role after such partial lesions.

In order to investigate more directly the involvement of the spinal cord in expressing locomotion after partial SCI, we devised a dual spinal lesion paradigm in which the spinal cord is first lesioned on one side (~lateral hemisection) at T10–T11 and then, some weeks later, a complete section at T13 (i.e., the same level as for previous spinal cats) is performed. The hypothesis underlying that paradigm was that if the spinal cord is changed to express locomotion after the hemisection, some of these changes should be detectable in the spinal cord after the subsequent complete spinalization. Indeed, we have shown

that after the complete section, cats can walk within 24 h (first recording session; Barrière et al., 2008, 2010; Martinez et al., 2011; Rossignol et al., 2009) whereas it normally takes a few weeks to achieve such a locomotor performance after a complete SCI (Barbeau and Rossignol, 1987; Belanger et al., 1996; de Leon et al., 1998). The kinematic and EMG parameters of walking after the hemisection indicate that robust compensatory changes occur in the hindlimbs on both sides. In brief, after hemisection, several asymmetries between hindlimbs take place. For example, the stance phase of the hindlimb on the hemilesioned side is shortened, while the swing phase is lengthened and reciprocal changes are observed on the other side. Three weeks after hemisection, cats were able to express an active locomotor pattern and the hindlimb on the lesioned side exhibited a gradual recovery approaching the locomotor performance recorded in the intact state (Fig. 3a and b). However, the locomotor asymmetries induced by the hemisection were not spontaneously (i.e., with no specific rehabilitative strategy) compensated even 3 weeks after hemisection. At this time point, a complete spinalization was performed in T13. Of great interest is that as early as 24 h after the complete spinal section, more than 50% of the cats reexpressed a bilateral locomotor pattern such as the locomotor asymmetries documented in the hemispinal state disappeared or even reversed although with overall shortened cycle as usually the case in spinal cats (Fig. 3c). Some changes were also seen in reflex responses after hemisection and some of these alterations persist for a few days after spinalization before becoming symmetrical again after spinalization (Frigon et al., 2009).

The experiments using the dual spinal lesion paradigm thus indicate that the spinal CPG itself is altered during the hemispinal period as shown by the profound changes seen after spinalization. This strongly suggests that after partial SCI, not only are there changes in remnant supraspinal structures and in the connectivity of descending

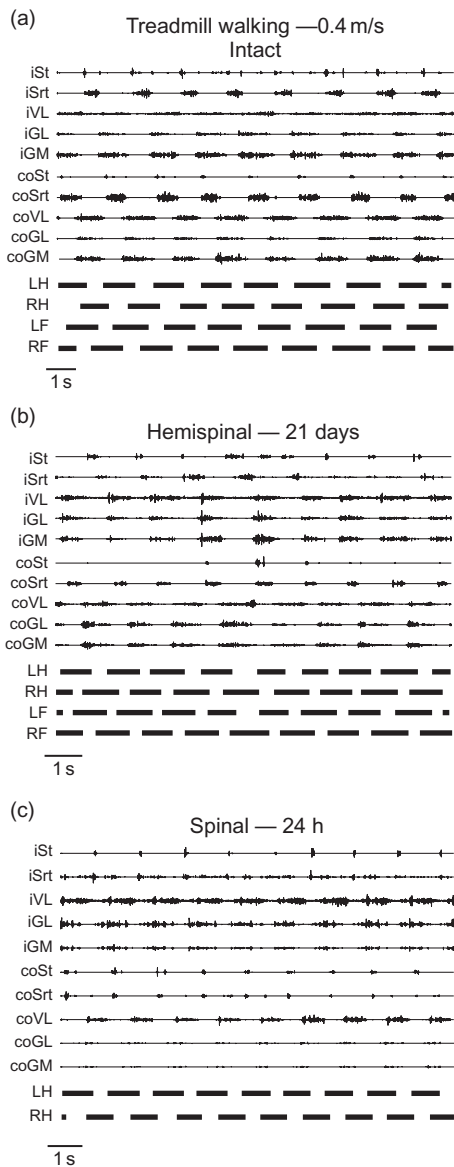


Fig. 3. Episodes of treadmill locomotion at different time of the dual lesion paradigm in a cat walking at 0.4 m/s. Top traces of electromyographic recordings obtained bilaterally from hindlimb flexor and extensor muscles at the intact (a), hemispinal (b), and early (c) spinal states. Duty cycles (black horizontal bars) below the EMGs illustrate the support periods (stance) of each limb. St, semitendinosus; Srt, sartorius; VL, vastus lateralis; GL, lateral gastrocnemius; GM, median gastrocnemius; LH, left hindlimb; RH, right hindlimb; LF, left forelimb; RF, right forelimb.

pathways but also within the spinal cord itself. BMI approaches to foster recovery of functions after various types of SCI (whether electrical or pharmacological) should take into account these changes at the various levels of the CNS. Thus, BMI devices may target some levels of the spinal cord and be adjustable so that excitability changes in spinal circuits are taken into account.

A question often raised is whether such notions apply to humans, especially when such a strong role is considered for a spinal cord CPG. As discussed in a recent paper (Nadeau et al., 2010), there are a number of indications that the isolated spinal cord of humans also contain rhythmogenic capabilities. Work by Dimitrijevic (Dimitrijevic et al., 1998) and work by Harkema and others (Harkema, 2008) rely on the existence of such spinal circuits to express locomotor rhythms that can be activated by BMI such as epidural stimulation. It can thus be concluded that BMI approaches to restore locomotor function are very promising especially when they take into consideration the built-in synergies at different levels of the CNS and the intrinsic changes that occur after SCI.

References

- Alvarez, F. J., Taylor-Blake, B., Fyffe, R. E., De Blas, A. L., & Light, A. R. (1996). Distribution of immunoreactivity for the beta 2 and beta 3 subunits of the GABA_A receptor in the mammalian spinal cord. *The Journal of Comparative Neurology*, 365, 392–412.
- Aoki, M., Fujito, Y., Kosaka, I., & Satomi, H. (1988). Does collateral sprouting from corticospinal fibers participate in motor recovery after spinal hemisection in monkeys? In H. Flohr (Ed.), *Post-lesion neural plasticity* (pp. 223–231). Springer-Verlag.
- Aoki, M., Fujito, Y., Mizuguchi, A., & Satomi, H. (1991). Recovery of hindlimb movement after spinal hemisection and collateral sprouting from corticospinal fibers in monkeys. In M. Shimamura, S. Grillner & V. R. Edgerton (Eds.), *Neurobiological basis of human locomotion* (pp. 401–405). Tokyo: Japan Scientific Societies Press.
- Ballermann, M., & Fouad, K. (2006). Spontaneous locomotor recovery in spinal cord injured rats is accompanied by anatomical plasticity of reticulospinal fibers. *The European Journal of Neuroscience*, 23, 1988–1996.

- Barbeau, H., & Rossignol, S. (1987). Recovery of locomotion after chronic spinalization in the adult cat. *Brain Research*, 412, 84–95.
- Bareyre, F. M., Kerschensteiner, M., Raineteau, O., Mettenleiter, T. C., Weinmann, O., & Schwab, M. E. (2004). The injured spinal cord spontaneously forms a new intraspinal circuit in adult rats. *Nature Neuroscience*, 7, 269–277.
- Barrière, G., Frigon, A., Leblond, H., Provencher, J., & Rossignol, S. (2010). Dual spinal lesion paradigm in the cat: Evolution of the kinematic locomotor pattern. *Journal of Neurophysiology*, 104, 1119–1133.
- Barrière, G., Leblond, H., Provencher, J., & Rossignol, S. (2008). Prominent role of the spinal central pattern generator in the recovery of locomotion after partial spinal cord injuries. *The Journal of Neuroscience*, 28, 3976–3987.
- Barthélemy, D., Leblond, H., Provencher, J., & Rossignol, S. (2006). Non-locomotor and locomotor hindlimb responses evoked by electrical microstimulation of the lumbar cord in spinalized cats. *Journal of Neurophysiology*, 96, 3273–3292.
- Barthélemy, D., Leblond, H., & Rossignol, S. (2007). Characteristics and mechanisms of locomotion induced by intraspinal microstimulation and dorsal root stimulation in spinal cats. *Journal of Neurophysiology*, 97, 1986–2000.
- Belanger, M., Drew, T., Provencher, J., & Rossignol, S. (1996). A comparison of treadmill locomotion in adult cats before and after spinal transection. *Journal of Neurophysiology*, 76, 471–491.
- Bregman, B. S., Kunkel-Bagden, E., McAtee, M., & O'Neill, A. (1989). Extension of the critical period for developmental plasticity of the corticospinal pathway. *The Journal of Comparative Neurology*, 282, 355–370.
- Brustein, E., & Rossignol, S. (1998). Recovery of locomotion after ventral and ventrolateral spinal lesions in the cat. I. Deficits and adaptive mechanisms. *Journal of Neurophysiology*, 80, 1245–1267.
- Brustein, E., & Rossignol, S. (1999). Recovery of locomotion after ventral and ventrolateral spinal lesions in the cat. II. Effects of noradrenergic and serotoninergic drugs. *Journal of Neurophysiology*, 81, 1513–1530.
- Calford, M. B., & Tweedale, R. (1988). Immediate and chronic changes in responses of somatosensory cortex in adult flying-fox after digit amputation. *Nature*, 332, 446–448.
- Calford, M. B., & Tweedale, R. (1991). Immediate expansion of receptive fields of neurons in area 3b of macaque monkeys after digit denervation. *Somatosensory & Motor Research*, 8, 249–260.
- Chau, C., Barbeau, H., & Rossignol, S. (1998a). Early locomotor training with clonidine in spinal cats. *Journal of Neurophysiology*, 79, 392–409.
- Chau, C., Barbeau, H., & Rossignol, S. (1998b). Effects of intrathecal α_1 - and α_2 -noradrenergic agonists and norepinephrine on locomotion in chronic spinal cats. *Journal of Neurophysiology*, 79, 2941–2963.
- Courtine, G., Gerasimenko, Y., van den, B. R., Yew, A., Musienko, P., Zhong, H., et al. (2009). Transformation of nonfunctional spinal circuits into functional states after the loss of brain input. *Nature Neuroscience*, 12, 1333–1342.
- Cowley, K. C., Zaporozhets, E., & Schmidt, B. J. (2008). Propriospinal neurons are sufficient for bulbospinal transmission of the locomotor command signal in the neonatal rat spinal cord. *The Journal of Physiology*, 586, 1623–1635.
- de Leon, R. D., Hodgson, J. A., Roy, R. R., & Edgerton, V. R. (1998). Locomotor capacity attributable to step training versus spontaneous recovery after spinalization in adult cats. *Journal of Neurophysiology*, 79, 1329–1340.
- Delivet-Mongrain, H., Leblond, H., & Rossignol, S. (2008). Effects of localized intraspinal injections of a noradrenergic blocker on locomotion of high decerebrate cats. *Journal of Neurophysiology*, 100, 907–921.
- Dimitrijevic, M. R., Gerasimenko, Y., & Pinter, M. M. (1998). Evidence for a spinal central pattern generator in humans. *Annals of the New York Academy of Sciences*, 860, 360–376.
- Donoghue, J. P., Suner, S., & Sanes, J. N. (1990). Dynamic organization of primary motor cortex output to target muscles in adult rats. II. Rapid reorganization following motor nerve lesions. *Experimental Brain Research*, 79, 492–503.
- Faggion, B. M., Nguyen, K. T., & Nicolelis, M. A. (1997). Immediate and simultaneous sensory reorganization at cortical and subcortical levels of the somatosensory system. *Proceedings of the National Academy of Sciences of the United States of America*, 94, 9428–9433.
- Forssberg, H., & Grillner, S. (1973). The locomotion of the acute spinal cat injected with clonidine i.v. *Brain Research*, 50, 184–186.
- Forssberg, H., Grillner, S., & Halbertsma, J. (1980). The locomotion of the low spinal cat. I. Coordination within a hindlimb. *Acta Physiologica Scandinavica*, 108, 269–281.
- Forssberg, H., Grillner, S., Halbertsma, J., & Rossignol, S. (1980). The locomotion of the low spinal cat: II. Interlimb coordination. *Acta Physiologica Scandinavica*, 108, 283–295.
- Fouad, K., Pedersen, V., Schwab, M. E., & Brosamle, C. (2001). Cervical sprouting of corticospinal fibers after thoracic spinal cord injury accompanies shifts in evoked motor responses. *Current Biology*, 11, 1766–1770.
- Franchi, G., & Veronesi, C. (2004). Long-term motor cortex reorganization after facial nerve severing in newborn rats. *The European Journal of Neuroscience*, 20, 1885–1896.
- Frigon, A., Barrière, G., Leblond, H., & Rossignol, S. (2009). Asymmetric changes in cutaneous reflexes after a partial spinal lesion and retention following spinalization during locomotion in the cat. *Journal of Neurophysiology*, 102, 2667–2680.

- Ghosh, A., Haiss, F., Sydekum, E., Schneider, R., Gullo, M., Wyss, M. T., et al. (2010). Rewiring of hindlimb corticospinal neurons after spinal cord injury. *Nature Neuroscience*, 13, 97–104.
- Ghosh, A., Sydekum, E., Haiss, F., Peduzzi, S., Zorner, B., Schneider, R., et al. (2009). Functional and anatomical reorganization of the sensory-motor cortex after incomplete spinal cord injury in adult rats. *The Journal of Neuroscience*, 29, 12210–12219.
- Giroux, N., Brustein, E., Chau, C., Barbeau, H., Reader, T. A., & Rossignol, S. (1998). Differential effects of the noradrenergic agonist clonidine on the locomotion of intact, partially and completely spinalized adult cats. In O. Kiehn, R. M. Harris-Warrick, L. M. Jordan, H. Hulborn & N. Kudo (Eds.), *Neuronal mechanisms for generating locomotor activity* (pp. 517–520). New York: Annals of the New York Academy of Sciences.
- Giroux, N., Rossignol, S., & Reader, T. A. (1999). Autoradiographic study of α_1 , α_2 -Noradrenergic and Serotonin1A receptors in the spinal cord of normal and chronically transected cats. *The Journal of Comparative Neurology*, 406, 402–414.
- Goldstein, B., Little, J. W., & Harris, R. M. (1997). Axonal sprouting following incomplete spinal cord injury: An experimental model. *The Journal of Spinal Cord Medicine*, 20, 200–206.
- Grillner, S. (1973). Locomotion in the spinal cat. In R. B. Stein, K. G. Pearson, R. S. Smith & J. B. Redford (Eds.), *Control of posture and locomotion. Advances in behavioural biology*, (Vol. 7, pp. 515–535). New York: Plenum Press.
- Grillner, S. (1981). Control of locomotion in bipeds, tetrapods, and fish. In J. M. Brookhart & V. B. Mountcastle (Eds.), *Handbook of physiology. The nervous system II* (pp. 1179–1236). Bethesda, Maryland: American Physiology Society.
- Grillner, S., & Zanger, P. (1979). On the central generation of locomotion in the low spinal cat. *Experimental Brain Research*, 34, 241–261.
- Guèvremont, L., Renzi, C. G., Norton, J. A., Kowalczewski, J., Saigal, R., & Mushahwar, V. K. (2006). Locomotor-related networks in the lumbosacral enlargement of the adult spinal cat: Activation through intraspinal microstimulation. *IEEE Transactions on Neural Systems and Rehabilitation Engineering*, 14, 266–272.
- Harkema, S. J. (2008). Plasticity of interneuronal networks of the functionally isolated human spinal cord. *Brain Research Reviews*, 57, 255–264.
- Harris, R. M., Little, J. W., & Goldstein, B. (1994). Spared descending pathways mediate locomotor recovery after subtotal spinal cord injury. *Neuroscience Letters*, 180, 37–40.
- Houle, J. D., & Jin, Y. (2001). Chronically injured supraspinal neurons exhibit only modest axonal dieback in response to a cervical hemisection lesion. *Experimental Neurology*, 169, 208–217.
- Jain, N., Catania, K. C., & Kaas, J. H. (1997). Deactivation and reactivation of somatosensory cortex after dorsal spinal cord injury. *Nature*, 386, 495–498.
- Jain, N., Florence, S. L., & Kaas, J. H. (1995). Limits on plasticity in somatosensory cortex of adult rats: Hindlimb cortex is not reactivated after dorsal column section. *Journal of Neurophysiology*, 73, 1537–1546.
- Jiang, W., & Drew, T. (1996). Effects of bilateral lesions of the dorsolateral funiculi and dorsal columns at the level of the low thoracic spinal cord on the control of locomotion in the adult cat: I. Treadmill walking. *Journal of Neurophysiology*, 76, 849–866.
- Kiehn, O. (2006). Locomotor circuits in the mammalian spinal cord. *Annual Review of Neuroscience*, 29, 279–306.
- Langlet, C., Leblond, H., & Rossignol, S. (2005). The mid-lumbar segments are needed for the expression of locomotion in chronic spinal cats. *Journal of Neurophysiology*, 93, 2474–2488.
- Lavrov, I., Courtine, G., Dy, C. J., Van den Brand, R., Fong, A. J., Gerasimenko, Y., et al. (2008). Facilitation of stepping with epidural stimulation in spinal rats: Role of sensory input. *The Journal of Neuroscience*, 28, 7774–7780.
- Marcoux, J., & Rossignol, S. (2000). Initiating or blocking locomotion in spinal cats by applying noradrenergic drugs to restricted lumbar spinal segments. *The Journal of Neuroscience*, 20, 8577–8585.
- Martinez, M., Brezun, J. M., Zennou-Azogui, Y., Baril, N., & Xerri, C. (2009). Sensorimotor training promotes functional recovery and somatosensory cortical map reactivation following cervical spinal cord injury. *The European Journal of Neuroscience*, 30, 2356–2367.
- Martinez, M., Delcour, M., Russier, M., Zennou-Azogui, Y., Xerri, C., Coq, J. O., et al. (2010). Differential tactile and motor recovery and cortical map alteration after C4-C5 spinal hemisection. *Experimental Neurology*, 221, 186–197.
- Martinez, M., Delivet-Mongrain, H., Leblond, H., & Rossignol, S. (2011). Recovery of hindlimb locomotion after incomplete spinal cord injury in the cat involves spontaneous compensatory changes within the spinal locomotor circuitry. *Journal of Neurophysiology*, in press.
- Menei, P., Montero-Menei, C., Whittemore, S. R., Bunge, R. P., & Bunge, M. B. (1998). Schwann cells genetically modified to secrete human BDNF promote enhanced axonal regrowth across transected adult rat spinal cord. *The European Journal of Neuroscience*, 10, 607–621.
- Merzenich, M. M., & Jenkins, W. M. (1993). Reorganization of cortical representations of the hand following alterations of skin inputs induced by nerve injury, skin island transfers, and experience. *Journal of Hand Therapy*, 6, 89–104.
- Murray, K. C., Nakae, A., Stephens, M. J., Rank, M., D'Amico, J., Harvey, P. J., et al. (2010). Recovery of

- motoneuron and locomotor function after spinal cord injury depends on constitutive activity in 5-HT(2C) receptors. *Nature Medicine*, 16, 694–700.
- Nacimiento, W., Sappok, T., Brook, G. A., Toth, L., Schoen, S. W., Noth, J., et al. (1995). Structural changes of anterior horn neurons and their synaptic input caudal to a low thoracic spinal cord hemisection in the adult rat: A light and electron microscopic study. *Acta Neuropathologica*, 90, 552–564.
- Nadeau, S., Jacquemin, G., Fournier, C., Lamarre, Y., & Rossignol, S. (2010). Spontaneous motor rhythms of the back and legs in a patient with a complete spinal cord transection. *Neurorehabilitation and Neural Repair*, 24, 377–383.
- Onifer, S. M., Zhang, Y. P., Burke, D. A., Brooks, D. L., Decker, J. A., McClure, N. J., et al. (2005). Adult rat forelimb dysfunction after dorsal cervical spinal cord injury. *Experimental Neurology*, 192, 25–38.
- Pike, F. H., Elsbern, C. A., McCulloch, W. S., & Rizzolo, A. (1929). Some observations on experimentally produced convulsions: The localization of the motor mechanisms from which the typical clonic movements of epilepsy arise. *The American Journal of Psychiatry*, 9, 259–283.
- Rossignol, S. (1996). Neural control of stereotyped limb movements. In L. B. Rowell & J. T. Shepherd (Eds.), *Handbook of physiology, section 12. Exercise: Regulation and integration of multiple systems* (pp. 173–216). New York: Oxford University Press.
- Rossignol, S. (2006). Plasticity of connections underlying locomotor recovery after central and/or peripheral lesions in the adult mammals. *Philosophical Transactions of the Royal Society of London. Series B, Biological Sciences*, 361, 1647–1671.
- Rossignol, S., Barriere, G., Alluin, O., & Frigon, A. (2009). Re-expression of locomotor function after partial spinal cord injury. *Physiology (Bethesda, MD)*, 24, 127–139.
- Rossignol, S., Chau, C., & Barbeau, H. (1995). Pharmacology of locomotion in chronic spinal cats. In A. Taylor, M. H. Gladden & R. Durbaba (Eds.), *Alpha and gamma motor systems* (pp. 449–455). New York, London: Plenum Press.
- Rossignol, S., Dubuc, R., & Gossard, J. P. (2006). Dynamic sensorimotor interactions in locomotion. *Physiological Reviews*, 86, 89–154.
- Rossignol, S., & Frigon, A. (2011). Recovery of locomotion after spinal cord injury: Some facts and mechanisms. *Annual Review of Neuroscience*, 34, 411–438.
- Saigal, R., Renzi, C., & Mushahwar, V. K. (2004). Intraspinal microstimulation generates functional movements after spinal-cord injury. *IEEE Transactions on Neural Systems and Rehabilitation Engineering*, 12, 430–440.
- Sanes, J. N., Suner, S., & Donoghue, J. P. (1990). Dynamic organization of primary motor cortex output to target muscles in adult rats. I. Long-term patterns of reorganization following motor or mixed peripheral nerve lesions. *Experimental Brain Research*, 79, 479–491.
- Schmidlin, E., Wannier, T., Bloch, J., & Rouiller, E. M. (2004). Progressive plastic changes in the hand representation of the primary motor cortex parallel incomplete recovery from a unilateral section of the corticospinal tract at cervical level in monkeys. *Brain Research*, 1017, 172–183.
- Sherrington, C. S., & Laslett, E. E. (1903). Observations on some spinal reflexes and the interconnection of spinal segments. *The Journal of Physiology*, 29, 58–96.
- Stein, R. B., & Mushahwar, V. (2005). Reanimating limbs after injury or disease. *Trends in Neurosciences*, 28, 518–524.
- Steward, O., Zheng, B., Tessier-Lavigne, M., Hofstadter, M., Sharp, K., & Matsudaira Yee, K. (2008). Regenerative growth of corticospinal tract axons via the ventral column after spinal cord injury in mice. *The Journal of Neuroscience*, 28, 6836–6847.
- Tillakaratne, N. J., Mouria, M., Ziv, N. B., Roy, R. R., Edgerton, V. R., & Tobin, A. J. (2000). Increased expression of glutamate decarboxylase (GAD(67)) in feline lumbar spinal cord after complete thoracic spinal cord transection. *Journal of Neuroscience Research*, 60, 219–230.
- Weidner, N., Ner, A., Salimi, N., & Tuszynski, M. H. (2001). Spontaneous corticospinal axonal plasticity and functional recovery after adult central nervous system injury. *Proceedings of the National Academy of Sciences of the United States of America*, 98, 3513–3518.
- Zaporozhets, E., Cowley, K. C., & Schmidt, B. J. (2006). Propriospinal neurons contribute to bulbospinal transmission of the locomotor command signal in the neonatal rat spinal cord. *The Journal of Physiology*, 572, 443–458.

CHAPTER 15

Modeling the potentiality of spinal-like circuitry for stabilization of a planar arm system

George A. Tsianos[†], Giby Raphael[‡] and Gerald E. Loeb^{†,*}

[†] Department of Biomedical Engineering, University of Southern California, Los Angeles, CA, USA

[‡] Advanced Brain Monitoring Inc., Carlsbad, CA, USA

Abstract: The design of control systems for limb prostheses seems likely to benefit from an understanding of how sensorimotor integration is achieved in the intact system. Traditional BMIs guess what movement parameters are encoded by brain activity and then decode them to drive prostheses directly. Modeling the known structure and emergent properties of the biological decoder itself is likely to be more effective in bridging from normal brain activity to functionally useful limb movement. In this study, we have extended a model of spinal circuitry (termed SLR for spinal-like regulator; see Raphael, G., Tsianos, G. A., & Loeb G. E. 2010, Spinal-like regulator facilitates control of a two-degree-of-freedom wrist. *The Journal of Neuroscience*, 30(28), 9431–9444.) to a planar elbow–shoulder system to investigate how the spinal cord contributes to the control of a musculoskeletal system with redundant and multiarticular musculature and interaction (Coriolis) torques, which are common control problems for multisegment linkages throughout the body. The SLR consists of a realistic set of interneuronal pathways (monosynaptic Ia-excitatory, reciprocal Ia-inhibitory, Renshaw inhibitory, Ib-inhibitory, and propriospinal) that are driven by unmodulated step commands with learned amplitudes. We simulated the response of a planar arm to a brief, oblique impulse at the hand and investigated the role of cocontraction in learning to resist it. Training the SLR without cocontraction led to generally poor performance that was significantly worse than training with cocontraction. Further, removing cocontraction from the converged solutions and retraining the system achieved better performance than the SLR responses without cocontraction. Cocontraction appears to reshape the solution space, virtually eliminating the probability of entrapment in poor local minima. The local minima that are entered during learning with cocontraction are favorable starting points for learning to perform the task when cocontraction is abruptly removed. Given the control system’s ability to learn effectively and rapidly, we hypothesize that it will generalize more readily to the wider range of tasks that subjects must learn to perform, as opposed to BMIs mapped to outputs of the musculoskeletal system.

*Corresponding author.

Tel.: +1-213-821-5311; Fax: +1-213-821-3897

E-mail: gloeb@usc.edu

Keywords: spinal cord; interneurons; regulator; controller; cocontraction.

Introduction

Moving limbs in a purposeful manner, whether it is a simple reaching movement or fine manipulation of an object, is an elaborate process that requires sophisticated integration of volitional commands and sensory feedback. The design of control systems for sensorimotor prostheses seems likely to benefit from an understanding of how such control is achieved in the intact system. Many regions of the brain participate in this process, but all of their output signals are integrated in the spinal cord. The spinal circuitry consists of a variety of reasonably well-characterized interneurons that are highly evolved and conserved throughout mammalian and even vertebrate evolution ([Pierrot-Deseilligny and Burke, 2005](#)). In particular, the large majority of corticospinal neurons have few or no direct projections to spinal motoneurons ([Rathelot and Strick, 2009](#)), projecting instead to spinal interneurons where their signals are integrated with various somatosensory afferents and recurrent motoneuron signals. Depending on one's perspective, any given muscle recruitment can be described either as the result of a descending command that has been modulated by segmental feedback or a segmental reflex whose gain has been set by descending commands; given the circuitry, they are functionally indistinguishable.

A brain-machine interface naturally focuses on the cortical command signals. Cortical activity recorded from nonhuman primates during trained motor behaviors can be correlated with experimental measures of the kinematics or kinetics of the performance. The decoded cortical signals can be used to recreate those kinematics or kinetics in a robotic or virtual simulation of the limb (see other chapters in this volume). Because of the mechanical coupling within the musculoskeletal system, however, similar correlations can be obtained with a wide variety of measures of the

task ([Churchland and Shenoy, 2007](#)). Further, the input-output relationships shift substantially with small changes to the task (e.g., changes in limb posture unrelated to the end-point trajectory being controlled; [Scott and Kalaska, 1997](#)). This suggests that the dimensionality of neural activity is significantly larger than the set of movement parameters that are hypothesized to be encoded (see [Churchland and Shenoy, 2007](#)). This also indicates that the correlations do not reflect the coordinate frame in which the brain normally computes command signals. Further, these correlations may actually reflect cortical inputs from higher motor planning centers (e.g., parietal cortex) and/or somatosensory feedback and efference-copy signals from lower centers such as the spinal cord.

Rather than guessing what coordinates the brain might use and building decoders based on correlations observed, we can start with the known structure of the biological decoder itself. Fortunately, a fair amount of spinal connectivity is known (see [Jankowska, 1992](#); [Pierrot-Deseilligny and Burke, 2005](#)). Modeling of musculoskeletal systems is sufficiently advanced to support the development of realistic model systems in which the potentiality of the components can be appreciated. Modeling tools can be used to gain insight into the spinal cord's contribution to various behavioral phenomena such as kinematic performance, stability, energy consumption, and learning. Alternatively, they can also give us insight into the extent to which these aspects need to be specified explicitly by higher centers or treated as emergent properties of the system being controlled.

In previous research, we obtained surprising results from a realistic model of the spinal circuitry operating a model of a two degree-of-freedom wrist with four muscles ([Raphael et al., 2010](#)). The model consisted of a realistic set of interneurons whose descending commands were simple step functions with learned amplitudes.

The model was called a “spinal-like regulator” (SLR) because it included elements that may actually be located in supraspinal circuits and excluded some known spinal interneurons whose connectivity or roles were less well characterized. Despite having an oversimplified brain whose outputs were limited to unmodulated steps, learning by adjusting one gain at a time rapidly discovered physiological solutions for a wide range of tasks. Even with a large number of control inputs, the simple learning algorithm always converged rapidly to solutions similar to published normal behavior regardless of the random starting point of the search. This is surprising because the large number of control inputs would theoretically create a complex solution space with many undesirable local minima. The fact that training always resulted in good performance implies that the structure of the spinal circuitry facilitates learning by crafting a solution space consisting of many local minima that are good enough for many common tasks. Further, details of muscle activity during the learned behaviors appeared to be physiological (e.g., minimal cocontraction) even though muscle activation was not included in the training criteria. This suggested that the structure of the spinal cord is predisposed toward metabolically efficient behavior.

In this study, we have extended this modeling scheme to a planar elbow–shoulder system to investigate how the spinal cord contributes to the control of a musculoskeletal system with redundant and multiarticular musculature and interaction (Coriolis) torques, which are common control problems for multisegment linkages throughout the body.

Methods

Simulation environment

The neuromusculoskeletal system shown schematically in Fig. 1 includes realistic models of muscles, proprioceptors, and spinal circuitry in conjunction with a simplified model of the brain. Models of

individual components have been described in other publications and are summarized here.

Musculoskeletal model

The musculoskeletal system represents an arm whose motion is constrained within the horizontal plane (see [Brown and Loeb, 2000](#)). The three-segment skeleton is made up of torso, upper and lower arm segments that are linked by hinge-like shoulder and elbow joints. Each joint is operated by a pair of antagonist muscles that provide flexion and extension torques. In addition, a pair of biarticular muscles provides flexion and extension torques across both muscles. See [Fig. 2](#) for a detailed description of the musculoskeletal parameters.

The muscle model used in this study ([Tsianos et al., 2011](#), in preparation) is a modified version of virtual muscle (VM) presented in [Cheng et al. \(2000\)](#). The new muscle model is more computationally efficient and computes energy consumption in addition to force over a wide range of stimulation conditions. It accurately captures the nonlinear effects of firing rate, kinematics, and fiber composition on force production and energy consumption. Tendon plus aponeurosis are modeled as a nonlinear elastic component in series with the contractile machinery. Under dynamic conditions, such series elasticity results in substantial differences between the kinematics of the whole muscle and of the muscle fascicles and spindles, which have significant effects on force production, energy consumption, and proprioceptor activity.

Proprioceptor models

Each muscle in our system includes models of muscle spindles ([Mileusnic et al., 2006](#)) and Golgi tendon organs (GTO; [Mileusnic and Loeb, 2009](#)). The muscle spindle model generates a response depending on fascicle kinematics and fusimotor excitation, with separate gamma static and gamma dynamic control of length and velocity

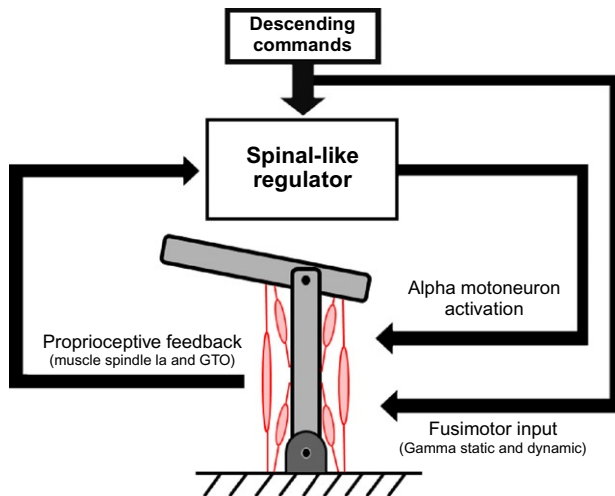


Fig. 1. Schematic overview of the neuromusculoskeletal system of a planar arm. Descending commands from the brain model and proprioceptive feedback from muscle spindle and Golgi tendon organ models project to interneurons in the spinal-like regulator (SLR). The interneurons integrate this information and send it to the alpha motoneurons that drive the muscles. The brain model also delivers fusimotor input to the muscle spindles, effectively setting their transduction sensitivity.

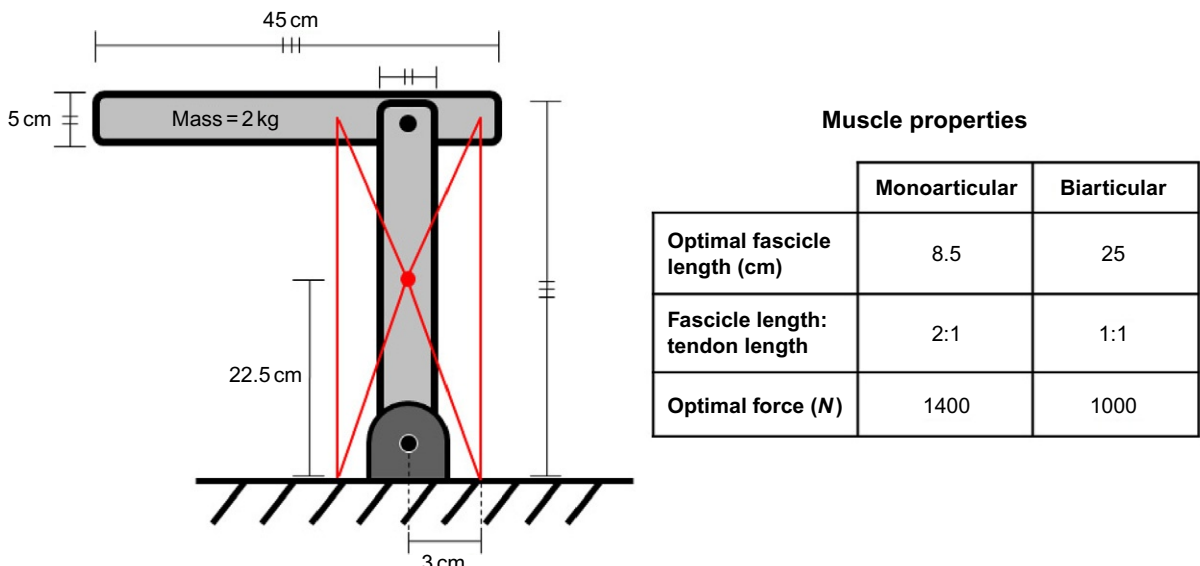


Fig. 2. Musculoskeletal system parameters. The proximal and distal arms have identical dimensions and mass, which is uniformly distributed over each segment. In the posture shown in the figure, the muscles are arranged symmetrically about the proximal segment. The monoarticular muscles have one attachment point at the center of the proximal segment and another one 3 cm away from the joint they actuate. The biarticular muscles attach 3 cm away from the elbow and shoulder joint on the same side of the proximal segment.

sensitivity, respectively. Although the model captures both group Ia and II afferent responses, we used only the Ia response in our system because we omitted spinal circuitry associated with group II feedback (see [Raphael et al., 2010](#)). The GTO model generates a response that represents activity from an ensemble of group Ib afferents in response to whole muscle tension.

Spinal cord model

The spinal cord model is composed of classical interneuronal circuitry described in the experimental literature plus fusimotor control for the muscle spindles. It includes the following pathways: monosynaptic Ia-excitatory, reciprocal Ia-inhibitory, Renshaw inhibitory, Ib-inhibitory, and propriospinal interneuronal pathways. These circuits between a given pair of muscles are largely defined by their functional relationship, which can be synergist, antagonist, or variable depending on task, which we term partial synergists. The connectivity of these relationships for each type of interneuronal circuit is described in detail in [Raphael et al. \(2010\)](#).

Given that the building blocks of the overall spinal network have already been defined, the major challenge in this study was to determine the functional relationships among the arm muscles to construct the network specific to this system. Although monoarticular muscles crossing a single joint are obviously antagonistic, the interaction torques among joints in the arm make it difficult to intuit the underlying muscle activity, hence whether and when a given pair of muscles acts as synergists or antagonists. Further, the system is kinetically redundant (meaning that multiple sets of muscle activation patterns can accomplish the same movement), which further complicates the relationships among the various muscles.

Kinetics and EMG studies of planar arm movement provide descriptions of muscle coordination patterns associated with reaching tasks, thus giving us insight into these functional relationships. We

used the active torque analysis presented in [Graham et al. \(2003\)](#) to identify the functional relationships among monoarticular muscles crossing different joints. The direction of active joint torques agreed with monoarticular muscle activity from several movements presented in [Karst and Hasan \(1991\)](#), therefore active torque direction was a good indicator of which muscle was being recruited. We found that although reaching movements typically require that the shoulder and elbow rotate in opposite directions, the direction of active torques was often the same. In fact, all combinations of active joint torque direction between the two joints were observed, suggesting that any given pair of muscles that cross different joints act as partial synergists. EMG data from Karst and Hasan (1991) were also used to gain insight into the relationships between these muscles and the biarticular muscles, whose individual contributions cannot be deduced with confidence from net joint torques. We found that biarticular muscles could be recruited in or out of phase with the monoarticular muscles that had the same actions at the joints they crossed, suggesting that they have partial synergist relationships with the rest of the set.

In summary, each monoarticular muscle is modeled as antagonist to the monoarticular muscle crossing the same joint and partial synergist to both monoarticular muscles crossing the other joint. Each biarticular muscle is modeled as a partial synergist to all muscles in the set, including each other. The overall network consists of 340 local projections (e.g., afferent and interneuronal pathways) whose activity is modulated by the brain (see next section). The local and descending projections are distributed among 24 interneurons (four classical types for each of the six muscles) and six motoneurons whose bias is also set by the brain model (see [Fig. 3](#)).

Brain model

The brain is modeled as a task planner that evaluates performance according to criteria defined for each task and an adaptive controller

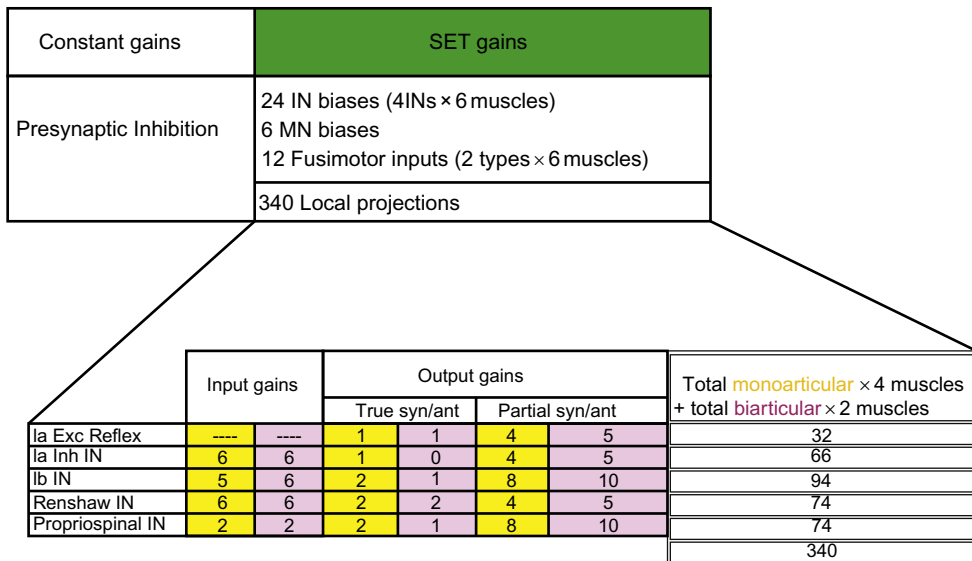


Fig. 3. Distribution of gains among the various interneurons and muscles. Gains are distributed into categories depending on whether they modulate the inputs or outputs of a given interneuron. Each category is subdivided further for monoarticular and biarticular muscles, as their connectivity with the rest of the muscles differs.

that adjusts its control inputs based on performance (see [Loeb et al., 1999](#)). The control inputs (normalized for the range -1 to 1) set the bias of interneurons and motoneurons (which have sigmoidal input/output functions) and the gains of the local projections within the spinal cord. The learning scheme for the adaptive controller has been described in detail in [Raphael et al. \(2010\)](#). Briefly, each control input is initialized at random within a relatively low range (-0.3 to 0.3) to avoid instability. The inputs are then tuned through a simple gradient descent process in which each gain is sequentially adjusted in the positive and negative direction and then left at the value that produces the best performance. One cycle through all the gains corresponds to one iteration. The model in this study was trained for three iterations and the size of the adjustments was 0.2, 0.2, and 0.1, respectively. Only three iterations were performed because they were sufficient for the model to converge on locally optimal solutions.

Modeled task

The response of a planar arm to a brief, oblique impulse ($100 \text{ N} \times 10 \text{ ms}$) at the hand was simulated, equivalent to $\sim 30 \text{ Nm}$ extension torque at each joint. The perturbation was applied at random between 0.5 and 1.5 s into the simulation to avoid anticipation and use of momentum in the opposite direction rather than spinal reflexes to resist the perturbation. The gains of the SLR were initially set at random and adjustments were evaluated according to quadratic cost (squared deviation of the hand from the initial position integrated from 0.5 s before the perturbation to 2 s after). See [Fig. 4](#) for a schematic overview of the task.

We also tested the response of the system when adding a modest level of cocontraction (20% activation to all muscles) to the SLR to simulate the experimental phenomenon where subjects cocontract more in the early phase of learning and to examine the effects it may have on the

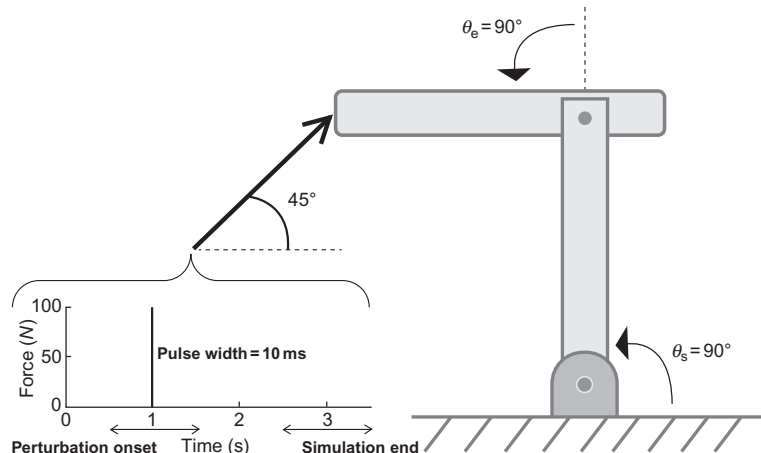


Fig. 4. Overview of the modeled task. An impulsive force ($100\text{ N} \times 10\text{ ms}$) is applied at the end point of a stationary arm at a random onset within a 1-s interval. Task performance is measured by integrating the displacement of the arm over two and half seconds (half a second before the perturbation to two seconds after).

adaptation process. The level of cocontraction was chosen to be as low as typically adopted by experimental subjects, which itself is insufficient to stabilize the arm on its own. To gain insight into its role once performance converges, we subsequently removed the cocontraction and ran an additional training session.

Results

Training the SLR without cocontraction led to generally poor performance (mean = 0.091, SD = 0.15) that was often worse than applying cocontraction alone (SLR gains fixed at zero; Fig. 5). Most of the converged solutions were mediocre with only two being acceptable (see exemplary solutions in Fig. 5). The criteria for acceptable performance was derived from human subjects performing a similar task in Lacquaniti and Soechting (1986; although they appeared to

use a much slower and smaller perturbing impulse, which was not quantified). When cocontraction was added to the SLR, the system's final performance was significantly better and less variable (mean = 0.006, SD = 0.005). All the converged solutions produced better performance than applying cocontraction alone, with over half of them being acceptable even by the strict performance criteria.

As shown in the learning curves in Fig. 5, in both cases, the initial cost did not correlate well with the cost of the converged solution. The trial with the best converged solution, for example, had one of the worst starting costs. Further, most initial starting points for the trials with cocontraction had a higher cost than those corresponding to the system being subjected to cocontraction alone. Thus, cocontraction by itself or added to a randomized SLR was not significantly better than the randomized SLR alone, but the addition of cocontraction to an SLR

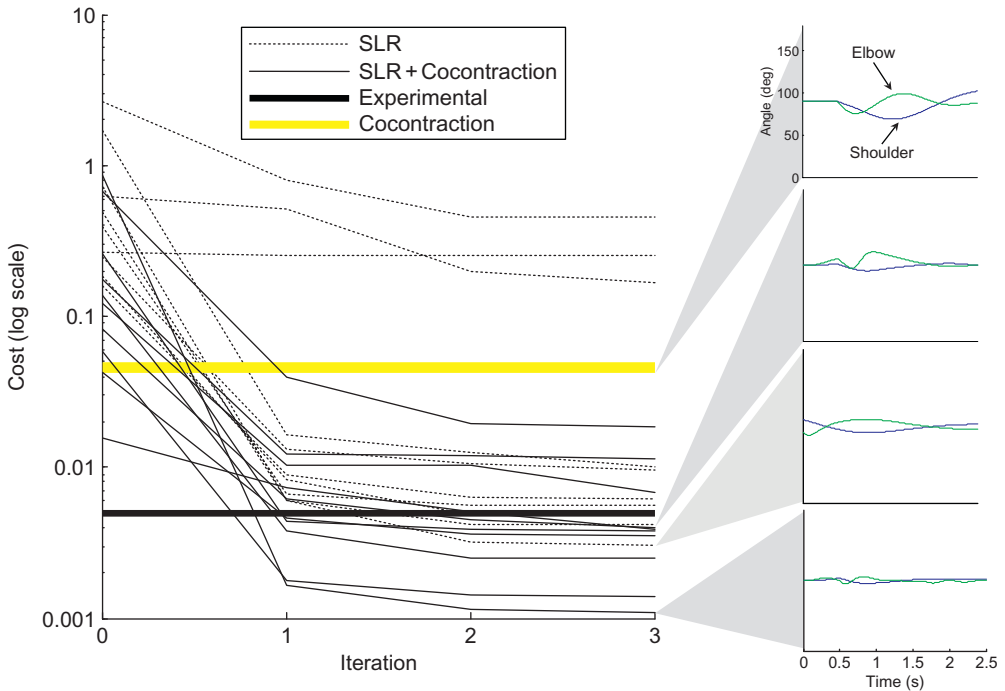


Fig. 5. Learning curves and exemplary joint angle trajectories for trials in which the spinal-like regulator was trained without (thin dotted lines) and with co-contraction (thin solid lines). The upper limit of experimental performance (derived from Lacquaniti & Soechting, 1986; thick black solid line) and modeled performance achieved when applying co-contraction alone (thick gray solid line) are also plotted for reference.

guaranteed that any randomized SLR would converge to a good performance with a modest amount of training.

Removing the cocontraction signal from a converged, well-performing system produced an immediate deterioration in performance (mean = 0.242, SD = 0.287; Fig. 6). Retraining the system using the previously converged solutions as starting points, however, achieved better performance (mean = 0.005, SD = 0.005) than the SLR responses without cocontraction. Surprisingly, they were even slightly (but not significantly) better than the SLR responses with cocontraction (SLR+cocontraction: mean = 0.006, SD = 0.005; retrained SLR following removal of cocontraction: mean = 0.005, SD = 0.005).

Discussion

Role of cocontraction in learning novel tasks

Cocontraction has been shown to be an effective strategy for stabilizing the arm in situations where external perturbations are applied (Franklin et al., 2003; Hasan, 2005; Lacquaniti and Soechting, 1986; Milner and Franklin, 2005) or a high level of accuracy is demanded (Gribble et al., 2003). Cocontraction has an obvious stabilizing effect because each muscle's viscoelastic properties, termed preflexes (see Brown and Loeb, 2000), intensifies with activation. The effects of cocontraction on learning, however, are not as intuitive because understanding them

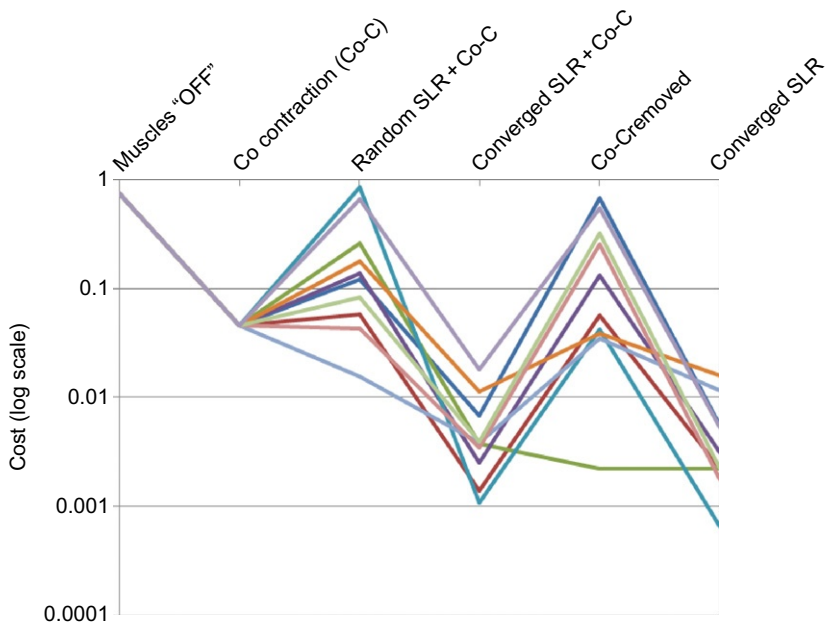


Fig. 6. Learning curves for 10 trials in which the SLR was first trained with cocontraction followed by removing the cocontraction and further training (traces from left to right). The performance achieved with inactive muscles (first point) and cocontraction alone (second point) is also shown for reference.

requires knowledge of the control points (e.g., descending inputs and reflex gains) in the sensorimotor system, their influence on the performance criteria of a given task (defined largely by the neural connectivity), and the means by which they are adjusted (i.e., type of adaptive controller). Franklin et al. (2008) show that by adjusting the degree of feedforward antagonist muscle coactivation based on position feedback, it is possible to reproduce some characteristics of physiological learning of novel tasks. This purely feedforward scheme, however, does not take into account the actual control points of the nervous system and the nature of the solution space thereby afforded. Therefore, it provides limited insight regarding the actual control problem that the nervous system encounters and the opportunity to learn to replace energetically expensive cocontraction with well-chosen gains for proprioceptive feedback.

Our results show that cocontraction reshapes the solution space, virtually eliminating the probability of entrapment in poor local minima. The local minima that are entered during learning with cocontraction are favorable starting points for learning to perform the task when cocontraction is abruptly removed. These results suggest that the tendency of subjects to resort initially to cocontraction when learning a new task (Franklin et al., 2003; Thoroughman and Shadmehr, 1999) may be an important step in the learning process that eventually results in mature strategies marked by little cocontraction and greatly decreased cortical activity.

Role of the spinal cord

The genetically specified and highly preserved connectivity of the mammalian spinal cord

appears to provide a high-dimensional control space that happens to facilitate rapid and successful learning of new motor tasks. This is true even when a simplified model of the SLR is controlled by a highly oversimplified model of the brain and the algorithm by which it learns. The relatively simple and local optimization algorithm applied in this study was successful at finding many good-enough solutions because the state space defined by the SLR consists mostly of good local minima. The complex sequencing of muscle activations required to resist the perturbation in the absence of cocontraction was produced by the SLR circuitry itself acting on afferent and efference-copy signals generated by the perturbing torque and the subsequent responses of the SLR, according to well-chosen but unmodulated gains preset by the controlling brain.

Limitations

The model of the brain used in this study was purposely chosen to be highly simplistic to investigate the emergent properties of the SLR. As shown in this study and in [Raphael et al. \(2010\)](#), the spinal cord appears to create a solution space that facilitates learning “good-enough solutions” rapidly; these are properties that are obviously useful and are presumably exploited by the brain.

The potentiality of spinal circuits may vary depending on the mechanics of the musculoskeletal system and the task. In the system described here, the added cocontraction signal (perhaps supplied by corticomotoneuronal cells in the biological system) was necessary at least initially to find good solutions with a high success rate. Interestingly, the SLR for a two-degree-of-freedom but concentric wrist joint did NOT require any initial cocontraction to enable its controller to learn effective strategies to resist those perturbations and the solutions that it produced did not include cocontraction. It is possible that the requirement for initial cocontraction arises from the mechanical instabilities that arise in

nonconcentric multiarticular systems subject to Coriolis forces.

If cocontraction is, indeed, an important feature of learning, then it would be useful for the brain itself to learn to apply and remove it according to the same learning algorithm used to adjust SLR gains. This can be accomplished by driving the learning process according to a cost function that includes both metabolic energy consumption and kinematic performance criteria. It may also be useful to employ a more biologically plausible learning algorithm in which the adaptive controller adjusts multiple SLR gains simultaneously instead of individually. These refinements of the model are currently underway and will be applied to the simple perturbation task described herein, as well as to the rich set of planar reaching tasks for which human performance data are available in the literature.

Implications for BMIs

The tasks that we have chosen to teach our model systems are similar to those that have been chosen by most researchers developing BMIs for neural prosthetic applications. It seems plausible that retraining the brain to perform tasks that it used to perform with the intact spinal cord and musculoskeletal system will be easier and more successful if the prosthetic system incorporates properties and functions similar to those being replaced or bypassed. The circuitry modeled in the SLR appears to be complex but useful. It is easily emulated in software algorithms. A subject learning to use any BMI must be trained by asking the subject to imagine performing a particular task. The recorded neural activity can then be taken as the solution to the problem of controlling the SLR. Iterative algorithms could then be used offline to find a mapping between the various BMI outputs and the available SLR inputs that successfully performs the task. We hypothesize that such a control system will generalize more readily to the wider range of tasks that

subjects must learn to perform, as opposed to BMIs mapped to outputs of the musculoskeletal system.

References

- Brown, I. E., & Loeb, G. E. (2000). A reductionist approach to creating and using neuromusculoskeletal models. In J. Winters & P. Crago (Eds.), *Biomechanics and neuro-control of posture and movement* (pp. 148–163). New York: Springer.
- Cheng, E., Brown, I. E., & Loeb, G. E. (2000). Virtual muscle: A computational approach to understanding the effects of muscle properties on motor control. *Journal of Neuroscience Methods*, 101, 117–130.
- Churchland, M. M., & Shenoy, K. V. (2007). Temporal complexity and heterogeneity of single-neuron activity in premotor and motor cortex. *Journal of Neurophysiology*, 97, 4235–4257.
- Franklin, D. W., Burdet, E., Tee, K. P., Osu, R., Chew, C. M., Milner, T. E., et al. (2008). CNS learns stable, accurate, and efficient movements using a simple algorithm. *The Journal of Neuroscience*, 28, 11165–11173.
- Franklin, D. W., Osu, R., Burdet, E., Kawato, M., & Milner, T. E. (2003). Adaptation to stable and unstable dynamics achieved by combined impedance control and inverse dynamics model. *Journal of Neurophysiology*, 90, 3270–3282.
- Graham, K. M., Moore, K. D., et al. (2003). Kinematics and kinetics of multijoint reaching in nonhuman primates. *Journal of Neurophysiology*, 89(5), 2667–2677.
- Gribble, P. L., Mullin, L. I., Cothros, N., & Mattar, A. (2003). Role of cocontraction in arm movement accuracy. *Journal of Neurophysiology*, 89, 2396–2405.
- Hasan, Z. (2005). The human motor control system's response to mechanical perturbation: Should it, can it, and does it ensure stability? *Journal of Motor Behavior*, 37(6), 484–493.
- Jankowska, E. (1992). Interneuronal relay in spinal pathways from proprioceptors. *Progress in Neurobiology*, 38, 335–378.
- Karst, G. M., & Hasan, Z. (1991). Timing and magnitude of electromyographic activity for two-joint arm movements in different directions. *Journal of Neurophysiology*, 66(5), 1594–1604.
- Lacquaniti, F., & Soechting, J. F. (1986). Responses of mono- and bi-articular muscles to load perturbations of the human arm. *Experimental Brain Research*, 65, 135–144.
- Loeb, G. E., Brown, I. E., & Cheng, E. (1999). A hierarchical foundation for models of sensorimotor control. *Experimental Brain Research*, 126, 1–18.
- Mileusnic, M. P., Brown, I. E., Lan, N., & Loeb, G. E. (2006). Mathematical models of proprioceptors: I. Control and transduction in the muscle spindle. *Journal of Neurophysiology*, 96, 1772–1788.
- Mileusnic, M. P., & Loeb, G. E. (2009). Force estimation from ensembles of Golgi tendon organs. *Journal of Neural Engineering*, 6, 1–15.
- Milner, T. E., & Franklin, D. W. (2005). Impedance control and internal model use during the initial stage of adaptation to novel dynamics in humans. *The Journal of Physiology*, 567, 651–664.
- Pierrot-Deseilligny, E., & Burke, D. (2005). *The circuitry of the human spinal cord, its role in motor control and movement disorders*. Cambridge, UK: Cambridge University Press.
- Raphael, G., Tsianos, G. A., & Loeb, G. E. (2010). Spinal-like regulator facilitates control of a two-degree-of-freedom wrist. *The Journal of Neuroscience*, 30(28), 9431–9444.
- Rathelot, J. A., & Strick, P. L. (2009). Subdivisions of primary motor cortex based on cortico-motoneuronal cells. *Proceedings of the National Academy of Sciences of the United States of America*, 106(3), 918–923.
- Scott, S. H., & Kalaska, J. F. (1997). Reaching movements with similar hand paths but different arm orientations. I. Activity of individual cells in motor cortex. *Journal of Neurophysiology*, 77(2), 826–852.
- Thoroughman, K. A., & Shadmehr, R. (1999). Electromyographic correlates of learning an internal model of reaching movements. *The Journal of Neuroscience*, 19, 8573–8588.
- Tsianos, G. A., Rustin, C., & Loeb G. E. (2011). Mammalian muscle model for predicting force and energetics during physiological behaviors. *IEEE Transactions on Neural Systems & Rehabilitation Engineering*, (in press).

CHAPTER 16

Advances in the use of electrical stimulation for the recovery of motor function

Dejan B. Popović^{†,‡,*} and Mirjana B. Popović^{†,‡,§}

[†] Faculty of Electrical Engineering, University of Belgrade, BE, Serbia

[‡] Aalborg University, Center for Sensory-Motor Interaction, AA, Denmark

[§] Institute for Multidisciplinary Research, BE, Serbia

Abstract: This chapter sheds light on several issues that are being explored to optimize the application of electrical stimulation in a motor neural prosthesis (MNP) for the restoration of movement in humans with paralysis. Although several MNPs are commercially available, there are issues that limit their use in therapy and/or daily assistance: (1) the users' intention of what and how to move needs to be effectively transmitted to the MNP controller; (2) interface to the neural pathways that leads to physiological-like activation should be improved; (3) artificial control of the MNP should match the biological control of the preserved biological systems; and (4) sensors information should be fused and provided to both the controller of the MNP and the user. We suggest that with the improved use of cortical or other physiological signals, application of multipad electrodes with special protocols, rule-based control that mimics biological control, and with the incorporation of micro- and nanotechnologies, wireless communications, and microcontrollers, the MNP operation can be greatly enhanced. The chapter specifically addresses the control of MNP for the upper extremities and provides details on the new surface multipad electrodes that are of interest for neurorehabilitation of stroke patients.

Keywords: neural prosthesis; functional electrical stimulation; control; upper extremities; man-machine interface.

Introduction

We start this chapter by bringing the reader's attention to the paper presented 44 years at the

Dubrovnik meeting (Reswick et al., 1967), where he introduced the “cybernetic actuation” of paralyzed muscles (Fig. 1, left panel). It is interesting to mention that Dr. Reswick “instrumented” himself before traveling from North America with intramuscular electrodes (shoulder muscles). Reswick demonstrated the use of the implanted interface by opening and closing the prosthetic

*Corresponding author.

Tel.: +381113218345; Fax: +381113248681
E-mail: dbp@efz.rs

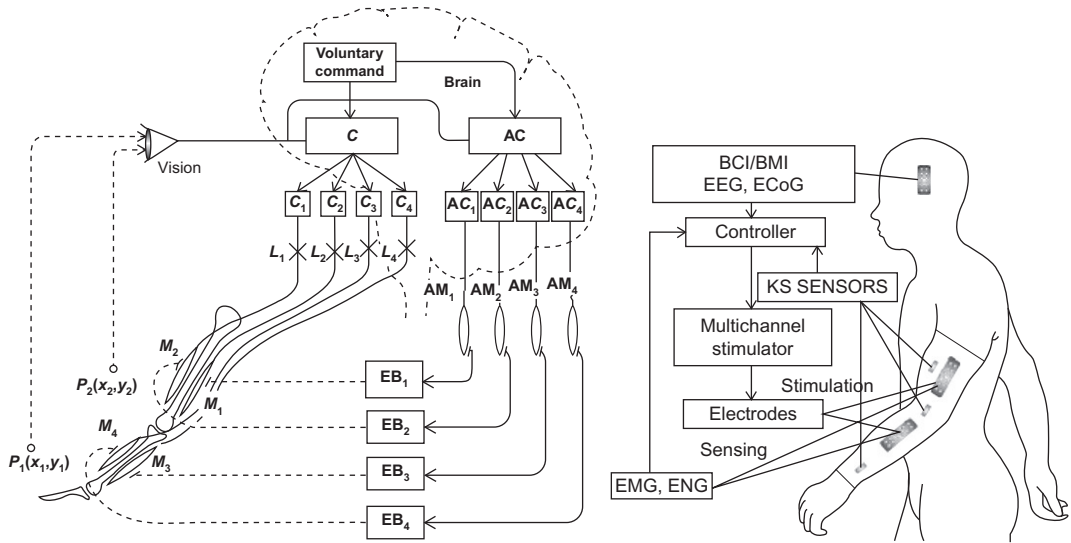


Fig. 1. Left panel: Cybernetic actuation of paralyzed muscles. C_i ($i=1, 2, 3, 4$) are the command signals from the central nervous system that activate muscles (M_i) in a healthy human. L_i indicates lesion that prevents the neural signal from reaching the target muscle. AC_i indicates “alternative communication” channels that need to be trained to operate the muscles (M_i). EB_i stands for the “electronic brain,” a special-purpose computer that detects signals from the alternative communication channels and generates the appropriate burst of electrical pulses to activate the muscle required for the function. P_j ($j=1,2$) are the points within the visual field related to the function, and they are included to indicate that the vision needs to be integrated into the control of the cybernetic actuation. Modified from Reswick et al. (1967), with permission. Right panel: The model of the motor neural prosthesis used in this chapter based on electrical stimulation. KS stands for “kinematics sensors.”

hand which was presented at the same meeting by Bottomley (1967). The opening and closing of the hand was triggered by voluntary contractions of the muscles with implants.

Since then, the technology for interfacing tissues using micro- and nanotechnologies, new materials, and computing power has been improved considerably; yet, the concept remains the same. The enhanced understanding of the effects of the external activation of tissues and the organization of sensory-motor control in healthy individuals and patients, based on electrophysiological and imaging evidence, has provided new insight into how to proceed with cybernetic actuation. A system for cybernetic actuation is today termed a neural prosthesis (NP). An NP controls the activation of neural pathways by inducing currents in the tissues to interact with motor systems (e.g., drop-foot stimulator) and

sensory systems (e.g., cochlear and visual prostheses). We discuss here the elements that need to be improved in making motor neural prostheses (MNPs) effective and practical. The model of the MNP (Fig. 1, right panel) that we discuss includes the interface with the user, hardware that is replacing the missing biological transmission channels (controller, multichannel stimulator, and electrodes), and sensors for feedback (kinematics sensors (KS), electrodes, and the appropriate amplifiers for recordings of the muscle activity (EMG)).

Command channel for the MNP

In most current MNPs, the command channel (user interface) is reduced to a simple switch, but this communication channel has limitations.

The suggested cybernetic actuation model of an advanced MNP has a hierarchical structure ([Fig. 1](#), right panel).

The top control level serves as the intention command channel and comes from the higher cortical structures. The command source is now often assumed to come directly from the cortical activity (brain computer interface (BCI) or brain machine interface (BMI)). This command is appealing because the signals are generated at the time when the movement needs to be initiated. An example of this command channel was recently described by [Pfurtscheller et al. \(2005\)](#). They showed that an EEG-based asynchronous (uncued, user-driven) BCI can trigger the grasping of a tetraplegic subject by means of an MNP. The patient was able to generate bursts of beta oscillations by imagining movement of his foot. This brain activity was captured by a single EEG channel system. When this activity exceeded a predefined threshold, a subsequent switching of a grasp sequence composed of four phases occurred. The patient was able to grasp a glass with the paralyzed hand assisted by an MNP completely on his own.

The command signal could be generated from the recordings of peripheral sensory-motor systems activity (e.g., muscle activity (EMG) and peripheral nerve activity (ENG)). An example of the EMG control of grasping was described by [Saxena et al. \(1995\)](#). Tetraplegic subjects were able to control opening/closing of the hand and the strength of the grasp. However, the surface EMG was shown to be prone to artifacts, to not be sufficiently robust and stable, and to be overall too complex for daily applications ([Saxena et al., 1995](#)). The use of EMGs and other command inputs with an implantable system was presented by [Hart et al. \(1998\)](#). They demonstrated that EMG signals can be used with success and showed that this control signal is robust and effective. Gesture recognition (e.g., recognition of wrist extension by means of the Hall effect sensor) is also a possible solution ([Prochazka et al., 1997](#)). Other command signals, such as voice

control, gaze control, and artificial vision, are also feasible alternatives.

Physiological-like electrical stimulation

The contractions of muscles in healthy humans follow the firing of motoneurons initiated by neural activities within the central nervous system. The slow, fatigue-resistant motor units are active at a lower voluntary effort than larger, fast, fatigable units. The largest fibers are more easily excited than the small fibers. The firing rate of individual motoneurons is low, and the motoneurons fire asynchronously.

The MNP replaces the missing activations coming from the higher centers and activates motoneurons by sending bursts of electrical charge. The frequency of pulses within the burst must be high enough to produce a fused contraction of the muscle. In human arm muscles, fusion occurs at about 16–18 Hz, while in the legs it starts at about 20 Hz. An inverse order of electrically induced recruitment is typical when applying an MNP. Muscle output increases at higher frequencies ($f < 100$ Hz), but muscle fatigue develops rapidly.

The electrical charge within the single pulse regulates the recruitment ([Baratta and Solomonow, 1990](#); [Crago et al., 1974, 1980](#)). A single pulse needs to be short (from about 50 μ s to about 500 μ s). The amplitude may be as low as a fraction of 1 mA when using intraneuronal electrodes to about 150 mA when large muscles are activated with surface electrodes ([Mortimer, 1981](#); [Scheiner et al., 1990](#)). Biphasic, charge-compensated stimulation is preferred over monophasic stimulation ([Scheiner et al., 1990](#)). The shape of the secondary (charge compensation) pulse is important because one would like the electrode reactions to be totally reversible, suggesting a rapid current reversal in the secondary phase.

The application of an MNP directly determines which MNP–motoneuron interface is more

appropriate. If an MNP is to be used for therapy, then a viable solution is the use of transcutaneous interfaces (surface electrodes), and if an MNP is meant to be used as an orthosis, then implantable electrodes are the preferred solution.

Subcutaneous (implantable) electrodes have good selectivity, have repeatable excitation effects, and create sensations that are less apparent to the users than those generated by surface electrodes. The amount of charge required for the production of functional force is also lower than that required by surface electrodes. Two types of widely used electrodes are intramuscular electrodes (Bowman and Erickson, 1985), which can be inserted nonsurgically with a hypodermic needle through closed skin or an open incision and epimysial electrodes (Grandjean and Mortimer, 1986), which typically have a disk-shaped metal plate (3–5 mm in diameter) with a reinforced polymer for attaching the electrode to the muscular fascia.

The invention of BION technology was an important step forward because it enabled implantable systems to be powered and controlled wirelessly (Loeb et al., 2001; Weber et al., 2005). BION technology allows the selective activation of bodily systems. The technological modifications to the original microstimulator design allow the recording of signals from the body and the relative positions among the units, which provide significant advantages in control. The specific value of BION technology is its minimally invasive implantation and minimal discomfort; hence, it can also be used for therapy.

Nerve electrodes have the potential to produce the most desired physiological response. Nerve electrodes are characterized by their placement relative to the nerve (encircling or intraneuronal). In most cases, cuff electrodes have longitudinal slits to allow their installation on the nerve. The cuff is made of a polymer (usually silicone rubber or polyamide). The electrodes in the cuff are made of metal, which is circumferential or forms a matrix of pads. A self-wrapping cuff is self-sizing, which eliminates the problem of selecting

the appropriate size (Naples et al., 1988). Advanced cuff electrodes with multiple contacts (array electrodes) aim to selectively stimulate individual fascicles in the same nerve (Sweeney et al., 1990; Veraart et al., 1993). A flat version of the cuff (FINE electrode; Tyler and Durand, 1997, 2002) reshapes the nerve into a flat geometry to increase the surface area and move central axon populations closer to the surface. Testing of the FINE electrode around the sciatic nerves of cats revealed the selective recruitment of each of the four main branches of the sciatic nerve.

Intraneuronal electrodes invade the epineurium and come close to individual axons. Branner and Normann (2000) investigated the feasibility of implanting a silicon-based array that contained 25 or 100 penetrating electrodes (1-mm long) into the peripheral nerves of the cat sciatic nerve (Utah electrode array). Current injections that were in the range of $10\ \mu\text{A}$ were sufficient to evoke muscle twitches. Dowden et al. (2009) tested the selectivity of stimulation in the sciatic nerve of a cat with the Utah electrode array. About 74% of the electrodes per implant evoked neural activation, and the muscles of interest were selectively recruited. It is important to note that several pins of an electrode array activate the same muscle, and hence, it is possible to asynchronously activate the stimulation electrodes and mimic natural recruitment. Other types of intraneuronal electrodes are being developed with promising characteristics: the longitudinal intrafascicular electrode (LIFE) introduced in the late 1990s (Nannini and Horch, 1991; Yoshida and Horch, 1993) and the fine-wire electrode for direct stimulation of the spinal cord (Mushahwar et al., 2000).

Recently, the Prochazka group (Gan et al., 2007) introduced the router system, which allows surface stimulation to be transmitted to neural tissues that need to be stimulated. This method minimizes the hardware that needs to be implanted. However, the surgery is relatively invasive, and the results are comparable to those obtained with other neural electrodes.

Surface electrodes are the solution for most therapeutic applications. Surface electrodes are not invasive, and they are easy to apply on a daily basis. Surface electrodes need to provide even distribution of current, flexibility to maintain skin contact, and easy application and removal, and should not cause skin irritation. Surface electrodes with conductive polymers have rather large surface areas ($2\text{--}100\text{ cm}^2$). The primary limitation encountered with surface electrodes is that small muscles generally cannot be selectively activated, and deep muscles cannot be activated without first exciting more superficial muscles. Further, a fine gradation of force can be difficult to achieve. Unpleasant sensations and pain can be limitations when applying surface electrodes.

The use of multicontact electrodes has been introduced many years ago with implantable technologies. This approach allows for various branches or even small groups of axons to be recruited (Branner and Normann, 2000). A practical solution for multipad surface electrodes was introduced and shown to be effective (Popović-Bijelić et al., 2005). The multipad arrays that cover relatively large skin areas, with a controller that allows the asynchronous activation of a desired combination of individual pads can activate different branches of subcutaneous motoneurons at lower frequencies ($\approx 5\text{--}10\text{ Hz}$). This stimulation results in fused muscle contraction and the selective activation of individual muscles. The array electrodes were tested for grasping control in tetraplegic and stroke patients (Popović and Popović, 2009). The assessment of grasping functionality demonstrated that the optimal electrode has a branched-tree shape, and the shapes were different from patient to patient (Popović and Popović, 2009). We illustrate here the operation of the multipad electrode with a set of representative recordings during the grasping of a juice can by a healthy subject and a tetraplegic patient stimulated with a four-channel stimulator via array electrodes positioned over the dorsal and volar aspects of the forearm (Fig. 2).

The reduced firing rate leads to slower development of muscle fatigue. This has been shown by Malešević et al. (2010), who reported that fatigue can be postponed when using electrode arrays to stimulate the quadriceps in paraplegic patients. The results showed that low-frequency stimulation through electrode arrays generated forces that were comparable to those generated when the same muscle group was stimulated through a pair of large electrodes at a higher frequency (25 Hz). The results also showed that muscles were able to generate more than 70% of the maximum force for three times longer time at a lower stimulation frequency applied via electrode arrays.

Artificial control for MNPs: Cloning biological control

An MNP controller needs to allow the following functions: (1) use of real-time analog data and sensors for sensory-driven feed-forward or closed-loop control; (2) use of switches for finite-state control; and (3) generation of signals that define the shape, amplitude, duration, and repetition rate of the impulses that are being delivered. A controller must produce a sufficient number of output signals that accommodate the stimulator's number of channels. Today, most microcontrollers can perform simple, real-time control, but most are incapable of executing complex, model-based control algorithms. Digital signal processors can be used, but at this stage, their power consumption is still inadequate for portable, self-contained systems (especially implantable systems).

The schema presented in Fig. 3 offers a more detailed view of the model shown in Fig. 1 (right panel). The analog engineering model is a hybrid hierarchical controller (HHC; Popović and Sinkjær, 2000). The adjective “hybrid” describes the behavior defined by the interaction of subsystems with both continuous dynamics and discrete-event dynamics.

The hierarchical organization of the controller helps manage its complexity, and higher levels in

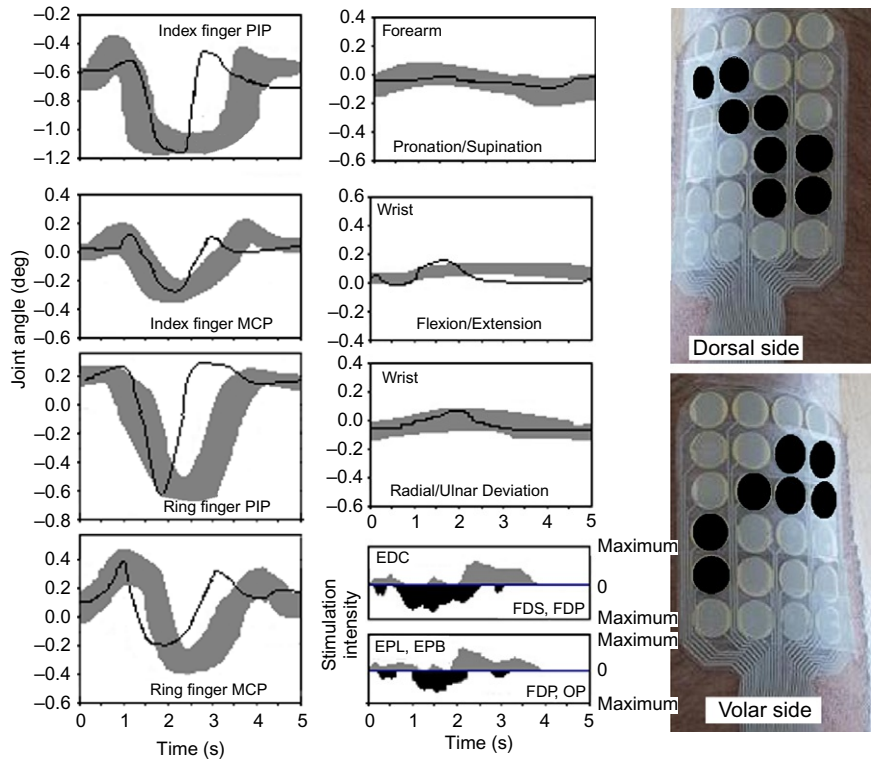


Fig. 2. Joint angle recordings in a healthy subject (solid lines) and a tetraplegic patient with a complete lesion at C4/C5 (gray area, 10 repetitions) and array electrodes during the grasp of a juice can. The right panels show the pads (black fields) that produced the selective desired activation of the finger extensors and flexors with minimum wrist joint interference. The stimulation pattern used for the grasping is shown in the middle-bottom panel. Acronyms used: EDC, extensor digitorum communis; FDS and FDP, flexors digitorum superficialis and profundus, respectively; EPL and EPB, extensors pollicis longus and brevis, respectively; OP, opponens m.

the hierarchy require less-detailed models (discrete abstractions) of the functions at the lower levels, necessitating the interaction of discrete and continuous components (Fig. 3). The extracted artificial part of the HHC that is used for movement incorporates three levels (Fig. 3, bottom panel). The entry of the artificial control structure is the interface between the user and the machine. This interface is a principal command channel, and it allows the user to continuously trigger or control its operation. The interface initiates the activity of a discrete, rule-based controller. This rule-based controller

operates as a discrete and simple data-feedback system, and its main role is to distribute the commands to the lowest actuator levels. The rule-based controller implements the finite-state model of the movement. The actuator level deals with the specific muscle groups that are responsible for the flexion or extension of a single joint. The actuator level implements continuous feedback control and structural modeling. This approach has been tested in several MNP applications for the upper and lower extremities (Kojoović et al., 2009; Popović et al., 2004; Popović and Popović, 1994, 2001).

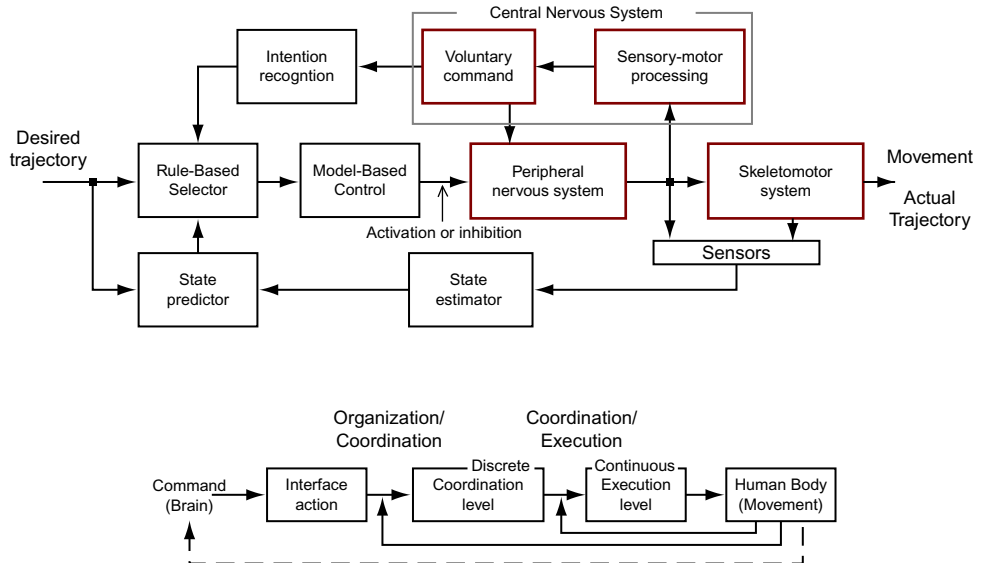


Fig. 3. A model of a hybrid hierarchical controller for an MNP. A rule-based selector implements the temporal and spatial synergies (discrete controller), while the activation and inhibition follow model-based control (continuous control). A state estimator is present where two subsystems interact. A model of a life-like hybrid hierarchical controller for an MNP is shown in the bottom panel.

The lower actuator-control level is responsible for executing the decisions that come from the coordination level. Executing commands (in the sense of artificial reflexes) mean that the electrical stimulation has to be delivered to a group of muscles that are controlling a joint. Single-joint control is achieved through the coordinated action of several muscles acting on neighboring segments.

We will illustrate the specifics of HHCs with MNPs for reaching and grasping function (Popović, 2003). In engineering terms, the nervous system solves the following three tasks during reach/grasp/release (RGR): (1) multimodal sensory integration (sensory intake); (2) complex transformations between different external and intrinsic spatial coordinate systems; and (3) motor commands that are adequate to accomplish the function (MacKenzie and Iberall, 1994). This translates into the following phases that need to be accomplished by the HHC: (1) RGR temporal

synchrony and (2) RGR spatial synergies. The RGR functional task can be divided into the following phases: (1) hand transport to the object location (positioning or reaching), hand orientation and opening (prehension), and hand closing (grasping of the object); (2) hand-with-object transport to the task location; (3) using the object (the actual task); (4) returning the object and releasing it at the object post; and (5) finally returning the hand to its initial position. These phases can be effectively determined with a velocity space model, as shown in Fig. 4. Phases 1 and 5 were defined as “no-object” phases, while the “object phase” label was assigned to phases 2, 3, and 4 for most of the RGR tasks.

Using the same data that determined the temporal synchrony, it was possible to determine the spatial synergies, as shown in Fig. 5. We show the synergies that are relevant to the external control of elbow joint rotation (Popović and Popović, 2001), prehension, grasp, and release.

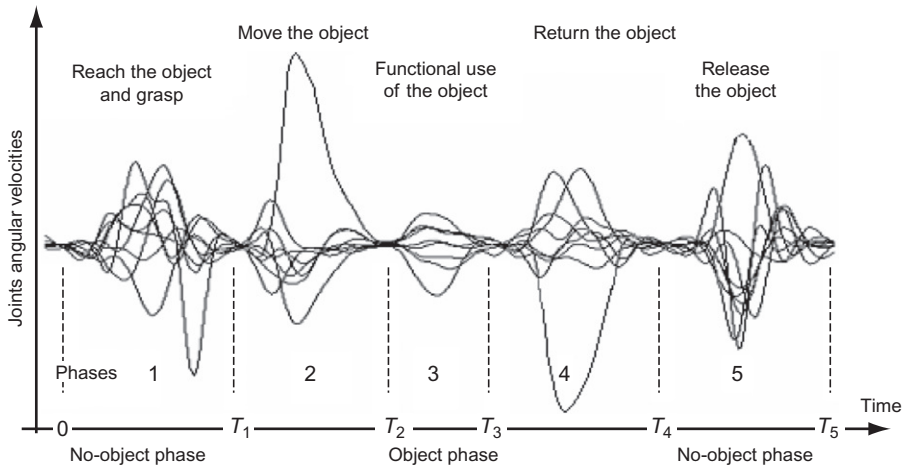


Fig. 4. The “temporal synchrony” model of the reach-to-grasp, use, and release of an object. The angular velocities are averaged and normalized recordings collected from arm and hand joints when reaching, grasping, drinking, returning, and releasing the juice can. The temporal description of this process has five phases.

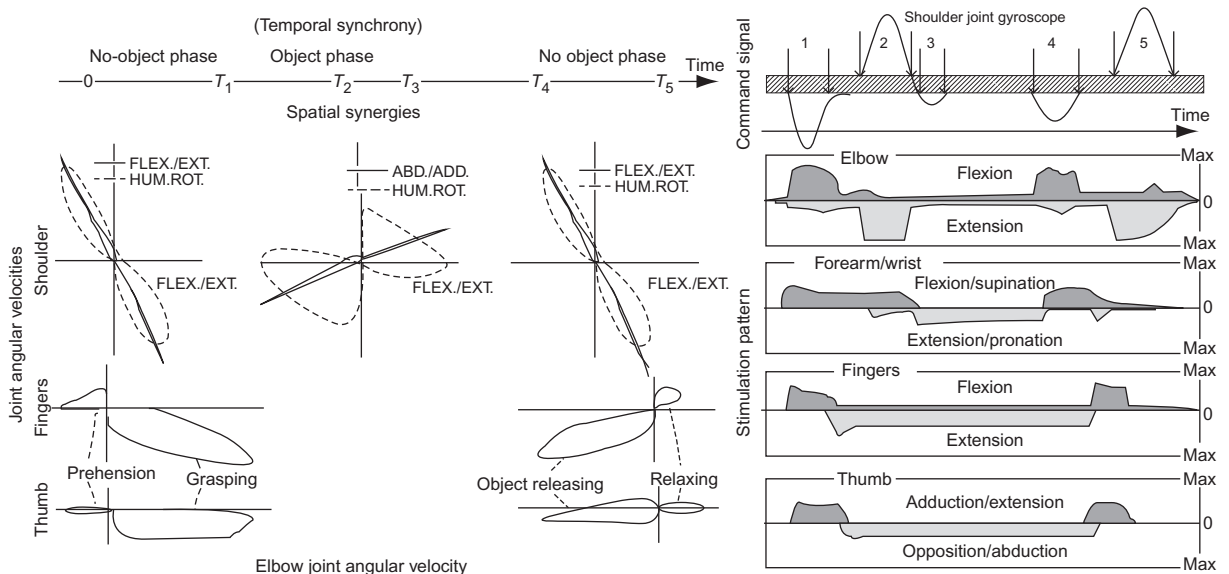


Fig. 5. Left: The spatial synergies for the “drinking from a juice can” task were used to synthesize electrical stimulation patterns for assisting the reach/grasp of tetraplegic and stroke patients. The top line shows the temporal synchrony (discrete) that triggers the adequate spatial synergy and is required for functional movement. Right: The stimulation patterns were used for the control of reaching and grasping in tetraplegic and stroke patients. The shaded areas are muscle activations that were normalized to the maximum force that can be generated by the muscle. The agonist and antagonist levels of activities are shown in opposite directions. FLEX, flexion; EXT, extension; ABD, abduction; ADD, adduction; HUM.ROT, humeral rotation.

This is an example of phase space plots formed in the angular velocity state spaces of the upper arm and forearm.

Testing this life-like control system on stroke patients showed that the stimulation patterns obtained using this technique produced smooth, natural movements (Popović et al., 2004). The stimulation profiles that were used in the clinical trials in stroke patients are presented in Fig. 5 (right panels). The top panel shows the command signal that followed the temporal synchrony, while the actual stimulation profiles were determined using modeling and heuristics.

The same methodology can be applied to other functional movements, such as standing and walking. The application of HHCs to the restoration of walking was described by Popović et al. (2003), in which a six-channel MNP (using goniometer and force-sensing resistor signals) allowed the automatic control of the walking in paraplegic patients. A more detailed description can be found in Popović and Sinkjær (2000).

Sensor systems

Sensors for MNP applications should provide both the control system and the user with information regarding the conditions of the NP. In some cases, it is not obvious that the user needs instant information (e.g., if the automatic execution follows the desired trajectory). However, if anything unexpected happens, the sensory warning may prevent catastrophic consequences. Sensors are needed in MNP systems for their command interfaces (e.g., activating the NP and changing the mode of operation). The optimal sensor system will use the natural information from the biological sensors (Hoffer et al., 1996).

The sensor system should provide various kinds of information, such as the contact force or pressure (grasp force and ground reaction force), the position of the joints (prehension, reaching, standing, and walking), and, perhaps, the activity of the muscle. The dynamic range,

resolution, and frequency response of the sensors must be determined at the start of the application. For example, the force sensors for walking and standing must withstand several times the user's body weight under dynamic loading, and the joint position sensors must allow unrestrained movement over the joint's entire range of motion.

The constraints imposed on the sensors for MNP systems are significant. The sensors must be cosmetically acceptable and easy to mount, they should be self-contained and consume little power, and they must provide adequate information. In most available MNP systems, the sensors are placed externally. A sensor positioned on the surface of the body is unsuitable for many situations. For example, an external force sensor on the digits of the hand requires donning and should work in variable temperature conditions and hazardous environments. The alternative is to use implanted sensors. These sensors have to meet the same performance specifications while functioning in a more hostile environment. These sensors should communicate with the remote control box with a wireless communication link. The ultimate solution is to use available biological sensors in the organism (i.e., to record from the nerves and muscles and process the information into a useful real-time signal). This solution requires the ability to interface with the nerves and interpret the signals that they are supplying to the central nervous system.

Conclusions

In this chapter, we presented the MNP as an effective instrument for the restoration of function in humans with paralysis caused by a central nervous system lesion. We presented components of the MNP that are the focus of active and ongoing research. Advances in the BCI and BMI, in addition to technological progress, are all facilitating innovative design of the hardware for

an MNP, but the integration of the artificial and biological systems still requires basic and applied research. The MNP is on its way to becoming acceptable for both health-care givers and individual home use.

Acknowledgment

This research was partly funded by the project No. 175016, Ministry of Science and Technological Development of the Republic of Serbia, Belgrade, Serbia, and the project InRES, SCOPES program, Swiss National Research Foundation.

References

- Baratta, R., & Solomonow, M. (1990). The dynamic response model of nine different skeletal muscles. *IEEE Transactions on Biomedical Engineering, BME-37*, 243–251.
- Bottomley, A. H. (1967). Design considerations for a prosthetic prehension device. In D. B. Popović (Ed.), *Proceedings of advances in external control of human extremities I-X* (pp. 82–89). Denmark: The Center for Sensory-Motor Interaction (SMI), Aalborg University8676210012.
- Bowman, B. R., & Erickson, R. C. D. (1985). Acute and chronic implantation of coiled wire intraneuronal electrodes during cyclical electrical stimulation. *Annals of Biomedical Engineering, 13*, 75–93.
- Branner, A., & Normann, R. A. (2000). A multielectrode array for intrafascicular recording and stimulation in sciatic nerve of cats. *Brain Research Bulletin, 51*(4), 293–306.
- Crago, P. E., Peckham, P. H., Mortimer, J. T., & Van der Meulen, J. (1974). The choice of pulse duration for chronic electrical stimulation via surface, nerve and intramuscular electrodes. *Annals of Biomedical Engineering, 2*, 252–264.
- Crago, P. E., Peckham, P. H., & Thrope, G. B. (1980). Modulation of muscle force by recruitment during intramuscular stimulation. *IEEE Transactions on Biomedical Engineering, BME-27*(12), 679–684.
- Dowden, B. R., Wilder, A. M., Hiatt, S. D., Normann, R. A., Brown, N. A. T., & Clark, A. (2009). Selective and graded recruitment of cat hamstring muscles with intrafascicular stimulation. *IEEE Transactions on Neural Systems and Rehabilitation Engineering, 17*(6), 545–552.
- Gan, L. S., Prochazka, A., Bornes, T. D., Denington, A. A., & Chan, K. M. (2007). A new means of transcutaneous coupling for neural prostheses. *IEEE Transactions on Biomedical Engineering, 54*(3), 509–517.
- Grandjean, P. A., & Mortimer, J. T. (1986). Recruitment properties of monopolar and bipolar epimysial electrodes. *Annals of Biomedical Engineering, 14*(1), 53–66.
- Hart, R. L., Kilgore, K. L., & Peckham, P. H. (1998). A comparison between control methods for implanted FES hand-grasp systems. *IEEE Transactions on Rehabilitation Engineering, 6*(2), 208–218.
- Hoffer, J. A., Stein, R. B., Haugland, K. K., Sinkjær, T., Durfee, W. K., Schwartz, A. B., et al. (1996). Neural signals for command control and feedback in functional electrical stimulation. *Journal of Rehabilitation Research, 33*(2), 145–157.
- Kojović, J., Djurić-Jovičić, M., Došen, S., Popović, M. B., & Popović, D. B. (2009). Sensor-driven four-channel stimulation of paretic leg: Functional electrical walking therapy. *Journal of Neuroscience Methods, 181*, 101–105.
- Loeb, G. E., Peck, R. A., Moore, W. H., & Hood, K. (2001). BION™ system for distributed neural prosthetic interfaces. *Medical Engineering & Physics, 23*(1), 9–18.
- MacKenzie, C., & Iberall, T. (1994). *The grasping hand. Advances in psychology* (Vol. 104). Amsterdam: North-Holland.
- Malešević, N., Popović, L., Schwirtlich, L., & Popović, D. B. (2010). Distributed low-frequency electrical stimulation delays muscle fatigue compared to conventional stimulation. *Muscle Nerve, 42*, 556–562.
- Mortimer, T. (1981). Motor prosthesis. In V. B. Brooks (Ed.), Bethesda: The American Physiological Society, pp. 3–14. (Sect 1, Vol. 11, part 1(5)).
- Mushahwar, V. K., Collins, D. F., & Prochazka, A. (2000). Spinal cord microstimulation generates functional limb movements in chronically implanted cats. *Experimental Neurology, 163*(2), 422–429.
- Nannini, N., & Horch, K. (1991). Muscle recruitment with intrafascicular electrodes. *IEEE Transactions on Biomedical Engineering, 38*, 769–776.
- Naples, G. G., Mortimer, J. T., Scheiner, A., & Sweeney, J. D. (1988). A spiral nerve cuff electrode for peripheral nerve stimulation. *IEEE Transactions on Biomedical Engineering, 35*, 905–916.
- Pfurtscheller, G., Müller-Putz, G. R., Pfurtscheller, J., & Rupp, R. (2005). EEG-based asynchronous BCI controls functional electrical stimulation in a tetraplegic patient. *EURASIP Journal on Applied Signal Processing, 19*, 3152–3155.
- Popović, M. B. (2003). Control of neural prostheses for grasping and reaching. *Medical Engineering & Physics, 25*, 41–50.
- Popović, M. B., & Popović, D. B. (1994). A new approach to reaching control for tetraplegic subjects. *Journal of Electromyography and Kinesiology, 4*, 242–253.
- Popović, M. B., & Popović, D. B. (2001). Control for an elbow neuroprosthesis: Cloning biological synergies. *IEEE Engineering in Medicine and Biology Magazine, 20*, 74–81.

- Popović, D. B., & Popović, M. B. (2009). Automatic determination of the optimal shape of the surface electrode: Selective stimulation. *Journal of Neuroscience Methods*, 178(1), 174–181.
- Popović, D. B., Popović, M. B., Sinkjær, T., Stefanović, A., & Schwirtlich, L. (2004). Therapy of paretic arm in hemiplegic subjects augmented with a neural prosthesis: A cross-over study. *Canadian Journal of Physiology and Pharmacology*, 82(8/9), 749–756.
- Popović, D. B., Radulović, M., Schwirtlich, L., & Jauković, N. (2003). Automatic vs. hand-controlled walking of paraplegics. *Medical Engineering & Physics*, 25(1), 63–74.
- Popović, D. B., & Sinkjær, T. (2000). *Control of movement for the physically disabled*. London, UK: Springer.
- Popović-Bijelić, A., Bijelić, G., Jorgovanović, N., Bojanić, D., Popović, D. B., & Popović, M. B. (2005). Multi-field surface electrode for selective electrical stimulation. *Artificial Organs*, 29(6), 448–452.
- Prochazka, A., Gauthier, M., Wieler, M., & Kenwell, Z. (1997). The bionic glove: An electrical stimulator garment that provides controlled grasp and hand opening in quadriplegia. *Archives of Physical Medicine and Rehabilitation*, 78(6), 608–614.
- Reswick, J. B., Ko, W., Vodovnik, L., McLeod, W., & Crochetiere, W. (1967). On the cybernetic restoration of human function in paralysis. In: *Proceedings of second international conference on external control of human extremities, Dubrovnik, Yugoslavia, September 1967*, Belgrade: Yugoslav Society for ETAN, pp. 3–14. Popović, D. B. (2002). *Advances in external control of human extremities I-X*, (CD). Reproduced in. In *The Center for Sensory-Motor Interaction (SMI)*. Denmark: Aalborg University ISBN: 8676210012.
- Saxena, S., Nikolić, S., & Popović, D. B. (1995). An EMG-controlled grasping system for tetraplegics. *Journal of Rehabilitation Research and Development*, 32, 17–24.
- Scheiner, A., Mortimer, J. T., & Roessmann, U. (1990). Imbalanced biphasic electrical stimulation: Muscle tissue damage. *Annals of Biomedical Engineering*, 18(4), 407–425.
- Sweeney, J. D., Ksieński, D. A., & Mortimer, J. T. (1990). A nerve cuff technique for selective excitation of peripheral nerve trunk regions. *IEEE Transactions on Biomedical Engineering*, 37, 706–715.
- Tyler, D. J., & Durand, D. M. (1997). A slowly penetrating interfascicular nerve electrode for selective activation of peripheral nerves. *IEEE Transactions on Rehabilitation Engineering*, 5, 51–61.
- Tyler, D. J., & Durand, D. M. (2002). Functionally selective peripheral nerve stimulation with a flat interface nerve electrode. *IEEE Transactions on Neural Systems and Rehabilitation Engineering*, 10(4), 204–213.
- Veraart, C., Grill, W. M., & Mortimer, J. T. (1993). Selective control of muscle activation with a multipolar nerve cuff electrode. *IEEE Transactions on Biomedical Engineering*, 40(7), 640–653.
- Weber, D. J., Stein, R. B., Chan, K. M., Loeb, G., Richmond, F., Rolf, R., et al. (2005). BIONic WalkAide for correcting foot drop. *IEEE Transactions on Neural Systems and Rehabilitation Engineering*, 13(2), 242–246.
- Yoshida, K., & Horch, K. (1993). Selective stimulation of peripheral nerve fibers using dual intrafascicular electrodes. *IEEE Transactions on Biomedical Engineering*, 40, 492–494.

CHAPTER 17

Intraspinal microstimulation for the recovery of function following spinal cord injury

Jeremy A. Bamford and Vivian K. Mushahwar*

*Department of Cell Biology and the Centre for Neuroscience, Faculty of Medicine & Dentistry, University of Alberta,
Edmonton, AB, Canada*

Abstract: Spinal cord injury is a devastating neurological trauma, often resulting in the impairment of bladder, bowel, and sexual function as well as the loss of voluntary control of muscles innervated by spinal cord segments below the lesion site. Research is ongoing into several classes of therapies to restore lost function. These include the encouragement of neural sparing and regeneration of the affected tissue, and the intervention with pharmacological and rehabilitative means to improve function. This review will focus on the application of electrical current in the spinal cord in order to reactivate extant circuitry which coordinates and controls smooth and skeletal muscle below the injury. We first present a brief historical review of intraspinal microstimulation (ISMS) focusing on its use for restoring bladder function after spinal cord injury as well as its utilization as a research tool for mapping spinal cord circuits that coordinate movements. We then present a review of our own results related to the use of ISMS for restoring standing and walking movements after spinal cord injury. We discuss the mechanisms of action of ISMS and how they relate to observed functional outcomes in animal models. These include the activation of fibers-in-passage which lead to the transsynaptic spread of activation through the spinal cord and the ability of ISMS to produce fatigue-resistant, weight-bearing movements. We present our thoughts on the clinical potential for ISMS with regard to implantation techniques, stability, and damage induced by mechanical and electrical factors. We conclude by suggesting improvements in materials and techniques that are needed in preparation for a clinical proof-of-principle and review our current attempts to achieve these.

Keywords: Electrical stimulation; lumbosacral enlargement; locomotor networks; standing; walking; muscle fatigue.

Introduction

Functional electrical stimulation (FES) refers to the application of electrical current to peripheral or central neural tissues to restore function after injury. Most commonly, FES is applied to peripheral

*Corresponding author.

Tel.: +1-780-492-4519; Fax: +1-780-492-1617
E-mail: vivian.mushahwar@ualberta.ca

nerve fibers; however, central stimulation may be advantageous as it affords the opportunity to activate directly the higher level circuitry which oversees and coordinates function. Intrap spinal microstimulation (ISMS) is an example of a central stimulation paradigm which employs fine microwires implanted into the lumbar spinal cord. This area of the spinal cord contains all of the motoneurons which innervate muscles of the lower limbs (Henneman and Mendell, 1981) along with the networks which coordinate muscles and produce multijoint synergies and locomotion (Jankowska, 1992; Kiehn, 2006). The lumbar cord also offers structural advantages as it is protected by the spinal column and is distant from actuated muscles, thus reducing the chance of damage or dislocation of the implanted microwires. The current work is a review of our results with ISMS and a commentary on the works of other groups employing ISMS to answer their own research questions.

A brief history of ISMS in research

ISMS has been used extensively as a research tool to explore spinal network pathways. As early as 1940, Renshaw used penetrating electrodes to stimulate in the spinal cord and measure the synaptic delay in reflex pathways (Renshaw, 1940). In the 1970s, Jankowska and colleagues undertook a series of mapping experiments designed to explore the connections between interneurons mediating reciprocal inhibition (Jankowska and Roberts, 1972) and to understand the way in which external current activates neuronal structures in the central nervous system (CNS) (Gustafsson and Jankowska, 1976).

The mapping of spinal cord networks

More recently, ISMS has been used by Bizzi and colleagues to investigate the organization of locomotor circuitry in the spinal cord of frog (Bizzi et al., 1991; Giszter et al., 1993; Lemay et al., 2001; Saltiel et al., 2001), rat (Tresch and Bizzi,

1999), and cat (Lemay and Grill, 2004; Lemay et al., 2009). These authors employed penetrating microelectrodes to stimulate in the intermediate gray matter (primarily lamina VII) and evoke movements around the hip, knee, and ankle joints. Forces were measured in a matrix of locations in order to calculate the isometric force vectors which resulted from ISMS of the intermediate gray matter. As a result of this work, these authors hypothesized that the intermediate gray matter is autonomously organized into circuits which, when activated individually, produce a finite number of convergent force fields that will direct the limb to an equilibrium point in space (Fig. 1). They termed these “movement primitives” and suggested that all movements were constructed from these simpler components (Bizzi et al., 1995). Further, descending connections could employ these circuits to construct more complex movements by activating movement primitives in combination.

Although the movement primitives hypothesis is attractive, experiments that we have performed led us to believe that the intermediate spinal gray matter does not contain discrete circuits that govern specified movements. Our results showed that the outcome of intermediate spinal cord stimulation depended strongly on the presence of descending input (Mushahwar et al., 2004). Further, the direction of movement could be altered by increasing stimulus amplitude. This suggests a complex and flexible network in the spinal cord, perhaps responsible for processing inputs in order to activate motoneuronal pools coordinately.

The restoration of bladder control

In the early 1970s, experiments were performed investigating the ability of penetrating spinal cord electrodes to produce voiding in spinal cord injured individuals. Trials were initially conducted in animals and early results proved promising (Fig. 2). Approximately 50% of the animals achieved functional voiding during acute experiments with spinally intact ($n=11$) and transected cats ($n=9$;

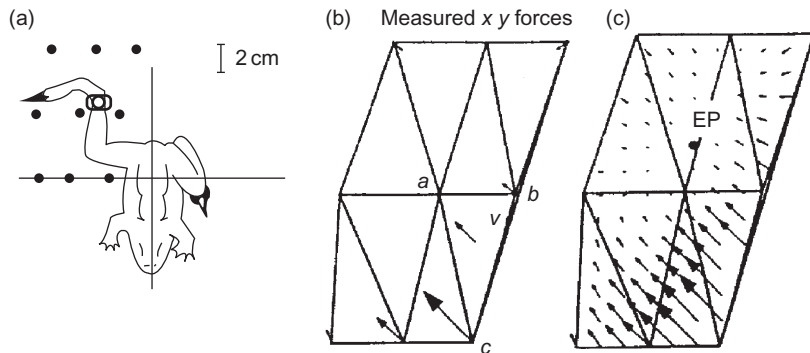


Fig. 1. Forces produced by stimulation of spinal cord gray matter in frog are measured at multiple locations in a grid. Force vectors are interpolated and a convergent force field is produced representing the equilibrium point for the generated movement. A limited number of distinct force fields (movement primitives) are identified. In theory, movement primitives could be combined in a modular manner to produce the full range of possible movements. Reproduced with permission from [Bizzzi et al. \(1995\)](#).

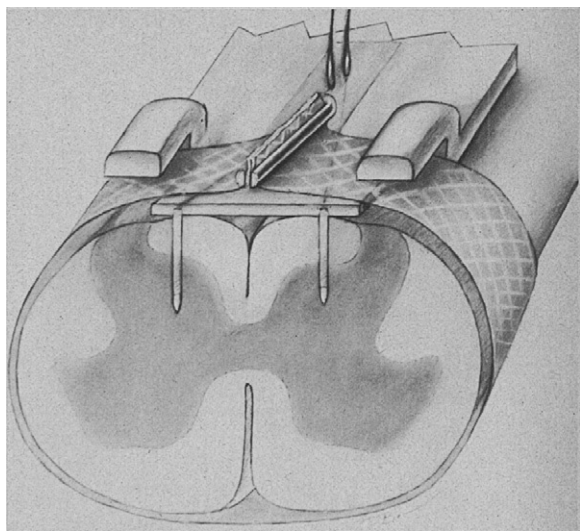


Fig. 2. ISMS for bladder control. A drawing of the early spinal stimulation methods used in animals and humans to restore bladder function after spinal cord injury. Reproduced with permission from [Nashold et al. \(1972\)](#).

[Friedman et al., 1972](#)). Chronic experiments in cats and dogs produced similar results and suggested that, given accurate placement, penetrating spinal cord electrodes might be an effective method of reestablishing normal voiding after spinal cord

injury (SCI) in humans. Based on this work, 27 human patients with paraplegia were implanted with bilateral penetrating electrodes at the S1 spinal cord level ([Nashold et al., 1981](#)). Adequate voiding was achieved in ~60% of these patients, the majority of the successful outcomes occurring in females (10 out of 15 successes were in women). Coactivation of the external urethral sphincter (EUS) necessitated further interventions such as partial sphincterotomies in some patients ([Nashold et al., 1981](#)). This, combined with the ~40% failure rate attributed to misplacement of the electrode tips, led the authors to conclude that other treatments could produce similar efficacy without the need for invasive spinal cord surgery ([Gaunt and Prochazka, 2006](#)).

More recent experiments have employed ISMS using smaller microwire electrodes. It was thought that the smaller surface area of the electrode tips ($1600\text{--}2400 \mu\text{m}^2$) might avoid the current spread likely responsible for the coactivation of bladder and EUS ([Pikov et al., 2007](#)). A number of sacral sites exist that might be targeted by ISMS in order to produce coordinated bladder contractions and EUS relaxation. In one report, sites along the sacral spinal cord were stimulated in α -chloralose anesthetized, spinally intact cats while bladder and urethral pressures were recorded ([Grill et al.,](#)

1999). The authors found moderate increases in bladder pressure; however, these were sometimes associated with increases in urethral pressure, indicating coactivation of the EUS. Nevertheless, distinct sites were located which produced solely increases in bladder pressure along with no increase or even small decreases in urethral pressure. Another group applied ISMS in the S2 region through a single microwire in both acute and chronically transected cats (Tai et al., 2004). Despite demonstrating large increases in bladder pressure, with small decreases in urethral pressure, voiding was limited due to coactivation of EUS. In a more recent report employing chronically implanted ISMS arrays, some degree of voiding was achieved with at least one microwire in 15 of 22 cats (Pikov et al., 2007). The authors of this study encountered results ranging from near-complete voiding to no voiding with any microwire. In some cases, ISMS produced sustained and large increases in bladder pressure and concomitant decreases in EUS tone, while in other animals, a sufficient combination of bladder pressure and EUS relaxation could not be achieved. The authors speculated that these mixed results were explained by having too few stimulation sites available in each animal. It is likely that a denser array of intraspinal stimulating sites would have produced a higher success rate. The authors concluded that interwire spacing of no greater than 300 µm should be employed (Pikov et al., 2007).

To date, ISMS has not proved effective in producing bladder voiding consistently better than established devices which employ anterior sacral root stimulation and often posterior rhizotomy (Ragnarsson, 2008). Therefore, some have concluded that employing it to restore lower urinary tract function after SCI in humans may not be worth the risks associated with long-term implantation (Gaunt and Prochazka, 2006). However, the possibility that ISMS can inhibit EUS contraction has persuaded other groups to continue to pursue multisite arrays which could provide the ability to selectively contract and relax the bladder and EUS, respectively, in order to produce continence or micturition (Pikov et al., 2007).

Use of intraspinal microstimulation for restoring leg movements

A description of surgical techniques

Over the past decade, our group has been actively investigating the use of ISMS for producing functional standing and walking movements after SCI. Testing was conducted in rats and cats, with or without an SCI, and the investigations involved short- and long-term ISMS implantation protocols. Below, we summarize the findings and experiences we have amassed.

Detailed explanations of our surgical methods in rat and cat have been published elsewhere (Bamford et al., 2010b; Guevremont and Mushahwar, 2008). What follows is a brief overview of the general implantation procedure. Microwires are manufactured manually from 30 µm diameter fine wire composed of stainless steel or 80%/20% platinum/iridium and insulated with a 4-µm layer of polyimide (California Fine Wire Company, Grover Beach, USA). Microwires are exposed by manually deinsulating 30–60 µm of the terminal end and sharpening the tips by cutting them to ~15°. Under anesthesia, a laminectomy is performed to expose the target region of the spinal cord. Intraspinal microwires are implanted in both sides of the spinal cord, spaced 2–4 mm apart, rostrocaudally. Arrays comprising multiple microwires are implanted with the tips targeting the motoneuronal pools along the lumbar spinal cord. Microwire tips are inserted individually and advanced to preset depths so that the epidural portion floats on the dorsal surface of the spinal cord. During implantation, test trains are delivered through each microwire to verify accurate targeting of its tip. For instance, trains of stimuli through a microwire tip resting in the quadriceps motoneuronal pool of cat or rat would produce selective activation of quadriceps muscle and evoke gradual increases in force in response to increasing stimulus amplitude. Individual microwires are fixed at their point of insertion to the dura mater with discrete

drops of cyanoacrylate glue. The microwires are further secured in bundles to the dura mater with 8–10 sutures at the base of the nearest rostral spinous process. At this spinous process, the microwires are routed through a silastic tube that is already anchored to the laminar surface of the process. The tube is subcutaneously routed to a headpiece anchored to the skull and the micro-wire connector is exteriorized through the skin to allow for electrical connections (Fig. 3).

Following chronic implantation, animals are administered analgesics and antibiotics and allowed to recover for 7 days. After the initial recovery period, test stimulus trains (typically 100–200 µA, charge-balanced, biphasic pulses with a width of 200 µs and frequency of 20–50 pulses/s) are delivered to ascertain the microwire responses. Direct observation and palpation ensure that the microwires continue to evoke specific and robust contractions of the target muscles and that force is recruited in a gradual manner. Changes in the direction of movement or the rate of the force recruitment likely indicate a shifting of the microwire tip during the recovery period.

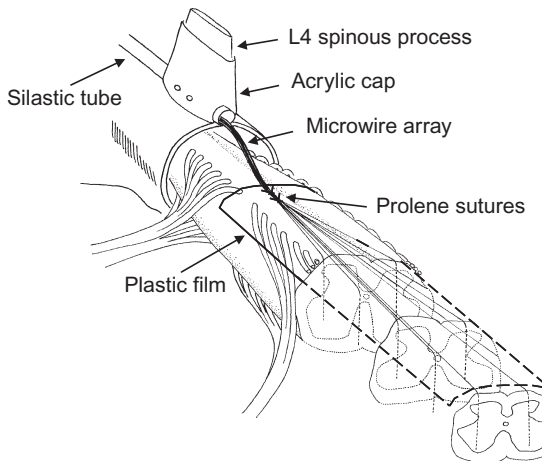


Fig. 3. A drawing of the ISMS implant array. Multiple microwires can be inserted at varying lengths along the spinal cord, creating a bilateral array of possible stimulation sites. The microwires are covered in plastic film and routed through a silicon tube to a headpiece. Reproduced with permission from Prochazka et al. (2001).

Typically, the movement patterns and force recruitment evoked by chronically implanted wires will not change after this initial recovery period (Mushahwar et al., 2000). However, stimulus thresholds may continue to rise in the 2- to 4-week period after implantation, a result we attribute to the gradual accumulation of connective tissue encapsulation around the microwire.

ISMS is best applied in the motoneuronal pools for evoking functional limb movements

In our experiments, ISMS is typically applied in lamina IX of the lumbosacral spinal cord. The motoneurons contained therein are organized into discrete columnar groups according to the muscles they innervate (Henneman and Mendell, 1981; Romanes, 1964). Motoneuronal pools are conserved across species, their locations having been confirmed in rats, cats, and humans (Nicolopoulos-Stournaras and Iles, 1983; Romanes, 1951; Sharrard, 1955; Vanderhorst and Holstege, 1997). We have shown previously that delivering current directly in the motoneuronal pools activates muscles selectively (Mushahwar and Horch, 2000b; Mushahwar et al., 2000), and recruits force gradually in response to increasing stimulus strength (Bamford et al., 2005; Mushahwar and Horch, 2000a; Snow et al., 2006). Further, a range of movements can be elicited; from single-joint flexion or extension, to weight-bearing and fatigue-resistant standing and stepping (Lau et al., 2007; Saigal et al., 2004; Guevremont et al., 2006; Fig. 4). All of these are routinely achieved in the absence of the pharmacological aids that are typically required to generate weight-bearing and functional movements via epidural or dorsal horn stimulation (Barthelemy et al., 2006, 2007; Gerasimenko et al., 2003; Ichiyama et al., 2008). Finally, in spinally intact cats, ISMS at amplitudes up to 300 µA produced no signs of pain or discomfort, suggesting that this method could be used in individuals with partial spinal cord injuries for functional rehabilitation (Mushahwar et al., 2000).

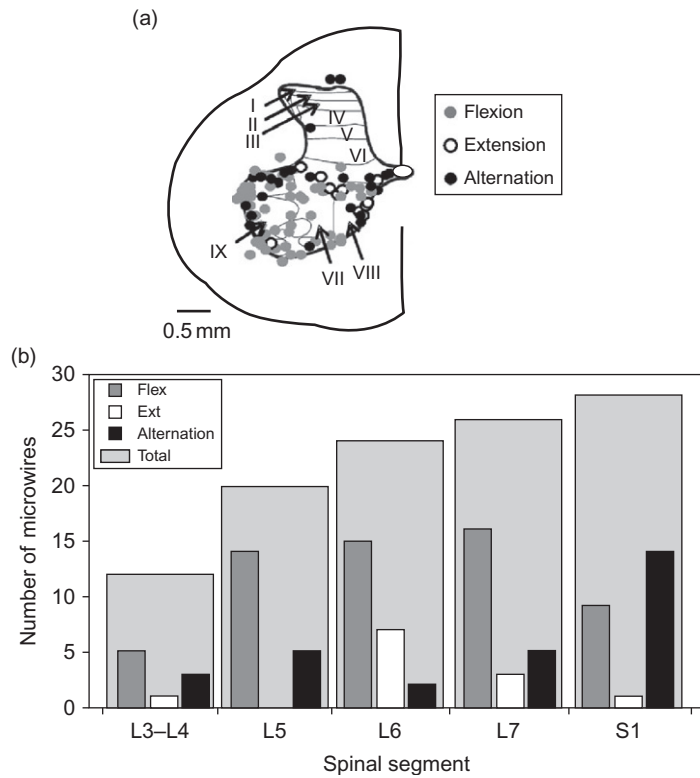


Fig. 4. Summary of ISMS microwire tip locations and evoked responses. The locations of stimulation across multiple cat experiments are displayed in (a). A variety of movements could be produced from microstimulation but the most reliable came from microstimulation of lamina IX. Flexion movements were most common at all spinal segments tested; however, extension and alternation could also be reliably produced (b). Reproduced with permission from [Guevremont et al. \(2006\)](#).

The movements recruited by ISMS

From single joints to functional stepping

Early work established that ISMS can selectively activate muscles and produce gradual force recruitment ([Mushahwar and Horch, 2000a,b](#)). Further, stimulation through single microwires can produce whole-limb synergies characterized by the production of weight-bearing torque at the joints of spinally intact cats ([Mushahwar et al., 2000](#)).

Interleaved stimulus trains through pairs of microwires in each side of the spinal cord

produced a mean standing duration of 21 min when a closed-loop control strategy was employed in spinally intact cats ([Lau et al., 2007](#)). In animals with chronically transected spinal cords, functional stepping was achieved by delivering interleaved stimulus trains through microwire arrays implanted in the lumbosacral cord ([Saigal et al., 2004](#)). Individual microwires producing extension, flexion, and limb-swing synergies were then activated coordinately to achieve stepping which was weight bearing and fatigue resistant over continuous bouts of 40 consecutive steps each. Stepping was achieved with only four microwires in each side of the

spinal cord. As confirmed later this is evidence that ISMS can activate locomotor networks and produce rhythmic, weight-bearing stepping when applied in the ventral horn of the lumbosacral enlargement (Guevremont et al., 2006).

Presumably, single-joint movements are achieved by activating discrete motoneuronal pools, whereas synergies are achieved by activating multiple pools through existing spinal connections. Alternating stepping movements are likely achieved by the activation of an even larger network involving ipsilateral and bilateral reciprocal inhibitory connections (Guevremont et al., 2006; Jankowska, 1992; Prochazka et al., 2002).

The advantages of interleaved stimulation

One of the advantages of ISMS is the ability to employ interleaved stimulation strategies. Interleaved electrical stimulation can be used to improve fatigue resistance and produce smooth, predictable movements (Mushahwar and Horch, 1997; Rack and Westbury, 1969). Interleaving involves the presentation of stimulus pulses from multiple electrodes at evenly spaced intervals such that the resultant frequency of muscle activation is the sum of the individual pulse trains. For example, two electrodes stimulating at 20 pulses/s, when interleaved, would produce an aggregate 40 twitches/s in the muscle. In order to employ interleaved stimulation, an FES system must be able to recruit independent populations of motor units selectively. Others have employed interleaved stimulation to increase the fatigue resistance of evoked movements (McDonnell et al., 2004; Yoshida and Horch, 1993). Likewise, we have found that the fatigue resistance of ISMS can be improved by employing interleaved stimulation (Lau et al., 2007; Mushahwar and Horch, 1997; Fig. 5). The improvements offered by interleaving the stimulus trains are dependent upon the ability of ISMS to activate different subsets of motor units.

Explaining the recruitment characteristics of ISMS

Another advantage of ISMS is the observation that the delivery of current from a point source within discrete motoneuronal pools is capable of generating complex synergistic movements. This suggests that ISMS is capable of exciting a large network of neurons that connect motoneuronal pools into functional groups. In addition to the columnar motoneuronal pools, the ventral gray matter is known to contain a dense network of axonal processes from a variety of interneurons, propriospinal neurons, and afferent projections. It has previously been established that networks do exist between synergistic motoneuronal pools and that they process the reciprocal activation of agonist and antagonist muscles (Jankowska, 1992). As one example, the branching of Ia afferents is known to be extensive as each axon synapses with every motoneuron in the homonymous motoneuronal pool and with a large proportion of motoneurons in pools of synergistic muscles (Mendell and Henneman, 1971). This suggests that motoneurons, in response to ISMS, are recruited transsynaptically via the excitation of fibers-in-passage, an attractive theory as it explains the following observations.

- (1) Gradual force recruitment. The force recruited by ISMS increases gradually in response to increasing stimulus strength (Bamford et al., 2005; Mushahwar and Horch, 2000a; Snow et al., 2006). We found that the slope of the average force recruitment curve in rats was 3.4 times and 4.9 times shallower than that derived from peripheral nerve stimulation (Bamford et al., 2010a, 2005). Further, as stimulus strength is increased, the duration of muscle twitches narrows and the proportion of fast-twitch fibers recruited by ISMS increases (Bamford et al., 2005; Mushahwar and Horch, 2000a). These responses approximate the small-to-large (and slow-to-fast) recruitment

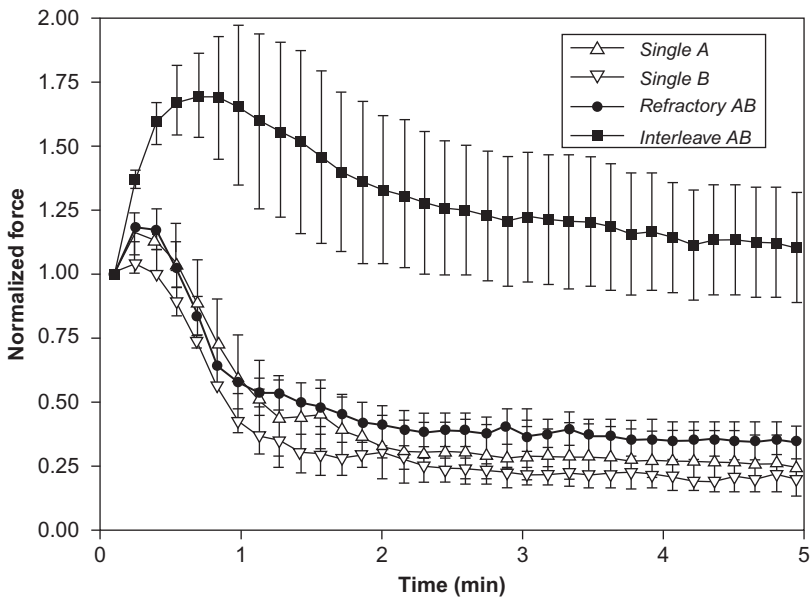


Fig. 5. Fatigue characteristics of interleaved stimulation. Normalized tetanic forces produced by stimulating cat spinal cord through two independent electrodes (A and B) are shown. Single forces were produced by stimulating through either electrode A or B individually at 50 Hz (single A and single B). Refractory AB forces were produced by stimulating electrode B at 50 Hz during the refractory period for neurons activated by electrode A. Interleaved stimulation was produced by stimulating through each electrode in an interleaved manner at 25 Hz, yielding an aggregate stimulation frequency of 50 Hz. Not only did interleaved stimulation produced greater force, but it also reduced fatigue. Reproduced with permission from [Mushahwar and Horch \(1997\)](#).

of motor units during reflex activation of a muscle, sometimes referred to as Henneman's size principle ([Gordon et al., 2004; Henneman et al., 1974](#)). As in Henneman's original experiments, our results could be explained by the indirect activation of motor units through afferent Ia projections (among other projections), which produce a normal, ordered recruitment ([Henneman, 1957](#)).

- (2) Whole-limb synergies can be generated by stimulating through a single microwire. Both flexion and extension synergies are readily achieved across a variety of neural contexts including spinally intact, spinally transected, and decerebrate cat preparations ([Mushahwar et al., 2000; Saigal et al., 2004; Stein et al., 2002](#)). The activation of distant motoneuronal pools required to achieve a synergy implies that

a network of propriospinal neurons, interneurons, and afferents is transmitting the original activation via transsynaptic mechanisms ([Mushahwar et al., 2002](#)). Moreover, these synergies are relatively robust to perturbations such as the addition of anesthesia or varying stimulus characteristics such as pulse amplitude or frequency. This is in contrast to what is achieved during stimulation of the intermediate gray matter where responses are altered following spinalization, decerebration, or even as a result of increasing stimulus amplitude ([Aoyagi et al., 2004; Mushahwar et al., 2004](#)).

The production of single-joint movements can be explained by the activation of a single motoneuronal pool. Nonetheless, the activation of complex synergies must involve a larger network. It is

understood that the first network elements activated by electrical stimulation are likely to be axons passing near the current source (fibers-in-passage; Gustafsson and Jankowska, 1976; Nowak and Bullier, 1998). The best explanation for the phenomena listed above is that ISMS activates motoneurons indirectly, that is, transsynaptically, through the excitation of fibers-in-passage, a result that has been demonstrated previously during stimulation of the spinal cord (Gaunt et al., 2006; Jankowska and Roberts, 1972).

The stability of ISMS implants

ISMS causes minimal histological damage

In chronic experiments, we have found that ISMS implants produce stable results and cause limited damage. We have performed postmortem histological examinations of spinal cord tissue obtained from chronically implanted cats and rats. We found evidence of ongoing inflammation limited to the area surrounding the microwire tracks in rats implanted for 30 days (Bamford et al., 2010b). In these experiments, rats were stimulated daily at levels sufficient to cause functional quadriceps contractions, but within safe limits for central neural stimulation (McCreery et al., 1990, 2004). In contrast to our rat experiments, we found no sign of ongoing inflammatory actions in cats implanted for up to 6 months and stimulated 2–3 times per week (Prochazka et al., 2001). This likely indicates that the inflammatory response endemic to centrally implanted, nonabsorbable structures such as microwires can be expected to subside over time so long as the applied electrical stimulus is within safe levels (Grill et al., 2009) and the implants are stable within the spinal cord tissue.

The flexibility of ISMS implants

Other investigations involving centrally implanted electrodes have shown lasting damage as

evidenced by a decrease in the neuronal density surrounding the implant (Biran et al., 2005, 2007). One difference between these implants and our own is their mechanical properties. Electrodes made of silicon, tungsten, or another brittle material may create a mechanical mismatch between the electrodes and the soft tissue into which they are implanted. In contrast to these experiments, the minimal level of damage incurred by chronic ISMS implants is comparable to that seen in postmortem analysis of deep brain stimulation implants in human subjects (Haberler et al., 2000). This work demonstrated the formation of a glial scar surrounding the electrodes, but no ongoing inflammatory response despite the persistent use of the implants over a period of up to 70 months. Both ISMS microwires and deep brain stimulation electrodes are characterized by a degree of flexibility which may ameliorate the mechanically adverse effects of implantation by absorbing micromotion in the system. In support of this view, an experiment showed that free-floating silicon implants produced less cortical neural damage than when the same implants were tethered to the skull (Biran et al., 2007). Presumably, the floating implant design was able to move freely with the cortical tissue, while the tethered design resisted any micromotion. With regard to ISMS, it is our view that a design where each microwire floats independently and is composed of the most flexible materials which make implantation practical should be employed in order to produce the least amount of damage.

The functional stability of ISMS

A further indication of microwire stability can be derived from the stability of functional measures over time. Presumably, stability in key characteristics of ISMS such as stimulus threshold, force recruitment, and the observable movements produced suggest that the underlying neural

structures recruited by ISMS have been maintained throughout the implantation period. Conversely, changes in these characteristics may indicate either movement of the microwire tip or damage to activated neural structures, or both. For instance, we determined that ISMS continues to recruit force gradually after chronic implantation and stimulation (Bamford et al., 2010b). Further, the functional movements elicited by ISMS microwires have been shown to be relatively stable as at least 67% of implanted microwires maintained the same responses over 6 month experiments in cats (Guevremont and Mushahwar, 2008; Mushahwar et al., 2000). In chronically implanted cats and rats, we have found that stimulus thresholds for activation have either risen (cats; Mushahwar et al., 2000) or fallen (rats; Bamford et al., 2010b) over the 30 days following implantation. While seemingly contradictory, these findings may be explained by the different stimulation durations employed in these experiments. In the cat experiments, the animals received little stimulation for the first 30 days following implantation and the increase in threshold for activation is presumably due to the encapsulation of microwires during this period. Following the initial rise, stimulus threshold was stable over the following months. In contrast, chronically implanted rats received 4 h of stimulation each day at levels sufficient to cause functional quadriceps activation. We speculate that daily stimulation may have induced a plastic response similar to that seen with daily step training in chronically transected cats and rats which resulted in a decrease in markers of inhibitory neurotransmitters in the spinal cord (Edgerton et al., 2004). Although stimulus threshold changes were altered in a statistically significant manner in both chronically implanted cats and rats, the alterations did not cause the stimulus amplitude required to produce functional responses to rise beyond safe levels for central stimulation (McCreery et al., 1990, 2004).

Moving toward clinical application

Improvements necessary for clinical translation

The results we summarize here encourage the continuation of research into ISMS with the goal of progressing toward clinical proof-of-principle in the future. However, a number of challenges must be addressed before clinical trials could be considered. These challenges require further engineering as they are primarily related to microwire manufacture, implantation, and post-implantation control strategies.

Our results suggest that centrally implanted electrodes should be manufactured from the most flexible, compliant materials possible and implanted in a manner that allows the microwires to individually float with spinal cord micromotion. Currently, we accomplish this by implanting each microwire individually and manually. This occasionally leads to misplacement of the microwire tips, an occurrence that is often due to difficulties in perceiving the relative vertical axis with respect to the spinal cord (Guevremont and Mushahwar, 2008). It would be desirable to simplify the procedure by implanting an array of microwires in one step, so long as the mechanical individuality of each microwire is maintained. Current work is proceeding into the development of implantation systems which could temporarily connect multiple microwires but then dissolve in the tissue, leaving the microwires separated. A bioabsorbable material such as a hydrogel or collagenous platform might serve to contain the microwires during implantation, dissolving thereafter.

The manufacture of ISMS arrays is currently a manual, challenging process requiring 2–3 days per array. Once constructed, the arrays are fragile and cannot be further customized during implantation. One advance that we are currently employing is the use of magnetic resonance imaging prior to implantation in order to acquire accurate dimensions with which to customize each

implant to the experimental animal. This allows us to manufacture fewer arrays and improves targeting success.

Conclusions

ISMS produces graded, fatigue-resistant force from selected muscles. Further, the movements generated include weight-bearing standing and stepping, despite the employment of relatively simple stimulation protocols and control strategies to date. We have found that chronic implantation of ISMS microwires is well tolerated by rat and cat spinal cord tissue and we believe that this is partly due to the flexible nature of our microwires. Advances in the materials and design of our implants will seek to capitalize on the inherent advantages of ISMS and aid in the development of a clinically viable procedure to restore motor function following SCI. If clinically successful, this technique could dramatically improve the quality of life and independence of those living with paralysis.

Acknowledgments

The authors would like to acknowledge funding from the Alberta Heritage Foundation for Medical Research (AHFMR), the Canadian Institutes of Health Research, the International Spinal Research Trust, and the National Institutes of Health. V. K. M. is an AHFMR Senior Scholar.

References

- Aoyagi, Y., Mushahwar, V. K., Stein, R. B., & Prochazka, A. (2004). Movements elicited by electrical stimulation of muscles, nerves, intermediate spinal cord, and spinal roots in anesthetized and decerebrate cats. *IEEE Transactions on Neural Systems and Rehabilitation Engineering*, 12, 1–11.
- Bamford, J. A., Putman, C. T., & Mushahwar, V. K. (2005). Intraspinal microstimulation preferentially recruits fatigue-resistant muscle fibres and generates gradual force in rat. *The Journal of Physiology*, 569, 873–884.
- Bamford, J. A., Putman, C. T., & Mushahwar, V. K. (2010a). Muscle plasticity in rat following spinal transection and chronic intraspinal microstimulation. *IEEE Transactions on Neural Systems and Rehabilitation Engineering*, 19, 79–83.
- Bamford, J. A., Todd, K. G., & Mushahwar, V. K. (2010b). The effects of intraspinal microstimulation on spinal cord tissue in the rat. *Biomaterials*, 31, 5552–5563.
- Barthelemy, D., Leblond, H., & Rossignol, S. (2007). Characteristics and mechanisms of locomotion induced by intraspinal microstimulation and dorsal root stimulation in spinal cats. *Journal of Neurophysiology*, 97, 1986–2000.
- Barthelemy, D., et al. (2006). Nonlocomotor and locomotor hindlimb responses evoked by electrical microstimulation of the lumbar cord in spinalized cats. *Journal of Neurophysiology*, 96, 3273–3292.
- Biran, R., Martin, D. C., & Tresco, P. A. (2005). Neuronal cell loss accompanies the brain tissue response to chronically implanted silicon microelectrode arrays. *Experimental Neurology*, 195, 115–126.
- Biran, R., Martin, D. C., & Tresco, P. A. (2007). The brain tissue response to implanted silicon microelectrode arrays is increased when the device is tethered to the skull. *Journal of Biomedical Materials Research. Part A*, 82, 169–178.
- Bizzi, E., Mussa-Ivaldi, F. A., & Giszter, S. (1991). Computations underlying the execution of movement: A biological perspective. *Science*, 253, 287–291.
- Bizzi, E., et al. (1995). Modular organization of motor behavior in the frog's spinal cord. *Trends in Neurosciences*, 18, 442–446.
- Edgerton, V. R., et al. (2004). Plasticity of the spinal neural circuitry after injury. *Annual Review of Neuroscience*, 27, 145–167.
- Friedman, H., Nashold, B. S. J., & Senechal, P. (1972). Spinal cord stimulation and bladder function in normal and paraplegic animals. *Journal of Neurosurgery*, 36, 430–437.
- Gaunt, R. A., & Prochazka, A. (2006). Control of urinary bladder function with devices: Successes and failures. *Progress in Brain Research*, 152, 163–194.
- Gaunt, R. A., et al. (2006). Intraspinal microstimulation excites multisegmental sensory afferents at lower stimulus levels than local α -motoneuron responses. *Journal of Neurophysiology*, 96, 2995–3005.
- Gerasimenko, Y. P., et al. (2003). Initiation of locomotor activity in spinal cats by epidural stimulation of the spinal cord. *Neuroscience and Behavioral Physiology*, 33, 247–254.
- Giszter, S. F., Mussa-Ivaldi, F. A., & Bizzi, E. (1993). Convergent force fields organized in the frog's spinal cord. *The Journal of Neuroscience*, 13, 467–491.
- Gordon, T., et al. (2004). The resilience of the size principle in the organization of motor unit properties in normal and reinnervated adult skeletal muscles. *Canadian Journal of Physiology and Pharmacology*, 82, 645–661.
- Grill, W. M., Bhadra, N., & Wang, B. (1999). Bladder and urethral pressures evoked by microstimulation of the sacral spinal cord in cats. *Brain Research*, 836, 19–30.

- Grill, W. M., Norman, S. E., & Bellamkonda, R. V. (2009). Implanted neural interfaces: Biochallenges and engineered solutions. *Annual Review of Biomedical Engineering*.
- Guevremont, L., & Mushahwar, V. K. (2008). Tapping into the spinal cord for restoring function after spinal cord injury. In D. J. DiLorenzo & J. D. Bronzino (Eds.), *Neuroengineering*. Boca Raton: CRC Press pp. 19-1 to 19-25.
- Guevremont, L., et al. (2006). Locomotor-related networks in the lumbosacral enlargement of the adult spinal cat: Activation through intraspinal microstimulation. *IEEE Transactions on Neural Systems and Rehabilitation Engineering*, 14, 266-272.
- Gustafsson, B., & Jankowska, E. (1976). Direct and indirect activation of nerve cells by electrical pulses applied extracellularly. *The Journal of Physiology*, 258, 33-61.
- Haberler, C., et al. (2000). No tissue damage by chronic deep brain stimulation in Parkinson's disease. *Annals of Neurology*, 48, 372-376.
- Henneman, E. (1957). Relation between size of neurons and their susceptibility to discharge. *Science*, 126, 1345-1347.
- Henneman, E., & Mendell, L. M. (1981). Functional organization of motoneuron pool and its inputs. In V. D. Brooks (Ed.), *Handbook of Physiology, Section 1, The Nervous System*. Vol II, Part I (pp. 423-507). Bethesda: American Physiological Society.
- Henneman, E., Clamann, H. P., Gillies, J. D., & Skinner, R. D. (1974). Rank order of motoneurons within a pool: Law of combination. *Journal of Neurophysiology*, 37, 1338-1349.
- Ichiyama, R. M., et al. (2008). Dose dependence of the 5-HT agonist quipazine in facilitating spinal stepping in the rat with epidural stimulation. *Neuroscience Letters*, 438, 281-285.
- Jankowska, E. (1992). Interneuronal relay in spinal pathways from proprioceptors. *Progress in Neurobiology*, 38, 335-378.
- Jankowska, E., & Roberts, W. J. (1972). An electrophysiological demonstration of the axonal projections of single spinal interneurones in the cat. *The Journal of Physiology*, 222, 597-622.
- Kiehn, O. (2006). Locomotor circuits in the mammalian spinal cord. *Annual Review of Neuroscience*, 29, 279-306.
- Lau, B., Guevremont, L., & Mushahwar, V. K. (2007). Strategies for generating prolonged functional standing using intramuscular stimulation or intraspinal microstimulation. *IEEE Transactions on Neural Systems and Rehabilitation Engineering*, 15, 273-285.
- Lemay, M. A., Grasse, D., & Grill, W. M. (2009). Hindlimb endpoint forces predict movement direction evoked by intraspinal microstimulation in cats. *IEEE Transactions on Neural Systems and Rehabilitation Engineering*, 17, 379-389.
- Lemay, M. A., & Grill, W. M. (2004). Modularity of motor output evoked by intraspinal microstimulation in cats. *Journal of Neurophysiology*, 91, 502-514.
- Lemay, M. A., et al. (2001). Modulation and vectorial summation of the spinalized frog's hindlimb end-point force produced by intraspinal electrical stimulation of the cord. *IEEE Transactions on Neural Systems and Rehabilitation Engineering*, 9, 12-23.
- McCreery, D. B., et al. (1990). Charge density and charge per phase as cofactors in neural injury induced by electrical stimulation. *IEEE Transactions on Biomedical Engineering*, 37, 996-1001.
- McCreery, D., et al. (2004). Arrays for chronic functional microstimulation of the lumbosacral spinal cord. *IEEE Transactions on Neural Systems and Rehabilitation Engineering*, 12, 195-207.
- McDonnell, D., Clark, G. A., & Normann, R. A. (2004). Selective motor unit recruitment via intrafascicular multielec-trode stimulation. *Canadian Journal of Physiology and Pharmacology*, 82, 599-609.
- Mendell, L. M., & Henneman, E. (1971). Terminals of single Ia fibers: Location, density, and distribution within a pool of 300 homonymous motoneurons. *Journal of Neurophysiology*, 34, 171-187.
- Mushahwar, V. K., Collins, D. F., & Prochazka, A. (2000). Spinal cord microstimulation generates functional limb movements in chronically implanted cats. *Experimental Neurology*, 163, 422-429.
- Mushahwar, V. K., & Horch, K. W. (1997). Proposed specifications for a lumbar spinal cord electrode array for control of lower extremities in paraplegia. *IEEE Transactions on Rehabilitation Engineering*, 5, 237-243.
- Mushahwar, V. K., & Horch, K. W. (2000a). Muscle recruitment through electrical stimulation of the lumbosacral spinal cord. *IEEE Transactions on Rehabilitation Engineering*, 8, 22-29.
- Mushahwar, V. K., & Horch, K. W. (2000b). Selective activation of muscle groups in the feline hindlimb through electrical microstimulation of the ventral lumbosacral spinal cord. *IEEE Transactions on Rehabilitation Engineering*, 8, 11-21.
- Mushahwar, V. K., et al. (2002). Intraspinal micro stimulation generates locomotor-like and feedback-controlled movements. *IEEE Transactions on Neural Systems and Rehabilitation Engineering*, 10, 68-81.
- Mushahwar, V. K., et al. (2004). Movements generated by intraspinal microstimulation in the intermediate gray matter of the anesthetized, decerebrate, and spinal cat. *Canadian Journal of Physiology and Pharmacology*, 82, 702-714.
- Nashold, B. S., Friedman, H., & Grimes, J. (1972). Electrical stimulation of the conus medullaris to control bladder emptying in paraplegia: a ten-year review. *Applied Neurophysiology*, 45, 40-43.
- Nashold, B. S. J., Friedman, H., & Grimes, J. (1981). Electrical stimulation of the conus medullaris to control the bladder in

- the paraplegic patient. A 10-year review. *Applied Neurophysiology*, 44, 225–232.
- Nicolopoulos-Stournaras, S., & Iles, J. F. (1983). Motor neuron columns in the lumbar spinal cord of the rat. *The Journal of Comparative Neurology*, 217, 75–85.
- Nowak, L. G., & Bullier, J. (1998). Axons, but not cell bodies, are activated by electrical stimulation in cortical gray matter. I. Evidence from chronaxie measurements. *Experimental Brain Research*, 118, 477–488.
- Pikov, V., Bullara, L., & McCreery, D. B. (2007). Intraspinal stimulation for bladder voiding in cats before and after chronic spinal cord injury. *Journal of Neural Engineering*, 4, 356–368.
- Prochazka, A., Mushahwar, V. K., & McCreery, D. B. (2001). Neural prostheses. *The Journal of Physiology*, 533, 99–109.
- Prochazka, A., Mushahwar, V., & Yakovenko, S. (2002). Activation and coordination of spinal motoneuron pools after spinal cord injury. *Progress in Brain Research*, 137, 109–124.
- Rack, P. M., & Westbury, D. R. (1969). The effects of length and stimulus rate on tension in the isometric cat soleus muscle. *The Journal of Physiology*, 204, 443–460.
- Ragnarsson, K. T. (2008). Functional electrical stimulation after spinal cord injury: Current use, therapeutic effects and future directions. *Spinal Cord*, 46, 255–274.
- Renshaw, B. (1940). Activity in the simplest spinal reflex pathways. *Journal of Neurophysiology*, 3, 373–387.
- Romanes, G. J. (1951). The motor cell columns of the lumbo-sacral spinal cord of the cat. *The Journal of Comparative Neurology*, 94, 313–363.
- Romanes, G. J. (1964). The motor pools of the spinal cord. *Progress in Brain Research*, 11, 93–119.
- Saigal, R., Renzi, C., & Mushahwar, V. K. (2004). Intraspinal microstimulation generates functional movements after spinal-cord injury. *IEEE Transactions on Neural Systems and Rehabilitation Engineering*, 12, 430–440.
- Saltiel, P., et al. (2001). Muscle synergies encoded within the spinal cord: Evidence from focal intraspinal NMDA iontophoresis in the frog. *Journal of Neurophysiology*, 85, 605–619.
- Sharrard, W. J. (1955). The distribution of the permanent paralysis in the lower limb in poliomyelitis: A clinical and pathological study. *The Journal of Bone and Joint Surgery, 37-B*, 540–558.
- Snow, S., Horch, K. W., & Mushahwar, V. K. (2006). Intraspinal microstimulation using cylindrical multielecetrodes. *IEEE Transactions on Biomedical Engineering*, 53, 311–319.
- Stein, R. B., et al. (2002). Limb movements generated by stimulating muscle, nerve and spinal cord. *Archives Italiennes de Biologie*, 140, 273–281.
- Tai, C., et al. (2004). Bladder and urethral sphincter responses evoked by microstimulation of S2 sacral spinal cord in spinal cord intact and chronic spinal cord injured cats. *Experimental Neurology*, 190, 171–183.
- Tresch, M. C., & Bizzi, E. (1999). Responses to spinal microstimulation in the chronically spinalized rat and their relationship to spinal systems activated by low threshold cutaneous stimulation. *Experimental Brain Research*, 129, 401–416.
- Vanderhorst, V. G., & Holstege, G. (1997). Organization of lumbosacral motoneuronal cell groups innervating hindlimb, pelvic floor, and axial muscles in the cat. *The Journal of Comparative Neurology*, 382, 46–76.
- Yoshida, K., & Horch, K. (1993). Reduced fatigue in electrically stimulated muscle using dual channel intrafascicular electrodes with interleaved stimulation. *Annals of Biomedical Engineering*, 21, 709–714.

CHAPTER 18

Interfacing neurons with carbon nanotubes: (re)engineering neuronal signaling

Alessandra Fabbro[†], Giada Cellot[†], Maurizio Prato[‡] and Laura Ballerini^{†,*}

[†] Life Science Department, Center for Neuroscience B.R.A.I.N., University of Trieste, TS, Italy

[‡] Department of Chemical and Pharmaceutical Sciences, University of Trieste, TS, Italy

Abstract: Carbon nanotubes (CNTs) are cylindrically shaped nanostructures made by sheets of graphene rolled up to form hollow tubes. Owing to their unique range of thermal, electronic, and structural properties, CNTs have been rapidly developing as a technology platform for biological and medical applications, including those designed to develop novel neuro-implantable devices. Depending on their structure, CNTs combine an incredible strength with an extreme flexibility. Further, these materials exhibit physical and chemical properties which allow them to efficiently conduit electrical current in electrochemical interfaces. CNTs can be organized in scaffolds made up of small fibers or tubes with diameters similar to those of neural processes such as axons and dendrites. Recently, CNT scaffolds have been found to promote growth, differentiation, and survival of neurons and to modify their electrophysiological properties. These features make CNTs an attractive material for the design of nano–bio hybrid systems able to govern cell-specific behaviors in cultured neuronal networks.

The leading scope of this short review is to highlight how nanotube scaffolds can impact on neuronal signaling ability. In particular, we will focus on the direct and specific interactions between this synthetic nanomaterial and biological cell membranes, and on the ability of CNTs to improve interfaces developed to record or to stimulate neuronal activity.

CNTs hold the potential for the development of innovative nanomaterial-based neurological implants. Therefore, it is particularly relevant to improve our knowledge on the impact on neuronal performance of interfacing nerve cells with CNTs.

Keywords: carbon nanotubes; neuronal network; spontaneous activity; hippocampal culture; afterdepolarization; neural interfaces.

*Corresponding author.

Tel: +39-040-558-2411/8750; Fax: +39-040-558-2011
E-mail: lballerini@units.it

Introduction

Among the emerging applications of nanotechnology to neuroscience, the development of artificial nanomaterials, such as carbon nanotubes (CNTs) or nanofibers, raises particular interest for their potential exploitation in next-generation scaffolds for nerve tissue engineering (Gilmore et al., 2008), or in long-term implants such as neural interfaces (Keefer et al., 2008; Kotov et al., 2009). The unique physical-chemical features of CNTs allow the development of a variety of miniaturized devices with remarkable properties (Krishnan et al., 1998). CNT soluble preparations have been also proposed for the fabrication of novel molecular sensing, diagnostic, or drug delivery devices (Pantarotto et al., 2004).

More recently, CNTs have shown the ability to govern several neuronal behaviors when used as platforms to support the growth in cultured cortical circuits (Cellot et al., 2009; Galvan-Garcia et al., 2007; Hu et al., 2004; Lovat et al., 2005; Mattson et al., 2000; Ni et al., 2005).

CNTs are cylindrical nanostructures, composed of a single graphene sheet rolled up and closed at each end by hemispherical fullerene caps. They show a radius of a few nanometers and are characterized by a high aspect ratio and a variable length, usually below 1 μm . In the past decade, two different types of CNTs have been extensively used in basic neuroscience research: (i) single-walled carbon nanotubes (SWCNTs) and (ii) multi-walled carbon nanotubes (MWCNTs), made up of multiple concentric graphite cylinders. SWCNTs' and MWCNTs' shape and size mimic the morphology of small neuronal processes (Gilmore et al., 2008) and their high electrical conductivity combined to the large surface area may increase charge injection capacity of CNT-based microelectrodes (Kotov et al., 2009). These features make CNTs intriguing candidates for nervous system applications.

CNT-based devices are expected to fulfill the requirements of safety of use, biocompatibility, and mechanical and electrochemical stability in a

biological environment, in order to be used for the development, implementation, and improvement of neuronal interfaces and electrodes (Keefer et al., 2008; Kotov et al., 2009; Lu et al., 2010; Nguyen-Vu et al., 2006). In this framework, it is highly relevant to improve our knowledge on the direct effects that nanotubes might have on neuronal signaling ability, by means of CNTs/cell membrane "direct" interactions, or, alternatively, on neurite formation ability, by instructing dendrites' and axons' growth and/or branching. SWCNTs- and MWCNTs-induced modulations may thus, in principle, alter neural signal integration at multiple levels.

This review will highlight the impact of CNTs on nerve cell functions (e.g., electrical regenerative properties and synaptic activity) and on nerve cell morphological features (e.g., adhesion, growing, and neurite/dendrite extension abilities) in cultured neuronal networks. We will also address the more recent issue regarding the application of CNTs as neural interfaces for recording and/or stimulating neuronal activity.

The biocompatibility of CNT-based substrates and the impact of CNTs on nerve cell signaling

The first report on CNT biocompatibility dates back to 2000, when Mattson et al. (2000) showed that dissociated hippocampal neurons attached and grew on glass coverslips coated with as-prepared MWCNTs or with 4-hydroxynonenal functionalized MWCNTs.

Several studies assessed and confirmed later, in cultured neurons, the biocompatibility of CNT growth platforms (Gheith et al., 2005; Hu et al., 2004; Lovat et al., 2005; Malarkey et al., 2009), but the properties of MWCNT/neurons hybrid networks from the electrophysiological and functional point of view were investigated for the first time only in 2005 by Lovat and collaborators. These authors studied how neurons reconstructed a functional network when integrated to non-functionalized MWCNTs (Lovat et al., 2005).

In this work, a homogeneous and purified meshwork of MWCNTs on glass (Fig. 1a) was obtained by first functionalizing CNTs by means of the 1,3-dipolar cycloaddition reaction, then dissolving them in dimethylformamide to allow purification, deposited on glass substrate and heated to eliminate residual functionalization (Fig. 1b). The authors cultured dissociated hippocampal neurons on MWCNT-covered glass substrates and recorded neuronal activity using traditional, single-cell electrophysiological techniques. They confirmed that cultured hippocampal circuits grew well on a conductive MWCNTs meshwork

and, remarkably, they report that the frequency of spontaneous synaptic activity (measured as postsynaptic currents) was always significantly enhanced when compared to that of control neurons grown on pure glass coverslips. This boost in spontaneous network activity was accompanied by an increase in the frequency of action potential firing (Fig. 1c). The subsequent work by Mazzatorta et al. (2007) demonstrated that SWCNTs were able to improve synaptic activity in cultured networks in a similar fashion. The hypothesis that the increased network activity found in neurons grown on CNT scaffolds

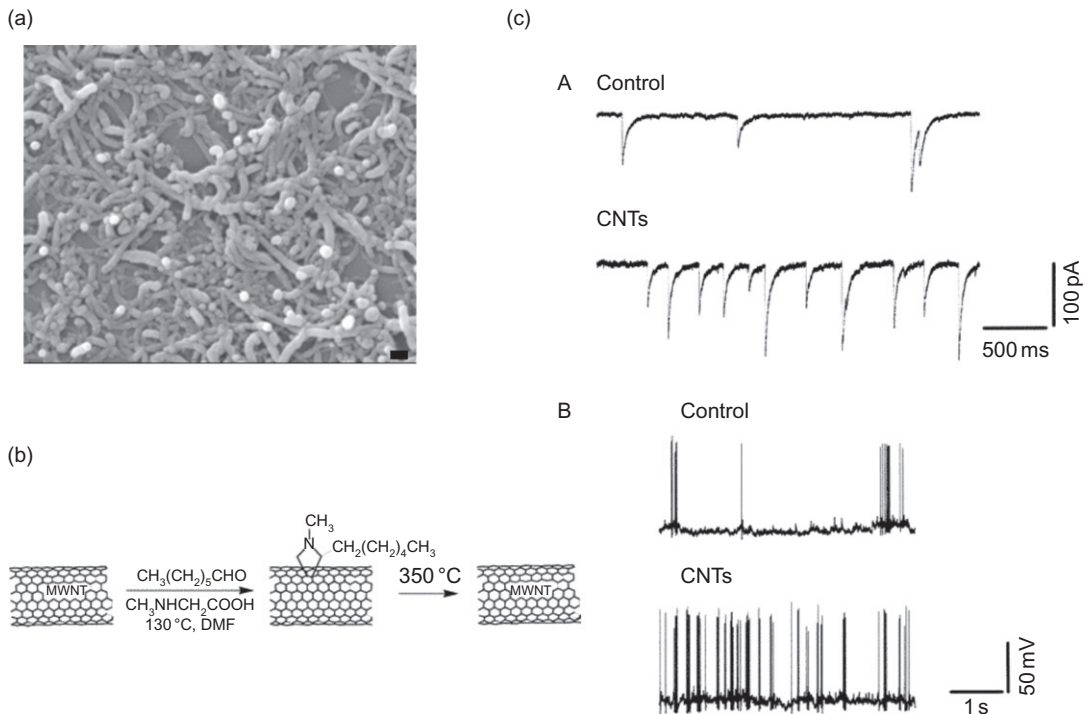


Fig. 1. Carbon nanotube impact on neuronal performance of cultured hippocampal networks. (a) SEM micrograph showing the appearance of a purified MWCNT layer, used as growing substrate for cultured hippocampal neurons. Scale bar: 200 nm. (b) Schematic representation of the protocol used for the preparation of homogeneous and purified carbon nanotubes meshwork by the 1,3-dipolar cycloaddition reaction. MWCNT is first functionalized to allow purification and then deposited on glass and heated to 350° , to eliminate the functionalization preserving the carbon nanotube network. (c)(A)) Spontaneous synaptic currents recorded from hippocampal neurons in control condition (glass) and on a carbon nanotubes (CNTs) layer like the one shown in (c)(A)). (c)(B)) Spontaneous firing activity of cultured neurons in control and on carbon nanotubes (CNTs). Note the large increase in the frequency of both spontaneous postsynaptic currents and action potentials. Adapted with permission from Lovat et al. (2005).

could be related to an increased number of neurons adhering on such substrates was ruled out by visualization and quantification of cultured neurons via immunocytochemistry experiments, where antibodies against specific protein markers were used (Lovat et al., 2005; Mazzatorta et al., 2007). These studies demonstrated that the detected functional differences were not merely due to the construction of networks of different sizes. In particular, a direct quantification of hippocampal cells, by labeling the cultures with antibodies targeted to microtubule-associated protein 2 (MAP-2), showed that the neuronal density did not differ between control and CNT cultures and that the general morphology of neurons, monitored as the distribution of cell body diameters (Mazzatorta et al., 2007) and the number of neurites departing from the neuronal soma (Lovat et al., 2005; Mazzatorta et al., 2007), were similar in the two growing conditions (control and SWCNTs or MWCNTs). Additionally, the electrophysiological characterization of the passive membrane properties of the recorded neurons (membrane capacitance, input resistance, and resting membrane potential), generally accepted as useful indicators of the cellular dimensions and health, were fully comparable between control and neurons developed on CNT films (Cellot et al., 2009; Lovat et al., 2005; Mazzatorta et al., 2007). Overall, these results indicated that the increased spontaneous activity detected in the presence of pure, non-functionalized, MWCNT or SWCNT scaffolds were not due to differences in neuronal density or cell morphology. Thus, other phenomena, regardless of network sizes, were governing the interplay between CNTs and neurons.

In this context, the occurrence of extensive, intimate, and tight contacts between neuronal membranes and CNT growth platforms was demonstrated by scanning and transmission electron microscopy (SEM and TEM, respectively) analysis (Cellot et al., 2009; Mazzatorta et al., 2007; Fig. 2) and suggested a direct (maybe even electrical) coupling of CNTs to neuronal

processes. Such interactions are potentially responsible for the effects of these scaffolds on neuronal performance, which relapse at the network level. A parallel work from Sorkin et al. (2009) supported this hypothesis, showing that process entanglement is a key mechanism by which neurons anchor to rough surfaces (such as CNTs), thus contributing to the physical interactions between neurons and nanotube substrates.

The work by Cellot et al. (2009) specifically addressed the emergence of an electrical coupling between CNTs and neuronal membranes. The authors used single-cell electrophysiology techniques to demonstrate that nanotubes are able to reengineer the integrative electrical abilities of hippocampal neurons maintained *in vitro*. In this study (Cellot et al., 2009), neurons were cultured on CNT substrates (SWCNTs or MWCNTs) or on control substrate (glass coverslips). Neurons were patched-clamped in whole cell configuration and forced to fire short trains of action potentials at variable frequencies (20–100 Hz) in order to maximize, at the single-cell level, the interactions between the regenerative properties of the proximal and distal cell compartments (Larkum et al., 1999). With these experiments, Cellot et al. (2009) showed that neurons grown onto CNT carpets were more prone to generate back-propagating action potentials, a neuronal regenerative property known to be involved in the regulation of local synaptic feedback and in the release of chemical messengers (Kuczewski et al., 2008; Waters et al., 2005; Zilberter et al., 2005). Back-propagating action potentials were unmasked due to the appearance of additional subthreshold somatic depolarization after short trains of action potentials (Fig. 3a and b; Cellot et al., 2009; Larkum et al., 1999). The authors also showed that the nanotube-induced modification of the dendritic electrogenic properties resulted in an increase in single-cell excitability: this effect may explain, at least in part, the boosting of spontaneous activity that was always observed in neurons

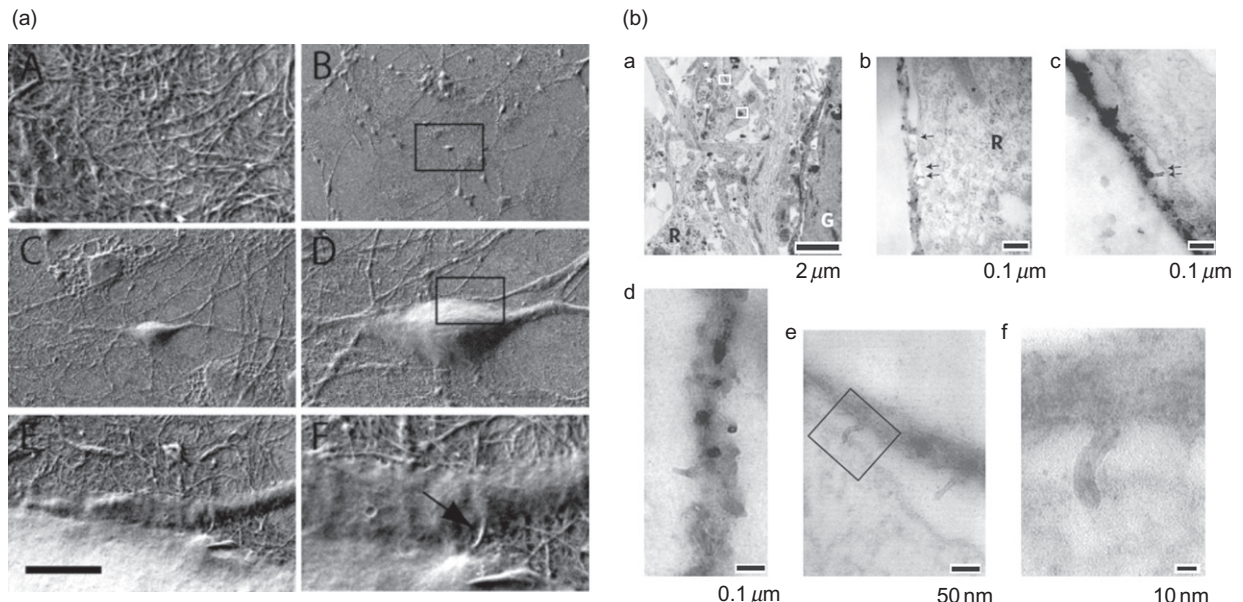


Fig. 2. Neuronal membranes of cultured hippocampal neurons make extensive and intimate contacts with the carbon nanotubes layer. (a) SEM images of hippocampal neurons cultured on carbon nanotubes. A, detail of the SWCNT layer; B–D, subsequent micrographs at higher magnifications of a hippocampal neuron grown on SWCNT. Note the extensive outgrowth of neurites on the carbon nanotube meshwork and the intimate contacts between carbon nanotube and neuronal membrane. Scale bar (in E): A, 1 μm ; B, 200 μm ; C, 25 μm ; D, 10 μm ; E, 2 μm ; F, 450 nm. Reproduced with permission from Mazzatorta et al. (2007). (b) TEM images of hippocampal neurons cultured on MWCNTs, showing healthy organization of neuronal networks. “R” indicates clusters of ribosomes and “G” a presumed glial cell (with the typical electron dense cytoplasm). b and c, TEM sagittal sections showing MWCNT-membrane contacts (arrows). d, MWCNT morphology. e and f, high-magnification micrographs showing MWCNT “pinching” neuronal membrane. Reproduced with permission from Cellot et al. (2009).

cultured on purified CNTs (Cellot et al., 2009; Lovat et al., 2005; Mazzatorta et al., 2007). Cellot et al. (2009) further explored which specific property of CNTs (i.e., their nanostructure, providing a characteristic nano-roughness to the scaffold surface, or their electrical conductivity) is the key one needed to successfully alter neuronal regenerative ability. To address this issue, neurons were cultured on materials different from CNTs, but presenting either comparable nano-roughness or comparable electrical conductivity. In particular, Cellot et al. (2009) used the self-assembling peptide RADA 16 substrates to mimic CNT-like three-dimensional nanostructure in the absence of electrical conductivity, and indium tin oxide (ITO) substrates to reproduce CNT-like

conductivity in the absence of a three-dimensional nanostructure. In both cases, these substrates were unable to replicate CNT effects on neuronal regenerative properties and excitability. The authors therefore suggested that both SWCNTs and MWCNTs mediated their effects via the coexistence of both conductivity and nanostructure (Cellot et al., 2009).

With a combination of electrophysiological techniques and theoretical modeling, Cellot et al. (2009) tried to correlate, even if speculatively, the effects detected at the single-cell level to those displayed at the network level. In particular, they succeeded in predicting by network modeling the impact of the improved dendritic regenerative properties brought about by CNT scaffolds on the

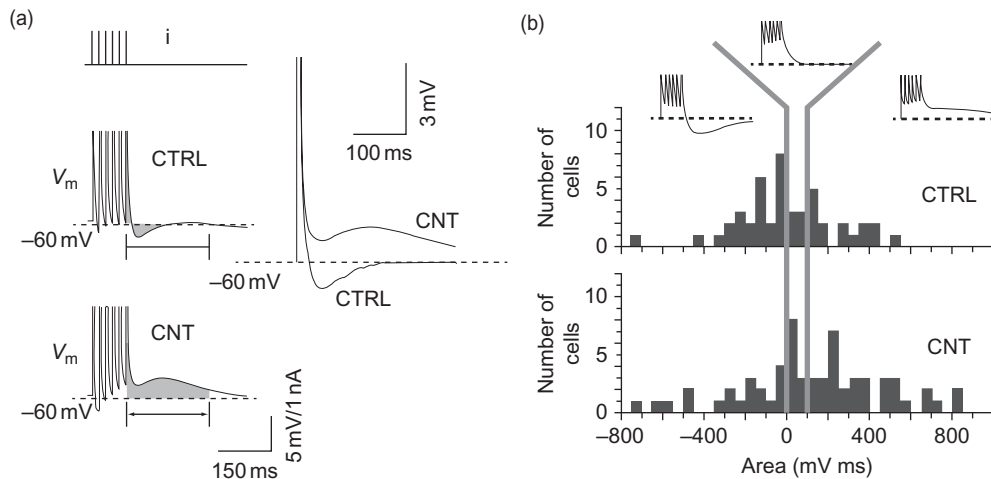


Fig. 3. Carbon nanotubes increase neuronal excitability. (a) hippocampal neurons cultured on glass (CTRL) or on a carbon nanotube (CNT) layer were forced to fire a regular train of six action potentials, to evaluate the presence of an additional hyperpolarization (afterhyperpolarization, AHP) or depolarization (afterdepolarization, ADP; shaded areas) after the last action potential of the train. Control neurons typically showed AHP; conversely, the majority of neurons grown on carbon nanotubes showed a marked ADP. (B) area distributions showing the frequency of occurrence of AHP (left), neutral response (center), or ADP (right). The distribution of carbon nanotube neurons is shifted to the right, indicating an increase in the occurrence of ADP, indicative of enhanced single-cell excitability. Reproduced with permission from [Cellot et al. \(2009\)](#).

emerging network behavior. In the proposed model, they enriched a circuit composed by randomly connected individual neurons with back-propagating action potentials. The resulting electrical activity generated by the modeled circuit showed the occurrence of bursting of synaptic events of prolonged duration, without a clear increase in the frequency of events. This prediction was confirmed by voltage clamp recordings performed on neuronal networks developed on SWCNT substrates ([Cellot et al., 2009](#)).

The molecular mechanisms underlying the generation of back-propagating action potentials in neurons grown on CNTs are still to be elucidated. Nonetheless, focusing on the excellent conductive properties of nanotubes and on their ability to form tight contacts with neuronal membranes, it is tempting to speculate that CNTs are able to facilitate the generation of back-propagating action potentials via promoting a direct electrical shortcut between adjacent compartments on

dendrites, a provocative hypothesis supported by theoretical modeling ([Cellot et al., 2009](#)).

Regardless of the mechanisms involved in CNTs/neurons interactions, it should be considered that back-propagating action potentials have been involved to various extents in the regulation of synaptic short- and long-term plasticity ([Kuczewski et al., 2008](#); [Waters et al., 2005](#); [Zilberter et al., 2005](#)). This issue should probably be explored in future studies, in order to deepen our knowledge of the mechanisms underlying CNTs long-term effects on the activity of neuronal networks.

CNTs as interfaces for neuronal stimulation and recording: improving electrode performance by CNTs

The extraordinary electrical conductivity, surface area, and strength of CNTs make them excellent candidates for interfacing neural systems, in view

of the development of robust and biocompatible neuroprosthetic devices. The fundamental requirements for further miniaturization of electrodes can be significantly improved by CNT coatings, since their high surface area can drastically increase charge injection capacity and decrease the interfacial impedance with neurons (Kotov et al., 2009). The understanding of the potentials linked to CNTs exploitation in neuro-electrode engineering, or to the development of nanotubes/neural interfaces, is far from the complete realization.

The possibility of delivering electrical stimulation to neurons through CNT layers was investigated by several groups (Liopo et al., 2006; Mazzatorta et al., 2007; Wang et al., 2006), which demonstrated that CNTs offer a suitable and efficient interface for the direct stimulation of neuronal cells seeded on the nanotubes themselves. An original approach to this issue is represented by the work of Gheith et al. (2006), who developed a layer-by-layer (LBL) technique to produce CNT films that were used as growing substrates for neurons. Using this LBL approach, the authors were able to stimulate neurons by direct applications of voltage steps to the CNT films, eliciting an extrinsic stimulation to neuronal cells. The authors hypothesized that this stimulation was due to a cation's influx inside the cell. More recently, Cho and Borgens (2010) blended MWCNTs with type IV collagen, and using this blend as substrate for PC12 cells culturing, they reported that the MWCNT/extracellular matrix molecule blend can be employed to electrically stimulate neurons.

A significant advance in the development of CNT/neural interfaces for the recording of neuronal activity was recently made by Keefer et al. (2008), who showed that CNTs coatings decreased electrode impedance and increased charge transfer, paving the way to an extensive and fruitful employment of SWCNTs and MWCNTs in the development of electrophysiological recording and stimulation techniques.

Recently, Lu et al. (2010) tested the suitability of the use of polypyrrole (PPy)/SWCNT films

for nanosurface modifications of electrodes. After showing that PC12 cells grown on PPy/SWCNT-covered ITO surfaces extended longer processes and constructed more complex neurite networks, when compared to control ITO surfaces, the authors studied the consequences of the implantation of PPy/SWCNT-covered Pt devices (where SWCNTs were electrodeposited on the electrodes) in the rat brain and compared it with the noncovered Pt implants. In this experimental model, the authors demonstrated that there was less gliosis and increased neuronal survival around the site of PPy/SWCNT implants, when compared to Pt alone. Even if the authors did not dissect the effects of PPy in itself from those of SWCNTs in itself, in terms of neuronal survival and gliosis, this study paves the way for developing systematic, long-term assessments of CNT-based interfaces on neuronal tissue *in vivo*.

In the last few years, several reports focused on the use of CNTs as nanostructured electrodes for the multisite delivering of electrical stimuli or for the recording of neuronal electrical signals. One of the first works dealing with this issue was that of Gabay and colleagues (2005), who described a novel class of microelectrodes based on high-density CNT islands deposited onto titanium nitride conductor-based chips, with a lithographically defined pattern, where CNT sites served as working electrodes. CNT-based electrodes were fully biocompatible and their enhanced electrochemical properties allowed high-fidelity extracellular recordings of electrical activity of cortical neurons, directly seeded on the electrodes.

One of the first works showing that SWCNTs are able to modify neuronal performance, when employed in the fabrication of recording electrodes was that of Khraiche et al. (2009). The authors cultured rat hippocampal neurons on micro electrode arrays (MEAs) in which several drops of SWCNTs solution were deposited at the tip of gold microelectrodes. The authors observed that the electrical activity of rat hippocampal neuronal networks developed on SWCNTs-modified MEAs was detected as soon

as 4 days after seeding and continued to grow till day 7, while neurons developed on control (bare gold) electrodes showed no electrical activity till day 7. The authors suggested that the increase in surface roughness due to SWCNTs immobilized on the microelectrodes provides cells with a larger surface area to adhere leading to an increase in the activation of adhesion molecules (such as integrins), which might in turn promote a faster neuronal differentiation (Khraiche et al., 2009).

An additional work where CNTs-modified MEAs were shown to significantly improve neuron/electrode interfacing and neuronal recordings is that reported by Shein et al. (2009). The authors coated MEA electrodes with CNTs, obtaining islands with a conductive, three-dimensional, exceptionally high surface area. Dissociated cortical neurons cultured on these arrays adhered only and directly to these islands, and self-assembled in neuronal network patterned on the CNT neurochip. Once the neurons had adhered and self-organized, the CNT-MEA allowed very high fidelity, direct recording of neuronal activity, and an effective electrical stimulation of neurons, at the electrode sites.

Notably, Shoval et al. (2009) took advantage from an analogous MWCNTs-modified MEA and showed the impact of this device on neuronal operation, by recording the activity of whole-mount retinas isolated from the neonatal mouse (Fig. 4a). After minutes from the placement of the retinas on the electrodes, Shoval et al. (2009) could obtain electrical recordings of the spontaneous, typical, propagating retinal waves. When compared to those detected from commercially available electrodes, recordings from MWCNTs-MEAs showed a consistently higher signal-to-noise ratio (Fig. 4b). Moreover, the authors observed a prominent increase in the amplitude of the recorded spikes over a period of minutes to hours. Shoval et al. (2009) proposed that this phenomenon is probably due to an

improvement in cell–electrode coupling, resulting from a dynamic interaction between MWCNTs and neurons. It should not be excluded however, that MWCNTs might have intrinsically modified neuronal network activity, because of their properties (see the section “The biocompatibility of CNT-based substrates and the impact of CNTs on nerve cell signaling”). In the same work, the authors also validated the suitability of their MWCNT electrodes for neuronal stimulation (Shoval et al., 2009).

The advantages of CNT-MEAs over metal electrodes in neuronal recordings were further confirmed by the work of Gabriel et al. (2009). These authors deposited SWCNTs directly on standard platinum electrodes to fabricate MEAs for electrophysiological recordings. In this report, the application of SWCNT-modified MEAs to record electrical activity from whole-mount rabbit retinas allowed a very low noise recording of multiunit activity in comparison with standard, platinum electrode-based MEAs (Gabriel et al., 2009).

The impact of CNTs on neuronal morphology and growth

In the perspective of employing CNT-based scaffolds to support neuronal network formation and to interface neuronal function, the ability of CNTs to promote neuronal attachment and neurite extension and/or branching is highly relevant. Several groups addressed this issue, employing either SWCNTs or MWCNTs, as-prepared or functionalized; alternatively, SWCNTs were even codeposited with (conductive) polymers (PEG, PPy, etc.; Lu et al., 2010; Malarkey et al., 2009; Ni et al., 2005).

The idea that different functionalizations may strongly affect CNT-mediated effects on neuronal morphology and survival (see e.g., Hu et al., 2004; Mattson et al., 2000; Ni et al., 2005) already emerged from these first studies. In their

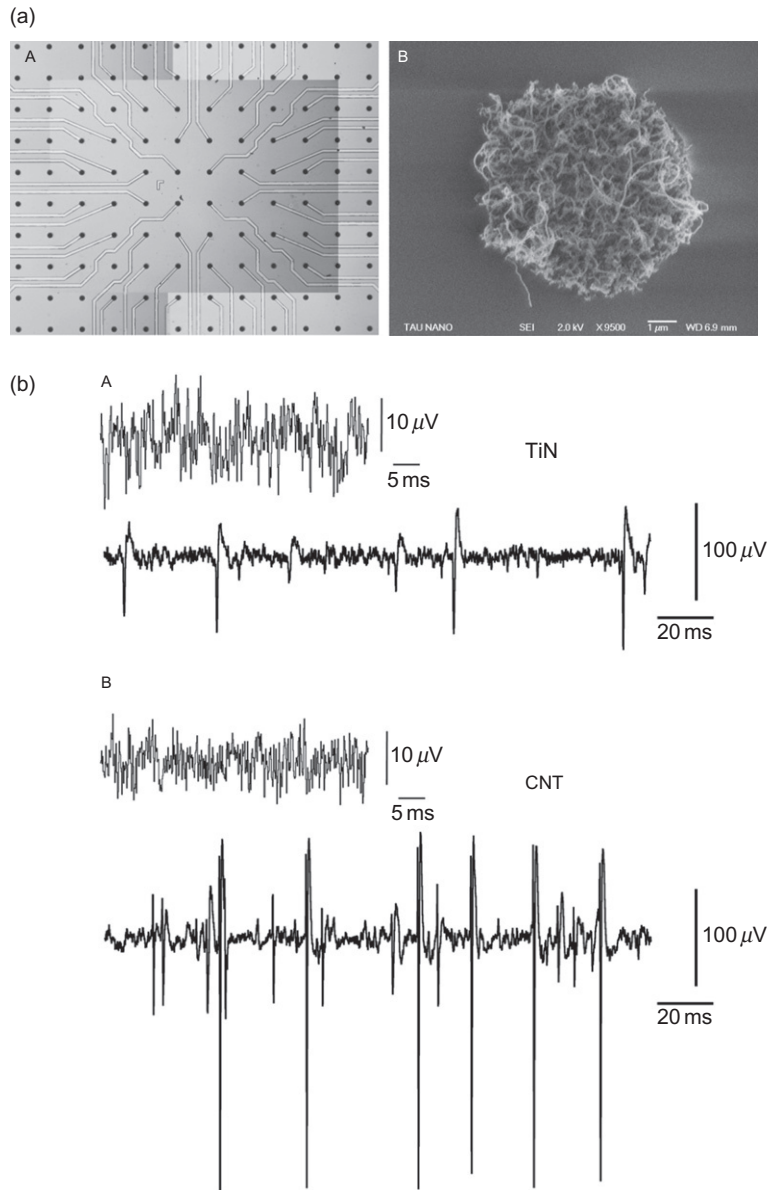


Fig. 4. Application of carbon nanotube-based MEAs for neuronal interfacing and recording. (a) Left, view of a carbon nanotube-MEA. Each of all 60 electrodes in the field ends with a carbon nanotubes island (black dots). Right, micrograph showing the three-dimensional and rough surface of an MWCNT island. (b) Application of the MWCNT-MEA to record neural activity from a whole-mount mouse retina. Top, recordings of spontaneous activity (unfiltered and filtered) with commercial titanium nitride (TiN) electrodes. Bottom, recordings (unfiltered and filtered) obtained with an MWCNT electrode. Note the striking increase in the signal-to-noise ratio. Reproduced from [Shoval et al. \(2009\)](#).

pioneering work, [Mattson et al. \(2000\)](#) showed that neurons grown on MWCNTs functionalized with 4-hydroxynonenal constructed more elaborated neuritic trees, with an increased number of processes, longer neurites, and higher branching occurrence, when compared to neurons grown on unmodified MWCNTs. In 2004, Hu and colleagues tested various functionalized MWCNTs in their ability to affect neuronal morphology. The authors tested at pH 7.35 negatively charged ($-COOH$), neutral (poly-*m*-aminobenzene sulfonic acid: PABS, zwitterionic), and positively charged (ethylenediamine: EN) functionalized MWCNTs, and demonstrated that the processes' average length was higher in neurons grown on positively charged MWCNT-EN and the amount of neurites' branching progressively increased from negatively (MWCNT-COOH) to neutral (MWCNT-PABS) and to positively charged (MWCNT-EN) CNTs.

The issue of the electrical charge and conductivity of SWCNTs as modulatory factors in mediating CNT effects on neuronal outgrowth was explored by [Malarkey et al. \(2009\)](#). These authors produced films of polyethylene glycol (PEG)-functionalized SWCNTs of increasing conductivities (from 0.3 to 42 S/cm) and cultured hippocampal neurons on these different substrates or on polyethylenimine (PEI) as control. They showed that the neurites' lengths and branches per neuron were significantly higher in neurons grown on PEG-SWCNTs with the smallest conductivity (0.3 S/cm) than those grown on PEI substrates (controls) or on PEG-SWCNTs with larger conductivity values.

It is interesting to note, however, the absence of such effects on neuronal morphology, growth, and branching, when using pure, non-functionalized CNTs. This issue was addressed in 2005 by Lovat and colleagues, who reported that the neuronal density of cultured hippocampal neurons seeded on defunctionalized MWCNTs is similar to that of neurons seeded on pure glass and that the number of neurites per neuron was again similar in both culture conditions. Similar

results were obtained by a subsequent study on SWCNTs ([Mazzatorta et al., 2007](#)).

Conclusions

The present review summarizes recent advances in the study of the impact of CNTs on neuronal performance, together with the first, pioneering evidences on the interactions between CNTs and neurons. MWCNT and SWCNT substrates are biocompatible and show the intriguing ability to increase single-cell excitability and spontaneous synaptic activity *in vitro* (thanks to both their conductive and nanostructural properties), suggesting their capacity to reengineer neuronal integrative properties. In addition, CNTs are a promising material for implementing neuronal interfaces and electrodes, to deliver electrical stimuli with improved neuronal-electrode interface contact or to record electrical signals with a remarkably high signal-to-noise ratio. Thanks to these properties, CNTs hold the potential of being used as a next-generation nanomaterial for biomedical applications, particularly in the field of neural prosthesis.

Acknowledgments

Financial support from NEURONANO-NMP4-CT-2006-031847 and CARBONANOBRIDGE-ERC-2008-227135 to L. B. and M. P. is gratefully acknowledged.

Abbreviations

ADP	afterdepolarization
AHP	afterhyperpolarization
CNT	carbon nanotube
CTRL	control
EN	ethylenediamine
ITO	indium tin oxide

LBL	layer-by-layer
MAP-2	microtubule-associated protein 2
MEA	micro electrode array
MWCNTs	multi-walled carbon nanotubes
PABS	poly- <i>m</i> -aminobenzene sulfonic acid
PC12 cells	pheochromocytoma 12 cells
PEG	polyethylene glycol
PEI	polyethylenimine
PPy	polypyrrole
Pt	platinum
SEM	scanning electron microscopy
SWCNTs	single-walled carbon nanotubes
TEM	transmission electron microscopy

References

- Celotto, G., Cilia, E., Cipollone, S., Rancic, V., Sucapane, A., Giordani, S., et al. (2009). Carbon nanotubes might improve neuronal performance by favouring electrical shortcuts. *Nature Nanotechnology*, *4*, 126–133.
- Cho, Y., & Borgens, R. B. (2010). The effect of an electrically conductive carbon nanotube/collagen composite on neurite outgrowth of PC12 cells. *Journal of Biomedical Materials Research. Part A*, *95*, 510–517.
- Gabay, T., Jakobs, E., Ben-Jacob, E., & Hanein, Y. (2005). Engineered self-organization of neural networks using CNT clusters. *Physica A*, *350*, 611–621.
- Gabriel, G., Gómez, R., Bongard, M., Benito, N., Fernández, E., & Villa, R. (2009). Easily made single-walled carbon nanotube surface microelectrodes for neuronal applications. *Biosensors and Bioelectronics*, *24*, 1942–1948.
- Galvan-Garcia, P., Keefer, E. W., Yang, F., Zhang, M., Fang, S., Zakhidov, A. A., et al. (2007). Robust cell migration and neuronal growth on pristine carbon nanotube sheets and yarns. *Journal of Biomaterials Science, Polymer Edition*, *18*, 1245–1261.
- Gheith, M. K., Pappas, T. C., Liopo, A. V., Sinani, V. A., Shim, B. S., Motamed, M., et al. (2006). Stimulation of neural cells by lateral currents in conductive layer-by-layer films of single-walled carbon nanotubes. *Advanced Materials*, *18*, 2975–2979.
- Gheith, M. K., Sinani, V. A., Wicksted, J. P., Matts, R. L., & Kotov, N. A. (2005). Single-walled carbon nanotube poly-electrolyte multilayers and freestanding films as a biocompatible platform for neuroprosthetic implants. *Advanced Materials*, *17*, 2663–2667.
- Gilmore, J. L., Yi, X., Quan, L., & Kabanov, A. V. (2008). Novel nanomaterials for clinical neuroscience. *Journal of Neuroimmune Pharmacology*, *3*, 83–94.
- Hu, H., Ni, Y., Montana, V., Haddon, R. C., & Parpura, V. (2004). Chemically functionalized carbon nanotubes as substrates for neuronal growth. *Nano Letters*, *4*, 507–511.
- Keefer, E. W., Botterman, B. R., Romero, M. I., Rossi, A. F., & Gross, G. W. (2008). Carbon nanotube coating improves neuronal recordings. *Nature Nanotechnology*, *3*, 434–439.
- Khraiche, M., Jackson, N., & Muthuswamy, J. (2009). Early onset of electrical activity in developing neurons cultured on carbon nanotube immobilized microelectrodes. In *The proceedings of the 31st annual international conference of the IEEE Engineering in Medicine and Biology Society*, (pp. 777–780), Minneapolis, Minnesota, USA.
- Kotov, N. A., Winter, J. O., Clements, I. P., Jan, E., Timko, B. P., Campidelli, S., et al. (2009). Nanomaterials for neural interfaces. *Advanced Materials*, *21*, 3970–4004.
- Krishnan, A., Dujardin, E., Ebbesen, T. W., Yianilos, P. N., & Treacy, M. M. J. (1998). Young's modulus of single-walled nanotubes. *Physical Review B*, *58*, 14013–14019.
- Kuczewski, N., Porcher, C., Ferrand, N., Fiorentino, H., Pellegrino, C., Kolarow, R., et al. (2008). Back-propagating action potentials trigger dendritic release of BDNF during spontaneous network activity. *The Journal of Neuroscience*, *28*, 7013–7023.
- Larkum, M. E., Kaiser, K. M., & Sakmann, B. (1999). Calcium electrogenesis in distal apical dendrites of layer 5 pyramidal cells at a critical frequency of back-propagating action potentials. *Proceedings of the National Academy of Sciences of the United States of America*, *96*, 14600–14604.
- Liopo, A. V., Stewart, M. P., Hudson, J., Tour, J. M., & Pappas, T. C. (2006). Biocompatibility of native functionalized single-walled carbon nanotubes for neuronal interface. *Journal of Nanoscience and Nanotechnology*, *6*, 1365–1374.
- Lovat, V., Pantarotto, D., Lagostena, L., Cacciari, B., Grandolfo, M., Righi, M., et al. (2005). Carbon nanotube substrates boost neuronal electrical signaling. *Nano Letters*, *5*, 1107–1110.
- Lu, Y., Li, T., Zhao, X., Li, M., Cao, Y., Yang, H., et al. (2010). Electrodeposited polypyrrole/carbon nanotubes composite films electrodes for neural interfaces. *Biomaterials*, *31*, 5169–5181.
- Malarkey, E. B., Fisher, K. A., Belyarova, E., Liu, W., Haddon, R. C., & Parpura, V. (2009). Conductive single-walled carbon nanotube substrates modulate neuronal growth. *Nano Letters*, *9*, 264–268.
- Mattson, M. P., Haddon, R. C., & Rao, A. M. (2000). Molecular functionalization of carbon nanotubes and use as substrates for neuronal growth. *Journal of Molecular Neuroscience*, *14*, 175–182.
- Mazzatorta, A., Giugliano, M., Campidelli, S., Gambazzi, L., Businaro, L., Markram, H., et al. (2007). Interfacing neurons with carbon nanotubes: Electrical signal transfer and

- synaptic stimulation in cultured brain circuits. *The Journal of Neuroscience*, 27, 6931–6936.
- Nguyen-Vu, T. D. B., Chen, H., Cassell, A. M., Andrews, R., Meyyappan, M., & Li, J. (2006). Vertically aligned carbon nanofiber arrays: An advance toward electrical–neural interfaces. *Small*, 2, 89–94.
- Ni, Y., Hu, H., Malarkey, E. B., Zhao, B., Montana, V., Haddon, R. C., et al. (2005). Chemically functionalized water soluble single-walled carbon nanotubes modulate neurite outgrowth. *Journal of Nanoscience and Nanotechnology*, 10, 707–712.
- Pantarotto, D., Singh, R., McCarthy, D., Erhardt, M., Briand, J. P., Prato, M., et al. (2004). Functionalized carbon nanotubes for plasmid DNA gene delivery. *Angewandte Chemie International Edition in English*, 43, 5242–5246.
- Shein, M., Greenbaum, A., Gabay, T., Sorkin, R., David-Pur, M., Ben-Jacob, E., et al. (2009). Engineered neuronal circuits shaped and interfaced with carbon nanotube microelectrode arrays. *Biomedical Microdevices*, 11, 495–501.
- Shoval, A., Adams, C., David-Pur, M., Shein, M., Hanein, Y., & Sernagor, E. (2009). Carbon nanotube electrodes for effective interfacing with retinal tissue. *Frontiers in Neuroengineering*, 2, 4.
- Sorkin, R., Greenbaum, A., David-Pur, M., Anava, S., Ayali, A., Ben-Jacob, E., et al. (2009). Process entanglement as a neuronal anchorage mechanism to rough surfaces. *Nanotechnology*, 20, 015101.
- Wang, K., Fishman, H. A., Dai, H., & Harris, J. S. (2006). Neural stimulation with a carbon nanotube microelectrode array. *Nano Letters*, 6, 2043–2048.
- Waters, J., Schaefer, A., & Sakmann, B. (2005). Back-propagating action potentials in neurones: Measurement, mechanisms and potential functions. *Progress in Biophysics and Molecular Biology*, 87, 145–170.
- Zilberman, Y., Harkany, T., & Holmgren, C. D. (2005). Dendritic release of retrograde messengers controls synaptic transmission in local neocortical networks. *The Neuroscientist*, 11, 334–344.

CHAPTER 19

Nanomodified surfaces and neurite outgrowth

Martin Kanje* and Fredrik Johansson

Department of Biology, University of Lund, Sölvegatan, LU, Sweden

Abstract: Here we describe our attempts to study the interaction of nanomodified surfaces with neurons and macrophages. Surfaces with nano-sized topographies produced by UV lithography, electrochemical etching, nanoimprint lithography, microdispensing, or by electrospinning of plastic nanofibers or by making plastic replicas of the extracellular matrix with nanoresolution were found to guide neurite outgrowth extending from the dorsal root and the superior cervical ganglion in tissue culture. Ordered arrays of nanowires acted as particularly potent guides for the neurites. Loose nanowires activated the macrophages. We conclude that relatively simple nanomodifications of surfaces can be utilized to guide neurites. This property could potentially be applied to guide neurite outgrowth on implants in the nervous system intended for recordings of electrical and/or chemical activities.

Keywords: nanostructured materials; nerve regeneration; ganglia DRG; neurite electrodes; implants.

Introduction

An overall aim of ours is to produce new types of biocompatible electrodes for chronic implantation, that is, a multiple electrode array (MEA) into the nervous system. This is a formidable task since any implant into the nervous system or elsewhere elicits a foreign body reaction. This reaction includes activation of inflammatory cells like microglia in the central nervous system (CNS) and macrophages in the peripheral nervous system (PNS). The implant is then

embedded either by fibroblasts/giant cells or by astrocytes, processes which result in poor electrode registrations; for review of the responses of brain tissue to electrodes, see Polikov et al. (2005). At present, there is no simple way by which these reactions can be controlled. There are also other demands on a MEA. Such a device intended for implantation in humans and restoration of lost neural functions must survive and function reliable for years. It must be nontoxic allowing the cells around the implant to stay alive. One cannot replace a MEA in the brain very often, thus it must be biosafe. Further, a MEA should have the capability to work bidirectionally, that is, be able to record and stimulate with high spatial and temporal resolution.

*Corresponding author.

Tel.: +46-462-229577/705-329577

E-mail: martinkanje@cob.lu.se

Our basic idea is that nanotechnology offers solutions to some of the challenges associated with the construction of a biocompatible MEA. We assume that it should be possible to use nanomodifications of the implant surface not only to increase the biocompatibility of the implant but also to anchor the implant in the tissue. The latter is important since electrodes which move along with the tissue (untethered ones) seem to give rise to less inflammation than electrodes which are tethered (Biran et al., 2007). Nanotechnology also offers the possibility to achieve very high spatial resolution with extremely small electrodes at high density. Finally, the possibility to use nanomodified surfaces to be able to sort and guide nerve fibers to the electrodes is very attractive. Guidance combined with sorting would allow individual nerve fibers to be addressed, for example, differentiate between motor and sensory fibers, and sensory fibers of different modalities.

In this chapter, we describe our studies on how neurons and macrophages, cells of the innate immune system, interact with nanomodified surfaces.

Methods

In our experimental strategy, we first construct an artificial nanomodified surface using a variety of techniques including UV lithography, electrochemical etching, nanoimprint lithography, microdispensing, and electrospinning, but we also make plastic replicas of the extracellular matrix (ECM) with nanoresolution. We then test how nerve cell processes (neurites) emanating from organ-cultured adult dorsal root ganglia (DRG) or the superior cervical ganglia (SCG) grow and behave on these surfaces. The DRG, removed from adult mouse, contain sensory nerve cell bodies while the SCG is a collection of sympathetic cell bodies. In organ culture, new neurites grow out from the ganglia onto the nanomodified surface. Outgrowth can be stimulated by the

addition of nerve growth factor (NGF) to the culture medium and can be visualized using immunocytochemistry for neurofilaments or beta-tubulin or by ultrastructural methods like scanning electron microscopy (SEM). In parallel experiments, the behavior of isolated intraperitoneal macrophages seeded onto the nanomodified surfaces may be studied. We also implant the nanomodified surfaces under the skin or into the sciatic nerve and then follow tissue regeneration and the foreign body reaction in rats. The experimental setup for evaluation of neurite outgrowth is shown in Fig. 1. The details of the various experimental processes are described elsewhere (Gustavsson et al., 2007; Johansson et al., 2005, 2006, 2008a; Prinz et al., 2008).

Results and discussion

Porous silicon surfaces

Silicon chip surfaces with pores of different sizes can be obtained through electrochemical etching (Johansson et al., 2005, 2008b; Prinz et al., 2008). This procedure increases the surface area dramatically, a property that is advantageous in the context of making efficient electrodes. Figure 2 shows such surfaces.

We tested how neurites grew on silicon chips with pores in the range from 100 to 1500 nm. Pore size proved important for neurite outgrowth. Neurites from DRG neurons stimulated by NGF preferred to grow on silicon with pore sizes in the range of 150–500 nm (Johansson et al., 2005, 2008b). By alternating stripes of smooth and porous silicon, it was also possible to separate neurites (Fig. 3).

Neurites are not the only structures which show reactions to nanopores. Sapelkin et al. (2006), for instance, noted that immortalized hippocampal neurons preferred to adhere to porous silicon over smooth silicon although the pore sizes were smaller (50–100 nm) than ours.

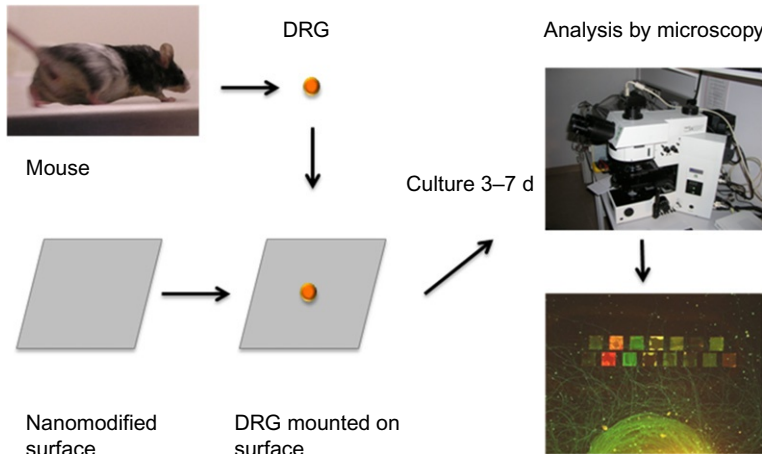


Fig. 1. Experimental setup for neurite regeneration *in vitro*. Mouse ganglia, DRG, or SCG are removed by dissection and mounted on various types of nanomodified surfaces. After 3–7 days, the preparations are fixed and nerve cell processes—neurites—are visualized by immunocytochemistry or investigated by SEM.

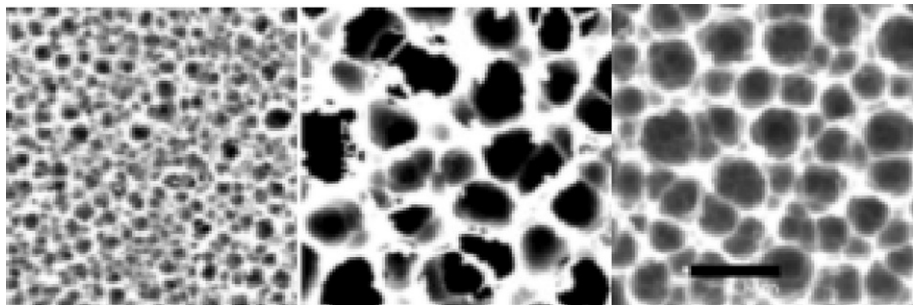


Fig. 2. Porous silicon. The pores were obtained by electrochemical etching of smooth silicon wafers for various periods of time in hydrofluoric acid and dimethylformamide with backside illumination. The diameter of the holes was measured from SEM images (scale bar: 2000 nm).

Ferraz et al. (2010) found that macrophages were activated by aluminum oxide surfaces with pores around 200 nm.

The mechanism by which pore size affects guidance and cell activation remains to be determined, but it should involve rearrangement of the cytoskeleton. Be that as it may, porous silicon seems to be an attractive material for electrode design considering its large surface area and the ease by which it can be doped.

Nanoimprint lithography

We used a silicon master stamp to make patterns in polymethylmethacrylate (PMMA 50) using nanoimprint lithography (Fig. 4; Johansson et al., 2006).

The imprinted pattern was 17 squares measuring $200 \times 200 \mu\text{m}$ containing ridges and grooves of different pitches and widths. DRG neurites aligned along the pattern and exhibited contact

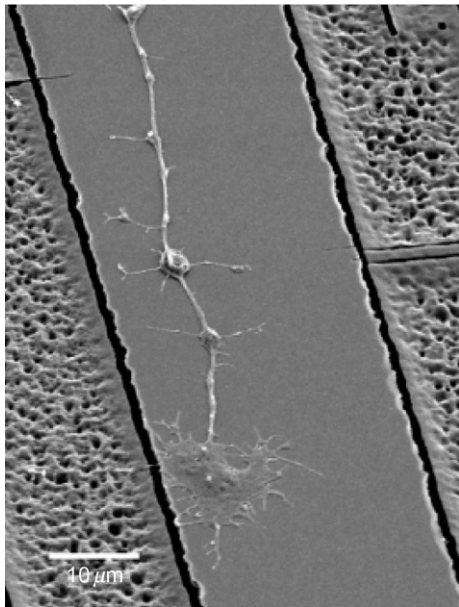


Fig. 3. Neurites on porous silicon. The neurite grows on the smooth silicon and avoids the surrounding silicon surfaces containing large pores. Note the prominent growth cone (SEM picture).

guidance (Fig. 5). The extent of guidance was dependent on neurite size. Small diameter neurites aligned better than did large ones.

The neurites preferred to grow on the edges and elevations. The SCG showed the same alignment and guidance as did the DRG neurites, as evaluated by immunocytochemistry and SEM. Contact guidance was observed very early (Harrison, 1911) in tissue culture. Cells align in scratches at the bottom of tissue culture dishes for instance. The smallest size of the structures which can induce contact guidance is not known. We have found that structures like nanowires with diameters around 50 nm affect guidance and induce the formation of focal adhesions (see below).

Microdispensing

Microdispensed protein patterns represent another type of nanomodifications of a surface. Any type of pattern can be printed and the thickness of the pattern could be one to several protein

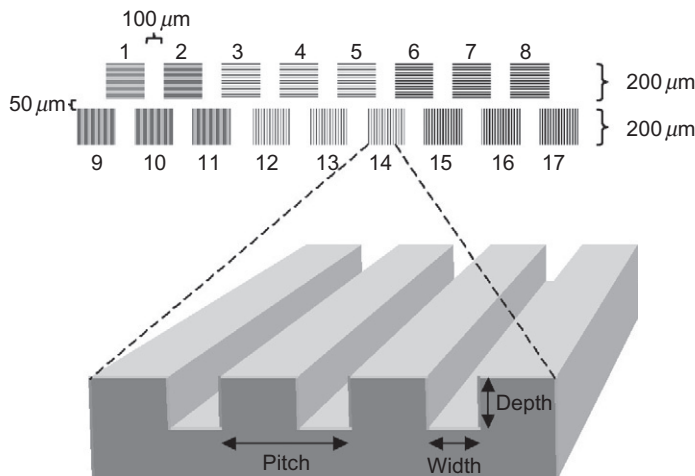


Fig. 4. Nanoimprinted patterns. A silicon master was employed to imprint the pattern into PMMA. The stamp consisted of 17 squares measuring $200 \times 200 \mu\text{m}^2$ with ridges and grooves with various width and pitches. The upper squares have patterns perpendicular to the lower squares in order to rule out any intrinsic orientation of regenerating neurites.

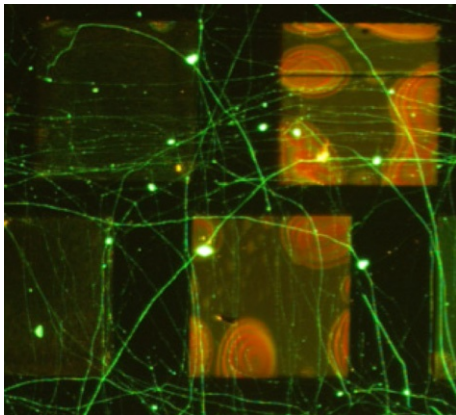


Fig. 5. Neurites grown on nanoimprinted patterns. Fluorescence microscopy. The neurites are green and the imprinted $200 \times 200 \mu\text{m}$ squares are visible. Note how the neurites align on the patterned squares and how they have turned 90° on the squares below. No alignment is observed outside the squares.

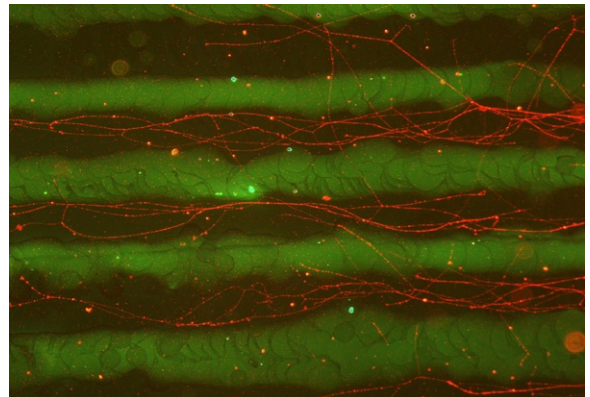


Fig. 6. Microdispensed pattern of bovine serum albumin (BSA). Alternating stripes ($50 \mu\text{m}$ broad) of bovine serum albumin (green) was printed on the bottom of a tissue culture dish. Neurites (red) from a DRG preferred to grow on the uncovered plastic and avoid the BSA territory. It is possible that chemical cues provided by different neurotrophic factors can be used to sort neurons.

layers thick. Drop size, in our case, 100 μl , and the free energy of the substrate determines the minimum resolution of the pattern. We printed protein patterns on tissue culture plastics (polystyrene) using a piezoelectric microdispenser (Gustavsson et al., 2007). Figure 6 shows neurite outgrowth from DRG in a tissue culture dish with microdispensed fluorescent bovine serum albumin in alternating stripes with the uncovered plastic surface. The neurites avoided the albumin. In contrast, when laminin was microdispensed, the neurites preferred to grow on the protein-covered stripes (not shown). Both attractive and inhibitory territories obtained by microdispensing on a MEA surface can thus be utilized for guidance and sorting of neurites. Such cues are utilized by neurons *in vivo* and several proteins which promote or inhibit neurite growth in the CNS are known. Proteoglycans have an inhibitory role as does myelin-associated glycoprotein and Nogo (Fawcett, 2009; Schwab, 2010). Protein-covered surfaces are prone to degradation and the proteins on the surface cannot be easily replenished. Therefore, protein-patterned chips

have a limited lifetime, as compared with more stable nanotopographies, obtained by etching in silicon, although the latter may not be as stable as assumed.

Electrospun fibers

Electrospinning is a very versatile method which can be utilized to spin fibers of nearly any polymers in the nanometer to micrometer range (for review see Teo and Ramakrishna, 2006). The principles of this technique are depicted in Fig. 7. If a DRG is mounted on electrospun fibers of polystyrene, the neurites align along the nanofibers (Fig. 8). At higher magnification, the individual neurites were seen to climb along the polystyrene fibers; in some cases, fascicle-like structures were observed on the fibers.

Electrospinning of thin fibers thus seem to be a very powerful way to guide neurites (Corey et al., 2007).

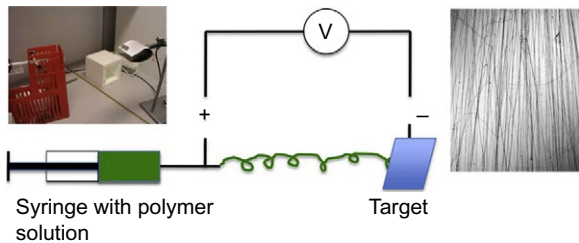


Fig. 7. Electrospinning of nanofibers. By injecting a polymer solution through a syringe into a strong electric field, electrospun fibers can be collected on the cathode. It is possible to control the alignment of the fibers by changing the geometry or dynamics of the cathode. Aligned fibers are shown to the right.

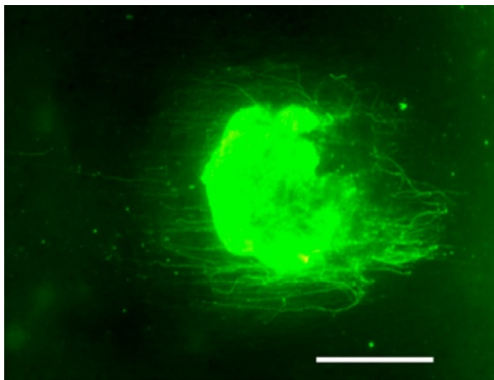


Fig. 8. Dorsal root ganglion on electrospun polystyrene. A DRG was mounted on parallel-aligned nanofibers and allowed to regenerate. The neurites are faithfully aligned along the nanofibers. At higher magnification (not shown), neurites forming fascicle-like structure were found on the electrospun fibers (scale bar: 500 μ m).

Such fibers can also be made into tubes and supplied with trophic factors. Further, they can be made of polymers like poly-L-lactide which is biodegradable *in vivo* and can then release loaded drugs and growth factors. Electrospun structures are also used for tissue reconstruction. The present results and those of others (Bockelmann et al., 2011; Corey et al., 2007) show that electrospun fibers can guide neurite outgrowth. Electrospinning is thus a potential

technique for the construction of new types of electrode surfaces. It is conceivable that electrospun nets or matrixes can also anchor implants.

Nanowires

Ordered arrays of nanowires made of group III-V materials, in our case GaP, are the most powerful guiding elements we have worked with (Hallstrom et al., 2007, 2009, 2010). Such constructions can also be used to measure cell-generated forces in the piconewton range (Hallstrom et al., 2010) by filming the deflection of the nanowires caused by their interaction with neurites or cells. Figure 9 shows such an array of nanowires made of GaP. These wires are around 50 nm in diameter and can be tailored to any height and diameter. Nanowires are potential electrodes and are thus interesting from the point of MEAs but also other aspects are worth consideration like anchoring and the spatial resolution they offer. We have found that neurons can be penetrated by nanowires and survive this ordeal for several days (Hallstrom et al., 2007). Figure 9 shows neurites emanating from a DRG and how they are aligned along the nanowires. Contact between the fibers and the nanowires is associated with the formation of adhesion spots. Based on these findings, it is tempting to suggest that nanowires may play an important role in the development of high-resolution MEAs.

In separate experiments, we have found that cells also can be aligned along magnetically ordered Ni-nanowires (Johansson et al., 2010).

Nanowires at large

The possibility that nanostructures including nanowires may be released from electrodes has been considered. This possibility may pose a threat if the loose wires cause inflammation, which may be detrimental for neurons. Indeed, Eriksson

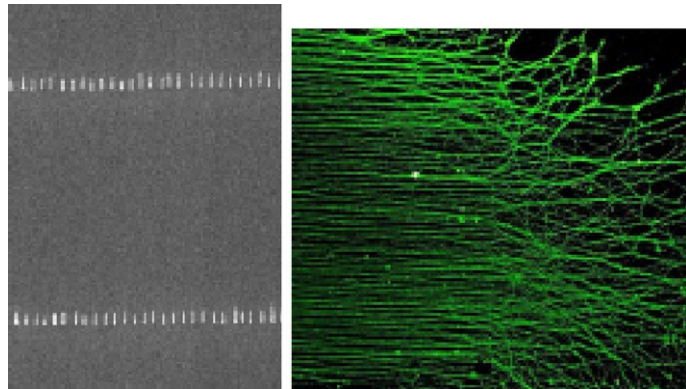


Fig. 9. GaP nanowires. Left, horizontally arranged GaP nanowires. Right neurites (green) from DRG are oriented along the GaP wires but not on the smooth GaP surface (to the right).

[Linsmeier et al. \(2009\)](#), who followed the fate of GaP nanowires injected into the brain, noticed an inflammatory response around the wires. We have studied the effects of free nanowires on cultured peritoneal macrophages. The wires were made of different materials like polystyrene, gold, nickel, and GaP. Exposure of nanowires caused activation of the macrophages *in vitro*. The wires were internalized by the macrophages ([Fig. 10](#)).

Biomimetic surfaces

Most cells are attached to the ECM. We speculated that artificial replicas of natural surfaces with nanometer resolution could be one option to explore for neurite guidance. To this end, we made polystyrene casts, in a two-step procedure, of sciatic nerve sections where only the ECM of the nerve remained ([Sondell et al., 1998](#)). The plastic replicas faithfully reproduced the ECM structure of the nerve section ([Fig. 11](#)). Neurites from the DRG aligned along the ECM structures. We assume that the neurites use the topographical cues provided by the replicas as there are no chemical cues available on the replicas. The replicas are stable and are not affected by proteolytic enzymes as would the ECM master be if

implanted. We obtained proofs of principle for our idea, but much work is required before this technique could be implemented in MEAs.

In vivo

Going from *in vitro* experiments to *in vivo* is a very difficult task. The cells of the innate immune system responsible for the initiation and maintenance of the foreign body reaction are not present *in vitro*. *In vivo* these cells cover the implant and it is not obvious that regenerating neurites come in contact with the MEA surface. To this end, we have investigated what happens if a porous chip is implanted into the severed sciatic nerve of the rat. A rectangular silicon chip, porous on one side and smooth on the other, was inserted into a tube which joined the proximal and distal ends of the cut sciatic nerve. The nerve was allowed to regenerate and two new nerve structures formed in the tube one on each side of the chip. The nerve structure on the smooth side had a thicker capsule on the side facing the tube than that on the porous side ([Johansson et al., 2009](#)). We hypothesize that this is due to the anchoring effect of the porous silicon resulting in less movement and against the tube

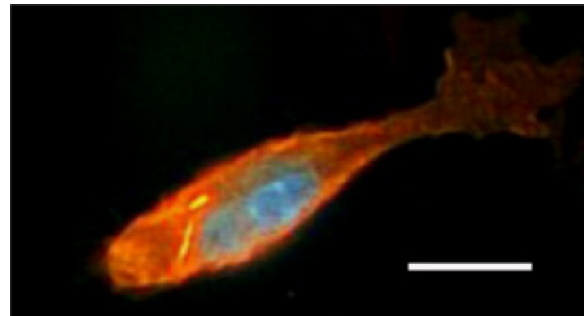


Fig. 10. A macrophage with internalized nanowires. Mouse peritoneal macrophages were exposed to fluorescently labeled polystyrene nanowires (yellow–orange). The wires were endocytosed by the cells. The nucleus (blue) is stained by bisbenzimide (scale bar: 5 μm).

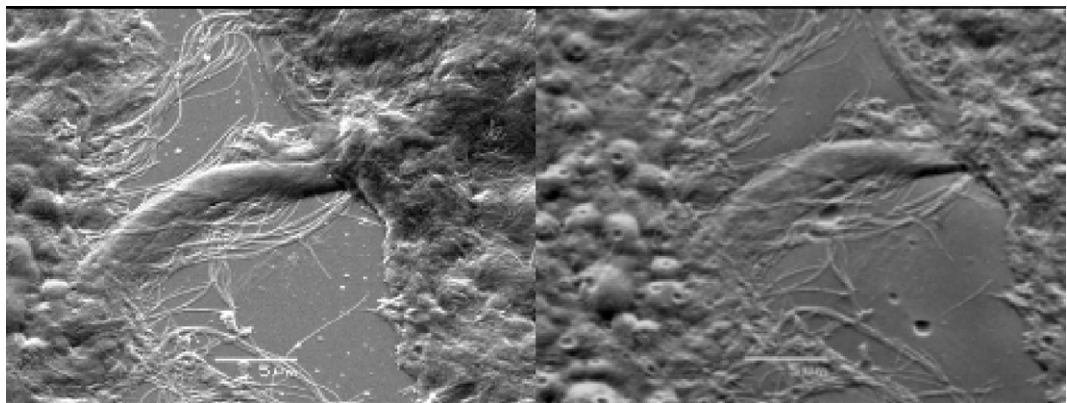


Fig. 11. Replica of the ECM of an extracted section of the sciatic nerve. The picture to the left shows the original preparation and that to the right the polystyrene replica. The treads are nanometer thick collagen fibers.

wall and therefore less inflammation than on the smooth side. The anchoring structures are shown in Fig. 12.

Conclusions

Fairly simple nanomodifications of surfaces can be used for guidance and sorting of nerve fibers–neurites *in vitro*. This includes topographical modifications and cues provided by grooves and ridges, aligned nanowires, and biomimetic

replicas of biosurfaces. Chemical cues like basal lamina components and neurotrophic factors on surfaces can also be utilized albeit such surfaces are less stable. In combination with recording devices, nanomodifications of MEA surfaces could be utilized to guide and sort neurites before they make contacts with sensors. *In vivo* implantation of a nanomodified surface (porous silicon) showed less of an inflammatory response probably due to an improved anchoring of the implant. Here, the innate immune system and the foreign body reaction are hard obstacles to overcome.

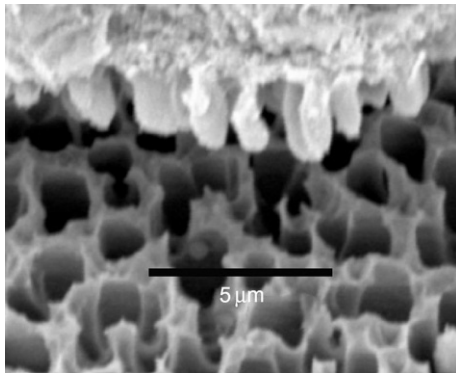


Fig. 12. Porous silicon surface after implantation *in vivo*. A new nerve surrounded by a capsule (perineurium?) has formed between the tube wall and the porous silicon side of the silicon chip. Note the nipple-like structures facing the porous silicon. These structures act as anchors.

Still, our initial assumption that nanotechnology offers solution to several of the challenges posed by the construction of high-resolution MEAs was substantiated by the presented findings.

Acknowledgment

The present studies were supported by grants from The Swedish Research Council 60012701, Knut and Alice Wallenberg's foundation 2004.011, and Crafoord foundation.

References

- Biran, R., Martin, D. C., & Tresco, P. A. (2007). The brain tissue response to implanted silicon microelectrode arrays is increased when the device is tethered to the skull. *Journal of Biomedical Materials Research. Part A*, 82, 169–178.
- Bockelmann, J., Klinkhammer, K., von Holst, A., Seiler, N., Faissner, A., Brook, G. A., et al. (2011). Functionalization of electrospun poly(epsilon-caprolactone) fibers with the extracellular matrix-derived peptide GRGDS improves guidance of Schwann cell migration and axonal growth. *Tissue Engineering. Part A*, 17, 475–486.
- Corey, J. M., Lin, D. Y., Mycek, K. B., Chen, Q., Samuel, S., Feldman, E. L., et al. (2007). Aligned electrospun nanofibers specify the direction of dorsal root ganglia neurite growth. *Journal of Biomedical Materials Research. Part A*, 83, 636–645.
- Eriksson Linsmeier, C., Prinz, C. N., Pettersson, L. M., Caroff, P., Samuelson, L., Schouenborg, J., et al. (2009). Nanowire biocompatibility in the brain—Looking for a needle in a 3D stack. *Nano Letters*, 9, 4184–4190.
- Fawcett, J. (2009). Molecular control of brain plasticity and repair. *Progress in Brain Research*, 175, 501–509.
- Ferraz, N., Hong, J., Santin, M., & Karlsson Ott, M. (2010). Nanoporosity of alumina surfaces induces different patterns of activation in adhering monocytes/macrophages. *International Journal of Biomaterials*, 2010, 402715.
- Gustavsson, P., Johansson, F., Kanje, M., Wallman, L., & Linsmeier, C. E. (2007). Neurite guidance on protein micro-patterns generated by a piezoelectric microdispenser. *Biomaterials*, 28, 1141–1151.
- Hallstrom, W., Lexholm, M., Suyatin, D. B., Hammarin, G., Hessman, D., Samuelson, L., et al. (2010). Fifteen-piconewton force detection from neural growth cones using nanowire arrays. *Nano Letters*, 10, 782–787.
- Hallstrom, W., Martensson, T., Prinz, C., Gustavsson, P., Montelius, L., Samuelson, L., et al. (2007). Gallium phosphide nanowires as a substrate for cultured neurons. *Nano Letters*, 7, 2960–2965.
- Hallstrom, W., Prinz, C. N., Suyatin, D., Samuelson, L., Montelius, L., & Kanje, M. (2009). Rectifying and sorting of regenerating axons by free-standing nanowire patterns: A highway for nerve fibers. *Langmuir*, 25, 4343–4346.
- Harrison, R. G. (1911). On the stereotropism of embryonic cells. *Science*, 34, 279–281.
- Johansson, F., Carlberg, P., Danielsen, N., Montelius, L., & Kanje, M. (2006). Axonal outgrowth on nano-imprinted patterns. *Biomaterials*, 27, 1251–1258.
- Johansson, F., Hallstrom, W., Gustavsson, P., Wallman, L., Prinz, C., Montelius, L., et al. (2008a). Nanomodified surfaces and guidance of nerve cell processes. *Journal of Vacuum Science & Technology B*, 26, 2558–2561.
- Johansson, F., Jonsson, M., Alm, K., & Kanje, M. (2010). Cell guidance by magnetic nanowires. *Experimental Cell Research*, 316, 688–694.
- Johansson, F., Kanje, M., Eriksson, C., & Wallman, L. (2005). Guidance of neurons on porous patterned silicon: Is pore size important? *Physica Status Solidi C*, 2, 3258–3262.
- Johansson, F., Kanje, M., Linsmeier, C. E., & Wallman, L. (2008b). The influence of porous silicon on axonal outgrowth *in vitro*. *IEEE Transactions on Biomedical Engineering*, 55, 1447–1449.
- Johansson, F., Wallman, L., Danielsen, N., Schouenborg, J., & Kanje, M. (2009). Porous silicon as a potential electrode material in a nerve repair setting: Tissue reactions. *Acta Biomaterialia*, 5, 2230–2237.

- Polikov, V. S., Tresco, P. A., & Reichert, W. M. (2005). Response of brain tissue to chronically implanted neural electrodes. *Journal of Neuroscience Methods*, 148, 1–18.
- Prinz, C., Hallstrom, W., Martensson, T., Samuelson, L., Montelius, L., & Kanje, M. (2008). Axonal guidance on patterned free-standing nanowire surfaces. *Nanotechnology*, 19, 345101.
- Sapelkin, A. V., Bayliss, S. C., Unal, B., & Charalambou, A. (2006). Interaction of B50 rat hippocampal cells with stain-etched porous silicon. *Biomaterials*, 27, 842–846.
- Schwab, M. (2010). Functions of the Nogo proteins and their receptors in the nervous system. *Nature Reviews Neuroscience*, 11, 799–811.
- Sondell, M., Lundborg, G., & Kanje, M. (1998). Regeneration of the rat sciatic nerve into allografts made acellular through chemical extraction. *Brain Research*, 795, 44–54.
- Teo, W. E., & Ramakrishna, S. (2006). A review on electrospinning design and nanofibre assemblies. *Nanotechnology*, 17, R89–R106.

CHAPTER 20

Direct local polymerization of poly(3,4-ethylenedioxothiophene) in rat cortex

Liangqi Ouyang[†], Rylie Green[‡], Kathleen E. Feldman[†] and David C. Martin^{†,*}

[†] Department of Materials Science and Engineering, The University of Delaware, Newark, DE, USA

[‡] Graduate School of Biomedical Engineering, University of New South Wales, Sydney, NSW, Australia

Abstract: Glial scar encapsulation is thought to be one of the major reasons for the failure of chronic brain-machine interfaces. Many strategies, including modification of the probe surface chemistry, delivery of anti-inflammatory drugs, and changes of probe geometry, have been employed to reduce glial scar formation. We have proposed that a possible means to establish long-term, reliable communication across the scar is the *in situ* polymerization of conjugated polymers such as PEDOT in neural tissue. Previously, we exposed entire brain slices to the EDOT monomer. Here, we demonstrate that PEDOT can be polymerized by the direct delivery of EDOT monomer to the reaction site. The monomer was delivered into rat cortex via microcannula and simultaneously electrochemically polymerized within the tissue using a microwire electrode. We found that the resulting PEDOT polymer cloud grew out from the working electrode tip and extended far out into the brain tissue, spanning distances more than 1 mm. We also examined the morphology of resulting polymer cloud by optical microscopy.

Keywords: cortical electrodes; biocompatibility; conjugated polymers; biointegration; electrochemical polymerization.

Introduction

Long-term implantation of neural probes in the brain is accompanied by a chronic foreign body reaction (Polikov et al., 2005), which is associated with increased system impedance (Lempka et al., 2009) and the deterioration of signal recording

quality (Ludwig et al., 2006; Schwartz, 2004). In cortex, the characteristic inflammatory reaction involves the formation of an insulating glial scar encapsulating the electrode (Biran et al., 2005; Turner et al., 1999) as well as the activation of microglia and macrophages proximal to the implant surface (Menei et al., 1994; Szarowski et al., 2003), presumably prohibiting the regeneration of neural axons (Fawcett and Asher, 1999). Thus, the encapsulation of electrodes, combined with the “kill zone” created by initial

*Corresponding author.
Tel: (302) 831-2062
E-mail: miltv@udel.edu

mechanical insertion of electrodes and the persistent strains at the interface between rigid, implanted devices in soft, living tissue (Edell et al., 1992; Polikov et al., 2005), is likely the major contributors to the reduction of neuronal cells around recording site (Liu et al., 1999; Winslow and Tresco, 2010). Hence, there have been continued issues associated with obtaining reliable, sensitive, chronic cortical recordings.

Many strategies have been employed to address these problems. One common method is to modify the probe surface with a relatively thin film in order to improve its biocompatibility: for example, growing conducting polymers on hydrogel-coated probes (Kim et al., 2004), electrochemically depositing conducting polymers and peptides on the probe (Cui et al., 2003; Green et al., 2009), immobilizing neural cell adhesion molecules such as L1 on probes (Azemi et al., 2010), or coating the probe surfaces with laminin (He et al., 2006). Another approach is to load the electrodes with anti-inflammatory drugs such as the peptide alpha-melanocyte stimulating hormone (alpha-MSH) (Zhong and Bellamkonda, 2005) or dexamethasone (Abidian et al., 2006; Kim and Martin, 2006). Also, dramatically changing the electrode geometry has been shown to be capable of reducing glial sheath formation (Seymour and Kipke, 2007).

Recently, our lab has investigated an *in situ* approach that has the potential to effectively bring the electrode out to the neural cells beyond the glial scar. In this approach, we have directly polymerized poly(3,4-ethylenedioxythiophene) (PEDOT), a conjugated, inherently conducting polymer, within living tissue. Our *in vitro* experiments showed that the neural cells could maintain 80% cell viability even after 24 h of exposure to 0.01 M EDOT monomer solution. Polymerizations could be done much more quickly than this (\sim 30 min), making it possible to encapsulate the cells in PEDOT while they were still viable. After polymerization, the cultured cells were embedded in the polymer matrix and remained viable for at least the next 120 h. The cells could then be removed from the polymer matrix. The resulting conducting

polymer substrate had a cell-shaped topology that can itself serve as an interesting template for neural regeneration (Richardson-Burns et al., 2007a). For the *in vivo* tests, rat brains were sliced and soaked in the monomer solution before polymerization. The direct polymerization of PEDOT in the brain tissue produced a dark PEDOT polymer cloud that grew for large distances (500 μm –1 mm or more) into the living tissue, more than sufficient to cross the glial scar sheath. The PEDOT filaments grew around the cells in the extracellular matrix, leaving the neuronal cells themselves intact. As the deposition charge increased, the PEDOT cloud also became darker. Electrical measurements showed that the formation of PEDOT significantly decreased the impedance and phase angle of the gold electrode, presumably because it leads to a large effective surface for efficient charge exchange between the ionically conducting neural cells and the electrically conducting metallic substrate (Richardson-Burns et al., 2007b).

In this chapter, the *in situ* approach was extended to allow simultaneous local monomer delivery and electrochemical deposition of the polymer. Our approach uses a microcannula with a microwire electrode attached on each side facilitating local delivery of the monomer solution while directly polymerizing PEDOT in the living tissue. Both formaldehyde-fixed brain tissue and recently extracted living rat brains were used as models to test the feasibility of this system. Additionally, the morphology of resulting PEDOT polymer cloud was examined.

Materials and methods

C315G-MS303/2/SP Simultaneous Electrode-Guide combinations were purchased from PlasticsOne[®] (Virginia, USA). Both the adjacent microelectrodes and microcannula were stainless steel. The electrodes had a diameter of 230 μm and the cannula guide was 26 gauge (with an inside diameter of 200 μm).

Monomer solution of 0.01 M EDOT was prepared by dissolving 21.4 μ L EDOT (Bayer) in 20 mL 1 \times PBS solution which served as both the dopant (through dissociated Cl⁻ ions) and the solvent.

Adult rat brains were provided by Dr. Amy Griffin's lab in the Department of Psychology at the University of Delaware. The preserved tissue was supplied following fixation in formalin. Prior to polymerization, the tissue was immersed into PBS solution for 15–30 min. During the polymerization, the tissue was mechanically stabilized in 1% gelatin. The insertion depth of electrodes in the brain tissue was kept constant at 1 mm.

Galvanostatic electrochemical polymerization of PEDOT in the brain tissue was carried out in 0.01 M EDOT PBS solution at a constant current of 0.01 mA (corresponding to 5.38 mA/cm²) generated by an Autolab Potentiostat/Galvanostat PGSTAT12 (Metrohm Autolab B.V., The Netherlands). The deposition time was varied from 10 min up to 1 h. Before the polymerization, EDOT monomer solution was delivered into the brain at 0.2 μ L/min for 30 min. The delivery rate was controlled by a Genie Plus syringe pump (Kent Scientific Corporation, Connecticut, USA). The flow of the solution was continued throughout the electrochemical polymerization. For the negative control group, PBS solution instead of EDOT solution was injected at the same rate. After 30 min of injection, the constant current was applied.

Positive controls were performed by depositing PEDOT on bare electrodes under potentiostatic conditions. Stainless steel electrodes were immersed in 0.01 M EDOT PBS solution, and a constant voltage of 1.2 V (vs. Ag/AgCl) was then applied. The depositions were performed for 10 min, and after deposition, the electrodes were taken out, washed with DI water, and dried at room temperature.

The working electrodes, controls, and positive controls were examined by cyclic voltammetry. Typically, the electrodes have been extracted from the tissue, rinsed with water, and dried at

room temperature, and then placed into phosphate buffered saline (PBS) solution for cyclic voltammetry (CV) tests. CV was performed on the same Autolab system with a platinum counter electrode and a saturated calomel reference electrode. Cycling was performed between -1 and +1 V with a scan rate of 0.1 V/s.

The brain tissue was sectioned into 40- μ m-thick slices (courtesy of Henry Hallock and Arun Asok from the Department of Psychology at the University of Delaware). Optical micrographs were taken on a Nikon Optiphot 2-POL optical microscope (Nikon Corporation, Tokyo, Japan) equipped with SPOT RT digital color camera using Spotv 3.2 software on a Dell PC. All the other pictures were taken on a Canon EOS 30D camera.

Results and discussion

We have previously described the *in situ* polymerization of PEDOT in living neural cell culture, where 3,4-ethylenedioxythiophene (EDOT) was delivered to the entire slice at one time (Richardson-Burns et al., 2007a,b). Here, we used the PlasticsOne® C315G-MS303/2/SP Simultaneous Electrode-Guide combinations as our local monomer delivery/electrochemical deposition system. As shown in Fig. 1, this is a guide cannula with an electrode attached on each side. An internal microcannula can be inserted through the

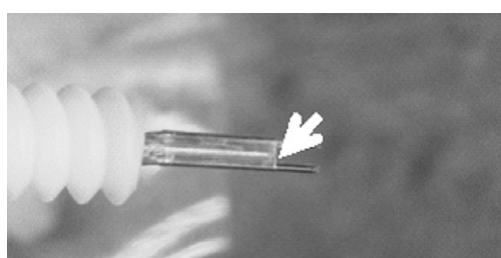


Fig. 1. Photo of a PlasticsOne® C315G-MS303/2/SP Simultaneous Electrode-Guide combination. The cannula guide is between the electrodes (red arrow).

guide cannula with adjustable insertion depth. Both plastic and metal internal cannulae are commercially available from PlasticsOne®. Initially, it was thought that the metal cannulae might interfere with the working electrode during electrochemical polymerization and electrical characterization. However, as the cannula was well isolated, it did not appear to have an effect on the depositions when compared to custom-made plastic cannulae, which were more difficult to handle than metal ones due to their high flexibility.

The EDOT monomer solution was delivered through the cannula at a constant flow rate controlled by a syringe pump. Ideally, the EDOT monomer delivery rate should be equal to the polymerization rate, such that no unreacted EDOT monomer remains in the tissue. As such, at the electrode/tissue interface, it would be desirable to have:

$$j_m = j_e \quad (1)$$

where j_m is the monomer delivery rate, and j_e is the electrochemical polymerization rate. Here, j_m is the product of Q_m and C , where Q_m is the total solution delivery rate (g/s, controlled by syringe pump), and C is the fractional concentration (controlled by mixing). The j_e is equal to $Q_c E_w / F$, where Q_c is the total current delivery rate (C/s, controlled by the AutoLab), E_w is the equivalent weight of monomer and dopant deposited per unit charge (g/C), and F is Faraday's constant (C/mol).

In order to understand the diffusion behavior of aqueous solutions through cortical tissue, colored food dye was delivered at a constant rate into agarose gels. The transparent 0.6 wt% agarose gel was chosen to mimic the tissue (Chen et al., 2004). As expected, at relatively low delivery rates (0.1–0.2 µL/min), the food color evenly and smoothly diffused into the gel matrix without causing any bubbling and cracking as depicted in Fig. 2. Interestingly, the color has a visibly higher diffusion rate back along the insertion tract demonstrating that this is the path of least

resistance rather than the desired path into the gel matrix. Thus, the fluid cloud dispersed in greater volume along the sides of the cannula than through the gel tissue model. Considering that the electrodes are on the flanks of the cannula, the diffusion toward the sides of the cannula may actually help the localized polymerization.

The brain tissue models we used were formaldehyde-fixed adult rat brains. The brain tissue was physically stabilized in gelatin gel (1 wt% in phosphate buffered saline, PBS; Fig. 3a). In order to electrochemically polymerize PEDOT on the working electrode, EDOT monomer needs to be within the interfacial region of the electrode. Cyclic voltammograms were used to estimate the optimal delivery time, indicated by an increase in tissue conductivity and charge storage capacity. The polymerization was done under galvanostatic conditions (~5.8 mA/cm²). At a delivery rate of 0.2 µL/min, it took approximately 30 min for the monomer solution to diffuse to the vicinity of the electrodes. As a result, EDOT monomer solution was delivered at 0.2 µL/min for 30 min prior to electrochemical polymerization. This equals a cumulative volume of 6 µL of solution and 60 nmols of EDOT monomer. As estimated by Noel et al. (2000), 2.3 electrons per EDOT monomer are required for polymerization, subsequently 13.3 mC are needed for the polymerization of 60 nmol EDOT. However, as the polymerization is unlikely to be 100% efficient throughout the deposition, more monomer was delivered at the same rate (0.2 µL/min).

The first evidence of successful polymerization was the appearance of a dark grayish-blue cloud at the insertion site (Fig. 3c, red arrow) while nothing was apparent in the PBS control group. A layer of dark polymer was also found at the end of the working electrode. To understand the morphology of polymer cloud growth, multiple depositions were carried out with increasing total charge passed, to produce a series of polymer clouds of increasing size in the same brain model. Three deposition charges, 6, 12, and 18 mC were used, and as predicted, the area of dark cloud

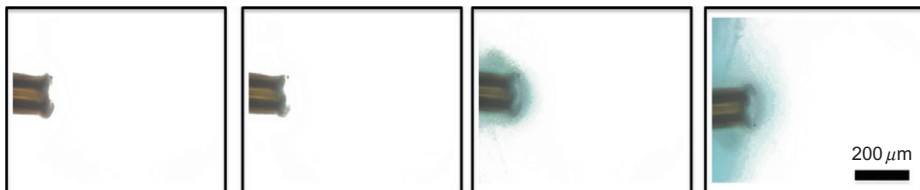


Fig. 2. Diffusion of blue food color dye in 0.6 wt% agarose gel. The food color was delivered at a rate of $0.2 \mu\text{L}/\text{min}$. Every frame represents 120 s.

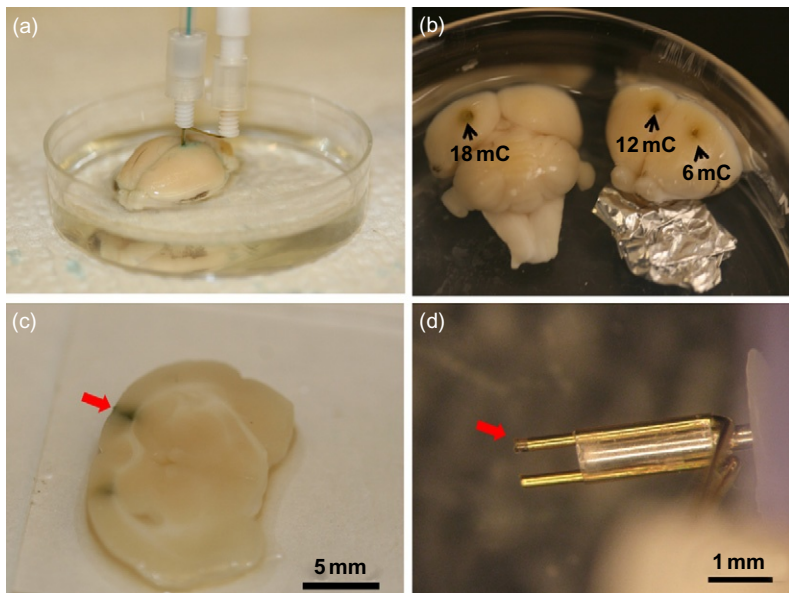


Fig. 3. Direct polymerization of PEDOT in rat brain. (a) An image of setup. The cannula was delivering food dye into the brain. Flanking the cannula are the working electrode and counter/reference electrode. (b) A rat brain (coronally sectioned into two parts, anterior and posterior) within which three PEDOT clouds were formed. The deposition charges were 6, 12, and 18 mC respectively. (c) A coronal section of another rat brain with PEDOT cloud in it (red arrow). This time, the polymer was deposited by applying constant voltage (2 V) for 20 min (about 18 mC of charge). All the other parameters are the same with the depositions in (b). The greenish cloud grew into the brain tissue, and the color spread around the cortex, while at the end of the electrode tip it appeared most dense. (d) PEDOT also formed on the working electrode tip (red arrow).

was also found to increase (Fig. 3b). The cloud morphology was similar in appearance for all depositions, being dense toward the center of working electrode, and then appearing more

diffuse as the polymer extended into the tissue. Coronal sections of the tissue show that the morphology of the polymer cloud was not a uniform sphere (Fig. 3c, red arrow). The color appeared

denser along the insertion tract, which is understandable: the flow was shown to have a higher diffusion rate along the insertion site. The electrode tip, where the polymerization started, thus had highest polymer density, which then decreased toward the cloud extremities as it became more and more difficult for the monomers to get close to the polymerizing center. It is hypothesized that the formation of the polymer itself may also hinder local mass transport, making this system somewhat self-limiting. The net result is that the polymer appeared to be spreading from the deposition site outward into the surrounding tissue. It is also worth noting that the brain itself is heterogeneous and anisotropic: the white matter is denser than the cortex and even the cortex can also be divided into different layers (Sykova and Nicholson, 2008). Further, the mass diffusion is much faster in the cortex, which also helps explain why there was little polymer that spread into the white matter.

In order to examine if the deposition on the working electrode tip (Fig. 3d) was PEDOT, the working electrode was extracted, and its CV was tested in PBS. Also, the control electrode, which was prepared by delivering 6 μ L of PBS followed by 6 mC of charge deposition on an electrode *in vivo*, and a positive control which had already been coated with PEDOT, were tested under the same CV condition. Following polymer deposition, a characteristic PEDOT oxidation peak appeared near -0.07 V (Fig. 4b, red arrow) which concurs with data presented in the literature (Groenendaal et al., 2003) as well as a reduction peak near -0.45 V. The positive control, stainless steel electrode coated with PEDOT showed the E^{ox} and E^{re} at -0.07 and -0.25 V (Fig. 4d, black arrows). However, the CV of the control group (Fig. 4a) was shown to have similar shape to the bare stainless steel electrode (Fig. 4c).

In order to understand the distribution of PEDOT in the brain tissue, PEDOT was polymerized in another fixed rat brain with a relatively larger amount of charge (36 mC, 0.01 mA

of constant current for 1 h). The brain tissue was then sectioned into 40 μ m thick slices. Optical micrographs (Fig. 5a,b) show that PEDOT formed filaments in the brain tissue. The polymer distribution was highly asymmetric: it formed a crescent-shaped dense contour near the cannula insertion site (Fig. 5a, red arrow), while away from the cannula, the polymer filaments gradually spread toward the surface of the cortex. Although the mechanisms leading to this shape are not yet well understood, it is proposed that this may be a result of the higher diffusion rate of the monomer solution along the insertion tracts rather than into the matrix. Also, considering the 1 mm insertion depth into the brain, it is thought that the cannula is close to the white matter, which is much more dense than the cortex. As such, the monomer flow may have a greater tendency than presented by the gel models to travel back along the insertion tract and thereafter diffuse into the cortex. The net result was that, around the cannula wall (insertion tract), there was always higher concentration of monomer. As such, when the rate of polymerization is significantly higher than the diffusion rate, polymerization will consume all the available monomer not long after the polymerization initiation. As a result, the polymerization process will change the existing monomer concentration gradient. Although initially the concentration is greater near the cannula insertion site and more diffuse away from the cannula, during the polymerization, the monomer being delivered via the cannula is driven by the concentration gradient toward the working electrode. However, once a given amount of EDOT is polymerized and the interstitial space is filled with PEDOT, more EDOT is not able to diffuse deeper into the tissue area (due to mass transport limitation.) Thus, the newly formed polymers were all accumulated on the initial crescent-shaped area, making it increasingly dense with time. In previous literature, PEDOT was directly polymerized in mouse brain slices that had been soaked into or injected with EDOT monomer (Richardson-Burns et al.,

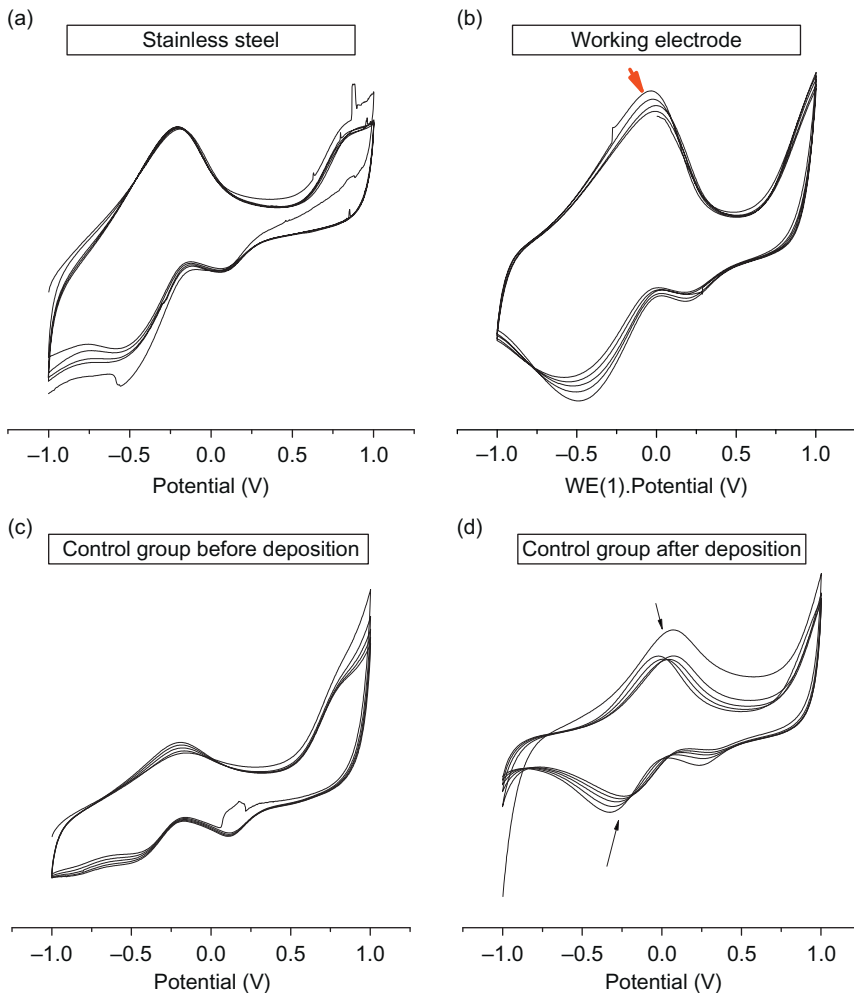


Fig. 4. (a) CV of a stainless steel electrode control (after 6 μ L of PBS solution injection followed by 12 mC deposition), (b) CV of a working electrode after localized deposition, (c) CV of a bare electrode, (d) CV of a PEDOT coated electrode. All the tests were performed in PBS solution, 0.1 V/s and five cycles.

2007a). The resulting polymer cloud was nearly spherical but had a dense outer contour. This dense contour concurs with the current finding that once the polymerization process consumed all the available monomers, the concentration gradients drove free monomers in other areas of the tissue toward the electrode, and on the surface of existing polymer cloud, these monomers

were polymerized and accumulated. By adjusting current density, we may be able to control the polymerization rate and obtain a more uniform polymer cloud.

Many voids appeared in the PEDOT cloud, while outside of the cloud, the tissue structure was more intact. As this deposition was done at extreme condition (36 mC of total charge), during

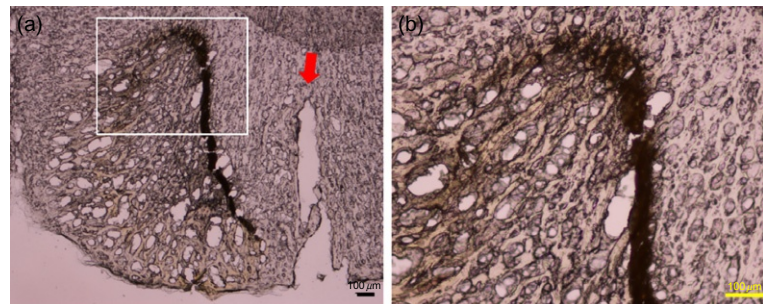


Fig. 5. Optical micrograph of a 40- μm -thick brain slice in which PEDOT was directly deposited. (a) thick crescent-shaped cloud of PEDOT polymer filaments formed in the rat cortex. The red arrow indicates the cannula insertion site. The electrode traces are not shown in this slice. (b) Higher magnification of the polymer cloud.

the deposition, the potential often went to as high as 2–3 V, well above the water window. It is thus likely that gas bubbles were formed during the deposition. These voids were not observed in cell culture (Richardson-Burns et al., 2007a) or living tissue depositions (Richardson-Burns et al., 2007b). It should also be pointed out that after fixation, the cells lost their elasticity and the space between them is reduced; thus, this model is more prone to being damaged by the strain caused by asymmetric polymerization.

Conclusions

In this chapter, we demonstrated the direct polymerization of PEDOT in rat brain tissue with a simultaneous delivery system. Results showed that PEDOT polymer clouds could be formed within the tissue and the size of the clouds are related to the charge applied. With more charge, a larger polymer cloud was observed. However, the shapes were not consistent. As the polymer is presumably deposited in the extracellular spaces, the mass transport and diffusion will also determinate the morphology of polymer clouds. It is necessary to limit the charge density at a certain range, so that the electrode and the tissue can be well preserved. Detailed relationship between

current density, polymerization rate, and mass diffusion will be studied on fresh brain tissue. In the future, we are going to further investigate the diffusion of monomer and the electrical properties of PEDOT clouds in living tissue. Besides PEDOT, other conducting polymers, especially bioinspired melanin derivatives, will also be investigated.

Acknowledgments

The authors gratefully acknowledge the contributions of Norman Meznarich, a graduate student in Materials Science and Engineering at the University of Michigan who helped us develop methods for the local delivery and polymerization of PEDOT in cortical tissue before our laboratory moved to the University of Delaware. We also acknowledge the efforts of Michelle Dee, an Undergraduate from USC who worked in our laboratory in the summer of 2010 on an NSF REU project. This work was supported in part by the Army MURI, the NSF, the University of Delaware, and an NIH EUREKA grant. D. C. M. is a Cofounder and Chief Scientific Officer of Biotectix LLC, a University of Michigan spin-off company in Ann Arbor that is developing

coatings for interfacing biomedical devices with living tissue.

References

- Abidian, M. R., Kim, D. H., & Martin, D. C. (2006). Conducting-polymer nanotubes for controlled drug release. *Advanced Materials*, 18, 405–409.
- Azemi, E., Lagenaur, C. F., & Cui, X. T. (2010). The surface immobilization of the neural adhesion molecule L1 on neural probes and its effect on neuronal density and gliosis at the probe/tissue interface. *Biomaterials*, 32, 681–692.
- Biran, R., Martin, D. C., & Tresco, P. A. (2005). Neuronal cell loss accompanies the brain tissue response to chronically implanted silicon microelectrode arrays. *Experimental Neurology*, 195, 115–126.
- Chen, Z. J., Gillies, G. T., Broaddus, W. C., Prabhu, S. S., Fillmore, H., Mitchell, R. M., et al. (2004). A realistic brain tissue phantom for intraparenchymal infusion studies. *Journal of Neurosurgery*, 101, 314–322.
- Cui, X. Y., Wiler, J., Dzaman, M., Altschulerb, R. A., & Martin, D. C. (2003). *In vivo* studies of polypyrrole/peptide coated neural probes. *Biomaterials*, 24, 777–787.
- Edell, D. J., Toi, V. V., McNeil, V. M., & Clark, L. D. (1992). Factors influencing the biocompatibility of insertable silicon microshafts in cerebral cortex. *IEEE Transactions on Biomedical Engineering*, 39, 635–643.
- Fawcett, J. W., & Asher, R. A. (1999). The glial scar and central nervous system repair. *Brain Research Bulletin*, 49, 377–391.
- Green, R. A., Lovell, N. H., & Poole-Warren, L. A. (2009). Cell attachment functionality of bioactive conducting polymers for neural interfaces. *Biomaterials*, 30(22), 3637–3644.
- Groenendaal, L. B., Zotti, G., Aubert, P. H., Waybright, S. M., & Reynolds, J. R. (2003). Electrochemistry of poly(3,4-ethylenedioxothiophene) derivatives: Past, present and future. *Advanced Materials*, 15, 855–879.
- He, W., McConnell, G. C., & Bellamkonda, R. V. (2006). Nanoscale laminin coating modulates cortical scarring response around implanted silicon microelectrode arrays. *Journal of Neural Engineering*, 3, 316–326.
- Kim, D. H., & Martin, D. C. (2006). Sustained release of dexamethasone from hydrophilic matrices using PLGA nanoparticles for neural drug delivery. *Biomaterials*, 27, 3031–3037.
- Kim, D. H., Abidian, M., & Martin, D. C. (2004). Conducting polymers grown in hydrogel scaffolds coated on neural prosthetic devices. *Journal of Biomedical Materials Research. Part A*, 71A, 577–585.
- Lempka, S. F., Miocinovic, S., Johnson, M. D., Vitek, J. L., & McIntyre, C. C. (2009). *In vivo* impedance spectroscopy of deep brain stimulation electrodes. *Journal of Neural Engineering*, 6, 1–11.
- Liu, X., McCreery, D. B., Carter, R. R., Bullara, L. A., Yuen, T. G. H., & Agnew, W. F. (1999). Stability of the interface between neural tissue and chronically implanted intracortical microelectrodes. *IEEE Transactions on Rehabilitation Engineering*, 7, 315–326.
- Ludwig, K. A., Uram, J. D., Yang, J., Martin, D. C., & Kipke, D. R. (2006). Chronic neural recordings using silicon microelectrode arrays electrochemically deposited with a poly(3,4-ethylenedioxothiophene) (PEDOT) film. *Journal of Neural Engineering*, 3, 59–70.
- Menei, P., Croue, A., Daniel, V., Pouplardbarthelaix, A., & Benoit, J. P. (1994). Fate biocompatibility of three types of microspheres implanted into the brain. *Journal of Biomedical Materials Research*, 28, 1079–1085.
- Noel, V., Randriamahazaka, H., & Chevrot, C. (2000). Composite films of iron(III) hexacyanoferrate and poly(3,4-ethylenedioxothiophene): Electrosynthesis and properties. *Journal of Electroanalytical Chemistry*, 489, 46–54.
- Polikov, V. S., Tresco, P. A., & Reichert, W. M. (2005). Response of brain tissue to chronically implanted neural electrodes. *Journal of Neuroscience Methods*, 148, 1–18.
- Richardson-Burns, S. M., Hendricks, J. L., Foster, B., Povich, L. K., Kim, D. H., & Martin, D. C. (2007). Polymerization of the conducting polymer poly(3,4-ethylenedioxothiophene) (PEDOT) around living neural cells. *Biomaterials*, 28, 1539–1552.
- Richardson-Burns, S. M., Hendricks, J. L., & Martin, D. C. (2007). Electrochemical polymerization of conducting polymers in living neural tissue. *Journal of Neural Engineering*, 4, L6–L13.
- Schwartz, A. B. (2004). Cortical neural prosthetics. *Annual Review of Neuroscience*, 27, 487–507.
- Seymour, J. P., & Kipke, D. R. (2007). Neural probe design for reduced tissue encapsulation in CNS. *Biomaterials*, 28, 3594–3607.
- Sykova, E., & Nicholson, C. (2008). Diffusion in brain extracellular space. *Physiological Reviews*, 88, 1277–1340.
- Szarowski, D. H., Andersen, M. D., Ritterer, S., Spence, A. J., Issacson, M., Craighead, H. G., et al. (2003). Brain responses to micromachined silicon devices. *Brain Research*, 983, 23–35.
- Turner, J. N., Shain, W., Szarowski, D. H., Andersen, M., Martins, S., Issacson, M., et al. (1999). Cerebral astrocyte response to micromachined silicon implants. *Experimental Neurology*, 156, 33–49.
- Winslow, B. D., & Tresco, P. A. (2010). Quantitative analysis of the tissue response to chronically implanted microwire electrodes in rat cortex. *Biomaterials*, 31, 1558–1567.
- Zhong, Y., & Bellamkonda, R. V. (2005). Controlled release of anti-inflammatory agent alpha-MSH from neural implants. *Journal of Controlled Release*, 106, 309–318.

Subject Index

- All channel microstimulation, 149
Alzheimer type dementia, 89–90
Amyotrophic lateral sclerosis (ALS), 27–28
Auditory neurons, 22
- Bayesian regression self-training method, 53
Brain–computer interfaces (BCIs). See also
 Brain–machine interface; Deep brain stimulation
 applications, 27–28
 communication, 27–28
 P300-BCI (see P300 based brain–computer interfaces)
Brain foreign body response, silicon
 microelectrode. See also Planar solid silicon microelectrode arrays, brain FBR
BBB integrity, 177
cellular and molecular features, 174–175
critical surface area concept model, 175
device-associated inflammation, 177–178
GFAP, intensity and spatial distribution, 177
IgG immunoreactivity, 177
inflammation, biotic-abiotic interface, 175
macrophage-secreted soluble factors, 175–177
neuronal viability, 177
tissue response, 174–175
- Brain–machine–brain interface (BMBI)*, 47–48
Brain–machine interface (BMI), 204
 artifact rejection, 6
 auditory neurons, 22
 biocompatibility
 definition, 182
 fixation mode, 182–183
 functional distance, 183
- implantation time, 183
implant size, 182
neural interface (*see Neural interface*)
data analysis
 ISIH, 7
 tonal and phoneme data analysis, 7–8
data collection sessions, 6–7
feedback, 21–22
human cortical neurons, 3
implantation target, 4–6
implanted electronic package, 4–6
incomplete SCI (*see Incomplete spinal cord injury (SCI), BMI approach*)
large-amplitude units, 19–20
mirror neurons, 22
neural prosthetic implications, 23–24
neurotrophic electrode,
 3–4, 5
paralyzed and communication-impaired subjects, 3
phoneme identification and speech production, 10
recording methodology, 6
single units, cellular origin, 17–19
single *vs.* multiunits, 22–23
spike sorting, 6
stability, 20–21
statistical analysis, 17
surgical implantation, 4–6
unit amplitudes and firing rates, 2, 8–10
whole body BMI (*see Whole body brain–machine interface*)
Brain model, 207–208

- Carbon nanotubes (CNTs)**
- back-propagating action potentials, 246
 - biocompatibility, 242–244
 - electrical coupling, 244, 245
 - network modeling, 245–246
 - neuronal excitability, 246
 - neuronal morphology and growth, 248–250
 - neuronal performance, 242–244
 - neuronal stimulation and recording
 - CNTs-modified MEAs, 248
 - electrical stimulation, 247
 - electrode impedance and charge transfer, 247
 - metal electrode vs. CNT-MEAs, 248
 - microelectrodes, 247
 - MWCNTs-modified MEA, 248, 249
 - nanotubes/neural interface, 246–247
 - polypyrrole (PPy)/SWCNT films, 247
 - SWCNTs-modified MEAs, 247–248
 - Physical–chemical features, 241–242
 - single-cell electrophysiology techniques, 244–245
 - soluble preparations, 241–242
 - structure, 242
 - types, 242
- Cochlear implant (CI)**
- brain function, 120–121
 - CIS strategy, 118, 119
 - cognitive neuroscience, 118
 - electric vs. acoustic stimulation, 119–120
 - neural prostheses, 117–118
 - postlingually deafened patients, 120
 - speech reception score, 120
 - tonotopic frequency, 118
 - topdown approach
 - brain imaging, 125–126
 - brain's capabilities, 121–122
 - brain stem-evoked response, 125
 - central auditory processing, 122
 - design process feedback, 126
 - electrophysiological hierarchy, 124–125
 - electrophysiological measure, 124
 - envelope cutoff frequency, 122
 - mismatch negativity, 124
 - neural activity, auditory periphery, 121
- Cognitive neuroscience**
- brain imaging, 125–126
 - brain's capabilities, 121–122
 - brain stem-evoked response, 125
 - central auditory processing, 122
 - design process feedback, 126
 - electrophysiological hierarchy, 124–125
 - electrophysiological measure, 124
 - envelope cutoff frequency, 122
 - mismatch negativity, 124
 - neural activity, auditory periphery, 121
 - plastic changes, brain function, 126–127
 - psychophysical task, 123–124
 - short-latency P1 wave, 124
- Constant phase element (CPE)**, 149–151, 160
- Continuous interleaved sampling (CIS) strategy**, 118, 119
- Corticospinal neurons**, 204
- Current source density (CSD) analysis**, 148, 154
- Deep brain stimulation (DBS)**
- Alzheimer type dementia, 89–90
 - brain–electrode interfaces, 76
 - brain–electrode–machine interface, 72, 73
 - depression, 75
 - 3D high-frequency stimulation, 76
 - ECoG recording
 - human BCI program, 79–80
 - primate BCI program, 78
 - rat BCI program, 77–78
 - epilepsy, 74
 - Göttingen minipig model, 101
 - impulse control disorders-OCD
 - bilateral excitotoxic lesion, 109–110
 - STN DBS, 111
 - STN inactivation, 110–111
 - stop-signal task, 111
 - motivation-addiction
 - bilateral STN lesion, 112
 - nucleus accumbens, 111–112
 - STN, 112–113

- MPTP, 105–106
 neuroprostheses, 80–81
 OCD, 74–75, 106
 optogenetics, 90–92
 Parkinson disease
 anti-Parkinsonian medication, 72–74
 beneficial effects, 107–108
 dystonia, 74
 five-choice serial RT task, 108–109
 hyperdirect pathway, 108
 implantation targets, 72
 Kaplan–Meier plot, 84, 85, 86
 levodopa therapy, 83–84
 LID, 72–74
 MR images, 84–88
 neural center, locomotor behavior, 84–88
 non-levodopa responsive symptoms, 84
 nonmotor function, 106–109
 pedunculopontine nucleus, 84–88
 STN DBS, 109
 STN electrolytic destruction, 72–74
 STN HFS, 106–107
 STN HFS effects, rat model, 107, 108
 STN lesion, 106
 tremor abolition, 72–74
 unilateral PPN DBS on UPDRS, 84–88
 psychosurgery evaluation, 75–76
 refractory depression
 cerebral blood flow, PET imaging, 88–89
 HRSD-17, 88–89
 sagittal T2-weighted MRI, 88–89
 safety and efficacy profile, 92–93
 subthalamic nucleus, 105–106
 Tourette syndrome, 75
 Depression, 75
 Dorsal root ganglia (DRG), 254
 Duke University Center for Neuroengineering (DUCN), 47–48
- Electrochemical impedance spectroscopy (EIS), 149
 Electrode encapsulation, 62–63
 Electrospun fibers, 257–258
 Embedded electrode, neural interface.
See Matrix-embedded electrode
- Encapsulated cell biodelivery (ECB), 98
 Epilepsy, 74
 External urethral sphincter (EUS) coactivation, 228–230
- Functional electrical stimulation (FES), 48, 55, 227–228
- Galvanostatic electrochemical polymerization, 265
 Gelatin-embedded electrode, 65–66
 Glial fibrillary acidic protein (GFAP)
 expression, 182
 Göttingen minipig model
 characteristics, 101
 neural and stem cell transplantation, 99–101
 neurobiological research animal, 98–99
 neurosurgery, 99
 scanning modality, 99
 spinal cord stimulation, 101
- Hamilton Rating Scale for Depression (HRSD-17), 88–89, 90
- Human brain enhancement. *See* Brain–machine interface
- Hybrid hierarchical controller (HHC) model
 actuator level, 219–220
 lower actuator-control level, 221
 reach/grasp/release phase, 221
 rule-based controller, 219–220
 spatial synergies, 221–223
 standing and walking, 223
 stroke, 223
 temporal synchrony model, 221, 222
 user and machine interface, 219–220
- Impulse control disorders (ICD)
 bilateral excitotoxic lesion, 109–110
 STN DBS, 111
 STN inactivation, 110–111
 stop-signal task, 111
- Incomplete spinal cord injury (SCI), BMI
 approach
 cortical area reorganization, 192–193
 damaged fibers reorganization, 196
 descending pathway reorganization

- Incomplete spinal cord injury (SCI), BMI approach (*Continued.*)
- remnant fibers, 195–196
 - synaptic efficiency changes, 193–195
 - locomotor control, 192
 - spinal circuitry
 - dual spinal lesion paradigm, 198–199
 - hindlimb locomotion, 198
 - rhythmogenic capability, 199
 - spinal locomotion, 198
 - treadmill locomotion, 199
- Internet browsing, P300-BCI
- ALS patient, 34–35
 - BCI2000 platform, 35–36
 - P300-based BCI, 34
 - QualiWorld accessibility software, 35–36
 - web browsing prototype, 36, 38
 - web browsing system, 34–35
- Intracortical microstimulation (ICMS), 55–57, 161. *See also* Multielectrode arrays (MEAs)
- based microstimulation
 - animal behavioral model, 147
 - audiogram, 148, 153
 - behavioral paradigm, 148
 - behavioral response, single electrode, 159
 - brain machine interfaces, 131
 - current source density analysis, 148, 154
 - electrophysiological markers, 159–162
 - functional sensory prosthesis, 152–155
 - histological markers, 159–162
 - histology, 148–149
 - impedance
 - chronically implanted electrode, 149
 - EIS, 149
 - equivalent circuit model, 149–151, 160
 - low-impedance interface, 151
 - Nyquist plot, 149, 158
 - impedance spectroscopy, 157–159
 - mean impedance, 162
 - microelectrodes, 132
 - multiple electrodes, 159
 - patterned microstimulation testing, 163
 - regression analysis, 148–149, 155
 - reliability of, 147
- sensory cortices stimulation, 146
- sensory prosthesis, 146
- short-term impedance, 162
- in situ* technique, 159
- threshold stability, 148, 156
- threshold task, 148
- voltage-gated sodium channel, 159–162
- Intraspinal microstimulation (ISMS)
- advantages, 233, 234
 - bladder control restoration, 229
 - bladder voiding, 230
 - external urethral sphincter coactivation, 228–229
 - microwire electrodes, 229–230
 - penetrating spinal cord electrodes, 228–229
 - clinical application, 236–237
 - historical aspects, 228
 - implants stability
 - flexibility, 235
 - functional stability, 235–236
 - minimal histological damage, 235
 - leg movement restoration
 - force recruitment, 231
 - implantation procedure, 230–231
 - ISMS implant array, 231
 - microwires, 230–231
 - motoneuronal pools, limb movement, 231, 232
 - lumbar spinal cord, 227–228
 - recruitment characteristics
 - gradual force recruitment, 233
 - single-joint movements, 234–235
 - whole-limb synergies, 234
 - from single joints to functional stepping
 - interleaved stimulus, 232–233
 - single-joint movements, 233
 - single microwires, 232
 - spinal cord network mapping, 228
- Kaplan–Meier plot, 84, 85, 86
- Komolgorov–Smirnov test, 149–151, 152

- Levodopa-induced dyskinesias (LID), 72–74
- Linear discriminant analysis (LDA), 31
- Macrophage, nanomodified surface. *See* Neurite outgrowth, nanomodified surface
- Matrix-embedded electrode
- drug delivery, 66–68
 - embedding technique, 66
 - gelatin-embedded electrode, 65–66
 - polymer based μ -foil electrode, 65–66, 67
 - umbrella electrode bundle, 65–66, 68
- 1-Methyl-4-phenyl-1,2,3,6-tetrahydropyridine (MPTP), 105–106
- Microdispensing, 256–257
- Mirror neurons, 22
- Mismatch negativity (MMN), 124
- Motor neural prosthesis (MNP)
- artificial control
 - controller functions, 219
 - HHC model (*see* Hybrid hierarchical controller model)
 - microcontrollers, 219
- command channel
- EEG channel system, 217
 - EMG signals, 217
 - hierarchical structure, 216–217
- electrical stimulation in physiological-like electrical stimulation
- BION technology, 218
 - electrical charge, 217
 - electrode arrays, 219
 - intraneural electrodes, 218
 - MNP-motoneuron interface, 217–218
 - motoneurons, 217
 - multicontact electrodes, 219
 - muscle contraction, pulse frequency, 217
 - nerve electrodes, 218
 - router system, 218
 - subcutaneous (implantable) electrodes, 218
 - surface electrodes, 219
 - sensor systems, 223
- Multichannel electrode, neural interface constructs and implantation procedure
- matrix-embedded electrode, 65–66
- surface configuration, 65
- ultrathin protrusions, 64–65
- electrode implant effect, 63, 64
- encapsulation, 62–63
- micromotions, 63
- nervous tissue stimulation, 62
- neuroanatomical technique, 69
- novel embedding technology, 68–69
- pathophysiological response, 62–63
- physiological state, 61
- plastic capacity, 62
- Multielectrode arrays (MEAs) based microstimulation
- action potential recordings
 - chronic timescales, 156, 158
 - microstimulated and non-microstimulated feline, 152–155
 - PCA-based t-distribution algorithm, 151
 - tissue viability, 159–162
 - chronic 1 kHz impedance, 152, 153, 154
 - data acquisition
 - electromyography, 148–149
 - electrophysiological recording, 148
 - impedance measurements, 148
 - data analysis
 - electromyographic data, 152
 - electrophysiological recording, 151
 - impedance, 149–151
 - electrode arrays, 147
- microstimulation
- all channel stimulation, 149
 - awake felines, 155–157
 - chronic stimulation, 149
 - evoked electromyographic response, 157–159
 - parallel stimulation, 149
 - stimulus waveforms, 149
 - neural system, 146
 - pre and postimpedance, 152
 - seizure, 162–163
 - surgical procedure, 147
 - thresholded action potential amplitudes, 159
- Multi-walled carbon nanotubes (MWCNTs), 242
- Musculoskeletal system, 206

- Nanowires, 258
- Nerve growth factor (NGF), 254
- NeuN immunoreactivity, 174
- Neural interface
 - BMI biocompatibility
 - DAPI staining, 186
 - fixation mode, 182–183
 - functional distance, 183
 - glial cells, 185
 - implantation time, 183
 - implant size, 182
 - neural density and inflammatory markers, 185–186
 - neurons counting, 186
 - tethered design strategy, 186–187
- multichannel electrode (*see also* Multichannel electrode, neural interface)
 - biocompatibility, 62–63
 - nervous tissue stimulation, 62
 - neuronal recording, 62
- Neural prosthetic implications, 23–24
- Neurite outgrowth, nanomodified surface
 - basal lamina components and neurotrophic factors, 260–261
 - biomimetic surfaces, 259
 - electrospun fibers, 257–258
 - foreign body reaction, 253
 - methods, 254, 255
 - microdispensing, 256–257
 - multiple electrode array, 253
 - nanoimprint lithography
 - contact guidance, 255–256
 - focal adhesions, 256
 - microdispensed pattern, BSA, 256, 257
 - nanoimprinted patterns, 256
 - nanowires, 258–259
 - porous silicon surfaces
 - electrochemical etching, 254, 255
 - macrophage activation, 255
 - neurite, 254, 256
 - pore sizes, 254
 - in vitro experiments, 259–260, 261
- Neuromodulation
 - cost-effective research model, 97
 - ECB, 98
- Göttingen minipig model
 - characteristics, 101
 - deep brain stimulation, 101
 - neural and stem cell transplantation, 99–101
 - neurobiological research animal, 98–99
 - neurosurgery, 99
 - scanning modality, 99
 - spinal cord stimulation, 101
- Parkinson disease, 98
 - stem cell transplantation, 98
- Neuronano Research Center, 63
- Neurotrophic electrode (NE), 3–4, 5
- Nonvisual p300-based BCI system, 40–41
- Obsessive-compulsive disorders (OCD), 74–75, 106**
- Optogenetics, 57, 90–92
- Parallel microstimulation, 149
- Parkinson disease
 - deep brain stimulation
 - anti-Parkinsonian medication, 72–74
 - beneficial effects, 107–108
 - dystonia, 74
 - five-choice serial RT task, 108–109
 - hyperdirect pathway, 108
 - implantation targets, 72
 - Kaplan-Meier plot, 84, 85, 86
 - levodopa therapy, 83–84
 - LID, 72–74
 - MR images, 84–88
 - neural center, locomotor behavior, 84–88
 - non-levodopa responsive symptoms, 84
 - nonmotor function, 106–109
 - pedunculopontine nucleus, 84–88
 - STN DBS, 109
 - STN electrolytic destruction, 72–74
 - STN HFS, 106–107
 - STN HFS effects, rat model, 107, 108
 - STN lesion, 106
 - tremor abolition, 72–74
 - unilateral PPN DBS on UPDRS, 84–88
 - neuromodulation, 98
 - P300 based brain-computer interfaces (BCIs)
 - brain activity translation, 27–28

- brain painting, 33–34
 checkerboard paradigm, 37–39
 dichotomous Hex-o-Spell, 37–39
 environmental control
 communication and control solution, 32–33
 information transfer rate, 32
 virtual quality, 32
 event related potential
 activation, centro-parietal regions, 28, 29
 advantage, 28
 feature extraction, 30–31
 letter matrix, 28, 30
 oddball paradigm, 28
 shrinkage linear discriminant analysis, 31
 signal conditioning, 29–30
 SWDA, 31
 internet browsing
 ALS patient, 34–35
 BCI2000 platform, 35–36
 P300-based BCI, 34
 QualiWorld accessibility software, 35–36
 web browsing prototype, 36, 38
 web browsing system, 34–35
 nonvisual p300-based BCI system, 40–41
 P300 BCI-based communication, 31–32
 physiological predictors, 39–40
 psychological variables, 39
 state-of-the-art technology, 41–42
 visual P300, 37–39
 PCA-based t-distribution algorithm, 151
 Planar elbow–shoulder system, SLR model
 BMI, 212–213
 cocontraction
 learning novel tasks, 210–211
 removal, 210–211
 converged solution, 209–210
 learning curves and exemplary joint angle trajectory, 209, 210
 limitations, 212
 modeled task
 cocontraction, 208–209
 impulsive force, 208
 simulation environment
 brain model, 207–208
 musculoskeletal system, 205, 206
 neuromusculoskeletal system, 206
 proprioceptor model, 205–207
 spinal cord model, 207, 208
 spinal cord role, 211–212
 Planar solid silicon microelectrode arrays, brain FBR. *See also* Brain foreign body response, silicon microelectrode
 animal surgery, 169
 BBB dysfunction, 171–173
 CD68, 171
 euthanasia and tissue preparation, 169–170
 GFAP immunoreactivity, 173
 immunohistochemistry, 170
 inflammation and reactive gliosis, 168
 microelectrodes, 169, 170
 NeuN immunoreactivity, 173–174
 neuronal *vs.* nonneuronal cell response, 174–175
 quantitative analysis
 fluorescent images, 170
 neuronal cell body distribution, 171
 staining intensity, 170–171
 recording instability, 168
 statistical analysis, 171
 tissue reaction, 168–169
 PlasticsOne^r C315G-MS303/2/SP Simultaneous Electrode-Guide combination, 265
 Polymer based μ-foil electrode, 65–66, 67
 Poly (3,4-ethylenedioxythiophene) (PEDOT)
 polymerization
 asymmetric polymerization, 269–270
 cyclic voltammograms, 266
 diffusion behavior, 266
 electrochemical polymerization rate, 266
 materials and methods
 adult rat brain tissue, 265
 cyclic voltammetry, 265
 EDOT solution, 265
 galvanostatic electrochemical polymerization, 265
 microelectrodes and microcannula, 264
 optical micrographs, 265
 positive controls, 265
 monomer delivery rate, 266
 optical micrographs, 268–269, 270

- Poly (3,4-ethylenedioxythiophene) (PEDOT) polymerization (*Continued*)
- PlasticsOne^r C315G-MS303/2/SP Simultaneous Electrode-Guide combination, 265–266
 - polymer cloud growth, 266–268, 270
 - stainless steel electrode control, CV, 268
- Proprioceptor model, 205–207
- QualiWorld accessibility software, 35–36
- Refractory depression
- cerebral blood flow, PET imaging, 88–89
 - HRSD-17, 88–89
 - sagittal T2-weighted MRI, 88–89
- Single-walled carbon nanotubes (SWCNTs), 242
- Spinal circuitry
- complete SCI
 - locomotor CPG localization, 197–198
 - and spinal CPG, 196–198
 - incomplete SCI
 - dual spinal lesion paradigm, 198–199
 - hindlimb locomotion, 198
 - rhythmogenic capability, 199
 - spinal locomotion, 198
 - treadmill locomotion, 199
- Spinal cord model, 208, 211–212
- Spinal-like circuitry
- behavioral phenomena, 204
 - cortical signals, 204
 - corticospinal neurons, 204
 - spinal-like regulator model
 - control inputs, 204–205
 - planar elbow-shoulder system (*see* Planar elbow-shoulder system, SLR model)
- Sputtered iridium oxide film (SIROF), 147
- Stepwise linear discriminant analysis (SWDA), 31
- Stimulus waveforms, 149
- Subthalamic nucleus (STN), 72–74
- Superior cervical ganglia (SCG), 254
- Tourette syndrome, 75
- Treadmill locomotion, 199
- Umbrella electrode bundle, 65–66, 68
- Unscented Kalman filter, 52, 53
- Whole body brain–machine interface (BMI)
- bimanual control, 53
 - bipedal locomotion
 - humanoid 51-DOF robot, 54
 - leg kinematics and EMGs, 54
 - paralysis treatment, 53–54
 - parameters of, 54
 - BMBIs, 47–48
 - classical paradigm, 49
 - decoders
 - autonomous controller, 53
 - Bayesian regression self-training method, 53
 - motor parameter, 52
 - multiple model-switching paradigm, 52
 - unscented Kalman filter, 52
 - functional electrical stimulation, 55
 - large-scale neuronal recording
 - chronic multielectrode longevity, 51–52
 - 3D recording cube, 49–51
 - neuroprosthetic device, 49–51
 - signal-to-noise ratio, 51, 52
 - VLSBA, 51–52
 - neuronal ensemble activity, 49
 - posture and balance, 55
 - primary motor cortex (M1), 47–48
 - sensorized neuroprosthetic
 - BMI-reaching tasks, 56
 - ICMS feedback, 56
 - optogenetic method, 57
 - positional signals, 56–57
 - somatosensory feedback channel, 55–56
 - somatosensory map, 56–57
 - whole-body neuroprosthetic
 - functional electrical stimulation, 48
 - magnetoencephalographic recording and fMRI, 48–49, 50
 - motor deficits, 48
 - paraplegic patient survey, 48
- Whole-limb synergy, 234
- Wilcoxon's signed rank test, 149–151, 152

- Volume 149: Cortical Function: A View from the Thalamus, by V.A. Casagrande, R.W. Guillery and S.M. Sherman (Eds.) – 2005 ISBN 0-444-51679-4.
- Volume 150: The Boundaries of Consciousness: Neurobiology and Neuropathology, by Steven Laureys (Ed.) – 2005, ISBN 0-444-51851-7.
- Volume 151: Neuroanatomy of the Oculomotor System, by J.A. Büttner-Ennever (Ed.) – 2006, ISBN 0-444-51696-4.
- Volume 152: Autonomic Dysfunction after Spinal Cord Injury, by L.C. Weaver and C. Polosa (Eds.) – 2006, ISBN 0-444-51925-4.
- Volume 153: Hypothalamic Integration of Energy Metabolism, by A. Kalsbeek, E. Fliers, M.A. Hofman, D.F. Swaab, E.J.W. Van Someren and R.M. Buijs (Eds.) – 2006, ISBN 978-0-444-52261-0.
- Volume 154: Visual Perception, Part 1, Fundamentals of Vision: Low and Mid-Level Processes in Perception, by S. Martinez-Conde, S.L. Macknik, L.M. Martinez, J.M. Alonso and P.U. Tse (Eds.) – 2006, ISBN 978-0-444-52966-4.
- Volume 155: Visual Perception, Part 2, Fundamentals of Awareness, Multi-Sensory Integration and High-Order Perception, by S. Martinez-Conde, S.L. Macknik, L.M. Martinez, J.M. Alonso and P.U. Tse (Eds.) – 2006, ISBN 978-0-444-51927-6.
- Volume 156: Understanding Emotions, by S. Anders, G. Ende, M. Junghofer, J. Kissler and D. Wildgruber (Eds.) – 2006, ISBN 978-0-444-52182-8.
- Volume 157: Reprogramming of the Brain, by A.R. Möller (Ed.) – 2006, ISBN 978-0-444-51602-2.
- Volume 158: Functional Genomics and Proteomics in the Clinical Neurosciences, by S.E. Hemby and S. Bahn (Eds.) – 2006, ISBN 978-0-444-51853-8.
- Volume 159: Event-Related Dynamics of Brain Oscillations, by C. Neuper and W. Klimesch (Eds.) – 2006, ISBN 978-0-444-52183-5.
- Volume 160: GABA and the Basal Ganglia: From Molecules to Systems, by J.M. Tepper, E.D. Abercrombie and J.P. Bolam (Eds.) – 2007, ISBN 978-0-444-52184-2.
- Volume 161: Neurotrauma: New Insights into Pathology and Treatment, by J.T. Weber and A.I.R. Maas (Eds.) – 2007, ISBN 978-0-444-53017-2.
- Volume 162: Neurobiology of Hyperthermia, by H.S. Sharma (Ed.) – 2007, ISBN 978-0-444-51926-9.
- Volume 163: The Dentate Gyrus: A Comprehensive Guide to Structure, Function, and Clinical Implications, by H.E. Scharfman (Ed.) – 2007, ISBN 978-0-444-53015-8.
- Volume 164: From Action to Cognition, by C. von Hofsten and K. Rosander (Eds.) – 2007, ISBN 978-0-444-53016-5.
- Volume 165: Computational Neuroscience: Theoretical Insights into Brain Function, by P. Cisek, T. Drew and J.F. Kalaska (Eds.) – 2007, ISBN 978-0-444-52823-0.
- Volume 166: Tinnitus: Pathophysiology and Treatment, by B. Langguth, G. Hajak, T. Kleinjung, A. Cacace and A.R. Möller (Eds.) – 2007, ISBN 978-0-444-53167-4.
- Volume 167: Stress Hormones and Post Traumatic Stress Disorder: Basic Studies and Clinical Perspectives, by E.R. de Kloet, M.S. Oitzl and E. Vermetten (Eds.) – 2008, ISBN 978-0-444-53140-7.
- Volume 168: Models of Brain and Mind: Physical, Computational and Psychological Approaches, by R. Banerjee and B.K. Chakrabarti (Eds.) – 2008, ISBN 978-0-444-53050-9.
- Volume 169: Essence of Memory, by W.S. Sossin, J.-C. Lacaille, V.F. Castellucci and S. Belleville (Eds.) – 2008, ISBN 978-0-444-53164-3.
- Volume 170: Advances in Vasopressin and Oxytocin – From Genes to Behaviour to Disease, by I.D. Neumann and R. Landgraf (Eds.) – 2008, ISBN 978-0-444-53201-5.
- Volume 171: Using Eye Movements as an Experimental Probe of Brain Function—A Symposium in Honor of Jean Büttner-Ennever, by Christopher Kennard and R. John Leigh (Eds.) – 2008, ISBN 978-0-444-53163-6.
- Volume 172: Serotonin-Dopamine Interaction: Experimental Evidence and Therapeutic Relevance, by Giuseppe Di Giovanni, Vincenzo Di Matteo and Ennio Esposito (Eds.) – 2008, ISBN 978-0-444-53235-0.
- Volume 173: Glaucoma: An Open Window to Neurodegeneration and Neuroprotection, by Carlo Nucci, Neville N. Osborne, Giacinto Bagetta and Luciano Cerulli (Eds.) – 2008, ISBN 978-0-444-53256-5.
- Volume 174: Mind and Motion: The Bidirectional Link Between Thought and Action, by Markus Raab, Joseph G. Johnson and Hauke R. Heekeren (Eds.) – 2009, 978-0-444-53356-2.
- Volume 175: Neurotherapy: Progress in Restorative Neuroscience and Neurology — Proceedings of the 25th International Summer School of Brain Research, held at the Royal Netherlands Academy of Arts and Sciences, Amsterdam, The Netherlands, August 25–28, 2008, by J. Verhaagen, E.M. Hol, I. Huitinga, J. Wijnholds, A.A. Bergen, G.J. Boer and D.F. Swaab (Eds.) – 2009, ISBN 978-0-12-374511-8.
- Volume 176: Attention, by Narayanan Srinivasan (Ed.) – 2009, ISBN 978-0-444-53426-2.
- Volume 177: Coma Science: Clinical and Ethical Implications, by Steven Laureys, Nicholas D. Schiff and Adrian M. Owen (Eds.) – 2009, 978-0-444-53432-3.
- Volume 178: Cultural Neuroscience: Cultural Influences On Brain Function, by Joan Y. Chiao (Ed.) – 2009, 978-0-444-53361-6.
- Volume 179: Genetic models of schizophrenia, by Akira Sawa (Ed.) – 2009, 978-0-444-53430-9.
- Volume 180: Nanoneuroscience and Nanoneuropharmacology, by Hari Shanker Sharma (Ed.) – 2009, 978-0-444-53431-6.

- Volume 181: Neuroendocrinology: The Normal Neuroendocrine System, by Luciano Martini, George P. Chrousos, Fernand Labrie, Karel Pacak and Donald W. Pfaff (Eds.) – 2010, 978-0-444-53617-4.
- Volume 182: Neuroendocrinology: Pathological Situations and Diseases, by Luciano Martini, George P. Chrousos, Fernand Labrie, Karel Pacak and Donald W. Pfaff (Eds.) – 2010, 978-0-444-53616-7.
- Volume 183: Recent Advances in Parkinson's Disease: Basic Research, by Anders Björklund and M. Angela Cenci (Eds.) – 2010, 978-0-444-53614-3.
- Volume 184: Recent Advances in Parkinson's Disease: Translational and Clinical Research, by Anders Björklund and M. Angela Cenci (Eds.) – 2010, 978-0-444-53750-8.
- Volume 185: Human Sleep and Cognition Part I: Basic Research, by Gerard A. Kerkhof and Hans P.A. Van Dongen (Eds.) – 2010, 978-0-444-53702-7.
- Volume 186: Sex Differences in the Human Brain, their Underpinnings and Implications, by Ivanka Savic (Ed.) – 2010, 978-0-444-53630-3.
- Volume 187: Breathe, Walk and Chew: The Neural Challenge: Part I, by Jean-Pierre Gossard, Réjean Dubuc and Arlette Kolta (Eds.) – 2010, 978-0-444-53613-6.
- Volume 188: Breathe, Walk and Chew; The Neural Challenge: Part II, by Jean-Pierre Gossard, Réjean Dubuc and Arlette Kolta (Eds.) – 2011, 978-0-444-53825-3.
- Volume 189: Gene Expression to Neurobiology and Behaviour: Human Brain Development and Developmental Disorders, by Oliver Braddick, Janette Atkinson and Giorgio M. Innocenti (Eds.) – 2011, 978-0-444-53884-0.
- Volume 190: Human Sleep and Cognition Part II: Clinical and Applied Research, by Hans P.A. Van Dongen and Gerard A. Kerkhof (Eds.) – 2011, 978-0-444-53817-8.
- Volume 191: Enhancing Performance for Action and perception: Multisensory Integration, Neuroplasticity and Neuroprosthetics: Part I, by Andrea M. Green, C. Elaine Chapman, John F. Kalaska and Franco Lepore (Eds.) – 2011, 978-0-444-53752-2.
- Volume 192: Enhancing Performance for Action and Perception: Multisensory Integration, Neuroplasticity and Neuroprosthetics: Part II, by Andrea M. Green, C. Elaine Chapman, John F. Kalaska and Franco Lepore (Eds.) – 2011, 978-0-444-53355-5.
- Volume 193: Slow Brain Oscillations of Sleep, Resting State and Vigilance, by Eus J.W. Van Someren, Ysbrand D. Van Der Werf, Pieter R. Roelfsema, Huibert D. Mansvelder and Fernando H. Lopes da Silva (Eds.) – 2011, 978-0-444-53839-0.